frontiers | Research Topics

Women in plant development and evodevo: 2022

Edited by
Jana Krajnakova, Raffaella Battaglia and Neusa Steiner

Published in
Frontiers in Plant Science

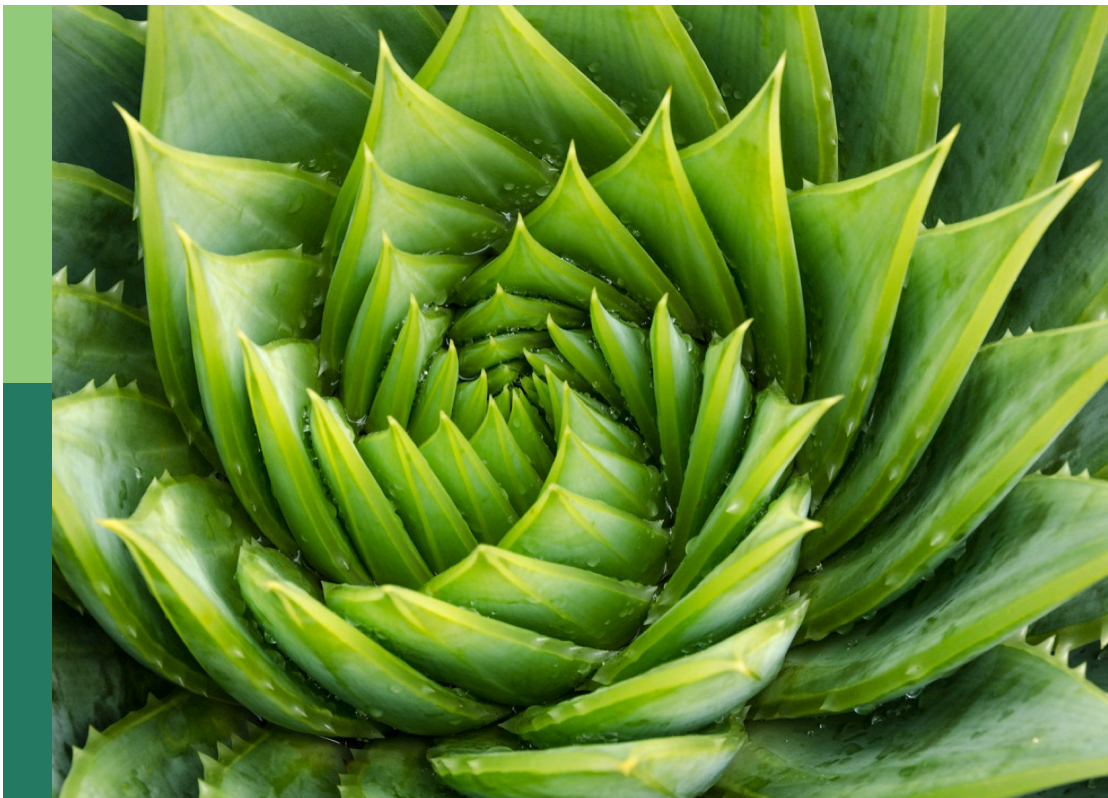

ISSN 1664-8714
ISBN 978-2-83251-955-4
DOI 10.3389/978-2-83251-955-4

About Frontiers

Frontiers is more than just an open access publisher of scholarly articles: it is a pioneering approach to the world of academia, radically improving the way scholarly research is managed. The grand vision of Frontiers is a world where all people have an equal opportunity to seek, share and generate knowledge. Frontiers provides immediate and permanent online open access to all its publications, but this alone is not enough to realize our grand goals.

Frontiers journal series

The Frontiers journal series is a multi-tier and interdisciplinary set of open-access, online journals, promising a paradigm shift from the current review, selection and dissemination processes in academic publishing. All Frontiers journals are driven by researchers for researchers; therefore, they constitute a service to the scholarly community. At the same time, the *Frontiers journal series* operates on a revolutionary invention, the tiered publishing system, initially addressing specific communities of scholars, and gradually climbing up to broader public understanding, thus serving the interests of the lay society, too.

Dedication to quality

Each Frontiers article is a landmark of the highest quality, thanks to genuinely collaborative interactions between authors and review editors, who include some of the world's best academicians. Research must be certified by peers before entering a stream of knowledge that may eventually reach the public - and shape society; therefore, Frontiers only applies the most rigorous and unbiased reviews. Frontiers revolutionizes research publishing by freely delivering the most outstanding research, evaluated with no bias from both the academic and social point of view. By applying the most advanced information technologies, Frontiers is catapulting scholarly publishing into a new generation.

What are Frontiers Research Topics?

Frontiers Research Topics are very popular trademarks of the *Frontiers journals series*: they are collections of at least ten articles, all centered on a particular subject. With their unique mix of varied contributions from Original Research to Review Articles, Frontiers Research Topics unify the most influential researchers, the latest key findings and historical advances in a hot research area.

Find out more on how to host your own Frontiers Research Topic or contribute to one as an author by contacting the Frontiers editorial office: frontiersin.org/about/contact

Women in plant development and evodevo: 2022

Topic editors

Jana Krajnakova — New Zealand Forest Research Institute Limited (Scion), New Zealand

Raffaella Battaglia — Council for Agricultural and Economics Research (CREA), Italy

Neusa Steiner — Federal University of Santa Catarina, Brazil

Citation

Krajnakova, J., Battaglia, R., Steiner, N., eds. (2023). *Women in plant development and evodevo: 2022*. Lausanne: Frontiers Media SA.

doi: 10.3389/978-2-83251-955-4

Table of contents

frontiers | Frontiers in Plant Science

ORIGINAL RESEARCH
published: 13 April 2022
doi: 10.3389/fpls.2022.865928

OsbZIP47 Is an Integrator for Meristem Regulators During Rice Plant Growth and Development

*Sandhan Prakash†, Rashmi Rai†, Mohamed Zamzam†, Owais Ahmad‡, Raghavaram Peesapati‡ and Usha Vijayraghavan**

Department of Microbiology and Cell Biology, Indian Institute of Science, Bengaluru, India

OPEN ACCESS

Edited by:
José Manuel Pérez-Pérez, Miguel Hernández University of Elche, Spain

Reviewed by:
Ram Kishor Yadav, Indian Institute of Science Education and Research Mohali, India
Weibing Yang, Institute of Plant Physiology and Ecology, Shanghai Institutes for Biological Sciences (CAS), China

***Correspondence:**
Usha Vijayraghavan
uvr@iisc.ac.in;
uvr123@gmail.com

†These authors share first authorship

‡These authors share second authorship

Specialty section:
This article was submitted to Plant Development and EvoDevo, a section of the journal Frontiers in Plant Science

Received: *30 January 2022*
Accepted: *09 March 2022*
Published: *13 April 2022*

Citation:
Prakash S, Rai R, Zamzam M, Ahmad O, Peesapati R and Vijayraghavan U (2022) OsbZIP47 Is an Integrator for Meristem Regulators During Rice Plant Growth and Development. Front. Plant Sci. 13:865928. doi: 10.3389/fpls.2022.865928

Stem cell homeostasis by the WUSCHEL–CLAVATA (WUS-CLV) feedback loop is generally conserved across species; however, its links with other meristem regulators can be species-specific, rice being an example. We characterized the role of rice *OsbZIP47* in vegetative and reproductive development. The knockdown (KD) transgenics showed meristem size abnormality and defects in developmental progression. The size of the shoot apical meristem (SAM) in 25-day *OsbZIP47KD* plants was increased as compared to the wild-type (WT). Inflorescence of KD plants showed reduced rachis length, number of primary branches, and spikelets. Florets had defects in the second and third whorl organs and increased organ number. *OsbZIP47KD* SAM and panicles had abnormal expression for CLAVATA peptide-like signaling genes, such as *FON2-LIKE CLE PROTEIN1* (*FCP1*), *FLORAL ORGAN NUMBER 2* (*FON2*), and hormone pathway genes, such as cytokinin (CK) *ISOPENTEYLTRANSFERASE1* (*OsIPT1*), *ISOPENTEYLTRANSFERASE 8* (*OsIPT8*), auxin biosynthesis *OsYUCCA6, OsYUCCA7* and gibberellic acid (*GA*) biosynthesis genes, such as *GRAIN NUMBER PER PANICLE1* (*GNP1/OsGA20OX1*) and *SHORTENED BASAL INTERNODE* (*SBI/OsGA2ox4*). The effects on *ABBERANT PANICLE ORGANIZATION1* (*APO1*), *OsMADS16,* and *DROOPING LEAF* (*DL*) relate to the second and third whorl floret phenotypes in *OsbZIP47KD*. Protein interaction assays showed OsbZIP47 partnerships with RICE HOMEOBOX1 (OSH1), RICE FLORICULA/LEAFY (RFL), and OsMADS1 transcription factors. The meta-analysis of KD panicle transcriptomes in *OsbZIP47KD*, *OsMADS1KD*, and *RFLKD* transgenics, combined with global OSH1 binding sites divulge potential targets coregulated by OsbZIP47, OsMADS1, OSH1, and RFL. Further, we demonstrate that OsbZIP47 redox status affects its DNA binding affinity to a *cis* element in *FCP1*, a target locus. Taken together, we provide insights on *OsbZIP47* roles in SAM development, inflorescence branching, and floret development.

Keywords: *Oryza sativa*, shoot apical meristem, panicle, floret, *PERIANTHIA*, *FASCIATED EAR4*, OsMADS1

INTRODUCTION

The post-embryonic shoot development in flowering plants depends on the balance between stem cell renewal in the central zone of above ground meristems and the adoption of specific differentiation programs in cells from the peripheral zone. The genetic framework of the basic WUSCHEL–CLAVATA (WUS-CLV) pathway for meristem maintenance is largely conserved in monocots and dicots, yet some functional differences are reported among cereal grass models, such as maize and rice. In maize, functions for *TASSEL DWARF1* (*TD1, CLV1* ortholog) and *FASCIATED EAR2* (*FEA2, CLV2* ortholog) in the shoot apical meristem (SAM) are not obvious in the respective mutants, yet mutants in these genes have significant and somewhat differential effects on the female *vs.* male inflorescence meristems (IMs) (Bommert et al., 2005; Dodsworth, 2009; Pautler et al., 2013; Chongloi et al., 2019). In rice, *FLORAL ORGAN NUMBER 1* (*FON1*) is the *CLV1* ortholog, while *FON2/FON4*, *FON2 SPARE1* (*FOS1*) and *FON2-LIKE CLE PROTEIN1* (*FCP1*) encode CLV3 peptide paralogs. FON2 signaling through FON1 majorly regulates the homeostasis of IMs whereas FCP1 triggered signaling regulates SAM through effects on *WUSCHEL RELATED HOMEOBOX* (*OsWOX4*), functionally related to *AtWUS* (Nagasawa et al., 1996; Suzaki et al., 2004, 2006; Ohmori et al., 2013). These tissue-specific effects of maize *TD1*, *FEA2,* and of rice *CLV3-like* genes exemplify species-specific innovations in signaling components of this core meristem regulatory circuit. In the SAM of Arabidopsis, AtWUS activates *SHOOT MERISTEMLESS (STM*), and both directly regulate *CLV3* expression to maintain constant stem cell number (Su et al., 2020). Integration of CLV-WUS pathway with the roles of class I *KNOTTED-1-LIKE HOMEOBOX* (*KNOX*) genes, Arabidopsis *STM*, rice *HOMEOBOX1* (*OSH1*), and maize *KNOTTED1* (*KN1*) in meristem maintenance is conserved across species (Vollbrecht et al., 2000; Brand et al., 2002; Tsuda et al., 2011). Similarly, the interlinking of WUS-CLV pathway with phytohormone-based meristem control, by cytokinin (CK), auxin (IAA/AUX), gibberellin (GA), brassinosteriod (BR) actions, is also conserved (Kurakawa et al., 2007; Gordon et al., 2009; Lee et al., 2009; Zhao et al., 2010; Yamaki et al., 2011; Somssich et al., 2016). OSH1 positively autoregulates itself directly by binding to evolutionarily conserved *cis*-elements within its locus (Tsuda et al., 2011). Further, OSH1 induces the expression of CK biosynthesis genes, such as *ADENOSINE PHOSPHATE ISOPENTENYL TRANSFERASE 2* (*OsIPT2*) and *OsIPT3* (Sakamoto et al., 2006). Interestingly, CK treatment of callus activates the transcription of rice *KNOX* genes (Tsuda et al., 2011). AtWUS and OsWOX4 also regulate CK signaling in Arabidopsis and rice, respectively (Leibfried et al., 2005; Ohmori et al., 2013). In the floral meristem center, the timing of the termination of stem cell activity is co-incident with carpel/ovule specification. This creates a determinate floral meristem for normal reproduction. Meristem termination is mediated by the concerted activity of floral organ identity genes (Class A, C, and E) whose regulatory effects on *WUS-CLV* and *WUS-KNOX* pathway genes operate in both monocots and eudicots [reviewed by Tanaka et al. (2013), Callens et al. (2018), and Chongloi et al. (2019)]. These genes are in turn spatially and temporally regulated. For example, Arabidopsis *LEAFY* (*LFY*) directly activates *APETALA1* (*AP1*) and *WUS* (Lenhard et al., 2001; Lohmann et al., 2001) while repressing the shoot meristem identity gene, *TERMINAL FLOWER1* (*TFL1*) (Moyroud et al., 2009, 2010). Furthermore, in young floral meristems, *LFY* together with *UNUSUAL FLORAL ORGAN* (*UFO*) and *WUS* activate *APETALA3* (*AP3*) and *AGAMOUS* (*AG*) gene expression in the third and fourth whorls of the developing meristem (Parcy et al., 1998; Busch et al., 1999; Wagner et al., 1999; Lenhard et al., 2001; Lohmann et al., 2001). In the later stages of floral meristem development, AG directly activates *KNUCKLES* (*KNU*) which leads to the repression of *WUS* by the recruitment of Polycomb group (PcG) chromatin modifiers (Ming and Ma, 2009; Sun et al., 2009, 2014; Liu et al., 2011; Zhang, 2014). Aside from LFY, the *AG* expression is also influenced by *PERIANTHIA* (*PAN*) that encodes a bZIP class TF, whose orthologs are *Oryza sativa basic LEUCINE ZIPPER* 47 (*OsbZIP47*) and maize *FASCIATED EAR4* (*ZmFEA4*). Floral meristem size and organ patterning defects in the Arabidopsis *pan-3 lfy-31* double the mutant, and in transgenics with modified PAN fusion proteins (repressive *vs.* activated forms) show roles of *AtPAN* in floral determinacy, meristem size, and floral organ patterning (Running and Meyerowitz, 1996; Chuang et al., 1999; Das et al., 2009; Maier et al., 2009, 2011). Maize *ZmFEA4* activates the expression of genes involved in AUX pathway and lateral organ differentiation and also regulates both SAM and IM size homeostasis (Pautler et al., 2015). Unlike Arabidopsis and maize, *OsbZIP47* (LOC_Os06g15480) is not well-characterized, and its interacting partners are largely unknown. Further, how inflorescence BM identity and transition regulators intersect with the two meristem maintenance pathways (CLV-WUS and KNOX1) is not much explored in rice. Here, functional characterization of *OsbZIP47* by RNA interference (dsRNAi)-based knockdown (KD) and identification of some meristem regulators, such as OsbZIP47 interacting partners sheds light on its role in meristem size and meristem developmental progression. Further, our transcriptome and meta-analysis uncovered downstream pathways that can be co-regulated by OsbZIP47 and OSH1, OsMADS1, or RFL.

MATERIALS AND METHODS

Plasmid Constructs Generation and Rice Transformation

For siRNA (interference) mediated KD of endogenous *OsbZIP47*, a gene-specific 226bp 3′UTR DNA fragment was cloned in the sense and in the antisense orientation in pBluescript vector, and were separated by a 270-bp linker. Subsequently, the insert in recombinant pBluescript was re-cloned in the binary rice expression vector, pUN downstream to the maize ubiquitin promoter for the expression of *OsbZIP47* hairpin RNAs (**Supplementary Figure 1**; Prasad et al., 2001). For the over-expression of *OsbZIP47*, the full length cDNA was cloned at *Bam*HI (blunted)-*Kpn*I sites in the pUN vector to create *pUbi:OsbZIP47* (**Supplementary Figure 4**). These constructs for KD and over-expression of *OsbZIP47* were transformed into

the *Agrobacterium tumefaciens* strain, LBA4404 and then co-cultivated with embryogenic calli from TP309 WT (*O. Sativa* var *japonica*) seeds as described by Prasad et al. (2001). Transgenic plants, dsRNAi *OsbZIP47* and Ox-*OsbZIP47*, were grown in IISc, Bangalore, Green house condition, approximately at 27°C during the months of January–May and July–October always with wild-type (WT) controls.

Phenotypic Characterization of Knockdown Transgenic

The transgenic plants, such as dsRNAi *OsbZIP47* and Ox-*OsbZIP47* were selected on half-strength MS medium containing 50 mg L^{-1} of hygromycin. Phenotypic analysis was done with T3 dsRNAi *OsbZIP47* transgenics and T1 Ox-*OsbZIP47* lines. Eosin-hematoxylin stained 25 DAG seedling tissue sections (7 μm, Lecia microtome; RM2045) were imaged by Apotome2 Zeiss. The cell size in the SAM was measured by ImageJ. The seedling height was measured at age eight DAG. Adult plant height, lamina joint angle, panicle length, branch characteristics, and spikelet numbers were measured after panicle booting. Pre-anthesis florets, in panicles prior to emergence from the flag leaf, were imaged using Leica Wild M3Z stereomicroscope.

RNA-Sequencing and RT-qPCR

Next Generation Sequencing (NGS) of RNA from *OsbZIP47* KD panicles (0.1–0.5 cm) was done for two biological replicates with matched WT panicles as controls. The total RNA was extracted using Trizol Reagent (Sigma) according to manufacturer's instructions. About 1 μg of total RNA was used for library preparation using rRNA depletion-based NEB Next UltraII RNA kit. The NGS was performed using Illumina Hi-Seq, pair-end 2 × 150 bp chemistry. After quality check (using FastQC and multiQC software), the reads were mapped against indexed *O. sativa* ssp. *japonica* cv. reference genome (RAP-DB)[1] using STAR2 (v2.5.3a). Further, differential gene expression (DGE) of read counts between WT and transgenics were computed using edgeR (v3.28.0) package with the absolute log2 fold change ≥ 1 with p-value ≤ 0.05. For real-time qPCR experiments, oligo(dT)-primed cDNAs were synthesized using 2 ug of total RNA with MMLV (reverse transcriptase, NEB). The qRT-PCR reactions were set up with 50–70 ng of cDNA, 250 nM gene-specific primers, and FastStart Universal Sybr Green Master (Rox) mix (Roche) in CFX384 real-time system (Biorad) or Applied Biosystems ViiA 7 system. Fold change in the transcript levels of deregulated genes was calculated as a difference in cycle threshold value between transgenic and wild type. To obtain normalized threshold value (ΔΔCt), first ΔCt value was calculated by subtracting the Ct value for internal control; *Ubiquitin5,* from the Ct value for each gene of interest (Gene Ct-Ubi5 Ct). Then ΔΔCt was calculated by subtracting the WT ΔCt value from the ΔCt value obtained from the transgenic tissue. The fold-change was calculated as $2^{\wedge -(\Delta\Delta Ct)}$. Primers used and their sequences are listed in **Supplementary Table 2**. The RNA sequencing raw data files used in this study have been deposited to Gene Expression Omnibus (GEO) database under the accession number GSE196747.

[1]https://rapdb.dna.affrc.go.jp/

RNA *in situ* Hybridization

To generate *OsbZIP47* riboprobes, a gene-specific 226bp DNA fragment from 3′UTR (1329-1555 bp) was PCR-amplified and cloned in the pBluescript KS + vector. Sense and antisense Digoxigenin-labeled (DIG-UTP, Roche) riboprobes were prepared by *in vitro* transcription using T3 and T7 RNA polymerases (NEB), respectively. Tissue processing and probe hybridizations was done according to the study by Prasad et al. (2005). Signal was developed using anti-digoxygenin-alkaline phosphatase (AP) conjugated antibodies (Roche) and 5-Bromo-4-chloro-3-indolyl phosphate (BCIP)-nitro blue tetrazolium (NBT) chromogenic substrates (Roche). Images were captured by Apotome2 Zeiss microscope system.

Bacterial Expression of OsbZIP47 Full-Length Protein and Studies of Oligomeric Status

For OsbZIP47 protein expression and purification from bacteria, *OsbZIP47* full-length (FL) CDS was cloned in the pET32a vector. Thioredoxin-His-tagged OsbZIP47FL was expressed from Rosetta (DE3) bacterial strain induced with 0.2 mM of isopropyl β- *d*-1-thiogalactopyranoside (IPTG) for 3 h at 37°C. Oligomeric states of OsbZIP47 protein was determined by analytical size-exclusion chromatography (SEC) performed at 4°C on a Superdex 200 increase column Cytiva (Formerly, GE Healthcare Life Sciences), Marlborough, United States pre-equilibrated with a buffer (25 mM of sodium phosphate (pH 7.4), 100 mM of NaCl, and 5% of glycerol). Approximately, 400 μg of protein, (∼2 mg/ml) was injected into AKTA purifiers Cytiva (Formerly, GE Healthcare Life Sciences), Marlborough, United States connected to the column. The flow rate was maintained at 0.3 ml/min and the protein elution profile was at 220 nm. The molecular weight was calculated using a standard plot. Molecular weight was calculated using the equation: $Y = -0.602X + 4.6036$, where $Y = V_e/V_o$ (V_e = Elution volume; V_o = Void volume) and X = Log of molecular weight in Dalton.

Electrophoretic Mobility Shift Assays

Escherichia coli rosetta (DE3) bacterial lysates with the Trx-His-OsbZIP47 FL was prepared in a buffer: 10mM of HEPES-KOH, pH 7.8, 50mM of NaCl, 0.5% of Non-idet P-40, 0.5 mM of EDTA, 1 mM of MgCl2, 10% of glycerol, 0.5 mM of DTT, and 1x protease inhibitor cocktail (Sigma). About 1–4 μl of lysate was incubated with 5'end P^{32} labeled DNA oligonucleotide probes for 30 min at 4°C in 1× EMSA buffer (20 mM of HEPES-KOH pH 7.8, 100 mM of KCl, 2 mM of DTT, 1 mM of ETDA, 0.1% of BSA, 10 ng of Herring sperm DNA, 10% of glycerol, 1× protease inhibitor cocktail) in 15 μl reactions. After binding, the reaction constituents were resolved on an 8% of native-PAGE gel in 0.5× Tris-borate EDTA (TBE) buffer at room temperature. Gel autoradiography was done in a phoshorimager (GE; Typhoon FLA 9500). The DNA probe sequences are listed in **Supplementary Table 2**.

Microscale Thermophoresis Assay

Escherichia coli rosetta (DE3)-expressed proteins (Trx-His-OsbZIP47 FL and Trx-His; **Supplementary Figure 9**) were added to the buffer: 10mM of HEPES-KOH pH 8.0, 50 mM of NaCl, 0.5% of TWEEN-20, 0.5 mM of EDTA, 1 mM of $MgCl_2$, 10% of glycerol, 2 mM of beta mercaptoethanol, and 1 mM of PMSF. About 10 mM of each protein was labeled with 5 mM of Red-NHS 2nd Generation primary amine labeling dye (NanoTemper GmbH, Cat# MO-L011), and then eluted in the buffer: 10 mM of HEPES-KOH pH 8.0, 50 mM of NaCl, 0.5% of TWEEN-20, 0.5 mM of EDTA, 1 mM of $MgCl_2$, 10% of glycerol, 1X PIC (ROSCHE), and a reducing/oxidizing agent (20 mM of DTT/1 mM of oxidized glutathione). The labeled protein was incubated with dsOsFCP1 oligonucleotides which was serially diluted from 100 μM to 3.05 nM in 16 steps and fluorescence was measured using Monolith NT.115Pico (NanoTemper GmbH). The excitation power was varied between 1 and 50% to obtain measurable fluorescence signal. The MST power was varied between medium to high, to achieve high signal to noise ratio. For OsbZIP47 FL, the initial fluorescence was measured which is indicative of rapid binding. For Trx-His tag, the response evaluation was done at default on time. MO Control v1.6.1 (NanoTemper GmbH) and MO Affinity Analysis v2.6 (NanoTemper GmbH) were used for the analysis.

Yeast Two-Hybrid Assays

The full length CDS of *OsbZIP47* was amplified from KOME clone, AK109719 using gene-specific primers, cloned into pBSKS vector and validated by restriction digestions and Sanger sequencing. The CDS was subsequently cloned into yeast two hybrid vectors, pGBDUC1 and pGADC1. Similarly, all the CDS fragments that would encode prey proteins, such as OsMADS1, OsETTIN1/2, RFL, OSH1, OsMADS15, OsMADS2, OSH15, and OsMADS15 were PCR-amplified from either KOME cDNA clones or from cDNA made from panicle tissue RNA, and subcloned into pGBDUC1 and pGADC-1 vectors. The bait clone, pGBDUC1 OsbZIP47 and indicated prey recombinants in pGADC1 were co-transformed into the yeast, pJ69-4A yeast two-hybrid (Y2H) strain (James et al., 1996). Transformants were selected on synthetic drop out media lacking leucine and uracil. Protein interactions were assessed in at least five purified transformants by serial dilution spotting of broth cultures onto SD/-Leu-Ura-His plates supplemented with 10 mM of 3AT and by the ONPG assay (**Supplementary Materials** and Methods).

Bimolecular Fluorescence Complementation Assays

The *OsbZIP47* cDNA with a truncated C domain (amino acid 199–385) was cloned into pSPYCE (M) (*C*-terminal fusion) and pSPYNE (R) 173 (*N*-terminal fusion) bimolecular fluorescence complementation (BiFC) vectors (Waadt et al., 2008). Similarly, the full-length CDS encoding prey proteins, such as OsMADS1, OsETTIN 2, RFL, OSH1, and OsMADS15 were subcloned into pSPYNE (R) 173 vector. Six combinations of cEYFP and nEYFP fusions, including positive and negative controls, were transiently co-expressed in onion (*Allium cepa*) epidermal cells by *Agrobacterium. tumefaciens* (C58C1) infiltration as described by Xu et al. (2014). Co-transformed tissues were incubated at 25°C in dark for 48 h before being assayed for YFP activity. Fluorescence images were screened using a confocal laser microscope (Zeiss LSM880, Airyscan) with 2AU 480 nm excitation and 520 nm emission for the detection of YFP signal.

Meta-Analysis

The published transcriptome datasets in dsRNAi*OsMADS1* and dsRNAi*RFL* panicles were adopted in this study to compare them with that of *OsbZIP47KD* transcriptome dataset. The differentially expressed genes (DEGs) from each dataset was taken up for pair-wise comparison to identify unique, or commonly (upregulated, or downregulated) downstream genes. The deregulated genes were also corelated with the published data on OSH1 genome-wide binding (**Supplementary Materials** and Methods). To align genes from the diverse datasets, i.e., transcriptomes downstream to *OsMADS1*, *RFL*, and genes bound by OSH1 for meta-analysis and for GO enrichment analyses, the gene IDs as per RAP-dB (see text footnote 1) were converted to their corresponding gene ID in MSU-TIGR v7.[2] After this curation, among the 2,800 RAP-dB ID genes, only 2,210 genes were also annotated in MSU-TIGR v7. The list of RAP-dB gene IDs and their corresponding MSU v7 LOC_IDs are presented in **Supplementary Dataset 1**.

RESULTS

OsbZIP47 Knockdown Plants Have Enlarged Shoot Apical Meristem Size

To investigate the developmental roles of *OsbZIP47,* we generated thirteen independent *OsbZIP47* KD transgenics (*OsbZIP47KD*) by RNA interference (dsRNAi, **Figure 1A**) specific to a unique region of *OsbZIP47* 3′UTR. Based on the degree of KD and seed viability in primary T0 transgenic lines, we chose two lines; *OsbZIP47*KD line #10 and *OsbZIP47*KD line #14 for detailed phenotypic analysis in T3 generation. As a representative, phenotypic data from the *OsbZIP47*KD line #14 is further discussed here. In pooled panicle tissues (0.1–0.5 cm) from this line, qRT-PCR showed approximately 24-fold downregulation of the endogenous *OsbZIP47* transcripts (**Supplementary Figure 1**). The earliest phenotype noted was the seedling height at 8 days after germination (DAG), which was significantly reduced in *OsbZIP47KD* as compared to the WT (**Figures 1B,C** and **Supplementary Table 1**). This observation led us to examine SAM in the histological sections of seedlings aged 25 days after germination (DAG) from both WT and *OsbZIP47KD* plants. First, we examined SAM size and found that SAM area was increased as compared to WT (**Figures 1D,F**). Consistent with SAM enlargement in *OsbZIP47KD* plants, SAM width and height showed significant and marginal increase, respectively (**Supplementary Table 1**). To understand the cellular differences that underlie meristem size abnormalities, the cell size of L1 layer in the upper central and the peripheral zone of

[2]http://rice.plantbiology.msu.edu/

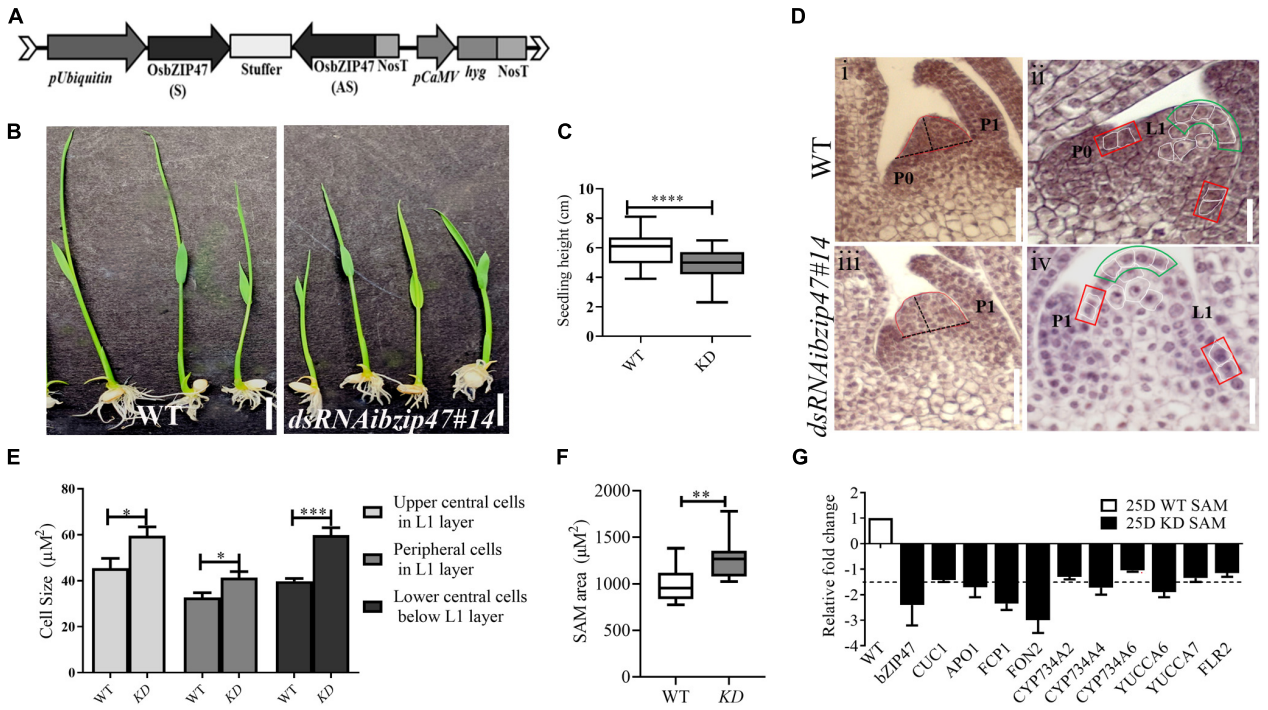

FIGURE 1 | *OsbZIP47* knockdown (KD) vegetative phenotypes. **(A)** Schematic representation of *dsRNAiOsbZIP47* transgene T-DNA segment. **(B)** Seedling height of 8-day *OsbZIP47KD* (*dsRNAibZIP47#14*) plants is shorter than that of wild-type (WT) plants. Scale bar = 1 cm. **(C)** Seedling height data shown as mean ± s.d., Student's *t*-tests, $^{****}P < 0.0001$, $n = 30$. **(D)** Representative histological sections of SAMs from WT and *dsRNAibZIP47#14*. SAM area in 25 days after germination (DAG) seedlings marked by red outline in panels **(i,iii)**. SAM height and width are marked by dashed black lines. Measured cells are marked with white outlines in panels ii and iv. Scale bar in panes **(i,iii)** are of 50 μM, and panels **(ii,iv)** are of 20 μM. **(E)** Comparison of L1 cell size in the central, and peripheral cells, and in the lower central cells underlying the central L1 layer. The statistical analysis of cell size, for cells in different regions of the meristem, was derived from 10 to 12 different sections. Data is shown as mean ± s.d. Student's *t*-tests. $^{*}P < 0.05$, $^{***}P < 0.001$. **(F)** Comparison of SAM area in *OsbZIP47KD* (*dsRNAibZIP47#14*) *vs.* WT in 25 DAG seedlings. Data is shown as mean ± s.d. Student's *t* tests, $^{**}P < 0.01$, $n = 10$. **(G)** RT-qPCR analyses of *CUC1, APO1, FCP1, FON2, CYP734A2, CYP734A4, CYP734A6, YUCCA6, DRUS2/FLR2*, and *FON2* transcripts in SAM from 25 DAG seedlings. Fold-change values were determined by comparing the normalized expression levels in *OsbZIP47KD* plants to WT plants.

the meristem and the internal cells underlying the L1 layer were measured. Intriguingly, the size of these cells was increased as compared to WT (**Figure 1E**). Further, the spatial distribution of dividing cells in 25DAG SAMs was assessed by RNA *in situ* hybridization for the cell cycle S-phase marker, HISTONE4 (H4) (**Supplementary Figure 2**). Compared to WT, the overall H4 transcript signal in the median longitudinal SAM sections of *OsbZIP47KD* seedlings was higher. Altogether, these results suggest that the increased SAM area in *OsbZIP47KD* seedlings is attributed to an increase in cell size and number. To understand some molecular corelates for SAM phenotypes, transcript levels for few known regulators of SAM size homeostasis were tested (**Figure 1G**) using SAM tissues from 25 DAG seedlings. The downregulation of *FCP1* and *FON2* (rice homologs of *CLV3*), *APO1* (*UFO1* homolog), *CYP734A4,* and *YUCCA6* was observed. Also, *CUC1,* the lateral meristem boundary marker (Aida et al., 1997; Takeda et al., 2011), showed a marginal reduction in expression. The downregulation of rice *CLV3* homologs in *OsbZIP47KD* SAM may contribute to the overall enlarged SAM size. Further, the increased cell size in L1 layer and its underlying cells could be attributed to a reduction in *CYP734A4* expression in SAM of *OsbZIP47KD* plants. Of note is the report that SAM cells in *CYP734A* RNAi plants are more vacuolated as compared to the WT which was suggested to indicate premature cell differentiation (Tsuda et al., 2014). Altogether, these gene expression effects of *OsbZIP47* can be related to abnormal SAM size homeostasis on its KD with novel effects on the components in the CLV-WUS pathway, on other meristem regulators, AUX, and BR phytohormone pathways.

Late Heading Date and Altered Panicle Architecture of *OsbZIP47* Knockdown Plants

OsbZIP47KD plants are delayed by 20 days for SAM to IM transition. At this stage, *OsbZIP47KD* plant height was reduced compared to WT (**Figures 2A–D**) suggesting that in the WT, *OsbZIP47* promotes developmental transition from the vegetative to reproductive phase. The shorter plant height was due to poor stem internode elongation in the KD transgenics without change in internode number (**Figure 2F**). The panicle of KD plants showed developmental abnormalities, i.e., reduced inflorescence axis (panicle rachis) length (**Figure 2E**), reduced number of primary branches, and spikelets (**Figures 3A,L,M** and

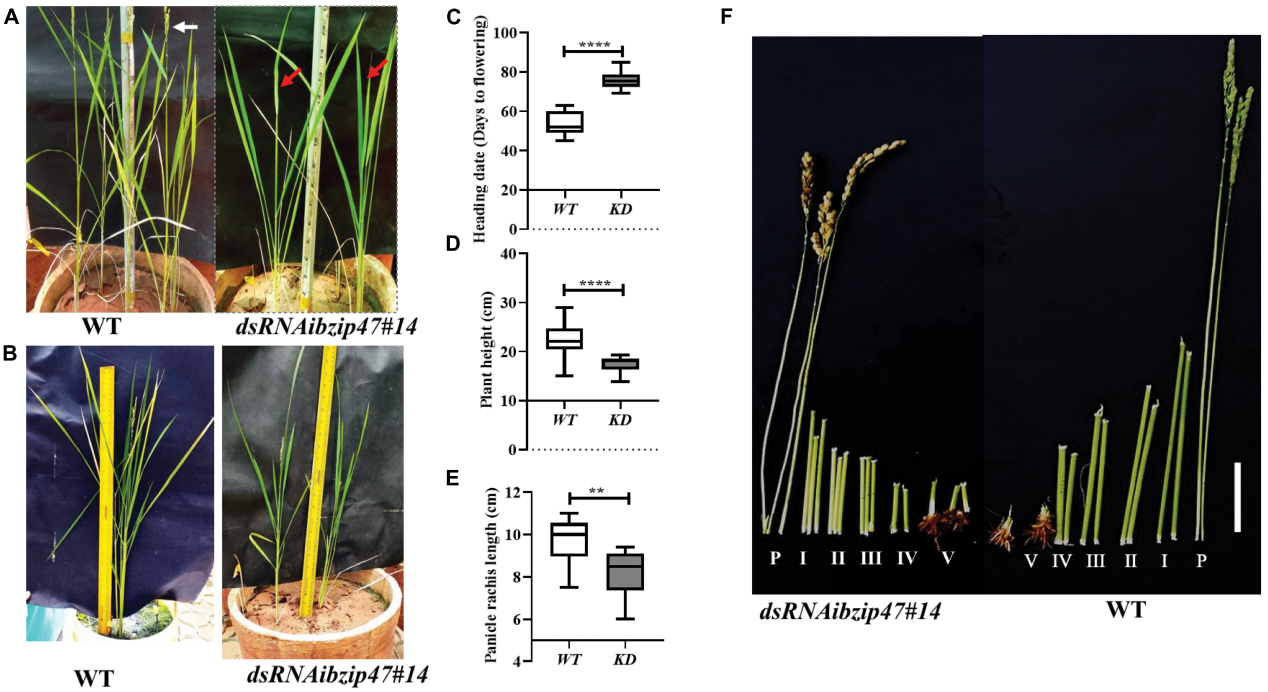

FIGURE 2 | Phenotypic effects of *OsbZIP47KD* on plant growth and floral transition. **(A)** Flowering timing (SAM to inflorescence meristem (IM)/panicle meristem transition) in *OsbZIP47KD* plants is delayed by approximately 22 days as compared to the WT. White arrow indicates the booted panicle in WT and red arrow points to the absence of the booted panicle in a *OsbZIP47KD* plant of the same age. **(B)** Height of mature flowering plants shows that as compared to the WT, *OsbZIP47KD* plants are shorter. Quantitation of heading dates **(C)**, plant height **(D)**, and panicle rachis length **(E)** in WT and *OsbZIP47KD* plants. Data are shown as the mean ± s.d. (Student's *t*-tests, $^{**}P < 0.01$, $^{****}P < 0.0001$, $n = 10$). **(F)** Internodes in mature flowering WT and *OsbZIP47KD* plants are displayed and are numbered from I to V from the apical end. P is the panicle bearing node and internode. Bar, 2.5 cm. Shorter internodes from I to V in *OsbZIP47KD* contributes to the reduced height.

Supplementary Table 1). Together, these phenotypes indicate early progression of primary branch meristems to spikelets in *OsbZIP47KD* plants and point to a possible role of *OsbZIP47* in the temporal control of branch meristem indeterminacy. Moreover, *OsbZIP47KD* plants had greater flag leaf lamina joint angle as compared to the WT (**Figures 3B,C,K**). KD plants of *CYP734A4* (Tsuda et al., 2014), a gene with reduced expression in *OsbZIP47KD* plants (**Figure 1G**), also share this phenotype and have abnormal meristems. Plant architecture, flowering time, leaf angle, and inflorescence architectures all impact yield, grain shape, and size (Harder and Prusinkiewicz, 2013; Sakuma and Schnurbusch, 2020). Interestingly, seeds from *OsbZIP47KD* plants were altered for the length/width (L/W) ratio as compared to WT (**Figures 3I,J**), suggesting *OsbZIP47* impedes cell proliferation in the grain width direction, which is supported by a recent finding of Hao et al. (2021). In later sections of our study on *dsRNAiOsbZIP47* lines, we identify some molecular links underlying cell proliferation in the developing grain. We propose that the role of *OsbZIP47* in restriction of cell proliferation is likely attributed to the positive regulation of *EL2*, encoding a plant cyclin-dependent kinase inhibitor, and negative regulation of some key cell-cycle regulators i.e., *CYCLIN-D7-1* (*CYCD7;1*) and *MITOGEN-ACTIVATED PROTEIN KINASE KINASE 10* (*MKK10-1*) in WT panicles (**Supplementary Dataset 1**). Rice EL2 cell cycle inhibitory functions are proposed to link cell cycle progression with biotic and abiotic stress responses (Peres et al., 2007). In Arabidopsis, *AtCYCD7* expression is transcriptionally regulated by cell type-specific transcription factors that confine its expression to appropriate developmental window as ectopic expression triggered division (Weimer et al., 2018). The OsMKK10-1 paralog, OsMKK10-2 phosphorylates OsMPK6 *in vivo* (Ma et al., 2017). This is interesting since mutations of *OsMPK6* impair differentiation of L1 layer cells during early embryogenesis (Yi et al., 2016).

OsbZIP47 Contributes to Second and Third Whorls, Lodicule, and Stamen Organ Development

OsbZIP47KD floret phenotypes were largely restricted to lodicules and stamens (**Figures 3D–H**). The organ defects were grouped into four classes. Class I, representing 40% of *OsbZIP4KD* florets, had mild deformed lodicule (distal elongation) with normal stamen number (**Supplementary Figure 3**). In class II (∼28%), mild lodicule elongation occurred with abnormal short stamens and poorly developed anthers (**Figure 3H**). Florets of class III (∼20%) had partially deformed lodicules with an increase in stamen number to 7 (**Figures 3E,G**). In class IV (∼12%) florets had mildly elongated lodicules and chimeric organs with lodicule and stamen characteristics

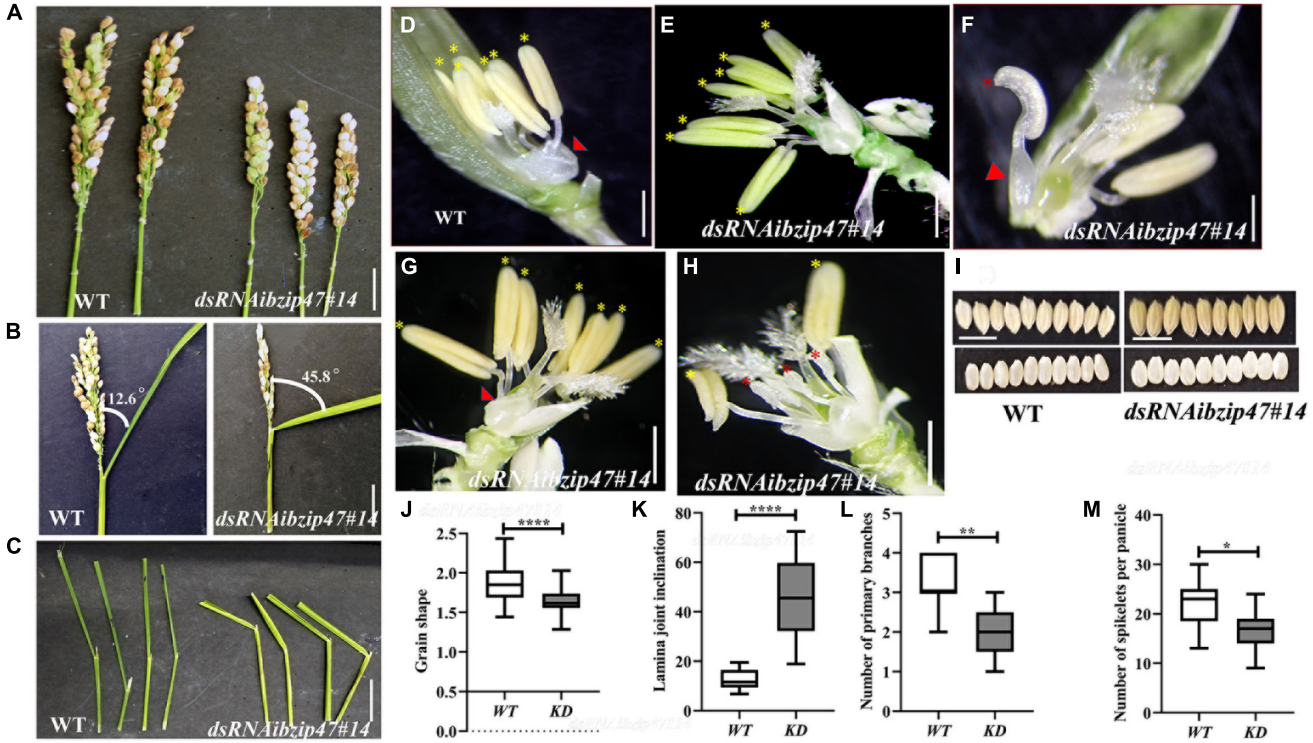

FIGURE 3 | Floret organ numbers and organ development in *OsbZIP47KD* plants. **(A)** Shorter panicle *OsbZIP47KD* with reduced number of primary branches and spikelet number per panicle as compared to the WT plant. **(B,C)** Flag leaf angle in fully headed panicles shows increased lamina joint angle in *OsbZIP47KD* plant as compared to the WT. **(D)** WT floret organs shown after removal of lemma and the spikelet sterile lemmas. Red arrow points to the pair of lodicules and yellow asterisks to the six normal stamens. **(E–H)** Organ phenotypes in *OsbZIP47KD* florets. **(E)** Floret with seven stamens (yellow asterisks) with normal filaments and anthers. **(F)** Floret with mildly deformed lodicule (red arrowhead), two of its six normal stamens (others were removed) and a chimeric second whorl organ with lodicule and stamenoid features (red asterisk). **(G)** Floret with deformed lodicule and seven normal stamens (yellow asterisk). **(H)** Floret with slightly deformed lodicule, short stamens, and shrunken anthers (red asterisk), two near normal stamens (yellow asterisk). **(I,J)** Grain morphology in *OsbZIP47KD* and WT plants. The length/width (L/W) ratio of *OsbZIP47KD* seeds was lower than that of WT seeds, suggesting increased grain width. Scale bar = 1 cm in panels **(A–I)**. **(J–M)** Statistical analysis (mean ± s. d.) of grain shape, lamina joint angle, primary branch number, and number of spikelets per panicles. Data in panels **(J)** [n = 40 in panel **(J)**], **(K)** (n = 10), **(L)** (n = 11), **(M)** (n = 9), Student's t-tests, $^{*}P < 0.05$, $^{**}P < 0.01$, $^{***}P < 0.001$.

(**Figure 3F**). Also, in most florets of all classes, the lodicules were abnormally fused with lemma making dissection of the lemma from the floret difficult. Altogether, these data suggest that *OsbZIP47* contributes to floral organ development in the second and third whorls. In a complementary analysis, we examined consequences of ubiquitous overexpression of full-length *OsbZIP47*cDNA in transgenic rice. Surprisingly, none of the *OsbZIP47OX* lines had any notable phenotypic changes from the WT despite ∼10-fold overexpression in *OsbZIP47OX* panicle tissues (**Supplementary Figure 4**). A speculation is that *OsbZIP47* functions may depend on partners or that some post-translational modifications (PTMs) may modulate its functions, as was concluded from overexpression studies of Arabidopsis *AtPAN* (Chuang et al., 1999).

Tissue Expression Profile of *OsbZIP47* Through Development

RNA *in situ* hybridization was performed to examine spatial distribution of *OsbZIP47* mRNA in various above ground meristems. These experiments confirmed transcripts in meristems that is consistent with the phenotypes of *OsbZIP47KD* plants. In SAM of wild type young seedlings (5 DAG and 25 DAG), transcripts were evenly distributed (**Figures 4A,B**). This pattern is somewhat different from maize *FEA4* where the signals are excluded from SAM stem cell niche and from incipient P0 leaf primordium (Pautler et al., 2015). During reproductive development, high levels of *OsbZIP47* transcripts are shown at the apical end of growing IM/rachis and at the ends of branch meristem (PBM and SBM, **Figures 4C,D**) which may relate to the poorly branched inflorescence of knockdown plants. In elongating primary and secondary branches (**Figure 4D**), transcript signal is mild and spatially uniform. In spikelet meristem (SM, Sp2, **Figure 4E**), and in floral meristems (Sp4-Sp6, **Figure 4F**), the signal is high and spatially uniform. However, in mature florets, *OsbZIP47* RNA was confined to the lodicule, stamen and carpel organ primordia, and differentiating organs (**Figure 4G**). Additionally, hybridization signal in carpel wall (c) and ovule (o) was observed (**Figure 4H**). Arabidopsis *pan* mutant flowers occasionally have multiple carpels up to three

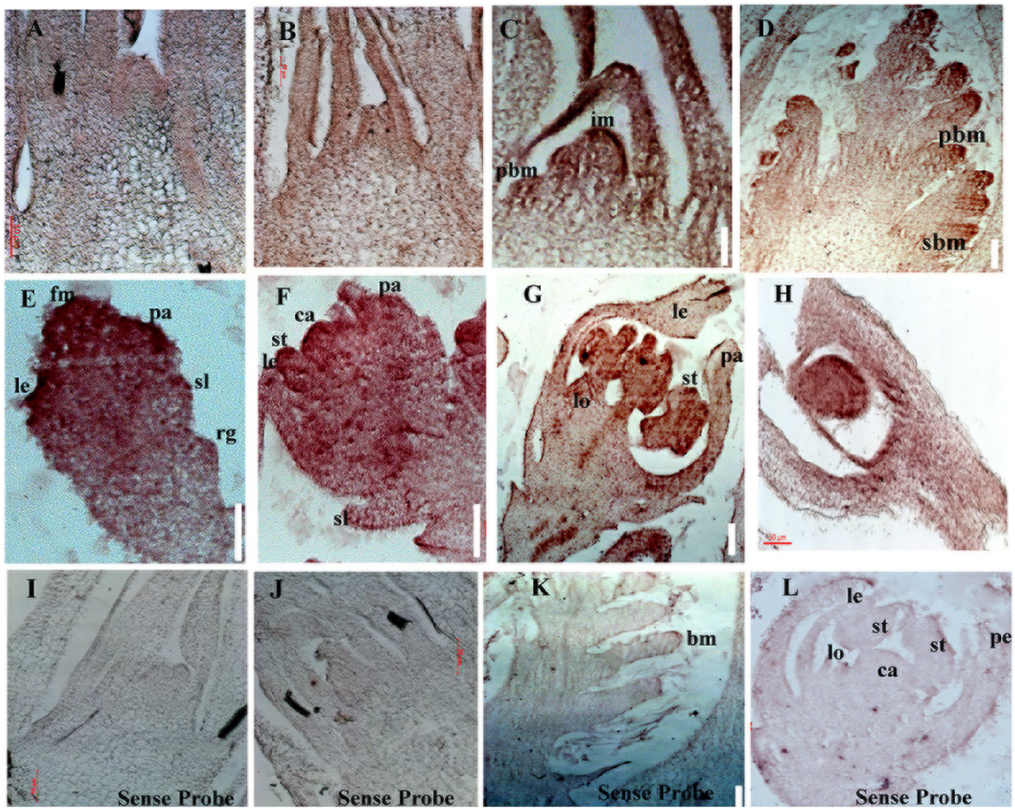

FIGURE 4 | Spatial distribution of *OsbZIP47* transcripts in meristems and florets. **(A,B)** *OsbZIP47 in situ* RNA hybridization signal in SAM tissues from 5 DAG and 25 seedlings. Expression in SAM and in emerging leaf primordia. **(C,D)** Inflorescence meristem (IM) with emerging primary branch meristems show expression of *OsbZIP47* in the elongation meristem and primary branch meristems (prb), secondary branch meristems (srb), and in young leaves. **(E)** *OsbZIP47* transcripts in very early floret meristem (FM) with uniform spatial distribution of signal. **(F)** Floret uniform signal in the well-formed stamens (st), lemma/palea (le and pa) organ primordia, and in the central early carpel primordia. **(G)** High level of *OsbZIP47* expression in the lodicule and in stamens, and lower signal in the near mature lemma and palea. **(H)** *OsbZIP47* transcripts in the ovary wall and ovule. **(I,J)** SAM in 5 DAG and 25 DAG plants probe with sense probe as a negative control. **(K,L)** IM and near mature floret, respectively probed with sense RNA.

with deviated gynoecium (Running and Meyerowitz, 1996). We speculate *OsbZIP47* may have a minor role in carpel development or could be functionally redundant with floral C-class function genes. Thus, *OsbZIP47* is expressed in various above-ground meristems reflecting its diverse roles in different meristems.

Heterodimerization of OsbZIP47 With Other Floral Meristem Regulators

Heterodimerization of transcription factors can modulate genome wide gene expression by modifying specificity and affinity to target DNA binding sites, and by integrating independent pathways controlled by two or more factors. Interacting partners of OsbZIP47 or of its Arabidopsis and Maize homologs are largely unknown. To understand molecular mechanism of OsbZIP47, we investigated its interaction with different transcription factors. Among the co-occurring motifs in genome-wide loci bound by OsMADS1, the motif for bZIP factor binding is enriched (Khanday et al., 2016). This was the basis for our hypothesis that OsMADS1 and members of OsbZIP family could function in complexes in early floral meristems. Further, the temporal co-expression profiles of *OsMADS1* and *OsbZIP47* overlap in developing panicles (Arora et al., 2007; Nijhawan et al., 2008); hence we tested interaction among these proteins using the heterologous yeast two hybrid assay (**Figure 5**). Additionally, to investigate possibility of OsbZIP47 heterodimerization with other meristem regulators, we relied on reports from genetic studies in Arabidopsis, maize and rice to curate and choose candidates for interaction assays (Das et al., 2009; Khanday et al., 2013; Deshpande et al., 2015; Pautler et al., 2015). OSH1, OsH15, ETTIN1, ETTIN2, and RFL emerged as candidates. We re-visited reports on the panicle and floret expression patterns of these meristem regulators to deduce if spatial co-expression of *OsbZIP47*, *OSH1* and *OSH15* could occur. RNA *in situ* patterns of *OSH1* in rice panicles and florets (Komatsu et al., 2001; Chu et al., 2006; Hu et al., 2015) and *OsbZIP47* transcript spatial profile (**Figure 4**) point to an overlap of *OsbZIP47* and *OSH1* transcripts in primary and secondary branch primordia and in a broad range of developing spikelet/floret meristems (Sp2–Sp8) (**Supplementary Figure 5**). Further, mutant *osh1* (Tsuda et al., 2011, 2014) and *OsbZIP47KD* plants share common phenotypes such as increased leaf lamina

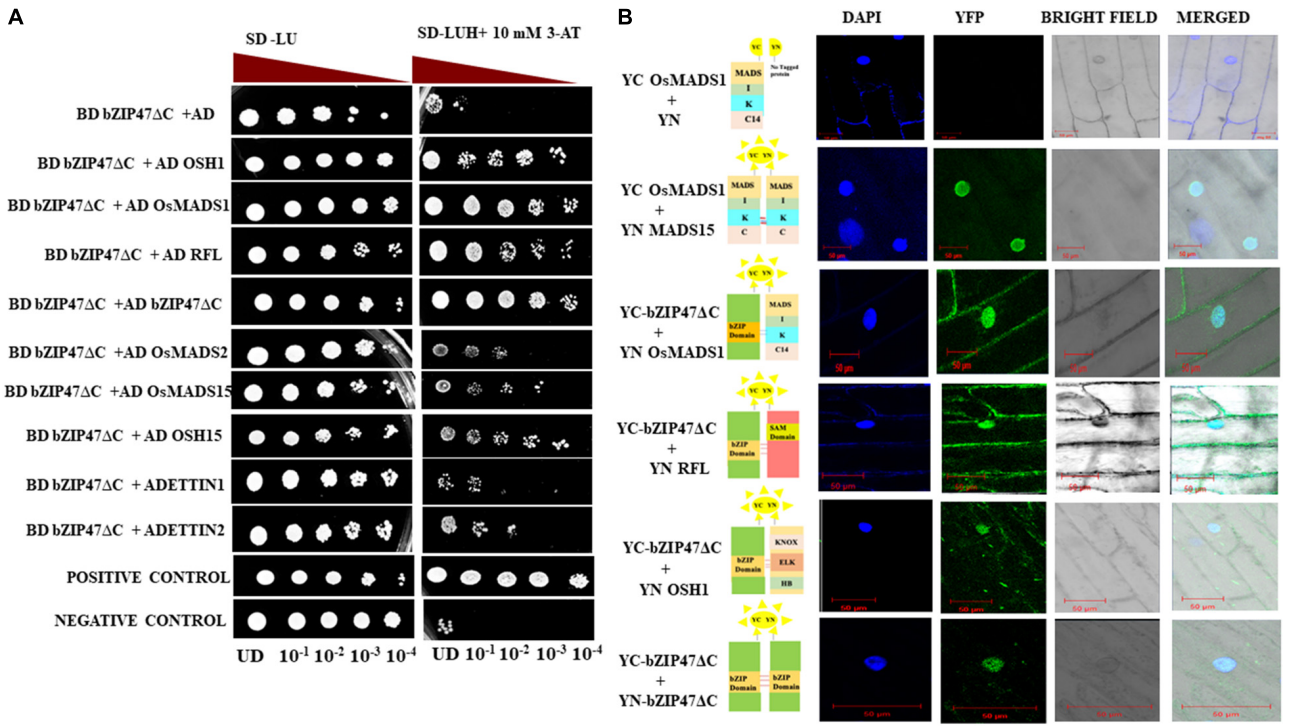

FIGURE 5 | Interaction of OsbZIP47 with other meristem factors. **(A)** Yeast two hybrid (Y2H) assays with OsbZIP47ΔC protein (lacking 186–380 amino acids in C terminal) and predicted protein partners, such as OsMADS1 (MIKC14 domain), RFL, OsETTIN1, OsETTIN2, OSH1, OsMADS2, OsMADS15, and OSH15. Serial dilutions of yeast cells (PJ694A) spotted on media lacking histidine and supplemented with 10 mM 3-AT. Growth after five days at 30°C is shown. Yeast transformants with OsMADS15 in pGBDUC1 vector and OsMADS1 MIKC14 in pGADC1vector served as positive control for protein interaction. A combination of pGADC1 and pGBDUC1 empty vectors (without protein fusion) was the negative control. **(B)** Validation of Y2H protein interactions by Bimolecular Fluorescence Complementation (BiFC) assays in onion epidermal cells. YFP fluorescence was detected when OsbZIP47ΔC-cYFP fusion protein was co-expressed with OsMADS1-nYFP, RFL-nYFP, and OSH1 nYFP. Absence of YFP fluorescence in the negative control i.e., OsbZIP47ΔCYC and YN domain alone was the negative control. Bars = 50 μm.

joint angle, short panicle with reduced number of spikelets and deformed stamens. Moreover, Pautler et al. (2015) reported that several gene loci are cobound by ZmKN1 (the ortholog of rice OSH1) and ZmFEA4 (ortholog of *OsbZIP47*). These findings together indicate likelihood of OsbZIP47 and OSH1 interactions for co-regulation of target genes. Also, OsH15, a closely related paralog of OSH1 (Tsuda et al., 2011), co-expresses with *OsbZIP47* in spikelet meristem/floret meristem stage 6 (Yoon et al., 2017; **Supplementary Figure 5**). As *OsbZIP47* KD caused abnormal floral phenotypes, it was intriguing to determine if OsbZIP47 could heterodimerize with OsH15. In Arabidopsis, *pan ettin* phenotypes suggest *AtPAN* and *AtETTIN/AUXIN-RESPONSIVE FACTOR3* (*ARF3*) redundantly regulate floral organ numbers and patterns (Sessions et al., 1997). Additionally, rice *ETTIN1* and *ETTIN2* RNAi lines have aberrant plant height, compromised panicle branching, and defects in stamen and carpel development (Khanday et al., 2013). Some of these phenotypes resembled those observed in *OsbZIP47KD* plants. Similarly, for mutants in *RFL,* the rice *AtLEAFY* ortholog, the alleles *apo2* and *ssc*, or the *RNAi RFL*KD (Kyozuka et al., 1998; Rao et al., 2008; Wang et al., 2017) plants share some phenotypes with *OsbZIP47KD* plants. The common phenotypes include shorter plant height, delayed flowering, reduced panicle rachis length, and branch complexity. Thus, we hypothesized that OsETTIN1, OsETTIN2, and RFL may interact with OsbZIP47 to modulate aspects of organ development. Based on these meta-analyses, protein partnership between OsbZIP47 and OSH1, OsH15, ETTIN1, ETTIN2, and RFL was tested by the Y2H assay. Moreover, we also tested the interactions of OsbZIP47 with OsMADS15 (an A Class APETALA1/FRUITFULL AP1/FUL-clade transcription factor) and OsMADS2 (a B class PISTILLATA/GLOBOSA-like protein). OsMADS15 regulates vegetative to reproductive floral transition and functions in specifying meristem identity (Kater et al., 2006; Kobayashi et al., 2012). OsMADS2 functions in partnership with OsMADS16/SUPERWOMAN1 (SPW) as a B-class complex (Lombardo et al., 2017; Kong et al., 2019). The delayed flowering phenotypes of *OsbZIP47KD* transgenics and the defects in the second and third whorl floral organs, justified our choice of OsMADS15 and OsMADS2, respectively. Since full length OsbZIP47 exhibited transcriptional transactivation activity in yeast (**Supplementary Figure 6A**), a C-terminal truncated version (OsZIP47ΔC) lacking 186-385 amino acids including the transcription activation domain was taken as bait protein in fusion with Gal4 BD. Prey proteins (OsMADS1, OSH1, OsH15, ETTIN1, ETTIN2, RFL, OsMADS15, or OsMADS2) were fused to GAL4 AD. The GAL4AD-OsMADS15 interaction

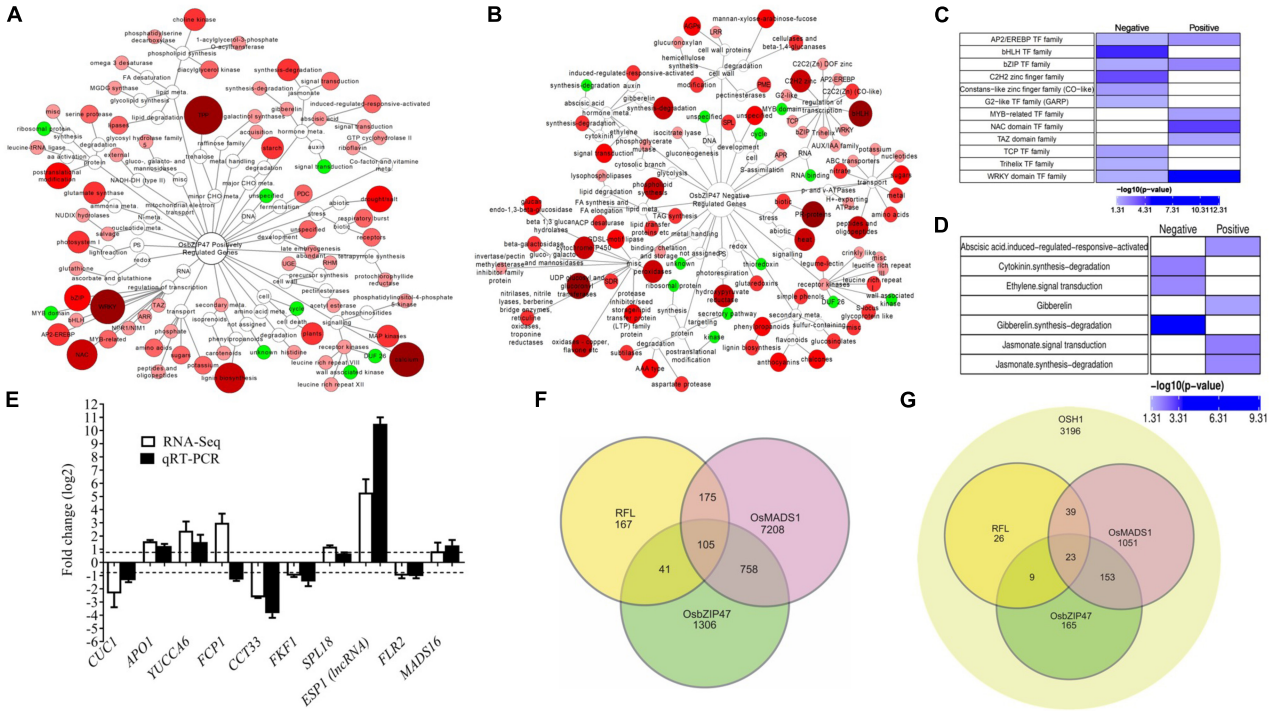

FIGURE 6 | Differentially expressed genes (DEGs) and GO enrichment analysis of pathways downstream to OsbZIP47. Enrichment networks depicting pathways regulated by OsbZIP47. **(A)** positively regulated, and **(B)** negatively regulated pathways. The red and green color nodes represent enriched and depleted functional categories, respectively ($P < 0.05$). The size and color intensity of the node correlates with the over-representation of genes within the given class. **(C)** Enrichment map of transcription factor (TF) genes shows those encoding members from bHLH, G2-like, C2H2 zinc finger, TCP, Trihelix are underrepresented, whereas TFs, such as AP2/EREBP, MYB-related, NAC domain, TAZ, WRKY, and bZIP were overrepresented. **(D)** The 2,210 DEGs annotated in MSU-TIGR v7 were taken for GO-enrichment analysis for phytohormone metabolism and signaling. Cytokinin (CK) degradation, ethylene signal transduction genes, and gibberellin (GA)-synthesis-degradation were enriched in negatively regulated dataset, whereas, abscisic acid (ABA), GA pathway, and jasmonate (JA) pathways predominate in the positively regulated set. **(E)** RT-qPCR analysis of the relative fold-change for transcripts from several candidate target genes of OsZIP47 in 0.1 to 0.5 cm panicles from *OsbZIP47KD* as compared to WT tissues. The normalization of transcript level of each gene was done using *UBQ5* transcript levels. Error bars represent the standard deviation. **(F)** Venn diagram showing unique and overlapping sets of differentially expressed genes (DEGs) derived from *OsMADS1, OsbZIP47,* and *RFL* transcriptome datasets (Rao et al., 2008; Khanday et al., 2013; this study). **(G)** Genes implicated to be coregulated by *OsMADS1, OsbZIP47,* and *RFL* and bound by *OSH1* (Rao et al., 2008; Khanday et al., 2013; Tsuda et al., 2014; this study).

with GAL4DB-OsMADS1 was taken as the positive control (Lim et al., 2000). In addition, homodimerization capability of OsbZIP47ΔC was tested. Growth pattern of transformed yeast cells on reporter media SD/-Leu-Ura-His + 10 mM3AT and the X-gal quantitative assays (**Supplementary Figure 6B**) suggested that OsbZIP47 can heterodimerize with OsMADS1, OSH1, and RFL. We also found a strong homodimerization of OsbZIP47ΔC protein (**Figures 5A,B**). Both OsMADS15 and OsH15 showed weak interactions with OsbZIP47 (**Figure 5A**), while ETTIN1, ETTIN2, and OsMADS2 showed no interaction. Further, we performed *in-planta* BiFC assays to substantiate the protein–protein interactions screened in Y2H assay. *OsbZIP47ΔC* was cloned upstream to the coding sequence of C-terminal region of split YFP to express *OsbZIP47ΔC*-cYFP fusion protein. The coding sequences of *OsMADS1*, *OsbZIP47ΔC*, *RFL, OsETTIN2*, and *OSH1* were cloned in frame downstream to the coding sequence of the N-terminal split YFP (nYFP) to express nYFP fusion proteins. These six different combinations of nYFP and cYFP fusion proteins were transiently co-expressed in onion epidermal cells. Nuclear YFP fluorescence signals confirmed protein interaction of OsbZIP47 with OsMADS1, OSH1, and RFL (**Figure 5B**). Thus, we suggest that OsbZIP47 partnership with OsMADS1, OSH1, and RFL could contribute to meristem functions, inflorescence complexity, and floret development.

Transcriptome of Developing Inflorescences of *OsbZIP47* Knockdown Lines

To capture gene expression landscape in *OsbZIP47KD* panicles, high throughput RNA-sequencing was carried out in two biological replicates of *OsbZIP47KD* and WT panicles (In2-In4, 1 mm to 5 mm panicles), and the DEGs (greater than two-fold change, *p*-value < 0.05) were extracted (**Supplementary Dataset 1**, **Supplementary Materials** and Methods). Further, DEGs were examined for gene ontology pathway enrichment. Among the DEGs, 1,945 genes were upregulated, and 855 genes were downregulated in *OsbZIP47KD* panicles (**Supplementary Figure 7**, **Supplementary Dataset 1**). Gene Ontology (GO) analysis of positively regulated gene

set (**Figures 6A,B** and **Supplementary Materials** and Methods, **Supplementary Dataset 2**) revealed enrichment of RNA (regulation of transcription), lipid, CHO metabolism, signaling, development, and hormone metabolism pathways (**Figure 6A**). Whereas in the negatively regulated set, genes related to secondary metabolism, transport, cell wall, signaling, stress, hormone metabolism, and miscellaneous factors were overrepresented (**Figure 6B**). Not surprisingly, genes involved in hormone signaling and metabolism were controlled by *OsbZIP47*, both positively and negatively (**Figures 6C,D**). Specifically, jasmonate (JA) and abscisic acid (ABA) pathway genes are overrepresented in the positively regulated gene set. CK degradation and ethylene signal transduction genes are notable in the negatively regulated gene set. Interestingly, genes of GA pathway were enriched in the positively regulated gene set, whereas genes for GA-synthesis-degradation were enriched in the negatively regulated gene set (**Figure 6D**). Examples of *OsbZIP47* downstream genes that could interlink hormone pathways for panicle and floret development include *APETALA-2-LIKE TRANSCRIPTION FACTOR39* (OsAP2-39), 9- cis-epoxycarotenoid dioxygenase3 (*OsNCED3*), and *ELONGATED UPPER MOST INTERNODE1* (*OsEUI1*). *AP2-39* balances the antagonistic relation between ABA and GA by modulating the expression levels of *OsNCED3* and *OsEUI1* to regulate plant height, yield, and seed germination (Yaish et al., 2010; Shu et al., 2016). We observed positive regulation of *OsAP2-39* and *OsNCED3,* and negative regulation of *EUI1* by *OsbZIP47*. Thus, we suggest that *OsbZIP47* may enhance ABA biosynthesis and modulate GA biosynthesis possibly to regulate plant height and panicle rachis elongation (**Figures 2D,E**). Examples of other *OsbZIP47* downstream genes linked to different phenotypes in *OsbZIP47KD* plants are further discussed. Interestingly, in *OsbZIP47KD* inflorescences, whole transcriptome analyses showed higher transcript levels for the *CLV3* paralog genes, *FON2/4* and *FCP1*. Moreover, genes from the KNOX-WUS pathway, and isopentenyl-transferases, *IPT6,* and IPT8 that encode CK-biosynthesis rate limiting enzymes were also upregulated. These results together, suggest the roles of *OsbZIP47* in the regulation of panicle primary branch meristems and secondary branch meristems. Reduced transcript expression was observed for *SQUAMOSA PROMOTER BINDING PROTEIN-LIKE 7* (*SPL7*), *OsMADS16,* and *YABBY* domain factor-*DROOPING LEAF* (*DL*) in *OsbZIP47KD*. The *SPL7* regulates inflorescence meristem and spikelet transition (Dai et al., 2018). *OsMADS16* and *DL* regulate lodicule, stamen, and carpel development (Nagasawa et al., 2003; Yamaguchi et al., 2004). Moreover, the F-box gene, *APO1* with roles in spikelet and floret development was also deregulated (**Supplementary Dataset 1** and **Figure 6E**; Ikeda et al., 2005, 2007). These findings corelate with the *OsbZIP47KD* inflorescence branching and floret organ defects (**Figures 2**, **3**). The positive regulation of *CUC1* by *OsbZIP47* supports plausible mechanism for its influence on organ whorl boundaries (Takeda et al., 2011; **Figure 6E** and **Supplementary Dataset 1**) and could explain the development of chimeric floral organs in *OsbZIP47KD* transgenics. Transcription factors control the dynamics of hormone signaling pathways by modulating gene expression levels. Transcription factors genes that are deregulated in *OsbZIP47KD* panicles include bHLH gene members (22 genes), Co-like Zn finger (5 genes), TCP class 1 (2 genes), and TCP class 2 (1 gene), trihelix (4 genes), C2H2 zinc (20 genes) (**Figure 6C** and **Supplementary Dataset 2**). The genes for transcription factors that are positively regulated by *OsbZIP47* are from NAC class, WRKY class, and MYB-related class genes. Among the latter class is OsLHY (LATE ELONGATED HYPOCOTYL)/CCA1 (CIRCADIAN CLOCK ASSOCIATED1) which functions in photoperiodic flowering, plant tillering, and grain yield (Wang et al., 2020; Sun et al., 2021). We speculate that the delayed flowering phenotype of *OsbZIP47KD* plants can be associated with the positive regulation of *OsLHY* by *OsbZIP47*. We also speculate that positive regulation of *DWARF AND RUNTISH SPIKELET2/FERONIA like Receptor 2* (*DRUS2/FLR2*) may contribute to architecture, fertility, and seed yield (Li et al., 2016; **Figure 6E** and **Supplementary Dataset 1**). To obtain a predicted list of candidate direct genes and targets of OsbZIP47, we queried the dataset of deregulated genes in *OsbZIP47KD* panicles for the occurrence of *cis* motif typical to the TGA-subclade within the large family of bZIP factors in the rice, Arabidopsis, and maize genomes. Arabidopsis TGA sub-family includes AtPAN, the homolog of OsbZIP47, and AtPAN binds to the core *cis* regulatory element TGACG (Gutsche and Zachgo, 2016). Among the 2,210 differentially expressed annotated (MSU-TIGR v7) genes, a large number displayed the core motif TGACG in their TSS-promoter proximal regions (-500 bp to + 100 bp from TSS; **Supplementary Dataset 3**). Interestingly, the TGACG core motif occurred three times in this region of the *FCP1* locus hinting that *FCP1* deregulation is likely a direct effect of OsbZIP47. Other predicted direct targets that relate to developmental functions of OsbZIP47 are *APO1*, *GNP1* (*GA20Ox1*), *CYCD7*, *OsSPL7*, *OsIAA20*, and *GRX6,* to name a few. Other gene targets could be regulated by degenerate *cis* elements related to "core motif" or by "core motif" in other distal regions of these loci. This *in silico* prediction of downstream targets of OsbZIP47 provides an extra level of confidence to the transcriptome-based deregulated gene set and can facilitate DNA–protein interaction studies. Overall, these results give a snapshot of *OsbZIP47* molecular functions in inflorescence tissues and give leads to its unique *vs.* evolutionarily conserved roles for panicle meristem transitions and floral organ development.

Comprehensive Datamining of Transcriptome Datasets of *OsMADS1*, *OsbZIP47*, *RFL,* and Genome Binding Dataset for *OSH1*

Extending our findings of OsbZIP47 interaction with OsMADS1, RFL, and OSH1, we carried out meta-analyses of published transcriptome datasets affected in mutants of these partner proteins. To identify candidate genes for co-regulation by these factors, the differential transcriptome in *dsRNAiOsbZIP47KD*, dsRNAi*OsMADS1*, and dsRNAi*RFL* panicles were examined (Rao et al., 2008; Khanday et al., 2013). First, we aligned genes from three different transcriptomic datasets for this meta-study (**Supplementary Materials** and Methods). The

2,210 (as annotated by MSU-TIGR v7) deregulated genes in *dsRNAiOsbZIP47KD* panicles were examined for overlap with 8,246 affected genes in *dsRNAiOsMADS1KD* transcriptome (**Figure 6F** and **Supplementary Dataset 4**; Khanday et al., 2013). Among 758 candidate genes co-regulated by both OsbZIP47 and OsMADS1 (**Figure 6F** and **Supplementary Dataset 4**), 204 genes were downregulated in both *OsbZIP47KD* and *OsMADS1KD* lines. These genes included Gibberellin-regulated protein precursor expressed (*GASR3*), auxin-responsive *SMALL AUXIN-UP RNA 11* (*OsSAUR11*), *DRUS2/FLR2,* and *JASMONATE ZIM-DOMAIN12* (*TIFY11D/OsJAZ12*) (ZIM domain transcription factor). Another group of genes (386 out of 758 genes) were upregulated in both *OsbZIP47KD* and *OsMADS1KD* panicle datasets. This sub-set includes *OsMADS16*, *GNP1* (*GRAIN NUMBER PER PANICLE1*) and genes that regulate hormone signaling, such as *OsIAA20, YUCCA7, PROBABLE AUXIN EFFLUX CARRIER COMPONENT 5B* (*PIN5B),* and *ETHYLENE INSENSITIVE LIKE 4* (*EIL*). Among the 758 candidate genes co-regulated by OsbZIP47 and OsMADS1, a subgroup of 153 genes (**Figure 6G**) are also bound by OSH1 (Tsuda et al., 2014). Striking among this sub-set are: *IAA20*, *YUCCA7, SPLIT-HULL* (*SPH*), and *DRUS2*/*FLR2*. Similarly, 41 genes (**Figure 6F**) are common to the DEGs in *OsbZIP47KD* panicles (RNA-Seq) and a low-density microarray study of panicles from dsRNAi*RFL* KD plants (Rao et al., 2008). Interestingly, 32 out of 41 genes were downregulated in both these datasets including ethylene signaling gene, *ACO1* which regulates internode elongation (Iwamoto et al., 2011), JA signaling gene, *TIFY11D* (Kim et al., 2009), and the *EMBRYOSAC1* (*OsEMSA1*) involved in embryo sac development (Zhu Q. et al., 2017). Finally, we identified 105 DEGs common to the differential transcriptome in *RFLKD*, *OsMADS1KD*, and *OsbZIP47KD* panicles (**Figure 6F**). The notable genes include *ETHYLENE INSENSITIVE-LIKE GENE 2* (*EIL2*), *ALLENE OXIDE SYNTHASE* (*AOS1*), and *GIBBERELLIN 2-OXIDASE 9* (*GA2OX9*). A subset of 23 genes are potentially regulated by OSH1 (**Figure 6G**; Tsuda et al., 2014). We infer that these transcription regulators possibly multimerize in one or more forms of complexes to regulate meristem development in rice. Overall, these findings hint that protein complexes, plausibly heterogeneous, with the combinations of OsbZIP47 and its varied partner factors may spatially and temporally co-ordinate downstream gene expression during panicle development, spikelet, and floret development.

Redox-Dependent DNA Binding of OsbZIP47

DNA binding by Arabidopsis AtPAN is redox-sensitive due to the five Cysteine residues in the extended N-terminal domain (Gutsche and Zachgo, 2016; **Supplementary Figure 8**). Unlike AtPAN homologs from diverse species, rice OsbZIP47 lacks this domain. All proteins share a conserved Cys in the C terminal transcription transactivation domain (AtPAN Cys340/OsbZIP47 Cys269). Cys17 in OsbZIP47 is conserved in monocot species, while Cys196 is unique to *OsbZIP47*. Thus, though the rice and *Arabidopsis* proteins are homologs, they differ in size and in the overall number of cysteine residues. To examine OsbZIP47 oligomerization and the effects of its redox status on binding to target gene *cis* DNA elements, the full length (FL) OsbZIP47 protein was expressed in bacteria. The DNA binding activity of AtPAN is regulated by *S*-glutathionylation of the conserved Cys340 by AtROXY1, a glutaredoxin redox enzyme (Li et al., 2009; Gutsche and Zachgo, 2016). The corresponding conserved Cys 269 in OsbZIP47 may also render the rice protein to be redox-sensitive for biochemical activity. To determine if OsbZIP47 FL protein forms higher order self-oligomers, SEC with the purified Trx-His OsbZIP47 (62 Kda) protein was done and the elution of the protein in the column void volume (**Figure 7A**) suggested either aggregation or the formation of high order oligomers in the given condition. To examine the latter possibility, the purified OsbZIP47-His-Trx protein was treated with 2 mM of diamide, an oxidizing agent. In parallel, another aliquot of the protein was treated with 20 mM DTT, a reducing agent, and both treated protein fractions were analyzed on a non-reducing SDS-PAGE gel. The oxidized OsbZIP47-His-Trx sample had slower mobility whereas the reduced OsbZIP47-His-Trx sample migrated with the expected mobility for a ∼68 Kda protein. Importantly, we found that the effects of the oxidizing agent (diamide) can be reversed by DTT treatment. These data show that OsbZIP47 oligomerization is affected by its redox status (**Figure 7B**). Recently, OsbZIP47 maize ortholog, FEA4 was shown to switch its oligomerization status following redox change (Yang et al., 2021). Next, we tested the DNA binding affinity of OsbZIP47 to the TGACGT *cis* motif (predicted for OsbZIP47 DNA binding) present at around -371 bp upstream of the start codon in the *OsFCP1* locus (**Figure 7C**). The latter is a downstream gene target whose expression levels are affected in the SAM and in the panicles of *OsbZIP47KD* plants. The OsbZIP47 FL protein status was altered by incubation with the reducing agent DTT (20 mM) or with the oxidant diamide (2 mM) for 30 min prior to the incubation with the TGACGT motif containing DNA substrate. OsbZIP47 FL protein bound to the TGACGT motif under reducing conditions. Interestingly, incubation with diamide decreased OsbZIP47 FL-DNA interaction. Thus, electrophoretic mobility shift assays showed redox-sensitive DNA-binding of the OsbZIP47 FL protein (**Figure 7D**). Further, we quantified the binding affinity of OsbZIP47 FL with *cis* element from the *OsFCP1* locus using microscale thermophoresis (MST). To this end, OsbZIP47 FL protein was labeled with the RED-NHS 2nd Generation Dye (MO-L011, Nanotemper GmbH) and was mixed with increasing concentrations of *OsFCP1* oligos until saturation. The fluorescent signals obtained with increasing ligand concentrations followed a clear sigmoidal binding curve. As expected, OsbZIP47 FL protein displayed a stronger binding affinity to the *OsFCP1* locus in its reduced state, with a dissociation constant K_d of 815 nM, as compared to K_d of 2.16 uM in the oxidized state (**Figure 7E**). The differential K_d values confirm a redox sensitive DNA–protein interaction. The Trx-His tag protein was taken as a negative control in these assays and no interaction between protein and ligand was detected (**Supplementary Figure 9**). Overall, the results of our qualitative and quantitative data suggest that affinity of *OsbZIP*47 FL binding to DNA was redox-dependent

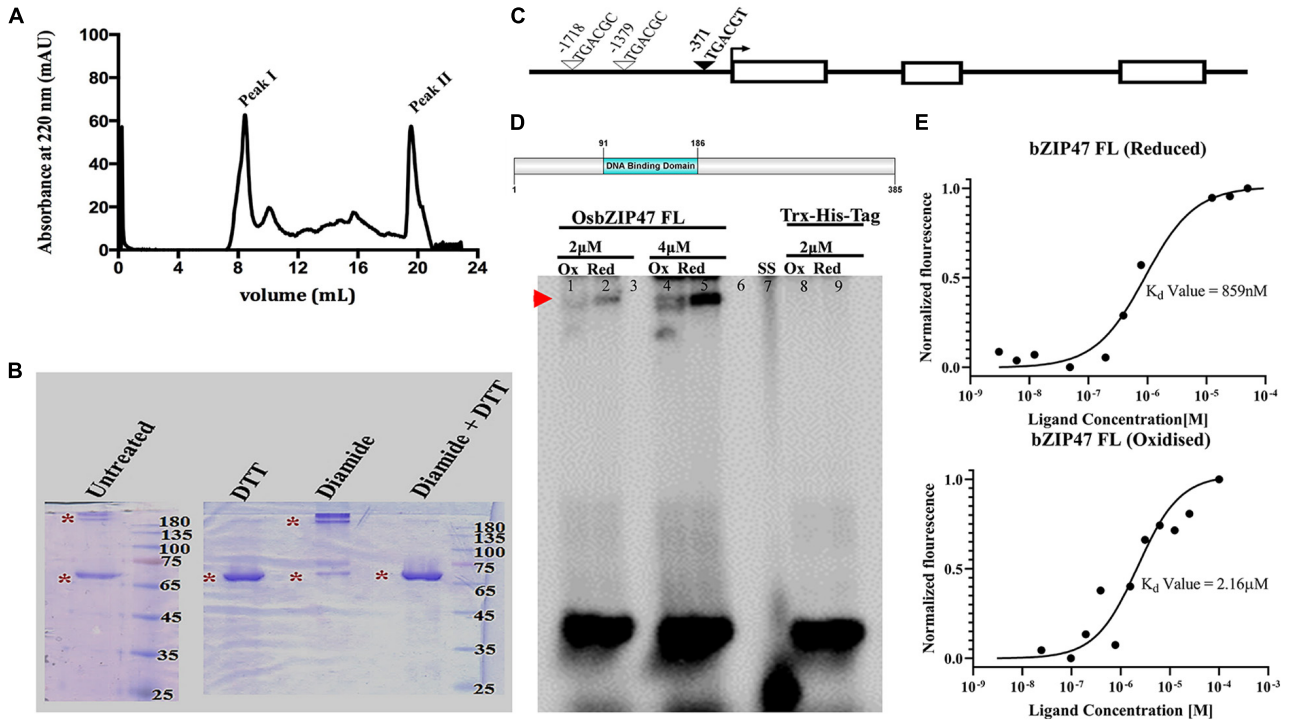

FIGURE 7 | OsbZIP47 oligomerization and the effects of its redox status on DNA binding. **(A)** Size-exclusion chromatography (SEC) profile for OsbZIP47 protein/oligomer on a Superdex 200 increase column. **(B)** Mobility of purified OsbZIP47-Trx protein on non-reducing 10% of SDS-PAGE after treatment with 2 mM of diamide (an oxidizing agent), or with 20 mM DTT (a reducing agent), or with 2 mM diamide followed by 20 mM DTT. **(C)** Schematic representation of the *FCP1* gene locus. Exons are open white boxes, introns are shown as black lines, and the predicted *cis* motifs for bZIP DNA binding domain (DBD) are represented as inverted triangles. The DNA binding properties of OsbZIP47FL protein was tested for the TGACGT *cis* motif located at -371bp of *FCP1* (marked with a filled inverted triangle). **(D)** Schematic representation of OsbZIP47 FL protein (amino acid 1 to 385) used for EMSA and microscale thermophoresis assays. EMSA assays with full-length OsbZIP47 (62 Kda protein) shows retarded mobility of DNA-protein complex for the OsFCP1 locus (as indicated by red arrow). Lanes 1 and 2 correspond to the oxidized and reduced form of bZIP47 FL protein incubated with 2 μM of oligo. Lanes 4 and 5 represent the oxidized and reduced form of the same protein, incubated with 4 μM of oligo. Lanes 8 and 9 correspond to Trx-Tag protein incubated with 4 μM of probe. Lanes 3 and 6 are blank. Unbound dsDNA oligonucleotide is at the bottom. **(E)** Microscale thermophoresis-based assay to determine the dissociation constant for OsbZIP47 full-length and OsFCP1 dsDNA oligo interaction. 80 nM of fluorescently labeled protein was taken for binding with DNA sequences from OsFCP1 locus taken at a wide concentration range (100 μM to 3.05 nM). The OsbZIP47 full length protein was reduced with 20 mM DTT or oxidized with 1mM of oxidized glutathione. OsbZIP47 full length protein shows increased binding in the reduced state as compared to the oxidized state.

despite the absence of the extended Cys rich N-terminal domain commonly found in homologs from other species. Recently, OsbZIP47 close ortholog, ZmFEA4 was shown to interact with three GRX proteins to modulate its redox status and DNA accessibility (Yang et al., 2021).

DISCUSSION

Arabidopsis PAN, maize FEA4, and rice bZIP47 proteins share a significant degree of similarity throughout their lengths with the most conserved region being the DNA binding domain (**Supplementary Figure 8**; Chuang et al., 1999; Nijhawan et al., 2008). Species-specific developmental roles for these factors may therefore arise from interacting co-regulators, from protein modification of these transcriptional regulators, and through variations in their downstream genes and pathways. Arabidopsis *AtPAN* has pleiotropic vegetative and reproductive growth effects. Flowers in the *pan* mutant are characterized by an increase in the floral organ number without a corresponding increase in FM size (Running and Meyerowitz, 1996; Chuang et al., 1999). Another study reported early flowering of *pan* mutant plants in long-day and short-day grown plants having an enlarged SAM and inflorescence meristems (Maier et al., 2011). Maize mutant *zmfea4* have enlarged vegetative SAMs, severely fasciated inflorescences, and florets with reduced stamen numbers (Pautler et al., 2015). We show that *OsbZIP47KD* plants have abnormalities in the shoot meristem size homeostasis similar to the enlarged SAM of maize *fea4* mutant. Yet, other phenotypes are unique to rice *OsbZIP47KD* lines, for instance, delayed flowering, increased stamen numbers, chimeric floral organs, and subtle changes to grain size and shape. Hence, despite redundancy of bZIP transcription factors, the phenotypes of single mutants, such as *atpan1*, *zmfea4*, and *OsbZIP47KD* indicate OsbZIP47 has evolutionarily conserved as well as unique roles in the vegetative and reproductive development. The partnership of OsbZIP47, with meristem regulators, OsMADS1, RFL, and OSH1 (KNOX1/STM), its oligomeric and redox

status could relate to its functions in different meristems. This partnership and the findings that emerge from the differential transcriptome in *OsbZIP47KD* panicles allowed us to map OsbZIP47-regulated downstream genes, and those potentially dependent on its co-regulators.

Meristem Development in Vegetative and Reproductive Phase

The enlarged SAM in *OsbZIP47KD* seedlings is superficially similar to that of maize *fea4*, yet there are underlying subtle differences in rice KD plants. A detailed phenotyping of SAMs from *OsbZIP47KD* seedlings showed increased cell size of L1 layer and its underlying cells suggesting precocious cell differentiation. Further, SAMs of *OsbZIP47KD* showed increased transcript signal of cell proliferation marker, H4 as indicated by *in situ* hybridization. The downregulation of *FON2*, *FCP1*, *YUCCA6, CUC1, APO1,* and *CYP734A4* in SAM, suggests several complex pathways by which OsbZIP47 contributes to SAM size and plant growth by modulating cell proliferation and differentiation. Notable here is the regulation of *CYP734A,* which as a direct target of OSH1 is suggested to repress premature cell differentiation in meristems (Tsuda et al., 2014). This observation together with our data on protein interactions between OsbZIP47 and OSH1 supports a plausible mechanism by which OsbZIP47-OSH1 partnership could regulate *CYP734A* expression with ensuing effects on meristem and lateral primordia development. Further, phytohormones, CK, AUX, and GA are also essential for cell division and organ differentiation (Leibfried et al., 2005; Zhao et al., 2010; Su et al., 2011). Transcriptome profiling of *OsbZIP47KD* panicles shows deregulated expression levels for different phytohormone related genes including *KNOTTED1-LIKE11*, *IPT1*, *IPT8*, *OsGA3OX2 OsGA2OX3*, *OsGA2OX4,* Os*GA20OX1*, *YUCCA6*, and *YUCCA7*. Plant meristems are under redox control by reactive oxygen species (ROS), the by-products of aerobic metabolism. ROS levels control the expression of *WUS* and the activity of TCP class1 transcription factors to balance cell proliferation and differentiation in Arabidopsis SAM (Viola et al., 2013; Zeng et al., 2017). Like TCP class1, proteins containing cysteines with low pKa values are sensitive to cellular redox status (Martins et al., 2018). Glutaredoxins (GRX) reduce cellular ROS level and interact with different proteins including AtPAN1, ZmFEA4, and OsbZIP47 to modulate their activity by modifying their redox state (Li et al., 2009; Laporte et al., 2012; Schippers et al., 2016; Hao et al., 2021; Yang et al., 2021). Arabidopsis *pan* and maize *fea4* mutants exhibited increased meristem size (Maier et al., 2011; Pautler et al., 2015). Contrastingly, single, double, and triple mutations of different GRX paralogs in maize showed progressive reduction of meristem size, proposing a model where GRXs balance redox status and activity of ZmFEA4 to control meristem size (Yang et al., 2021). Interestingly, in transcriptome profiling of *OsbZIP47KD* panicles, *OsGRX6* was downregulated whereas *OsGRX16* and *OsGRX20* were upregulated (**Supplementary Dataset 1**), suggesting a mechanism by which *OsbZIP47* could be regulating meristem development. We propose OsbZIP47 functions as an integrator of the WUS-CLV and KNOX pathways for meristem development as it regulates the expression levels of key signaling factors in both pathways. Also, genes predicted to have roles in floral organ primordia differentiation such as *OsBLH1* (*BEL1*-like homeodomain), *OsKANADI1,* and *CUC1* are deregulated in *OsbZIP47KD* panicle tissues. Interestingly, reproductive panicle branching phenotypes of *OsbZIP47KD* panicles resemble *apo1* and *apo2/rfl* mutants (Ikeda et al., 2005, 2007; Rao et al., 2008; Ikeda-Kawakatsu et al., 2009; Deshpande et al., 2015). Thus, the interactions between RFL and OsbZIP47 could positively regulate the panicle meristem branch identity and its developmental transitions. One example of a target gene for co-regulation by OsbZIP47 and RFL is *CUC1*. Further, the elevated transcript levels of *APO1* in *OsbZIP47KD* panicle tissues hints that *OsbZIP47* in the WT panicle suppresses the expression of *APO1* which we speculate may affect the partnership with *APO2/RFL*. From this, we anticipate that *OsbZIP47* could have evolved to regulate some unique molecular pathways for vegetative and reproductive phase meristem growth and development.

Transition of Shoot Apical Meristem to Inflorescence Meristem

Knockdown of rice *OsbZIP47* showed delayed flowering (**Figure 2A**). This trait is common in mutants or KD transgenics in *OsMADS1* and *APO2/RFL* that encode OsbZIP47 protein partners (Jeon et al., 2000; Rao et al., 2008; Ikeda-Kawakatsu et al., 2012; Kannan et al., 2021). These observations support our hypothesis that these factors function in "one or more" complexes. Panicle transcript analysis in KD transgenics indicates that *OsbZIP47* can promote flowering by fine-tuning the expression of several flowering time regulators that are upstream to florigens, *HEADING DATE* 3a (*Hd3a*) and *RICE FLOWERING LOCUS* (*RFT*), and by controlling the expression of circadian clock-associated genes. Examples of genes from these two categories are *O. sativa LATE FLOWERING* (*OsLF*), *LATERAL ORGAN BOUNDARY DOMAIN* (*OsLBD38*), *INDETERMINATE DOMAIN 6* (*OsIDD6*), *FLAVIN-BINDING, KELCH REPEAT F-BOX1* (*OsFKF1*), *PHYTOCLOCK 1*(*OsPCL1*), and *OsLHY*/*CCA1*. Several rice flowering time quantitative trait loci (QTLs) also influence grain traits (Chen et al., 2014; Zhu Y.J. et al., 2017; Ma et al., 2019). The effect of *OsbZIP47KD* on rice grain shape is not reported for maize *fea* kernels suggesting unique effects of *OsbZIP47* on grain size and shape in rice as also reported by Hao et al. (2021). Our transcriptomic analysis identified a set of grain shape genes regulated by *OsbZIP47*. Examples of this category are *LONG GRAIN 3* (*OsLG3*), *GRAIN SHAPE GENE ON CHROMOSOME 9* (*GS9*), *GRAIN WIDTH QTL on chromosome 7* (*GW*) and *FLOURY ENDOSPERM 2* (*FLO2*). *GS9 positively* controls the grain size by altering the cell division along with BR signaling (Zhao et al., 2018). Interestingly, we noted increased expression of *CYCD7;1* in *OsbZIP47KD* panicles (**Supplementary Dataset 1**). This is remarkable as in Arabidopsis, the tissue and stage-specific control of this G1-S phase cell cycle gene controls the cell division in different contexts, with ectopic expression driving increased cell division and expansion in the embryo and the endosperm

(Collins et al., 2012; Weimer et al., 2018). With this, we postulate that *OsbZIP47* links flowering time, cell cycle, and BR signaling to regulate grain shape.

Regulation of Inner Floral Organ Identity and Specification

Consistent with *OsbZIP47* expression in the second and third whorl organs of near mature florets (Sp6–Sp8), we observed lodicule and stamen differentiation defects in *dsRNAiOsbZIP47* florets. Increased stamen numbers, with degenerated anthers on short filaments and lodicule-stamen chimeric organs support roles for OsbZIP47 in organ differentiation. Interestingly, in *OsbZIP47KD* florets, the higher transcript abundance of *OsMADS16* (homolog of *AtAP3*) and *DL*, a contributor to Class C function in rice florets (**Supplementary Dataset 2**), are indicative of some distinct effects in rice florets. Overexpression of *OsMADS16* can increase stamen numbers and form stamenoid carpels without any effects on lodicules (Lee et al., 2003). More recently, rice transgenics with a modified repressive *OsMADS16* (OsMADS16-SDX repressor domain fusion) exhibited indehiscent anthers (Sato et al., 2012). These phenotypes are akin to third whorl organ differentiation defects seen in *OsbZIP47KD* florets. Microsporogenesis in anthers of Arabidopsis flowers requires *SPOROCYTELESS/NOZZLE* (*SPL/NZZ*), a target of Class B and C organ identity factors (Ito et al., 2004). In line with this, we noted upregulation of *OsSPL*, possibly an effect of increased *OsMADS16* in *OsbZIP47KD* florets. Since we did not detect OsbZIP47 interaction with OsMADS2 in the Y2H assay, we speculate that OsbZIP47 regulates stamen differentiation by modulating the expression of *OsMADS16*. Upstream regulators of *OsMADS16* are *OsDL* and *FON2* (Ikeda et al., 2007; Xu et al., 2017). Both are upregulated in *OsbZIP47KD* inflorescence. The upregulated transcript of *FON2* in *OsbZIP47KD* inflorescence suggests that *OsbZIP47KD* stamen phenotypes are *OsMADS16*-mediated.

Biochemical Properties of OsbZIP47 Can Underlie Its Unique Functions and Downstream Effects

Multiple sequence alignment shows that OsbZIP47 shares nearly 50% of amino acid identity with homologs across diverse species. A common feature among many bZIP47 proteins, except OsbZIP47 and Bamboo PH01000727G0540, is a variably extended N terminal domain (**Supplementary Figure 8**). DNA binding activity of Arabidopsis PAN is redox-sensitive due to the presence of five Cysteine (Cys) amino acids in the extended N-ter domain and the conserved C-ter Cys340 in the transcription transactivation domain (Gutsche and Zachgo, 2016). OsbZIP47 protein has only three Cys (Cys17, Cys196, and Cys269). Cys17 is represented in all the monocot species. Cyse269 (Cys 340 of AtPAN) is conserved in all homologs compared here (**Supplementary Figure 8**). Cys196 is unique to OsbZIP47. Interestingly, among proteins compared here, wheat TAE56722G002 has the maximum number of 11 Cys. These observations hint that the number of Cys residues in this clade of bZIP proteins may have evolved for species-specific roles, plausibly for the adoption of unique structures with effects on tissue-specific target gene expression. Despite being a shorter protein with fewer Cys residues, OsbZIP47 showed redox-dependent DNA binding to *OsFCP1*, a downstream gene whose expression was upregulated in *OsbZIP47KD* panicles. Yang et al. (2021) demonstrated that OsbZIP47 maize ortholog, FEA4 interacts with three GRX proteins to modulate its redox status and DNA accessibility proposing a model by which redox status of FEA4 mediate meristem size. In rice, OsGRX19 or MICROSPORELESS1 (OsMIL1) is a potential glutaredoxin redox enzyme for OsbZIP47 as it is a homolog of the glutaredoxin redox enzyme, AtROXY1 and ZmMSCA1 from Arabidopsis and maize, respectively (Timofejeva et al., 2013; Yang et al., 2015). Interaction between OsMIL1 and TGA1 in yeast and the reduction of glutathionylation of OsbZIP47 by ROXY homolog, WG1 are both established (Hong et al., 2012; Hao et al., 2021). Indehiscent anthers phenotype is common to *OsbZIP47KD* and *mil1* mutant (Hong et al., 2012) leading us to propose S-glutathionylation of OsbZIP47 could be important for the development of anther. Overall, we uncover conserved as well as unique functions and mechanisms of OsbZIP47 that support meristem growth and determinacy during vegetative and reproductive development leading to grain formation. Together, these functions make OsbZIP47 a potential locus for allele mining and crop improvement.

DATA AVAILABILITY STATEMENT

The datasets presented in this study can be found in online repositories. The names of the repository/repositories and accession number(s) can be found below: https://www.ncbi.nlm.nih.gov/geo/query/acc.cgi?acc=GSE196747.

AUTHOR CONTRIBUTIONS

UV, SP, RR, MZ, and OA designed the research. SP, RR, MZ, and OA performed research and experiments. RP performed bioinformatic analyses. Data analyses and manuscript preparation was done by SP, RR, MZ, RP, and UV. All authors read and approved the final manuscript.

FUNDING

This work was funded by the Department of Biotechnology, Ministry of Science and Technology, Government of India project entitled, Functional Analysis of Gene Regulatory Networks During Flower and Seed Development in Rice, Project number: BT/AB/FG-1 (PH-II)/2009 to UV. University Grants Commission, Delhi was acknowledged for DS Kothari postdoctoral research fellowship to RR; Project ID: No. F.42/2006 (BSR)/BL/1718/0151. Research fellowship to RP and MZ was

from the Indian Institute of Science. Fellowship to OA was from the Council for Industrial and Scientific Research.

ACKNOWLEDGMENTS

Inputs from Grace Chongloi and other members of the UVR laboratory during the course of the study are acknowledged. Divya is thanked for assistance with confocal imaging and Murthy and Jagadeesh are thanked for assistance in plant growth and care. We acknowledge the DBT-IISc Partnership Divisional Bio-imaging and Greenhouse Facilities.

SUPPLEMENTARY MATERIAL

The Supplementary Material for this article can be found online at: https://www.frontiersin.org/articles/10.3389/fpls.2022.865928/full#supplementary-material

REFERENCES

Aida, M., Ishida, T., Fukaki, H., Fujisawa, H., and Tasaka, M. (1997). Genes involved in organ separation in *Arabidopsis*: an analysis of the cup-shaped cotyledon mutant. *Plant Cell* 9, 841–857. doi: 10.1105/tpc.9.6.841

Arora, R., Agarwal, P., Ray, S., Singh, A. K., Singh, V. P., Tyagi, A. K., et al. (2007). MADS-box gene family in rice: genome-wide identification, organization and expression profiling during reproductive development and stress. *BMC Genomics* 8:242. doi: 10.1186/1471-2164-8-242

Bommert, P., Satoh-Nagasawa, N., Jackson, D., and Hirano, H. Y. (2005). Genetics and evolution of inflorescence and flower development in grasses. *Plant Cell Physiol.* 46, 69–78. doi: 10.1093/pcp/pci504

Brand, U., Grunewald, M., Hobe, M., and Simon, R. (2002). Regulation of CLV3 expression by two homeobox genes in *Arabidopsis*. *Plant Physiol.* 129, 565–575. doi: 10.1104/pp.001867

Busch, M. A., Bomblies, K., and Weigel, D. (1999). Activation of a floral homeotic gene in *Arabidopsis*. *Science* 285, 585–587. doi: 10.1126/science.285.5427.585

Callens, C., Tucker, M. R., Zhang, D., and Wilson, Z. A. (2018). Dissecting the role of MADS-box genes in monocot floral development and diversity. *J. Exp. Bot.* 69, 2435–2459. doi: 10.1093/jxb/ery086

Chen, J. Y., Guo, L., Ma, H., Chen, Y. Y., Zhang, H. W., Ying, J. Z., et al. (2014). Fine mapping of qHd1, a minor heading date QTL with pleiotropism for yield traits in rice (*Oryza sativa* L.). *Theor. Appl. Genet.* 127, 2515–2524. doi: 10.1007/s00122-014-2395-7

Chongloi, G. L., Prakash, S., and Vijayraghavan, U. (2019). Regulation of meristem maintenance and organ identity during rice reproductive development. *J. Exp. Bot.* 70, 1719–1736. doi: 10.1093/jxb/erz046

Chu, H., Qian, Q., Liang, W., Yin, C., Tan, H., Yao, X., et al. (2006). The floral organ number4 gene encoding a putative ortholog of *Arabidopsis* CLAVATA3 regulates apical meristem size in rice. *Plant Physiol.* 142, 1039–1052. doi: 10.1104/pp.106.086736

Chuang, C. F., Running, M. P., Williams, R. W., and Meyerowitz, E. M. (1999). The PERIANTHIA gene encodes a bZIP protein involved in the determination of floral organ number in *Arabidopsis thaliana*. *Genes Dev.* 13, 334–344. doi: 10.1101/gad.13.3.334

Collins, C., Dewitte, W., and Murray, J. A. (2012). D-type cyclins control cell division and developmental rate during *Arabidopsis* seed development. *J. Exp. Bot.* 63, 3571–3586. doi: 10.1093/jxb/ers015

Dai, Z., Wang, J., Yang, X., Lu, H., Miao, X., and Shi, Z. (2018). Modulation of plant architecture by the miR156f-OsSPL7-OsGH3.8 pathway in rice. *J. Exp. Bot.* 69, 5117–5130. doi: 10.1093/jxb/ery273

Das, P., Ito, T., Wellmer, F., Vernoux, T., Dedieu, A., Traas, J., et al. (2009). Floral stem cell termination involves the direct regulation of AGAMOUS by PERIANTHIA. *Development* 136, 1605–1611. doi: 10.1242/dev.035436

Deshpande, G. M., Ramakrishna, K., Chongloi, G. L., and Vijayraghavan, U. (2015). Functions for rice RFL in vegetative axillary meristem specification and outgrowth. *J. Exp. Bot.* 66, 2773–2784. doi: 10.1093/jxb/erv092

Dodsworth, S. (2009). A diverse and intricate signalling network regulates stem cell fate in the shoot apical meristem. *Dev. Biol.* 336, 1–9. doi: 10.1016/j.ydbio.2009.09.031

Gordon, S. P., Chickarmane, V. S., Ohno, C., and Meyerowitz, E. M. (2009). Multiple feedback loops through cytokinin signaling control stem cell number within the *Arabidopsis* shoot meristem. *Proc. Nat. Acad. Sci. U.S.A.* 106, 16529–16534. doi: 10.1073/pnas.0908122106

Gutsche, N., and Zachgo, S. (2016). The N-Terminus of the floral *Arabidopsis* TGA transcription factor PERIANTHIA mediates redox-sensitive DNA-binding. *PLoS One* 11:e0153810. doi: 10.1371/journal.pone.0153810

Hao, J., Wang, D., Wu, Y., Huang, K., Duan, P., Li, N., et al. (2021). The GW2-WG1-OsbZIP47 pathway controls grain size and weight in rice. *Mol. Plant* 14, 1266–1280. doi: 10.1016/j.molp.2021.04.011

Harder, L. D., and Prusinkiewicz, P. (2013). The interplay between inflorescence development and function as the crucible of architectural diversity. *Ann. Bot.* 112, 1477–1493. doi: 10.1093/aob/mcs252

Hong, L., Tang, D., Zhu, K., Wang, K., Li, M., and Cheng, Z. (2012). Somatic and reproductive cell development in rice anther is regulated by a putative glutaredoxin. *Plant Cell* 24, 577–588. doi: 10.1105/tpc.111.093740

Hu, Y., Liang, W., Yin, C., Yang, X., Ping, B., Li, A., et al. (2015). Interactions of OsMADS1 with floral homeotic genes in rice flower development. *Mol. Plant* 8, 1366–1384. doi: 10.1016/j.molp.2015.04.009

Ikeda, K., Ito, M., Nagasawa, N., Kyozuka, J., and Nagato, Y. (2007). Rice ABERRANT PANICLE ORGANIZATION 1, encoding an F-box protein, regulates meristem fate. *Plant J.* 51, 1030–1040. doi: 10.1111/j.1365-313X.2007.03200.x

Ikeda, K., Nagasawa, N., and Nagato, Y. (2005). ABERRANT PANICLE ORGANIZATION 1 temporally regulates meristem identity in rice. *Dev. Biol.* 282, 349–360. doi: 10.1016/j.ydbio.2005.03.016

Ikeda-Kawakatsu, K., Maekawa, M., Izawa, T., Itoh, J., and Nagato, Y. (2012). ABERRANT PANICLE ORGANIZATION 2/RFL, the rice ortholog of *Arabidopsis* LEAFY, suppresses the transition from inflorescence meristem to floral meristem through interaction with APO1. *Plant J.* 69, 168–180. doi: 10.1111/j.1365-313X.2011.04781.x

Ikeda-Kawakatsu, K., Yasuno, N., Oikawa, T., Iida, S., Nagato, Y., Maekawa, M., et al. (2009). Expression level of ABERRANT PANICLE ORGANIZATION1 determines rice inflorescence form through control of cell proliferation in the meristem. *Plant Physiol.* 150, 736–747. doi: 10.1104/pp.109.136739

Ito, T., Wellmer, F., Yu, H., Das, P., Ito, N., Alves-Ferreira, M., et al. (2004). The homeotic protein AGAMOUS controls microsporogenesis by regulation of SPOROCYTELESS. *Nature* 430, 356–360. doi: 10.1038/nature02733

Iwamoto, M., Kiyota, S., Hanada, A., Yamaguchi, S., and Takano, M. (2011). The multiple contributions of phytochromes to the control of internode elongation in rice. *Plant Physiol.* 157, 1187–1195. doi: 10.1104/pp.111.184861

James, P., Halladay, J., and Craig, E. A. (1996). Genomic libraries and a host strain designed for highly efficient two-hybrid selection in yeast. *Genetics* 144, 1425–1436. doi: 10.1093/genetics/144.4.1425

Jeon, J. S., Jang, S., Lee, S., Nam, J., Kim, C., Lee, S. H., et al. (2000). leafy hull sterile1 is a homeotic mutation in a rice MADS box gene affecting rice flower development. *Plant Cell* 12, 871–884. doi: 10.1105/tpc.12.6.871

Kannan, P., Chongloi, G. L., Majhi, B. B., Basu, D., Veluthambi, K., and Vijayraghavan, U. (2021). Characterization of a new rice OsMADS1 null mutant generated by homologous recombination-mediated gene targeting. *Planta* 253:39. doi: 10.1007/s00425-020-03547-3

Kater, M. M., Dreni, L., and Colombo, L. (2006). Functional conservation of MADS-box factors controlling floral organ identity in rice and *Arabidopsis*. *J. Exp. Bot.* 57, 3433–3444. doi: 10.1093/jxb/erl097

Khanday, I., Das, S., Chongloi, G. L., Bansal, M., Grossniklaus, U., and Vijayraghavan, U. (2016). Genome-wide targets regulated by the OsMADS1 transcription factor reveals its DNA recognition properties. *Plant Physiol.* 172, 372–388. doi: 10.1104/pp.16.00789

Khanday, I., Yadav, S. R., and Vijayraghavan, U. (2013). Rice LHS1/OsMADS1 controls floret meristem specification by coordinated regulation of transcription factors and hormone signaling pathways. *Plant Physiol.* 161, 1970–1983. doi: 10.1104/pp.112.212423

Kim, E. H., Kim, Y. S., Park, S. H., Koo, Y. J., Choi, Y. D., Chung, Y. Y., et al. (2009). Methyl jasmonate reduces grain yield by mediating stress signals to alter spikelet development in rice. *Plant Physiol.* 149, 1751–1760. doi: 10.1104/pp.108.134684

Kobayashi, K., Yasuno, N., Sato, Y., Yoda, M., Yamazaki, R., Kimizu, M., et al. (2012). Inflorescence meristem identity in rice is specified by overlapping functions of three AP1/FUL-like MADS box genes and PAP2, a SEPALLATA MADS box gene. *Plant Cell* 24, 1848–1859. doi: 10.1105/tpc.112.097105

Komatsu, M., Maekawa, M., Shimamoto, K., and Kyozuka, J. (2001). The LAX1 and FRIZZY PANICLE 2 genes determine the inflorescence architecture of rice by controlling rachis-branch and spikelet development. *Dev. Biol.* 231, 364–373. doi: 10.1006/dbio.2000.9988

Kong, L., Duan, Y., Ye, Y., Cai, Z., Wang, F., Qu, X., et al. (2019). Screening and analysis of proteins interacting with OsMADS16 in rice (*Oryza sativa* L.). *PLoS One* 14:e0221473. doi: 10.1371/journal.pone.0221473

Kurakawa, T., Ueda, N., Maekawa, M., Kobayashi, K., Kojima, M., Nagato, Y., et al. (2007). Direct control of shoot meristem activity by a cytokinin-activating enzyme. *Nature* 445, 652–655. doi: 10.1038/nature05504

Kyozuka, J., Konishi, S., Nemoto, K., Izawa, T., and Shimamoto, K. (1998). Down-regulation of RFL, the FLO/LFY homolog of rice, accompanied with panicle branch initiation. *Proc. Nat. Acad. Sci. U.S.A.* 95, 1979–1982. doi: 10.1073/pnas.95.5.1979

Laporte, D., Olate, E., Salinas, P., Salazar, M., Jordana, X., and Holuigue, L. (2012). Glutaredoxin GRXS13 plays a key role in protection against photooxidative stress in *Arabidopsis*. *J. Exp. Bot.* 63, 503–515. doi: 10.1093/jxb/err301

Lee, B. H., Johnston, R., Yang, Y., Gallavotti, A., Kojima, M., Travencolo, B. A., et al. (2009). Studies of aberrant phyllotaxy1 mutants of maize indicate complex interactions between auxin and cytokinin signaling in the shoot apical meristem. *Plant Physiol.* 150, 205–216. doi: 10.1104/pp.109.137034

Lee, S., Jeon, J.-S., An, K., Moon, Y.-H., Lee, S., Chung, Y.-Y., et al. (2003). Alteration of floral organ identity in rice through ectopic expression of OsMADS16. *Planta* 217, 904–911. doi: 10.1007/s00425-003-1066-8

Leibfried, A., To, J. P., Busch, W., Stehling, S., Kehle, A., Demar, M., et al. (2005). WUSCHEL controls meristem function by direct regulation of cytokinin-inducible response regulators. *Nature* 438, 1172–1175. doi: 10.1038/nature04270

Lenhard, M., Bohnert, A., Jurgens, G., and Laux, T. (2001). Termination of stem cell maintenance in *Arabidopsis* floral meristems by interactions between WUSCHEL and AGAMOUS. *Cell* 105, 805–814. doi: 10.1016/s0092-8674(01)00390-7

Li, C., Wang, L., Cui, Y., He, L., Qi, Y., Zhang, J., et al. (2016). Two FERONIA-like receptor (FLR) genes are required to maintain architecture, fertility, and seed yield in rice. *Mol. Breeding* 36:151. doi: 10.1007/s11032-016-0580-x

Li, S., Lauri, A., Ziemann, M., Busch, A., Bhave, M., and Zachgo, S. (2009). Nuclear activity of ROXY1, a glutaredoxin interacting with TGA factors, is required for petal development in *Arabidopsis thaliana*. *Plant Cell* 21, 429–441. doi: 10.1105/tpc.108.064477

Lim, J., Moon, Y. H., An, G., and Jang, S. K. (2000). Two rice MADS domain proteins interact with OsMADS1. *Plant Mol. Biol.* 44, 513–527. doi: 10.1023/a:1026517111843

Liu, X., Kim, Y. J., Muller, R., Yumul, R. E., Liu, C., Pan, Y., et al. (2011). AGAMOUS terminates floral stem cell maintenance in *Arabidopsis* by directly repressing WUSCHEL through recruitment of Polycomb Group proteins. *Plant Cell* 23, 3654–3670. doi: 10.1105/tpc.111.091538

Lohmann, J. U., Hong, R. L., Hobe, M., Busch, M. A., Parcy, F., Simon, R., et al. (2001). A molecular link between stem cell regulation and floral patterning in *Arabidopsis*. *Cell* 105, 793–803. doi: 10.1016/s0092-8674(01)00384-1

Lombardo, F., Kuroki, M., Yao, S. G., Shimizu, H., Ikegaya, T., Kimizu, M., et al. (2017). The superwoman1-cleistogamy2 mutant is a novel resource for gene containment in rice. *Plant Biotechnol. J.* 15, 97–106. doi: 10.1111/pbi.12594

Ma, H., Chen, J., Zhang, Z., Ma, L., Yang, Z., Zhang, Q., et al. (2017). MAPK kinase 10.2 promotes disease resistance and drought tolerance by activating different MAPKs in rice. *Plant J.* 92, 557–570. doi: 10.1111/tpj.13674

Ma, X., Feng, F., Zhang, Y., Elesawi, I. E., Xu, K., Li, T., et al. (2019). A novel rice grain size gene OsSNB was identified by genome-wide association study in natural population. *PLoS Genet.* 15:e1008191. doi: 10.1371/journal.pgen.1008191

Maier, A. T., Stehling-Sun, S., Offenburger, S. L., and Lohmann, J. U. (2011). The bZIP transcription factor PERIANTHIA: a multifunctional hub for meristem control. *Front. Plant Sci.* 2:79. doi: 10.3389/fpls.2011.00079

Maier, A. T., Stehling-Sun, S., Wollmann, H., Demar, M., Hong, R. L., Haubeiss, S., et al. (2009). Dual roles of the bZIP transcription factor PERIANTHIA in the control of floral architecture and homeotic gene expression. *Development* 136, 1613–1620. doi: 10.1242/dev.033647

Martins, L., Trujillo-Hernandez, J. A., and Reichheld, J. P. (2018). Thiol based redox signaling in plant nucleus. *Front. Plant Sci.* 9:705. doi: 10.3389/fpls.2018.00705

Ming, F., and Ma, H. (2009). A terminator of floral stem cells. *Genes Dev.* 23, 1705–1708. doi: 10.1101/gad.1834409

Moyroud, E., Kusters, E., Monniaux, M., Koes, R., and Parcy, F. (2010). LEAFY blossoms. *Trends Plant Sci.* 15, 346–352. doi: 10.1016/j.tplants.2010.03.007

Moyroud, E., Tichtinsky, G., and Parcy, F. (2009). The LEAFY floral regulators in angiosperms: conserved proteins with diverse roles. *J. Plant Biol.* 52, 177–185. doi: 10.1007/s12374-009-9028-8

Nagasawa, N., Miyoshi, M., Kitano, H., Satoh, H., and Nagato, Y. (1996). Mutations associated with floral organ number in rice. *Planta* 198, 627–633. doi: 10.1007/BF00262651

Nagasawa, N., Miyoshi, M., Sano, Y., Satoh, H., Hirano, H., Sakai, H., et al. (2003). SUPERWOMAN1 and DROOPING LEAF genes control floral organ identity in rice. *Development* 130, 705–718. doi: 10.1242/dev.00294

Nijhawan, A., Jain, M., Tyagi, A. K., and Khurana, J. P. (2008). Genomic survey and gene expression analysis of the basic leucine zipper transcription factor family in rice. *Plant Physiol.* 146, 333–350. doi: 10.1104/pp.107.112821

Ohmori, Y., Tanaka, W., Kojima, M., Sakakibara, H., and Hirano, H. Y. (2013). WUSCHEL-RELATED HOMEOBOX4 is involved in meristem maintenance and is negatively regulated by the CLE gene FCP1 in rice. *Plant Cell* 25, 229–241. doi: 10.1105/tpc.112.103432

Parcy, F., Nilsson, O., Busch, M. A., Lee, I., and Weigel, D. (1998). A genetic framework for floral patterning. *Nature* 395, 561–566. doi: 10.1038/26903

Pautler, M., Eveland, A. L., LaRue, T., Yang, F., Weeks, R., Lunde, C., et al. (2015). FASCIATED EAR4 encodes a bZIP transcription factor that regulates shoot meristem size in maize. *Plant Cell* 27, 104–120. doi: 10.1105/tpc.114.132506

Pautler, M., Tanaka, W., Hirano, H. Y., and Jackson, D. (2013). Grass meristems I: shoot apical meristem maintenance, axillary meristem determinacy and the floral transition. *Plant Cell Physiol.* 54, 302–312. doi: 10.1093/pcp/pct025

Peres, A., Churchman, M. L., Hariharan, S., Himanen, K., Verkest, A., Vandepoele, K., et al. (2007). Novel plant-specific cyclin-dependent kinase inhibitors induced by biotic and abiotic stresses. *J. Biol. Chem.* 282, 25588–25596. doi: 10.1074/jbc.M703326200

Prasad, K., Parameswaran, S., and Vijayraghavan, U. (2005). OsMADS1, a rice MADS-box factor, controls differentiation of specific cell types in the lemma and palea and is an early-acting regulator of inner floral organs. *Plant J.* 43, 915–928. doi: 10.1111/j.1365-313X.2005.02504.x

Prasad, K., Sriram, P., Kumar, C. S., Kushalappa, K., and Vijayraghavan, U. (2001). Ectopic expression of rice OsMADS1 reveals a role in specifying the lemma and palea, grass floral organs analogous to sepals. *Dev. Genes Evol.* 211, 281–290. doi: 10.1007/s004270100153

Rao, N. N., Prasad, K., Kumar, P. R., and Vijayraghavan, U. (2008). Distinct regulatory role for RFL, the rice LFY homolog, in determining flowering time and plant architecture. *Proc. Natl. Acad. Sci. U.S.A.* 105, 3646–3651. doi: 10.1073/pnas.0709059105

Running, M. P., and Meyerowitz, E. M. (1996). Mutations in the PERIANTHIA gene of *Arabidopsis* specifically alter floral organ number and initiation pattern. *Development* 122, 1261–1269. doi: 10.1242/dev.122.4.1261

Sakamoto, T., Sakakibara, H., Kojima, M., Yamamoto, Y., Nagasaki, H., Inukai, Y., et al. (2006). Ectopic expression of KNOTTED1-like homeobox protein induces expression of cytokinin biosynthesis genes in rice. *Plant Physiol.* 142, 54–62. doi: 10.1104/pp.106.085811

Sakuma, S., and Schnurbusch, T. (2020). Of floral fortune: tinkering with the grain yield potential of cereal crops. *New Phytol.* 225, 1873–1882. doi: 10.1111/nph.16189

Sato, H., Yoshida, K., Mitsuda, N., Ohme-Takagi, M., and Takamizo, T. (2012). Male-sterile and cleistogamous phenotypes in tall fescue induced by chimeric repressors of SUPERWOMAN1 and OsMADS58. *Plant Sci.* 183, 183–189. doi: 10.1016/j.plantsci.2011.08.010

Schippers, J. H., Foyer, C. H., and van Dongen, J. T. (2016). Redox regulation in shoot growth, SAM maintenance and flowering. *Curr. Opin. Plant Biol.* 29, 121–128. doi: 10.1016/j.pbi.2015.11.009

Sessions, A., Nemhauser, J. L., McColl, A., Roe, J. L., Feldmann, K. A., and Zambryski, P. C. (1997). ETTIN patterns the *Arabidopsis* floral meristem and reproductive organs. *Development* 124, 4481–4491. doi: 10.1242/dev.124.22.4481

Shu, K., Chen, Q., Wu, Y., Liu, R., Zhang, H., Wang, P., et al. (2016). ABI4 mediates antagonistic effects of abscisic acid and gibberellins at transcript and protein levels. *Plant J. Cell Mol. Biol.* 85, 348–361. doi: 10.1111/tpj.13109

Somssich, M., Je, B. I., Simon, R., and Jackson, D. (2016). CLAVATA-WUSCHEL signaling in the shoot meristem. *Development* 143, 3238–3248. doi: 10.1242/dev.133645

Su, Y. H., Liu, Y. B., and Zhang, X. S. (2011). Auxin-cytokinin interaction regulates meristem development. *Mol. Plant* 4, 616–625. doi: 10.1093/mp/ssr007

Su, Y. H., Zhou, C., Li, Y. J., Yu, Y., Tang, L. P., Zhang, W. J., et al. (2020). Integration of pluripotency pathways regulates stem cell maintenance in the *Arabidopsis* shoot meristem. *Proc. Nat. Acad. Sci. U.S.A.* 117, 22561–22571. doi: 10.1073/pnas.2015248117

Sun, B., Looi, L. S., Guo, S., He, Z., Gan, E. S., Huang, J., et al. (2014). Timing mechanism dependent on cell division is invoked by Polycomb eviction in plant stem cells. *Science* 343:1248559. doi: 10.1126/science.1248559

Sun, B., Xu, Y., Ng, K. H., and Ito, T. (2009). A timing mechanism for stem cell maintenance and differentiation in the *Arabidopsis* floral meristem. *Genes Dev.* 23, 1791–1804. doi: 10.1101/gad.1800409

Sun, C., Zhang, K., Zhou, Y., Xiang, L., He, C., Zhong, C., et al. (2021). Dual function of clock component OsLHY sets critical day length for photoperiodic flowering in rice. *Plant Biotechnol. J.* 19, 1644–1657. doi: 10.1111/pbi.13580

Suzaki, T., Sato, M., Ashikari, M., Miyoshi, M., Nagato, Y., and Hirano, H. Y. (2004). The gene FLORAL ORGAN NUMBER1 regulates floral meristem size in rice and encodes a leucine-rich repeat receptor kinase orthologous to *Arabidopsis* CLAVATA1. *Development* 131, 5649–5657. doi: 10.1242/dev.01441

Suzaki, T., Toriba, T., Fujimoto, M., Tsutsumi, N., Kitano, H., and Hirano, H. Y. (2006). Conservation and diversification of meristem maintenance mechanism in *Oryza sativa*: function of the FLORAL ORGAN NUMBER2 gene. *Plant Cell Physiol.* 47, 1591–1602. doi: 10.1093/pcp/pcl025

Takeda, S., Hanano, K., Kariya, A., Shimizu, S., Zhao, L., Matsui, M., et al. (2011). CUP-SHAPED COTYLEDON1 transcription factor activates the expression of LSH4 and LSH3, two members of the ALOG gene family, in shoot organ boundary cells. *Plant J.* 66, 1066–1077. doi: 10.1111/j.1365-313X.2011.04571.x

Tanaka, W., Pautler, M., Jackson, D., and Hirano, H. Y. (2013). Grass meristems II: inflorescence architecture, flower development and meristem fate. *Plant Cell Physiol.* 54, 313–324. doi: 10.1093/pcp/pct016

Timofejeva, L., Skibbe, D. S., Lee, S., Golubovskaya, I., Wang, R., Harper, L., et al. (2013). Cytological characterization and allelism testing of anther developmental mutants identified in a screen of maize male sterile lines. *G3 (Bethesda)* 3, 231–249. doi: 10.1534/g3.112.004465

Tsuda, K., Ito, Y., Sato, Y., and Kurata, N. (2011). Positive autoregulation of a KNOX gene is essential for shoot apical meristem maintenance in rice. *Plant Cell* 23, 4368–4381. doi: 10.1105/tpc.111.090050

Tsuda, K., Kurata, N., Ohyanagi, H., and Hake, S. (2014). Genome-wide study of KNOX regulatory network reveals brassinosteroid catabolic genes important for shoot meristem function in rice. *Plant Cell* 26, 3488–3500. doi: 10.1105/tpc.114.129122

Viola, I. L., Guttlein, L. N., and Gonzalez, D. H. (2013). Redox modulation of plant developmental regulators from the class I TCP transcription factor family. *Plant Physiol.* 162, 1434–1447. doi: 10.1104/pp.113.216416

Vollbrecht, E., Reiser, L., and Hake, S. (2000). Shoot meristem size is dependent on inbred background and presence of the maize homeobox gene, knotted1. *Development* 127, 3161–3172. doi: 10.1242/dev.127.14.3161

Waadt, R., Schmidt, L. K., Lohse, M., Hashimoto, K., Bock, R., and Kudla, J. (2008). Multicolor bimolecular fluorescence complementation reveals simultaneous formation of alternative CBL/CIPK complexes in planta. *Plant J.* 56, 505–516. doi: 10.1111/j.1365-313X.2008.03612.x

Wagner, D., Sablowski, R. W., and Meyerowitz, E. M. (1999). Transcriptional activation of APETALA1 by LEAFY. *Science* 285, 582–584. doi: 10.1126/science.285.5427.582

Wang, F., Han, T., Song, Q., Ye, W., Song, X., Chu, J., et al. (2020). The rice circadian clock regulates tiller growth and panicle development through strigolactone signaling and sugar sensing. *Plant Cell* 32, 3124–3138. doi: 10.1105/tpc.20.00289

Wang, J., Wang, R., Wang, Y., Zhang, L., Zhang, L., Xu, Y., et al. (2017). Short and Solid Culm/RFL/APO2 for culm development in rice. *Plant J.* 91, 85–96. doi: 10.1111/tpj.13548

Weimer, A. K., Matos, J. L., Sharma, N., Patell, F., Murray, J. A. H., Dewitte, W., et al. (2018). Lineage- and stage-specific expressed CYCD7;1 coordinates the single symmetric division that creates stomatal guard cells. *Development* 145:dev160671. doi: 10.1242/dev.160671

Xu, K., Huang, X., Wu, M., Wang, Y., Chang, Y., Liu, K., et al. (2014). A rapid, highly efficient and economical method of *Agrobacterium*-mediated in planta transient transformation in living onion epidermis. *PLoS One* 9:e83556. doi: 10.1371/journal.pone.0083556

Xu, W., Tao, J., Chen, M., Dreni, L., Luo, Z., Hu, Y., et al. (2017). Interactions between FLORAL ORGAN NUMBER4 and floral homeotic genes in regulating rice flower development. *J. Exp. Bot.* 68, 483–498. doi: 10.1093/jxb/erw459

Yaish, M. W., El-Kereamy, A., Zhu, T., Beatty, P. H., Good, A. G., Bi, Y. M., et al. (2010). The APETALA-2-like transcription factor OsAP2-39 controls key interactions between abscisic acid and gibberellin in rice. *PLoS Genet.* 6:e1001098. doi: 10.1371/journal.pgen.1001098

Yamaguchi, T., Nagasawa, N., Kawasaki, S., Matsuoka, M., Nagato, Y., and Hirano, H. Y. (2004). The YABBY gene DROOPING LEAF regulates carpel specification and midrib development in *Oryza sativa*. *Plant Cell* 16, 500–509. doi: 10.1105/tpc.018044

Yamaki, S., Nagato, Y., Kurata, N., and Nonomura, K. (2011). Ovule is a lateral organ finally differentiated from the terminating floral meristem in rice. *Dev. Biol.* 351, 208–216. doi: 10.1016/j.ydbio.2010.12.006

Yang, F., Bui, H. T., Pautler, M., Llaca, V., Johnston, R., Lee, B. H., et al. (2015). A maize glutaredoxin gene, abphyl2, regulates shoot meristem size and phyllotaxy. *Plant Cell* 27, 121–131. doi: 10.1105/tpc.114.130393

Yang, R. S., Xu, F., Wang, Y. M., Zhong, W. S., Dong, L., Shi, Y. N., et al. (2021). Glutaredoxins regulate maize inflorescence meristem development via redox control of TGA transcriptional activity. *Nat. Plants* 7, 1589–1601. doi: 10.1038/s41477-021-01029-2

Yi, J., Lee, Y. S., Lee, D. Y., Cho, M. H., Jeon, J. S., and An, G. (2016). OsMPK6 plays a critical role in cell differentiation during early embryogenesis in *Oryza sativa*. *J. Exp. Bot.* 67, 2425–2437. doi: 10.1093/jxb/erw052

Yoon, J., Cho, L. H., Antt, H. W., Koh, H. J., and An, G. (2017). KNOX protein OSH15 induces grain shattering by repressing lignin biosynthesis genes. *Plant Physiol.* 174, 312–325. doi: 10.1104/pp.17.00298

Zeng, J., Dong, Z., Wu, H., Tian, Z., and Zhao, Z. (2017). Redox regulation of plant stem cell fate. *EMBO J.* 36, 2844–2855. doi: 10.15252/embj.201695955

Zhang, X. (2014). Delayed gratification—waiting to terminate stem cell identity. *Science* 343, 498–499. doi: 10.1126/science.1249343

Zhao, D.-S., Li, Q.-F., Zhang, C.-Q., Zhang, C., Yang, Q.-Q., Pan, L.-X., et al. (2018). GS9 acts as a transcriptional activator to regulate rice grain shape and appearance quality. *Nat. Commun.* 9:1240. doi: 10.1038/s41467-018-03616-y

Zhao, Z., Andersen, S. U., Ljung, K., Dolezal, K., Miotk, A., Schultheiss, S. J., et al. (2010). Hormonal control of the shoot stem-cell niche. *Nature* 465, 1089–1092.

Zhu, Q., Zhang, X. L., Nadir, S., DongChen, W. H., Guo, X. Q., Zhang, H. X., et al. (2017). A LysM domain-containing gene OsEMSA1 involved in embryo sac development in rice (*Oryza sativa* L.). *Front. Plant Sci.* 8:1596. doi: 10.3389/fpls.2017.01596

Zhu, Y. J., Fan, Y. Y., Wang, K., Huang, D. R., Liu, W. Z., Ying, J. Z., et al. (2017). Rice Flowering Locus T 1 plays an important role in heading date influencing yield traits in rice. *Sci. Rep.* 7:4918. doi: 10.1038/s41598-017-05302-3

Conflict of Interest: The authors declare that the research was conducted in the absence of any commercial or financial relationships that could be construed as a potential conflict of interest.

Publisher's Note: All claims expressed in this article are solely those of the authors and do not necessarily represent those of their affiliated organizations, or those of the publisher, the editors and the reviewers. Any product that may be evaluated in this article, or claim that may be made by its manufacturer, is not guaranteed or endorsed by the publisher.

frontiers | Frontiers in Plant Science

ORIGINAL RESEARCH
published: 29 April 2022
doi: 10.3389/fpls.2022.889066

Candidate Genes Modulating Reproductive Timing in Elite US Soybean Lines Identified in Soybean Alleles of *Arabidopsis* Flowering Orthologs With Divergent Latitude Distribution

*Nicholas Dietz[1], Yen On Chan[2,3], Andrew Scaboo[1], George Graef[4], David Hyten[4], Mary Happ[4], Brian Diers[5], Aaron Lorenz[6], Dechun Wang[7], Trupti Joshi[2,3,8,9] and Kristin Bilyeu[10]**

[1] Division of Plant Science and Technology, University of Missouri, Columbia, MO, United States, [2] Christopher S. Bond Life Sciences Center, University of Missouri, Columbia, MO, United States, [3] MU Data Science and Informatics Institute, University of Missouri, Columbia, MO, United States, [4] Department of Agronomy and Horticulture, University of Nebraska, Lincoln, NE, United States, [5] Department of Crop Sciences, University of Illinois, Urbana, IL, United States, [6] Department of Agronomy and Plant Genetics, University of Minnesota, Saint Paul, MN, United States, [7] Department of Plant, Soil and Microbial Sciences, Michigan State University, East Lansing, MI, United States, [8] Department of Electrical Engineering and Computer Science, University of Missouri, Columbia, MO, United States, [9] Department of Health Management and Informatics, School of Medicine, University of Missouri, Columbia, MO, United States, [10] USDA/ARS Plant Genetics Research Unit, Columbia, MO, United States

OPEN ACCESS

Edited by:
Michael Gerard Muszynski, University of Hawai'i at Mānoa, United States

Reviewed by:
Richard Macknight, University of Otago, New Zealand
Kyuya Harada, Osaka University, Japan

***Correspondence:**
Kristin Bilyeu
kristin.bilyeu@usda.gov;
bilyeuk@missouri.edu

Specialty section:
This article was submitted to Plant Development and EvoDevo, a section of the journal Frontiers in Plant Science

Received: 03 March 2022
Accepted: 08 April 2022
Published: 29 April 2022

Citation:
Dietz N, Chan YO, Scaboo A, Graef G, Hyten D, Happ M, Diers B, Lorenz A, Wang D, Joshi T and Bilyeu K (2022) Candidate Genes Modulating Reproductive Timing in Elite US Soybean Lines Identified in Soybean Alleles of Arabidopsis Flowering Orthologs With Divergent Latitude Distribution. Front. Plant Sci. 13:889066. doi: 10.3389/fpls.2022.889066

Adaptation of soybean cultivars to the photoperiod in which they are grown is critical for optimizing plant yield. However, despite its importance, only the major loci conferring variation in flowering time and maturity of US soybean have been isolated. By contrast, over 200 genes contributing to floral induction in the model organism *Arabidopsis thaliana* have been described. In this work, putative alleles of a library of soybean orthologs of these *Arabidopsis* flowering genes were tested for their latitudinal distribution among elite US soybean lines developed in the United States. Furthermore, variants comprising the alleles of genes with significant differences in latitudinal distribution were assessed for amino acid conservation across disparate genera to infer their impact on gene function. From these efforts, several candidate genes from various biological pathways were identified that are likely being exploited toward adaptation of US soybean to various maturity groups.

Keywords: development, soybean, flowering time, vegetative phase, reproductive phase, genomics, orthologs

INTRODUCTION

Flowering time is a key trait for maximizing yield potential in many crop species. Extensive research into the genetic mechanisms controlling reproductive timing in the long-day-flowering model organism *Arabidopsis thaliana* has blazed the trail for understanding the flowering process and has been instrumental in identifying these genes in other species. At least six major pathways

coordinate to modulate flowering, including the photoperiod, ambient temperature, vernalization, autonomous, aging, and gibberellins pathways (reviewed in Fornara et al., 2010). Together, members of these pathways integrate environmental and endogenous signals and converge upon key floral integrator genes to promote flowering under optimum conditions (**Figure 1**).

The circadian clock complex is composed of three distinct groups of genes, the morning loop, central loop, and evening loop, which regulate one another to maintain an endogenous 24-h oscillation period. *LATE ELONGATED HYPOCOTYL* (*LHY*) and *CIRCADIAN CLOCK-ASSOCIATED 1* (*CCA1*) promote expression of members of the morning loop, while *TIMING OF CAB EXPRESSION 1* (*TOC1*) regulates members of the evening loop (Alabadì et al., 2001; Gendron et al., 2012). Reciprocal regulation between these three loops ensures proper expression of day/night developmental programs. Photoreceptors in the photoperiod pathway, such as the phytochrome and cryptochrome molecules, perceive different wavelengths of light and, together with output from the circadian clock, affect stabilization of the *CONSTANS* (*CO*) protein in the leaf (Valverde et al., 2004). The relative balance of *CO*, a floral promoter, and the *TEMPRANILLO* (*TEM1*, *TEM2*) repressor genes regulates expression of *FLOWERING LOCUS T* (*FT*), a key florigen producing gene, in response to daylength (Castillejo and Pelaz, 2008). *FLOWERING LOCUS C* (*FLC*) integrates signaling from both the vernalization and autonomous pathways and, when expressed, functions to delay flowering by repressing key floral integrators *SUPPRESSOR OF OVEREXPRESSION OF CONSTANS 1* (*SOC1*) and *FT* expression (Lee et al., 2000).

Under optimum flowering conditions, *FT* is expressed in the leaf and produces a mobile florigen that travels to the meristem by way of the phloem. Once in the meristem, *FT*, in concert with *SOC1* and *LEAFY* (*LFY*), stimulate the floral meristem transition and activate homeotic genes that give rise to the various floral organs (Parcy et al., 1998; Liu C. et al., 2009). Like *FT*, gibberellins, a class of hormone involved in broad developmental regulation throughout the plant, are produced in the leaf and travel to the meristem where they promote floral induction by upregulation of *SOC1* (Mutasa-Göttgens and Hedden, 2009).

In contrast to *Arabidopsis*, soybean begins its reproductive period in response to short day photoperiods and lacks a vernalization requirement for proper seed germination. Despite this evolutionary divergence, nearly all the isolated flowering time genes in soybean are orthologs of *Arabidopsis* genes. *GmFT2a* (*E9*) and *GmFT5a* are two such orthologs of the *Arabidopsis FT* gene which promote flowering in response to environmental and endogenous signals under appropriate conditions (Takeshima et al., 2016; Zhao et al., 2016). *E1*, a legume-specific B3-related transcription factor, mediates the photoperiod response to suppress *GmFT2a* and *GmFT5a* expression during long days (Xia et al., 2012). Once days shorten past a critical threshold, *E1* is suppressed, which derepresses *GmFT2a* and *GmFT5a* to allow flowering.

Tof11 and *Tof12* are recently isolated paralogs which contributed to soybean domestication (Lu et al., 2020). These genes are orthologs of the *Arabidopsis* circadian clock gene *PSEUDO RESPONSE REGULATOR 3* (*PRR3*), which function upstream of the central loop oscillator *GmLHY*. *GmPHYA3* (*E3*) and *GmPHYA2* (*E4*) are orthologs of the *Arabidopsis PHYA* gene (Liu et al., 2008; Watanabe et al., 2009). These phytochrome molecules perceive red and far-red light, which, in concert with the *Tof11*, *Tof12*, and *GmLHY*, mediate *E1* expression to coordinate flowering in response to daylength. Like *Tof11* and *Tof12*, *GmGIa* (*E2*) is a circadian clock-associated member of the evening loop in soybean and is a paralog of the *Arabidopsis GIGANTEA* (*GI*) gene (Watanabe et al., 2011). *GmGIa* contributes to flowering in response to photoperiod by delaying expression of *GmFT2a* under long days. The *J* locus (*E6*) is an ortholog of *EARLY FLOWERING 3* (*ELF3*), another circadian clock gene which delays flowering under short day photoperiods and is used to extend the vegetative phase of soybean grown in low latitude production environments (Lu et al., 2017).

Five mutant alleles of the *E1* gene have been identified, including alleles containing a frameshift mutation (*e1-fs*), a missense mutation (*e1-as*), a retrotransposon insertion (*e1-re*), a likely regulatory mutation (*e1-p*), and a complete deletion of the *E1* gene (*e1-nl*) (Tsubokura et al., 2013). A recessive allele of *E2* contains a single base substitution resulting in a non-sense mutation (Watanabe et al., 2011). The *E3* gene has two variant alleles that differ in their amino acid sequences, relative to the Williams 82 reference: a rare allele containing a non-sense mutation in third exon (*e3-mo*), and an allele containing a large ∼13 kb deletion after the third exon, resulting in a truncated protein (*e3-tr*) (Watanabe et al., 2009; Tsubokura et al., 2013). A single mutant allele of the *E4* gene contains retrotransposon insertion in its first exon (*e4-SORE-1*) (Liu et al., 2008).

Soybean varieties are adapted to narrow latitudinal ranges, referred to as Maturity Group (MG), due to their propensity to flower and mature in response to photoperiod. In US soybean production, *E1, E2, and E3* confer most of the observed variation in flowering time and maturity; no variation in the *E4* gene has been detected in US soybean cultivars (Langewisch et al., 2017). In each case, the dominant allele confers later flowering and maturity. *e1-as*, a partially functional recessive allele of *E1*, contains a single missense mutation in its nuclear localization sequence, impairing its ability to enter the nucleus to suppress *GmFT2a*, and resulting in earlier flowering (Xia et al., 2012). The non-sense mutation in the *E2* gene results in a non-functional protein and confers early flowering (Watanabe et al., 2011). The predominant recessive allele of *E3* among US soybean, *e3-tr*, produces a truncated non-functional protein which confers early flowering (Watanabe et al., 2009). However, given the inability of short-read sequencing data to capture large insertions and deletions, the *e3-tr* mutant allele was not incorporated in this study.

Allelic combinations of these three genes are the major loci conferring adaptation to the various MGs in US soybean varieties (Langewisch et al., 2017). The dominant alleles of all three genes are present in the late flowering cultivars of the south (MG V through MG VIII), whereas accruement of additional recessive alleles confers earlier flowering of cultivars in northern MGs (MG 0–MG IV). Despite this knowledge, our understanding of the loci which confer modest changes in flowering time, such

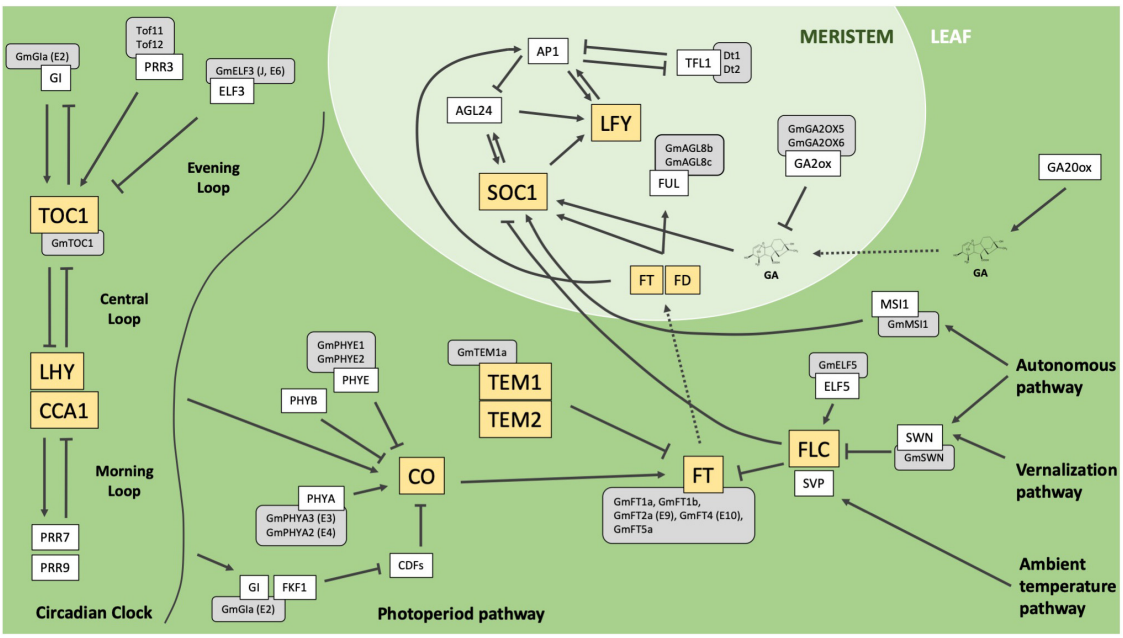

FIGURE 1 | Simplified depiction of characterized pathways and genes which influence flowering in the model organism *Arabidopsis thaliana* (adapted from Fornara et al., 2010). Sharp boxes represent *Arabidopsis* genes. Gray rounded boxes represent orthologous genes in soybean. Yellow boxes highlight key integrators or regulators in their respective pathways. Solid arrows indicate positive regulation, T-bars represent negative regulation, dotted arrows represent mobility from leaf to meristem. *Arabidopsis* genes: *Gigantea* (*GI*), *Pseudo Response Regulator 3* (*PRR3*), *Early Flowering 3 (ELF3), Timing of CAB Expression 1 (TOC1), Late Elongated Hypocotyl (LHY), Circadian Clock Associated 1 (CCA1), Pseudo Response Regulator 7 (PRR7), Pseudo Response Regulator 9 (PRR9), Flavin-binding, Kelch Repeat, F-Box 1 (FKF1), Cycling DOF Factors (CDFs), Phytochrome A (PHYA), Phytochrome B (PHYB), Phytochrome E (PHYE), Constans (CO), Tempranillo 1 (TEM1), Tempranillo 2 (TEM2), Flowering Locus T (FT), Flowering Locus C (FLC), Early Flowering 5 (ELF5), Short Vegetative Phase (SVP), Swinger (SWN), Multicopy Suppressor of IRA 1 (MSI1), Gibberellin 20-oxidase (GA20ox), Gibberellin 2-oxidase (GA2ox), Fruitful (FUL), Flowering Locus D (FD), Suppressor of Constans 1 (SOC1), Leafy (LFY), Agamous-like 24 (AGL24), Apetala 1 (AP1), Terminal Flower 1 (TFL1).* Soybean genes: *Gigantea A (GmGla, E2), Time of Flowering 11 (Tof11), Time of Flowering 12 (Tof12), Early Flowering 3 (GmELF3, J, E6), Timing of CAB Expression 1 (GmTOC1), Phytochrome A3 (GmPHYA3, E3), Phytochrome A2 (GmPHYA2, E4), Phytochrome E1 (PHYE1), Phytochrome E2 (PHYE2), Tempranillo 1a (GmTEM1a), Flowering Locus T 1a (GmFT1a), Flowering Locus T 1b (GmFT1b), Flowering Locus T 2a (GmFT2a, E9), Flowering Locus T 4 (GmFT4, E10), Flowering Locus T 5a (GmFT5a), Early Flowering 5 (GmELF5), Swinger (GmSWN), Multicopy Suppressor of IRA1 (GmMSI1), Gibberellins 2-oxidase 5 (GmGA2OX5), Gibberellins 2-oxidase 6 (GmGA2OX6), Agamous-like 8b (GmAGL8b), Agamous-like 8c (GmAGL8c), Determinant 1 (Dt1), Determinant 2 (Dt2).*

as those within MGs or between adjacent maturity groups, is still lacking. In this work, we utilized resequencing data from 264 elite US soybean lines, converted into a specialized "allele" format, to test soybean orthologs of *Arabidopsis* flowering genes for differences in latitudinal adaptation between lines differing for alleles. Here, latitude was utilized as a proxy for relative flowering time. For genes with significant *p* values, weblogos were generated from multiple sequence alignments to determine which mutations occurred in conserved peptide domains and were thus likely to impact protein function. Based on these criteria, we present a set of eight high confidence genes which warrant further investigation as targets for optimizing flowering time and maturity in US soybean cultivars.

MATERIALS AND METHODS

Curation of Imputed Resequencing Dataset

As part of a parallel effort to catalog the extent of genetic variation in wild and cultivated soybean, our research group previously developed a diversity panel derived from two sets of publicly available resequenced soybean accessions (Zhou et al., 2015; Valliyodan et al., 2021). In this work we used 772 accessions from this diversity panel as a core set of accessions, from which we obtained a total of ∼35.7 M SNP and InDel positions (Škrabišová et al., 2022). We genotyped an additional 518 resequenced accessions at those ∼35.7 Mil positions from other published datasets (Happ et al., 2019; Liu et al., 2020) or from our own skim resequencing efforts (**Supplementary Table 1**). The set of 65 accessions resequenced by our research group were predominantly elite US soybean lines (ELs) derived from the public university soybean breeding programs in Minnesota, Michigan, Illinois, and Missouri.

Raw reads for publicly available accessions were obtained from NCBI SRA (projects: SRP062245, SRP105183, SRP045129, PRJNA512147) or from the National Genomics Data Center Genome Sequence Archive (project: PRJCA002030). All reads were aligned to the Wm82.a2.v1 Phytozome reference genome using BWA Mem v0.7.17. Variants were called using GATK HaplotypeCaller v4.1.9.0 in "-ERC GVCF" mode. Any identified variant positions which were exclusive to the 518 non-reference

panel accessions (i.e., those positions which were not part of the ∼35.7 M SNPs and InDels called from the reference panel) were excluded. Imputation with Beagle v5.2 was performed on the ∼35.7 M positions using the core set of 772 accessions as a reference panel to fill in any missing genotype data derived from regions of poor read coverage or quality. The effect of each of these variants was predicted using the software utility SNPEff v4.3.1t and the Ensembl GTF annotation file for the Wm82.a2.v1 reference genome.[1] Variant annotations were restricted to the primary transcript only.

Conversion of Variants to Alleles

The full set of ∼35.7 Mil variant positions was filtered to only include those positions predicted to cause some non-conservative amino acid change in a gene product. This includes all exonal InDels, non-sense mutations, splice site mutations, loss or gain of either a start or stop codon, and non-conservative missense mutations (as defined by groups in **Supplementary Table 2**). For all accessions, the remaining variant positions in each gene were concatenated to create a putative allele for all ∼55k genes in the genome. The full accession panel was then filtered to obtain only the subset of ELs for which state of origin could be determined; these 264 ELs were then used for subsequent analyses.

Latitude Assignment and Rescaling of 264 Elite US Soybean Lines

For 141 of the 264 resequenced ELs, we were able to obtain days to maturity or relative maturity scores directly from the breeders who developed them (**Supplementary Table 3**). In such cases, we used those maturity scores to expand the relative latitude values of each EL to the latitudinal range encompassed by the approximate northern and southern border of their respective state. **Supplementary Figure 1** illustrates this methodology using 12 resequenced ELs derived from Dr. Brian Diers' breeding program in Illinois as an example. The northern border of Illinois has a latitude of 42.496369°N, while the southern border has a latitude of 37.231888°N. The earliest maturing EL resequenced from Dr. Diers' program had a relative maturity (RM) value of 2.5, while the latest maturing EL was assigned an RM of 4.0. The two ELs with RM 2.5 and RM 4.0 were assigned latitude values of 42.496369°N and 37.231888°N, respectively, while the other ten ELs' latitudes were scaled to this latitudinal range based on their RM values. ELs for which breeders provided days to maturity data, instead of RM values, were treated similarly. In such cases, ELs with the fewest number of days to maturity were assigned a latitude corresponding to the northern border of the state and ELs with the largest number of days to maturity were assigned a latitude corresponding to the southern border of the state. All ELs which matured between the earliest and latest ELs were rescaled to the latitudinal range of the state, according to their respective days to maturity score. ELs which were assigned scaled latitudes based on available maturity information are denoted by "maturity-scaled latitude" in the "LATITUDE_TYPE" column of **Supplementary Table 4**. ELs for which maturity scores were not available were assigned a latitude value corresponding to the centroidal latitude of the state that the EL originated from (denoted as "centroidal latitude" in the "LATITUDE_TYPE" column of **Supplementary Table 4**).

[1] http://ftp.ebi.ac.uk/ensemblgenomes/pub/release-51/plants/gtf/glycine_max

E1 and *E2* Genotype Assignment of Elite US Soybean Lines From Resequencing Data

E1 and *E2* genotypes for all 264 ELs were determined from resequencing results. In addition to the characterized T75R substitution in the *E1* gene (Xia et al., 2012), three ELs in our resequencing panel had a frameshift mutation in *E1*, resulting from a string of adenosine repeats (**Supplementary Table 5**). Given that InDels which arise from sequence repeats are often artifacts of read alignment error, as well as the low frequency of this mutation among our resequencing panel, only the T75R mutation (06:20207322) was considered when assigning *e1-as/E1* genotypes to ELs. Variation at two positions in the *E2* gene was present among our resequencing panel: the previously characterized K528* non-sense mutation (10:45310798) leading to the *e2* allele (Watanabe et al., 2011), and an isoleucine to valine substitution of amino acid 220 (**Supplementary Table 6**). As previously stated, only non-conservative mutations were considered when differentiating alleles (as defined by amino acid groups in **Supplementary Table 2**). As such, *E2* genotypes were assigned solely based on the K528* non-sense mutation.

A Curated List of Soybean Orthologs of *Arabidopsis* Flowering Time Genes Tested for Latitudinal Disparity

Wu et al. (2019) identified 420 soybean orthologs of the 215 *Arabidopsis* genes involved in flowering from a reciprocal BLASTP query. In this study, we curated an expanded list containing the 420 soybean genes identified by Wu et al., plus an additional 29 orthologs identified from a manual search of the literature (**Supplementary Table 7**). Genes in this list were excluded from further analysis if (1) they lacked non-conservative mutations, or (2) they lacked at least one alternate allele (i.e., non-reference allele) present in ten or more ELs. These filtering criteria resulted in a final list of 139 genes. These genes were then tested for latitudinal disparity between alleles of the subset of ELs containing the *E* genotype *e1-as/E2*. Mean comparisons were carried out using a student *t*-test (genes with two alleles) or an *ANOVA* (genes with more than two alleles). The *t*- or *f*-statistic representing the 95% confidence interval for each gene was empirically determined by randomization using 1,000 permutations. For genes with more than two alleles, significance letters were obtained from a test for least significant difference. All statistics were conducted using the "stats" package in R v4.0.2 and boxplots for genes with significant *p* values ($p < 0.05^*$) were generated using ggplot2 v3.3.2.

Weblogo Generation for Genes of Interest

Wm82.a2.v1 peptide sequences for full genes, based on the primary transcript, were pulled from Ensembl using the biomaRt

v2.44.4 package. Orthologous sequences were obtained from an NCBI BLASTP query using the command line utility Protein-Protein BLAST v2.10.1. For each returned genus, the orthologous sequence with the highest percent identity was selected, while redundant sequences from each genus were discarded. Multiple sequence alignments for each gene were generated using the msa v1.20.1 R package. Weblogos were generated by clipping the multiple sequence alignment to approximately ten amino acids on either side of each variant, except in cases where variants fell within ten amino acids of the beginning or end of the aligned sequence.

RESULTS

A Curated Set of Resequenced Elite US Soybean Lines

The objective for this work was to identify additional genes that may be contributing to flowering time in US soybean production environments. We performed variant calling and effect annotation on the genome sequence of 264 elite US soybean lines (ELs) from other published works (Zhou et al., 2015; Liu et al., 2020; Valliyodan et al., 2021) and from our own resequencing efforts (**Supplementary Table 4**). This resulted in a total of ∼11.3 Mil SNPs and InDels. Alleles were defined by the subset of SNPs and InDels which resulted in amino acid changes for each gene. This collection of ELs represents MG's 0 through VIII and spans a latitudinal range from approximately 27.6°N to 48.9°N. A subset of 31 of these ELs have the maturity genotype *E1*/*E2*, 187 ELs have *e1-as*/*E2*, and 41 ELs have *e1-as*/*e2* (**Supplementary Table 8**). The 5 ELs with the maturity genotype *E1*/*e2* were excluded from further analysis (Langewisch et al., 2017).

Soybean Orthologs of *Arabidopsis* Flowering Genes Tested for Latitudinal Disparity Between Alleles

Alleles for 139 orthologs of *Arabidopsis* flowering genes (**Supplementary Table 9**) were tested for significant latitudinal disparity (difference in mean latitudes based on reference or alternate allele(s) of each gene) among the 187 resequenced ELs within the *E* genotype group *e1-as/E2*. For genes that were significant ($p < 0.05^*$) for disparities in mean latitude between alleles, a weblogo was created for the variants comprising each allele to determine whether each variant occurred within a conserved sequence domain which is likely important for protein function (Shaner et al., 1993). We identified a set of soybean genes likely playing a role in modulating flowering time in these ELs by taking into consideration latitudinal disparity between alleles, degree of amino acid conservation, and functional annotation of the *Arabidopsis* orthologs. Only the subset of identified genes, based on the criteria mentioned above, are discussed in further detail here; there were 19 other genes with significant latitudinal disparity that failed to meet our other criteria (**Supplementary Figure 2**).

E1 and *E2* Show Latitudinal Disparity Between Alleles for Elite US Soybean Lines

Mutant alleles of *E1* (Glyma.06G207800) and *E2* (Glyma.10G221500) confer earlier flowering than their functional counterparts and are exploited to shorten the life cycle of soybean grown in northern US production environments (Watanabe et al., 2011; Xia et al., 2012; Langewisch et al., 2017). As a proof of concept, we analyzed the latitudinal disparity of alleles of *E1* and *E2* to assess whether latitude was a suitable proxy for flowering time. Among our full resequencing panel, 36 ELs had the functional allele of *E1*, while 228 ELs had the *e1-as* missense allele (**Supplementary Table 8**). A means comparison revealed a significant difference in mean latitude ($p < 0.001^{***}$), where ELs with the *e1-as* allele had an average latitude that was 4.6°N higher than those with the *E1* allele (**Figure 2A**). A similar assessment for the *E2* gene was conducted using only those ELs containing the *e1-as* allele of *E1*. There were 187 ELs in our resequencing panel that had the functional *E2* allele, while 41 ELs had the non-sense *e2* allele (**Supplementary Table 8**). Like *E1*, alleles of *E2* showed a significant difference in mean latitude ($p < 0.001^{***}$), where ELs containing *e2* were adapted to 2.5°N higher latitude, on average, than ELs containing *E2* (**Figure 2B**). Our findings concur with previous reports describing the allelic distribution of *E1* and *E2* among US soybean cultivars and validated our strategy of using latitude as a proxy for relative flowering time and maturity in this study (Langewisch et al., 2017). Furthermore, to avoid the large confounding effect that variation in *E1* and *E2* would have when assessing the latitudinal disparity of other genes, only the 187 ELs containing the *E* genotype *e1-as/E2* were included in further analysis.

Modulation of Flowering Time by Members of the Autonomous Pathway

The autonomous pathway broadly modulates the plant's ability to perceive and respond to signaling from other pathways, principally through regulation of *FLOWERING LOCUS C* (*FLC*), but also through genes that act in pathways parallel to *FLC* (**Figure 1**; reviewed in Simpson, 2004). *MULTICOPY SUPPRESSOR OF IRA 1* (*MSI1*), one such *FLC*-independent gene, is involved in epigenetic reprogramming of the key floral integrator gene *SUPPRESSOR OF OVEREXPRESSION OF CONSTANS 1* (*SOC1*) (Bouveret et al., 2006). *GmMSI1* on chromosome 05 (Glyma.05G131200) was identified as a putative ortholog of the *Arabidopsis MSI1* gene (Wu et al., 2019). Among our panel of resequenced ELs, 174 ELs contained the Williams 82 reference allele of *GmMSI1*, while 20 ELs contained a single methionine to threonine substitution of amino acid 37. We discovered a significant difference ($p < 0.05^*$) in mean latitude between ELs with contrasting alleles of *GmMSI1*, where ELs with the M37T substitution were adapted to 0.76°N higher, on average, than ELs with the reference allele (**Figure 3A**). A weblogo generated from 237 genera showed the threonine residue at position 38, as well as the surrounding peptide domain, were highly conserved in this protein and thus likely important for protein function (**Figure 3B**).

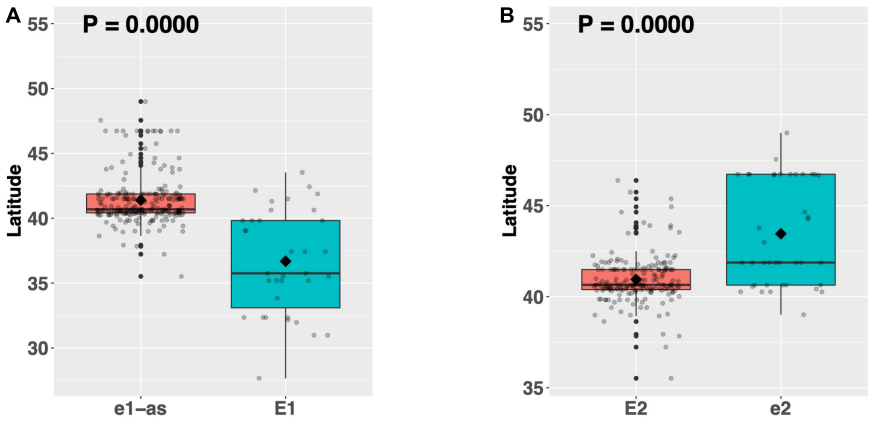

FIGURE 2 | Latitudinal distribution of major alleles of **(A)** the *E1* gene and **(B)** the *E2* gene among 264 resequenced ELs. Latitude of origination was used a proxy for relative flowering time. Latitude values were estimated based on state of origin and, where available, were scaled according to maturity info provided by breeders that developed the ELs (see Experimental Procedures). Means comparisons were conducted using a student *t*-test, where the *t*-statistic representing the 95% confidence interval was empirically derived by randomization. Transparent dots represent the latitude of each accession. Boxplots show the mean (diamond), median (solid line), quartile span (box), range (vertical lines), and outliers (solid dots). The Williams 82 reference allele is on the left and the box filled with red.

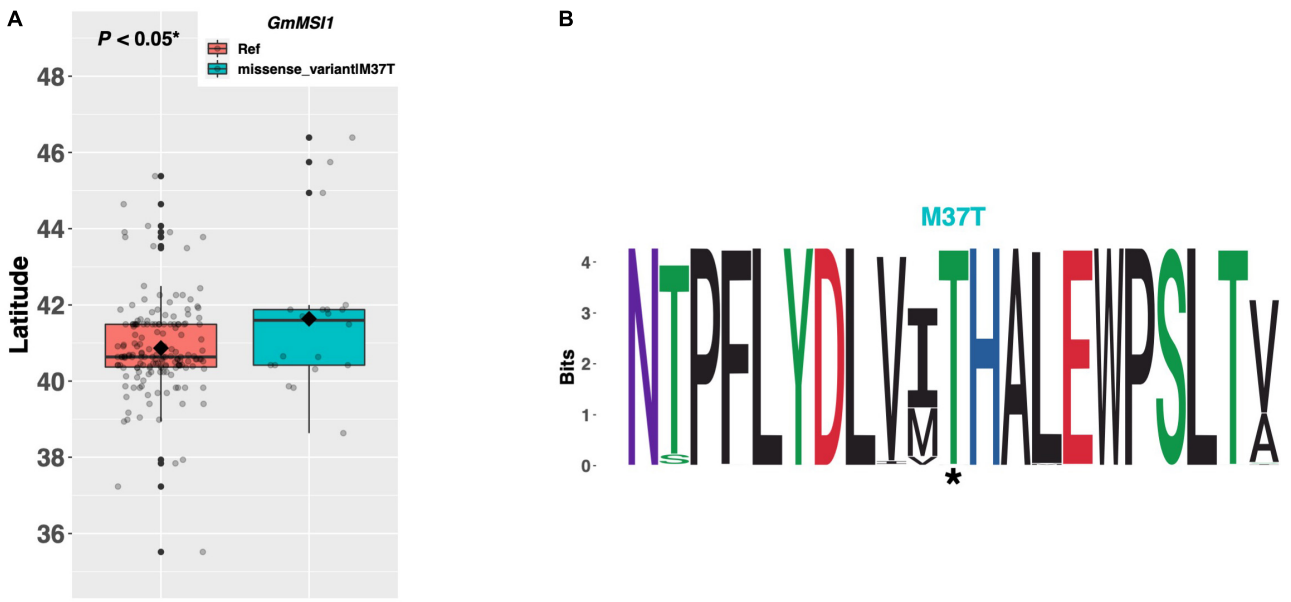

FIGURE 3 | (A) Latitudinal distribution of *GmMSI1* alleles among 187 resequenced ELs with the maturity genotype *e1-as/E2*. Latitude of origination was used a proxy for relative flowering time. Latitude values were estimated based on state of origin and, where available, were scaled according to maturity info provided by breeders that developed the ELs (see Experimental Procedures). Means comparison was conducted using a student *t*-test, where the *t*-statistic representing the 95% confidence interval was empirically derived by randomization. Transparent dots represent the latitude of each accession. Boxplots show the mean (diamond), median (solid line), quartile span (box), range (vertical lines), and outliers (solid dots). Inset legend shows the collection of mutations which make up each allele, where "Ref" refers to the Wm82.a2.v1 reference allele. **(B)** Weblogo depicting degree of amino acid conservation of the domain surrounding each mutation (asterisk) in *GmMSI1*.

FLOWERING LOCUS C, a potent repressor of *FT* and *SOC1*, is a key floral integrator of endogenous and external signaling from several pathways in *Arabidopsis* (**Figure 1**; Lee et al., 2000). Chromatin remodeling of the *FLC* locus by members of the Polycomb Repressive Complex (PRC), including the histone methyltransferase gene *SWINGER* (*SWN*), results in *FLC* silencing and derepression of *FT* and *SOC1* (Chanvivattana et al., 2004). *GmSWN* on chromosome 03 (Glyma.03G224300) was identified as a putative ortholog of the *Arabidopsis SWN* gene (Wu et al., 2019). Our resequencing panel revealed one alternate allele, in addition to the Williams 82 reference allele, containing a threonine to alanine substitution of amino acid 677. There were 37 ELs in the resequencing panel that had the reference allele, while 144 ELs had the T677A missense mutation (**Figure 4A**). ELs containing the alternate allele of *GmSWN* were adapted to 0.58°N higher latitude, on average, than ELs containing the

reference allele ($p < 0.05^{*}$), and a weblogo generated from 92 genera showed that the T677A substitution occurred in a region of strong conservation, where alanine was the conserved residue (**Figure 4B**).

EARLY FLOWERING 5 (*ELF5*) is a member of the autonomous pathway in *Arabidopsis* which has been postulated to post-transcriptionally upregulate *FLC* to delay flowering (**Figure 1**; Noh et al., 2004). There are two alternate alleles of the soybean ortholog *GmELF5* (Glyma.05G031100) among our resequencing panel, in addition to the Williams 82 reference allele. Both alternate alleles share a glycine to lysine substitution of amino acid 242, a serine to proline substitution of amino acid 202, a serine to leucine substitution of amino acid 282, and an inframe insertion of several amino acids between amino acids 166 and 167 (**Figure 5**). In addition to these shared mutations, one allele has a mutated splice site and an additional inframe insertion between amino acids 404 and 405, while the other allele has a lysine to asparagine substitution of amino acid 122. A significant latitudinal disparity ($p < 0.001^{***}$) was observed between the reference allele and the alternate allele containing the splice site mutation, where ELs containing the splice site mutation were adapted to 0.88°N higher latitude than ELs containing the reference allele (**Figure 5A**). ELs with the alternate allele with the K122N missense mutation were adapted to a similar latitude as the reference allele. A weblogo depicting each of these mutations reveals that the S202P, Q242K, S282L, and the S166_S167 insertion occur in regions of low conservation (**Supplementary Figure 3**). By contrast, both the P404_P405 insertion and the K122N substitution occur in apparent conserved regions, suggesting that these positions may be important for protein function (**Figure 5B**).

The reference allele has an intact splice site, while the allele with the splice donor variant has a single threonine insertion between the second and third nucleotide in the splice site (**Figure 5C**).

Modulation of Flowering Time by Genes in the Photoperiod and Circadian Clock Pathways

The *TEMPRANILLO* genes (*TEM1*/*TEM2*) are a family of *RAV* class transcription factors which play a complex role in mediating signaling from several pathways to delay flowering in *Arabidopsis* (**Figure 1**; Castillejo and Pelaz, 2008; Osnato et al., 2012). However, despite their key role in *Arabidopsis*, the effect of *TEM* orthologs on flowering time in soybean, especially *GmTEM1a* (Glyma.20G186200), is still underexplored. One alternate allele of *GmTEM1a* was discovered among the resequenced ELs in the *e1-as*/*E2* genotype group containing a glutamine to proline substitution of amino acid 184 (**Figure 6A**). ELs with the Q184P substitution were adapted to 0.59°N higher latitude, on average, than ELs with the reference allele ($p < 0.05^{*}$). A weblogo generated from 124 genera revealed that the proline residue at position 184, as well as the surrounding region, is highly conserved and that the Williams 82 reference line has the non-conserved allele (**Figure 6B**).

In *Arabidopsis*, *PHYTOCHROME E* (*PHYE*) is a photoreceptor molecule which participates broadly in plant developmental responses to light (**Figure 1**; Devlin et al., 1998). The soybean ortholog *GmPHYE1* on chromosome 09 (Glyma.09G088500) has a single alternate allele possessing a histidine to tyrosine substitution of amino acid 708, which is present in 53 ELs in our resequencing panel (**Figure 7A**). An assessment of latitudinal disparity between the Williams 82 reference allele of *GmPHYE1* and the H708Y alternate allele revealed a significant difference in mean latitudes ($p < 0.05^{*}$), where ELs with the reference allele were adapted 0.58°N higher than ELs with the missense mutation, on average. A weblogo generated from 109 genera showed that the H708Y missense mutation occurred in a conserved protein domain, where the tyrosine residue was conserved and the histidine residue present in Williams 82 was the non-conserved residue (**Figure 7B**).

TIMING OF CAB EXPRESSION 1 (*TOC1*) is a core member of the circadian clock complex in *Arabidopsis* and is responsible for promoting expression of genes in the evening complex (**Figure 1**; Gendron et al., 2012). The soybean ortholog *GmTOC1* (Glyma.06G196200) has a single alternate allele among our resequencing panel, which contains a leucine to serine substitution of amino acid 56 and an isoleucine to serine substitution of amino acid 473 (**Figure 8A**). An assessment of latitudinal disparity between the Williams 82 reference allele and the alternate allele revealed a significant difference in mean latitude ($p < 0.001^{***}$), where ELs containing the alternate allele were adapted to 0.64°N higher than ELs with the reference allele (**Figure 8A**). A weblogo generated from 134 genera showed that the I473S mutation occurred in a region of low conservation, whereas the L56S mutation occurred in a region of high conservation, where the serine residue appeared to be conserved (**Figure 8B**).

Modulation of Flowering Time by Genes in the Gibberellin Pathway

Gibberellins are a class of hormone responsible for modulating many developmental programs throughout the plant. *GmGA2OX5* and *GmGA2OX6* are orthologs of the *Arabidopsis GA2OX2* and *GA2OX1* genes, respectively, which metabolize gibberellic acid in the apical meristem and delay flowering (**Figure 1**). *GmGA2OX5* (Glyma.13G218200) has a single alternate allele present in 16 ELs in our resequencing panel, which contains a tryptophan to cysteine substitution of amino acid 307 (**Figure 9A**). We observed a significant difference in mean latitude ($p < 0.05^{*}$) between ELs containing the Williams 82 reference allele and the alternate allele, where ELs with the reference allele were adapted to 0.67°N higher, on average, than ELs with the alternate allele (**Figure 9A**). A weblogo generated from 100 genera revealed that the W307C mutation occurred in a region of high conservation, where the tryptophan residue was almost perfectly conserved (**Figure 9B**).

Among ELs in our resequencing panel, a single alternate allele of *GmGA2OX6* (Glyma.13G259400) existed containing an aspartate to asparagine substitution of amino acid 31, and a proline to alanine substitution of amino acid 182 (**Figure 10A**).

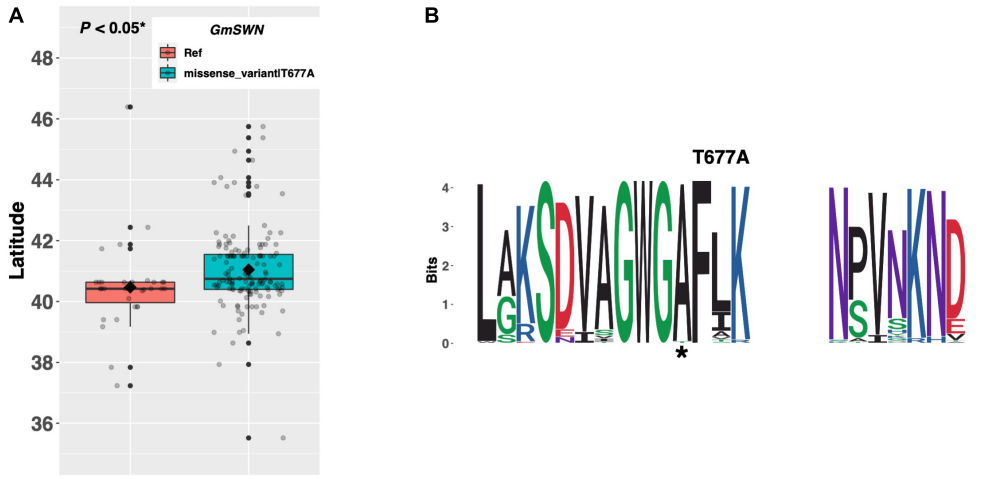

FIGURE 4 | (A) Latitudinal distribution of *GmSWN* alleles among 187 resequenced ELs with the maturity genotype *e1-as/E2*. Latitude of origination was used a proxy for relative flowering time. Latitude values were estimated based on state of origin and, where available, were scaled according to maturity info provided by breeders that developed the ELs (see Experimental Procedures). Means comparisons were conducted using a student *t*-test, where the *t*-statistic representing the 95% confidence interval was empirically derived by randomization. Transparent dots represent the latitude of each accession. Boxplots show the mean (diamond), median (solid line), quartile span (box), range (vertical lines), and outliers (solid dots). Inset legend shows the collection of mutations which make up each allele, where "Ref" refers to the Wm82.a2.v1 reference allele. **(B)** Weblogo depicting degree of amino acid conservation of the domain surrounding each mutation (asterisks) in *GmSWN*.

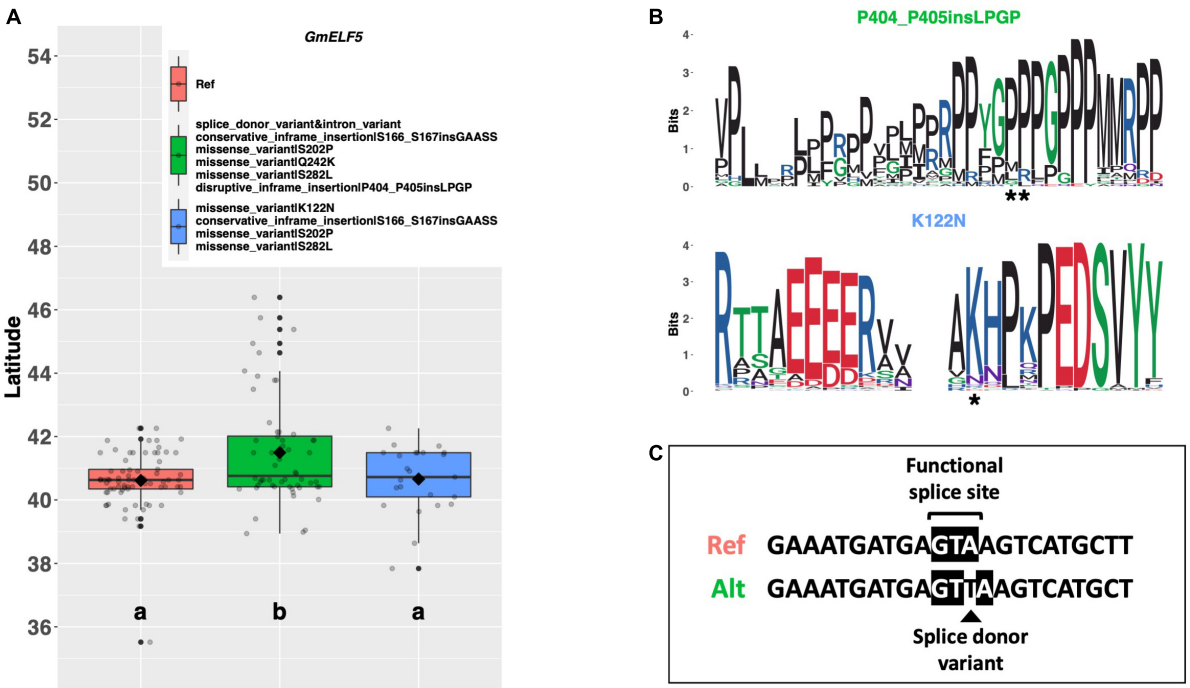

FIGURE 5 | (A) Latitudinal distribution of *GmELF5* alleles among 187 resequenced ELs with the maturity genotype *e1-as/E2*. Latitude of origination was used a proxy for relative flowering time. Latitude values were estimated based on state of origin and, where available, were scaled according to maturity info provided by breeders that developed the ELs (see Experimental Procedures). Means comparison was conducted using an ANOVA, where the *f*-statistic representing the 95% confidence interval was empirically derived by randomization. Significance letters were obtained from a test of least significant difference. Transparent dots represent the latitude of each accession. Boxplots show the mean (diamond), median (solid line), quartile span (box), range (vertical lines), and outliers (solid dots). Inset legend shows the collection of mutations which make up each allele, where "Ref" refers to the Wm82.a2.v1 reference allele. **(B)** Weblogo depicting degree of amino acid conservation of the domain surrounding prioritized mutations (asterisk) in *GmELF5*. **(C)** Comparison of the splice site sequence at the second exon/intron boundary in the Williams 82 Ref sequence and alternate allele containing the splice donor variant.

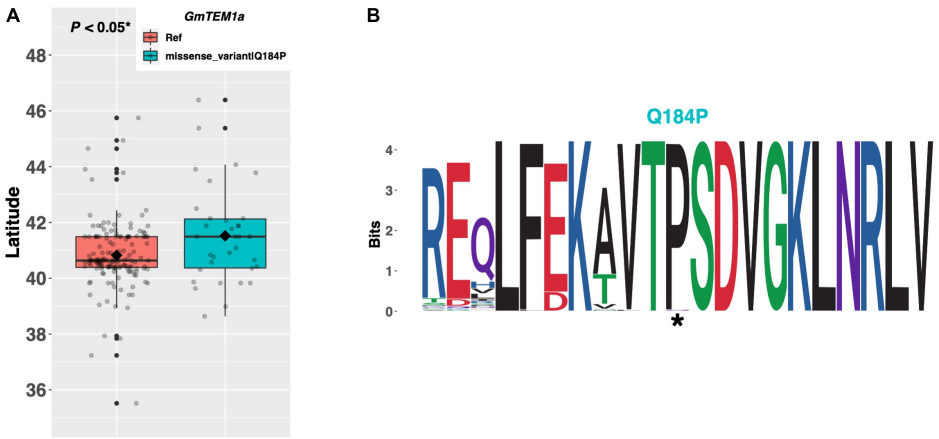

FIGURE 6 | (A) Latitudinal distribution of *GmTEM1a* alleles among 186 resequenced ELs with the maturity genotype *e1-as/E2*. Latitude of origination was used a proxy for relative flowering time. Latitude values were estimated based on state of origin and, where available, were scaled according to maturity info provided by breeders that developed the ELs (see Experimental Procedures). Means comparison was conducted using a student *t*-test, where the *t*-statistic representing the 95% confidence interval was empirically derived by randomization. Transparent dots represent the latitude of each accession. Boxplots show the mean (diamond), median (solid line), quartile span (box), range (vertical lines), and outliers (solid dots). Inset legend shows the collection of mutations which make up each allele, where "Ref" refers to the Wm82.a2.v1 reference allele. **(B)** Weblogo depicting degree of amino acid conservation of the domain surrounding each mutation (asterisks) in *GmTEM1a*.

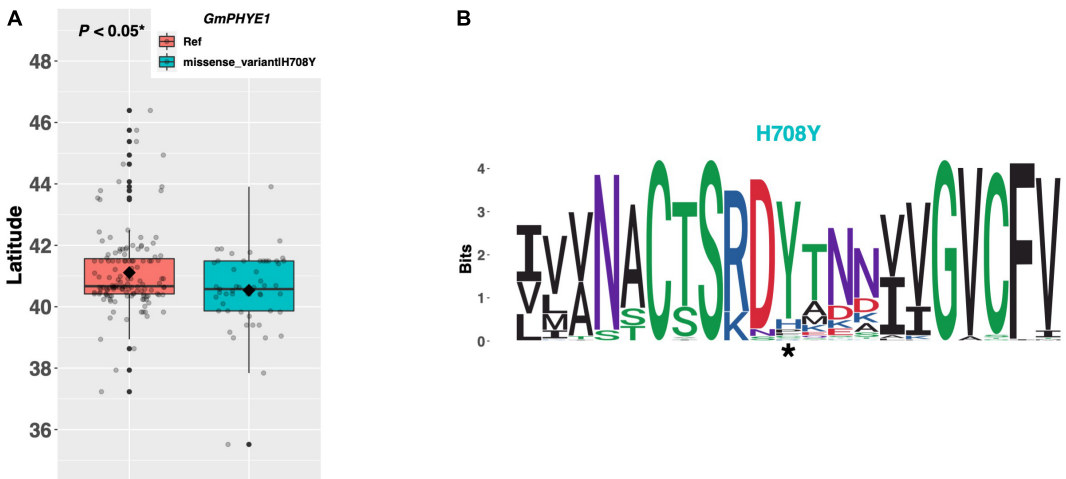

FIGURE 7 | (A) Latitudinal distribution of *GmPHYE1* alleles among 187 resequenced ELs with the maturity genotype *e1-as/E2*. Latitude of origination was used a proxy for relative flowering time. Latitude values were estimated based on state of origin and, where available, were scaled according to maturity info provided by breeders that developed the ELs (see Experimental Procedures). Means comparison was conducted using a student *t*-test, where the *t*-statistic representing the 95% confidence interval was empirically derived by randomization. Transparent dots represent the latitude of each accession. Boxplots show the mean (diamond), median (solid line), quartile span (box), range (vertical lines), and outliers (solid dots). Inset legend shows the collection of mutations which make up each allele, where "Ref" refers to the Wm82.a2.v1 reference allele. **(B)** Weblogo depicting degree of amino acid conservation of the domain surrounding each mutation (asterisk) in *GmPHYE1*.

An assessment of latitudinal disparity revealed a significant difference in mean latitude ($p < 0.05^*$) between ELs containing the Williams 82 reference allele and ELs containing the alternate allele, where ELs with the alternate allele were adapted to 0.41°N higher latitude, on average. A weblogo generated from 102 genera revealed that both missense mutations occurred in regions of high amino acid conservation, where the aspartate and proline residues were conserved at positions 31 and 182, respectively (**Figure 10B**).

DISCUSSION

In this study, we identified an allelic series for soybean orthologs of *Arabidopsis* flowering time genes from high quality SNPs and InDels derived from resequencing analysis of the genomes of 264 elite US soybean lines (ELs). A total of 139 genes, for which allelic variation was present in high frequency among our resequencing panel, were assessed to determine the likelihood of their utilization to modulate flowering time and maturity in

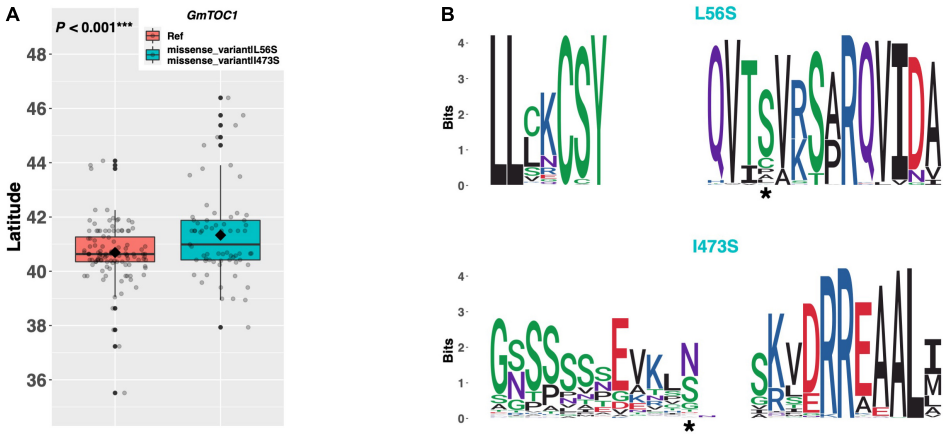

FIGURE 8 | (A) Latitudinal distribution of *GmTOC1* alleles among 187 resequenced ELs with the maturity genotype *e1-as/E2*. Latitude of origination was used a proxy for relative flowering time. Latitude values were estimated based on state of origin and, where available, were scaled according to maturity info provided by breeders that developed the ELs (see Experimental Procedures). Means comparison was conducted using a student *t*-test, where the *t*-statistic representing the 95% confidence interval was empirically derived by randomization. Transparent dots represent the latitude of each accession. Boxplots show the mean (diamond), median (solid line), quartile span (box), range (vertical lines), and outliers (solid dots). Inset legend shows the collection of mutations which make up each allele, where "Ref" refers to the Wm82.a2.v1 reference allele. **(B)** Weblogo depicting degree of amino acid conservation of the domain surrounding each mutation (asterisk) in *GmTOC1*.

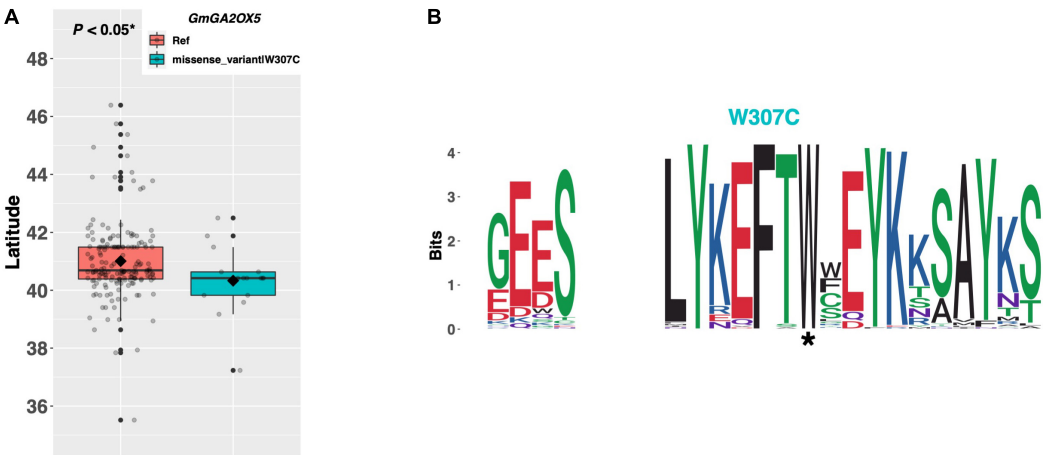

FIGURE 9 | (A) Latitudinal distribution of *GmGA2OX5* alleles among 187 resequenced ELs with the maturity genotype *e1-as/E2*. Latitude of origination was used a proxy for relative flowering time. Latitude values were estimated based on state of origin and, where available, were scaled according to maturity info provided by breeders that developed the ELs (see Experimental Procedures). Means comparison was conducted using a student *t*-test, where the *t*-statistic representing the 95% confidence interval was empirically derived by randomization. Transparent dots represent the latitude of each accession. Boxplots show the mean (diamond), median (solid line), quartile span (box), range (vertical lines), and outliers (solid dots). Inset legend shows the collection of mutations which make up each allele, where "Ref" refers to the Wm82.a2.v1 reference allele. **(B)** Weblogo depicting degree of amino acid conservation of the domain surrounding each mutation (asterisk) in *GmGA2OX5*.

modern US soybean. Eight genes in various biological pathways were identified based on latitudinal disparity between alleles, amino acid conservation of identified mutations, and their function in the model organism *A. thaliana*. It should be noted that our analysis does not preclude the possibility that enrichment for these alleles in different latitudinal groups could be the consequence of breeder selection for particular alleles of linked genes, rather than selection for the genes identified in this study. However, the degree of sequence conservation, as determined by the weblogos for each variant, suggests these mutations occur in important amino acid domains of their respective proteins and thus likely have an impact on flowering time, regardless of whether they were the intended targets of selection.

Functional Conservation and Divergence of Genes in the Autonomous Pathway

In *Arabidopsis*, *MSI1* promotes flowering *via* direct upregulation of *SOC1* and *msi1* mutants resulted in delayed flowering (Bouveret et al., 2006). Our results show that ELs with the

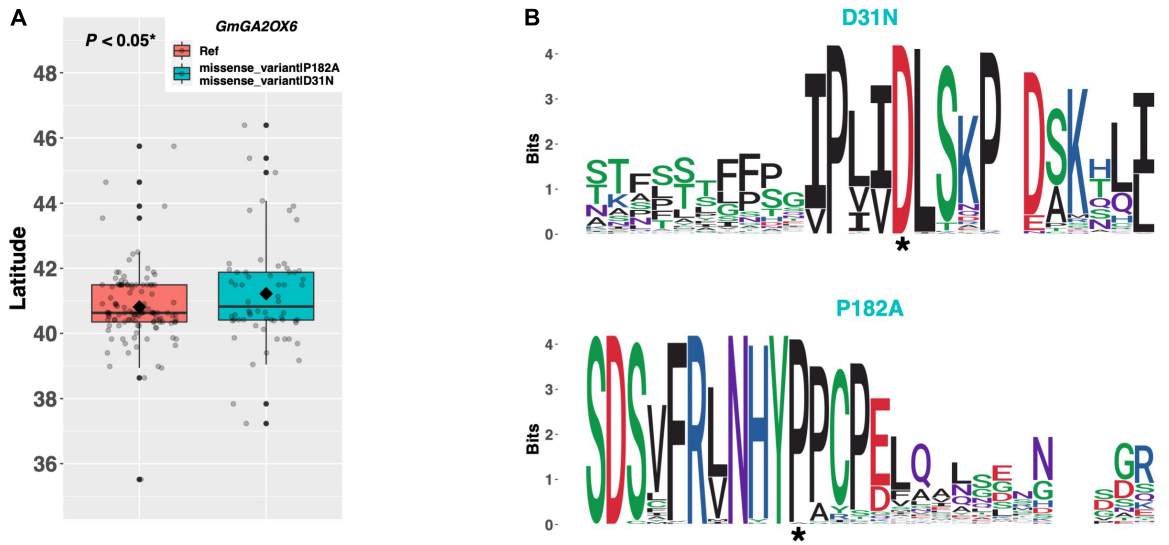

FIGURE 10 | (A) Latitudinal distribution of *GmGA2OX6* alleles among 187 resequenced ELs with the maturity genotype *e1-as/E2*. Latitude of origination was used a proxy for relative flowering time. Latitude values were estimated based on state of origin and, where available, were scaled according to maturity info provided by breeders that developed the ELs (see Experimental Procedures). Means comparison was conducted using a student *t*-test, where the *t*-statistic representing the 95% confidence interval was empirically derived by randomization. Transparent dots represent the latitude of each accession. Boxplots show the mean (diamond), median (solid line), quartile span (box), range (vertical lines), and outliers (solid dots). Inset legend shows the collection of mutations which make up each allele, where "Ref" refers to the Wm82.a2.v1 reference allele. **(B)** Weblogo depicting degree of amino acid conservation of the domain surrounding each mutation (asterisk) in *GmGA2OX6*.

putative functional allele of *GmMSI1* (i.e., those containing the threonine residue at position 37) are adapted to higher latitudes than ELs with the methionine residue and likely flower and mature earlier. These data suggest that the ability of *GmMSI1* to promote floral induction may be conserved in soybean and warrants further investigation as a potential target for optimizing flowering time. As is characteristic of members of chromatin remodeling complexes, mutations in *MSI1* pleiotropically affect traits other than flowering time in *Arabidopsis*, including fertilization and seed development (Köhler et al., 2003). While this seems to suggest that utilizing *GmMSI1* to optimize flowering time in soybean may result in developmental abnormalities, the fact that there is significant variation in this gene among ELs, and multiple orthologs of *MSI1* exist in soybean, suggests that this gene may have diverged substantially in function from the ancestral state.

In soybean, *GmFLC-like* acts similarly to *FLC* by physically interacting with the promoter of *GmFT2a* to inhibit its expression and delay flowering (Lyu et al., 2020). In *Arabidopsis*, the *SWN* gene is expressed in the leaf primordia and apical meristem of young seedlings, as well as in the inflorescence and floral meristems (Chanvivattana et al., 2004). By contrast, *GmSWN* transcripts were not detected in the Williams 82 reference line (Severin et al., 2010), which contains the putative non-functional allele (i.e., the allele with the threonine residue). The fact that ELs with the putative functional allele (i.e., those with the alanine residue) tend to be adapted to higher latitudes than ELs with the threonine residue, suggests that floral promotion by *GmSWN via* downregulation of *GmFLC-like* may be conserved in soybean.

elf5 mutants in *Arabidopsis* exhibit early flowering in both long and short days at least in part by reduced promotion of the floral repressor *FLC* (Noh et al., 2004). In soybean cv. Williams 82, *GmELF5* is highly expressed in most major tissues throughout the plant (Severin et al., 2010). Our resequencing data indicated several mutations defined two distinct alternate alleles of this gene, in addition to the reference allele. Of particular interest is a mutation in a splice site region defining the second exon/intron boundary, which occurs in one of the alternate alleles. That ELs with this putative null allele are adapted to higher latitudes and likely flower earlier suggests that the function of *ELF5* to delay flowering may be conserved in soybean. The second alternate allele contained an asparagine residue in place of a conserved lysine residue at position 122; however, ELs containing this allele seem to be adapted to similar latitudes as ELs with the reference allele. This is at odds with the theory that the function of *GmELF5* to delay flowering is conserved, because we would expect ELs with the non-conserved asparagine residue to be adapted to higher latitudes. Further experimentation is needed to determine how *GmELF5* and the alleles described herein affect flowering time in soybean.

Functional Conservation and Divergence of Genes in the Photoperiod Pathway

When functional, TEM1/TEM2 compete with the CO protein to inhibit FT expression and delay flowering in Arabidopsis (Castillejo and Pelaz, 2008). Regulatory variation in a light-responsive promoter element of the GmTEM1a paralog, GmTEM1b (also known as GmRAV), was recently shown

to promote flowering time and maturity in soybean (Wang et al., 2021), confirming that the native function of GmTEM1b in delaying flowering is conserved between Arabidopsis and soybean. In contrast, ELs with the putative functional allele of GmTEM1a (i.e., those with the proline residue at position 184) are adapted to higher latitudes on average and appear to flower earlier than ELs with the glutamine residue. This finding suggests a possible divergence in function between GmTEM1a and both GmTEM1b and the Arabidopsis TEM1 gene, whereby GmTEM1a may function to promote flowering when functional. Consistent with this idea, Wu et al. showed that, among Clark near-isogenic lines containing contrasting alleles of either E1, E2, or E3, GmTEM1a was differentially expressed under long days in both the E1 and E2 NILs (Wu et al., 2019). By contrast, GmTEM1b was not differentially expressed in any of the three Clark NILs under long days. Taken together, these results suggest that GmTEM1a and GmTEM1b are regulated independently and lends credence to the theory that these genes may have divergent function.

Five phytochrome genes (*PHYA* to *PHYE*) exist in *Arabidopsis*, where *PHYA/PHYC* and *PHYB/PHYD/PHYE* form two distinct phylogenetic clades, indicating that the *PHYE* gene is most closely related to *PHYB* and *PHYD* (Mathews, 2006). In *Arabidopsis*, *phye* single mutants are identical to wild-type plants but flower early in a *phya phyb* background, revealing that the function of *PHYE* overlaps with that of *PHYA* and *PHYB* to delay flowering (Devlin et al., 1998). ELs in our resequencing panel which contained the putative functional allele of *GmPHYE1* (i.e., those with the conserved tyrosine residue) were adapted to lower latitudes, and thus likely flower later, than those containing the reference allele. *GmPHYE1* is expressed in several tissues throughout the Williams 82 reference line, including in the leaves and flowers (Severin et al., 2010). Taken together, these results suggest that the function of *PHYE* to delay flowering is likely conserved in the soybean ortholog *GmPHYE1*.

The *Arabidopsis TOC1* gene is a core component of the circadian clock involved in reciprocal regulation of genes that stimulate the morning complex (*CCA1* and *LHY*), and impairment of which results in a shortened circadian period and concomitant early flowering (Strayer et al., 2000; Gendron et al., 2012). A novel allele of *GmTOC1* (Glyma.06G196200) containing a conserved serine residue at position 56 was identified among ELs in our resequencing panel, and ELs containing this allele were adapted to higher latitudes than ELs with the leucine residue at this position. Liu H. et al. (2009) identified a conserved pseudo-receiver domain near the N terminus of the *GmTOC1* paralog on chromosome 04 (Glyma.04G166300) and demonstrated that its expression peaks in the evening, similar to that of *TOC1* in *Arabidopsis*. These data suggest that the function of *TOC1* to maintain appropriate circadian period, and thus to delay flowering, appears to be conserved in at least the *GmTOC1* gene on chromosome 04. By contrast, those ELs in our resequencing panel with the putative functional allele of the *GmTOC1* gene on chromosome 06 (i.e., those with the serine residue) appear to flower earlier, suggesting that there may be divergence in function between *GmTOC1* on chromosome 06 and the *Arabidopsis TOC1* gene.

Functional Conservation and Divergence of Genes in the Gibberellin Pathway

Biosynthesis of florigenic gibberellic acid (GA) is mediated by *GA20OX2* in the leaves of *Arabidopsis*, the loss of function of which delays flowering modestly under long days and dramatically under short days (Rieu et al., 2008b). By contrast, the *GA2OX* class of oxidases inactivate GA, and mutants of which result in earlier flowering, especially in short days (Rieu et al., 2008a). However, reports describing the activity of GA reveal that the effects and precise mechanism by which GA influences photoperiod-dependent flowering have significantly diverged between species (reviewed in Mutasa-Göttgens and Hedden (2009)). Our results revealed a single alternate allele in each of two *GA2OX* orthologs, *GmGA2OX5* and *GmGA2OX6*. ELs in our resequencing panel containing the putative functional allele of *GmGA2OX5* (i.e., those with the tryptophan residue at position 307) are adapted to higher latitudes and likely flower earlier than those with the cysteine residue, suggesting that *GmGA2OX5* may have diverged in function from its *Arabidopsis* ortholog, *GA2OX*. By contrast, ELs containing the putative functional allele of *GmGA2OX6* (i.e., those with the aspartate residue at position 31 and the proline residue at position 182) were adapted to lower latitudes than ELs with the putative impaired allele, suggesting that *GmGA2OX6* may delay flowering, similar to its *Arabidopsis* ortholog *GA2OX*. However, further work is needed to test how each of these genes and the alleles described here affect flowering time in cultivated soybean.

Future Research

The candidate genes identified from this exploratory analysis constitute the preliminary framework needed to further define the genetic architecture of flowering time in US soybean. Given that the latitudinal separation between alleles of these genes is generally smaller than that of *E1* and *E2*, it's likely that these candidates are minor effect genes, however, further work is needed to validate these as modulators of flowering time and to characterize the magnitude of their effects under natural photoperiods. The fact that eight candidate genes were identified means there are a multitude of allele combinations that may be present in any one accession. When investigating the allele status for the combination those eight genes, accessions with a larger number of the "northern" alleles (the allele with the higher mean latitude) were generally adapted to more northern latitudes, and those with fewer "northern" alleles were adapted to more southern latitudes. Three accessions had the "northern" alleles of all eight candidate genes (PI548540, SS202, and Amcor89), while five accession had just one "northern" allele (PI597382, PI548387, PI548565, Avery, and SA17-15682). Without further research to understand the impact of each identified candidate gene individually, it is difficult to model what is likely to be complex interactions of these genes in relation to photoperiod response. Recent work established a regulatory link between the *GmTEM1a* ortholog, *GmTEM1b* (*GmRAV*), and several gibberellins-associated genes in the modulation of plant height in soybean (Xue et al., 2022). It would be interesting to investigate whether there is a similar link between the *GmTEM1a*,

GmGA2OX5, and *GmGA2OX6* genes identified in this study in the control of flowering.

DATA AVAILABILITY STATEMENT

The datasets presented in this study can be found in online repositories. The names of the repository/repositories and accession number(s) can be found below: https://soykb.org/public_data.php, KB100.

AUTHOR CONTRIBUTIONS

ND and KB conceived and designed experiments, analyzed data, and wrote the manuscript. YC and TJ developed the resequencing analysis pipelines, generated the combined sequence data files, and provided data quality control. AS, GG, BD, AL, DW, DH, and MH provided germplasm and phenotypes for the analysis. All authors have read and approved the manuscript.

ACKNOWLEDGMENTS

The USDA is an equal opportunity provider and employer.

SUPPLEMENTARY MATERIAL

The Supplementary Material for this article can be found online at: https://www.frontiersin.org/articles/10.3389/fpls.2022.889066/full#supplementary-material

Supplementary Figure 1 | Example of latitudinal rescaling according to days to maturity or relative maturity scores. Skim resequenced US cultivars (dots) derived from Dr. Brian Diers' breeding program. Latitude values **(left)** were scaled according to their Relative Maturity values **(right)** to fit the approximate latitudinal range of the state of Illinois.

Supplementary Figure 2 | Boxplots of genes with a significant latitudinal disparity between alleles from among 187 resequenced ELs with the maturity genotype *e1-as/E2*. Latitude of origination was used a proxy for relative flowering time. Latitude values were estimated based on state of origin and, where available, were scaled according to maturity info provided by breeders that developed the cultivars (see Experimental Procedures). Means comparison was conducted using an *ANOVA*, where the *t*-statistic representing the 95% confidence interval was empirically derived by randomization. *P* value refers to significance between alleles with the largest difference in means. Transparent dots represent the latitude of each accession. Boxplots show the mean (diamond), median (solid line), quartile span (box), range (vertical lines), and outliers (solid dots). Inset legend shows the collection of mutations which make up each allele.

Supplementary Figure 3 | Weblogo depicting degree of amino acid conservation of the domain surrounding each mutation (asterisk) in *GmELF5*.

REFERENCES

Alabadì, D., Oyama, T., Yanovsky Marcelo, J., Harmon Franklin, G., Más, P., and Kay Steve, A. (2001). Reciprocal regulation between *TOC1* and *LHY/CCA1* within the *Arabidopsis* circadian clock. *Science* 293, 880–883. doi: 10.1126/science.1061320

Bouveret, R., Schönrock, N., Gruissem, W., and Hennig, L. (2006). Regulation of flowering time by *Arabidopsis MSI1*. *Development* 133, 1693–1702. doi: 10.1242/dev.02340

Castillejo, C., and Pelaz, S. (2008). The balance between CONSTANS and TEMPRANILLO activities determines FT expression to trigger flowering. *Curr. Biol.* 18, 1338–1343. doi: 10.1016/j.cub.2008.07.075

Chanvivattana, Y., Bishopp, A., Schubert, D., Stock, C., Moon, Y.-H., Sung, Z. R., et al. (2004). Interaction of polycomb-group proteins controlling flowering in *Arabidopsis*. *Development* 131, 5263–5276. doi: 10.1242/dev.01400

Devlin, P. F., Patel, S. R., and Whitelam, G. C. (1998). Phytochrome E influences internode elongation and flowering time in Arabidopsis. *Plant Cell* 10, 1479–1487. doi: 10.1105/tpc.10.9.1479

Fornara, F., de Montaigu, A., and Coupland, G. (2010). SnapShot: control of flowering in *Arabidopsis*. *Cell* 141, 550–550.e2.

Gendron, J. M., Pruneda-Paz, J. L., Doherty, C. J., Gross, A. M., Kang, S. E., and Kay, S. A. (2012). *Arabidopsis* circadian clock protein, TOC1, is a DNA-binding transcription factor. *Proc. Natl. Acad. Sci. U.S.A.* 109, 3167–3172. doi: 10.1073/pnas.1200355109

Happ, M. M., Wang, H., Graef, G. L., and Hyten, D. L. (2019). Generating high density, low cost genotype data in soybean [*Glycine max* (L.) Merr.]. *G3 Genes Genom. Genet.* 9, 2153–2160. doi: 10.1534/g3.119.400093

Köhler, C., Hennig, L., Bouveret, R., Gheyselinck, J., Grossniklaus, U., and Gruissem, W. (2003). *Arabidopsis* MSI1 is a component of the MEA/FIE *Polycomb* group complex and required for seed development. *EMBO J.* 22, 4804–4814. doi: 10.1093/emboj/cdg444

Langewisch, T., Lenis, J., Jiang, G.-L., Wang, D., Pantalone, V., and Bilyeu, K. (2017). The development and use of a molecular model for soybean maturity groups. *BMC Plant Biol.* 17:91. doi: 10.1186/s12870-017-1040-4

Lee, H., Suh, S.-S., Park, E., Cho, E., Ahn, J. H., Kim, S.-G., et al. (2000). The AGAMOUS-LIKE 20 MADS domain protein integrates floral inductive pathways in *Arabidopsis*. *Genes Dev.* 14, 2366–2376. doi: 10.1101/gad.813600

Liu, B., Kanazawa, A., Matsumura, H., Takahashi, R., Harada, K., and Abe, J. (2008). Genetic redundancy in soybean photoresponses associated with duplication of the phytochrome a gene. *Genetics* 180, 995–1007. doi: 10.1534/genetics.108.092742

Liu, C., Xi, W., Shen, L., Tan, C., and Yu, H. (2009). Regulation of floral patterning by flowering time genes. *Dev. Cell* 16, 711–722. doi: 10.1016/j.devcel.2009.03.011

Liu, H., Wang, H., Gao, P., Xü, J., Xü, T., Wang, J., et al. (2009). Analysis of clock gene homologs using unifoliolates as target organs in soybean (*Glycine max*). *J. Plant Physiol.* 166, 278–289. doi: 10.1016/j.jplph.2008.06.003

Liu, Y., Du, H., Li, P., Shen, Y., Peng, H., Liu, S., et al. (2020). Pan-genome of wild and cultivated soybeans. *Cell* 182, 162–176.e13. doi: 10.1016/j.cell.2020.05.023

Lu, S., Dong, L., Fang, C., Liu, S., Kong, L., Cheng, Q., et al. (2020). Stepwise selection on homeologous PRR genes controlling flowering and maturity during soybean domestication. *Nat. Genet.* 52, 428–436. doi: 10.1038/s41588-020-0604-7

Lu, S., Zhao, X., Hu, Y., Liu, S., Nan, H., Li, X., et al. (2017). Natural variation at the soybean J locus improves adaptation to the tropics and enhances yield. *Nat. Genet.* 49, 773–779. doi: 10.1038/ng.3819

Lyu, J., Cai, Z., Li, Y., Suo, H., Yi, R., Zhang, S., et al. (2020). The floral repressor *GmFLC-like* is involved in regulating flowering time mediated by low temperature in soybean. *Int. J. Mol. Sci.* 21:1322. doi: 10.3390/ijms21041322

Mathews, S. (2006). Phytochrome-mediated development in land plants: red light sensing evolves to meet the challenges of changing light environments. *Mol. Ecol.* 15, 3483–3503. doi: 10.1111/j.1365-294X.2006.03051.x

Mutasa-Göttgens, E., and Hedden, P. (2009). Gibberellin as a factor in floral regulatory networks. *J. Exp. Bot.* 60, 1979–1989. doi: 10.1093/jxb/erp040

Noh, Y.-S., Bizzell, C. M., Noh, B., Schomburg, F. M., and Amasino, R. M. (2004). *EARLY FLOWERING* 5 acts as a floral repressor in *Arabidopsis*. *Plant J.* 38, 664–672. doi: 10.1111/j.1365-313X.2004.02072.x

Osnato, M., Castillejo, C., Matías-Hernández, L., and Pelaz, S. (2012). *TEMPRANILLO* genes link photoperiod and gibberellin pathways to control flowering in *Arabidopsis*. *Nat. Commun.* 3:808. doi: 10.1038/ncomms1810

Parcy, F., Nilsson, O., Busch, M. A., Lee, I., and Weigel, D. (1998). A genetic framework for floral patterning. *Nature* 395, 561–566. doi: 10.1038/26903

Rieu, I., Ruiz-Rivero, O., Fernandez-Garcia, N., Griffiths, J., Powers, S. J., Gong, F., et al. (2008b). The gibberellin biosynthetic genes *AtGA20ox1* and *AtGA20ox2* act, partially redundantly, to promote growth and development throughout the Arabidopsis life cycle. *Plant J.* 53, 488–504. doi: 10.1111/j.1365-313X.2007.03356.x

Rieu, I., Eriksson, S., Powers, S. J., Gong, F., Griffiths, J., Woolley, L., et al. (2008a). Genetic analysis reveals that C19-GA 2-oxidation is a major gibberellin inactivation pathway in *Arabidopsis*. *Plant Cell* 20, 2420–2436. doi: 10.1105/tpc.108.058818

Severin, A. J., Woody, J. L., Bolon, Y.-T., Joseph, B., Diers, B. W., Farmer, A. D., et al. (2010). RNA-Seq atlas of *Glycine max*: a guide to the soybean transcriptome. *BMC Plant Biol.* 10:160. doi: 10.1186/1471-2229-10-160

Shaner, M. C., Blair, I. M., and Schneider, T. D. (1993). "Sequence logos: a powerful, yet simple, tool," in *Proceedings of the Twenty-Sixth Hawaii International Conference on System Sciences*, (Los Alamitos, CA: IEEE Computer Society Press).

Simpson, G. G. (2004). The autonomous pathway: epigenetic and post-transcriptional gene regulation in the control of *Arabidopsis* flowering time. *Curr. Opin. Plant Biol.* 7, 570–574. doi: 10.1016/j.pbi.2004.07.002

Škrabišová, M., Dietz, N., Zeng, S., On Chan, Y., Wang, J., Liu, Y., et al. (2022). A novel synthetic phenotype association study approach reveals the landscape of association for genomic variants and phenotypes. *J. Adv. Res.* doi: 10.1016/j.jare.2022.04.004

Strayer, C., Oyama, T., Schultz Thomas, F., Raman, R., Somers David, E., Más, P., et al. (2000). Cloning of the *Arabidopsis* clock gene *TOC1*, an autoregulatory response regulator homolog. *Science* 289, 768–771. doi: 10.1126/science.289.5480.768

Takeshima, R., Hayashi, T., Zhu, J., Zhao, C., Xu, M., Yamaguchi, N., et al. (2016). A soybean quantitative trait locus that promotes flowering under long days is identified as *FT5a*, a *FLOWERING LOCUS T* ortholog. *J. Exp. Bot.* 67, 5247–5258. doi: 10.1093/jxb/erw283

Tsubokura, Y., Watanabe, S., Xia, Z., Kanamori, H., Yamagata, H., Kaga, A., et al. (2013). Natural variation in the genes responsible for maturity loci E1, E2, E3 and E4 in soybean. *Ann. Bot.* 113, 429–441. doi: 10.1093/aob/mct269

Valliyodan, B., Brown, A. V., Wang, J., Patil, G., Liu, Y., Otyama, P. I., et al. (2021). Genetic variation among 481 diverse soybean accessions, inferred from genomic re-sequencing. *Sci. Data* 8:50. doi: 10.1038/s41597-021-00834-w

Valverde, F., Mouradov, A., Soppe, W., Ravenscroft, D., Samach, A., and Coupland, G. (2004). Photoreceptor regulation of CONSTANS protein in photoperiodic flowering. *Science* 303, 1003–1006. doi: 10.1126/science.1091761

Wang, Y., Xu, C., Sun, J., Dong, L., Li, M., Liu, Y., et al. (2021). GmRAV confers ecological adaptation through photoperiod control of flowering time and maturity in soybean. *Plant Physiol.* 187, 361–377. doi: 10.1093/plphys/kiab255

Watanabe, S., Hideshima, R., Xia, Z., Tsubokura, Y., Sato, S., Nakamoto, Y., et al. (2009). Map-based cloning of the gene associated with the soybean maturity locus E3. *Genetics* 182, 1251–1262. doi: 10.1534/genetics.108.098772

Watanabe, S., Xia, Z., Hideshima, R., Tsubokura, Y., Sato, S., Yamanaka, N., et al. (2011). A map-based cloning strategy employing a residual heterozygous line reveals that the *GIGANTEA* gene is involved in soybean maturity and flowering. *Genetics* 188, 395–407. doi: 10.1534/genetics.110.125062

Wu, F., Kang, X., Wang, M., Haider, W., Price, W. B., Hajek, B., et al. (2019). Transcriptome-enabled network inference revealed the *GmCOL1* feed-forward loop and its roles in photoperiodic flowering of soybean. *Front. Plant Sci.* 10:1221. doi: 10.3389/fpls.2019.01221

Xia, Z., Watanabe, S., Yamada, T., Tsubokura, Y., Nakashima, H., Zhai, H., et al. (2012). Positional cloning and characterization reveal the molecular basis for soybean maturity locus E1 that regulates photoperiodic flowering. *Proc. Natl. Acad. Sci. U.S.A.* 109, E2155–E2164. doi: 10.1073/pnas.1117982109

Xue, Y., Zhang, Y., Shan, J., Ji, Y., Zhang, X., Li, W., et al. (2022). Growth repressor GmRAV binds to the GmGA3ox promoter to negatively regulate plant height development in soybean. *Int. J. Mol. Sci.* 23:1721. doi: 10.3390/ijms23031721

Zhao, C., Takeshima, R., Zhu, J., Xu, M., Sato, M., Watanabe, S., et al. (2016). A recessive allele for delayed flowering at the soybean maturity locus E9 is a leaky allele of *FT2a*, a *FLOWERING LOCUS T* ortholog. *BMC Plant Biol.* 16:20. doi: 10.1186/s12870-016-0704-9

Zhou, Z., Jiang, Y., Wang, Z., Gou, Z., Lyu, J., Li, W., et al. (2015). Resequencing 302 wild and cultivated accessions identifies genes related to domestication and improvement in soybean. *Nat. Biotechnol.* 33, 408–414. doi: 10.1038/nbt.3096

Conflict of Interest: The authors declare that the research was conducted in the absence of any commercial or financial relationships that could be construed as a potential conflict of interest.

Publisher's Note: All claims expressed in this article are solely those of the authors and do not necessarily represent those of their affiliated organizations, or those of the publisher, the editors and the reviewers. Any product that may be evaluated in this article, or claim that may be made by its manufacturer, is not guaranteed or endorsed by the publisher.

frontiers | Frontiers in Plant Science

ORIGINAL RESEARCH
published: 29 April 2022
doi: 10.3389/fpls.2022.851960

BUMPY STEM Is an Arabidopsis Choline/Ethanolamine Kinase Required for Normal Development and Chilling Responses

*Christina Rabeler[1], Mingjie Chen[2] and Nick Kaplinsky[1]**

[1] Department of Biology, Swarthmore College, Swarthmore, PA, United States, [2] College of Life Sciences, Xinyang Normal University, Xinyang, China

Phospholipid biosynthesis is a core metabolic pathway that affects all aspects of plant growth and development. One of the earliest step in this pathway is mediated by choline/ethanolamine kinases (CEKs), enzymes in the Kennedy pathway that catalyze the synthesis of the polar head groups found on the most abundant plant phospholipids. The Arabidopsis genome encodes four *CEK*s. *CEK1-3* have been well characterized using viable mutants while *CEK4* encodes an essential gene, making it difficult to characterize its effects on plant development and responses to the environment. We have isolated an EMS-induced allele of *CEK4* called *bumpy stem* (*bst*). *bst* plants are viable, allowing the effects of decreased *CEK4* function to be characterized throughout the Arabidopsis life cycle. *bst* mutants have a range of developmental defects including ectopic stem growths at the base of their flowers, reduced fertility, and short roots and stems. They are also sensitive to cold temperatures. Supplementation with choline, phosphocholine, ethanolamine, and phosphoethanolamine rescues *bst* root phenotypes, highlighting the flow of metabolites between the choline and ethanolamine branches of the Kennedy pathway. The identification of *bst* and characterization of its phenotypes defines new roles for *CEK4* that go beyond its established biochemical function as an ethanolamine kinase.

Keywords: choline/ethanolamine kinase, *CEK4*, At2g26830, chilling, pedicel stem junction, phospholipid biosynthesis

OPEN ACCESS

Edited by:
Patricia Springer, University of California, Riverside, United States

Reviewed by:
Ying-Chen Lin, University of Oxford, United Kingdom
Hai Anh Ngo, Institute of Plant and Microbial Biology, Academia Sinica, Taiwan

****Correspondence:***
Nick Kaplinsky
nkaplin1@swarthmore.edu

Specialty section:
This article was submitted to Plant Development and EvoDevo, a section of the journal Frontiers in Plant Science

Received: *10 January 2022*
Accepted: *17 March 2022*
Published: *29 April 2022*

Citation:
Rabeler C, Chen M and Kaplinsky N (2022) BUMPY STEM Is an Arabidopsis Choline/Ethanolamine Kinase Required for Normal Development and Chilling Responses. Front. Plant Sci. 13:851960. doi: 10.3389/fpls.2022.851960

INTRODUCTION

Biological membranes compartmentalize cells and, in concert with embedded and associated protein complexes, regulate transport and signal transduction between cells and cellular compartments. Membranes are composed of a phospholipid bilayer consisting of a hydrophobic core sandwiched between hydrophilic head groups. Phosphatidylethanolamine (PtdEtn) and phosphatidylcholine (PtdCho) are the two most abundant phospholipids found in eukaryotic membranes. Their polar head groups, phosphoethanolamine and phosphocholine, are synthesized in the earliest steps of the Kennedy pathway when ethanolamine and choline, respectively, are phosphorylated by choline/ethanolamine kinases (CEKs). Later in the pathway these phosphorylated head groups are enzymatically coupled to the diacylglycerol to create PtdEtn

and PtdCho which are subsequently incorporated into membranes (Gibellini and Smith, 2010). Mutations in *CEK*s and other Kennedy pathway enzymes result in a wide range of phenotypes in plants as well as heritable genetic diseases in humans, highlighting the importance of this core biosynthetic pathway in all eukaryotes (Kwon et al., 2012; Lin et al., 2015, 2020; Yunus et al., 2016; Tavasoli et al., 2020; Tannert et al., 2021). Extensive efforts to characterize the Kennedy pathway have revealed that most organisms have multiple CEK isoforms encoded by distinct *CEK* genes.

The Arabidopsis genome encodes four *CEK*s numbered *CEK1-4*. These genes are expressed at different levels compared to each other and exhibit tissue-specific and environmentally responsive expression patterns, suggesting that each enzyme plays a distinct role in choline and ethanolamine metabolism (Tasseva et al., 2004; Lin et al., 2020). Examples of sub-specialization in this gene family include diverse substrate specificities among the CEKs as well as their differential effects on plant growth and development. *In vitro*, *CEK1* and *CEK2* have both choline and ethanolamine kinase activity while *CEK3* and *CEK4* have substrate specificity for choline and ethanolamine alone, respectively. Neither *CEK1* or *CEK2* exhibited detectable ethanolamine kinase activity *in vivo*, suggesting that *CEK4* is the principal ethanolamine kinase in Arabidopsis (Lin et al., 2019, 2020). Similar enzymatic specialization has also been described in *Glycine max*, suggesting that it is widespread in plants (Wharfe and Harwood, 1979). Complementing this biochemical approach, reverse genetics has also been used to reveal the developmental and biochemical roles of the Arabidopsis CEKs. *cek2* and *cek3* single mutants have short roots while *cek1* mutant roots are normal. This shows that at least two of the Arabidopsis *CEK*s are required for normal growth and development. Additional insights into CEK function have come from a chemical rescue experiment. In this experiment *cek3* seedlings were grown on media containing phosphocholine, which rescued the *cek3* short-root phenotype. This experiment's results are consistent with the biochemical characterization of *CEK3* as a choline kinase. *cek* mutants have also been used to provide *in vivo* support for the *in vitro* biochemical characterization. *cek1* single mutant and *cek1 cek3* double mutant plants were shown to have decreased choline kinase activity *in vivo* (Lin et al., 2020).

Compared to *CEK1-3*, *CEK4* remains relatively uncharacterized. This is because *cek4* loss of-function mutants are embryo lethal (Meinke et al., 2008; Lin et al., 2015; Meinke, 2020). The viability of *cek1*, *cek2*, and *cek3* T-DNA loss-of-function mutants coupled with the lack of detectable changes in lipid content in their single mutants suggests that *cek1-3* have partially overlapping functions in lipid metabolism and plant development (Lin et al., 2015, 2020). *CEK4* stands out from the other Arabidopsis *CEK*s as the functional alleles of *CEK1*, *CEK2*, and *CEK3* in *cek4* mutants cannot compensate for the loss of *CEK4* activity. Fundamental differences between *CEK4* and the other *CEKs* are also suggested by the observation that *CEK4* is phylogenetically distant from the other Arabidopsis *CEK*s (Lin et al., 2015). Combined with *CEK4*'s ethanolamine substrate specificity *in vitro*, it appears that *CEK4* plays unique and important roles in plant biochemistry and development. These roles are only partially understood. *CEK4* is expressed throughout the plant, including throughout heart stage and later embryos. High expression levels are found in the reproductive organs and in pollen, roots, and trichomes (Honys and Twell, 2004; Marks et al., 2009; Gilding and Marks, 2010; Lin et al., 2015). A 35S:*CEK4* line that complemented *cek4* embryonic arrest was shown to result in increased levels of both PtdEtn and PtdCho in seedlings and increased levels of PtdCho in mature siliques, consistent with a predicted function as a CEK (Lin et al., 2015). No further phenotypes were reported for this overexpression line and, to the best of our knowledge, no roles in post-embryonic plant development or responses to the environment have been described for *CEK4*.

Here we describe the isolation of a viable EMS induced allele of *CEK4* that appears to result in a partial loss of function. This novel allele reveals important post-embryonic developmental functions as well as a role in chilling responses for *CEK4*.

MATERIALS AND METHODS

EMS Mutagenesis

EMS mutagenesis was performed as described in Silverblatt-Buser et al. (2018).

Plant Growth

Plants were grown on soil under standard long-day greenhouse conditions with supplemental lighting. Plants grown on plates were grown on 0.5× Murashige and Skoog (0.5× MS) media containing 1% sucrose at 22°C under constant light conditions in E-30B growth chambers (Percival Scientific).

bumpy stem Mapping and Cloning

DNA from 412 individuals with mutant phenotypes in a *bst* mapping population was prepared using a DNeasy Plant Maxi Kit (Qiagen). A NEBNext DNA library prep set for Illumina (NEB) was used to prepare the sequencing library that was sequenced using an Illumina HiSeq (Illumina). Reads were mapped to the TAIR10 reference genome using SHORE and *bst* was mapped using SHOREmap (Schneeberger et al., 2009).

Scanning Electron Microscopy

Fresh tissue was imaged using low vacuum mode on a Quanta 200 scanning electron microscope (FEI) equipped with a cooled stage.

Chemical Complementation

Ler and *bst* seeds were sterilized and plated on 0.5× MS media, stratified at 4°C for 2 days, and transferred to an incubator for vertical growth at 22°C. After 3 days, seedlings were transferred to treatment plates containing either 100 μM or 1 mM of choline chloride (Cho), phosphocholine chloride calcium salt tetrahydride (PCho), monoethanolamine (MEA), or *O*-phosphorylethanolamine (PEA) (Sigma, St. Louis, MO, United States). The position of root tips were marked at transplanting. Seven days after transplanting the plates were scanned using an Epson V600 scanner with a black piece of felt

as a background and root growth was measured using ImageJ (Schneider et al., 2012). These experiments were repeated three times with 10–12 seedlings in each replicate.

Rosette Size Measurements

Rosette sizes were measured from images using ImageJ (Schneider et al., 2012) by measuring the Feret diameter of the smallest oval that completely surrounded each rosette.

RESULTS

bumpy stem Is a Recessive Mutant With Pleiotropic Developmental Phenotypes

bumpy stem (*bst*) was identified as a mutant with bumpy and twisted stem during a genetic screen unrelated to phospholipid head group biosynthesis. In this screen, *bob1-3* mutants in a Ler background were mutagenized with EMS and screened for synthetic developmental phenotypes (Silverblatt-Buser et al., 2018). Although *bst* does not exhibit a genetic interaction with *bob1-3*, we decided to characterize and clone the mutant gene because it had such an unusual phenotype. We back crossed *bst* into both Col-0 and Ler five times in order to remove *bob1-3* and other unlinked EMS induced mutations and their phenotypes from our analysis. *bst* phenotypes, while similar in both Col-0 and Ler backgrounds, are consistently stronger in Ler. F_1 plants of *bst*/*bst* × +/+ crosses did not display *bst* phenotypes and *bst* phenotypes segregate in a mendelian fashion in F_2 families. This suggests that they are caused by a single recessive mutation. The most striking phenotype in *bst* mutants is the abnormal patterning of the inflorescence stem.

bumpy stem inflorescence stems are irregularly swollen and bumpy compared to Col-0 inflorescence stems. In Col-0 plants the phyllotactic patterning of flowers on the flanks of the stem is regular (**Figure 1A**). The regular spacing between flowers observed in Col-0 plants is irregular in the mutant, resulting in clusters of flowers with disrupted phyllotactic patterning (**Figure 1B**). Closer inspection of the stem/pedicel boundary revealed a disruption of this boundary in *bst* plants. Col-0 plants have a distinct boundary between the stem and the floral pedicels. This boundary lines up with the lateral edge of the stem (**Figure 1C**). In *bst* plants this boundary is moved away from the edge of the stem. Unlike wild-type plants, *bst* plants have bumps of tissue that extend from the edge of the stem. The boundary between this ectopic tissue and the floral pedicels is a clearly visible notch separating the stem bumps and the pedicels. Instead of being in line with the edge of the stem, this boundary is displaced laterally (**Figure 1D**). In addition to flowers, Arabidopsis inflorescences also have secondary or axillary inflorescences that emerge from their flanks. The boundary between axillary inflorescences and the primary inflorescence stem is similar in *bst* and Col-0 plants with no ectopic growth subtending *bst* axillary inflorescences (**Figures 1E,F**).

bumpy stem plants have several other phenotypes associated with their inflorescences. Compared to the trichomes found on Col-0 stems *bst* trichomes have swollen bases (**Figures 1E,F**). *bst*

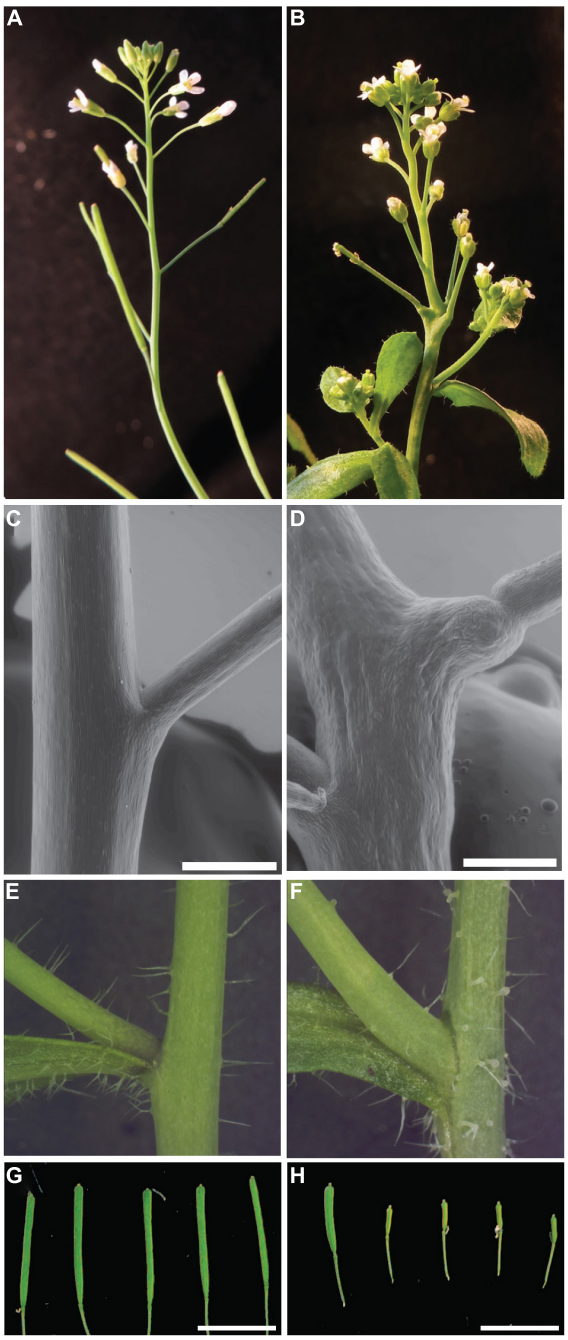

FIGURE 1 | *bumpy stem* inflorescence phenotypes. Normal Col-0 inflorescences exhibit spiral phyllotaxy with flowers separated from each other along the inflorescence **(A)**. *bst* flowers are found in clusters on the inflorescence and exhibit disrupted phyllotactic patterning **(B)**. The boundary between the pedicel and stem is flush with the side of the stem in Col-0 plants **(C)**. In *bst* mutants the notch defining the boundary is displaced, occurring at the tip of ectopic stem tissue that extends from the side of the stem **(D)**. No displacement is observed at the boundary between the main stem and axillary stems **(E,F)**. Compared to Col-0 trichomes **(E)**, *bst* trichomes have swollen bases **(F)**. Wild-type Ler plants are fertile and have filled and expanded siliques **(G)**. *bst* mutants in a Ler background are semi sterile, resulting in short siliques containing few seeds (left silique) and many sterile unexpanded siliques (right siliques) **(H)**. Scale bars are 0.5 mm in **C,D** and 1 mm in **G,H**.

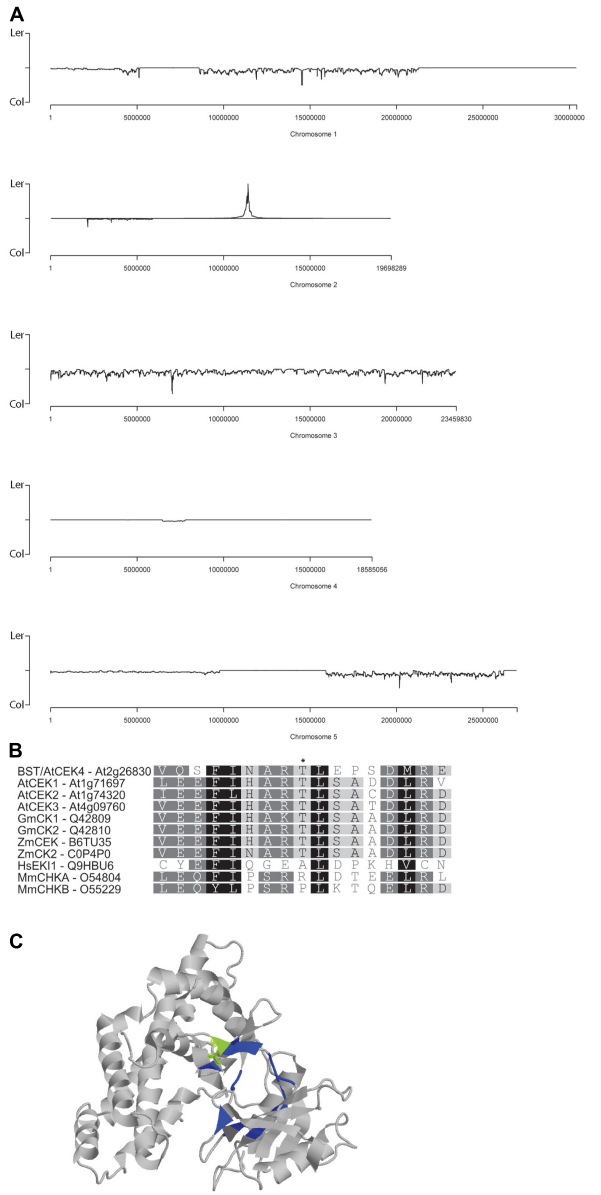

FIGURE 2 | Cloning and characterization of *bst*. *bst* was simultaneously mapped and cloned using a NGS approach. *bst* was generated in a Ler background and its position on chromosome 2 can be seen as peak of enrichment in Ler SNPs **(A)**. A protein alignment of CEKs from Arabidopsis (At), soybean (Gm), maize (Zm), humans (Hs), and mice (Mm) centered on T144 (indicated with a *) which is the site of the T144I mutation in *bst* **(B)**. CEK4 structure with the ATP binding pocket visible. Residues that participate in ATP binding are shaded blue and T141 is shaded green. Image generated using the molecule viewer at bar.utoronto.ca/eplant (Waese et al., 2017) **(C)**.

plants are also semi-sterile. In the more severe Ler background only some siliques (16%, $n = 93$), most frequently from later flowers, produce seeds. The *bst* siliques that do make seeds and elongate are significantly shorter than Ler siliques (Ler 1.23 ± 0.15 cm, *bst* 0.82 ± 0.19 cm, two-tailed *t*-test $p < 1 \times 10^{-5}$, **Figures 1G,H**). In the less severe and more fertile Col-0 background all siliques contain seeds. However, *bst* siliques are shorter than wild-type siliques (Col-0 1.36 ± 0.18 cm, *bst* 0.57 ± 0.24 cm, two-tailed *t*-test $p < 1 \times 10^{-4}$). In addition to these phenotypes, *bst* mutants also have smaller leaves, shorter inflorescences, and shorter roots compared to normal plants (**Figures 3**, **4**).

A Point Mutation in the Choline/Ethanolamine Kinase At2g26830/*CEK4*/*emb1187* Causes *bumpy stem* Phenotypes

To map and clone *bst* we generated a mapping population by crossing *bst* twice into a Col-0 background. Pooled genomic DNA from 412 mutants isolated from this mapping population was sequenced to ∼100-fold coverage. SHOREmap (Schneeberger et al., 2009) was used to simultaneously map and identify putative causal mutations in the sequence data using Col-0/Ler SNPs as mapping markers. A single mapping peak was identified at 11.4 Mb on chromosome 2 (**Figure 2A**). Of the two non-synonymous mutations within 250 kb of the mapping peak, the 422C>T mutation in At2g26830 turned out to be the *bst* causal mutation (see below). The mutation results in a T141I substitution, converting the polar threonine residue at this position into isoleucine (which is hydrophobic). The threonine at position 141 in *CEK4* is invariant in the four Arabidopsis *CEK*s as well as in corn (*Zea mays*) and soybean (*G. max*) *CEK*s (**Figure 2B**). It lies outside of the CEK catalytic domains d-6 and d-7 (Aoyama et al., 2004) at a position that directly interacts with ATP and forms part of the nucleotide binding pocket in the crystalized human choline kinase (Malito et al., 2006; **Figure 2C**).

In order to confirm that the mutation in *CEK4* was responsible for *bst* phenotypes we used two previously identified *cek4* T-DNA alleles in a genetic complementation experiment. Both alleles have embryo-lethal phenotypes. The first, *cek4-1* (SALK_057727), arrests at the heart stage (Lin et al., 2015). The second, *emb1187* (CS16107), arrests at the globular stage (Meinke et al., 2008; Meinke, 2020). As both of these T-DNA alleles are in a Col-0 background, we crossed each to *bst* introgressed into Col-0. Both lines failed to complement *bst* mutant phenotypes including short roots, small rosettes, short inflorescences, and bumpy stems. Each of these phenotypes was more severe in *bst*/*emb1187* and *bst*/*SALK_057727* plants than in *bst*/*bst* plants and the transheterozygous plants were completely sterile (**Figure 3**). The enhancement of the *bst* phenotype by two loss of function T-DNA alleles demonstrates that genetically, *bst* is a partial loss of function or hypomorphic allele (Muller, 1932).

Supplementation With Choline, Phosphocholine, Ethanolamine, and Phosphoethanolamine Rescues *bumpy stem* Root Growth Phenotypes

CEK4 has ethanolamine kinase activity *in vivo* and does not appear to function as a choline kinase (Lin et al., 2020). We took advantage of the viability of *bst* plants to test the hypothesis that *CEK4* functions as an ethanolamine kinase in plants using

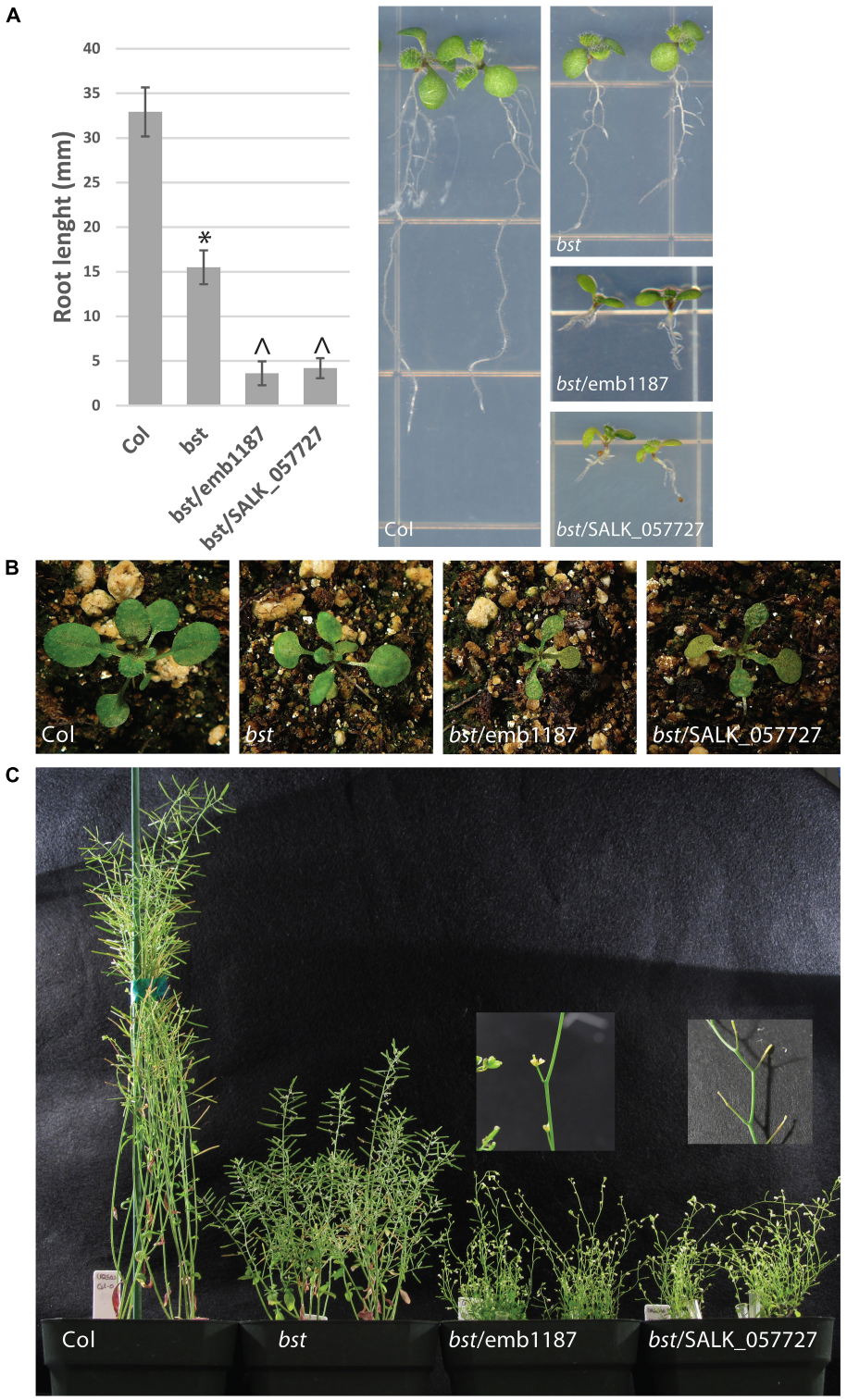

FIGURE 3 | *bumpy stem* root and shoot phenotypes and genetic complementation. *bst* plants were crossed to heterozygous emb1187 and SALK_057727 plants, both of which contain T-DNA insertions in *CEK4*. Seven day old *bst*/*bst* plants were imaged and their root lengths were measured. Root lengths were compared using unpaired two-tailed *t*-tests. The symbol "*" indicates a difference from Col with a *p*-value $< 10^{-10}$. The symbol "^" indicates a difference from both Col and *bst* with a *p*-value $< 10^{-7}$. Error bars are SD **(A)**. *bst* vegetative rosettes are smaller than wild-type. This phenotype is enhanced when the *bst* allele is combined with either *emb1187* or SALK_057727 **(B)**. The height of mature plants is reduced in *bst* plants and even more so in *bst*/*emb1187* and *bst*/SALK_057727 plants. *bst*/*emb1187* and *bst*/SALK_057727 plants are sterile **(C)**.

a chemical supplementation approach. The simplest model is that *bst* phenotypes are caused by a lack of ethanolamine kinase activity. This would make low phosphoethanolamine levels the proximal deficiency causing phenotypes. If this is the case then phosphoethanolamine supplementation should rescue *bst* phenotypes, just as phosphocholine can rescue *cek3* root phenotypes and ethanolamine and choline can rescue *serine decarboxylase 1* mutants (Kwon et al., 2012; Lin et al., 2020). We decided to test this by quantitating root growth rates in wild-type and *bst* seedlings after supplementing them with polar head group precursors. Seedlings in a Ler background were germinated and then transferred to plates containing either choline, phosphocholine, ethanolamine, or phosphoethanolamine. Treatment with 100 μM choline or phosphocholine resulted in significant increases in *bst* root growth rates, nearly completely rescuing the short root mutant phenotype. The same effect was observed at 1 mM concentrations of choline and phosphocholine, suggesting that 100 μM concentrations are sufficient for the observed phenotypic rescue (**Figure 4A**). In contrast, treatment with 100 μM phosphoethanolamine or ethanolamine did not significantly change *bst* root growth rates. Increasing the concentration of ethanolamine or phosphoethanolamine to 1 mM resulted in significant increases in *bst* root growth rates. However, the effect of ethanolamine or phosphoethanolamine supplementation at 1 mM was much smaller than that seen with either choline or phosphocholine treatment at either 100 μM or 1 mM (**Figure 4B**).

bumpy stem Mutants Have a Chilling Sensitive Phenotype

The composition of phospholipid bilayers is known to change as a compensatory response to a wide range of abiotic stresses. Temperature extremes, both high and low, result in alterations in membrane lipids (Welti et al., 2002). Gene expression profiling in response to a range of abiotic stresses showed that *CEK4* is strongly induced by cold temperatures (4°C) but not by other abiotic stresses (**Figure 5**; Kilian et al., 2007). This suggests that *CEK4* may have important functions in low temperature responses and that *bst* mutants might have chilling inducible phenotypes. To test this hypothesis we germinated and grew plants on soil for 15 days at 23°C before transferring them to 6°C for an additional 35 days. *bst* plants in both Col-0 and Ler backgrounds grew similarly to wild-type when grown at 23°C for 29 days. Differences between wild-type and *bst* plants were apparent after 35 days of growth at 6°C. After extended growth at low temperatures, *bst* plants were stunted compared to wild-type plants and their leaves were covered with cold induced lesions (**Figure 5**). While every Col-0 and Ler plant grown at 6°C continued to make new leaves that expanded and turned green, none of the *bst* plants in either genetic background did so. Instead, their apices became discolored and ceased to produce visible new leaves. The rosette sizes of cold grown plants were significantly smaller than those of untreated plants for all genotypes and growth reductions were larger in *bst* than in normal plants in both genetic backgrounds (Ler 55% reduction, *bst*^Ler 63% reduction, Col-0 46% reduction, *bst*^Col-0 55% reduction, two-tailed *t*-test $p < 0.002$ for all genotypes). The interaction between genotype and treatment on rosette size was significant in a Ler background [$f(1) = 6.414$, $p = 0.015$] but not in a Col background, consistent with the increased severity of other phenotypes in Ler.

DISCUSSION

CEK4 is the least well characterized choline/ethanolamine kinase in Arabidopsis because it is required for embryonic viability and, up to now, only T-DNA loss of function alleles have been available. This has made it hard to establish what roles it plays in plant growth and development. In this study we isolated *bst*, a partial loss of function allele of *CEK4*, and used it to demonstrate that *CEK4* plays roles in post-embryonic developmental patterning and cold responses.

CEK4 had previously been shown to be required for embryogenesis as *cek4* T-DNA mutant embryos arrest early during development (Lin et al., 2015). While it is not surprising that a key enzyme in a core biosynthetic pathway would be an essential gene, there are three other *CEK* genes in the Arabidopsis genome which could compensate for a loss of CEK4 activity. The observation that they don't suggests that *CEK4* has specialized functions that overlap minimally, if at all, with those of the other *CEK*s. The *bst* allele of *CEK4* behaves as a partial loss of function, demonstrated by the increased phenotypic severity when it is combined with a loss of function allele. *bst* is a point mutant, altering a key residue in the ATP binding pocket of the enzyme. The biochemical consequences of this change are uncharacterized but presumably the mutation results in decreased kinase activity due to altered ATP binding. This hypothesis could be tested in the future by directly assaying the effects of the *bst* T141I substitution on ATP binding and ethanolamine kinase activity, either *in vitro* or *in vivo*. We have not determined if *bst* mutant plants have alterations in their membranes. An analysis of any alterations may provide insights into the role that *CEK4* plays in the biological pathways that are affected in *bst* mutants.

bumpy stem plants have pleiotropic phenotypes, consistent with *CEK4* expression throughout plant development. These phenotypes include short roots and stems, swollen trichome bases, partial sterility, stem bumps at stem/pedicel junctions, and decreased chilling tolerance. These results suggest that the correct flux of metabolites through the Kennedy pathway is important not only for membrane biosynthesis but also for a variety of higher order processes in plants. Although we did not generate mechanistic insights into how *bst* results in decreased chilling tolerance, there are examples that illustrate the role of temperature dependent changes in phospholipid composition on temperature dependent responses. One example is temperature dependent flowering. The florigen *FT* has been shown to bind to membrane phospholipids at low temperatures, preventing it from moving and functioning as a signal. This serves as a mechanism that allows plants to delay flowering in response to chilling (Nakamura et al., 2014; Susila et al., 2021). Changes in the phospholipid composition of membranes could have direct

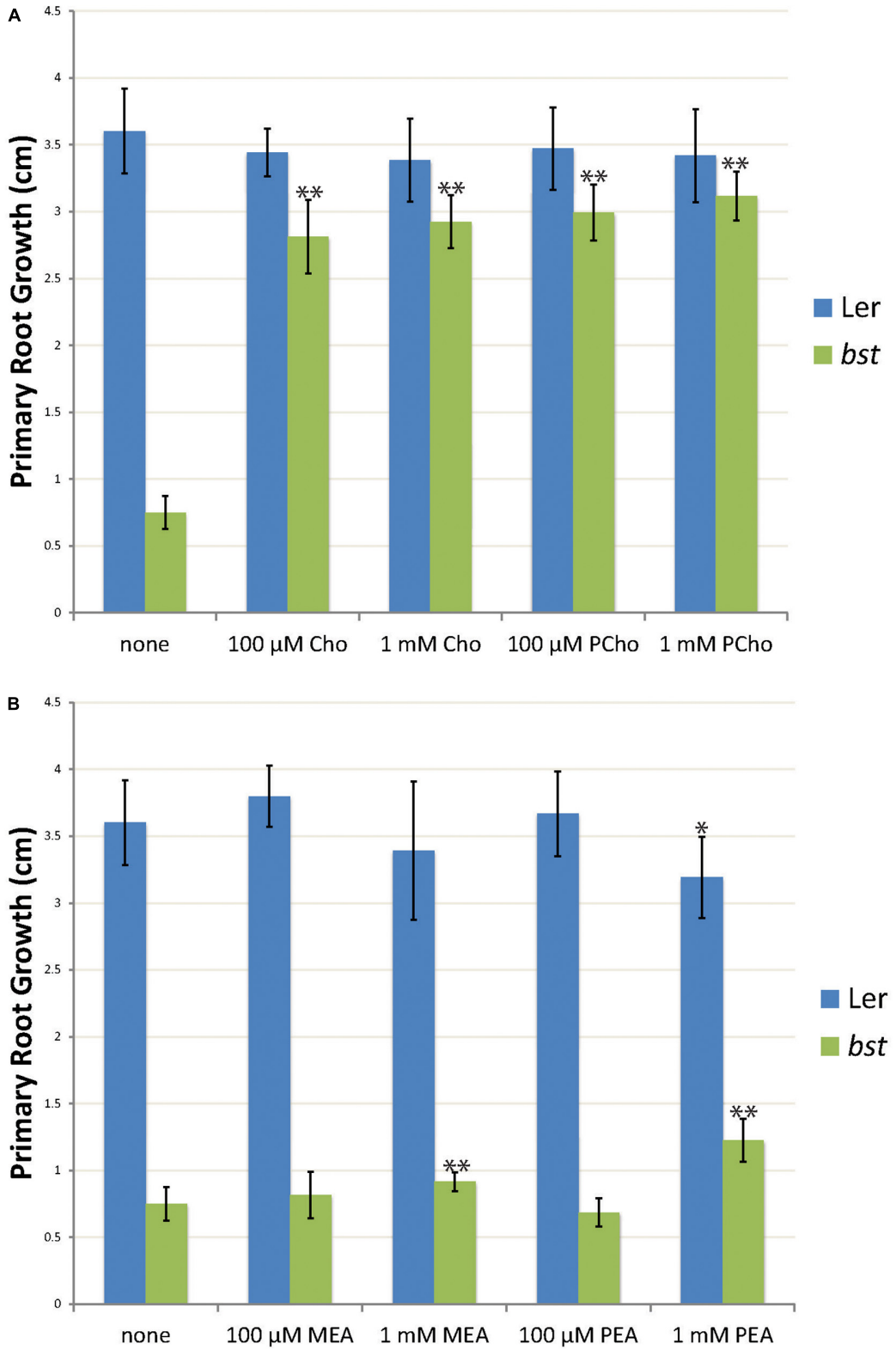

FIGURE 4 | The effects of choline, phosphocholine, ethanolamine, and phosphoethanolamine supplementation on root growth. Three day old seedlings were transplanted to plates containing choline (Cho) or phosphocholine (PCho) **(A)** or ethanolamine (MEA) or phosphoethanolamine (PEA) **(B)**. Primary root growth was measured after seven days of growth. The root length of treated plants was compared to untreated plants of the same genotype using unpaired *t*-tests. "*" indicates a *p*-value < 0.01 and "**" indicates a *p*-value < 0.001. Error bars are SD.

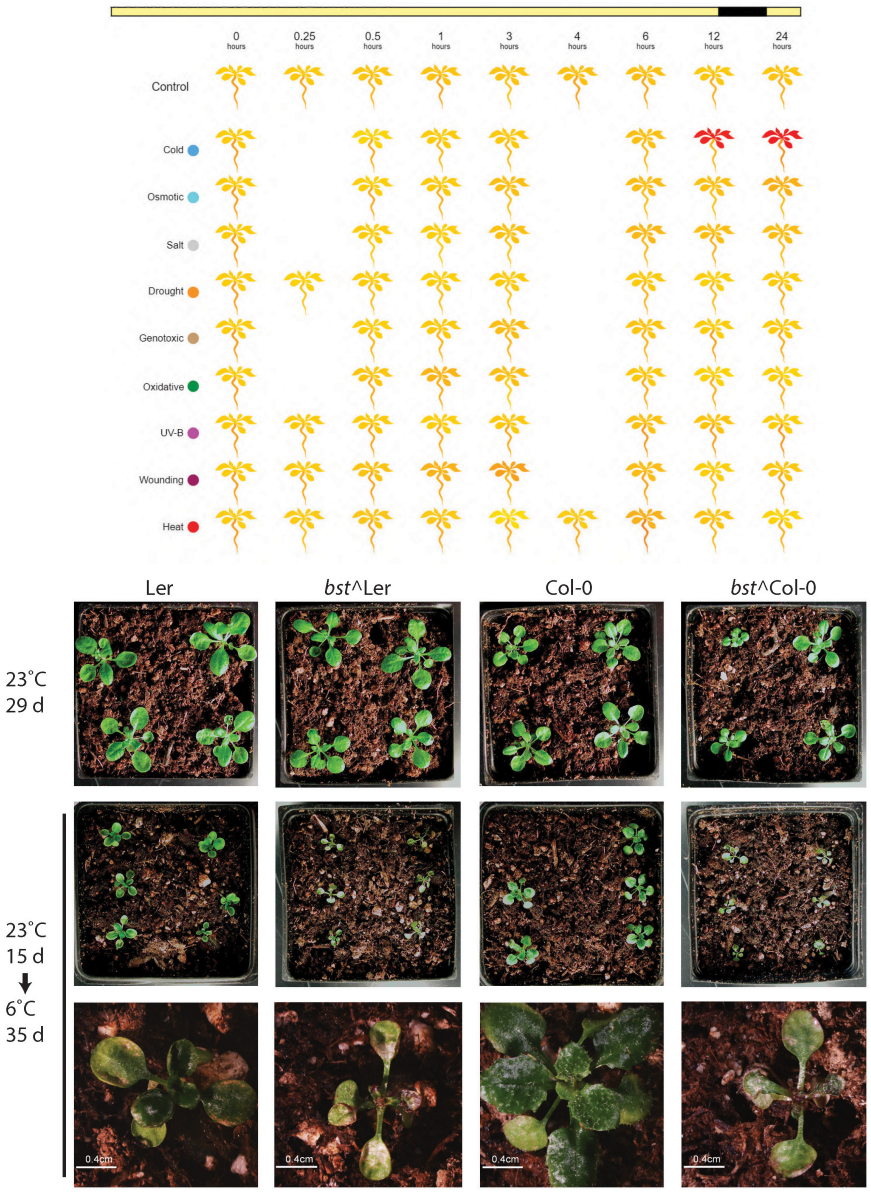

FIGURE 5 | *bumpy stem* responses to low temperatures. *bst* expression is induced by cold temperatures but not by other abiotic stresses. Yellow indicates low expression and red indicates high expression [data from Kilian et al. (2007), image generated using eplant at bar.utoronto.ca/eplant (Waese et al., 2017)]. Normal plants and *bst* plants in both Ler or Col-0 backgrounds were grown for 15 days at 23°C. Untreated plants were grown for an additional 14 days at 23°C while cold treated plants were transferred to 6°C and grown for an additional 35 days.

functional effects on the protein machinery embedded in or associated with them which, in turn, may alter intra- and inter-cellular signaling (Champeyroux et al., 2020). In addition, there are many well established examples of lipids functioning directly as signaling molecules in plants (Wang and Chapman, 2013; Ruelland and Valentova, 2016). These examples include roles for lipids in responding to abiotic stresses such as chilling and freezing responses (Welti et al., 2002; Hou et al., 2016).

CEK4 has been shown to have ethanolamine kinase but no detectable choline kinase activity *in vitro* (Lin et al., 2020). This does not mean that mutations in *CEK4* will only affect phosphoethanolamine production as phosphoethanolamine can be converted to phosphocholine by phosphoethanolamine *N*-methyltransferases (PMTs) (**Figure 6**). The observation that *pmt1* mutants have short roots (Cruz-Ramírez et al., 2004) demonstrates that normal levels of phosphocholine, produced from phosphoethanolamine, are required for robust root growth. Arabidopsis *pmt1 pmt3* double mutant plants have reduced phosphocholine levels and exhibit developmental phenotypes including small roots and shoots, but not bumpy stems, that can be rescued by choline or phosphocholine supplementation (Chen et al., 2018, 2019). *pmt1 pmt2 pmt3* triple mutants are seedling

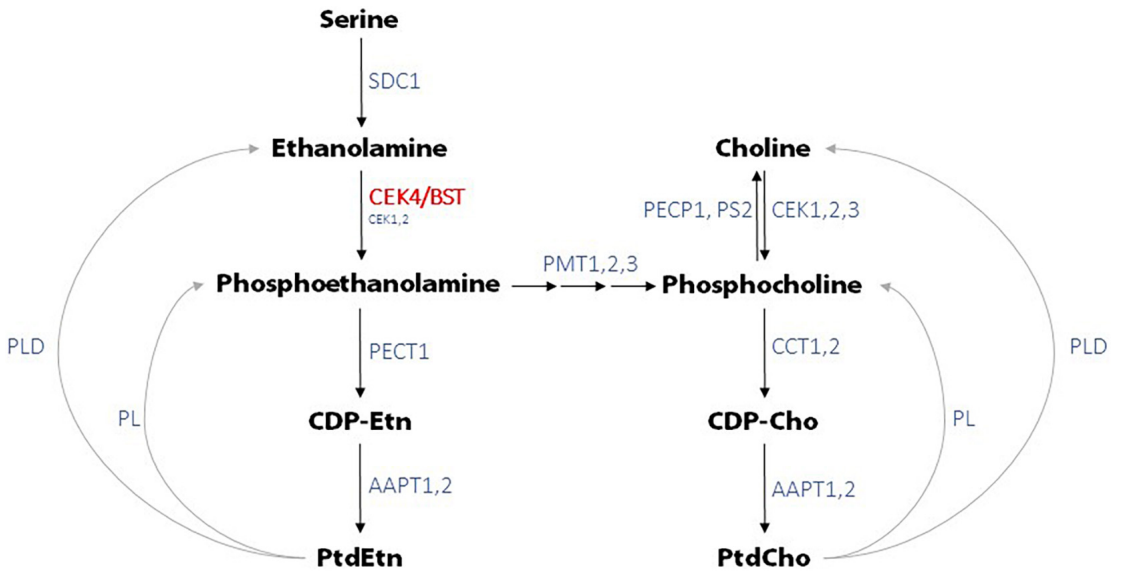

FIGURE 6 | Phosphatidylethanolamine (PtdEtn) and phosphatidylcholine (PtdCho) biosynthetic pathways in Arabidopsis. CEK4/BST functions as the principal ethanolamine kinase, directly producing phosphoethanolamine which is used to generate PtdEth. Through the activity of PMTs, CEK4/BST is also responsible for the production of PtdCho and other choline containing compounds. Enzymes not defined in the text are SDC1, serine decarboxylase 1; PECT1, CTP:phosphorylethanolamine cytidylyltransferase 1; AAPT1,2, aminoalcohol aminophosphotransferase 1,2; PL, phospholipase; PLD, phospholipase D; PECP1, phosphoethanolamine/phosphocholine phosphatase 1; PS2, phosphate starvation-induced gene 2; CCT1,2, CTP:phosphorylcholine cytidylyltransferase 1,2. CDP-Cho is cytidine diphosphocholine and CDP-Etn is cytidine diphosphoethanolamine. Adapted from models presented in Lin et al. (2015), Chen et al. (2019), and Liu et al. (2019).

lethal and exhibit up to 80% reductions in phosphocholine levels. This suggests that the bulk, if not all of, the phosphocholine found in Arabidopsis is produced from phosphoethanolamine and that decreased ethanolamine kinase activity will result in decreased phosphocholine levels (Liu et al., 2018, 2019; Chen et al., 2019). The conversion of phosphoethanolamine to phosphocholine by PMTs probably explains why *CEK4* overexpression in Arabidopsis resulted in both increased PtdEth as well as increased PtdCho levels even though *CEK4* only has ethanolamine kinase activity (Lin et al., 2015).

We tested the prediction that the *bst* short root phenotype would be rescued by supplementation with phosphoethanolamine, CEK4's predicted product. Surprisingly, phosphoethanolamine only partially rescued *bst* root phenotypes and only did so at relatively high concentrations (1 mM). The same was true for ethanolamine, CEK4's predicted substrate. We also supplemented *bst* seedlings with choline and phosphocholine. Rescue with both of these compounds was nearly complete at relatively low concentrations (100 μM). These unexpected results do not provide clear insights into *bst*'s root phenotypes; understanding them better will require a detailed metabolic analysis. One possible interpretation of these results is that, although *CEK4* functions principally or solely as an ethanolamine kinase, much of the phosphoethanolamine it produces is subsequently used as a substrate for the choline branch of the Kennedy pathway (**Figure 6**). Since a reduction in PMT generated phosphocholine results in short roots (Cruz-Ramírez et al., 2004; Chen et al., 2019; Liu et al., 2019), the *bst* phenotype could be principally due to reduced levels of choline containing compounds as opposed to ethanolamine containing compounds. This could explain the rescue with lower concentrations of choline containing compounds than ethanolamine containing compounds. Presumably only some of the supplemental phosphoethanolamine would be converted to phosphocholine by PMTs, reducing the efficiency of rescue with ethanolamine containing compounds relative to choline containing compounds. This idea could be tested by supplementation with labeled compounds followed by a metabolic analysis. Combining such an analysis with chemical inhibition of PMTs (Liu et al., 2019) or by using *bst pmt* double mutants could further refine our understanding of the flux of metabolites in the Kennedy pathway on plant growth and development. When combined with mutations in other *CEK* genes, *bst* may also provide insights into the *in planta* functions of this important gene that are shared with the other *CEK*s.

The viability of the *bst* allele provides a useful tool for further investigation of *CEK4* functions in development and responses to the environment. This study did not attempt to define the defects that underlie the developmental, reproductive, or chilling phenotypes we identified. Of special interest is the bumpy stem phenotype that this allele was named for. This phenotype is unusual and we are not aware of other Arabidopsis mutants that display this phenotype. Organ boundaries in plants are delineated by *LOB* gene expression (Shuai et al., 2002) and regulated by a complex genetic network that includes *CUC* and other genes (Hepworth and Pautot, 2015). Investigating the expression domains of *LOB*, *CUC*, and other boundary network genes in *bst* mutants could provide insights into the developmental signaling

mechanisms that link phospholipid head group metabolism and the establishment of boundaries between organs.

DATA AVAILABILITY STATEMENT

Strains described in this manuscript have been deposited at the ABRC with accession numbers CS73151 (*bst^*Col-0) and CS73152 (*bst^*Ler). The sequence data generated in the course of mapping and cloning *bst* have been deposited in the NCBI SRA as BioProject PRJNA796015.

AUTHOR CONTRIBUTIONS

CR and MC conceived of and performed the experiments and edited the manuscript. NK conceived of and performed the experiments, supervised the work, wrote the original draft, and edited the manuscript. All authors contributed to the article and approved the submitted version.

FUNDING

Research reported in this study was supported by the National Institute of General Medical Sciences of the National Institutes of Health award R15GM112173.

ACKNOWLEDGMENTS

We would like to thank the staff of the Swarthmore Biology Department for their excellent support.

REFERENCES

Aoyama, C., Liao, H., and Ishidate, K. (2004). Structure and function of choline kinase isoforms in mammalian cells. *Prog. Lipid Res.* 43, 266–281. doi: 10.1016/j.plipres.2003.12.001

Champeyroux, C., Stoof, C., and Rodriguez-Villalon, A. (2020). Signaling phospholipids in plant development: small couriers determining cell fate. *Curr. Opin. Plant Biol.* 57, 61–71. doi: 10.1016/J.PBI.2020.05.007

Chen, W., Salari, H., Taylor, M. C., Jost, R., Berkowitz, O., Barrow, R., et al. (2018). NMT1 and NMT3 N-Methyltransferase Activity Is Critical to Lipid Homeostasis, Morphogenesis, and Reproduction. *Plant Physiol.* 177, 1605–1628. doi: 10.1104/PP.18.00457

Chen, W., Taylor, M. C., Barrow, R. A., Croyal, M., and Masle, J. (2019). Loss of phosphoethanolamine n-methyltransferases abolishes phosphatidylcholine synthesis and is lethal. *Plant Physiol.* 179, 124–142. doi: 10.1104/pp.18.00694

Cruz-Ramírez, A., López-Bucio, J., Ramírez-Pimentel, G., Zurita-Silva, A., Sánchez-Calderon, L., Ramírez-Chávez, E., et al. (2004). The xipotl Mutant of Arabidopsis Reveals a Critical Role for Phospholipid Metabolism in Root System Development and Epidermal Cell Integrity. *Plant Cell* 16, 2020–2034. doi: 10.1105/TPC.103.018648

Gibellini, F., and Smith, T. K. (2010). The Kennedy pathway-De novo synthesis of phosphatidylethanolamine and phosphatidylcholine. *IUBMB Life* 62, 414–428. doi: 10.1002/iub.337

Gilding, E. K., and Marks, M. D. (2010). Analysis of purified glabra3-shapeshifter trichomes reveals a role for NOECK in regulating early trichome morphogenic events. *Plant J.* 64, 304–317. doi: 10.1111/J.1365-313X.2010.04329.X

Hepworth, S. R., and Pautot, V. A. (2015). Beyond the divide: boundaries for patterning and stem cell regulation in plants. *Front. Plant Sci.* 6:1052. doi: 10.3389/fpls.2015.01052

Honys, D., and Twell, D. (2004). Transcriptome analysis of haploid male gametophyte development in Arabidopsis. *Genome Biol.* 5, 1–13. doi: 10.1186/GB-2004-5-11-R85

Hou, Q., Ufer, G., and Bartels, D. (2016). Lipid signalling in plant responses to abiotic stress. *Plant Cell Environ.* 39, 1029–1048. doi: 10.1111/PCE.12666

Kilian, J., Whitehead, D., Horak, J., Wanke, D., Weinl, S., Batistic, O., et al. (2007). The AtGenExpress global stress expression data set: protocols, evaluation and model data analysis of UV-B light, drought and cold stress responses. *Plant J.* 50, 347–363. doi: 10.1111/j.1365-313X.2007.03052.x

Kwon, Y., Yu, S., Lee, H., Yim, J. H., Zhu, J.-K. K., and Lee, B. H. (2012). Arabidopsis Serine Decarboxylase Mutants Implicate the Roles of Ethanolamine in Plant Growth and Development. *Int. J. Mol. Sci.* 13, 3176–3188. doi: 10.3390/ijms13033176

Lin, Y. C., Araguirang, G. E., Ngo, A. H., Lin, K. T., Angkawijaya, A. E., and Nakamura, Y. (2020). The four Arabidopsis choline/ethanolamine kinase isozymes play distinct roles in metabolism and development. *Plant Physiol.* 183, 152–166. doi: 10.1104/pp.19.01399

Lin, Y.-C., Kanehara, K., and Nakamura, Y. (2019). Arabidopsis CHOLINE/ETHANOLAMINE KINASE 1 (CEK1) is a primary choline kinase localized at the endoplasmic reticulum (ER) and involved in ER stress tolerance. *New Phytol.* 223, 1904–1917. doi: 10.1111/nph.15915

Lin, Y. C., Liu, Y. C., and Nakamura, Y. (2015). The choline/ethanolamine kinase family in arabidopsis: essential role of CEK4 in phospholipid biosynthesis and embryo development. *Plant Cell* 27, 1497–1511. doi: 10.1105/tpc.15.00207

Liu, Y. C., Lin, Y. C., Kanehara, K., and Nakamura, Y. (2018). A pair of phosphobase methyltransferases important for phosphatidylcholine biosynthesis in Arabidopsis. *Plant J.* 96, 1064–1075. doi: 10.1111/TPJ.14090

Liu, Y. C., Lin, Y. C., Kanehara, K., and Nakamura, Y. (2019). A methyltransferase trio essential for phosphatidylcholine biosynthesis and growth 1. *Plant Physiol.* 179, 433–445. doi: 10.1104/pp.18.01408

Malito, E., Sekulic, N., Too, W. C. S., Konrad, M., and Lavie, A. (2006). Elucidation of Human Choline Kinase Crystal Structures in Complex with the Products ADP or Phosphocholine. *J. Mol. Biol.* 364, 136–151. doi: 10.1016/J.JMB.2006.08.084

Marks, M. D., Wenger, J. P., Gilding, E., Jilk, R., and Dixon, R. A. (2009). Transcriptome Analysis of Arabidopsis Wild-Type and gl3–sst sim Trichomes Identifies Four Additional Genes Required for Trichome Development. *Mol. Plant* 2:803. doi: 10.1093/MP/SSP037

Meinke, D., Muralla, R., Sweeney, C., and Dickerman, A. (2008). Identifying essential genes in Arabidopsis thaliana. *Trends Plant Sci.* 13, 483–491. doi: 10.1016/j.tplants.2008.06.003

Meinke, D. W. (2020). Genome-wide identification of EMBRYO-DEFECTIVE (EMB) genes required for growth and development in Arabidopsis. *New Phytol.* 226, 306–325. doi: 10.1111/nph.16071

Muller, H. J. (1932). Further studies on the nature and causes of gene mutations. *Int. Congr. Genet.* 61, 213–255.

Nakamura, Y., Andrés, F., Kanehara, K., Liu, Y. C., Dörmann, P., and Coupland, G. (2014). Arabidopsis florigen FT binds to diurnally oscillating phospholipids that accelerate flowering. *Nat. Commun.* 5:3553. doi: 10.1038/ncomms4553

Ruelland, E., and Valentova, O. (2016). Editorial: lipid Signaling in Plant Development and Responses to Environmental Stresses. *Front. Plant Sci.* 7:324. doi: 10.3389/FPLS.2016.00324

Schneeberger, K., Ossowski, S., Lanz, C., Juul, T., Petersen, A. H., Nielsen, K. L., et al. (2009). SHOREmap: simultaneous mapping and mutation identification by deep sequencing. *Nat. Methods* 6, 550–551. doi: 10.1038/nmeth0809-550

Schneider, C. A., Rasband, W. S., and Eliceiri, K. W. (2012). NIH Image to ImageJ: 25 years of image analysis. *Nat. Methods* 9, 671–675. doi: 10.1038/nmeth.2089

Shuai, B., Reynaga-Pe| na, C. G., and Springer, P. S. (2002). The Lateral Organ Boundaries Gene Defines a Novel, Plant-Specific Gene Family. *Plant Physiol.* 129, 747–761. doi: 10.1104/PP.010926

Silverblatt-Buser, E. W., Frick, M. A., Rabeler, C., and Kaplinsky, N. J. (2018). Genetic interactions between BOB1 and multiple 26S proteasome subunits suggest a role for proteostasis in regulating Arabidopsis development. *G3 Genes Genomes Genet.* 8, 1379–1390. doi: 10.1534/g3.118.300496

Susila, H., Jurić, S., Liu, L., Gawarecka, K., Chung, K. S., Jin, S., et al. (2021). Florigen sequestration in cellular membranes modulates temperature-responsive flowering. *Science* 373, 1137–1142. doi: 10.1126/SCIENCE.ABH4054

Tannert, M., Balcke, G. U., Tissier, A., and Köck, M. (2021). At4g29530 is a phosphoethanolamine phosphatase homologous to PECP1 with a role in flowering time regulation. *Plant J.* 107, 1072–1083. doi: 10.1111/TPJ.15367

Tasseva, G., Richard, L., and Zachowski, A. (2004). Regulation of phosphatidylcholine biosynthesis under salt stress involves choline kinases in Arabidopsis thaliana. *FEBS Lett.* 566, 115–120. doi: 10.1016/j.febslet.2004.04.015

Tavasoli, M., Lahire, S., Reid, T., Brodovsky, M., and McMaster, C. R. (2020). Genetic diseases of the Kennedy pathways for membrane synthesis. *J. Biol. Chem.* 295, 17877–17886. doi: 10.1074/JBC.REV120.013529

Waese, J., Fan, J., Pasha, A., Yu, H., Fucile, G., Shi, R., et al. (2017). ePlant: visualizing and Exploring Multiple Levels of Data for Hypothesis Generation in Plant Biology. *Plant Cell* 29, 1806–1821. doi: 10.1105/TPC.17.00073

Wang, X., and Chapman, K. D. (2013). Lipid signaling in plants. *Front. Plant Sci.* 4:216. doi: 10.3389/FPLS.2013.00216

Welti, R., Li, W., Li, M., Sang, Y., Biesiada, H., Zhou, H. E., et al. (2002). Profiling membrane lipids in plant stress responses: role of phospholipase Dα in freezing-induced lipid changes in arabidopsis. *J. Biol. Chem.* 277, 31994–32002. doi: 10.1074/jbc.M205375200

Wharfe, J., and Harwood, J. L. (1979). Lipid metabolism in germinating seeds: purification of ethanolamine kinase from soya bean. *Biochim. Biophys. Acta Lipids Lipid Metab.* 575, 102–111. doi: 10.1016/0005-2760(79)90135-8

Yunus, I. S., Liu, Y. C., and Nakamura, Y. (2016). The importance of SERINE DECARBOXYLASE1 (SDC1) and ethanolamine biosynthesis during embryogenesis of Arabidopsis thaliana. *Plant J.* 88, 559–569. doi: 10.1111/TPJ.13278

Conflict of Interest: The authors declare that the research was conducted in the absence of any commercial or financial relationships that could be construed as a potential conflict of interest.

Publisher's Note: All claims expressed in this article are solely those of the authors and do not necessarily represent those of their affiliated organizations, or those of the publisher, the editors and the reviewers. Any product that may be evaluated in this article, or claim that may be made by its manufacturer, is not guaranteed or endorsed by the publisher.

frontiers | Frontiers in Plant Science

TYPE Review
PUBLISHED 24 August 2022
DOI 10.3389/fpls.2022.951844

OPEN ACCESS

EDITED BY
Neusa Steiner,
Federal University of Santa Catarina, Brazil

REVIEWED BY
Mohammad Rashed Hossain,
Bangladesh Agricultural University, Bangladesh
Ling Qin,
Beijing University of Agriculture, China

*CORRESPONDENCE
Rita Lourenço Costa
rita.lcosta@iniav.pt

†These authors share first authorship

SPECIALTY SECTION
This article was submitted to Plant Development and EvoDevo, a section of the journal Frontiers in Plant Science

RECEIVED 24 May 2022
ACCEPTED 29 July 2022
PUBLISHED 24 August 2022

CITATION
Fernandes P, Colavolpe MB, Serrazina S and Costa RL (2022) European and American chestnuts: An overview of the main threats and control efforts. *Front. Plant Sci.* 13:951844. doi: 10.3389/fpls.2022.951844

European and American chestnuts: An overview of the main threats and control efforts

Patrícia Fernandes[1,2,3†], Maria Belén Colavolpe[1†], Susana Serrazina[4] and Rita Lourenço Costa[1,5*]

[1]Instituto Nacional de Investigação Agrária e Veterinária, I.P., Oeiras, Portugal, [2]Green-It Bioresources for Sustainability, ITQB NOVA, Oeiras, Portugal, [3]Department of Environmental Biology, State University of New York College of Environmental Science and Forestry, Syracuse, NY, United States, [4]BioISI – Biosystems and Integrative Sciences Institute, Faculdade de Ciências da Universidade de Lisboa, Lisbon, Portugal, [5]Centro de Estudos Florestais, Instituto Superior de Agronomia, Universidade de Lisboa, Lisbon, Portugal

Chestnuts are multipurpose trees significant for the economy and wildlife. These trees are currently found around the globe, demonstrating their genetic adaptation to different environmental conditions. Several biotic and abiotic stresses have challenged these species, contributing to the decline of European chestnut production and the functional extinction of the American chestnut. Several efforts started over the last century to understand the cellular, molecular, and genetic interactions behind all chestnut biotic and abiotic interactions. Most efforts have been toward breeding for the primary diseases, chestnut blight and ink disease caused by the pathogens, *Cryphonectria parasitica* and *Phytophthora cinnamomi*, respectively. In Europe and North America, researchers have been using the Asian chestnut species, which co-evolved with the pathogens, to introgress resistance genes into the susceptible species. Breeding woody trees has several limitations which can be mostly related to the long life cycles of these species and the big genome landscapes. Consequently, it takes decades to improve traits of interest, such as resistance to pathogens. Currently, the availability of genome sequences and next-generation sequencing techniques may provide new tools to help overcome most of the problems tree breeding is still facing. This review summarizes European and American chestnut's main biotic stresses and discusses breeding and biotechnological efforts developed over the last decades, having ink disease and chestnut blight as the main focus. Climate change is a rising concern, and in this context, the adaptation of chestnuts to adverse environmental conditions is of extreme importance for chestnut production. Therefore, we also discuss the abiotic challenges on European chestnuts, where the response to abiotic stress at the genetic and molecular level has been explored.

KEYWORDS

breeding, *Castanea*, climate change, chestnut blight, *Cryphonectria parasitica*, drought, ink disease, *Phytophthora cinnamomi*

Introduction

The genus *Castanea* belongs to the Fagaceae family, and it is constituted of three sections: *Eucastanon* (chestnuts), *Balanocastanon* (chinquapins), and *Hypocastanon* (the Henry chestnut). The most representative species and of greater economic importance are included in *Eucastanon*: European chestnut (*Castanea sativa* Mill.), the American chestnut [*Castanea dentata* (Marshall) Borkh.], the Chinese chestnut (*Castanea mollissima* Blume), and the Japanese chestnut (*Castanea crenata* Sieb. and Zucc.) (Vieitez and Merkle, 2005; Mellano et al., 2012). Recently, researchers may have discovered a new chestnut species. *Castanea alabamensis*, was considered a hybrid between *Castanea dentata* and *Castanea pumila* Mill. (Allegheny chinquapin), but it was identified as a distinct genetic and morphological group in North America (Perkins et al., 2021).

Chestnuts originated in eastern Asia (Japan and China), from where they dispersed and diverge through Europe and North America (Lang et al., 2007). Nowadays, they are found across the northern hemisphere. *Castanea sativa* is distributed in temperate and Mediterranean regions of Europe and Western Asia; *Castanea dentata*'s natural range is across the Appalachian Mountain region; *Castanea mollissima* is native to China; and *Castanea crenata* is distributed in the Korean Peninsula, Japan, and the temperate region of East Asia (Pereira-Lorenzo et al., 2012).

In Asia and Europe, chestnuts have been cultivated for decades and have great economical value for their nutritious nuts and quality timber. In North America, they were treasured for being a multipurpose key-stone forest tree very important for populations and wildlife in its natural range (Anagnostakis, 1987). In 2020, the total chestnut plantation area in the world was approximately 582,545 ha, and more than half of this area belongs to China. This translated into an annual world production of approximately 2,300,000 tons, where China is the leading producer with almost 1,750,000 tons, followed by Spain with 189,000 tons (Food and Agriculture Organization of the United Nations, 2022).

The American and European chestnuts are the most susceptible species to several stresses, mainly biotic. The once dominant American chestnut was decimated in the 20th century (Anagnostakis, 1987), while in Europe *C. sativa* was chastised and nut production declined 251,549 tons from 1961 to 2015 (Food and Agriculture Organization of the United Nations, 2022). Biotic and abiotic stresses in forest systems have not been as well studied at a genomic level as it has for herbaceous crops. The recent technological advances in molecular biology and next-generation sequencing (NGS) technologies (Grabherr et al., 2011) helped overcome several difficulties inherent to studying woody species such as chestnuts. The transcriptome is modifiable under different conditions, making it a great tool to explore stress response. Association mapping and genome-wide association studies (GWASs) allow the association between molecular markers and phenotype in complex populations (Badenes et al., 2016), which can help understand the genetic architecture of stresses. The genomic resources gathered in the last decades have increased our knowledge about *Castanea* spp. genetic diversity, phenology, adaptation, and interaction with biotic and abiotic stresses. Transcriptomes during stress response (Barakat et al., 2009, 2012; Santamaría et al., 2011; Serrazina et al., 2015), development of molecular markers (Martin et al., 2010; Pereira-lorenzo et al., 2010, Pereira-Lorenzo et al., 2011; Nishio et al., 2011; Kubisiak et al., 2013; Santos et al., 2015b), mapping and identification of Quantitative Trait Loci (QTL) (Kubisiak et al., 1997; Casasoli et al., 2004, 2006; Zhebentyayeva et al., 2014, 2019; Santos et al., 2017b) have set us a step closer to using genomic selection in breeding programs. Biotechnologies implemented in chestnuts also include large-scale micropropagation of improved genotypes and genetic transformation. Several *in vitro* culture techniques such as axillary shoot propagation, organogenesis, and somatic embryogenesis have been reported over the last decades (reviewed in Corredoira et al., 2017) and recent advances are still being published (Fernandes et al., 2020b; Liu et al., 2022). Genetic transformation can be a powerful tool to study the function of a gene or for crop improvement and has been an important milestone in chestnut research (Powell et al., 2019; Pavese et al., 2021a).

The research and breeding efforts made in the last decades seem to be having a positive impact since, in Europe, chestnut production has been increasing since 2015 for the first time in many decades (Food and Agriculture Organization of the United Nations, 2022). The purpose of this review is to provide a synopsis of the understanding gathered so far about chestnuts' main biotic and abiotic challenges. The section on biotic stresses will have ink disease and chestnut blight as the main focus, while the abiotic section will mainly focus on Southern Europe, where there is a majority of reports. The development and application of biotechnologies are also discussed as they relate to the efforts of fighting European chestnut's decline and revive the American species. **Figure 1** briefly summarizes the main topics discussed in this review.

Biotic stresses

Castanea species are challenged by several biotic stresses but the most destructive are *Cryphonectria parasitica* (Murr.) Barr. (*CP*) and *Phytophthora cinnamomi* Rands (*PC*), the pathogens causing chestnut blight and ink disease (also known as chestnut canker and root rot, respectively). Leaf spot (*Marssonina ochroleuca*), twig canker (*Cryptodiaporthe castanea*), and chestnut mosaic virus (ChMV) also affect chestnuts, however, the damage they cause is not as severe as the previously mentioned diseases (Serdar et al., 2019).

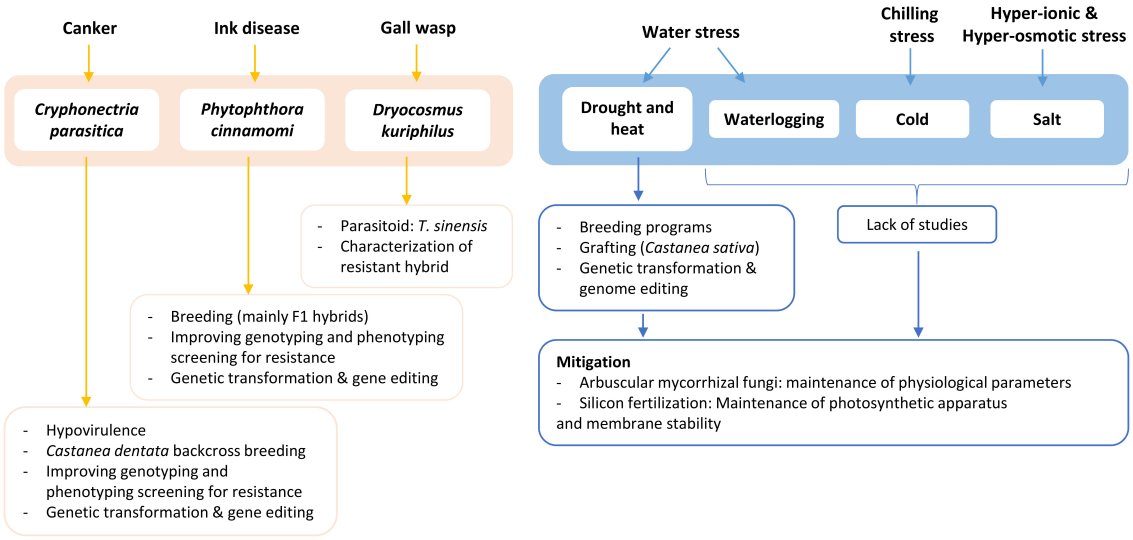

FIGURE 1
Schematic overview of the main topics discussed in this review. Information includes disease/stress, causal agent, and efforts for control/mitigation, in process or in perspective.

CP is a necrotrophic bark-inhabiting fungus whose primary hosts are *C. dentata, C. sativa, C. crenata,* and *C. mollissima,* although it also infects oaks (*Quercus* spp.), maples (*Acer* spp.), European hornbeam (*Carpinus betulus*) and chinquapins (*C. pumila* and *Castanea ozarkensis*). It is native to Eastern Asia, and it spread to North America and Europe due to imported infected chestnuts (Rigling and Prospero, 2018). *CP* was first described in 1904 in American chestnut in New York (Anagnostakis, 1987; Rigling and Prospero, 2018). In 50 years, it caused one of the most enormous economic and ecological devastations, leaving the American chestnut functionally extinct by killing an estimated 4 billion trees (Anagnostakis, 1987). This species now survives as stump sprouts (due to repeated blight infections) which are reservoirs of germplasm (Kubisiak and Roberds, 2006). *CP* was detected in Europe for the first time in 1938 in Italy, from where it rapidly spread to the rest of the continent to countries such as France, Switzerland, Portugal, Spain, and Turkey (Rigling and Prospero, 2018). It threatened the European chestnut stands, affecting production. Still, *C. sativa* recovered from the disease. This recovery was mainly related to the natural occurrence of mycoviruses in Europe that can infect this fungus and attenuate its virulence (hypovirulence, a viral disease that makes the pathogen less aggressive) (Robin and Heiniger, 2001; Milgroom and Cortesi, 2004). Also, *C. sativa* has lower susceptibility to the pathogen when compared to *C. dentata* (Waldboth and Oberhuber, 2009). Nowadays, *CP* is spread across Europe, North America, Africa (Tunisia), Asia and Australia (Eppo Global Database, 2022).

PC is a devastating hemibiotrophic pathogen with an extensive host range of close to 5,000 plant species (Hardham and Blackman, 2018). It has significant environmental and economic impacts (Weste and Marks, 1987; Hardham, 2005; Kamoun et al., 2015) by infecting plants important for forestry, and agriculture, such as chestnut, avocado, macadamia, oak, peach and pineapple [reviewed in Hardham and Blackman (2018)], causing annual damages of billions of dollars. *PC* is considered one of the Top 10 Oomycete plant pathogens (Kamoun et al., 2015). Its origin remains uncertain, but evidence indicates it originated near Papua New Guinea and South-East Asian regions (Ko et al., 1978; Zentmyer, 1988; Hardham, 2005). Ink disease was observed in American chestnuts and chinquapins in the southern United States since about 1850 [Milburn and Gravatt, 1932 as cited in Anagnostakis (2012)] and in Portugal since 1853 [Prunet, 1904 as cited in Anagnostakis (2012)]. But the first reports on this disease being caused by *PC* were a few years later. In European chestnuts, it was in 1860 [Grent, 1961 as cited in Burgess et al. (2017)], and in American chestnuts in 1986 [Corsa, 1986 as cited in Anagnostakis (2001)]. *PC* was introduced in all continents by plant-moving, except for Antarctica, becoming invasive worldwide (Eppo Global Database, 2022).

Castanea species have different susceptibility levels to these pathogens. The Asian species are the most resistant, probably due to their co-evolution with the pathogens (Crandall et al., 1945; Huang et al., 1996). In the specific case of chestnut blight, varying levels of quantitative resistance have been reported for Asian species, however, Chinese chestnut is considered more blight-resistant than Japanese chestnut (Huang et al., 1996).

Breeding for pathogen resistance in Europe and North America has different goals. The first focus on development and preservation of cultivars and ink disease-resistant rootstocks to reduce mortality, improve orchard production, and avoid

further decline of the species; the latter seeks to restore the American chestnut as a forest species. What is common in these efforts is the use of the Asian species resistance and the high interspecies crossability, to introgress resistance genes into the susceptible European and American species (Burnham et al., 1986; Fernández-López et al., 2001; Pereira-lorenzo et al., 2010; Costa et al., 2011; Steiner et al., 2017). In Europe, blight infection has been under control due to hypovirulence and consequently, most research is focused on understanding the interaction with *PC*, mainly in *C. sativa* and *C. crenata*. Contrary to North America, where dedication goes to *C. dentata* and *C. mollissima* responses to *CP*. Nevertheless, in recent years North Americans realized that *PC* will be a problem to the cultivation of the American chestnut with improved blight resistance, mainly in the south where temperatures allow ink disease establishment (Jeffers et al., 2009).

During the last decades, chestnut breeding programs have been looking into *Castanea* spp. cellular and molecular responses to *CP* and *PC*, which may be comparable since Oomycetes and Fungi share similar infection mechanisms (Latijnhouwers et al., 2003). Several hypotheses have been proposed so far and are discussed in the next sections.

Biotic stresses also include several pests such as the gall wasp [*Dryocosmus kuriphilus* (Yasumatsu)], chestnut tortrix moths (*Cydia splendana*, *Cydia fagiglandana*, and *Pammene fasciana*), the chestnut weevil (*Curculio elephas*) and ambrosia beetles [*Anisandrus* (*Xyleborus*) *dispar*]. Less damaging pests currently affecting chestnuts are the potato leafhopper (*Empoasca fabae*), Japanese beetle (*Popillia japonica*), Rose chafer (*Macrodactylus subspinosus*) and spider mites. Also, Peach moth (*Dichocrocis punctiferalis*) and goat moth (*Cossus cossus*) were reported as important pests in Japan and Turkey, respectively [reviewed in Serdar et al. (2019)]. The gall wasp is the most globally significant pest. It attacks European, American, and Asian chestnut species, and their hybrids, reducing the quality and quantity of timber (Kato and Hijii, 1997) and nuts (Battisti et al., 2014). The gall wasp does not kill the trees and for that, it has been given less attention than the previously referred pathogens. However, its spread may erase all the breeding efforts toward European and American chestnut sustainability due to the reduced nut production. Also, galls can be an entry point for *CP* increasing branch mortality (Meyer et al., 2015). The next sections provide an overview of our current knowledge of the chestnut's interaction with these three biotic stresses, with a focus on the pathogens.

Castanea spp. and *Cryphonectria parasitica*

Infection progress and symptoms

The histopathology of *CP* infection progress is described in American and Chinese chestnuts (Hebard et al., 1984). After spore germination, the fungus develops mycelial fans, which, by physical pressure, colonize the host cells progressing intercellularly through the bark and cambium. The extent and frequency of mycelial fan formation are essential for the enlargement of cankers. The host responses against the infection are lignification of cell walls succeeded by wound periderm formation. Lignification only blocks individual or small aggregates of hyphae, and only fully formed wound periderm can stop mycelial fans (Hebard et al., 1984). The advance of the mycelial fans kills the host cells by releasing toxins and cell wall-degrading enzymes (Roane et al., 1986) and when the host does not develop deep wound periderms allows the pathogen to keep obtaining nutrients from dying and dead chestnut cells (necrotrophy) (Hebard et al., 1984). Oxalate (oxalic acid) was considered linked with *CP* virulence when researchers suggested it had a toxic effect on host cells and enhanced cell wall degradation (Havir and Anagnostakis, 1983). This was later confirmed in knockout mutants of the pathogen (Chen et al., 2010).

CP only infects above-ground tree parts, producing orange/reddish-brown cankers (necrotic lesions) on the bark (**Figure 2**) and killing smaller branches. An early symptom of infection is the wilted and hanging leaves on infected dead branches. Trees react by producing numerous epicormic shoots below the cankers (Rigling and Prospero, 2018). Blight-resistant chestnuts typically survive infection with minimal internal damage, developing superficial lesions or cankers on the trunk. In blight-susceptible species, disease symptoms usually progress rapidly, resulting in host mortality. Also, symptoms in susceptible hosts may vary depending on the virulence of the fungus, tree size, longevity, health, and environmental factors (Roane et al., 1986; Clark et al., 2019). *CP* can survive and sporulate on the bark of dead or recently dead chestnut branches or stems for more than 1 year (Prospero et al., 2006).

Chestnut blight control

Quarantine regulations were implemented worldwide to control the movement and trade of plant material infected with blight. Unfortunately, these measures were ineffective due to asymptomatic infected plants (Rigling and Prospero, 2018). In natural ecosystems, attempts to eradicate the pathogen or apply fungicides are not feasible. Cutting and burning infected trees is a management alternative, but only viable in orchards. The use of chemicals is restricted in forests because it can cause phytotoxicity, and may induce resistance.

Efforts to develop control methods for *CP* are summarized in **Table 1**. In Europe, the disease is successfully managed due to the sizeable natural occurrence of hypovirulence, a viral disease in *CP* population caused by double-stranded RNA viruses which reduces virulence and sporulation of strains. Contrary to North America where hypovirulence was only found outside the American chestnut range and there is limited success in viral transfer between different vegetatively incompatible

FIGURE 2
Castanea dentata infected with *Cryphonectria parasitica* presenting an orange canker on the main trunk. This picture was taken at the Lafayette Experimental Road Station – SUNY-ESF (Syracuse, NY, United States).

fungus strains (Milgroom and Cortesi, 2004). Recent reports described a modification using genetically engineered "super donor" fungal strains that may help overcome these difficulties (Stauder et al., 2019).

Due to the hypovirulence success in Europe most efforts to manage blight are focused on the study of hypovirulent strains of *CP* (Robin and Heiniger, 2001; Bryner et al., 2012; Murolo et al., 2018). North America is focused in developing a blight-resistant chestnut through traditional backcross breeding and genetic engineering. For this reason, the following sections on *CP* will be mainly focused on North American reports.

Traditional breeding for *Cryphonectria parasitica* resistance

American chestnut breeding for blight resistance has been ongoing for over 100 years. Inter-species crosses with Asian chestnut species (mainly Chinese) were started by the United States Department of Agriculture (USDA) and the Connecticut Agricultural Experiment Station (CAES) [reviewed in Jacobs et al. (2013)]. However, these programs failed to produce a blight-resistant tree that retained American chestnuts' growth and quality timber. Besides the difficulties in finding the ideal candidate tree, nowadays we know there are other problems inherent to hybrid breeding that can turn restoration even more difficult such as male sterility (Sisco et al., 2014), internal kernel breakdown (IKB) (Fulbright et al., 2014) and intermediate traits (Cipollini et al., 2017).

In 1989 The American Chestnut Foundation (TACF) backcross breeding started at the Meadowview station by using two backcross hybrids (BC) [BC_1 (*C. dentata* × *C. mollissima*) × *C. dentata*] from the USDA and CAES programs as two different sources of blight resistance: the 'Clapper' and 'Graves' (from *C. mollissima* variety 'Nanking' and 'Mahogany,' respectively). To achieve a population with Chinese chestnut resistance and the American chestnut phenotype, the original breeding plan (Burnham et al., 1986) proposed successive hybrid backcrossing with several pure American chestnut lines (to ensure genetic diversity), selecting for blight resistance and American phenotype in every progeny. This plan was based on the assumption that the alleles for resistance were partially dominant and only two genes were involved. Nowadays, we know that chestnut blight resistance is quantitative, involving three main resistance loci (of up to seven in total) (Kubisiak et al., 1997, 2013), which changed the backcross breeding stages to include three backcross generations. The third backcross would be intercrossed to produce a BC_3F_2 population in which a fraction of the trees was predicted to be homozygous for the Asian resistance alleles. The selected resistant individuals would be planted in seed orchards producing a BC_3F_3 generation that would be essentially American chestnut morphologically and blight-resistant enough to start restoration [reviewed in Jacobs et al. (2013)]. Indeed, the American phenotype was recovered in 96% of the BC_3 generation, which resembled 24 measured traits (Diskin et al., 2006). Approximately 64,000 BC_3F_2 from both 'Clapper' and 'Graves' selections were planted between 2002 and 2018, and 7,600 trees remained as of 2018 (Westbrook et al., 2020b). Orchard trials of open-pollinated BC_3F_3 were made to estimate the genetic resistance of the selected BC_3F_2 trees, but after inoculations, the highest blight tolerance was more like American chestnut than Chinese chestnut. These findings suggested that blight resistance segregates at more loci than initially predicted and phenotypic selection has not been accurate enough (Steiner et al., 2017). This differs from 8-year-old BC_3F_3 forest reintroduction trials made in three locations in the southeastern United States, where the resistance of the trees was more like Chinese chestnut (Clark et al., 2019). TACF has ongoing field trials in 35 locations in the eastern United States but are still too young to assess blight resistance (Westbrook et al., 2020b). Nowadays, additional *C. mollissima* genotypes are being used as resistance sources (Steiner et al., 2017) at the Meadowview breeding station. This program has also been reproduced at 16 other locations by the different chapters of the foundation. After decades of breeding, the current goal is to select 1% of the 7,600 BC_3F_2 that are most blight-resistant, intercross the selected trees and increase BC_3F_3 blight resistance

TABLE 1 Summary of efforts to control *Cryphonectria parasitica* (*CP*).

Source of resistance/ Plant material	Approach for improvement	Resources related to resistance		Current status/ Outcomes	References
		Type of data	Description		
NA	Hypovirulence	NA	NA	Study of native hypovirulent strains of *CP*	Robin and Heiniger, 2001; Bryner et al., 2012; Murolo et al., 2018
NA	Hypovirulence: improve viral transfer in *CP*	NA	NA	Genetically engineered *CP* strain developed – "Super donor"	Stauder et al., 2019
Castanea mollissima varieties 'Nanking' and 'Mahogany'	Backcross breeding of *Castanea dentata*	NA	NA	Selecting most resistant BC_3F_2 to intercross	Burnham et al., 1986; Diskin et al., 2006; Westbrook et al., 2020b
C. mollissima × *C. dentata* F2 hybrids	Study genetic architecture of *CP* resistance; future MAS	Genetic linkage map	3 QTLs: *Cbr1* (LG B), *Cbr2* (LG F), *Cbr3* (LG G)	NA	Kubisiak et al., 1997, 2013; Sisco et al., 2005
		Sequencing of *Cbr1*, *Cbr2*, *Cbr3*	Genes annotated with the term "defense response". *Cbr1*: 8; *Cbr2*: 4; *Cbr3*: 3	NA	Staton et al., 2015
C. dentata and *C. mollissima*	Identification of resistance genes; future MAS	Transcriptome	Candidate genes related to: Cell wall biosynthesis, ROS, signaling of SA, ET, JA and ABA, HR, and PCD	NA	Barakat et al., 2009, 2012
C. mollissima × *C. dentata* BC_3F_2 generation and progeny (BC_3F_3)	Genomic prediction model for blight phenotypes	*C. dentata* draft genome; SNPs	GBS and phenotyping for canker severity on BC_3F_2, plus phenotyping BC_3F_3	Improving model: genotyping more BC_3F_2 trees	Westbrook et al., 2020b
Oxalate oxidase (*OxO*) gene from wheat	*C. dentata* genetic transformation	NA	NA	Tolerant American Chestnut waiting deregulation for restoration purposes	Powell et al., 2019; Newhouse et al., 2020

Source of resistance/plant material, approach for improvement, resources gathered, and current status and/or outcomes of these efforts are presented. NA, none applied; MAS, marker-assisted selection; QTL, quantitative trait loci; LG, linkage group; GBS, genotyping by sequencing; ROS, reactive oxygen species; SA, salicylic acid; ET, ethylene; JA, jasmonic acid; ABA, abscisic acid; HR, hypersensitive response; PCD, programmed cell death.

(Westbrook et al., 2020b). Also, selected blight-resistant hybrids are being evaluated for resistance to *PC* (Jeffers et al., 2009).

Screening for *Cryphonectria parasitica* resistant genotypes

Traditional screening for blight resistance can be determined by field inoculation of the stems/trunks (Griffin, 1983; Anagnostakis, 1992). These inoculations usually allow the evaluation of parameters such as mean canker length and width (canker expansion rate), stromata production, canker superficiality and swelling, and canker severity (Kubisiak et al., 1997; Steiner et al., 2017; Westbrook et al., 2020b). These methods are accurate but can only be performed in trees with at least 3 years of growth and cankers can take several months to develop. Alternative techniques can test younger plants (Powell et al., 2007; Newhouse et al., 2014). *CP* lesion progression can be accessed by small stem inoculations in trees with approximately 1-year-old and results can be collected in 3–4 weeks (Powell et al., 2007). However, this may harm the tree even if it has moderate levels of resistance. Alternatively, excised leaves from a few month-old seedlings can be inoculated (Newhouse et al., 2014). Leaves are not *CP*'s primary organ of infection. Nevertheless, results can be obtained in less than a week and correlate to stem inoculations (Newhouse et al., 2014), representing an expedited way to predict levels of blight resistance in big populations.

Improving characterization of *Cryphonectria parasitica* resistance

Kubisiak et al. (1997) developed a genetic linkage map with F_2 hybrids from the backcross breeding program, mapping 184 molecular markers. In three different linkage groups (LG) seven QTLs related to blight resistance were reported. Three major QTLs explained about 40% of the phenotypic variation in canker size. This map was later expanded by Sisco et al. (2005) and Kubisiak et al. (2013) and the three major QTLs identified were sequenced (**Table 1**; Staton et al., 2015). Of 782 annotated genes, 15 were related to defense response, giving further insight about the candidate resistance genes (Staton et al., 2015). Barakat et al. (2009, 2012) also identified candidate

genes for blight resistance by comparing American and Chinese chestnuts transcriptomes after *CP* challenge. The candidate genes were associated with response to biotic stimuli belonging to several pathways (**Table 1**; Barakat et al., 2012).

Westbrook et al. (2020b) recently suggested that blight resistance is a polygenic inherited trait. The population under study was the BC_3F_2 generation (mentioned in Section "Improving characterization of *Cryphonectria parasitica* resistance"). Genotyping-by-sequencing (GBS) and evaluation of different blight phenotypes in the BC_3F_2 population, along with canker severity assessment of their progeny (BC_3F_3), allowed the development of a genomic prediction model for blight resistance breeding (**Table 1**). They also performed GBS on *C. dentata* and *C. mollissima* to estimate hybrid indices.

Castanea spp. and *Phytophthora cinnamomi*

Infection process and symptoms

The *PC* can saprophytically grow in the soil, and when conditions are favorable (high soil moisture and temperatures above 10°C) to sporulate it produces biflagellate motile zoospores (asexual spores) which seek out roots by chemotactically attracting to suitable infection sites (Carlile, 1983). The early stages of the infection process during *PC* infection have been characterized at the cellular level for *C. sativa* and *C. crenata* (Fernandes et al., 2021b). The zoospores shed their flagella, encyst, and grow a germ tube on the root surface until the development of an appressorium-like swelling that allows the rhizodermis penetration, initiating the infection process. The zoospores can identify and infect susceptible and resistant *Castanea* roots as quickly as 3.5 h after root inoculation. Hyphae develop until they reach the vascular tissues of the susceptible European chestnut on the third day of infection. At this stage, *PC* switches from biotrophy to necrotrophy, characterized by cellular collapse and it starts producing resistance structures (chlamydospores) in *C. sativa* (Fernandes et al., 2021b). Chlamydospores allow *PC* to persist in plant material and the soil for up to 6 years (Zentmyer and Mircetich, 1966). In the resistant chestnut, *C. crenata,* the infection progress is slower because the host can induce early defense responses, such as callose deposition, hypersensitive response-like, and production of phenolic-like compounds. Nevertheless, *PC* can still reach the vascular tissues (Fernandes et al., 2021b). After reaching the vascular tissues of susceptible chestnuts, the pathogen continues colonizing the roots until it obstructs xylem vessels (Gomes-Laranjo et al., 2004), preventing root growth and interfering with water and nutrient uptake to the shoot. The roots and root collar start to rot, resulting in a progressive decline of the tree (Hardham, 2005). The first above-ground symptom is the chlorosis and wilting of leaves at the top followed by the dieback of branches, defoliation, and gradual decline until the host dies (**Figure 3**; Gomes-Laranjo et al., 2004). In resistant chestnuts the progression of the lesion caused by *PC* seems to stop at the roots or root collar level (Santos et al., 2015a), preventing further decline of the tree.

FIGURE 3
Castanea sativa shows symptoms of ink disease such as discoloration of leaves and dieback of branches. This picture was taken in Bragança, Trás-os-Montes region, Portugal.

Ink disease control

Control measures to prevent/restrain the pathogen have not been successful so far, mainly due to the easy development and migration of zoospores in humid conditions (especially during rainfalls) and to the resistance structures difficult to eradicate. Phosphite and metalaxyl have been the most efficient chemicals against *PC* [reviewed in Hardham (2005) and Hardham and Blackman (2018)]. However, the continuous use of these two chemicals has led to resistance development by the pathogen (Hardham and Blackman, 2018).

Until this date, there is no known effective biological control. Still, promising results were reported with soil inoculated with the bacteria *Byssochlamys nivea* or *Scopulariopsis brumptii*, which appears to decrease mortality in chestnuts inoculated with *PC* (Bosso et al., 2016). More common control approaches are the correct management of nurseries/orchards, the use of resistant rootstocks for propagation, or planting of resistant hybrids for production (Hardham, 2005).

Traditional breeding programs for *Phytophthora cinnamomi* resistance

In Europe several first-generation Euro-Asian hybrids have been produced by conventional breeding. Large backcross breeding programs have not been carried out to obtain a nearly wild-type disease-resistant European chestnut, and this may have cost a loss in specific characteristics of the European chestnut. However, many of the obtained hybrids have been successfully used as resistant rootstocks for European varieties, or as nut producing trees for having both resistance to the pathogen and sweet-tasting nuts. The most known example of this is the Euro-Japanese hybrid, CA04 or 'Bouche de Bétizac' (BB) developed by INRA (France) in 1962 (**Table 2**; Breisch et al., 1995). This hybrid became popular for having very large, sweet-tasting nuts and fast production. Cultivar selection has also been extensive in Italy, Spain, and Portugal, and regional favorites are developed mainly from local wild populations with large-caliber nuts.

In 1925 the first crosses started in France (Camus, 1929) and in 1926 started in Spain by Gallastegui, initiating the hybridization program between *C. crenata* and *C. sativa* (Pereira-lorenzo et al., 2010). After the 1940s, several breeding programs settled across Europe (Schad et al., 1952; Urquijo-Landaluze, 1957; Viéitez, 1960; Molina and Viéitez, 1967; Taveira-Fernándes, 1972; Salesses et al., 1993). Some of these programs obtained hybrid genotypes with low tolerance to cold (Breisch et al., 1995) and poor adaptability to the European environmental conditions in general, mainly because these were F1 hybrids (*C. crenata* × *C. sativa*) with 50% of their genetic information from Japanese chestnuts, a species with low tolerance to cold and drought (Fei et al., 2012). Several clones (111-1, 7521, 2671, and 1483) from Spanish breeding programs developed in the mid-20th century are still widely used as rootstocks for their high tolerance to ink disease and very high rootstock compatibility with fruit varieties (Serdar et al., 2019).

In Portugal, the first interspecific crosses were in 1947 by Bernardino Gomes, who used *C. crenata* (Tamba variety) as pollen donor (Vieira Natividade, 1947; Gomes Guerreiro, 1948, 1957). Later, in the 1990s, Professor Lopes Gomes started a breeding program at the University Trás-os-Montes e Alto Douro developing 53 genotypes resistant to ink disease (**Table 2**; Gomes Laranjo et al., 2007; Martins et al., 2009). More recently, in 2006, a breeding program was initiated (Costa et al., 2011) from which four F1 hybrids were selected for large-scale propagation due to their ability to multiply and root *in vitro*, field development and *PC* resistance levels (**Table 2**; Santos et al., 2015a; Fernandes et al., 2020a, 2021a).

As a consequence of breeding programs, the introgression of Asian alleles has been reported in a natural *C. sativa* forest (Alcaide et al., 2022). Adult and juvenile (offspring) trees were genotyped and *PC* resistance was detected. Back in the 1940s, *C. crenata* and *C. mollissima* were planted in the studied forest, which justifies the presence of only 70.6 and 28.6% of adults and juveniles, respectively, classified as pure *C. sativa* in this area. Alcaide et al. (2022) also reported more than 40% of juveniles as *C. sativa* × *C. crenata* hybrids and about 10% *C. sativa* × *C. mollissima* hybrids. Ten private alleles to Asian species were found in offspring, eight were exclusive to *C. crenata,* and two were found in *C. crenata* and *C. mollissima* species (Alcaide et al., 2022). The studied forest may benefit from the transfer of alleles involved in ink-disease resistance, and this advantage may be present in other European forests and orchards. However, more forest assessments should be performed to ensure that the European genotypes are not lost over generations.

Screening for *Phytophthora cinnamomi* resistant genotypes

With the increasing demand to support and accelerate breeding, phenotyping chestnut genotypes has been performed using different techniques. Symptom severity scales and measurements for subsequent accurate molecular marker: trait associations were reported turning screening for *Phytophthora* spp. resistance more efficient. Either by root inoculation of intact seedlings (Vettraino et al., 2001; Santini et al., 2003; Robin et al., 2006; Jeffers et al., 2009), root inoculation of rooted cuttings (Miranda-Fontaíña et al., 2007) or rooted shoots from *in vitro* culture (Cuenca et al., 2009; Santos et al., 2015a). Also, excised, or intact shoot from seedlings or clones were directly inoculated on its top (Ramos Guedes-Lafargue and Salesses, 1999; Fernández-López et al., 2001; Vettraino et al., 2001; Robin et al., 2006; Miranda-Fontaíña et al., 2007; Cuenca et al., 2009; Santos et al., 2015a). Phenotyping assays in chestnuts are usually performed at leaf-falling time (autumn) and after budburst (spring) (Santos et al., 2015a). According to Santos et al. (2015a), the root inoculation test was the best-resulted method to mimic the infection process in nature. However, this evaluation is expensive, laborious, and sometimes it is not feasible at the population level.

Studies performing the evaluation of responses after root inoculations reported a decrease in the severity of symptoms from the root to shoots. Also, different root-lesion phenotypes were observed depending on genotype susceptibility to the pathogen. The most resistant genotypes can confine or stop the spreading of the pathogen in the roots and from roots to root-collar, unlike the more susceptible ones that usually present their root system majorly affected, and consequently wilting of leaves (Miranda-Fontaíña et al., 2007; Santos et al., 2015a). Furthermore, control plants grow more than those subjected to inoculation (Robin et al., 2006; Miranda-Fontaíña et al., 2007; Santos et al., 2015a), which is expected as one of the consequences of the disease is the reduction of water and nutrient uptake, that consequently affects photosynthetic yield and plant growth (Santos et al., 2015a).

Depending on the phenotyping method (root or excised shoot), different metrics can be used to score the disease damage,

TABLE 2 Summary of efforts to control *Phytophthora cinnamomi*.

Source of resistance/ Plant material	Approach for improvement	Resources related to resistance			Current status/ Outcomes	References
		Marker type and loci	Gene	Gene function (putative)		
Castanea crenata	Controlled crosses with *C. sativa*	NA	NA	NA	F1 hybrids used as resistant rootstocks (e.g., Bouche de Bétizac)	Breisch et al., 1995
C. crenata	Controlled crosses with *C. sativa*	NA	NA	NA	53 resistant F1 hybrids (e.g., Colutad)	Gomes Laranjo et al., 2007; Martins et al., 2009
C. crenata *C. mollissima*	Controlled crosses with *C. sativa*	NA	NA	NA	SC55, SC914, SC1202 SM904: F1 hybrids with different levels of resistance	Costa et al., 2011; Santos et al., 2015a; Fernandes et al., 2020a, 2021a
BC_1F_1 *C. dentata* × *C. dentata-mollissima* 'Nanking'	Study genetic architecture of *PC* resistance; future MAS	SSRs LG_E	NA	NA	NA	Kubisiak, 2010
BC_1, BC_4 'Nanking' and 'Mahogany'		SNPs LG_E	NA	NA	NA	Zhebentyayeva et al., 2014
C. sativa × *C. crenata* F_1 hybrids		SNPs; EST-SSRs LG_E: (1) CC_3129_774 (2) CmSNP00773E (3) CC_48142_849 (4) CmSNP00522E (5) AC_32934_470 (6) AC_36335_960 LG_K: (7) CC_46475_1222 (8) CC_6279_2669 (9) AC_14650_453	NA	(1) Hormone signaling (2) PAF1 protein (3) Resistance protein NDR1/HIN1-Like protein 3 (4) Transport of phospholipids (5) Zinc finger, PHD-type (6) Contains a Myb/SANT-like domain (7) Uncharacterized (8) Cellulose synthase (9) Ribosomal_L6_N	NA	Santos et al., 2017b
BC_1F_1 BC_3F_1 *C. dentata* × *C. dentata-mollissima* 'Nanking' and 'Mahogany'		SNPs LG_A: hb52208; hb39959 LG_C: nk12394 LG_E: h25723; h54539; hb54410; jb79599; jb32342; jb43327; jb18453; jb13258; nk29352; nk35044; nk19473 LG_K: h31744; hb7814; hb27106	NA	NA	NA	Zhebentyayeva et al., 2019
C. crenata *C. sativa* *F1 hybrids*	Identification of resistance genes; future MAS	NA	(1) *Cast_C2CD* (2) *Cast_LRR-RLK* (3) *Cast_ABR1* (4) *Cast_Myb4* (5) *Cast_WRKY 31* (6) *Cast_RNF5* (7) *Cast_PE-2* (8) *Cast_Gnk2-like*	(1, 2) Pathogen recognition (3, 4, 5) Transcription factor (6) Ubiquitination regulator (7) Cell wall modification enzyme (8) Antifungal protein	NA	Santos et al., 2017a
C. crenata	Identification of resistance genes; future MAS	NA	*CcAOS*	Enzyme in JA pathway	Overexpression Increased tolerance in *Arabidopsis*	Serrazina et al., 2021

Source of resistance/plant material, approach for improvement, resources gathered, and current status and/or outcomes of these efforts are presented. NA, none applied. LG, linkage group; MAS, marker-assisted selection; JA, jasmonic acid.

and there are dissimilar opinions about which variable should be considered the main discriminator of resistance to *PC*. Previous studies specified the root or collar rot level should be considered the primary discriminator of resistance to *Phytophthora* sp. in chestnut (Robin et al., 2006; Miranda-Fontaíña et al., 2007; Cuenca et al., 2009). Other studies consider plant survival the primary indicator of resistance (Vettraino et al., 2001; Santos et al., 2015a). Santos et al. (2015a) stated the variable 'days of survival' was an excellent parameter to define resistance because the difference in the response of the genotypes is accentuated, and the heritability values are high (0.9 ± 0.04). In this work, shoot internal lesion-symptom was evaluated for the first time and it was considered crucial because it showed the advance of the disease lesion from roots and collar to aerial plant organs through the vascular system (Santos et al., 2015a).

Improving characterization of *Phytophthora cinnamomi* resistance

After realizing the importance of breeding for ink disease, North American TACF researchers started analyzing their trees from the backcross breeding program for *PC* resistance. In 2010, a preliminary study reported in a single major effect QTL in LG_E that explained more than 30% of the variation in a backcross population (**Table 2**; Kubisiak, 2010). These findings were later supported by Zhebentyayeva et al. (2014) who identified a major effect QTL for ink disease resistance in the same LG by studying several populations segregating for ink disease resistance (**Table 2**). In 2015, in Europe, Santos et al. (2015b) developed Simple-Sequence Repeats from Expressed Sequenced Tags (EST-SSR). These, together with Single Nucleotide Polymorphism (SNP) markers, were later used to construct an interspecific linkage map where two QTLs for *PC* resistance were identified (Santos et al., 2017b). The markers associated with QTL in LG_E and LG_K may enclose candidate genes to *PC* resistance, and genes putatively involved with the regulation of gene expression, respectively (**Table 2**; Santos et al., 2017b).

The arrival of next-generation sequencing revolutionized several research areas, including the detection and validation of genetic markers in wild and hybrid populations. Using GBS, Zhebentyayeva et al. (2019) increased the number of available markers for linkage analysis, mapping 7,715 sequence-based SNPs on eight parental genetic maps. Seventeen QTLs were associated with ink disease resistance on LG_A, LG_C, LG_E, and LG_K (**Table 2**). The most consistent QTLs were detected on LG_E and LG_K, which overlapped with QTLs previously reported by Santos et al. (2017b). The authors suggest the genetic architecture of *PC*'s resistance in Chinese chestnut × American chestnut hybrid progeny is due to some dominant QTLs together with quantitatively inherited partial resistance conferred by multiple small-effect QTLs (Zhebentyayeva et al., 2019).

In Europe, root transcriptomes of *C. crenata* and *C. sativa* inoculated and non-inoculated with *PC* were compared, resulting in the discovery of 283 differentially expressed genes as candidates for *PC* resistance (Serrazina et al., 2015). In 2017, eight of those genes were selected for further study and by using digital PCR their expression was evaluated in chestnut roots before and during infection (**Table 2**; Santos et al., 2017a). The authors suggest that European and Japanese chestnuts have the same defense mechanisms to *PC* but with different timings. The upregulation of a set of candidate genes after infection, such as *Cast_Gnk2-like* (anti-fungal function) and *Cast_C2CD* (pathogen recognition protein), suggests that *C. crenata* triggers HR-like cell death. The high expression of these genes in non-inoculated *C. crenata* compared to non-inoculated *C. sativa*, suggests improved constitutive defense mechanisms by the Japanese chestnut (Santos et al., 2017a). Indeed, these hypotheses were confirmed by Fernandes et al. (2021b) at the cellular level, who reported shared host responses in these two species following pathogen challenge (e.g., callose deposition and phenolic-like compounds accumulation). *Cast_Gnk2-like*, was identified as the best discriminator between susceptible and resistant genotypes to ink disease (Santos et al., 2017a), and efforts for the validation of its function in chestnuts are ongoing (**Table 2**; McGuigan et al., 2020). The gene *Allene oxide synthase* (*CcAOS*), an ortholog of a key enzyme of the JA pathway, was also selected from 2015 transcriptomes (Serrazina et al., 2015). The importance of this gene in plant defense responses against *PC* was demonstrated after being overexpressed in a susceptible *Arabidopsis* ecotype (Ler-0), resulting in a delay of infection progression and an increase in tolerance (**Table 2**; Serrazina et al., 2021).

Reports on ink disease molecular analysis discussed so far have been focused on root inoculations because it mimics what happens in nature. Saiz-Fernández et al. (2020) presented an alternative by inoculating European chestnut stems and collecting tissues bordering the infection site and away from it. Proteomic, metabolomic, and targeted hormone analysis showed that *PC* led to an accumulation of SA and JA and a massive reprogramming of the chestnut's proteome. Twenty-five proteins were identified as oppositely regulated in the areas next to and away from the infection site (Saiz-Fernández et al., 2020).

When studying plant-pathogen interactions, the first and most common approach is to unveil the host resistance mechanisms. To date, plant susceptibility (S) genes were only studied in a few woody species, as discussed by Pavese et al. (2021b). S-genes allow the compatibility of the pathogen to the host, facilitating infection. A mutated or lost S-gene may limit the pathogen's ability to induce host disease. The authors identified and characterized S-genes in *C. sativa* based on sequence homology, functional domain detection, and phylogenetic relationships. Transcript levels of S-genes after pathogen infection (both *PC* and *CP*) were generally higher in *C. sativa* when compared to *C. crenata*. Two genes were selected

for future studies on their putative role as S-genes in chestnut-pathogen interactions: *Powdery mildew resistance 4* (*pmr4*) and *Downy Mildew Resistance 6* (*dmr6*) which are suggested to act as negative regulators of SA pathway, consequently leading to susceptibility (Pavese et al., 2021b).

Genetic transformation as a tool for pathogen control

The emerging progress of genetic transformation systems for chestnuts has been an extremely encouraging story and nowadays genes can be tested for their ability to confer pathogen resistance. The progress of embryogenic regeneration systems for chestnut species [reviewed in Corredoira et al. (2017)] has provided fitting target material for transformation experiments. Carraway et al. (1994) did the first attempt on *Castanea* spp. genetic transformation, however, only obtained transgenic calli by using microprojectile bombardment in cultures of American chestnut. Since then, chestnut researchers have been dedicated to improving genetic transformation of this recalcitrant species. The first report of successful *Agrobacterium*-mediated transformation in *Castanea* spp. showed transgenic European chestnut shoots regenerated from hypocotyls but, transformation efficiencies were very low, and the number of chimeras was high (Seabra and Pais, 1998). This was followed by the transformation of European chestnut somatic embryos that were regenerated into whole plants and micropropagated (Corredoira et al., 2004). The authors recorded a maximum of 25% transformation efficiency after somatic embryo co-culture with *Agrobacterium* liquid suspension for 4 days (Corredoira et al., 2004). The first successful genetic transformed American chestnut was reported in 2006 by co-culturing somatic embryos with *Agrobacterium* liquid suspension (for 1 h) followed by a 2-day desiccation method (Polin et al., 2006). Rothrock et al. (2007) also transformed American chestnut by flooding the embryos with *Agrobacterium* liquid culture while still in semi-solid multiplication media. After these protocols, several works were published on the transformation of chestnut with pathogen resistance genes or to validate gene function. Genetic transformation studies for pathogen control are summarized in **Table 3**.

The rise of genetic transformation had a big impact, but public perception of the use of transgenes is not unanimous. Nowadays researchers are looking more into the use of cisgenes (transgenes from related species) (Corredoira et al., 2012, 2016; Steiner et al., 2017), trying to answer public concerns. Corredoira et al. (2012, 2016) obtained cisgene overexpressing lines with a (1) thaumatin-like protein (*CsTL1*) gene (**Table 3**; Corredoira et al., 2012); and (2) an endochitinase gene (*CsCh3*) (**Table 3**; Corredoira et al., 2016). More recently, McGuigan et al. (2020) transformed American chestnut with *Cast_Gnk2-like* (**Table 3**), a candidate resistance gene for *PC* (Santos et al., 2017a). In McGuigan et al. (2020) the authors also report two alternative methods for transformant selection by using liquid selection medium instead of semi-solid medium like the previously mentioned protocols. After the Agro-kill step, embryos were transferred to temporary immersion bioreactor systems (RITA® bioreactors, Sigma-Aldrich, St. Louis, MO, United States) or We Vitro containers cultivated by Magenta® (We Vitro Inc., Guelph, ON, Canada) where they were intermittently flooded and rocked, respectively. Although the treatments were not significantly different, the liquid medium protocols had more selection efficiency (McGuigan et al., 2020). As the genetic transformation techniques improve, targeted promoters that can replace the most common constitutive promotors also arise. An example of this is the *win3.12* inducible promotor from poplar (*Populus deltoides*), which has positively driven the gene oxalate oxidase (*OxO*) in American chestnut, showing a low level of baseline expression and being only induced by wounding and pathogen infection (**Table 3**; Carlson et al., 2021).

The genetically engineered American chestnut – The Darling 58

North American researchers have allied their breeding efforts to genetic transformation as this can be a quicker way to restoration when compared to just the traditional backcross breeding. In 1990, the TACF New York Chapter and the State University of New York-College of Environmental Science and Forestry (SUNY-ESF) started working on this alternative approach for restoration. A blight-resistant American chestnut tree (Darling 58, named after Herb Darling) was developed by genetic transformation (Polin et al., 2006; Rothrock et al., 2007; McGuigan et al., 2020) by adding to the genome a gene from wheat that encodes for a detoxifying enzyme, oxalate oxidase (*OxO*), to counter the major virulence factor of the pathogen (Powell et al., 2019). Oxalate oxidase degrades oxalic acid, a toxin produced by *CP* during infection (Rigling and Prospero, 2018), limiting the pathogen's damage without killing it. Currently, these trees are in regulated field plots awaiting deregulation for restoration purposes (**Table 1**; Newhouse et al., 2020). Crosses of transgenic chestnuts with wild-type American chestnuts are being performed in these plots (Westbrook et al., 2020a). The progeny is 100% American chestnut and approximately 50% of the offspring inherits *OxO* (which is rapidly detected by PCR or enzymatic assays; Zhang et al., 2013a). To increase genetic diversity, up to 4 transgenic chestnuts will be crossed with 1500 wild-type trees over up to 5 generations (Westbrook et al., 2020a). Transgenic pollen can be produced in less than a year (Baier et al., 2012; Pilkey, 2021), which helps expedite the process. Deregulation of the Darling American chestnut represents an important step toward restoring the species. However, public perception of introgressing a transgenic tree into the forest is not unanimous [discussed in Newhouse and Powell (2021)].

TABLE 3 Genetic transformation studies performed in European and American chestnuts with the goal of developing pathogen control strategies.

Explant	Approach	Gene (origin)	Gene function	Targeted pathogen	References
C. dentata somatic embryos	*Agrobacterium*-mediated transformation	*OxO* (wheat)	Detoxifying enzyme; degrades oxalic acid	*Cryphonectria parasitica*	Polin et al., 2006; Rothrock et al., 2007
					McGuigan et al., 2020
		OxO (wheat) (wound inducible promotor)			Carlson et al., 2021
C. sativa somatic embryos	*Agrobacterium*-mediated transformation	*CsCh3* (*C. sativa* cotyledons)	Chitinase-like protein; hydrolyses chitin from pathogen's cell wall	*Cryphonectria parasitica*	Corredoira et al., 2016
C. sativa somatic embryos	*Agrobacterium*-mediated transformation	*CsTL1* (*C. sativa* cotyledons)	Thaumatin-like protein; promotes osmotic rupture in the pathogen	*Phytophthora cinnamomi*	Corredoira et al., 2012
C. dentata somatic embryos	*Agrobacterium*-mediated transformation	*Cast_Gnk2-like* (*C. crenata* roots)	Antifungal	*Phytophthora cinnamomi*	McGuigan et al., 2020

Initial explant, inserted gene and origin, gene function, and target pathogen are presented.

Gene editing

Another exciting news for chestnut genome editing is the first proof of concept of CRISPR/Cas9, where the authors obtained albino plants by inducing a point mutation in *phytoene desaturase* (*pds*), a gene that disrupts chlorophyll biosynthesis (Pavese et al., 2021a). This new approach opens a new path for the functional characterization of genes involved in plant-pathogen interaction. The same research team characterized and selected two S-genes in *C. sativa* after *PC* and *CP* infection (*pmr4* and *dmr6* referred to in Section "Improving characterization of *Phytophthora cinnamomi* resistance"; Pavese et al., 2021a) which are potential candidates for functional characterization *via* CRISPR/Cas9 knockdown. This approach and the study of S-genes might help us understand if *PC* is adapted to the susceptible chestnuts and how it is interfering with their immunity and possibly inducing Effector Triggered Susceptibility.

Pests – *Castanea* spp. and *Dryocosmus kuriphilus*

The chestnut gall wasp *Dryocosmus kuriphilus* Yasumatsu, accidentally introduced into Italy and first reported in 2002 (Brussino et al., 2002), represents a limiting pest for the European chestnut, due to the severe yield losses it creates, as *C. sativa* has a low tolerance. **Figure 4** shows a chestnut infected by the gall wasp. It quickly spread to all Italian regions and later into the surrounding countries, causing a remarkable decrease in production (−60% in 2014 in Italy). Studies on biological control aimed at introducing the parasitoid wasp *Torymus sinensis* Kamijus, and also the genetic improvement for resistance to the cynipid were promptly started to solve the problem (Marinoni et al., 2020). The susceptibility to the chestnut gall wasp was evaluated in *C. sativa* and hybrid cultivars. Out of 62 cultivars, two *C. sativa*, one *C. crenata*, and four hybrids (*C. sativa* × *C. crenata*) showed total resistance (Sartor et al., 2015).

Resistance to the gall wasp was found in the hybrid cultivar Bouche de Bétizac (BB; *C. sativa* × *C. crenata*) (Dini et al., 2012) and studied by developing genetic linkage maps using a population derived from a cross between BB and the susceptible

FIGURE 4
Castanea spp. presenting a gall on the leaf (arrow) after *Dryocosmus kuriphilus* infection.

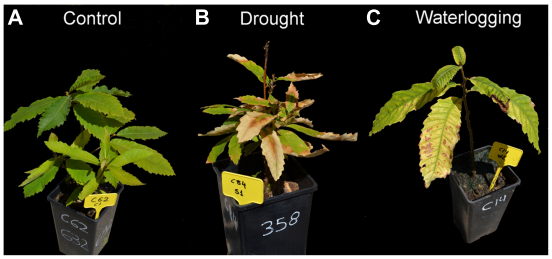

FIGURE 5
Castanea sativa seedlings under regular watering **(A)**, drought **(B)**, and waterlogging **(C)**, from Camisón et al. (2020). Control plants present green and turgid leaves. Leaves of drought plants present wilting and some may fall. Dieback can be observed. Leaves of plants with waterlogging present chlorosis, chlorophyll degradation in the central part of leaves, necrotic borders and senescence.

cultivar 'Madonna' (M; *C. sativa*) (Marinoni et al., 2020). The high-density genetic maps were constructed using double-digest restriction site-associated DNA-seq and simple sequence repeat markers. The map of BB consisted of 1,459 loci and spanned 809.6 cM; the map of 'Madonna' consisted of 1,089 loci and spanned 753.3 cM. In both maps, 12 linkage groups were identified. A single major QTL (Rdk1) was identified on the BB map, explaining up to 67–69% of the phenotypic variance of the resistance trait. The Rdk1 QTL region includes eleven scaffolds and two candidate genes putatively involved in the resistance (Marinoni et al., 2020). Acquadro et al. (2020) presented *de novo* assembly of the chestnut transcriptome of the resistant Euro-Japanese hybrid BB and the susceptible cultivar M, collecting RNA from buds, at different stages of budburst to investigate the plant response and understand which factors can lead the plant to develop or not the gall, to reconstruct the transcriptome of *C. sativa* buds under biotic stress (i.e., in the presence/absence of the chestnut gall wasp). The two transcriptomes were assembled into 34,081 (BB) and 30,605 (M) unigenes, respectively. The transcriptomes of both cultivars were properly assembled, and while the BB unigenes set was selected for the functional characterization, the M was just used for RNA-seq data analysis, highlighting the presence of 1,444 putative resistance gene analogs (RGAs) and about 1,135 unigenes, as putative miRNA targets. A global quantitative transcriptome profiling revealed some Gene Ontology enrichments as "response to stimulus" and "developmental processes" (e.g., post-embryonic development). Many up-regulated genes appeared to be transcription factors (e.g., *RAV1*, *AP2/ERF*, and *WRKY33*) or protein regulators (e.g., *RAPTOR1B*) and storage proteins (e.g., LEA D29) involved in "post-embryonic development." Dini et al. (2012) highlighted the occurrence of HR in BB as a response to the cynipid infestation, resulting in cell and larvae death. This fact was confirmed by Acquadro et al. (2020), since more than 100 genes appeared to be associated with "death" and "apoptosis" processes, including genes for HR response. The analysis was able to provide 7k simple sequence repeat SSR and 335k SNP/INDEL markers and generated the first reference unigene catalog for the European chestnut.

Gall wasp, apart from representing a severe constraint factor for the production of chestnut orchards, can also impact negatively the favorable effect of hypovirulence in *Cryphonectria parasitica*-*C. sativa* pathosystem, by the progressive weakening of the trees, caused by intensive attacks of *Dryocosmus kuriphilus*. Blight damage recurrences were observed in different Italian chestnut areas (in Piemonte, Trentino, and Toscana regions which were highly infested by the Chinese wasp; Turchetti et al., 2010). The use of effective biological control of the parasite with parasitoids like *T. sinensis*, is essential for the management of chestnut orchards to allow the survival of the trees and their productivity.

Abiotic stresses of *C. sativa*

The preponderance of reports on abiotic stresses focuses on the European chestnut. Since the beginning of the millennium and the awareness of climate change scenarios, studies on its impact on the species flourished (e.g., Casasoli et al., 2004; Lauteri et al., 2004). *C. sativa* is susceptible to climate change (Camisón et al., 2020; Castellana et al., 2021), raising the probability of abiotic stress events. Prolonged water deprivation or waterlogging and chill hour reduction, combined with rainfall deficit and extreme summer heat in Europe, may cause and prejudice nut and timber productivity and quality (Vázquez et al., 2016; Castellana et al., 2021). These extreme climate scenarios are predicted to be most frequent in Southern Europe (European Commission, 2022), where chestnut orchards have a great representation (Pérez-Girón et al., 2020). The review in this section will mainly focus on this European area.

Climate change is also predicted to significantly impact chestnut pests and pathogens (Burgess et al., 2017; Bonsignore et al., 2020), leading to differences in disease expressions since new strains and infection mechanisms are more likely to arise.

Three flexible domestication levels of *C. sativa* are considered: fruit orchards, coppice, and natural forests (Eriksson et al., 2005; Gomes-Laranjo et al., 2012). The flexibility among levels is related to the exchange of genetic material between the three types of populations, even though genetic variability is higher in natural forests (excluding the American species) and lower in orchards, which originated from domestication. Genetic variability encloses the capacity to adapt to adverse environmental conditions, maintaining homeostasis and reproduction, and the potential to evolve. Changes in morphology and physiology in response to abiotic stresses involve complex molecular processes under genetic and epigenetic control. Besides knowledge at the physiological level, knowledge of the response to the stress at the genetic and

molecular level in detail is essential to drive efficient tolerance to threatened species.

C. sativa natural adaptation to different environmental areas

The genetic resources of *C. sativa* natural populations represent the existing variation in adaptive traits (Eriksson et al., 2005). They may be the starting material for breeding programs to address tolerance to abiotic stress in elite varieties. Many studies characterize *C. sativa* ecotypes from the Iberian Peninsula, Italy, Greece, and Turkey (e.g., Villani et al., 1991; Eriksson et al., 2005; Fernandez-Lopez et al., 2005; Pereira-Lorenzo et al., 2011; Míguez-Soto et al., 2019; Castellana et al., 2021).

The environment influences adaptative traits such as annual biomass production, juvenile phenology growth, water use efficiency (WUE), and carbon isotype discrimination (Δ). European chestnut is a temperate-climate tree that requires relatively cool winters for dormancy and then warmer temperatures in spring, allowing physiological and phenological development as bud break, flowering, fruit set, and maturation (Gomes-Laranjo et al., 2012). Phenology depends on temperature, nutritional state, photoperiod, hormones, phytochromes, and others and can represent seasonal and environmental adaptation (Santamaría et al., 2009). WUE is the ratio of plant carbon (C) gain to water loss and is inversely related with Δ, which is affected by CO_2 assimilation and stomatal conductance (g_s) (Lauteri et al., 2004). From research mainly on non-cultivated populations, several European chestnut ecotypes are adapted to different climates, corresponding to different evolutionary pressures in the genome. In the Iberian Peninsula, Italy, Greece and Turkey, and based on morphological, physiological and/or molecular markers' studies (SSRs, EST-SSRs), hotter Mediterranean regions with lower water availability or drought drove populations to xeric ecotypes (early phenology, slow growth, high root development, high Δ, low WUE and longer juvenile periods). In comparison, populations in colder Atlantic regions with more water availability are mesophytic or mesic (later phenology, higher growth, low Δ) (Lauteri et al., 2004; Fernandez-Lopez et al., 2005; Gomes-Laranjo et al., 2012; Míguez-Soto et al., 2019; Camisón et al., 2021). Lauteri et al. (2004) suggest that mesic ecotypes respond strongly to favorable climatic conditions by increasing growth, while xeric ecotypes respond slowly to reduce the risk of damage after drought (e.g., xylem embolism, C starvation). This is in accordance with Pérez-Girón et al. (2020). They compared essential physiological parameters in orchards from two regions of the Iberian Peninsula: northern Spain and Portugal, and southern and central Spain. The authors found the highest annual photosynthesis rate and net primary production (net C stored after respiration and transformed into biomass) in the northern ecosystems. Water availability and temperature were the climatic variables that most influenced the two parameters.

Different European chestnut ecotypes may have origin in an overall high genetic diversity (Villani et al., 1991; Pereira-lorenzo et al., 2010; Cuestas et al., 2017; Poljak et al., 2017; Alessandri et al., 2020; Bouffartigue et al., 2020). Dinis et al. (2011a) and Pereira-Lorenzo et al. (2011) found, with the use of SSR markers, that the diversity in chestnut orchards was greatly due to hybridization and discretely due to mutations. *C. sativa* genetic diversity, with many alleles and a high level of polymorphism and heterozygosity (Casasoli et al., 2006), provides gene pools useful for establishing future conservation strategies. The ecotypes' traits correspond to adaptations that have the potential to be introgressed in threatened chestnut stands, potentially providing adaptation to climate change.

C. sativa response to drought

Most of the reports about *C. sativa* diseases related to abiotic stress describe the response to drought. *C. sativa* is strongly represented in the European Mediterranean area, which has been experiencing long and dry summers (high temperatures and low precipitation levels) with increasing drought conditions, causing a negative impact on *C. sativa* survival, productivity, and biodiversity (Ciordia et al., 2012; Alcaide et al., 2019; Castellana et al., 2021). *C. sativa* tree growth may be severely affected when the drought period is higher than two consecutive months (Menéndez-Miguélez et al., 2015), with most probable negative consequences on the development of leaves and fruits (Dinis et al., 2011a). Drought response is complex to analyze, as it may be influenced by population history, frequency of drought events, and phenotypic plasticity (Casasoli et al., 2006; Alcaide et al., 2019; Müller and Gailing, 2019).

Physiological and biochemical responses to drought

Martínez-Sancho et al. (2017) consider *C. sativa* a relatively anisohydric species in the physiological responses to high temperature and drought, meaning that stomata closing is not readily achieved after water deprivation unless under severe drought conditions. Low water potentials (Ψ) in seedlings resulted in an overall native loss of hydraulic conductivity and probable vessel embolism, accompanied by height and stem diameter decrease compared to controls. The authors suggest that the hydraulic conductivity can be potentially recovered in the next growing season with new earlywood vessels and xylem renovation.

Maurel et al. (2004) report that g_s, transpiration rate (E), hydraulic conductance (K) from soil to leaf, leaf Ψ, and root biomass decreased in *C. sativa* subjected to drought, whereas

abscisic acid (ABA) concentration in xylem increased. The authors also showed that g_s was regulated by the root-sourced ABA and by hydraulic signals, namely the relative sap flux from root to leaves. Leaf transpiration is an essential factor in establishing Ψ, or the flow of water from the soil to the roots, stems, leaves (stomata) and atmosphere, with the purpose of mineral uptake and regulation of leaf temperature. During water deprivation, E became seriously compromised, contributing to a significant decrease in overall plant metabolism and productivity (Gomes-Laranjo et al., 2012).

Ciordia et al. (2012) and Gomes-Laranjo et al. (2012) studied progenies of *C. sativa* cultivars (seedlings) from two areas in the Iberian Peninsula, North (Asturias and Galicia, with mesic or moderately humid environment) and Central/South (Canary Islands and Andalusia, with xeric and drier environment). Merging the results from both studies, restricted water supply reduced the Ψ, K (especially in xeric plantlets), CO_2 assimilation rate (A), E, g_s and, consequently, photosynthetic efficiency. Gomes-Laranjo et al. (2012) associated the reduced efficiency of Photosystem II (PII, low F_v/F_m) with an internal CO_2 concentration increase (Ci) and lower C assimilation, especially in Northern plant leaves. During water deprivation there is a need to reduce light absorption to avoid heat accumulation, resulting in the reduction of PSII efficiency or even photooxidative reduction in extreme conditions. An expected consequence is a reduction of growth (height and dry weight, except stem diameter) (Ciordia et al., 2012). Also, both studies found a reduction of leaf area, number (with no leaf fall) and sprouting, attributed to lower absorption of nutrients. The morphology of the leaves suffered modifications, with an increase in leaf lobation, resulting in a smaller boundary layer and more efficient heat exchange. The root:shoot ratio increased due to biomass distribution changes in response to the low water content in the soil, promoting root biomass that may improve the capacity to absorb water (Ciordia et al., 2012). The same authors consider that the north cultivars are more tolerant to drought than the Central ones, as the first demonstrated a better ability to recover Ψ after re-watering. Both mesic and xeric groups demonstrate phenotypic plasticity that is consistent with the genetic variation found using SSR and EST-SSR (Martin et al., 2010; Pereira-lorenzo et al., 2010), providing such stands the potential to respond to drought stress (Ciordia et al., 2012).

Camisón et al. (2020) (**Figure 5**) found that in drought-tolerant *C. sativa* seedlings (of the xeric ecotype from central Spain) the g_s was close to zero, associated with a decrease in relative water content (RWC), height and weight loss, increase in stem diameter, leaf wilting with occasional drop and plant dieback. Stomatal closure was associated with the reduction of A and soluble sugar accumulation in leaves, which may impair C supply. The authors suggest that soluble sugar accumulation in leaves and stems may have a role in plant osmoregulation. A decrease in leaf biomass was accompanied by an augment in nitrogen (N) levels in leaves due to N transport from senescent to green leaves. The peak of soluble sugar levels in leaves and stems coincided with the highest reduction in starch levels, probably due to starch mobilization as a source of soluble sugars for cell metabolism, osmotic adjustment, and consequent xylem vessel water refilling after drought-induced embolism. High respiration levels in stressed plants are related to the metabolism of soluble sugars to counteract the stress. The authors did not observe changes in total carbohydrate content or C starvation attributable to drought-tolerant species in non-extreme drought conditions.

Economically important chestnut orchards for nut production in Southern Europe are distributed through regions of provenance, many with several decades old, and established recurring to grafting without a conscient concern about the effects of global climate change. Camisón et al. (2021) analyzed if drought tolerance in *C. sativa* could be improved using drought-tolerant scions and rootstocks from xeric populations (X) from southern Spain, in comparison with drought-sensitive scions and rootstocks from humid populations (H, with mesic ecotype) from northern Spain, based in the research of Alcaide et al. (2019). Grafted and non-grafted 2 years old plants were used in the drought treatments. When X scions or rootstocks were used in these conditions, budbreak occurred earlier, and higher g_s and lower plant mortality were observed. *C. sativa* families of X origin advance budbreak phenology and may be used to induce early flushing in scions of H origin. Benefits could be attributed to the use of X rootstocks to advance budbreak in mesic areas, especially if enhanced growth, flowering, and fruit production are obtained. Grafted plants with X rootstocks (H/X and X/X) showed higher A, g_s, F_v/F_m of PII and leaf RWC than plants with H rootstocks (X/H and H/H). Rootstocks from xeric areas increase drought tolerance and survival of the more drought-susceptible material of mesic origin. On other hand, H used as rootstock lead to minimum values of leaf RWC and F_v/F_m levels, confirming its susceptibility to drought. Concerning scion, grafts with X rootstock wilted less than grafts with H rootstocks. Scions of xeric origin may also have the potential to improve drought-susceptible rootstocks. Grafting may be implemented as an adaptative tool to surpass climate change's effects (Camisón et al., 2021).

Camisón et al. (2021) also analyzed constitutive and drought-induced hormones [ABA, SA, JA, its conjugate (+)-7-iso-jasmonoyl-L-isoleucine (JA-Ile)], and the amino acid proline in leaves and roots of grafted and non-grafted plants of X and H origin. Before drought induction, in watered plants, leaf ABA and proline contents were higher in X than in H plants, in non-grafted and grafted material. The constitutive higher levels of ABA in X material may have contributed to lower g_s and the delay in plant dehydration in X rootstocks after drought treatment (Allario et al., 2013). The same rationale may be applied to proline, which may have conferred to X rootstocks a more effective osmotic adjustment when drought was applied (Amudha and Balasubramani, 2011). After drought treatments,

ABA and proline levels increased in leaves and roots of all materials. H/H plant presented the highest levels of ABA in roots and proline in leaves, which points to extreme stress. SA levels were higher in H, H/H and X/H plants. SA increase along with ABA has been reported in citrus response to drought (Santana-Vieira et al., 2016; Neves et al., 2017). JA-Ile level was higher in leaves, especially in H/H plants. JA-Ile in leaves under drought stress, allied to ABA, is involved in stomatal closure modulation (de Ollas et al., 2013). JA-Ile and JA levels in roots generally decreased, and the lowest value was found in H and H/H plants. More studies are needed to understand the hormone crosstalk in *C. sativa* response to drought.

Genomic aspects of drought response

Casasoli et al. (2004) performed a QTL analysis for three adaptative traits (bud burst, growth, and Δ), for 3 years, in an F1 progeny of *C. sativa* originated from two Turkish populations adapted to drought (female parent) and humid (male parent) environment. Thirty-five distinct QTLs were identified for phenology, 28 for growth, and 17 for Δ. The authors report phenotypic correlations and co-localization among QTLs for the three adaptative traits related to the genetic adaptation of the female parent to drought. Moreover, the adaptative traits seem to be regulated by several genes or gene groups of low and moderate effects, suggesting that the adaptation, and consequently the response to abiotic stress at the genetic level is highly complex in chestnuts.

Santamaría et al. (2011), after analyzing the transcriptome of dormant and non-dormant tree buds in *C. sativa* trees of Asturias (North of Spain), suggest that bud dormancy is associated with abiotic stress tolerance. There was a high representation of genes involved in low-temperature stress and dehydration protection of cellular structures: Late embryogenesis abundant proteins (*LEA*), including Dehydrins and Em protein, Heat shock proteins (*HSP*), and transcription factors that control the expression of HSPs [reviewed in Kalemba and Pukacka (2007)]. Also, galactinol synthase (*GOLS*) and Raffinose family oligosaccharides (*RFOs*) are involved in desiccation tolerance through protection to oxidative damage (Vinson et al., 2020).

Alcaide et al. (2019) quantified drought response in populations of *C. sativa* localized in contrasting environment regions of the North (lower average temperature and higher precipitation level) and South (higher average temperature and lower precipitation level) of Spain. In 1-year-old seedlings from selected trees, they found a direct correlation between leaf wilting and resprout with survival, indicative of drought tolerance. Individuals from populations in the South with xeric ecotype, thriving in severe drought conditions, were selected as a drought-tolerant resource. Allied to the data on phenotypic tolerance to drought, EST-SSR MAS permitted separation of North and South populations. Four markers were classified as significantly involved in the differentiation of *C. sativa* individuals to drought tolerance (**Table 4**). *FIR080* showed one allele for drought susceptibility and may correspond to a *Ricin B-like lectin EULS3*, involved in drought stress response through stomatal closure in *Arabidopsis thaliana* (van Hove et al., 2015). *VIT057* corresponds to *Ethylene-responsive transcription factor ERF017*, may act as a transcriptional activator and may be involved in gene regulation by stress factors[1]. *GOT045*, a *probable E3 ubiquitin-protein ligase*, may be involved in regulating ABA-mediated drought stress through ubiquitination (Lee and Kim, 2011; Seo et al., 2012). *FIR059* is putatively linked to the RH7 gene of the DEAD-box-RNA helicase family, which has been implicated in RNA processing and related to abiotic stress responses (Kim et al., 2008). Three alleles of *FIR059* were linked to drought-susceptible individuals, while two alleles were linked to drought-tolerant ones. *FIR059* is pointed as the best marker to identify putative drought-tolerant unstressed trees.

Castellana et al. (2021) associated *C. sativa* EST-SSR markers previously related with drought stress (Martin et al., 2010; Alcaide et al., 2019) with xeric or mesophytic natural populations in Spain, Greece and Turkey. Those EST-SSRs differentiated three genetic clusters: group I form areas with low precipitation and high temperatures along the year (**Table 4**); group II with low temperatures and low precipitations; and group III with moderate-low temperatures and high precipitations. Relations were found between climatic variables and alleles in the locus *FIR059* above mentioned: allele 152 was associated with heavy rain, allele 181 with warm and dry areas, and allele 185 with mild temperatures. Moreover, alleles 152 and 176 were associated to drought-tolerant plants, while allele 160 was linked to drought susceptibility.

C. sativa response to waterlogging

Global climate change will cause, among others, extreme rainfall events with a higher probability of long-term waterlogging in winter and spring, and short-term flooding events during summer (Christensen and Christensen, 2003; Kundzewicz et al., 2005). As *C. sativa* naturally grows on well-drained mid-sloped soils, it has a low tolerance to waterlogging (Glenz et al., 2006). Chestnut orchards established in floodplains can be severely affected by soil flooding, and there are still few studies that characterize the species response to this abiotic stress. Camisón et al. (2020), already mentioned before for analyzing drought stress in *C. sativa*, also analyzed waterlogging effects. The two stresses caused some analogous effects on 1-year-old seedlings with progeny from central Spain, with xeric ecotype: reduced g_s, A, and growth. The main negative effect of waterlogging in trees is oxygen deprivation in roots (hypoxia, Kreuzwieser and Rennenberg, 2014), causing a decrease in root

1 https://www.uniprot.org/uniprotkb/Q84QC2/entry

TABLE 4 Summary of the tolerance to abiotic stresses in *Castanea sativa* and *C. dentata*.

Abiotic stress/ Source of tolerance	Approach for improvement	Resources related to resistance			References
		Marker type and loci	Gene	Gene function	
Drought					
Castanea sativa forest populations, xeric ecotype, Hervás (Central Spain)	NA	NA	NA	NA	Camisón et al., 2020
Castanea sativa forest populations, xeric ecotype: Constantina, Sierra Norte (South Spain), Hervás (Central Spain), Holomontas Hortiatis (North Greece), Bursa (Northeast Turkey)	Identification of tolerance genes	EST-SSR MAS: *FIR080*, *VIT057*, *GOT045*, *FIR059*	*Ricin B-like lectin EULS3; Ethylene-responsive transcription factor ERF017; probable E3 ubiquitin-protein ligase; RH7* gene of the DEAD-box-RNA helicase family	Stomatal closure; transcriptional activator regulated by stress factors; regulation of ABA-mediated drought stress; RNA processing related to abiotic stress responses.	Alcaide et al., 2019; Castellana et al., 2021
Castanea sativa forest populations, xeric ecotype, Constantina (South Spain)	Future grafting: rootstocks and scions	NA	NA	NA	Camisón et al., 2021
Castanea dentata forest site, Reedsburg, WI, United States	Future breeding for introgression of trait in hybrids of *C. dentata* × *C. mollissima* resistant to *CP*	NA	NA	NA	Bauerle et al., 2006
NA	Future seedling inoculation with ectomycorrhizal fungi	NA	NA	NA	Aryal, 2017
Heat and cold					
n.a.	Identification of tolerance genes	NA	Small heat-shock protein *CsHSP17.5*	Prevent irreversible aggregation reactions between stress-labile proteins, maintaining the cytosolic proteins soluble	Soto et al., 1999
Heat					
Castanea sativa forest populations, xeric ecotype: Almería (South Spain)	Identification of tolerance genes	EST-SSR: *VIT099*, *POR016*	*NAC domain-containing protein78*; heat shock protein 70k (*HSP70*)	Regulation of flavonoid biosynthesis and 20S and 26S proteasomes in response to photooxidative stress; involved in stomatal closure and modulation of ABA-dependent physiological responses that may result in, e.g., thermotolerance	Dorado et al., 2022
NA	Future soil fertilization with Si	NA	NA	NA	Gomes-Laranjo et al., 2018

Sources of tolerant material, genomic data and possible solutions for stress mitigation are presented. Only references directly related to the respective stress are considered. NA, none applied.

hydraulic conductivity, xylem sap flow, and phloem transport. Consequently, the first responses to waterlogging include stomatal closure, followed by a decrease in net CO_2 assimilation and transpiration. The decrease in g_s was not associated with low water content in soil/roots, and Camisón et al. (2020) point to the involvement of chemical signals that regulate g_s in waterlogged plants.

Contrary to *C. sativa* plants with drought stress, lower N content and C/N ratio in leaves of waterlogged plants were observed (Camisón et al., 2020; **Figure 6**). This can also be attributed to the disturbances in CO_2 processing and N uptake by roots. There was also an initial augment of soluble sugar content in all tissues (glucose and sucrose) in waterlogged plants and later an accumulation of starch in stems and

FIGURE 6
Castanea sativa seedling under heat stress conditions described in Dorado et al. (2022).

roots. This was attributed to an active allocation of C for reserve formation, given the low A rates, and the inability of *C. sativa* to use carbohydrates for respiration and growth during waterlogging. Typically, susceptible plants decrease the activities of key enzymes for glycolysis in leaves and roots during the stress, not stimulating fermentative pathways as an alternative to producing energy (ATP) (Kreuzwieser and Rennenberg, 2014). Although and unexpectedly for susceptible plants, chestnuts formed aerenchyma at the root collar, pointing to the ability of the use of soluble sugars as C sources. When compared to drought-stressed plants, reduced respiration rates in waterlogged chestnuts, were attributed to a low use of soluble carbohydrates, as already mentioned. Another effect in *C. sativa* waterlogged plants was chlorophyll degradation (Camisón et al., 2020). This effect, allied to soluble sugar accumulation in leaves, may have resulted in A reduction. A visible related symptom in waterlogged plants was leaf shedding and chlorosis.

Camisón et al. (2020) consider that the susceptibility of *C. sativa* to waterlogging is related to the residual use of non-structural carbohydrates and the active allocation of C to reserve formation, resulting in an overall dropdown of net primary production and growth. Stress-sensitive trees cannot maintain carbohydrate availability resulting in the decrease of anabolic processes and the dieback of stressed tissues (Kreuzwieser and Rennenberg, 2014).

As drought stress response, the waterlogging stress response, is a highly complex process at the molecular and metabolic levels. The physiological adaptations of trees to waterlogging have a lack of data and data interpretation at the -omics level to advance in the understanding of the tolerance processes that serve as guidance to tree improvement programs.

C. sativa response to heat, cold and salt stress

Soto et al. (1999) describes *C. sativa* response to heat, cold and salt stress. The study focuses on a small heat-shock protein (sHSP) gene purified from mature *C. sativa* cotyledons, named *CsHSP17.5*. sHSP are stress-inducible proteins that can prevent irreversible aggregation reactions between stress-labile proteins, maintaining the cytosolic proteins soluble. They are also denominated ATP-independent molecular chaperones (Santhanagopalan et al., 2015). *CsHSP17.5* was overexpressed in *Escherichia coli* and improved viability under heat stress at 50°C and cold stress at 4°C. On the other hand, *C. sativa* seedlings under 1 year-old were subjected to heat-stress treatments (32°C or 40°C and 80% of relative humidity for 8 h), cold-treatments (4°C for up to 4 weeks) and salt-stress treatments (watering with 200 mM NaCl for up to 48 h). In vegetative organs of chestnut plantlets, transcripts hybridized with a *CsHSP17.5* cDNA probe in heat, cold, but not in salt stress. Despite the complexity and polygenic response of plants to abiotic stresses, *CsHSP17.5* is an interesting candidate to consider for biotechnological approaches to chestnut improvement to heat, drought (to which heat is mostly allied) and cold stresses (**Table 4**).

In a just released report (Dorado et al., 2022) where heat stress was tested, a significant increase in the osmolyte proline was observed in *C. sativa* leaves from humid forests, less thermophilic-tolerant. No variation was noted in *C. sativa* of xeric origin. Two EST-SSR markers are suggested to be included in the early selection of tolerant chestnuts to heat stress: locus *VIT099* (NAC domain-containing protein 78) and *POR016* (Heat shock protein 70 k) (**Table 4** and **Figure 6**).

Cumulative abiotic and biotic stresses may impact chestnut populations

Natural populations of European chestnut seem to adapt better to dry climates than to waterlogging (Vázquez et al., 2016; Camisón et al., 2020). Waterlogging is especially challenging for chestnuts susceptible to *Phytophthora* spp. growing in favorable edaphoclimatic conditions, as the pathogen causes high mortality in those scenarios (Vázquez et al., 2016). Drought and waterlogging negatively influence plant growth and induce loss of plant vigor, which causes susceptibility to pests and diseases (Maurel et al., 2001; Gomes-Laranjo et al., 2004, 2012; Dinis et al., 2011b).

C. sativa infected with hypovirulent strains of *CP*, located in the Central Eastern Alps in Italy, showed increased mortality

caused by a synergistic effect of blight infection and drought stress (Waldboth and Oberhuber, 2009). The trees were standing in regions with low precipitation during winter and high temperatures in spring and summer. Gomes-Laranjo et al. (2004) suggest that *PC* infectious capacity may increase with drought and heat, as plants have superior water uptake by roots and higher E, and the root damage caused by the pathogen action may accelerate plant decay. Moreover, Vázquez et al. (2016) report that if drought-stressed *C. sativa* seedlings are infected with *PC* and drought conditions are prolonged or waterlogging is applied, the mortality caused by the pathogen is highly significant.

Camisón et al. (2019) made an interesting study in which they assessed the drought stress tolerance in offspring of *PC*-infected *C. sativa* trees (from a forest in Southwest Spain of the xeric ecotype). Despite the increased tolerance to the pathogen in 1 year-old plants, suggesting the response was triggered in the subsequent generation, increased tolerance to water stress was not verified, therefore the infection did not influence dehydration stress memory.

Asian Chestnut species have different edaphoclimatic growth conditions when compared to *C. sativa*, being adapted to more humid environments. Pereira-lorenzo et al. (2010), Fernandez-Lopez (2011) and Vázquez et al. (2016) reveal that Euro-Asian hybrids bred for *PC* resistance, are susceptible to the frequently occurring summer water stresses in Southern latitudes of Spain. Deep studies on the impact of abiotic stresses in those hybrid clones cultivated in Europe, compared to *C. sativa*, need to come to light.

Contrary to the chestnuts in Europe, a different positive scenario occurs for the *C. dentata* x *C. mollissima* blight-resistant hybrids of the backcross breeding program previously mentioned. These hybrids, ∼94% *C. dentata* and 6% *C. mollissima*, are indistinguishable from the original *C. dentata*. Bauerle et al. (2006) studied the ecophysiological response of *C. dentata* seedlings to drought. They found that seedlings can decrease g_s and maintain Ψ, permitting a balance between transpiration and photosynthesis rate (A), and consequently increase WUE and C gain. The results point to drought tolerance of *C. dentata*, and if the trait is introgressed in blight-resistant hybrids, the reintroduction of the species in climate change scenarios predicted for the native *C. dentata* sites of the eastern United States may be facilitated (Brown et al., 2014) (**Table 4**).

Mitigation of abiotic stresses

Castanea mycorrhizae as sustainable helpers in the defense against abiotic stress

Arbuscular mycorrhizal fungi (AMF) are part of the soil microbiome and the symbiotic association with the rooting system of forest species is essential to plant nutrition and growth. AMF also helps recovery of abiotic stresses in plants, such as drought, flooding, extreme temperatures, salinity, heavy metals (Diagne et al., 2020), and biotic stresses caused by soil pathogens such as *PC* (e.g., in *C. sativa*, Branzanti et al., 1999). Equally important is that AMF improves soil aggregation and establishes interactions with beneficial soil microorganisms, upgrading the ecosystem (Diagne et al., 2020).

The AMF increases plant tolerance to extreme temperatures (heat and cold) by maintaining water and nutrient uptake, photosynthesis capacity, alleviating oxidative damage, increasing osmolytes' level, and consequently, improving growth. In plants subjected to high salinity, AMF enhances water and nutrient uptake, the accumulation of osmoregulators such as proline and sugars, and ionic homeostasis, including reducing Na^+ and Cl^- uptake (Diagne et al., 2020).

C. dentata × *C. mollissima* seedlings inoculated with ectomycorrhizal fungi (*Pisolithus tinctorius* and four *Rhizopogon* species), and subjected to drought, recovered faster than non-inoculated plants after rewetting (Aryal, 2017) (**Table 4**). The author based the conclusions on chlorophyll fluorescence levels (F_v/F_m).

At the genetic level, *C. sativa* in symbiosis with the AMF *Pisolithus tinctorius* may regulate the expression of genes related to abiotic stress (Sebastiana et al., 2009), as *Cystatin*, coding a cysteine protease inhibitor that may limit stress-induced proteolysis (Kunert et al., 2015), and *Lipid transfer/seed storage/trypsin-alpha amylase inhibitor*, corresponding to soluble proteins that facilitate the transfer of fatty acids (García-Olmedo et al., 1995). Curiously, Pernas et al. (2000) reported that non-mycorrhized *C. sativa* plantlets subjected to cold-, saline- and heat-shocks strongly upregulated a cystatin in roots and leaves, pointing to a relevant role of cystatins in abiotic stress mitigation.

Silicon fertilization as a prophylactic agent against abiotic stresses

Silicon (Si) is being studied as an ally for the resilience of crops to abiotic and biotic stresses, such as drought, high temperature, cold, salinity, heavy metal toxicity [reviewed in Choudhury et al. (2020)] and fungi, bacteria and herbivores [reviewed in Ma (2004)]. Recently it has been found that the described effects of Si in the alleviation of abiotic and biotic stresses are related to the modulation and regulation of genes involved in photosynthesis, transcription, water transport, phenylpropanoid- and ABA-dependent pathway (Manivannan and Ahn, 2017).

Zhang et al. (2013b) evaluated the foliar application of Sili-K solution on leaves after short but intense water deprivation, in potted plants of the genotype Ca90 (*C. sativa* × *C. crenata*, *PC*-resistant). They observed mitigation in heat stress: the

improved leaf growth was related to the increase in A. Si may have increased g_s and E, allowing more CO_2 to enter in the leaf, decreasing leaf temperature and increasing the transport of nutrients to leaves, respectively. The improved A was also associated with higher F_v/F_m of PSII and chlorophyll a and b content, suggested by a higher proportion of stacking in thylakoid membranes with less photo inhibitory damage. Moreover, Si may participate in the thermal stability of phospholipids in membranes. However, the foliar application of Si also increases the susceptibility to drought. Si application in potted plants with restricted space for root growth resulted in a lower concentration of soluble sugars, which was related to a lower osmotic pressure that may have decreased the cellular turgor and lowered leaf sap osmotic pressure, causing the plant to lose water more quickly (Zhang et al., 2013b).

Gomes-Laranjo et al. (2018) noted that chestnut roots have a good ability to absorb and accumulate Si in the plant. Two-month-old *C. sativa* were subjected to high temperatures and the soil was fertilized with Si. The authors observed the deposition of phytoliths in leaves and conducting vessels, which was associated with the increase of chlorophyll a/b and carotenoid content, and with the protection of the photosynthetic apparatus from oxidative damage. Also, a lower decrease in A and the increase of WUE was reported when compared to non-fertilized plants. The presence of phytoliths was also involved in the regulation of the stomatal movement, increase of cuticle thickness, and decrease in water loss, related to the lower values of *E* and g_s. Moreover, Si fertilization resulted in plants with a higher level of unsaturated lipids, improving membrane stability and integrity under high temperatures (Gomes-Laranjo et al., 2018) (**Table 4**).

In a later report, (Carneiro-Carvalho et al., 2019) verified the recovery capacity of 2-month-old *C. sativa* plants after a turnover from a high temperature to an adequate temperature. Si-fertilized plants showed a better recovery rate when compared to non-fertilized plants, reducing the oxidative damage and improving osmoregulation through the increase in the activity of antioxidant enzymes and metabolites such as catalase, ascorbate peroxidase, peroxidase, and phenols. These may have contributed to the reduction of electrolyte leakage, lipid peroxidation, and reactive oxygen species content.

Si fertilization seems to be absent of negative secondary effects for the environment or human health, making it sustainable for agriculture purposes.

Conclusion and future perspectives

Although many biotic and abiotic stresses threaten chestnuts, many efforts are being developed to overcome the challenges and save these important species. The incidence of *PC* and *CP* infections might become more severe in the context of climate change with the possible rise of new strains. Increasing the number of genetic and genomic resources combined with the development of high-throughput phenotyping technologies will help us reach marker-assisted selection (MAS). Screening individual trees within a breeding population and identifying the genetic basis of important traits should become faster, possibly reducing the number of BC needed in traditional breeding programs. The *de novo* transcriptome assembly provided a significant contribution, however, future studies can now rely on genomes of *C. mollissima* (Xing et al., 2019; Staton et al., 2020), *C. crenata* (Shirasawa et al., 2021), and *C. dentata* (Sandercock et al., 2022).

The potential of new approaches such as CRISPR/Cas systems in trees can result in desired changes such as introducing a gene of interest or targeted gene(s) knockouts of undesirable genes in plants (Limera et al., 2017). Added to gene silencing, the activation of genes and overexpression of proteins can be achieved by CRISPR/dCas9 (nuclease-dead Cas9), conferring new possibilities for gene functional analysis and characterization (Moradpour and Abdulah, 2020). The integrated use of these technological developments with biotic and abiotic stresses will help expand our capabilities of response to chestnut challenges.

The next steps for chestnut breeding may include improving resistance to both pathogens and looking for durable resistance. After screening Asian-American hybrid seedlings with improved blight resistance to *PC*, TACF found out that many of their hybrids were resistant to the oomycete (Zhebentyayeva et al., 2014, 2019). Researchers now believe that traditional breeding could be used to combine resistance (Steiner et al., 2017). It is also suggested that this could be achieved by stacking multiple resistance genes now that chestnut genetic transformation techniques have been optimized (Powell et al., 2019; McGuigan et al., 2020). There is also an increasing interest in cisgenes possibly because the deregulation process would be more straightforward. Moreover, the public perception may not be as fragmented as it is on the use of transgenics. Stacking cisgenes related to different defense mechanisms can help enhance resistance by different mechanisms. However, it is not expected that any of these genes will confer full resistance to the pathogens. For example, *OxO* is still the gene demonstrating the highest levels of resistance to blight disease (Steiner et al., 2017). Thus, we should just take advantage of all tools and combine transgenes and cisgenes.

The future roadmap for *Castanea*-pathogen studies may benefit from exploring the pathogen's virulence/avirulence factors specific to chestnut interactions. The available genomes of *PC* (Engelbrecht et al., 2021) and *CP* (Crouch et al., 2020) may bring some insight. Additionally, dual RNA sequencing enables the determination of responses and changes in the cellular networks of both organisms, which has already

helped understand ink disease in other plants (Meyer et al., 2016; Evangelisti et al., 2017). Identifying *CP* molecular weapons might increase the understanding of the vegetative incompatibility system. Consequently, this may improve hypovirulence biological control in North America where there is high vegetative incompatibility among the fungus strains (Milgroom and Cortesi, 2004). Success with hypovirulence may help keep the surviving American chestnuts alive while breeding for blight resistance is still ongoing.

It is also important to start making more efforts toward the understanding of gall wasp. Sequencing the genome of Ozark chinquapin (*C. ozarkensis*) will be an important tool since this species of chestnuts is resistant to the gall wasp (Anagnostakis, 2001).

The response of plants to abiotic stress is complex, and its complexity rises in tree species with long life cycles as chestnuts. In the case of *C. sativa*, there is a lack of systematic research on expressed genes and proteins, and involved metabolites and microbiome, allied to morphological and physiological responses to abiotic stresses. More studies in these subjects would permit directional genetic modification strategies for a more expedited species improvement besides breeding strategies (**Figure 1**), to cope with the rapidly advancing global climate change.

The chestnut species with more reports on abiotic stresses is *C. sativa*, most of them related to drought. Advances have been made in QTL identification and MAS has been used, however, a small number of genes involved in drought tolerance have been identified. The molecular markers used, reflect a limited part of the genome for such a complex stress. GBS of large sets of individuals was already used in *Castanea* species. This cost-effective technique could potentially improve the estimation of genetic diversity based on hundreds to thousands of genetic markers (Müller and Gailing, 2019).

Ultimately, global climate change will differently affect the ecosystems in which chestnut stands. Chestnut may adapt *via* alterations of physical traits, or it will occupy other ecosystems in new favorable geographical locations. The latter may be the most probable hypothesis (Pérez-Girón et al., 2020), which may guide the establishment of new chestnut orchards. The established regions of chestnut provenance are at risk of being seriously affected or even eliminated with climate change (Pérez-Girón et al., 2020). Their resilience and adaptation will depend on the extension of the climatic variations.

The contributions gathered for the past 40 years have given chestnut researchers great tools to support restoration and programs for developing sustainable control measures of biotic and abiotic stresses. This research also represents valuable knowledge that may be applied to other forest species, mainly related members of the Fagaceae family.

Author contributions

PF wrote the introduction. PF and MC compiled and wrote the information regarding the biotic stresses. SS compiled and wrote the information regarding the abiotic stresses. RC compiled the work done on Dryocosmus kuriphilus. All authors reviewed the successive drafts of the manuscript, contributed to the article, and approved the submitted version.

Funding

This publication was funded by Fundação para a Ciência e Tecnologia (FCT/MCTES/PIDDAC, Portugal) under the project 414103 FCT-Lx-FEDER-28760, Ph.D. grant SFRH/BD/115424/2016 (awarded to PF) and work contract 2477 of the contract-program 12345/20181 defined by DL nr. 57/2016 (awarded to SS).

Acknowledgments

The authors would like to thank Alejandro Solla and Javier Dorado [Faculty of Forestry, Institute for Dehesa Research (INDEHESA), Universidad de Extremadura, Spain] for gently providing images for **Figures 5**, **6**.

Conflict of interest

The authors declare that the research was conducted in the absence of any commercial or financial relationships that could be construed as a potential conflict of interest.

Publisher's note

References

Acquadro, A., Torello Marinoni, D., Sartor, C., Dini, F., Macchio, M., and Botta, R. (2020). Transcriptome characterization and expression profiling in chestnut cultivars resistant or susceptible to the gall wasp Dryocosmus kuriphilus. *Mol. Genet. Genomics* 295, 107–120. doi: 10.1007/s00438-019-01607-2

Alcaide, F., Solla, A., Cuenca, B., and Martín, M. Á (2022). Molecular evidence of introgression of Asian germplasm into a natural Castanea sativa forest in Spain. *Forestry* 95, 95–104. doi: 10.1093/forestry/cpab030

Alcaide, F., Solla, A., Mattioni, C., Castellana, S., and Martín, M. Á (2019). Adaptive diversity and drought tolerance in Castanea sativa assessed through EST-SSR genic markers. *Forestry* 92, 287–296. doi: 10.1093/FORESTRY/CPZ007

Alessandri, S., Krznar, M., Ajolfi, D., Cabrer, A. M. R., Pereira-Lorenzo, S., and Dondini, L. (2020). Genetic Diversity of Castanea sativa Mill. Accessions from the Tuscan-Emilian Apennines and Emilia Romagna Region (Italy). *Agronomy* 10:1319. doi: 10.3390/AGRONOMY10091319

Allario, T., Brumos, J., Colmenero-Flores, J. M., Iglesias, D. J., Pina, J. A., Navarro, L., et al. (2013). Tetraploid Rangpur lime rootstock increases drought tolerance *via* enhanced constitutive root abscisic acid production. *Plant Cell Environ.* 36, 856–868. doi: 10.1111/PCE.12021

Amudha, J., and Balasubramani, G. (2011). Recent molecular advances to combat abiotic stress tolerance in crop plants. *Biotechnol. Mol. Biol. Rev.* 6, 31–58. doi: 10.3389/fpls.2017.01768

Anagnostakis, S. L. (1987). Chestnut Blight: The Classical Problem of an Introduced Pathogen. *Mycologia* 79:23. doi: 10.2307/3807741

Anagnostakis, S. L. (1992). Measuring resistance of chestnut trees to chestnut blight. *Can. J. of Forest Res.* 22, 568–571. doi: 10.1139/x92-075

Anagnostakis, S. L. (2001). The effect of multiple importations of pests and pathogens on a native tree. *Biol. Invasions* 3, 245–254. doi: 10.1023/A:1015205005751

Anagnostakis, S. L. (2012). Chestnut Breeding in the United States for Disease and Insect Resistance. *Plant Dis.* 96, 1392–1403. doi: 10.1094/PDIS-04-12-0350-FE

Aryal, P. (2017). *Evaluation of Ecto-Mycorrhizae as a Determinant of Chestnut Growth and Stress Response*. Ph.D thesis Charleston, IL : Eastern Illinois University.

Badenes, M. L., Fernández i Martí, A., Ríos, G., and Rubio-Cabetas, M. J. (2016). Application of genomic technologies to the breeding of trees. *Front Genetics* 7:198. doi: 10.3389/FGENE.2016.00198/BIBTEX

Baier, K., Maynard, C., Powell, W., Barakat, A., Staton, M., Cheng, C.-H., et al. (2012). Early flowering in chestnut species induced under high dose light in growth chambers. *J. Am. Chestnut. Foundation* 12, 8–10. doi: 10.1186/1471-2229-12-38

Barakat, A., Diloreto, D. S., Zhang, Y., Smith, C., Baier, K., Powell, W. A., et al. (2009). Comparison of the transcriptomes of American chestnut (Castanea dentata) and Chinese chestnut (Castanea mollissima) in response to the chestnut blight infection. *BMC Plant Biol* 9:51 doi: 10.1186/1471-2229-9-51

Barakat, A., Staton, M., Cheng, C.-H., Park, J., Yassin, N. B. M., Ficklin, S., et al. (2012). Chestnut resistance to the blight disease: Insights from transcriptome analysis. *BMC Plant Biol.* 12:38. doi: 10.1186/1471-2229-12-38

Battisti, A., Benvegnù, I., Colombari, F., and Haack, R. A. (2014). Invasion by the chestnut gall wasp in Italy causes significant yield loss in Castanea sativa nut production. *Agricultural Forest Entomol.* 16, 75–79. doi: 10.1111/afe.12036

Bauerle, W. L., Wang, G. G., Bowden, J. D., and Hong, C. M. (2006). An analysis of ecophysiological responses to drought in American Chestnut. *Ann. Forest Sci.* 63, 833–842. doi: 10.1051/FOREST:2006066

Bonsignore, C. P., Vizzari, G., Vono, G., and Bernardo, U. (2020). Short-Term Cold Stress Affects Parasitism on the Asian Chestnut Gall Wasp Dryocosmus kuriphilus. *Insects* 11:841. doi: 10.3390/INSECTS11120841

Bosso, L., Scelza, R., Varlese, R., Meca, G., Testa, A., Rao, M. A., et al. (2016). Assessing the effectiveness of Byssochlamys nivea and Scopulariopsis brumptii in pentachlorophenol removal and biological control of two Phytophthora species. *Fungal Biol.* 120, 645–653. doi: 10.1016/J.FUNBIO.2016.01.004

Bouffartigue, C., Debille, S., Fabreguette, O., Cabrer, A. R., Pereira-Lorenzo, S., Flutre, T., et al. (2020). High admixture between forest an cultivated chestnut (Castanea sativa Mill.) in France. *bioRxiv* [Preprint]. doi: 10.1101/792259

Branzanti, B., Rocca, E., Pisi, A., Branzanti, M. B., Rocca, E., and Pisi, A. (1999). Effect of ectomycorrhizal fungi on chestnut ink disease. *Mycorrhiza* 9, 103–109. doi: 10.1007/S005720050007

Breisch, H., Boutitie, A., Reyne, J., Salesses, G., and Vaysse, P. (1995). Châtaignes et marrons. Paris, RA: CTIFL Centre Technique des Fruits et Légumes

Brown, C. E., Mickelbart, M. V., and Jacobs, D. F. (2014). Leaf physiology and biomass allocation of backcross hybrid American chestnut (Castanea dentata) seedlings in response to light and water availability. *Tree Physiol.* 34, 1362–1375. doi: 10.1093/TREEPHYS/TPU094

Brussino, G., Bosio, G., Baudino, M., Giordano, R., Ramello, F., and Melika, G. (2002). Dangerous exotic insect for the European chestnut. *Inf. Agrario* 58, 59–61.

Bryner, S. F., Rigling, D., and Brunner, P. C. (2012). Invasion history and demographic pattern of Cryphonectria hypovirus 1 across European populations of the chestnut blight fungus. *Ecol. Evol.* 2, 3227–3241. doi: 10.1002/ece3.429

Burgess, T. I., Scott, J. K., Mcdougall, K. L., Stukely, M. J. C., Crane, C., Dunstan, W. A., et al. (2017). Current and projected global distribution of Phytophthora cinnamomi, one of the world's worst plant pathogens. *Glob. Change Biol.* 23, 1661–1674. doi: 10.1111/gcb.13492

Burnham, C., French, D., and Rutter, P. (1986). Breeding blight-resistant chestnuts. *Plant Breed Rev.*, 4, 347–397

Camisón, Á, Ángela Martín, M., Dorado, F. J., Moreno, G., and Solla, A. (2020). Changes in carbohydrates induced by drought and waterlogging in Castanea sativa. *Trees Struct. Funct.* 34, 579–591. doi: 10.1007/S00468-019-01939-X/FIGURES/6

Camisón, Á, Martín, M. Á, Flors, V., Sánchez-Bel, P., Pinto, G., Vivas, M., et al. (2021). Exploring the use of scions and rootstocks from xeric areas to improve drought tolerance in Castanea sativa Miller. *Environ. Exp. Bot.* 187:104467. doi: 10.1016/J.ENVEXPBOT.2021.104467

Camisón, Á, Martín, M. Á, Sánchez-Bel, P., Flors, V., Alcaide, F., Morcuende, D., et al. (2019). Hormone and secondary metabolite profiling in chestnut during susceptible and resistant interactions with Phytophthora cinnamomi. *J. Plant Physiol.* 241:153030. doi: 10.1016/J.JPLPH.2019.153030

Camus, A. (1929). *Les chataigniers. Monographie des genres Castanea et Castanopsis*. Paris: Paul Lechevalier.

Carlile, M. J. (1983). "Motility, taxis, and tropism in Phytophthora," in *Phytophthora: its Biology, Ecology, and Pathology. St. Paul, MN, USA: The American Phytopathological Society*, eds D. C. Erwin, S. Barticki-Garcia, and P. H. Tsao 95–107. doi: 10.3/JQUERY-UI.JS

Carlson, E., Stewart, K., Baier, K., McGuigan, L., Culpepper, T., and Powell, W. (2021). Pathogen-induced expression of a blight tolerance transgene in American chestnut. *Mol. Plant Pathol.* 23, 370–382. doi: 10.1111/MPP.13165

Carneiro-Carvalho, A., Anjos, R., Aires, A., Marques, T., Pinto, T., and Gomes-Laranjo, J. (2019). Ecophysiological study of the impact of SiK§fertilization on Castanea sativa Mill. seedling tolerance to high temperature. *Photosynthetica* 57, 1165–1175. doi: 10.32615/PS.2019.099

Carraway, D., Wilde, H., and Merkle, S. (1994). Somatic embryogenesis and gene transfer in American chestnut. *J. Am. Chestnut. Found.* 8, 29–33.

Casasoli, M., Derory, J., Morera-Dutrey, C., Brendel, O., Porth, I., Guehl, J.-M., et al. (2006). Comparison of quantitative trait loci for adaptive traits between oak and chestnut based on an expressed sequence tag consensus map. *Genetics* 172, 533–546. doi: 10.1534/genetics.105.048439

Casasoli, M., Pot, D., Plomion, C., Monteverdi, M. C., Barreneche, T., Lauteri, M., et al. (2004). Identification of QTLs affecting adaptive traits in Castanea sativa Mill. *Plant Cell Environ.* 27, 1088–1101. doi: 10.1111/j.1365-3040.2004.01214.x

Castellana, S., Martin, M. Á, Solla, A., Alcaide, F., Villani, F., Cherubini, M., et al. (2021). Signatures of local adaptation to climate in natural populations of sweet chestnut (Castanea sativa Mill.) from southern Europe. *Ann. Forest Sci.* 78:27. doi: 10.1007/S13595-021-01027-6/FIGURES/12

Chen, C., Sun, Q., Narayanan, B., Nuss, D. L., and Herzberg, O. (2010). Structure of Oxalacetate Acetylhydrolase, a Virulence Factor of the Chestnut Blight Fungus. *J. Biol. Chem.* 285:26685. doi: 10.1074/JBC.M110.117804

Choudhury, M., Brahma, R., and Ahmed, P. (2020). Silicon nutrition for alleviation of abiotic stress in plants: A review. *J. Pharmacogn. Phytochem.* 9, 1374–1381.

Christensen, J. H., and Christensen, O. B. (2003). Severe summertime flooding in Europe. *Nature* 421, 805–806. doi: 10.1038/421805a

Ciordia, M., Feito, I., Pereira-Lorenzo, S., Fernández, A., and Majada, J. (2012). Adaptive diversity in Castanea sativa Mill. half-sib progenies in response to drought stress. *Environ. Exp. Bot.* 78, 56–63. doi: 10.1016/J.ENVEXPBOT.2011.12.018

Cipollini, M., Dingley, N. R., Felch, P., and Maddox, C. (2017). Evaluation of phenotypic traits and blight-resistance in an American chestnut backcross

orchard in Georgia. *Glob. Ecol. Conserv.* 10, 1–8. doi: 10.1016/J.GECCO.2017.01.004

Clark, S. L., Schlarbaum, S. E., Saxton, A. M., and Baird, R. (2019). Eight-year blight (Cryphonectria parasitica) resistance of backcross-generation American chestnuts (Castanea dentata) planted in the southeastern United States. *Forest Ecol. Manag.* 433, 153–161. doi: 10.1016/J.FORECO.2018.10.060

Corredoira, E., Martínez, M., Cernadas, M., and San José, M. (2017). Application of Biotechnology in the Conservation of the Genus Castanea. *Forests* 8:394. doi: 10.3390/f8100394

Corredoira, E., Montenegro, D., San-José, M. C., Vieitez, A. M., and Ballester, A. (2004). Agrobacterium-mediated transformation of European chestnut embryogenic cultures. *Plant Cell Rep.* 23, 311–318. doi: 10.1007/s00299-004-0804-0

Corredoira, E., San José, M. C., Vieitez, A. M., Allona, I., Aragoncillo, C., and Ballester, A. (2016). Agrobacterium-mediated transformation of European chestnut somatic embryos with a Castanea sativa (Mill.) endochitinase gene. *New Forests* 47, 669–684. doi: 10.1007/s11056-016-9537-5

Corredoira, E., Valladares, S., Allona, I., Aragoncillo, C., Vieitez, A. M., and Ballester, A. (2012). Genetic transformation of European chestnut somatic embryos with a native thaumatin-like protein (CsTL1) gene isolated from Castanea sativa seeds. *Tree Physiol.* 32, 1389–402. doi: 10.1093/treephys/tps098

Costa, R., Santos, C., Tavares, F., Machado, H., Gomes-Laranjo, J., Kubisiak, T., et al. (2011). Mapping and transcriptomic approches implemented for understanding disease resistance to Phytophthora cinammomi in Castanea sp. *BMC Proc.* 5:O18 doi: 10.1186/1753-6561-5-S7-O18

Crandall, B. S., Gravatt, G. F., and Ryan, M. M. (1945). Root disease of Castanea species and some coniferous and broadleaf nursery stocks, caused by Phytophthora cinnamomi. *Phytopathology* 35, 162–180.

Crouch, J. A., Dawe, A., Aerts, A., Barry, K., Churchill, A. C. L., Grimwood, J., et al. (2020). Genome sequence of the chestnut blight fungus Cryphonectria parasitica EP155: A fundamental resource for an archetypical invasive plant pathogen. *Phytopathology* 110, 1180–1188. doi: 10.1094/PHYTO-12-19-0478-A/ASSET/IMAGES/LARGE/PHYTO-12-19-0478-A_T1.JPEG

Cuenca, B., Fernández, M., and Ocaña, L. (2009). "Testaje de resistencia a *Phytophthora cinnamomi* de genotipos adultos seleccionados de *Castanea sativa* Mill," in *Proceedings of the 5th Congreso Forestal Español*, Avila, 1–10.

Cuestas, M. I., Mattioni, C., Martín, L. M., Vargas-Osuna, E., Cherubini, M., and Martín, M. A. (2017). Short communication: Functional genetic diversity of chestnut (Castanea sativa Mill.) populations from southern Spain. *Forest Syst.* 26:eSC06. doi: 10.5424/FS/2017263-11547

de Ollas, C., Hernando, B., Arbona, V., and Gómez-Cadenas, A. (2013). Jasmonic acid transient accumulation is needed for abscisic acid increase in citrus roots under drought stress conditions. *Physiol. Plantarum* 147, 296–306. doi: 10.1111/J.1399-3054.2012.01659.X

Diagne, N., Ngom, M., Djighaly, P. I., Fall, D., Hocher, V., and Svistoonoff, S. (2020). Roles of Arbuscular Mycorrhizal Fungi on Plant Growth and Performance: Importance in Biotic and Abiotic Stressed Regulation. *Diversity* 12:370. doi: 10.3390/D12100370

Dini, F., Sartor, C., and Botta, R. (2012). Detection of a hypersensitive reaction in the chestnut hybrid 'Bouche de Bétizac' infested by Dryocosmus kuriphilus Yasumatsu. *Plant Physiol. Biochem.* 60, 67–73. doi: 10.1016/j.plaphy.2012.07.023

Dinis, L. T., Peixoto, F., Pinto, T., Costa, R., Bennett, R. N., and Gomes-Laranjo, J. (2011a). Study of morphological and phenological diversity in chestnut trees ('Judia' variety) as a function of temperature sum. *Environ. Exp. Bot.* 70, 110–120. doi: 10.1016/J.ENVEXPBOT.2010.08.003

Dinis, L. T., Peixoto, F., Zhang, C., Martins, L., Costa, R., and Gomes-Laranjo, J. (2011b). Physiological and biochemical changes in resistant and sensitive chestnut (Castanea) plantlets after inoculation with Phytophthora cinnamomi. *Physiol. Mol. Plant Pathol.* 75, 146–156. doi: 10.1016/j.pmpp.2011.04.003

Diskin, M., Steiner, K. C., and Hebard, F. V. (2006). Recovery of American chestnut characteristics following hybridization and backcross breeding to restore blight-ravaged Castanea dentata. *Forest Ecol. Manag.* 223, 439–447. doi: 10.1016/J.FORECO.2005.12.022

Dorado, F. J., Solla, A., Alcaide, F., and Martín, M. A. (2022). Assessing heat stress tolerance in Castanea sativa. *Forestry* cac021. doi: 10.1093/forestry/cpac021

Engelbrecht, J., Duong, T. A., Prabhu, S. A., Seedat, M., and van den Berg, N. (2021). Genome of the destructive oomycete Phytophthora cinnamomi provides insights into its pathogenicity and adaptive potential. *BMC Genomics* 22:302. doi: 10.1186/s12864-021-07552-y

Eppo Global Database (2022). *Cryphonectria parasitica. Distribution*. Available online at: https://gd.eppo.int/taxon/ENDOPA/distribution (accessed on Feb 15, 2022).

Eriksson, G., Pliura, A., Villani, F., Bucci, G., Casasoli, M., Cherubini, M., et al. (2005). Management of genetic resources of the multi-purpose tree species castanea sativa mill. *Acta Horticulturae* 693, 373–386. doi: 10.17660/ACTAHORTIC.2005.693.47

European Commission (2022). *Consequences of climate change*. Available online at: https://ec.europa.eu/clima/climate-change/climate-change-consequences_en (accessed on May 21, 2022).

Evangelisti, E., Gogleva, A., Hainaux, T., Doumane, M., Tulin, F., Quan, C., et al. (2017). Time-resolved dual transcriptomics reveal early induced Nicotiana benthamiana root genes and conserved infection-promoting Phytophthora palmivora effectors. *BMC Biol.* 15:39. doi: 10.1186/s12915-017-0379-1

Fei, S., Liang, L., Paillet, F. L., Steiner, K. C., Fang, J., Shen, Z., et al. (2012). Modelling chestnut biogeography for American chestnut restoration. *Divers. Distrib.* 18, 754–768. doi: 10.1111/j.1472-4642.2012.00886.x

Fernandes, P., Amaral, A., Colavolpe, B., Balonas, D., Serra, M., Pereira, A., et al. (2020a). Propagation of New Chestnut Rootstocks with Improved Resistance to Phytophthora cinnamomi–New Cast Rootstocks. *Silva Lusit.* 28, 15–29. doi: 10.1051/silu/20202801015

Fernandes, P., Amaral, A., Colavolpe, B., Pereira, A., and Costa, R. (2021a). Avaliação agronómica de genótipos de castanheiro selecionados do programa de melhoramento genético para a resistência à tinta. *Vida Rural* 76–82.

Fernandes, P., Machado, H., do Céu Silva, M., and Costa, R. L. (2021b). A histopathological study reveals new insights into responses of chestnut (Castanea spp.) to root infection by Phytophthora cinnamomi. *Phytopathology* 111, 345–355. doi: 10.1094/PHYTO-04-20-0115-R

Fernandes, P., Tedesco, S., da Silva, I. V., Santos, C., Machado, H., and Costa, R. L. (2020b). A new clonal propagation protocol develops quality root systems in chestnut. *Forests* 11:826. doi: 10.3390/F11080826

Fernandez-Lopez, J. (2011). Identification of the genealogy of interspecific hybrids between Castanea sativa, Castanea crenata and Castanea mollissima. *Forest Syst.* 20, 65–80. doi: 10.5424/fs/2011201-9136

Fernández-López, J., Vazquez-Ruiz-De-Ocenda, R. A., Díaz-Vázquez, R., and Pereira-Lorenzo, S. (2001). Evaluation of resistance of Castanea sp. clones to Phytophthora sp. using excised chestnut shoots. *For. Snow Landsc. Res.* 76, 451–454.

Fernandez-Lopez, J., Zas, R., Diaz, R., Villani, F., Cherubini, M., Aravanopoulos, F. A., et al. (2005). Geographic variability among extreme european wild chestnut populations. *Acta Hortic.* 693, 181–186. doi: 10.17660/ACTAHORTIC.2005.693.21

Food and Agriculture Organization of the United Nations (2022). *Food and agriculture data*. Available online at: http://www.fao.org/faostat/en/#data/QC (accessed on Feb 15, 2022)

Fulbright, D. W., Stadt, S., Medina-Mora, C., Mandujano, M., Donis-González, I. R., and Serdar, U. (2014). Kernel breakdown appears when hybrid Castanea cultivars are pollinized by Castanea mollissima. *Acta Hortic.* 1019, 91–97.

García-Olmedo, F., Molina, A., Segura, A., and Moreno, M. (1995). The defensive role of nonspecific lipid-transfer proteins in plants. *Trends Microbiol.* 3, 72–74. doi: 10.1016/S0966-842X(00)88879-4

Glenz, C., Schlaepfer, R., Iorgulescu, I., and Kienast, F. (2006). Flooding tolerance of Central European tree and shrub species. *Forest Ecol. Manag.* 235, 1–13. doi: 10.1016/J.FORECO.2006.05.065

Gomes Guerreiro, M. (1948). *Alguns estudos do género Castanea. Relatório. Tomos I e II, 111*, Vol. XV. Alcobaça: Publicação da Direcção Geral dos Serviços Florestais e Aquícolas, Tipografia Alcobacence Lda.

Gomes Guerreiro, M. (1957). *Castanheiros. Alguns estudos sobre a sua ecologia e o seu melhoramento genético. Dissertation presented for the title of Aggregate Professor to the Instituto Superior de Agronomia*. Lisboa.

Gomes Laranjo, J., Ferreira Cardoso, J., Portela, E., and Abreu, C. (2007). *Castanheiros. Edição Programa AGRO 499–Contributo para difusão do conhecimento das cultivares portuguesas de castanheiro*. 373.

Gomes-Laranjo, J., Araujo-Alves, J., Ferreira-Cardoso, J., Pimentel-Pereira, M., Abreu, C. G., and Torres-Pereira, J. (2004). Effect of Chestnut Ink Disease on Photosynthetic Performance. *J. Phytopathol.* 152, 138–144. doi: 10.1111/j.1439-0434.2004.00814.x

Gomes-Laranjo, J., Dinis, L. T., Marques, T., Mota, M., Carvalho, A., Pinto, T., et al. (2018). Increasing chestnut resilience to climate change with innovative management practices. *Acta Hortic.* 1220, 163–176. doi: 10.17660/ACTAHORTIC.2018.1220.24

Gomes-Laranjo, J., Dinis, L., Martins, L., Portela, E., Pinto, T., Ara, M. C., et al. (2012). "Characterization of chestnut behavior with photosynthetic traits," in *Applied Photosynthesis*, ed. M. M. Najafpour (London: IntechOpen). doi: 10.5772/26227

Grabherr, M. G., Haas, B. J., Yassour, M., Levin, J. Z., Thompson, D. A., Amit, I., et al. (2011). Full-length transcriptome assembly from RNA-Seq data without a reference genome. *Nat. Biotechnol.* 29, 644–652. doi: 10.1038/NBT.1883

Griffin, G. J. (1983). Survival of American Chestnut Trees: Evaluation of Blight Resistance and Virulence in Endothia parasitica. *Phytopathology* 73:1084. doi: 10.1094/PHYTO-73-1084

Hardham, A. R. (2005). Phytophthora cinnamomi. *Mol. Plant Pathol.* 6, 589–604. doi: 10.1111/j.1364-3703.2005.00308.x

Hardham, A. R., and Blackman, L. M. (2018). Phytophthora cinnamomi. *Mol. Plant Pathol.* 19, 260–285. doi: 10.1111/mpp.12568

Havir, E. A., and Anagnostakis, S. L. (1983). Oxalate production by virulent but not by hypovirulent strains of Endothia parasitica. *Physiol. Plant Pathol.* 23, 369–376. doi: 10.1016/0048-4059(83)90021-8

Hebard, F. V., Griffin, G. J., and Elkins, J. R. (1984). Developmental Histopathology of Cankers Incited by Hypovirulent and Virulent Isolates of Endothia parasitica on Susceptible and Resistant Chestnut Trees. *Phytopathology* 74:140. doi: 10.1094/Phyto-74-140

Huang, H., Carey, W. A., Dane, F., and Norton, J. D. (1996). Evaluation of Chinese chestnut cultivars for resistance to Cryphonectria parasitica. *Plant Dis.* 80, 45–47. doi: 10.1094/PD-80-0045

Jacobs, D. F., Dalgleish, H. J., and Nelson, C. D. (2013). A conceptual framework for restoration of threatened plants: The effective model of American chestnut (Castanea dentata) reintroduction. *New Phytol.* 197, 378–393. doi: 10.1111/nph.12020

Jeffers, S. N., James, J. B., and Sisco, P. H. (2009). "Screening for resistance to Phytophthora cinnamomi in hybrid seedlngs of American chestnut," in *in Proceedings of the Fourth Meeting of the International Union of Forest Research Organizations (IUFRO) Working Party S07.02.09*, (Monterey), 188–194.

Kalemba, E. M., and Pukacka, S. (2007). 3 LEA PROTEINS AND sHSPs IN SEED PROTECTION Possible roles of LEA proteins and sHSPs in seed protection: A short review. *Biological. Lett.* 44, 3–16.

Kamoun, S., Furzer, O., Jones, J. D. G., Judelson, H. S., Ali, G. S., Dalio, R. J. D., et al. (2015). The Top 10 oomycete pathogens in molecular plant pathology. *Mol. Plant Pathol.* 16, 413–434. doi: 10.1111/mpp.12190

Kato, K., and Hijii, N. (1997). Effects of gall formation by Dryocosmus kuriphilus Yasumatsu (Hym., Cynipidae) on the growth of chestnut trees. *J. Appl. Entomol.* 121, 9–15. doi: 10.1111/j.1439-0418.1997.tb01363.x

Kim, J. S., Kim, K. A., Oh, T. R., Park, C. M., and Kang, H. (2008). Functional Characterization of DEAD-Box RNA Helicases in Arabidopsis thaliana under Abiotic Stress Conditions. *Plant Cell Physiol.* 49, 1563–1571. doi: 10.1093/PCP/PCN125

Ko, W. H., Chang, H. S., and Su, H. J. (1978). Isolates of Phytophthora cinnamomi from Taiwan as evidence for an Asian origin of the species. *Trans. Br. Mycol. Soc.* 71, 496–499. doi: 10.1016/S0007-1536(78)80080-1

Kreuzwieser, J., and Rennenberg, H. (2014). Molecular and physiological responses of trees to waterlogging stress. *Plant Cell Environ.* 37, 2245–2259. doi: 10.1111/PCE.12310

Kubisiak, T. (2010). "QTL analysis of Phytophthora resistance in a BC1 population," in *NE-1033 Annual Meeting Minutes*, (Maggie Valley).

Kubisiak, T. L., and Roberds, J. H. (2006). "Genetic structure of American chestnut populations based on neutral DNA markers. in Restoration of American Chestnut to Forest Lands,"in *Proceedings of a Conference and Workshop held at The North Carolina Arboretum, Asheville, North Carolina, U. S. A., May 4–6, 2004. Natural Resources Report NPS/NCR/CUE/NRR–2006/001, 109–122*, (Washington, DC: National Park Service).

Kubisiak, T. L., Hebard, F. V., Nelson, C. D., Zhang, J., Bernatzky, R., Huang, H., et al. (1997). Molecular Mapping of Resistance to Blight in an Interspecific Cross in the Genus Castanea. *Phytopathology* 87, 751–759. doi: 10.1094/PHYTO.1997.87.7.751

Kubisiak, T. L., Nelson, C. D., Staton, M. E., Zhebentyayeva, T., Smith, C., Olukolu, B. A., et al. (2013). A transcriptome-based genetic map of Chinese chestnut (*Castanea mollissima*) and identification of regions of segmental homology with peach (*Prunus persica*). *Tree Genet. Genomes* 1019, 557–571. doi: 10.1007/s11295-012-0579-3

Kundzewicz, Z. W., Ulbrich, U., Brücher, T., Graczyk, D., Krüger, A., Leckebusch, G. C., et al. (2005). Summer Floods in Central Europe–Climate Change Track? *Nat. Hazards* 36, 165–189. doi: 10.1007/S11069-004-4547-6

Kunert, K. J., van Wyk, S. G., Cullis, C. A., Vorster, B. J., and Foyer, C. H. (2015). Potential use of phytocystatins in crop improvement, with a particular focus on legumes. *J. Exp. Bot.* 66, 3559–3570. doi: 10.1093/JXB/ERV211

Lang, P., Dane, F., Kubisiak, T. L., and Huang, H. (2007). Molecular evidence for an Asian origin and a unique westward migration of species in the genus Castanea *via* Europe to North America. *Mol. Phylogenet. Evol.* 43, 49–59. doi: 10.1016/J.YMPEV.2006.07.022

Latijnhouwers, M., de Wit, P. J. G. M., and Govers, F. (2003). Oomycetes and fungi: Similar weaponry to attack plants. *Trends Microbiol.* 11, 462–469. doi: 10.1016/J.TIM.2003.08.002

Lauteri, M., Pliura, A., Monteverdi, M. C., Brugnoli, E., Villani, F., and Eriksson, G. (2004). Genetic variation in carbon isotope discrimination in six European populations of Castanea sativa Mill. originating from contrasting localities. *J. Evol. Biol.* 17, 1286–1296. doi: 10.1111/J.1420-9101.2004.00765.X

Lee, J. H., and Kim, W. T. (2011). Regulation of abiotic stress signal transduction by E3 ubiquitin ligases in Arabidopsis. *Mol. Cells* 31, 201–208. doi: 10.1007/S10059-011-0031-9

Limera, C., Sabbadini, S., Sweet, J. B., and Mezzetti, B. (2017). New biotechnological tools for the genetic improvement of major woody fruit species. *Front. Plant Sci.* 8:1418. doi: 10.3389/FPLS.2017.01418/BIBTEX

Liu, Z., Bi, W.-L., Shukla, M. R., and Saxena, P. K. (2022). *In Vitro* Technologies for American Chestnut (*Castanea dentata* (Marshall) Borkh) Conservation. *Plants* 11:464. doi: 10.3390/plants11030464

Ma, J. F. (2004). Role of silicon in enhancing the resistance of plants to biotic and abiotic stresses. *Soil Sci. Plant Nutr.* 50, 11–18. doi: 10.1080/00380768.2004.10408447

Manivannan, A., and Ahn, Y. K. (2017). Silicon regulates potential genes involved in major physiological processes in plants to combat stress. *Front. Plant Sci.* 8:1346. doi: 10.3389/FPLS.2017.01346/BIBTEX

Marinoni, D. T., Nishio, S., Valentini, N., Shirasawa, K., Acquadro, A., Portis, E., et al. (2020). Development of High-Density Genetic Linkage Maps and Identification of Loci for Chestnut Gall Wasp Resistance in Castanea spp. *Plants* 9:1048. doi: 10.3390/PLANTS9081048

Martin, M. A., Mattioni, C., Cherubini, M., Taurchini, D., and Villani, F. (2010). Genetic diversity in European chestnut populations by means of genomic and genic microsatellite markers. *Tree Genet. Genomes* 6, 735–744. doi: 10.1007/s11295-010-0287-9

Martínez-Sancho, E., Navas, L. K. V., Seidel, H., Dorado-Liñán, I., and Menzel, A. (2017). Responses of Contrasting Tree Functional Types to Air Warming and Drought. *Forests* 8:450. doi: 10.3390/F8110450

Martins, L., Anjos, R., Costa, R., and Gomes-Laranjo, J. (2009). "Colutad. Um clone de castanheiro resistente à doença da tinta," in *Castanheiros. Técnicas e Práticas*, eds J. Gomes-Laranjo, F. Peixoto, and J. Ferreira-Cardoso (Vila Real: Pulido Consulting - Indústria Criativa and Universidade Trás-os-Montes e Alto Douro), 135–142.

Maurel, M., Robin, C., Capdevielle, X., Loustau, D., and Desprez-Loustau, M. L. (2001). Effects of variable root damage caused by Phytophthora cinnamomi on water relations of chestnut saplings. *Ann. For. Sci.* 58, 639–651. doi: 10.1051/FOREST:2001151

Maurel, M., Robin, C., Simonneau, T., Loustau, D., Dreyer, E., and Desprez-Loustau, M. L. (2004). Stomatal conductance and root-to-shoot signalling in chestnut saplings exposed to Phytophthora cinnamomi or partial soil drying. *Funct. Plant Biol.* 31, 41–51. doi: 10.1071/FP03133

McGuigan, L., Fernandes, P., Oakes, A., Stewart, K., and Powell, W. (2020). Transformation of american chestnut (Castanea dentata (marsh.) borkh) using RITA® temporary immersion bioreactors and we vitro containers. *Forests* 11:1196. doi: 10.3390/f11111196

Mellano, M. G., Beccaro, G. L., Donno, D., Marinoni, D. T., Boccacci, P., Canterino, S., et al. (2012). Castanea spp. biodiversity conservation: Collection and characterization of the genetic diversity of an endangered species. *Genet. Resour. Crop Evol.* 59, 1727–1741. doi: 10.1007/s10722-012-9794-x

Menéndez-Miguélez, M., Álvarez-Álvarez, P., Majada, J., and Canga, E. (2015). Effects of soil nutrients and environmental factors on site productivity in Castanea sativa Mill. coppice stands in NW Spain. *New For.* 46, 217–233. doi: 10.1007/S11056-014-9456-2/TABLES/2

Meyer, F. E., Shuey, L. S., Naidoo, S., Mamni, T., Berger, D. K., Myburg, A. A., et al. (2016). Dual RNA-sequencing of Eucalyptus nitens during Phytophthora cinnamomi challenge reveals pathogen and host factors influencing compatibility. *Front. Plant Sci.* 7:191. doi: 10.3389/fpls.2016.00191

Meyer, J. B., Gallien, L., and Prospero, S. (2015). Interaction between two invasive organisms on the European chestnut: Does the chestnut blight fungus benefit from the presence of the gall wasp? *FEMS Microbiol. Ecol.* 91:fiv122. doi: 10.1093/femsec/fiv122

Míguez-Soto, B., Fernández-Cruz, J., and Fernández-López, J. (2019). Mediterranean and Northern Iberian gene pools of wild Castanea sativa Mill. are two differentiated ecotypes originated under natural divergent selection. *PLoS One* 14:e0211315. doi: 10.1371/JOURNAL.PONE.0211315

Milburn, M., and Gravatt, G. F. (1932). Preliminary note on a *Phytophthora* root disease of chestnut. *Phytopathology* 22, 977–978.

Milgroom, M. G., and Cortesi, P. (2004). Biological control of chestnut blight with hypovirulence: A critical analysis. *Annu. Rev. Phytopathol.* 42, 311–338. doi: 10.1146/ANNUREV.PHYTO.42.040803.140325

Miranda-Fontaíña, M. E., Fernández-López, J., Vettraino, A. M., and Vannini, A. (2007). Resistance of Castanea clones to Phytophthora cinnamomi: Testing and genetic control. *Silvae Genet.* 56, 11–21. doi: 10.1515/sg-2007-0002

Molina, F., and Viéitez, E. (1967). *Defense du chataignier contre ses maladies en Espagne. Atti Convegno Internazionallesul Castagno*. Cuneo: Ottobre.

Moradpour, M., and Abdulah, S. N. A. (2020). CRISPR/dCas9 platforms in plants: Strategies and applications beyond genome editing. *Plant Biotechnol. J.* 18, 32–44. doi: 10.1111/PBI.13232

Müller, M., and Gailing, O. (2019). Abiotic genetic adaptation in the Fagaceae. *Plant Biol.* 21, 783–795. doi: 10.1111/PLB.13008

Murolo, S., Angelini, R. M., de, M., Faretra, F., and Romanazzi, G. (2018). Phenotypic and molecular investigations on hypovirulent cryphonectria parasitica in Italy. *Plant Dis.* 102, 540–545. doi: 10.1094/PDIS-04-17-0517-RE

Neves, D. M., Almeida, L. A. D. H., Santana-Vieira, D. D. S., Freschi, L., Ferreira, C. F., Soares Filho, W. D. S., et al. (2017). Recurrent water deficit causes epigenetic and hormonal changes in citrus plants. *Sci. Rep.* 7:13684. doi: 10.1038/s41598-017-14161-x

Newhouse, A. E., and Powell, W. A. (2021). Intentional introgression of a blight tolerance transgene to rescue the remnant population of American chestnut. *Conserv. Sci. Pract.* 3:e348. doi: 10.1111/CSP2.348

Newhouse, A. E., Maynard, C. A., and Powell, W. A. (2014). Chestnut Leaf Inoculation Assay as a Rapid Predictor of Blight Susceptibility. *Plant Dis.* 98, 4–9. doi: 10.1094/PDIS-01-13-0047-RE

Newhouse, A., Coffey, V., McGuigan, L., Oakes, A., Breda, K., Matthews, D., et al. (2020). *Petition for Determination of Nonregulated Status for Blight-Tolerant Darling 58 American Chestnut (Castanea dentata)*. Available Online at: https://www.regulations.gov/document/APHIS-2020-0030-0002 (accessed on Oct 16, 2021).

Nishio, S., Yamamoto, T., Terakami, S., Sawamura, Y., Takada, N., Nishitani, C., et al. (2011). Novel genomic and EST-derived SSR markers in Japanese chestnuts. *Sci. Hortic.* 130, 838–846. doi: 10.1016/J.SCIENTA.2011.09.012

Pavese, V., Moglia, A., Corredoira, E., Martínez, M. T., Torello Marinoni, D., and Botta, R. (2021a). First Report of CRISPR/Cas9 Gene Editing in Castanea sativa Mill. *Front. Plant Sci.* 12:1752. doi: 10.3389/fpls.2021.728516

Pavese, V., Moglia, A., Gonthier, P., Marinoni, D. T., Cavalet-Giorsa, E., and Botta, R. (2021b). Identification of Susceptibility Genes in Castanea sativa and Their Transcription Dynamics following Pathogen Infection. *Plants* 10:913. doi: 10.3390/PLANTS10050913

Pereira-Lorenzo, S., Ballester, A., Corredoira, E., Vieitez, A. M., Agnanostakis, S., Costa, R., et al. (2012). "Chestnut," in *Handbook of Plant Breeding - Fruit Breeding*, eds M. L. Badenes and D. H. Byrne (Berlin: Springer Science), 729–769. doi: 10.1007/978-1-4419-0763-9_19

Pereira-Lorenzo, S., Costa, R. M. L., Ramos-Cabrer, A. M., Ciordia-Ara, M., Ribeiro, C. A. M., Borges, O., et al. (2011). Chestnut cultivar diversification process in the Iberian Peninsula. Canary Islands, and Azores. *Genome* 54, 301–315. doi: 10.1139/g10-122

Pereira-lorenzo, S., Costa, R., Ramos-Cabrer, A. M., Ribeiro, C., Silva, M., Manzano, G., et al. (2010). Variation in grafted European chestnut and hybrids by microsatellites reveals two main origins in the Iberian Peninsula. *Tree Genet. Genomes* 6, 701–715. doi: 10.1007/s11295-010-0285-y

Pérez-Girón, J. C., Álvarez-Álvarez, P., Díaz-Varela, E. R., and Mendes Lopes, D. M. (2020). Influence of climate variations on primary production indicators and on the resilience of forest ecosystems in a future scenario of climate change: Application to sweet chestnut agroforestry systems in the Iberian Peninsula. *Ecol. Indic.* 113:106199. doi: 10.1016/J.ECOLIND.2020.106199

Perkins, M. T., Zhebentyayeva, T., Sisco, P. H., and Craddock, J. H. (2021). Genome-Wide Sequence-Based Genotyping Supports a Nonhybrid Origin of Castanea alabamensis. *Syst. Bot.* 46, 973–984. doi: 10.1600/036364421X16370109698524

Pernas, M., Sánchez-Monge, R., and Salcedo, G. (2000). Biotic and abiotic stress can induce cystatin expression in chestnut. *FEBS Lett.* 467, 206–210. doi: 10.1016/S0014-5793(00)01157-1

Pilkey, H. (2021). *Developing and Optimizing Conservation Outcrossing Methods to Produce Diversified Blight-Tolerant American Chestnut Trees (Castanea Dentata [Marsh.] Borkh.)*, Ph.D thesis, New York NY: State University of New York-College of Environmental Science and Forestry. Syracuse.

Polin, L. D., Liang, H., Rothrock, R. E., Nishii, M., Diehl, D. L., Newhouse, A. E., et al. (2006). Agrobacterium-mediated transformation of American chestnut (Castanea dentata (Marsh.) Borkh.) somatic embryos. *Plant Cell Tissue Organ Cult.* 84, 69–79. doi: 10.1007/s11240-005-9002-1

Poljak, I., Idžojtić, M., Šatović, Z., Ježić, M., Ćurković-Perica, M., Simovski, B., et al. (2017). Genetic diversity of the sweet chestnut (Castanea sativa Mill.) in Central Europe and the western part of the Balkan Peninsula and evidence of marron genotype introgression into wild populations. *Tree Genet. Genomes* 13:18. doi: 10.1007/S11295-017-1107-2/FIGURES/3

Powell, W. A., Morley, P., King, M., and Maynard, C. A. (2007). Small stem chestnut blight resistance assay. *J. Am. Chestnut Foundation* 21, 34–38. doi: 10.1007/978-1-4939-1658-0_13

Powell, W. A., Newhouse, A. E., and Coffey, V. (2019). Developing Blight-Tolerant American Chestnut Trees. *Cold Spring Harb. Perspect. Biol.* 11:a034587. doi: 10.1101/CSHPERSPECT.A034587

Prospero, S., Conedera, M., Heiniger, U., and Rigling, D. (2006). Saprophytic Activity and Sporulation of Cryphonectria parasitica on Dead Chestnut Wood in Forests with Naturally Established Hypovirulence. *Phytopathology®* 96, 1337–1344. doi: 10.1094/PHYTO-96-1337

Prunet, A. (1904). Le reconstitution des Châtaigneries. *Bul. Mensuel de L'Office de Reseignements Agricoles* 3, 536–541.

Ramos Guedes-Lafargue, M., and Salesses, G. (1999). ink disease resistance: Some preliminary elements from the study of different crosses. *Acta Hortic.* 494, 355–362. doi: 10.17660/ActaHortic.1999.494.54

Rigling, D., and Prospero, S. (2018). Cryphonectria parasitica, the causal agent of chestnut blight: Invasion history, population biology and disease control. *Mol. Plant Pathol.* 19, 7–20. doi: 10.1111/mpp.12542

Roane, M., Griffin, G., and Elkins, J. (1986). *Chestnut blight, other Endothia diseases, and the genus Endothia*. Saint Paul, MIN: APS Press.

Robin, C., and Heiniger, U. (2001). Chestnut blight in Europe: Diversity of Cryphonectria parasitica, hypovirulence and biocontrol. *For. Snow Landsc. Res.* 76, 361–367.

Robin, C., Morel, O., Vettraino, A. M., Perlerou, C., Diamandis, S., and Vannini, A. (2006). Genetic variation in susceptibility to Phytophthora Cambivora in European chestnut (*Castanea sativa*). *For. Ecol. Manag.* 226, 199–207. doi: 10.1016/j.foreco.2006.01.035

Rothrock, R. E., Polin-McGuigan, L. D., Newhouse, A. E., Powell, W. A., and Maynard, C. A. (2007). Plate flooding as an alternative Agrobacterium-mediated transformation method for American chestnut somatic embryos. *Plant Cell Tissue Organ Cult.* 88, 93–99. doi: 10.1007/s11240-006-9170-7

Saiz-Fernández, I., Milenković, I., Berka, M., Černý, M., Tomšovský, M., Brzobohatý, B., et al. (2020). Integrated Proteomic and Metabolomic Profiling of Phytophthora cinnamomi Attack on Sweet Chestnut (*Castanea sativa*) Reveals Distinct Molecular Reprogramming Proximal to the Infection Site and Away from It. *Int. J. Mol. Sci.* 21:8525. doi: 10.3390/ijms21228525

Salesses, G., Ronco, L., Chauvin, J., and Chapa, J. (1993). Amélioration génétique du chataignier misse aupoint de tests d'évaluation du comportement vis-á-vis dela maladie de l'encre. *L'Arboric. Fruitiére* 458, 23–31.

Sandercock, A., Westbrook, J., Zhang, Q., Johnson, H., Saielli, T., Scrivani, J., et al. (2022). Whole-genome resequencing reveals the population structure, genomic diversity, and demographic history of American chestnut (*Castanea dentata*). *bioRxiv* [Preprint]. doi: 10.1101/2022.02.11.480151

Santamaría, M. E., Hasbún, R., Valera, M. J., Meijón, M., Valledor, L., Rodríguez, J. L., et al. (2009). Acetylated H4 histone and genomic DNA methylation patterns during bud set and bud burst in Castanea sativa. *J. Plant Physiol.* 166, 1360–1369. doi: 10.1016/J.JPLPH.2009.02.014

Santamaría, M. E., Rodríguez, R., Cañal, M. J., and Toorop, P. E. (2011). Transcriptome analysis of chestnut (Castanea sativa) tree buds suggests a putative role for epigenetic control of bud dormancy. *Ann. Bot.* 108, 485–498. doi: 10.1093/aob/mcr185

Santana-Vieira, D. D. S., Freschi, L., da Hora, Almeida, L. A., Moraes, D. H. S., de, et al. (2016). Survival strategies of citrus rootstocks subjected to drought. *Sci. Rep.* 6:38775. doi: 10.1038/srep38775

Santhanagopalan, I., Basha, E., Ballard, K. N., Bopp, N. E., and Vierling, E. (2015). "Model Chaperones: Small Heat Shock Proteins from Plants," in *The Big Book on Small Heat Shock Proteins. Heat Shock Proteins*, eds R. Tanguay and L. Hightower (Cham: Springer), 119–153. doi: 10.1007/978-3-319-16077-1_5

Santini, A., Barzanti, G. P., and Capretti, P. (2003). Susceptibility of some mesophilic hardwoods to alder phytophthora. *J. Phytopathol.* 151, 406–410. doi: 10.1046/j.1439-0434.2003.00739.x

Santos, C., Duarte, S., Tedesco, S., Fevereiro, P., and Costa, R. L. (2017a). Expression profiling of Castanea genes during resistant and susceptible interactions with the oomycete pathogen Phytophthora cinnamomi reveal possible mechanisms of immunity. *Front. Plant Sci.* 8:515. doi: 10.3389/fpls.2017.00515

Santos, C., Machado, H., Correia, I., Gomes, F., Gomes-Laranjo, J., and Costa, R. (2015a). Phenotyping Castanea hybrids for Phytophthora cinnamomi resistance. *Plant Pathol.* 64, 901–910. doi: 10.1111/ppa.12313

Santos, C., Nelson, C. D., Zhebentyayeva, T., Machado, H., Gomes-Laranjo, J., and Costa, R. L. (2017b). First interspecific genetic linkage map for Castanea sativa x Castanea crenata revealed QTLs for resistance to Phytophthora cinnamomi. *PLoS One* 12:e0184381. doi: 10.1371/journal.pone.0184381

Santos, C., Zhebentyayeva, T., Serrazina, S., Nelson, C. D., and Costa, R. (2015b). Development and characterization of EST-SSR markers for mapping reaction to Phytophthora cinnamomi in Castanea spp. *Sci. Hortic.* 194, 181–187. doi: 10.1016/j.scienta.2015.07.043

Sartor, C., Dini, F., Torello Marinoni, D., Mellano, M. G., Beccaro, G. L., Alma, A., et al. (2015). Impact of the Asian wasp Dryocosmus kuriphilus (Yasumatsu) on cultivated chestnut: Yield loss and cultivar susceptibility. *Sci Hortic.* 197, 454–460. doi: 10.1016/j.scienta.2015.10.004

Schad, C., Solignat, G., Grente, J., and Venot, P. (1952). Recherches sur le chataignier a la station de Brive. *Annales de L'amélioration des plantes* 3, 369–458.

Seabra, R. C., and Pais, M. S. (1998). Genetic transformation of European chestnut. *Plant Cell Rep*. 17, 177–182.

Sebastiana, M., Figueiredo, A., Acioli, B., Sousa, L., Pessoa, F., Baldé, A., et al. (2009). Identification of plant genes involved on the initial contact between ectomycorrhizal symbionts (Castanea sativa–European chestnut and Pisolithus tinctorius). *Eur. J. Soil Biol.* 45, 275–282. doi: 10.1016/J.EJSOBI.2009.02.001

Seo, D. H., Ryu, M. Y., Jammes, F., Hwang, J. H., Turek, M., Kang, B. G., et al. (2012). Roles of Four Arabidopsis U-Box E3 Ubiquitin Ligases in Negative Regulation of Abscisic Acid-Mediated Drought Stress Responses. *Plant Physiol.* 160, 556–568. doi: 10.1104/PP.112.202143

Serdar, Ü, Saito, T., Cuenca, B., Akyüz, B., Laranjo, J. G., Beccaro, G., et al. (2019). "Advances in cultivation of chestnuts," in *Achieving sustainable cultivation of tree nuts*, (Sawston: Burleigh Dodds Science Publishing Limited), 349–388. doi: 10.19103/as.2018.0042.22

Serrazina, S., Machado, H., Costa, R. L., Duque, P., and Malhó, R. (2021). Expression of Castanea crenata Allene Oxide Synthase in Arabidopsis Improves the Defense to Phytophthora cinnamomi. *Front. Plant Sci.* 12:149. doi: 10.3389/fpls.2021.628697

Serrazina, S., Santos, C., Machado, H., Pesquita, C., Vicentini, R., Pais, M. S., et al. (2015). Castanea root transcriptome in response to Phytophthora cinnamomi challenge. *Tree Genet. Genomes* 11:6. doi: 10.1007/s11295-014-0829-7

Shirasawa, K., Nishio, S., Terakami, S., Botta, R., Marinoni, D. T., and Isobe, S. (2021). Chromosome-level genome assembly of Japanese chestnut (Castanea crenata Sieb. et Zucc.) reveals conserved chromosomal segments in woody rosids. *DNA Res.* 28:dsab016. doi: 10.1093/DNARES/DSAB016

Sisco, P. H., Neel, T. C., Hebard, F. V., Craddock, J. H., and Shaw, J. (2014). Cytoplasmic male sterility in interspecific hybrids between american and asian Castanea species is correlated with the american d chloroplast haplotype. *Acta Hortic.* 1019, 215–222. doi: 10.17660/ACTAHORTIC.2014.1019.32

Sisco, P., Kubisiak, T., and Casasoli, M. (2005). "An improved genetic map for Castanea mollissima/Castanea dentata and its relationship to the genetic map of Castanea sativa," in *Proceedings of the III International Chestnut Congress*, eds C. G. Abreu, E. Rosa, and A. A. Monteiro (Leuven: Acta Horticulturae), 693.

Soto, A., Allona, I., Collada, C., Guevara, M. A., Casado, R., Rodriguez-Cerezo, E., et al. (1999). Heterologous Expression of a Plant Small Heat-Shock Protein Enhances *Escherichia coli* Viability under Heat and Cold Stress. *Plant Physiol.* 120, 521–528. doi: 10.1104/PP.120.2.521

Staton, M., Addo-Quaye, C., Cannon, N., Yu, J., Zhebentyayeva, T., Huff, M., et al. (2020). A reference genome assembly and adaptive trait analysis of Castanea mollissima 'Vanuxem,' a source of resistance to chestnut blight in restoration breeding. *Tree Genet. Genomes* 16:57 . doi: 10.1007/S11295-020-01454-Y/FIGURES/10

Staton, M., Zhebentyayeva, T., Olukolu, B., Fang, G. C., Nelson, D., Carlson, J. E., et al. (2015). Substantial genome synteny preservation among woody angiosperm species: Comparative genomics of Chinese chestnut (Castanea mollissima) and plant reference genomes. *BMC Genomics* 16:744. doi: 10.1186/s12864-015-1942-1

Stauder, C. M., Nuss, D. L., Zhang, D.-X., Double, M. L., MacDonald, W. L., Metheny, A. M., et al. (2019). Enhanced hypovirus transmission by engineered super donor strains of the chestnut blight fungus, Cryphonectria parasitica, into a natural population of strains exhibiting diverse vegetative compatibility genotypes. *Virology* 528, 1–6. doi: 10.1016/j.virol.2018.12.007

Steiner, K. C., Westbrook, J. W., Hebard, F. V., Georgi, L. L., Powell, W. A., and Fitzsimmons, S. F. (2017). Rescue of American chestnut with extraspecific genes following its destruction by a naturalized pathogen. *New Forests* 48, 317–336. doi: 10.1007/S11056-016-9561-5/FIGURES/4

Taveira-Fernándes, C. (1972). *Aspects de l'ameliorationdu chataignier pour la résistance a la maladie de l'encre. In In Actas III Congr Un Fitopat*. Oeiras: Medit, 313–320.

Turchetti, T., Addario, A., and Maresi, M. (2010). Interazioni tra cinipide galligeno e cancro della corteccia: Una nuova criticità per il castagno. *Forest@ J. Silvic. Forest Ecol.* 7:252. doi: 10.3832/EFOR0642-007

Urquijo-Landaluze, P. (1957). La regeneración del castaño. *Boletín de Patología Vegetal y Entomología Agrícola* 22, 217–232.

van Hove, J., de Jaeger, G., de Winne, N., Guisez, Y., and van Damme, E. J. M. (2015). The Arabidopsis lectin EULS3 is involved in stomatal closure. *Plant Sci.* 238, 312–322. doi: 10.1016/J.PLANTSCI.2015.07.005

Vázquez, A., Martín, L. M., and Solla, A. (2016). Influencia de escenarios cambiantes de estrés hídrico y encharcamiento en la susceptibilidad de Castanea sativa a Phytophthora cinnamomi. *Cuadernos de la Sociedad Española de Ciencias Forestales* 43, 227–234. doi: 10.31167/CSEF.V0I42.17478

Vettraino, A. M., Natili, G., Anselmi, N., and Vannini, A. (2001). Recovery and pathogenicity of Phytophthora species associated with a resurgence of ink disease in Castanea sativa in Italy. *Plant Pathol.* 50, 90–96. doi: 10.1046/j.1365-3059.2001.00528.x

Vieira Natividade, J. (1947). *Quatro anos na defesa da campanha e reconstituição dos soutos. Junta Nacional das Frutas (Ed.)*. Sintra: Tipografia Medina, 18.

Viéitez, E. (1960). "Obtención de castaños resistentes a la enfermedad de la tinta," in *investigaciones y experiencias forestales de Lourizán, Pontevedra, Spain*, ed. C. R. Estudios (Sucesores de Rivadeneyra S.A: Madrid).

Vieitez, F. J., and Merkle, S. A. (2005). "Fagaceae," in *Biotechnology of Fruit and Nut Crops*, ed. R. E. Litz (Wallingford, UK: CAB International), 263–296.

Villani, F., Pigliucci, M., Benedettelli, S., and Cherubini, M. (1991). Genetic differentiation among Turkish chestnut (Castanea sativa Mill.) populations. *Heredity* 66, 131–136. doi: 10.1038/hdy.1991.16

Vinson, C. C., Mota, A. P. Z., Porto, B. N., Oliveira, T. N., Sampaio, I., Lacerda, A. L., et al. (2020). Characterization of raffinose metabolism genes uncovers a wild Arachis galactinol synthase conferring tolerance to abiotic stresses. *Sci. Rep.* 10:15258. doi: 10.1038/s41598-020-72191-4

Waldboth, M., and Oberhuber, W. (2009). Synergistic effect of drought and chestnut blight (Cryphonectria parasitica) on growth decline of European chestnut (Castanea sativa). *Forest Pathol.* 39, 43–55. doi: 10.1111/j.1439-0329.2008.00562.x

Westbrook, J. W., Holliday, J. A., Newhouse, A. E., and Powell, W. A. (2020a). A plan to diversify a transgenic blight-tolerant American chestnut population using citizen science. *Plants People Planet* 2, 84–95. doi: 10.1002/PPP3.10061

Westbrook, J. W., Zhang, Q., Mandal, M. K., Jenkins, E. V., Barth, L. E., Jenkins, J. W., et al. (2020b). Optimizing genomic selection for blight resistance in American chestnut backcross populations: A trade-off with American chestnut ancestry implies resistance is polygenic. *Evol. Appl.* 13, 31–47. doi: 10.1111/eva.12886

Weste, G., and Marks, G. C. (1987). The Biology of Phytophthora cinnamomi in Australasian Forests. *Annu. Rev. Phytopathol.* 25, 207–229. doi: 10.1146/annurev.py.25.090187.001231

Xing, Y., Liu, Y., Zhang, Q., Nie, X., Sun, Y., Zhang, Z., et al. (2019). Hybrid de novo genome assembly of Chinese chestnut (Castanea mollissima). *Gigascience* 8:giz112. doi: 10.1093/gigascience/giz112

Zentmyer, G. A. (1988). Origin and distribution of four species of Phytophthora. *Trans. Br. Mycol. Soc.* 91, 367–378. doi: 10.1016/S0007-1536(88)80111-6

Zentmyer, G. A., and Mircetich, S. M. (1966). Saprophytism and persistence in soil by Phytophthora cinnamomi. *Phytopathology* 56, 710–712.

Zhang, B., Oakes, A. D., Newhouse, A. E., Baier, K. M., Maynard, C. A., and Powell, W. A. (2013a). A threshold level of oxalate oxidase transgene expression reduces Cryphonectria parasitica-induced necrosis in a transgenic American chestnut (Castanea dentata) leaf bioassay. *Transgenic. Res.* 22, 973–982. doi: 10.1007/s11248-013-9708-5

Zhang, C., Moutinho-Pereira, J. M., Correia, C., Coutinho, J., Gonçalves, A., Guedes, A., et al. (2013b). Foliar application of Sili-K§increases chestnut (Castanea spp.) growth and photosynthesis, simultaneously increasing susceptibility to water deficit. *Plant Soil* 365, 211–225. doi: 10.1007/S11104-012-1385-2/FIGURES/4

Zhebentyayeva, T. N., Sisco, P. H., Georgi, L. L., Jeffers, S. N., Perkins, M. T., James, J. B., et al. (2019). Dissecting Resistance to Phytophthora cinnamomi in Interspecific Hybrid Chestnut Crosses Using Sequence-Based Genotyping and QTL Mapping. *Phytopathology®* 109, 1594–1604. doi: 10.1094/PHYTO-11-18-0425-R

Zhebentyayeva, T., Chandra, A., Abbott, A. G., Staton, M. E., Olukolu, B. A., Hebard, F. V., et al. (2014). Genetic and genomic resources for mapping resistance to Phytophthora cinnamomi in chestnut. *Acta Hortic.* 1019, 263–270.

frontiers | Frontiers in Plant Science

TYPE Review
PUBLISHED 26 August 2022
DOI 10.3389/fpls.2022.906087

OPEN ACCESS

EDITED BY
Raffaella Battaglia,
Council for Agricultural and Economics Research (CREA), Italy

REVIEWED BY
Shigeyuki Betsuyaku,
Ryukoku University,
Japan
Rafael Cruz,
University of Edinburgh,
United Kingdom

*CORRESPONDENCE
Madhumitha Narasimhan
madhumitha.narasimhan@hhu.de

SPECIALTY SECTION
This article was submitted to Plant Development and EvoDevo, a section of the journal Frontiers in Plant Science

RECEIVED 28 March 2022
ACCEPTED 08 August 2022
PUBLISHED 26 August 2022

CITATION
Narasimhan M and Simon R (2022) Spatial range, temporal span, and promiscuity of CLE-RLK signaling.
Front. Plant Sci. 13:906087.
doi: 10.3389/fpls.2022.906087

Spatial range, temporal span, and promiscuity of CLE-RLK signaling

Madhumitha Narasimhan[1]* and Rüdiger Simon[2]

[1]Institute for Developmental Genetics, Heinrich-Heine University, Düsseldorf, Germany, [2]Institute for Developmental Genetics and Cluster of Excellence in Plant Sciences, Heinrich-Heine University, Düsseldorf, Germany

CLAVATA3/EMBRYO SURROUNDING REGION-RELATED (CLE) signaling through receptor-like kinases (RLKs) regulates developmental transitions and responses to biotic and abiotic inputs by communicating the physiological state of cells and tissues. CLE peptides have varying signaling ranges, which can be defined as the distance between the source, i.e., the cells or tissue that secrete the peptide, and their destination, i.e., cells or tissue where the RLKs that bind the peptide and/or respond are expressed. Case-by-case analysis substantiates that CLE signaling is predominantly autocrine or paracrine, and rarely endocrine. Furthermore, upon CLE reception, the ensuing signaling responses extend from cellular to tissue, organ and whole organism level as the downstream signal gets amplified. CLE-RLK-mediated effects on tissue proliferation and differentiation, or on subsequent primordia and organ development have been widely studied. However, studying how CLE-RLK regulates different stages of proliferation and differentiation at cellular level can offer additional insights into these processes. Notably, CLE-RLK signaling also mediates diverse non-developmental effects, which are less often observed; however, this could be due to biased experimental approaches. In general, CLEs and RLKs, owing to the sequence or structural similarity, are prone to promiscuous interactions at least under experimental conditions in which they are studied. Importantly, there are regulatory mechanisms that suppress CLE-RLK cross-talk *in vivo,* thereby eliminating the pressure for co-evolving binding specificity. Alternatively, promiscuity in signaling may also offer evolutionary advantages and enable different CLEs to work in combination to activate or switch off different RLK signaling pathways.

KEYWORDS

CLE, RLK, proliferation, differentiation, spatial range, non-developmental effects, promiscuity, co-evolution

Introduction

Cell to cell communication in plants is co-ordinated by several mobile signals, such as peptides, hormones, RNAs, and proteins. The CLE family of peptides in plants is central for communication and mediation of a wide range of processes that are essential for development, and in response to biotic and abiotic stimuli. The CLE pre-propeptides with a size of 80–100 amino acids are first synthesized in the rough endoplasmic reticulum in

an inactive form, and then proteolytically processed and have been, in some cases, shown to be glycosylated in the secretory pathway to form an active peptide of 12 or 13 amino acids, consisting of a highly conserved CLE domain as it reaches the apoplast. CLE peptides then bind to plasma membrane-localized RLKs on the CLE-secreting or adjacent cells, or are transported *via* the phloem to trigger intracellular signaling cascades in distant target tissues (Rojo et al., 2002; Gao and Guo, 2012; Notaguchi and Okamoto, 2015). Based on their function and sequence similarities, CLE peptides can be broadly classified into A-type (CLAVATA3 (CLV3) and CLV3-likes) that promote differentiation, or B-type (TRACHEARY ELEMENT DIFFERENTIATION INHIBITORY FACTOR (TDIF) and TDIF-likes) that promote proliferation when applied exogenously (Whitford et al., 2008). CLE peptides are often perceived by leucine-rich repeat (LRR)-RLKs, which contain an extracellular ligand-binding domain consisting of LRRs, a transmembrane domain, and an intracellular kinase domain (Poliushkevich et al., 2020). In this review, we will focus on CLE interaction with LRR-RLKs (hereafter referred to as CLE-RLK). CLE peptide perception may also require additional receptors for its perception and initiation of signaling cascade, such as the receptor-like protein CLAVATA 2 (CLV2), which contains an extracellular receptor domain, a transmembrane domain, and a small cytoplasmic tail, and the receptor-like pseudokinase CORYNE (CRN), which contains a transmembrane domain and a kinase domain. While CLE peptides almost exclusively bind and signal through members of the RLK subfamily XI, the co-receptors are from other subfamilies (Poliushkevich et al., 2020; Furumizu et al., 2021). RLKs can form homomers at the plasma membrane and interact with CLV2-CRN heteromers in the absence of the peptide ligand; notably, these preformed complexes cluster after CLE peptide binding (Bleckmann et al., 2010; Somssich et al., 2015; Hu et al., 2018). However, the precise function of the CLV2-CRN pseudo-receptor heteromeric complex is not yet known.

CLE-RLK signaling and effects

CLE-RLK signaling is a spatially co-ordinated process and its effects are highly temporally correlated. The spatial dimension constitutes the cells/tissue layers that send out the CLE signal, and those that perceive these signals through RLKs and respond to them, i.e., the signaling range (Müller and Schier, 2011). CLE peptides can be secreted and perceived by the same cell or a group of cells (autocrine). Alternatively, the peptide molecules can diffuse to the nearby cells to signal (paracrine), or can travel long-distance to different organs (endocrine). In this section, we have done a case-by-case analysis of some imperative and recent studies pertaining to the origin and the destination of the CLE signal.

The events following CLE perception have a wide temporal range. For example, activation of transcription factors (TFs) and subsequent induction of responsive genes happens in minutes, control of cell division occurs after hours, establishment of primordium occur in a day, formation of new organs require several days. Thus, the ensuing cell to organ level effects vary as the downstream signal gets amplified and spreads through intercellular communication (Plieth, 2010; Van Norman et al., 2011). This section highlights the temporal dimension of CLE-RLK signaling and their multiple effects—from molecular or cellular level (considered as short-term effect) to tissue, organ, or organism level (considered as long-term effect)—Table 1.

Regulation of proliferation and differentiation

Proliferation is the increase in the number of cells with the same identity as a result of continuous symmetric cell divisions, whereas differentiation involves symmetric or asymmetric formative divisions resulting in cells with different identities. CLE-RLK signaling regulates proliferation and differentiation of meristems, the region that embodies pluripotent stem cells, which continuously supply proliferating cells in the plant body. Plant and non-plant CLE peptides also regulate primordium formation in the root during bacterial symbiosis and nematode infections. Such CLE-RLK mediated regulation of proliferation and differentiation have been reported largely at the organ and tissue levels (Fletcher, 2020; Whitewoods, 2021; Willoughby and Nimchuk, 2021). However, the regulatory events occurring at the cellular level in controlling cell division and differentiation have not been understood well.

There are several stages that lead to cell division and differentiation or proliferation at cellular level. When the need for proliferation and differentiation is evaluated, CLE peptides, in addition to other signaling factors, can be secreted to signal the decision. Then the stem cell that will undergo formative division (stage 1—Figure 1A) receives the signal. Formative divisions, which can be asymmetric or symmetric, give rise to daughter cells of different identities. During asymmetric divisions, external signals, such as CLE peptides from the surrounding cells, together with the differentially inherited and intrinsic proteins and microRNAs initially polarize the cell. Then the orientation of cell division sets and the cell divides forming daughter cells with two distinct identities (stage 2—Figure 1A; De Veylder et al., 2007; De Smet and Beeckman, 2011; Kajala et al., 2014; Xu et al., 2021). The freshly divided stem cells are initially endowed with plastic identity with which they proliferate. These cells, through cues from CLE peptides based on the needs of the surrounding cells, can remain uncommitted to their identity (stage 3—Figure 1A). But over time, the cells commit to their identity through several morphological changes and differentiate, which can also be regulated by CLE (stage 4—Figure 1A). However, fully differentiated plant cells are capable of de−/redifferentiation (Gilbert, 2000; De Smet and Beeckman, 2011; Furuta et al., 2014; Gujas et al., 2020; Seo et al., 2020). A similar set of events occurs during the proliferation process of meristematic stem cells or the

TABLE 1 Summary of CLE-RLK signaling.

CLE peptide	RLK and/or other receptors involved	Origin of the peptide	Destination of the peptide/location of RLK Signaling range	Short-term (molecular, cellular) and long-term (tissue, organ, organism) effects
In the apical meristem of *Marchantia*				
MpCLE2	Signals through MpCLV1	The apical notch but outside the central region that hosts central subapical cells	The meristem with the apical and subapical cells where *MpCLV1* is expressed **Paracrine signaling**	Short-term: Inhibits differentiation of the subapical cells **Long-term: Mediates accumulation of subapical cells and enables their subsequent differentiation and dichotomous branching**
MpCLE1	Signals through MpTDR	The ventral part around the apical cell	Dorsal part where *MpTDR* is expressed **Both auto- and paracrine signaling**	Short-term: Inhibits proliferation of the apical meristem **Long-term: Regulates expansion of the thallus and proper formation of gametangiophores and gemma cups**
During *Physcomitrium* gametophore formation				
PpCLEs 1, -2, and -7	(PpCLE1 to -7) Signal through PpRPK2 and	Different regions in the gametophores	Gametophore	Short-term: Initiation of formative division, maintenance of CD orientation and specification of cell fate **Long-term: 1. Mediates formation of properly sized mature gametophores 2. Inhibits proliferative divisions in gametophore, thus maintaining gametophore and leaf size**
PpCLE6	PpCLV1a and -b	Protonemal filament	Likely gametophore	
PpCLE 3, -4, and -5		Not characterized	Likely gametophore	
In the SAM of *Arabidopsis*				
CLE40	Signals through (and likely binds) BAM1	PZ of IFM and SAM	PZ where *BAM1* is expressed **Likely autocrine signaling**	Short-term: 1. Induces *WUS* in the OC 2. Promotes proliferation and suppresses differentiation of stem cells **Long-term: 1. Promotes SAM growth 2. Proper formation of floral organs**
CLV3	Binds and signals through CLV1; signals through RPK2, CLV2/CRN	CZ of IFM and SAM	OC where it binds and signals through CLV1 **Paracrine signaling**	Short-term: 1. Represses *WUS* and its expansion into CZ 2. Suppresses proliferation of stem cells and enables their differentiation **Long-term: 1. Inhibits SAM growth 2. Regulates proper formation of floral organs**
In the root apical meristem of *Arabidopsis*				
CLE45	Binds BAM3; signals through CLV2/CRN, RPK2	PSE and SPC	1. PSE and SPC where it binds and signals through BAM3 **Autocrine signaling**	Short-term: 1. Inhibits periclinal, formative division of SPC into proto- and metaphloem cells 2. Inhibits the acquisition of morphological changes during PSE differentiation **Long-term: 1. Regulates PSE cell file formation 2. Regulates PRM development**
			2. Likely CC and PPP where *RPK2* is expressed **Likely paracrine signaling**	Short-term: Inhibits CC and PPP differentiation into PSE **Long-term: Maintains a reservoir of phloem cells with plastic identity for future needs**
CLE25	Signals through CIK and CLV2	In root: SPCs and its lineage; In stem: sieve elements	Not characterized	Short-term: Regulates periclinal, formative division of SPC into proto- and metaphloem cells **Long-term: Regulates PRM development, phloem transport and starch immobilization**
In the vascular meristem				
CLE41	Signals through PXY	Phloem	Cambium where *PXY* is expressed **Paracrine signaling**	Short-term: 1. Triggers proliferation of procambium/cambium by upregulating *WOX4* 2. Inhibits its differentiation into xylem 3. Controls orientation of procambial cell division **Long-term: 1. Organized vascular patterning 2. Maintenance of stele size and radial growth of the vascular system**

(Continued)

TABLE 1 Continued

CLE peptide	RLK and/or other receptors involved	Origin of the peptide	Destination of the peptide/location of RLK Signaling range	Short-term (molecular, cellular) and long-term (tissue, organ, organism) effects
PttCLE41	Likely signals through PttPXY	Phloem	Likely vascular cambium where *PttPXY* is expressed **Likely paracrine signaling**	Short-term: Likely induces proliferation of cambial cells, which then differentiate into xylem cells **Long-term: 1. Maintains overall secondary vascular growth and stem diameter 2. Regulates the internodal length and height of the plant**
PtrCLE20	Likely signals through PtrCLV2	Xylem	Vascular cambium **Paracrine signaling**	Short-term: Likely suppresses cambial cell proliferation leading to a decreased rate of xylem differentiation **Long-term: Maintains overall secondary vascular growth and stem diameter 2. Regulates the internodal length and height of the plant**
CLE9	Binds BAM1; signals through BAM2 and -3	Xylem precursors, particularly of protoxylem cell file positions	Likely xylem precursors of protoxylem cell file positions, where it binds and signals through BAM1, although BAM1 is broadly expressed in vascular and pericycle cells **Likely autocrine signaling**	Short-term: Prevents peri- and anticlinal divisions of xylem precursors that increases xylem and procambial cell number **Long-term: 1. Regulates the number of xylem and procambium cell files 2. Regulates the overall plant growth**
In stomatal lineage development				
CLE9	Binds HSL1-SERK1, the RLK-coreceptor complex	MMC, meristemoids and GCs	MMC and meristemoids, where it binds and signals through HSL1 **Likely autocrine signaling**	Short-term: 1. Destabilizes SPCH to prevent MMC from acquiring its identity 2. Prevents its further asymmetric divisions **Long-term: Regulates the density of GCs and PCs in leaves**
In root nodulation				
MtCLE12 and -13	Signals through MtSUNN, MtCRN	Nodule primordium in root	Likely shoot where *MtSUNN* is expressed **Likely endocrine signaling**	Short-term: MtCLE13 suppresses the proliferative divisions likely right after the initial cell divisions of the cortex and pericycle **Long-term: 1. Both peptides inhibit nodule primordium development 2. Decrease the nodule numbers, thus establishing N homeostasis**
LjCLE-RS1 and -2	Binds LjHAR1; signals through LjKLV and LjCLV2	Nodule primordium in root	Shoot, likely in leaf phloem, where *LjHAR1* is expressed **Endocrine signaling**	Short-term: LjCLE-RS1 and −2 peptides negatively regulate continuous cortical cell divisions after a few rounds of initial divisions **Long-term: 1. Both peptides inhibit nodule primordium development 2. Decrease the nodule numbers, thus establishing N homeostasis**
In nematode infection				
HsCLEB	Signals through TDR, CLV1, RPK2, CLV2/CRN	Nematode esophageal gland	Likely procambial cells in the root and/or the syncytial cells expressing TDR	Short-term: Induces procambial proliferative divisions **Long-term: Induces syncytia formation and increases rate of infection**
In organ primordium and organ development				
CLE26	Can bind and possibly signals through BAM1 and -2	Phloem pole of the stele in basal meristem	Not characterized	Short-term: Affects the PIN1 protein level in the root **Long-term: 1. Alters the auxin distribution in roots 2. Regulates PR length and LR density**
CLE3	Signals through CLV1	Pericycle cells in PR and LR	Likely companion cells where *CLV1* is expressed **Likely paracrine signaling**	Short-term: Not characterized **Long-term: 1. Inhibits LR emergence 2. Prevents root expansion in low N conditions**

(Continued)

TABLE 1 Continued

CLE peptide	RLK and/or other receptors involved	Origin of the peptide	Destination of the peptide/location of RLK Signaling range	Short-term (molecular, cellular) and long-term (tissue, organ, organism) effects
CLE5	Not characterized	Bases of young rosette leaves, of cauline leaves and of cotyledons of mature embryo; at both the adaxial and abaxial domains of vegetative shoot apex in developing rosette leaves	Not characterized	Short-term: Not characterized **Long-term: Regulates leaf width and symmetry**
CLE6	Not characterized	Bases of young rosette leaves and floral organs; only at the adaxial domain of vegetative shoot apex in developing rosette leaves	Not characterized	Short-term: Not characterized **Long-term: Regulates leaf width, symmetry and curvature**
Not characterized	CLV2/CRN	Not characterized	Not characterized	Short-term: 1. Upregulates auxin synthesis genes in the IFM cells 2. Maintains PIN1 protein levels in the IFM cells **Long-term: 1. Maintains overall auxin signaling in the IFM 2. Mediates flower primordia outgrowth and complete flower formation**
CLV3 and other CLEs	Signal through BAM1, -2, and -3	Not characterized	Not characterized	Short-term: Not characterized **Long-term: 1. Mediate flower primordia outgrowth and complete flower formation**
In regulation of non-developmental responses				
CLE25	Signals through BAM1 and -3	Vascular procambium of, possibly, the root	Leaf where *BAM1* and -2 are expressed **Endocrine signaling**	Short-term: 1. Promotes ABA synthesis 2. Enables stomatal closure **Long-term: Reduces water loss and ensures overall survival of the plant during water deficiency**
CLE9	Not characterized	Stomatal GCs	Likely the stomatal GCs **Likely autocrine signaling**	Short-term: 1. Activates *MPK3,−6* 2. Enables stomatal closure by signaling through effectors, such as, ABA, NO, H_2O_2 **Long-term: Prevents excessive water loss, thus conferring resistance to drought stress**
MtCLE53	Signals through MtSUNN	Vascular tissue with increased expression near colonization sites	Not characterized	(MtCLE53/-33) Short-term: 1. Upregulates *MtSUNN* 2. Suppresses the expression of strigolactone biosynthetic genes
MtCLE33	Signals through MtSUNN	Vascular tissue with strong expression in pericycle and xylem parenchyma (no change due to colonization)	Not characterized	**(MtCLE53/-33) Long-term: Suppresses excessive AM fungal colonization thus attaining Pi homeostasis**
RiCLE1	Not characterized	Fungi colonizing the root	Likely the epidermal and cortical cells	Short-term: Not characterized **Long-term: 1. Modulates root architecture by promoting PR and LR branching 2. Promotes the entry and spread of the fungi**
CLE45	Binds SKM1 and signals through SKM1 and -2	Stigma of the pistil at 22°C and expanded to the transmitting tract where pollen elongates at 30°C	Pollen where it binds SKM1 **Paracrine signaling**	Short-term: Retains mitochondrial dehydrogenase activity at high temperature, thus prolonging pollen viability 2. Sustains pollen performance and increases the chances of pollen tubes reaching the ovules **Long-term: Ensures stable seed production**

The list of CLE peptides and RLKs and other receptors they bind and/or signal through, their signaling range, the origin of the peptide and its destination where it exerts its effect, the short- and long-term effects covering the molecular, cellular, tissue, organ, and organism levels. ABA, abscisic acid; AM, arbuscular mycorrhiza; BAM, BARELY ANY MERISTEM; CC, companion cells; CD, cell division; CIK, CLAVATA3 INSENSITIVE RECEPTOR KINASES; CLE, CLAVATA3/EMBRYO SURROUNDING REGION-RELATED; CRN, CORYNE; CLV, CLAVATA; CZ, central zone; GC, guard cell; HSL, HAESA-LIKE 1; IFM, inflorescence meristem; LR, lateral root; MMC, meristemoid mother cell; MPK, MITOGEN-ACTIVATED PROTEIN KINASE; OC, organizing center; PC, pavement cell; PIN, PIN-FORMED; PPP, phloem pole pericycle; PRM, proximal root meristem; PSE, protophloem sieve element; PXY, PHLOEM INTERCALATED WITH XYLEM; PZ, peripheral zone; RLK, receptor-like kinase; RPK2, RECEPTOR-LIKE PROTEIN KINASE 2; SAM, shoot apical meristem; SKM, STERILITY-REGULATING KINASE MEMBER; SPC, sieve element precursor cell; SPCH, SPEECHLESS; SERK, SOMATIC EMBRYOGENESIS RECEPTOR KINASE; SUNN, SUPER NUMERIC NODULES; TDR, TDIF RECEPTOR; WOX, WUSCHEL-related HOMEOBOX 4; WUS, WUSCHEL. The name of the CLE peptide, its signaling range and the long term effects it mediates are described in bold letters.

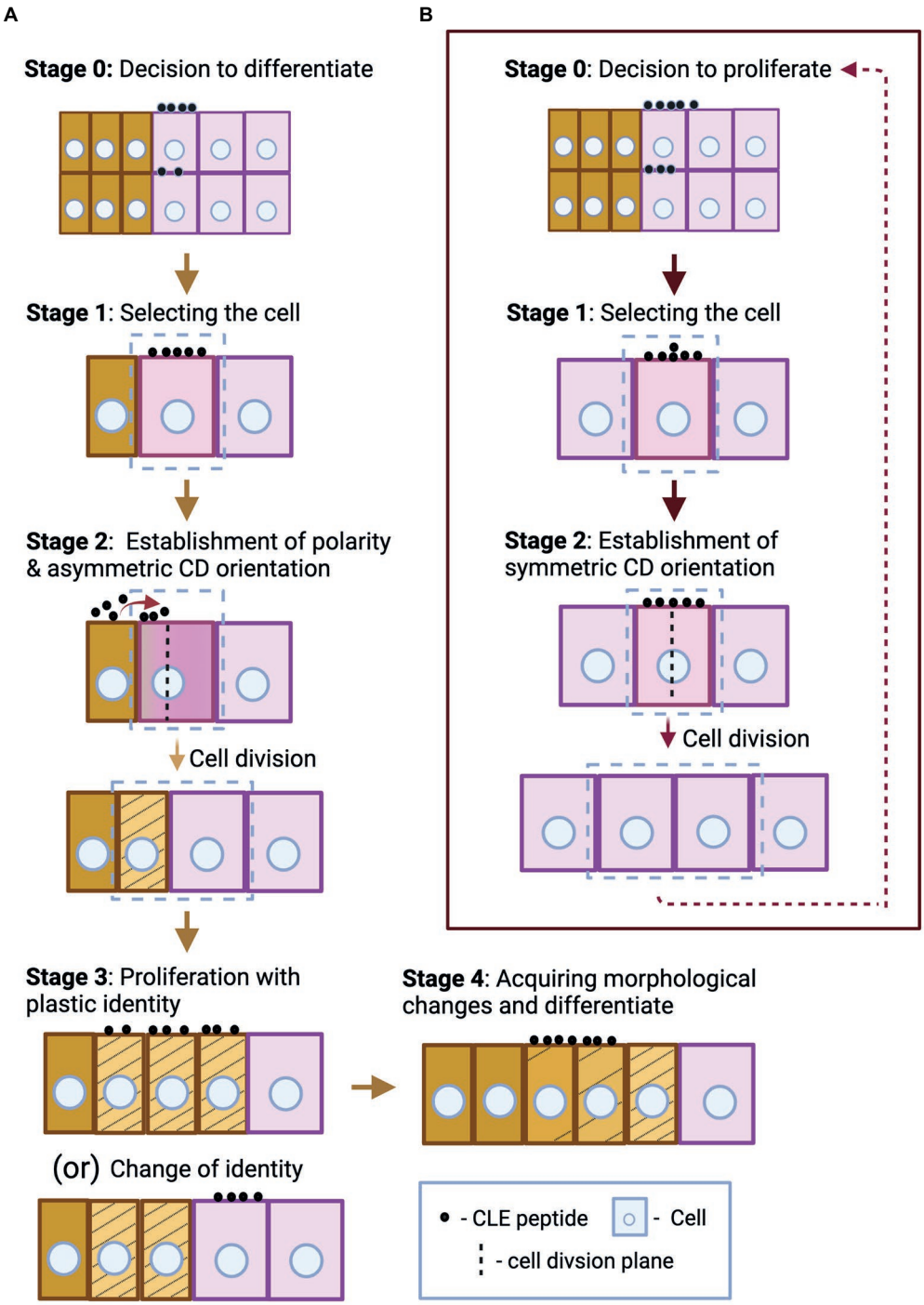

FIGURE 1
Schematic representation of some key aspects of different stages of asymmetric stem cell division and differentiation **(A)**, and symmetric cell division during proliferation **(B)**. **(A)** In stage 0, the CLE peptides that originate from the same or the surrounding cells send the signal to differentiate. Following the signal, the stem cell undergoes differentiation, and this process can be divided into four basic stages. First, the cell to undergo asymmetric formative division is selected (marked by a box)—stage 1. Based on the positional cues offered by neighboring cells through secreted CLE peptides (their origin and direction of diffusion are indicated by red arrow), the cell polarity and the cell division orientation are established. The cell divides producing daughter cells of unequal sizes with distinct identity (represented by striped yellow and pink cells)—stage 2. When the freshly divided stem cells are endowed with plastic identity (represented by stripes), they proliferate with the same plastic identity, or a particular cell (striped yellow) switches its identity to that of the surrounding cell (pink), under certain circumstances—stage 3. The cells further differentiate and reach its destination identity (unstriped yellow) by acquiring several morphological changes over time—stage 4. Stages 3 and 4 may also be regulated by CLE peptides, but the origin and directionality of the CLE peptides regulating stages 0, 3, and 4 are not defined in this figure as these can be case specific. **(B)** After the decision-making CLE peptides signal to proliferate—stage 0, the stem cells undergo proliferation, and this process comprises of two basic stages. First, the cell to undergo symmetric division is selected—stage 1. Then a symmetric cell division plane is set and the cell divides to form identical daughter cells—stage 2. The stem cells proliferate by continuous repetition of the two cell division stages. CLE peptides can induce or inhibit any of these stages of differentiation and proliferation processes.

cells forming the primordium (Figure 1B; De Veylder et al., 2007; Desvoyes et al., 2021). In addition to CLE peptides, several factors like hormones and TFs have been shown to regulate proliferation and differentiation at various stages (De Smet and Beeckman, 2011; Xu et al., 2021). This section highlights the influence of CLE-RLK signaling on stages of cell division and differentiation at the cellular level, in addition to the eventual tissue, organ and organism level effects (Figure 2; Table 1).

In the apical meristem of *Marchantia*

The genome of the liverwort *Marchantia polymorpha* encodes two CLE peptides: (1) *MpCLE1*, a TDIF-like peptide and (2) *MpCLE2*, a CLV3-like peptide, and two RLKs: *MpTDIF RECEPTOR* (*TDR*) and *MpCLAVATA 1* (*CLV1*). The apical meristem, hosted by the apical notch, is located at the growing tip of the gametophyte body (thallus). The apical notch, apart from being responsible for the radial expansion of the thallus, also produces gametangiophores, which are the reproductive structures developed from the thalli (Shimamura, 2016; Hirakawa et al., 2019). Hirakawa et al. (2019) showed that *Mpcle1* mutant exhibited thickening of the thallus and overgrowth of gametangiophores, whereas overexpression of *MpCLE1* resulted in small convoluted and distorted thalli. *MpCLE1*, expressed in the ventral part around the apical cell likely diffuses to the dorsal part where *MpTDR* is expressed to signal for suppression of proliferation (paracrine signaling; Hirakawa et al., 2019).

MpCLE2 inhibits differentiation of the dorsal and ventral derivatives at the apical meristem. The apical notch laterally expanded upon *MpCLE2* overexpression as undifferentiated anticlinally divided subapical cells over-accumulated. This resulted in multichotomous branching, whereas subapical cells, after reaching threshold cell numbers, immediately divide periclinally to differentiate and undergo dichotomous branching. *MpCLE2* is normally expressed outside of the central subapical stem cell region and signals *via* MpCLV1, which is expressed in the central region. MpCLE2 likely moves to the central region to elicit inhibition of differentiation (paracrine signaling; Hirakawa et al., 2020).

To summarize, MpCLE1 and MpCLE2 signal through MpTDR and MpCLV1 to inhibit proliferation and differentiation processes, respectively. However, it is not clear at which stage of cell division from stage 0 to 2 they act.

During *Physcomitrium* gametophore formation

CLE peptides regulate both differentiation and proliferation in moss. Whitewoods et al. (2018) showed that multiple CLE-like peptide mutants and CLV1-like receptor mutants exhibited defects in 3D development during gametophore formation. Fewer mutant gametophores were formed, and they had a significantly reduced height. Gametophore initiation was inhibited due to defects in orientation of cell division already at the 2-cell and 4-cell stages during which cell identity is defined. Moreover, the mutants formed a callus-like mass at the gametophore base, indicating defective proliferation and cell identity regulation. Furthermore, external application of the CLE peptides resulted in stunted gametophore development to which the RLK mutant, *Ppreceptor-like protein kinase 2* (*Pprpk2*) was resistant, implying that PpCLEs regulate proliferation through PpRPK2 (Whitewoods et al., 2018). This indicates that components and functions of CLE signaling networks regulating both proliferation and differentiation balance are conserved across clades during land plant evolution. Therefore, additionally understanding at what stages each of the PpCLE peptides operate to influence differentiation and proliferation processes will inform us of the common courses of action that complex land plants could have evolved.

In the shoot apical meristem of *Arabidopsis*

In the *Arabidopsis* inflorescence meristem (IFM), two key CLE peptides, CLV3 and CLE40, are expressed in complementary regions: *CLV3* is expressed in the central zone (CZ), where stem cells proliferate at a very slow rate. Stem cell daughters can shift to the peripheral zone (PZ) where the cells proliferate at a higher rate and start acquiring organ identities (flower meristem or leaf primordium; Fletcher et al., 1999; DeYoung et al., 2006; Deyoung and Clark, 2008; Schlegel et al., 2021). In the PZ, the cells express the CLE40 peptide. The homedomain TF WUSCHEL (WUS) is expressed in the organizing center (OC) and moves to the CZ to promote stem cell proliferation and *CLV3* expression (Mayer et al., 1998). CLE40 from the PZ promotes *WUS* expression in the OC by signaling through the RLK BARELY ANY MERISTEM1 (BAM1) in the PZ (likely autocrine signaling), thus indirectly promoting stem cell proliferation at the CZ (Deyoung and Clark, 2008; Schlegel et al., 2021). CLV3 diffuses from the CZ to the OC where it binds to CLV1 and signals to repress *WUS* (paracrine signaling; Figure 2A), limiting the WUS activity in the CZ, thereby restricting stem cell proliferation to decrease the IFM size (Clark et al., 1995, 1997; Fletcher et al., 1999; Brand et al., 2000; Schoof et al., 2000; Rojo et al., 2002). Correspondingly, *cle40* mutant exhibited smaller SAM and *clv3* mutant had enlarged SAM with extra floral organs (Clark et al., 1995; Schlegel et al., 2021). CLV2/CRN, RPK2 and a family of co-receptors, CLAVATA3 INSENSITIVE RECEPTOR KINASES1-4 (CIKs) are also involved in CLV3 signaling (Kayes and Clark, 1998; Brand et al., 2000; Muller et al., 2008; Kinoshita et al., 2010; Shinohara and Matsubayashi, 2015; Nimchuk, 2017; Hu et al., 2018). The number of proliferating cells in the CZ, and by extension the amount of CLV3 they secrete continuously determine the amount of WUS being expressed, which in turn promotes stem cell proliferation. Thus, the CLV3 signal coming from stem cells determines their proliferation rate. Similarly, CLE40 secreted by the differentiating cells also control *WUS* expression, thus determining the proliferation rate of stem cells that will eventually differentiate. Together, CLV3 and CLE40 signaling can convey the current proliferation and differentiation status of CZ and PZ, respectively, thereby influencing decisions to proliferate or differentiate further (stage 0—Figure 1).

Furthermore, WUS promotes *CLV3* expression and suppresses *CLE40* expression (Yadav et al., 2011; Schlegel et al., 2021). These two interconnected negative feedback loops equilibrate the levels

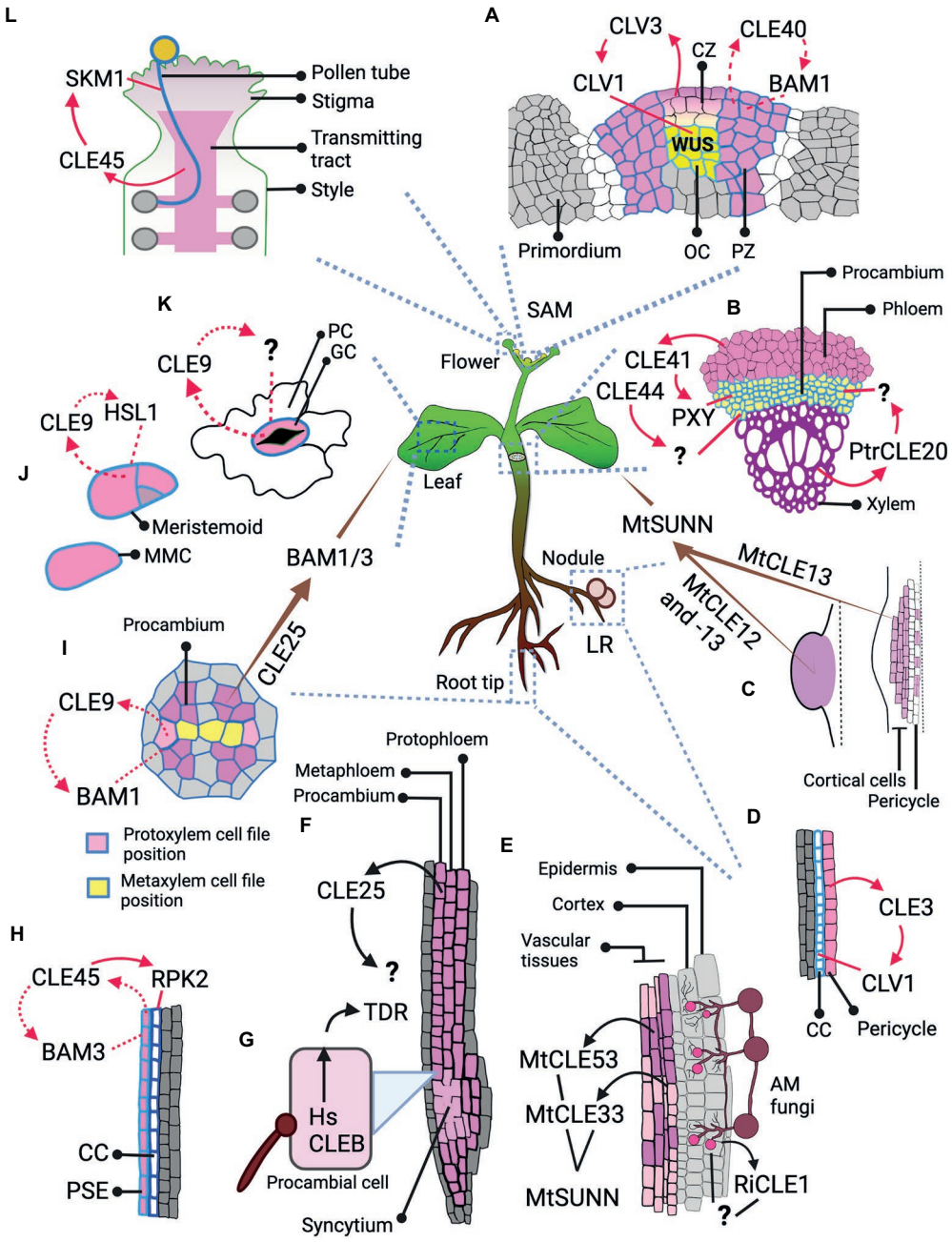

FIGURE 2
Spatial dimension of CLE signaling. The figure illustrates the cell or tissue of origin of the CLE peptide and its destination, and the RLK it binds to at the destination, thus defining whether the signaling type is autocrine, paracrine or endocrine. **(A)** Signaling in IFM: CLV3, as a paracrine signal from CZ, signals through CLV1 at the OC; CLE40, likely as an autocrine signal, signals through BAM1 at the PZ. **(B)** Paracrine signaling in vascular development: *Arabidopsis* CLE41 and CLE44 move from phloem to signal in procambium. CLE41 signals through PXY but the RLK through which CLE44 signals is unknown. In *Populus*, PtrCLE20 from xylem signals through an unknown RLK in procambium. **(C)** AON signaling from nodules: MtCLE13 from the cortical and pericycle cells of the developing nodule primordium (on the right), and both MtCLE12, -13 from young, round nodule (on the left) likely act as an endocrine signal and signal through MtSUNN in the shoot. **(D)** Signaling in LR: CLE3 from pericycle likely acts as a paracrine signal and moves to phloem CC to signal through CLV1. **(E)** Signaling during AM fungal symbiosis: *Rhizophagus irregularis* secretes RiCLE1 likely into the epidermal and cortical layers of the *Medicago* root, but the RLK that receives the CLE signal is unknown. *MtCLE53* and *-33* are expressed in the vascular tissues, while *MtCLE53* is upregulated close to the fungal infection sites. These CLEs signal through MtSUNN the localization of which is unknown. **(F,H)** Signaling during root protophloem development: **(F)** CLE25 is expressed in SPC lineage—protophloem, metaphloem, and procambium, but where and through which RLK it signals remains unknown. **(H)** CLE45, expressed in PSE, mediates an autocrine signaling regulation through BAM3 and likely a paracrine signaling regulation in CC through RPK2. **(G)** Signaling by nematode: HsCLEB, secreted by nematodes into the procambial cells, signals through TDR but it is not clear where it is expressed. **(I)** Autocrine signal in vascular development: CLE9, expressed in xylem precursors, signals through BAM1 expressed in vascular cells including xylem precursors. **(I–K)** Signaling in leaf: **(I)** CLE25, expressed in vascular procambium of root, acts as an endocrine signal and signals through BAM1/3 expressed in leaves for stomatal

(Continued)

FIGURE 2 Continued
closure. **(J)** CLE9 expressed in MMCs and meristemoid cells binds HSL1 expressed in the same cells and likely mediates an autocrine signaling regulation during stomatal development. **(K)** CLE9 likely mediates an autocrine signal through uncharacterized RLK in stomatal GCs for stomatal closure. **(L)** Paracrine signaling in pollen. CLE45 that expands into the transmitting tract signals through SKM1 in pollen. Various shades of pink mark the cells expressing different CLEs. Cell outlines with varying shades of blue represents different RLKs. The arrows indicate the signaling type. The brown tapering arrow—endocrine signaling; red solid arrow—paracrine signaling; red dotted arrow—autocrine signaling; black arrows—unknown signaling type due to lack of data on the RLK and/or its localization. Abbreviated cells and tissues: CZ, central zone; CC, companion cell; GC, guard cell; LR, lateral root; MMC, meristemoid mother cell; PC, pavement cell; PSE, protophloem sieve element; PZ, peripheral zone.

of WUS, CLE40 and CLV3 in the SAM, in order to balance the rates of proliferation and differentiation.

In the root apical meristem

In *Arabidopsis* roots, *CLE40* is expressed by the stele cells in the differentiation zone and mediates proliferation of the proximal root meristem (PRM—the root meristem part that extends from the quiescent center toward shoot, as opposed to the distal root meristem, DRM, that extends toward the root tip; Hobe et al., 2003; Stahl et al., 2009). *cle40* loss-of-function mutants exhibit a prematurely differentiated and therefore shorter proximal meristem. However, external application or overexpression of *CLE40* and, notably, of all the A-type peptides resulted in highly differentiated PRM, which depends on CRN-CLV2 (Fiers et al., 2005; Ito et al., 2006). In contrast, external application of *Arabidopsis* or poplar TDIFs induced proliferation and elongation of the PRM (Liu et al., 2016; Yang et al., 2020). Yang et al. (2020) further showed that TDIFs promote proximal and DRM size by regulating PIN-FORMED (PIN) mediated polar auxin transport. Thus, exogenous application of A-type or B-type peptide triggers a very generalized response in regulating differentiation and proliferation of the entire meristem, but how they regulate these processes at a cellular level is not yet understood.

CLE45 is expressed in the sieve element precursor cell (SPC) and its descendant cells in the PRM, and it has been shown to mediate both auto and paracrine regulatory signaling (Figure 2H). SPC undergoes periclinal division to form proto- and metaphloem cells. Protophloem cells then proliferate with a "plastic" protophloem sieve element (PSE) identity (in the meristematic zone) and these cells eventually undergo subsequent differentiation and commitment to PSE cell file identity (in the transition and differentiation zones). The RLK BAM3 is also expressed in SPC and its descendant cells, binds CLE45 (Figure 2H) and inhibits differentiation of the PSE cell file in diverse ways. At the cellular level, CLE45 suppresses periclinal division of SPC and the eventual formation of the PSE cell file. Additionally, CLE45 inhibits cells from committing to PSE identity in the differentiation zone by preventing them from acquiring morphological changes like cell wall thickening (Depuydt et al., 2013; Rodriguez-Villalon et al., 2014; Gujas et al., 2020). Furthermore, at tissue level, CLE45 signaling inhibits PRM development and elongation; however, this might be an indirect consequence of the lack of a PSE cell file (Depuydt et al., 2013; Hazak et al., 2017). CLV2 and CRN are essential in mediating CLE45 signaling (Fiers et al., 2005; Hazak et al., 2017), and interestingly, CRN promotes BAM3 localization at the plasma membrane (Hazak et al., 2017). Another plasma membrane-localized protein, OCTOPUS (OPS), sequesters CRN thus interfering with CLE45 signaling. Higher OPS activity or protein level antagonizes the CLE45 signaling effect. Moreover, *ops* mutants have increased BAM3 level and also frequently fail to form PSE (Hazak et al., 2017; Breda et al., 2019). This illustrates that the interplay between OPS and CLE45 signaling components retains a balance in PSE identity commitment in the phloem.

In addition to CLE45 inhibiting SPC descendants from acquiring PSE identity through autocrine signaling, CLE45 also inhibits the companion cells (CC) and phloem pole pericycle (PPP) cells from differentiating into PSE likely through paracrine signaling. Cell files surrounding PSE have the ability to reprogram and acquire PSE identity. CLE45 from PSE cell file signals to the neighboring CC and PPP cell files expressing RPK2 (Figure 2H) to prevent these cells from switching their identity to PSE, thus retaining a pool of plastic phloem cells (Gujas et al., 2020). During PSE formation, CLE45-BAM3 signaling controls different stages of cellular differentiation processes. It can inhibit the switch of the plastic CC and PPP identity into PSE, which occurs at stage 3 of cellular differentiation, or it can inhibit the PSE cells from acquiring morphological changes, which is stage 4 of cellular differentiation (Figure 1A). It also can suppress SPC formative division—at some point from stages 0 to 2—of cell differentiation process.

Similar to CLE45, CLE25 also affects PSE formation and consequently PRM development. *CLE25* is expressed in sieve elements of roots (Figure 2F) and stems and the *cle25* mutant exhibited a mild delay in PSE development. However, the mutant version $CLE25_{G6T}$ caused more pronounced defective downstream signaling (Ren et al., 2019). Plants expressing $CLE25_{G6T}$ sustained suppression of periclinal division of SPC into proto- and metaphloem (stage 0, 1, or 2). This further led to defects in PSE differentiation during early seedling development. However, at later stages, these earlier PSE defects resulted in significant accumulation of starch in leaves due to compromised starch remobilization caused by defective phloem transport (Ren et al., 2019).

In vascular development

The procambial and cambial cells constitute the vascular meristems. During primary growth, the plant mainly develops along the apical-basal axis. Once primary growth stops, cambium differentiates from procambium and actively proliferates and differentiates into secondary xylem and phloem, thus causing radial thickening of roots and stems, which occurs massively in woody plants (Miyashima et al., 2013; Růžička et al., 2015).

In *Arabidopsis*, the TDIF peptides (CLE41 and -44) have been shown to diffuse from phloem to procambium and promote proliferation of procambial/cambial cells by inducing *WUSCHEL-related HOMEOBOX4* (*WOX4*) expression; in parallel, they also inhibit differentiation of cambial cells into xylem (Hirakawa et al., 2008, 2010; Kondo et al., 2014). Similarly, in poplar trees, PttCLE41 peptide produced in the phloem also likely moves to cambium to induce cambial cell proliferation. Cambial cells express the RLK *PttPHLOEM INTERCALATED WITH XYLEM* (*PttPXY*). Etchells et al. (2015) observed that overexpressing *PttCLE41* or *PttPXY* in hybrid poplar resulted in taller trees with increased stem diameter due to higher cambial cell proliferation and xylem cell formation (Etchells et al., 2015). Zhu et al. (2020) observed an A-type peptide, PtrCLE20, produced by the secondary xylem moving into vascular cambium (Figure 2B) which suppresses its proliferation. Plants overexpressing *PtrCLE20* were shorter with decreased stem diameter due to significantly fewer vascular cambium and xylem cell layers (Zhu et al., 2020). Together, two poplar CLE peptides act in a complementary manner to retain an optimum number of dividing vascular cambium and differentiated xylem layers. However, it is not clear which stage of proliferative cell division each of the poplar CLEs regulate.

In addition to triggering proliferation of procambium/cambium and controlling its eventual differentiation, as discussed above, CLE41 also provides positional cues to control orientation of formative division. CLE41 diffuses from phloem to cambium (Figure 2B), thus potentially establishing a gradient and signals *via* PXY in the dividing cambial cells. This may alert them of the orientation of phloem and xylem tissues, thus assigning their plane of division, and signal to the daughter cell closest to the phloem to differentiate into a phloem cell. When Etchells et al. (2015) expressed *CLE41* ubiquitously, cell division orientations were disorganized and the arrangement of phloem, procambium and xylem was disarrayed (Etchells and Turner, 2010; De Smet and Beeckman, 2011; Etchells et al., 2015; Xu et al., 2021). In summary, like CLV3 in SAM, it is possible that CLE41 is secreted as a decision-making paracrine signal to proliferate procambium based on the current phloem differentiation status (stage 0—Figure 1B). In addition, during cambium differentiation into phloem and xylem, CLE41 could act as a polarizing signal to orient the cell division plane during stage 2 of cellular differentiation (Figure 1A).

In the meristematic zone of the root, xylem precursors in the protoxylem cell file position undergo periclinal divisions to increase the xylem file number of the metaxylem cell file positions. CLE9 is expressed in xylem precursors (particularly of the protoxylem cell file positions) and suppresses these divisions by binding BAM1, which is expressed widely across the vascular zone including xylem precursors (Figure 2I). BAM2 and -3 are also involved in this process. Thus, CLE9-BAM signaling restricts the xylem precursor cell proliferation, thereby preventing the formation of excessive number of differentiated metaxylem cell files (Qian et al., 2018). At the cellular level, CLE9-BAM1 signaling could be regulating any of the stages of proliferation—by suppressing the decision to proliferate or by regulating the cell cycle or any other cellular process (stages 0–2).

In stomatal lineage development

Meristemoid mother cells (MMC) are the stomatal lineage stem cells which give rise to the majority of the pavement cells (PC) in leaves by undergoing proliferative divisions and subsequent differentiation. An MMC first divides asymmetrically into a large stomata lineage ground cell (SLGC) and a smaller meristemoid cell, which in turn may undergo further rounds of asymmetric divisions forming more meristemoid cells. SLGC and meristemoid cells then differentiate into PCs and stomatal guard cells (GC), respectively (Lau and Bergmann, 2012). CLE9, expressed in MMCs, meristemoids and GCs, binds and signals *via* the RLK HAESA-LIKE 1 (HSL1) expressed in MMCs, meristemoids and PCs likely in an autocrine manner (Figure 2J). CLE9-HSL1 binding, which is enhanced by the SOMATIC EMBRYOGENESIS RECEPTOR KINASE 1 (SERK1) co-receptor, phosphorylates and destabilizes the TF SPEECHLESS (SPCH). SPCH is crucial for preserving MMC identity, and it also enables MMC to undergo subsequent asymmetric divisions that maintain the density of GCs and PCs in leaves (Qian et al., 2018). Thus, CLE9-HSL1 autocrine signaling in MMCs, by removing their own identity, unmarks themselves from being selected for formative divisions. Thereby, MMC differentiation is inhibited already at stage 1, when the cell to undergo division gets selected (Figure 1A).

In root nodulation

Nodules are specialized root organs that enable leguminous plants to enter symbiotic relationship with rhizobial bacteria. In response to rhizobial infection, some root cortical cells dedifferentiate, proliferate and finally form nodule primordia which host the bacteria. Nodulation is a costly process; hence plants exert a tight control over it through a process called autoregulation of nodulation (AON), which suppresses excessive nodulation (Ferguson et al., 2010; Reid et al., 2011). In *Medicago truncatula*, MtCLE12,-13 and -35 are expressed in the root in response to rhizobium and they mediate AON by signaling (by possibly binding) *via* the CLV1-like RLK SUPER NUMERIC NODULES (MtSUNN) expressed in the shoot. Thus, AON is likely the result of endocrine signaling from root to shoot (Imin et al., 2018; Lebedeva et al., 2020a; Mens et al., 2021). Similarly, in *Lotus japonicus*, root-derived arabinosylated LjCLE-RS1 and -2 are transported through xylem to the shoot where it binds and signals *via* CLV1-like HYPERNODULATION ABERRANT ROOT FORMATION 1 (LjHAR1), which is likely expressed in the leaf phloem (Krusell et al., 2002; Searle et al., 2003; Nontachaiyapoom et al., 2007; Okamoto et al., 2013). Observations on AON regulation by root-shoot CLE-RLK signaling in leguminous plants, demonstrated a novel role for CLE peptides as an endocrine signal (Okamoto et al., 2016). Moreover, the CRN and CLV2 orthologues in *M. truncatula*, MtCLV2 and MtCRN interact with MtSUNN; and mutation in *MtCRN* resulted in hypernodulation (Crook et al.,

2016). Similarly, in *Lotus japonicus,* mutations in *LjCLV2* and in *RPK2* orthologue, *KLAVIER* (*LjKLV*) also resulted in hypernodulation. Moreover, LjKLV and LjHAR1 interact with each other (Miyazawa et al., 2010; Krusell et al., 2011). This indicates that nodulation is regulated by CLE signaling through CLV1-like RLKs and other receptors, such as CRN, CLV2, and KLV.

MtCLE13 is already expressed in initial stages of nodule development. In the incipient and developing nodule primordium, *MtCLE13* is expressed strongly in the dividing cortical cells and mildly in pericycle cells around the regions of bacterial infection. But in the later young, round nodule stage, it is expressed throughout. However, *MtCLE12* is not expressed in the developing nodules, but in the later young, round nodule stage where, like *MtCLE13*, it is also expressed throughout the mature primordium (Mortier et al., 2010). It is likely that different CLE peptides produced by proliferating and differentiating cells during different stages of primordia development send paracrine AON activation signals in response (Figure 2C; Reid et al., 2011). Consistently, in response to AON activation, downstream hormones, TFs and miRNA (as observed in different leguminous plants) suppress nodule development (Suzaki et al., 2012; Takahara et al., 2013; Tsikou et al., 2018; Lebedeva et al., 2020b). Notably, in *Lotus japonicus*, this suppression was shown to occur after a few initial cortical cell divisions preventing the ensuing proliferative divisions, thus suppressing nodule primordium formation. Understanding which specific stage of cell division is being suppressed and the molecular mechanisms behind it will give us deeper insights into AON response signaling.

In nematode infection

Parasitic nematodes, such as root knot and cyst nematodes (RKN and CN, respectively) invade plant roots. The juvenile nematodes typically select a pericycle or procambial cell and inject several effector proteins including CLE peptide mimics into the cells through their stylet. The CLE mimics then reach the apoplast (Figure 2G) and manipulate the root vasculature development by inducing dedifferentiation and further proliferative divisions. The proliferated cells dissolve their cell wall and fuse to form a differentiated multinucleate feeding cell called a giant cell (in RKN) or syncytium (in CN), which serve as a nutrient source (Davis and Mitchum, 2005; de Almeida Engler and Gheysen, 2013; Frey and Favery, 2021).

In CN, A-type CLE mimics were identified in esophageal gland cell (Wang et al., 2005; Lu et al., 2009). Recently, Guo et al. (2015) identified also a B-type (TDIF)-mimic called *HsCLEB* (Figure 2G). They also observed high expression of *TDR* in the early syncytial stages in *Arabidopsis* after infection. TDR, CLV1, CLV2/CRN and RPK2 and WOX4 were shown to be crucial for syncytium growth and infection efficiency (Replogle et al., 2011; Guo et al., 2015, 2017). Furthermore, A-type HsCLE2 jointly with B-type HsCLEB could synergistically induce massive procambial cell proliferation through TDR (Whitford et al., 2008; Guo et al., 2017). Thus, it is likely that the CN TDIF mimic together with type-A CLE mimics hijacks the plant TDIF-TDR-WOX4 pathway to mediate syncytia formation during nematode infection (Guo et al., 2017). At the same time, in both galls and syncytia, there is an induced expression of procambial identity genes. This indicates that the nematodes maintain a pool of procambial stem cells by inducing proliferation possibly *via* the TDIF-TDR pathway for feeding cell formation (Yamaguchi et al., 2017). Learning how plant CLE-RLK signaling controls proliferation and at which stage(s) (Figure 1B) could support the generation of nematode resistant plant varieties in the future.

In organ primordium and organ development

Primordia and lateral organ development require controlled regulation of a series of processes: dedifferentiation, symmetric, asymmetric and proliferative divisions, and formative divisions and subsequent differentiation (Kwiatkowska, 2006; Torres-Martínez et al., 2019). CLE peptides have been observed to be functional in lateral root primordia (LRP) and lateral root (LR) development, and in flower and leaf primordia and correspondingly in flower and leaf outgrowths.

Lateral root primordium

CLE26 is expressed at the phloem pole in the stele and increases LR density by controlling primary root (PR) length and LR numbers. It is hypothesized that CLE26 controls auxin transport, thus modulating the auxin distribution during LR initiation (Czyzewicz et al., 2015). Similarly, CLE41, CLE44 and a poplar-derived TDIF-like peptide have also been shown to promote LRP establishment and increase LR length by mediating auxin redistribution along the LR initiation sites and in emerging LRs (Yang et al., 2020).

LR development is also controlled by CLE peptides responding to environmental factors, such as nutrient availability and symbiosis with arbuscular mycorrhizal (AM) fungi and rhizobia (Araya et al., 2014; de Bang et al., 2017; Dong et al., 2019; Le Marquer et al., 2019). Araya et al. (2014) reported that CLE3-CLV1 signaling suppresses the number and length of emergent LRs, thus likely preventing the roots from expanding in low nutritional environment. *CLE3* was upregulated in N-deficient conditions particularly in pericycle cells of both PR and LR. Furthermore, CLE3 likely moves and signals *via* CLV1, localized in the phloem companion cells of both PR and LR (Paracrine signaling; Figure 2D). *clv1* showed a significant increase in LR length under N-deficient condition and the suppression of LR length by CLE3 was alleviated in *clv1*. However, it is not clear how the signaling operates at the cellular level (Figure 1) to influence root emergence past stage VII of LR development (Araya et al., 2014). Dong et al. (2019) reported similar results in S-deficient conditions. Upon S-starvation, the LR density decreased and *CLE2* and *-3* genes were upregulated. On the other hand, the rate of LR formation was enhanced upon S-starvation in *clv1* mutants. This shows that CLV1 suppresses LR formation in S-deficient condition (Dong et al., 2019). In summary, CLV1 and several CLE peptides are essential for lateral root formation in response to S and N in the environment.

Leaf primordium

Two CLE peptides with different but overlapping expression and activity in lateral organ primordia affect leaf shape. *CLE6* is

expressed at the bases of young rosette leaves and of floral organs, whereas *CLE5* is expressed at the bases of young rosette leaves and of cauline leaves. CLE5 and 6 act downstream of leaf patterning factors in the leaf primordium to fine tune final leaf morphology. The mutants *cle5* and *cle5;cle6* show mild defects in leaf width, curvature and symmetry (DiGennaro et al., 2018). Details on CLE regulation of leaf morphology, such as how and where the leaf primordia-RLK(s) perceive CLE, and whether the cellular and tissue level effects they mediate are through regulation of proliferation or differentiation processes, remain open for investigation.

Flower primordium

Jones et al. (2021) reported temperature-oriented regulatory pathways directing reproductive development. *CRN* is expressed in early incipient primordium and throughout primordium formation, and was found to be required for primordial outgrowth and continuous flower production at lower temperatures (16°C–24°C). It functions in parallel with CLAVATA signaling in mediating these processes. Several CLE peptides, including CLV3, and the RLKs BAM1, -2 and CLV1 are involved in this CLAVATA signaling pathway although how they interact to regulate flower primordium outgrowth and complete flower formation is not yet characterized. At higher temperatures, these processes are controlled by the transcriptional repressor EARLY FLOWERING 3 (ELF3) that bypasses CLV2/CRN signaling (Jones et al., 2021).

Regulation of non-developmental responses

Widely observed effects of CLE-RLK signaling pertain to proliferation or differentiation processes through cell division regulation. Accordingly, the ancestral role of CLE-RLK signaling, surmised by tracing back its effects in moss, is speculated to be regulation of meristematic cell division (Whitewoods et al., 2018; Whitewoods, 2021). However, this hypothesis stems from widely used experimental approaches in studying plants that relied on strong discernible phenotypes that predominantly involved proliferation or differentiation during meristem or primordium development. This may have led to a slightly skewed perspective, namely that CLE signaling predominantly affects plant development. However, plants continuously adapt to various external stimuli and respond to their changing needs. Therefore, refocusing on non-developmental transitory and conditional plant responses will broaden our understanding of CLE-RLK signaling. In the next paragraph, we discuss the roles of CLE-RLK signaling in dehydration response, phosphate homeostasis and temperature stress through processes besides proliferation or differentiation control.

In dehydration response and stomatal closure

CLE-RLK signaling facilitates dehydration stress response. After a few hours of dehydration stress, *CLE25* is upregulated in procambium of the vascular tissue in roots and it is transported through the vasculature to reach the leaves (Figures 2I,K), where CLE25 upregulates abscisic acid (ABA) biosynthesis enabling stomatal closure. In *cle25* mutants, ABA response to dehydration was abolished and the plants suffered heavy water loss. This CLE25-mediated stomatal response occurs through BAM1 and -3 in leaves (Figures 2I,K). Thus, CLE25 can convey water-deficiency signals from the root to the leaves acting as a long-range endocrine signal (Takahashi et al., 2018). Similar to *CLE25*, *CLE9* expressed directly in stomatal GCs also regulate stomatal closure (Figure 2K) during dehydration stress by activating *MITOGEN-ACTIVATED PROTEIN KINASE 3* and *– 6* (*MPK3/6*) and *via* other downstream regulators, including ABA. *CLE9* overexpressing plants generally had smaller stomatal apertures and the leaves exhibited lower rate of water loss. Notably, unlike in the case of CLE25, BAMs are not the mediators of CLE9 signaling. Although the two CLEs might share the same downstream signaling components, the RLK that responds to CLE9 is not yet identified (Zhang et al., 2019). In brief, during dehydration stress, two disparate CLE peptides—CLE25 and -9—through disparate molecular events facilitate the same stomatal closure response. Thus, CLE peptides can also act as stress responders that signal specific cells or tissues to enable counteracting responses that does not involve cellular proliferation or differentiation regulation.

During AM fungal symbiosis

Plants enter symbiotic relationship with AM for phosphate acquisition, and this symbiosis is maintained through several regulatory signals including CLE peptides (Besserer et al., 2006; Genre et al., 2013; Kobae et al., 2018; Le Marquer et al., 2019; Müller et al., 2019). Strigolactone produced by the plant promotes fungal symbiosis (Akiyama et al., 2005). The phosphorous status of the plant and also the level of fungal colonization itself positively or negatively regulate the fungal symbiotic development (Menge et al., 1978; Breuillin et al., 2010). In *M. truncatula*, *MtCLE53* and *MtCLE33* are upregulated in response to fungal colonization and excess phosphate acquisition. Both genes were expressed in vascular tissue and *MtCLE53* was particularly upregulated near fungal colonies (Figure 2E). These peptides reduce the fungal colonization by downregulating genes involved in strigolactone biosynthesis and secretion. Overexpression of *MtCLE53* and *– 33* resulted in significant reduction in the number of fungal entry sites together with increased expression of the RLK *MtSUNN*. The working model is that, as the AM fungal colonization rises, levels of MtCLE53 gradually increase in response. Subsequently, MtCLE53-MtSUNN signals to further upregulate *MtSUNN* expression (positive feedback) and suppress strigolactone levels, thus reducing the rate of colonization (negative feedback; Müller et al., 2019).

CLE genes have been identified also in some species of AM fungi, which enable them to manipulate plant processes for symbiosis. The CLE peptides *RiCLE1 and GrCLE1*from *Rhizophagus irregularis* and *Gigaspora rosea* are expressed at higher levels during the mycorrhizal state of the plant (Figure 2E). *Medicago truncatula* roots pre-treated with the peptide and further exposed to the spores

showed higher number of fungal entry points with longer colonization sites (Le Marquer et al., 2019). To recapitulate, these root-acting CLEs produced during AM symbiosis respond transiently to the nutritional status of the plants and mediate phosphate homeostasis by directly regulating the fungal colonization. This exemplifies a CLE-RLK-mediated non-developmental effect.

In pollen tube viability

CLE-RLK signaling also mediates adaptational response to high-temperature stress. *CLE45*, expressed in stigma, expands its expression domain to the pollen tube transmitting tract after a shift toward higher temperature. CLE45 then acts as a paracrine signal and binds to the RLK STERILITY-REGULATING KINASE MEMBER1 (SKM1) expressed in pollen. CLE45 signaling *via* SKM1 and SKM2, which are both expressed in pollen, have been shown to prolong pollen tube viability at high temperatures by maintaining its mitochondrial activity until it reaches the ovules (Figure 2L). This is essential for pollen-embryo sac interactions and loss of CLE45 or the RLKs resulted in aberrant seed production (Endo et al., 2013). Thus, this heat-inducible CLE45-SKM1/2 system exemplifies CLE-RLK signaling in mediating a non-developmental response to abiotic stress.

Conclusion and remarks: Temporal and spatial dimensions

1. The temporal dimension: Has it been seconds, minutes, hours, or days?

Cellular effects: The temporal dimension illustrates the time elapsed from the perception of CLE signal by the RLK—seconds to weeks, which correlates with the extent of the CLE effect across plant body organization—from molecular to organ or organism level. The most studied effects of CLE signaling are the regulation of proliferation and differentiation at tissue and organ level. However, detailed studies into the molecular mechanisms behind CLE mediating cell level changes might provide unique insights on proliferation and differentiation processes.

Non-developmental effects: Current research approaches that involve tracing the signaling events resulting in strong developmental phenotypes, very often, lead to uncovering defects in cell division regulation, hence limiting our understanding of the full range of CLE-RLK signaling effects. Signaling events that produce non-developmental effects which occur specifically during a narrow time window or after an external stimulus remain underestimated due to lack of a strong observable phenotypes. Therefore, exposing the plants to diverse conditions and analyzing their transcriptome and following the CLE peptide expression patterns would provide us with an extensive array of its molecular to organ level effects. So far, there are a few studies, as discussed in this review, that show CLE-RLK mediated non-developmental responses. Further studies in this respect across different clades (lycophytes, ferns and gymnosperms, including bryophytes) will provide a greater prospect of defining the ancestral role.

2. The spatial dimension: Who initiates the CLE signal, who receives it and how?

Understanding the spatial aspect of a signaling process is essential as it enables us to delineate the cells, tissue or organs that are in direct communication. For example, induction of stem cell proliferation in a given tissue could be a consequence of CLE peptide produced by the neighboring tissue (paracrine signal) where rapid differentiation takes place.

On the other hand, how the CLE signal reaches the destination is an essential part of the signaling process. The overall analysis of CLE signaling range show that auto- and paracrine CLE signaling is more common than endocrine. It is likely that establishing long-distance communication is challenging as it depends on several factors such as (1) controlling the expression level and concentration of the peptide which further depends on its stability (half-time), dilution during transport through xylem, duration, consistency and level of expression of the peptide (2) post-translational modification of the peptide (3) access to the transport system which includes expression pattern of both the peptide and RLKs, as they should be expressed in the vicinity of vascular tissue: CLE peptide for its extensive transport and RLK for conveniently binding the transported peptide molecules (4) conditions in the destination cells or tissue where further dilution or concentration of the peptide molecules can take place (Müller and Schier, 2011; Notaguchi and Okamoto, 2015; Okamoto et al., 2015, 2016). However, the factors that restrict or expand the CLE signaling range remain so far unknown.

Promiscuity in CLE-RLK interaction

An important attribute of the CLE-RLK interaction is promiscuity. Promiscuity is a broad term used in two main contexts (Copley, 2015):

1. "Broader specificity"—This is when a protein can bind multiple ligands or interact with different proteins to mediate different effects. For example, "hub" proteins that contain disordered regions, which offer them conformational plasticity to serve as centers of signaling networks (Tsai et al., 2009; Schreiber and Keating, 2011).
2. "Physiologically irrelevant interactions"—This is when a protein interacts with a substrate in an artificial test scenario, which will not occur in the natural system. For example, a group of enzymes that are expressed as a part of an operon and function together will perform a particular process in the natural system. But one isolated enzyme, in a new environment, might perform an entirely new function owing to its active binding site that could bind another substrate (Copley, 2015).

Promiscuous interactions among proteins in a given system could be influenced by: (a) Sequence and/or structural similarity among the possible binding partners, which decides the binding

affinity to a specific interacting partner compared to other proteins (Schreiber and Keating, 2011; Copley, 2015), (b) Co-evolution of the binding interfaces of the interacting proteins, which promotes binding specificity through positive or negative selection of binding residues (Moyle et al., 1994; Yosef et al., 2009; Schreiber and Keating, 2011), (c) Post-translational modifications that offer interaction specificity (Tsai et al., 2009; Schreiber and Keating, 2011), (d) Concentration of the interacting protein in the local environment. High affinity binding occurs in the nM to μM range. If the concentration of other molecules or proteins is in excess amount, it can lead to non-specific interactions (Schreiber and Keating, 2011).

Examples of promiscuity in CLE signaling

Promiscuity has been observed among CLEs and RLKs during their interactions—be it natural or forced, such as in experimental simulations. Here, we have illustrated some of the common observations with examples.

- *Several CLE peptides (from the same or different species) causing the same effect*—Examples: Exogenous application of CLE25, CLV3, CLE46, and TDIF upregulate *NCED3* expression in leaves (Takahashi et al., 2018). Exogenous application of AtCLV3 and overexpression of *MpCLE2* result in the same effect—lateral expansion of the apical notch—in *Marchantia* (Hirakawa et al., 2020). Although these observations suggest that the same RLK perceives several CLEs, their interactions are physiologically irrelevant. This is because these interactions are likely the result of very high local peptide concentrations perceived in non-specific tissue layers leading to non-specific promiscuous interactions.
- *A peptide binding to different RLKs with strong affinities*—Examples: Through binding experiments, CLE9 has been shown to bind to both BAM1 and HSL1 with high affinities; Similarly, CLE45 can bind to both BAM3 and SKM1 (Shinohara et al., 2012; Endo et al., 2013; Hazak et al., 2017; Qian et al., 2018). This could be the result of RLKs and CLEs not establishing strict negative or positive selection during co-evolution. However, it is to be noted that co-receptor binding has been shown to offer higher binding affinities in the case of CLE9-HSL1 interaction (Qian et al., 2018) and importantly RLKs and the CLEs might undergo post-translational modifications that could confer binding specificity.
- *One RLK replacing the other spatially and functionally*—Examples: In *clv1* mutant, *BAM1* is upregulated and its expression shifts from PZ to OC and at least partially suppresses IFM expansion by binding CLV3 and signaling in the CLV pathway (DeYoung et al., 2006; Nimchuk et al., 2015; Schlegel et al., 2021). Furthermore, all meristem defects of *clv3* mutants were fully rescued by *CLE40* when expressed from the *CLV3* promoter (Hobe et al., 2003). These observed functional compensation mechanisms are the results of broader specificity of CLV3 and CLE40 in binding to BAM1 and CLV1—two closely related RLKs of the same subfamily, but *BAM1* and *CLV1* are naturally expressed in different zones, and they will therefore, *in vivo*, likely interact with only one of these CLEs, respectively.
- *Multiple CLEs signaling through same RLKs*—Example: Several redundant CLEs have been shown to compensate for CLV3 loss-of-function in suppressing IFM expansion. These redundant genes have been implicated to be consistently expressed in the inflorescence apices and not simply upregulated as a consequence to CLV3 loss, i.e., in *clv3*. CLV3 and these non-paralogous CLEs signal through (likely by binding to) CLV1 and BAM family of RLKs (Rodriguez-Leal et al., 2019). This observation suggests broader binding specificity of RLKs to several CLEs in a natural system, *in vivo*.

In summary, some of these observations exemplify promiscuous CLE-RLK interactions, albeit with lower binding affinity or at physiologically irrelevant concentration or at extraneous expression domains and time. However, other promiscuous interactions are on the account of their high structural similarity among peptides or RLKs of the same subfamilies.

Regulatory aspects of CLE-RLK interaction that promote signaling specificity

Why do CLEs and RLKs exhibit promiscuous interactions? It could be because of residual interactive motifs that are relics of ancestral functions. In an environment of highly similar proteins, avoiding cross-interaction through "perfect" binding site might be impossible and might be a costly process. Importantly, natural selection moderates the traits that lower the fitness of the organism. Hence, if the promiscuity does not disrupt the CLE-RLK downstream signaling due to cross-talk or antagonism, there will be no selective pressure against it (Copley, 2015). To that end, there are several regulatory aspects to CLE-RLK interaction that minimizes their cross-talk and fosters specificity in downstream signaling. In this section, we have described such observed regulatory aspects that likely prevent detrimental effects due to cross-talk, thereby bypassing the selective pressure toward binding specificity (Figure 3).

Regulating the concentration of CLEs

Several CLEs and RLKs function in proximity from each other. If the concentration of a secreted CLE increases over a threshold, there could be non-specific interactions with neighboring RLKs resulting in detrimental effects, which might lead to negative selection pressure necessitating co-evolution of binding specificity. There are established feedback loops and other repressive controls in CLE-RLK signaling networks, which maintain stable CLE concentration. For example: the CLV3-CLV1-WUS negative feedback loop maintains stable CLV3 concentration in *Arabidopsis* SAM. Similarly, SlCLV3 negative feedback represses its own expression (*SlCLV3*) and of its closest paralogue *SlCLE9* in tomato SAM (Yadav et al., 2011; Rodriguez-Leal et al., 2019).

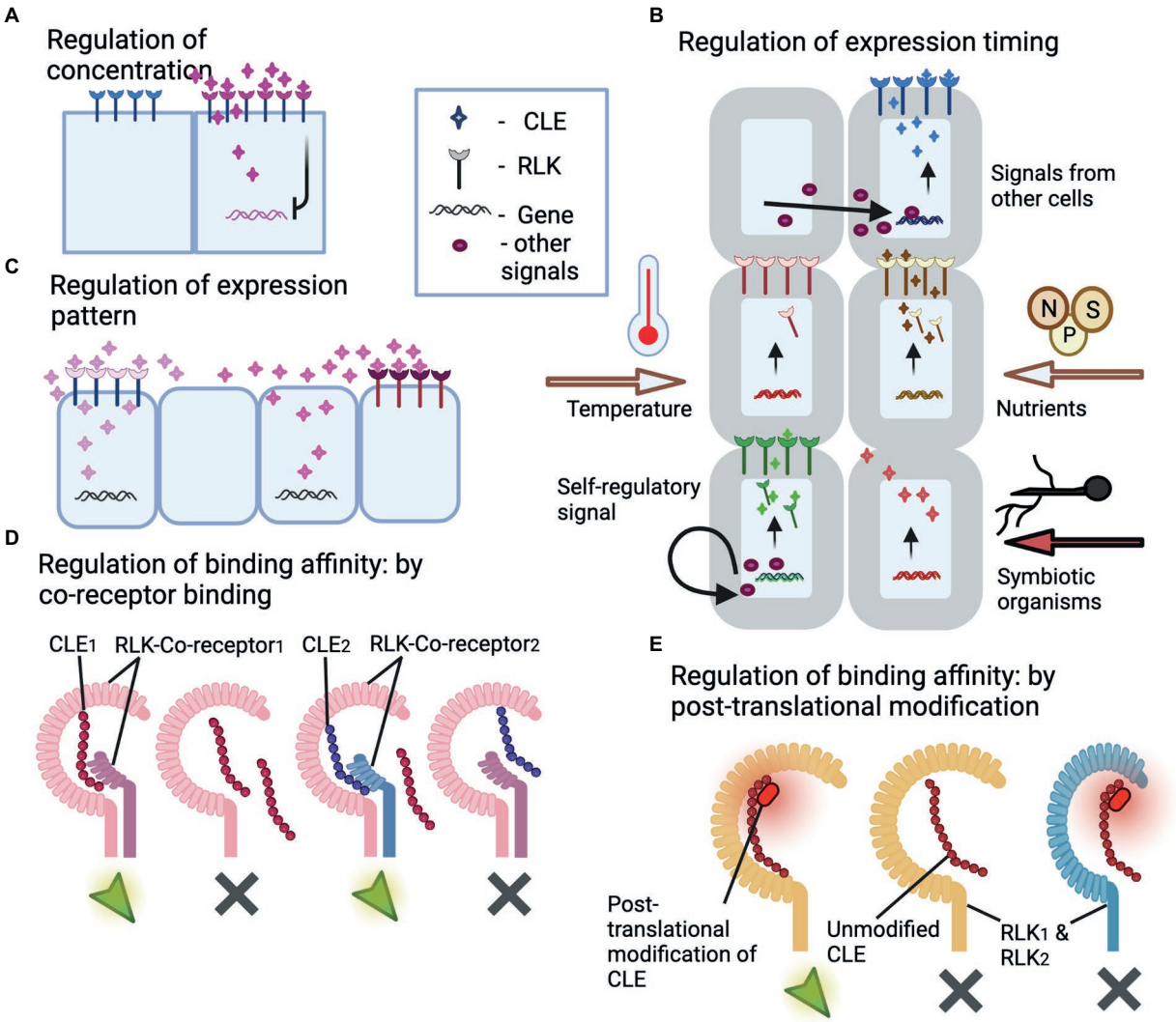

FIGURE 3
Illustrations of regulatory mechanisms that prevent cross-talk between CLE peptides and RLKs. **(A)** Regulation of CLE peptide concentration. The illustration depicts CLE peptide regulating its own synthesis through negative feedback loop, thus containing itself from excessive expression and spreading leading to cross-talk with other RLKs. **(B)** Regulation of the timing of CLE and/or RLK expression. The illustration depicts CLE and RLK expression controlled by external stimuli like temperature, nutrient availability, colonization by a symbiotic organism, or after certain regulatory signals produced by the same or other cells. Thus, the temporal control of expression pattern prevents cross-talk and competitive binding. **(C)** Regulation of the spatial expression pattern of CLEs and RLKs. This illustration depicts spatially separated expression of two similar CLEs avoiding cross-talk with the other RLK. Thus, the spatial control of expression pattern prevents cross-talk and competitive binding. **(D)** Regulation of CLE-RLK binding affinity through co-receptor binding. The illustration depicts co-receptors offering high binding affinity and thus high specificity to CLE-RLK interaction leading to activation of downstream signaling with no cross-talk. CLEs exhibit high affinity to the RLK that is bound with the corresponding co-receptor (co-receptor1 for CLE_1; co-receptor2 for CLE_2), whereas they exhibit low binding affinity to the co-receptor unbound RLK or to the RLK bound to a different co-receptor (co-receptor1 for CLE_2). **(E)** Regulation of CLE binding affinity through post-translational modifications. The illustration depicts post-translational modification offering high binding affinity and thus high specificity to CLE-RLK interaction leading to activation of downstream signaling with no cross-talk. The CLE peptide with post-translational modification binds to the corresponding RLK (RLK_1) with higher affinity compared to its unmodified counterpart and thus avoids cross-talk with the non-specific RLK_2. The green arrows and gray crosses in **(D,E)** represent activated and non-activated downstream signaling.

Regulating the timing of CLE/RLK expression

Controlling when each CLE/RLK is expressed limits the possibility of cross-talk and competition with other CLEs/RLKs. Several external stimuli (nutrients, temperature, symbiosis, etc.) and internal developmental signals trigger CLE/RLK expression, thus controlling their expression timing—Table 1. Example: *CLE25* is upregulated in root vasculature only during dehydration stress.

Regulating the CLE/RLK spatial expression pattern

Similar to the timing of expression, the spatial expression pattern also limits non-specific interactions. CLE/RLK expression in cells/tissue is directly controlled by TFs, which in turn are regulated by the developmental and physiological needs. Example: WUS restricts the *CLE40* expression zone in the PZ in response to

the proliferation/differentiation status of the SAM (Schlegel et al., 2021).

Co-receptor binding

Co-receptors regulate the binding specificity of RLKs toward peptides possibly by binding to and conferring a conformational change of the RLKs, thereby making it more or less specific for certain CLEs (Olsson et al., 2019). To that end, SERK1 increased the binding affinity between CLE9/10 and HSL1. But another RLK, BAM1, while binding to the same CLE9/10 peptide, did not recruit SERKs; hence, BAM1 functions either without any co-receptor recruitment or recruits some other co-receptor that subsequently increases its affinity to CLE9/10. Thus, co-receptors confer differential binding affinities for RLKs to mediate specific CLE-RLK interaction, thereby preventing RLK cross-talk with other CLEs.

Post-translational modifications of CLEs

Post-translational modifications alter the conformational properties of the proteins and change their binding specificities (Tsai et al., 2009; Schreiber and Keating, 2011). CLE peptides have been shown to undergo different post-translational modifications, some of which strengthen their binding affinity with the RLKs (Stührwohldt et al., 2020). Example: Tri-arabinosylated CLV3 binds CLV1 receptor with higher affinity than unmodified CLV3 *in vitro* (Ohyama et al., 2009). Such post-translational modifications could also possibly result in specific binding of CLEs to their respective RLKs, thus effectively preventing cross-talk with other RLKS.

Conclusion and remarks: CLE-RLK interaction and signaling

In conclusion, the CLE expression level, timing and spatial pattern, together with co-receptor binding limits CLE-RLK interactions to a specific region, time and type; thereby non-specific interactions or cross-talks are prevented *in vivo*. This has largely eliminated the evolutionary pressure to improve binding specificity between CLEs and RLKs, which has resulted in a general promiscuity in CLE-RLK interaction.

On the other hand, promiscuity or broader binding specificity among the signaling ligands and their receptors might offer an evolutionary advantage. It was shown that, in bone morphogenetic pathway, "combinations of different ligands" act more efficiently when signaling to a group of cells of different types expressing different receptors, compared to "one-to-one" ligand-receptor specific binding. Varied concentrations and combination of ligands were able to activate or deactivate different receptors and their downstream signaling (Su et al., 2022). Similar to their observations, it is possible that several CLEs together mediate such a complex combinatorial regulation during IFM development when several CLEs are expressed, and possibly during other processes too. In that case, mutagenesis and over expression analyses might be non-viable for studying CLE-RLK interaction and signaling. Synergistic effects of CLE peptides have been reported before (Whitford et al., 2008). However, attempting to reproduce *in vivo* levels and combinations is pivotal in understanding the nuances in promiscuous CLE-RLK signaling.

Recently several strides have been made toward understanding co-receptors regulating CLE-RLK signaling (Olsson et al., 2019; Gou and Li, 2020). There are still several avenues of CLE-RLK interactions that remain unexplored:

i. Post-translational modifications in CLEs and RLKs: What are the different ways in which both RLKs and CLEs are modified? How are these modifications regulated? How do they affect CLE-RLK interaction?
ii. RLK level in the cell/tissue: How are RLK turnover, inactivation/activation and expression level controlled? And how do they affect CLE signaling?
iii. Can variations in concentration and combination of multiple CLEs expressed in a region activate/deactivate the RLKs of that region?
iv. How is the signaling range (auto−/para−/endocrine) controlled? Can it be achieved solely by regulating the CLE-RLK expression pattern and levels?
v. What are the downstream signaling components of CLE-RLK and, by extension, the downstream effects that are conserved across clades? Understanding the differences in closely related non-angiosperm vascular plants will already be insightful.

Author contributions

MN and RS conceived the idea. MN wrote the manuscript and made the figures. All authors contributed to the article and approved the submitted version.

Funding

MN was supported by the DFG through a grant within the CRC1208 to RS.

Acknowledgments

We thank Yvonne Stahl for helpful suggestions. All the figures were created with BioRender.com.

Conflict of interest

The authors declare that the research was conducted in the absence of any commercial or financial relationships that could be construed as a potential conflict of interest.

Publisher's note

References

Akiyama, K., Matsuzaki, K., and Hayashi, H. (2005). Plant sesquiterpenes induce hyphal branching in arbuscular mycorrhizal fungi. *Nature* 435, 824–827. doi: 10.1038/nature03608

Araya, T., Miyamoto, M., Wibowo, J., Suzuki, A., Kojima, S., Tsuchiya, Y. N., et al. (2014). CLE-CLAVATA1 peptide-receptor signaling module regulates the expansion of plant root systems in a nitrogen-dependent manner. *Proc. Natl. Acad. Sci. U. S. A.* 111, 2029–2034. doi: 10.1073/pnas.1319953111

Besserer, A., Puech-Pagès, V., Kiefer, P., Gomez-Roldan, V., Jauneau, A., Roy, S., et al. (2006). Strigolactones stimulate arbuscular mycorrhizal fungi by activating mitochondria. *PLoS Biol.* 4:e226. doi: 10.1371/journal.pbio.0040226

Bleckmann, A., Weidtkamp-Peters, S., Seidel, C. A., and Simon, R. (2010). Stem cell signaling in Arabidopsis requires CRN to localize CLV2 to the plasma membrane. *Plant Physiol.* 152, 166–176. doi: 10.1104/pp.109.149930

Brand, U., Fletcher, J. C., Hobe, M., Meyerowitz, E. M., and Simon, R. (2000). Dependence of stem cell fate in Arabidopsis on a feedback loop regulated by CLV3 activity. *Science* 289, 617–619. doi: 10.1126/science.289.5479.617

Breda, A. S., Hazak, O., Schultz, P., Anne, P., Graeff, M., Simon, R., et al. (2019). A cellular insulator against CLE45 peptide signaling. *Curr. Biol.* 29, 2501.e3–2508.e3. doi: 10.1016/j.cub.2019.06.037

Breuillin, F., Schramm, J., Hajirezaei, M., Ahkami, A., Favre, P., Druege, U., et al. (2010). Phosphate systemically inhibits development of arbuscular mycorrhiza in Petunia hybrida and represses genes involved in mycorrhizal functioning. *Plant J.* 64, 1002–1017. doi: 10.1111/j.1365-313X.2010.04385.x

Clark, S. E., Running, M. P., and Meyerowitz, E. M. (1995). CLAVATA3 is a specific regulator of shoot and floral meristem development affecting the same processes as CLAVATA1. *Development* 121, 2057–2067. doi: 10.1242/dev.121.7.2057

Clark, S. E., Williams, R. W., and Meyerowitz, E. M. (1997). The CLAVATA1 gene encodes a putative receptor kinase that controls shoot and floral meristem size in Arabidopsis. *Cell* 89, 575–585. doi: 10.1016/s0092-8674(00)80239-1

Copley, S. D. (2015). An evolutionary biochemist's perspective on promiscuity. *Trends Biochem. Sci.* 40, 72–78. doi: 10.1016/j.tibs.2014.12.004

Crook, A. D., Schnabel, E. L., and Frugoli, J. A. (2016). The systemic nodule number regulation kinase SUNN in Medicago truncatula interacts with MtCLV2 and MtCRN. *Plant J.* 88, 108–119. doi: 10.1111/tpj.13234

Czyzewicz, N., Shi, C. L., Vu, L. D., Van De Cotte, B., Hodgman, C., Butenko, M. A., et al. (2015). Modulation of Arabidopsis and monocot root architecture by CLAVATA3/EMBRYO SURROUNDING REGION 26 peptide. *J. Exp. Bot.* 66, 5229–5243. doi: 10.1093/jxb/erv360

Davis, E. L., and Mitchum, M. G. (2005). Nematodes. Sophisticated parasites of legumes. *Plant Physiol.* 137, 1182–1188. doi: 10.1104/pp.104.054973

de Almeida Engler, J., and Gheysen, G. (2013). Nematode-induced endoreduplication in plant host cells: why and how? *Mol. Plant Microbe Interact.* 26, 17–24. doi: 10.1094/mpmi-05-12-0128-cr

de Bang, T. C., Lundquist, P. K., Dai, X., Boschiero, C., Zhuang, Z., Pant, P., et al. (2017). Genome-wide identification of Medicago peptides involved in macronutrient responses and nodulation. *Plant Physiol.* 175, 1669–1689. doi: 10.1104/pp.17.01096

De Smet, I., and Beeckman, T. (2011). Asymmetric cell division in land plants and algae: the driving force for differentiation. *Nat. Rev. Mol. Cell Biol.* 12, 177–188. doi: 10.1038/nrm3064

De Veylder, L., Beeckman, T., and Inzé, D. (2007). The ins and outs of the plant cell cycle. *Nat. Rev. Mol. Cell Biol.* 8, 655–665. doi: 10.1038/nrm2227

Depuydt, S., Rodriguez-Villalon, A., Santuari, L., Wyser-Rmili, C., Ragni, L., and Hardtke, C. S. (2013). Suppression of Arabidopsis protophloem differentiation and root meristem growth by CLE45 requires the receptor-like kinase BAM3. *Proc. Natl. Acad. Sci. U. S. A.* 110, 7074–7079. doi: 10.1073/pnas.1222314110

Desvoyes, B., Echevarría, C., and Gutierrez, C. (2021). A perspective on cell proliferation kinetics in the root apical meristem. *J. Exp. Bot.* 72, 6708–6715. doi: 10.1093/jxb/erab303

DeYoung, B. J., Bickle, K. L., Schrage, K. J., Muskett, P., Patel, K., and Clark, S. E. (2006). The CLAVATA1-related BAM1, BAM2 and BAM3 receptor kinase-like proteins are required for meristem function in Arabidopsis. *Plant J.* 45, 1–16. doi: 10.1111/j.1365-313X.2005.02592.x

Deyoung, B. J., and Clark, S. E. (2008). BAM receptors regulate stem cell specification and organ development through complex interactions with CLAVATA signaling. *Genetics* 180, 895–904. doi: 10.1534/genetics.108.091108

DiGennaro, P., Grienenberger, E., Dao, T. Q., Jun, J. H., and Fletcher, J. C. (2018). Peptide signaling molecules CLE5 and CLE6 affect Arabidopsis leaf shape downstream of leaf patterning transcription factors and auxin. *Plant Direct* 2:e00103. doi: 10.1002/pld3.103

Dong, W., Wang, Y., and Takahashi, H. (2019). CLE-CLAVATA1 signaling pathway modulates lateral root development under sulfur deficiency. *Plants* 8:103. doi: 10.3390/plants8040103

Endo, S., Shinohara, H., Matsubayashi, Y., and Fukuda, H. (2013). A novel pollen-pistil interaction conferring high-temperature tolerance during reproduction via CLE45 signaling. *Curr. Biol.* 23, 1670–1676. doi: 10.1016/j.cub.2013.06.060

Etchells, J. P., Mishra, L. S., Kumar, M., Campbell, L., and Turner, S. R. (2015). Wood formation in trees is increased by manipulating PXY-regulated cell division. *Curr. Biol.* 25, 1050–1055. doi: 10.1016/j.cub.2015.02.023

Etchells, J. P., and Turner, S. R. (2010). The PXY-CLE41 receptor ligand pair defines a multifunctional pathway that controls the rate and orientation of vascular cell division. *Development* 137, 767–774. doi: 10.1242/dev.044941

Ferguson, B. J., Indrasumunar, A., Hayashi, S., Lin, M. H., Lin, Y. H., Reid, D. E., et al. (2010). Molecular analysis of legume nodule development and autoregulation. *J. Integr. Plant Biol.* 52, 61–76. doi: 10.1111/j.1744-7909.2010.00899.x

Fiers, M., Golemiec, E., Xu, J., van der Geest, L., Heidstra, R., Stiekema, W., et al. (2005). The 14-amino acid CLV3, CLE19, and CLE40 peptides trigger consumption of the root meristem in Arabidopsis through a CLAVATA2-dependent pathway. *Plant Cell* 17, 2542–2553. doi: 10.1105/tpc.105.034009

Fletcher, J. C. (2020). Recent advances in Arabidopsis CLE peptide signaling. *Trends Plant Sci.* 25, 1005–1016. doi: 10.1016/j.tplants.2020.04.014

Fletcher, J. C., Brand, U., Running, M. P., Simon, R., and Meyerowitz, E. M. (1999). Signaling of cell fate decisions by CLAVATA3 in Arabidopsis shoot meristems. *Science* 283, 1911–1914. doi: 10.1126/science.283.5409.1911

Frey, N. F. D., and Favery, B. (2021). Plant-parasitic nematode secreted peptides hijack a plant secretory pathway. *New Phytol.* 229, 11–13. doi: 10.1111/nph.16842

Furumizu, C., Krabberød, A. K., Hammerstad, M., Alling, R. M., Wildhagen, M., Sawa, S., et al. (2021). The sequenced genomes of nonflowering land plants reveal the innovative evolutionary history of peptide signaling. *Plant Cell* 33, 2915–2934. doi: 10.1093/plcell/koab173

Furuta, K. M., Yadav, S. R., Lehesranta, S., Belevich, I., Miyashima, S., Heo, J. O., et al. (2014). Plant development. Arabidopsis NAC45/86 direct sieve element morphogenesis culminating in enucleation. *Science* 345, 933–937. doi: 10.1126/science.1253736

Gao, X., and Guo, Y. (2012). CLE peptides in plants: proteolytic processing, structure-activity relationship, and ligand-receptor interaction. *J. Integr. Plant Biol.* 54, 738–745. doi: 10.1111/j.1744-7909.2012.01154.x

Genre, A., Chabaud, M., Balzergue, C., Puech-Pagès, V., Novero, M., Rey, T., et al. (2013). Short-chain chitin oligomers from arbuscular mycorrhizal fungi trigger nuclear Ca2+ spiking in Medicago truncatula roots and their production is enhanced by strigolactone. *New Phytol.* 198, 190–202. doi: 10.1111/nph.12146

Gilbert, S. F. (2000). "The developmental mechanics of cell specification," in *Developmental Biology. 6th Edn.* ed. S. Associates (Sunderland (MA)), 341.

Gou, X., and Li, J. (2020). Paired receptor and Coreceptor kinases perceive extracellular signals to control plant development. *Plant Physiol.* 182, 1667–1681. doi: 10.1104/pp.19.01343

Gujas, B., Kastanaki, E., Sturchler, A., Cruz, T. M. D., Ruiz-Sola, M. A., Dreos, R., et al. (2020). A reservoir of pluripotent phloem cells safeguards the linear developmental trajectory of Protophloem sieve elements. *Curr. Biol.* 30, 755.e4–766.e4. doi: 10.1016/j.cub.2019.12.043

Guo, X., Chronis, D., De La Torre, C. M., Smeda, J., Wang, X., and Mitchum, M. G. (2015). Enhanced resistance to soybean cyst nematode Heterodera glycines in transgenic soybean by silencing putative CLE receptors. *Plant Biotechnol. J.* 13, 801–810. doi: 10.1111/pbi.12313

Guo, X., Wang, J., Gardner, M., Fukuda, H., Kondo, Y., Etchells, J. P., et al. (2017). Identification of cyst nematode B-type CLE peptides and modulation of the vascular

stem cell pathway for feeding cell formation. *PLoS Pathog.* 13:e1006142. doi: 10.1371/journal.ppat.1006142

Hazak, O., Brandt, B., Cattaneo, P., Santiago, J., Rodriguez-Villalon, A., Hothorn, M., et al. (2017). Perception of root-active CLE peptides requires CORYNE function in the phloem vasculature. *EMBO Rep.* 18, 1367–1381. doi: 10.15252/embr.201643535

Hirakawa, Y., Fujimoto, T., Ishida, S., Uchida, N., Sawa, S., Kiyosue, T., et al. (2020). Induction of Multichotomous branching by CLAVATA peptide in Marchantia polymorpha. *Curr. Biol.* 30, 3833.e4–3840.e4. doi: 10.1016/j.cub.2020.07.016

Hirakawa, Y., Kondo, Y., and Fukuda, H. (2010). TDIF peptide signaling regulates vascular stem cell proliferation via the WOX4 homeobox gene in Arabidopsis. *Plant Cell* 22, 2618–2629. doi: 10.1105/tpc.110.076083

Hirakawa, Y., Shinohara, H., Kondo, Y., Inoue, A., Nakanomyo, I., Ogawa, M., et al. (2008). Non-cell-autonomous control of vascular stem cell fate by a CLE peptide/receptor system. *Proc. Natl. Acad. Sci. U. S. A.* 105, 15208–15213. doi: 10.1073/pnas.0808444105

Hirakawa, Y., Uchida, N., Yamaguchi, Y. L., Tabata, R., Ishida, S., Ishizaki, K., et al. (2019). Control of proliferation in the haploid meristem by CLE peptide signaling in Marchantia polymorpha. *PLoS Genet.* 15:e1007997. doi: 10.1371/journal.pgen.1007997

Hobe, M., Müller, R., Grünewald, M., Brand, U., and Simon, R. (2003). Loss of CLE40, a protein functionally equivalent to the stem cell restricting signal CLV3, enhances root waving in Arabidopsis. *Dev. Genes Evol.* 213, 371–381. doi: 10.1007/s00427-003-0329-5

Hu, C., Zhu, Y., Cui, Y., Cheng, K., Liang, W., Wei, Z., et al. (2018). A group of receptor kinases are essential for CLAVATA signalling to maintain stem cell homeostasis. *Nat. Plants* 4, 205–211. doi: 10.1038/s41477-018-0123-z

Imin, N., Patel, N., Corcilius, L., Payne, R. J., and Djordjevic, M. A. (2018). CLE peptide tri-arabinosylation and peptide domain sequence composition are essential for SUNN-dependent autoregulation of nodulation in Medicago truncatula. *New Phytol.* 218, 73–80. doi: 10.1111/nph.15019

Ito, Y., Nakanomyo, I., Motose, H., Iwamoto, K., Sawa, S., Dohmae, N., et al. (2006). Dodeca-CLE peptides as suppressors of plant stem cell differentiation. *Science* 313, 842–845. doi: 10.1126/science.1128436

Jones, D. S., John, A., VanDerMolen, K. R., and Nimchuk, Z. L. (2021). CLAVATA signaling ensures reproductive development in plants across thermal environments. *Curr. Biol.* 31, 220.e5–227.e5. doi: 10.1016/j.cub.2020.10.008

Kajala, K., Ramakrishna, P., Fisher, A., Bergmann, D., De Smet, I., Sozzani, R., et al. (2014). Omics and modelling approaches for understanding regulation of asymmetric cell divisions in Arabidopsis and other angiosperm plants. *Ann. Bot.* 113, 1083–1105. doi: 10.1093/aob/mcu065

Kayes, J. M., and Clark, S. E. (1998). CLAVATA2, a regulator of meristem and organ development in Arabidopsis. *Development* 125, 3843–3851. doi: 10.1242/dev.125.19.3843

Kinoshita, A., Betsuyaku, S., Osakabe, Y., Mizuno, S., Nagawa, S., Stahl, Y., et al. (2010). RPK2 is an essential receptor-like kinase that transmits the CLV3 signal in Arabidopsis. *Development* 137, 3911–3920. doi: 10.1242/dev.048199

Kobae, Y., Kameoka, H., Sugimura, Y., Saito, K., Ohtomo, R., Fujiwara, T., et al. (2018). Strigolactone biosynthesis genes of Rice are required for the punctual entry of Arbuscular Mycorrhizal fungi into the roots. *Plant Cell Physiol.* 59, 544–553. doi: 10.1093/pcp/pcy001

Kondo, Y., Ito, T., Nakagami, H., Hirakawa, Y., Saito, M., Tamaki, T., et al. (2014). Plant GSK3 proteins regulate xylem cell differentiation downstream of TDIF-TDR signalling. *Nat. Commun.* 5:3504. doi: 10.1038/ncomms4504

Krusell, L., Madsen, L. H., Sato, S., Aubert, G., Genua, A., Szczyglowski, K., et al. (2002). Shoot control of root development and nodulation is mediated by a receptor-like kinase. *Nature* 420, 422–426. doi: 10.1038/nature01207

Krusell, L., Sato, N., Fukuhara, I., Koch, B. E., Grossmann, C., Okamoto, S., et al. (2011). The Clavata2 genes of pea and Lotus japonicus affect autoregulation of nodulation. *Plant J.* 65, 861–871. doi: 10.1111/j.1365-313X.2010.04474.x

Kwiatkowska, D. (2006). Flower primordium formation at the Arabidopsis shoot apex: quantitative analysis of surface geometry and growth. *J. Exp. Bot.* 57, 571–580. doi: 10.1093/jxb/erj042

Lau, O. S., and Bergmann, D. C. (2012). Stomatal development: a plant's perspective on cell polarity, cell fate transitions and intercellular communication. *Development* 139, 3683–3692. doi: 10.1242/dev.080523

Le Marquer, M., Bécard, G., and Frey, N. F. D. (2019). Arbuscular mycorrhizal fungi possess a CLAVATA3/embryo surrounding region-related gene that positively regulates symbiosis. *New Phytol.* 222, 1030–1042. doi: 10.1111/nph.15643

Lebedeva, M., Azarakhsh, M., Yashenkova, Y., and Lutova, L. (2020a). Nitrate-induced CLE peptide systemically inhibits nodulation in Medicago truncatula. *Plants* 9:1456. doi: 10.3390/plants9111456

Lebedeva, M., Yashenkova, Y. S., Dodueva, I., and Lutova, L. (2020b). Molecular dialog between root and shoot via regulatory peptides and its role in systemic control of plant development. *Russ. J. Plant Physiol.* 67, 985–1002. doi: 10.1134/S1021443720060114

Liu, Y., Yang, S., Song, Y., Men, S., and Wang, J. (2016). Gain-of-function analysis of poplar CLE genes in Arabidopsis by exogenous application and over-expression assays. *J. Exp. Bot.* 67, 2309–2324. doi: 10.1093/jxb/erw045

Lu, S. W., Chen, S., Wang, J., Yu, H., Chronis, D., Mitchum, M. G., et al. (2009). Structural and functional diversity of CLAVATA3/ESR (CLE)-like genes from the potato cyst nematode Globodera rostochiensis. *Mol. Plant Microbe Interact.* 22, 1128–1142. doi: 10.1094/mpmi-22-9-1128

Mayer, K. F., Schoof, H., Haecker, A., Lenhard, M., Jürgens, G., and Laux, T. (1998). Role of WUSCHEL in regulating stem cell fate in the Arabidopsis shoot meristem. *Cell* 95, 805–815. doi: 10.1016/s0092-8674(00)81703-1

Menge, J., Steirle, D., Bagyaraj, D., Johnson, E., and Leonard, R. (1978). Phosphorus concentrations in plants responsible for inhibition of mycorrhizal infection. *New Phytol.* 80, 575–578. doi: 10.1111/j.1469-8137.1978.tb01589

Mens, C., Hastwell, A. H., Su, H., Gresshoff, P. M., Mathesius, U., and Ferguson, B. J. (2021). Characterisation of Medicago truncatula CLE34 and CLE35 in nitrate and rhizobia regulation of nodulation. *New Phytol.* 229, 2525–2534. doi: 10.1111/nph.17010

Miyashima, S., Sebastian, J., Lee, J. Y., and Helariutta, Y. (2013). Stem cell function during plant vascular development. *EMBO J.* 32, 178–193. doi: 10.1038/emboj.2012.301

Miyazawa, H., Oka-Kira, E., Sato, N., Takahashi, H., Wu, G. J., Sato, S., et al. (2010). The receptor-like kinase KLAVIER mediates systemic regulation of nodulation and non-symbiotic shoot development in Lotus japonicus. *Development* 137, 4317–4325. doi: 10.1242/dev.058891

Mortier, V., Den Herder, G., Whitford, R., Van de Velde, W., Rombauts, S., D'Haeseleer, K., et al. (2010). CLE peptides control Medicago truncatula nodulation locally and systemically. *Plant Physiol.* 153, 222–237. doi: 10.1104/pp.110.153718

Moyle, W. R., Campbell, R. K., Myers, R. V., Bernard, M. P., Han, Y., and Wang, X. (1994). Co-evolution of ligand-receptor pairs. *Nature* 368, 251–255. doi: 10.1038/368251a0

Muller, R., Bleckmann, A., and Simon, R. (2008). The receptor kinase CORYNE of Arabidopsis transmits the stem cell–limiting signal CLAVATA3 independently of CLAVATA1. *Plant Cell* 20, 934–946. doi: 10.1105/tpc.107.057547

Müller, L. M., Flokova, K., Schnabel, E., Sun, X., Fei, Z., Frugoli, J., et al. (2019). A CLE-SUNN module regulates strigolactone content and fungal colonization in arbuscular mycorrhiza. *Nat. Plants* 5, 933–939. doi: 10.1038/s41477-019-0501-1

Müller, P., and Schier, A. F. (2011). Extracellular movement of signaling molecules. *Dev. Cell* 21, 145–158. doi: 10.1016/j.devcel.2011.06.001

Nimchuk, Z. L. (2017). CLAVATA1 controls distinct signaling outputs that buffer shoot stem cell proliferation through a two-step transcriptional compensation loop. *PLoS Genet.* 13:e1006681. doi: 10.1371/journal.pgen.1006681

Nimchuk, Z. L., Zhou, Y., Tarr, P. T., Peterson, B. A., and Meyerowitz, E. M. (2015). Plant stem cell maintenance by transcriptional cross-regulation of related receptor kinases. *Development* 142, 1043–1049. doi: 10.1242/dev.119677

Nontachaiyapoom, S., Scott, P. T., Men, A. E., Kinkema, M., Schenk, P. M., and Gresshoff, P. M. (2007). Promoters of orthologous Glycine max and Lotus japonicus nodulation autoregulation genes interchangeably drive phloem-specific expression in transgenic plants. *Mol. Plant Microbe Interact.* 20, 769–780. doi: 10.1094/mpmi-20-7-0769

Notaguchi, M., and Okamoto, S. (2015). Dynamics of long-distance signaling via plant vascular tissues. *Front. Plant Sci.* 6:161. doi: 10.3389/fpls.2015.00161

Ohyama, K., Shinohara, H., Ogawa-Ohnishi, M., and Matsubayashi, Y. (2009). A glycopeptide regulating stem cell fate in *Arabidopsis thaliana*. *Nat. Chem. Biol.* 5, 578–580. doi: 10.1038/nchembio.182

Okamoto, S., Shinohara, H., Mori, T., Matsubayashi, Y., and Kawaguchi, M. (2013). Root-derived CLE glycopeptides control nodulation by direct binding to HAR1 receptor kinase. *Nat. Commun.* 4:2191. doi: 10.1038/ncomms3191

Okamoto, S., Suzuki, T., Kawaguchi, M., Higashiyama, T., and Matsubayashi, Y. (2015). A comprehensive strategy for identifying long-distance mobile peptides in xylem sap. *Plant J.* 84, 611–620. doi: 10.1111/tpj.13015

Okamoto, S., Tabata, R., and Matsubayashi, Y. (2016). Long-distance peptide signaling essential for nutrient homeostasis in plants. *Curr. Opin. Plant Biol.* 34, 35–40. doi: 10.1016/j.pbi.2016.07.009

Olsson, V., Joos, L., Zhu, S., Gevaert, K., Butenko, M. A., and De Smet, I. (2019). Look closely, the beautiful may be small: precursor-derived peptides in plants. *Annu. Rev. Plant Biol.* 70, 153–186. doi: 10.1146/annurev-arplant-042817-040413

Plieth, C. (2010). Signal percolation through plants and the shape of the calcium signature. *Plant Signal. Behav.* 5, 379–385. doi: 10.4161/psb.5.4.10717

Poliushkevich, L., Gancheva, M., Dodueva, I., and Lutova, L. (2020). Receptors of CLE peptides in plants. *Russ. J. Plant Physiol.* 67, 1–16. doi: 10.1134/S1021443720010288

Qian, P., Song, W., Yokoo, T., Minobe, A., Wang, G., Ishida, T., et al. (2018). The CLE9/10 secretory peptide regulates stomatal and vascular development through distinct receptors. *Nat. Plants* 4, 1071–1081. doi: 10.1038/s41477-018-0317-4

Reid, D. E., Ferguson, B. J., Hayashi, S., Lin, Y. H., and Gresshoff, P. M. (2011). Molecular mechanisms controlling legume autoregulation of nodulation. *Ann. Bot.* 108, 789–795. doi: 10.1093/aob/mcr205

Ren, S. C., Song, X. F., Chen, W. Q., Lu, R., Lucas, W. J., and Liu, C. M. (2019). CLE25 peptide regulates phloem initiation in Arabidopsis through a CLERK-CLV2 receptor complex. *J. Integr. Plant Biol.* 61, 1043–1061. doi: 10.1111/jipb.12846

Replogle, A., Wang, J., Bleckmann, A., Hussey, R. S., Baum, T. J., Sawa, S., et al. (2011). Nematode CLE signaling in Arabidopsis requires CLAVATA2 and CORYNE. *Plant J.* 65, 430–440. doi: 10.1111/j.1365-313X.2010.04433.x

Rodriguez-Leal, D., Xu, C., Kwon, C. T., Soyars, C., Demesa-Arevalo, E., Man, J., et al. (2019). Evolution of buffering in a genetic circuit controlling plant stem cell proliferation. *Nat. Genet.* 51, 786–792. doi: 10.1038/s41588-019-0389-8

Rodriguez-Villalon, A., Gujas, B., Kang, Y. H., Breda, A. S., Cattaneo, P., Depuydt, S., et al. (2014). Molecular genetic framework for protophloem formation. *Proc. Natl. Acad. Sci. U. S. A.* 111, 11551–11556. doi: 10.1073/pnas.1407337111

Rojo, E., Sharma, V. K., Kovaleva, V., Raikhel, N. V., and Fletcher, J. C. (2002). CLV3 is localized to the extracellular space, where it activates the Arabidopsis CLAVATA stem cell signaling pathway. *Plant Cell* 14, 969–977. doi: 10.1105/tpc.002196

Růžička, K., Ursache, R., Hejátko, J., and Helariutta, Y. (2015). Xylem development - from the cradle to the grave. *New Phytol.* 207, 519–535. doi: 10.1111/nph.13383

Schlegel, J., Denay, G., Wink, R., Pinto, K. G., Stahl, Y., Schmid, J., et al. (2021). Control of Arabidopsis shoot stem cell homeostasis by two antagonistic CLE peptide signalling pathways. *Elife* 10:e70934. doi: 10.7554/eLife.70934

Schoof, H., Lenhard, M., Haecker, A., Mayer, K. F., Jürgens, G., and Laux, T. (2000). The stem cell population of Arabidopsis shoot meristems in maintained by a regulatory loop between the CLAVATA and WUSCHEL genes. *Cell* 100, 635–644. doi: 10.1016/s0092-8674(00)80700-x

Schreiber, G., and Keating, A. E. (2011). Protein binding specificity versus promiscuity. *Curr. Opin. Struct. Biol.* 21, 50–61. doi: 10.1016/j.sbi.2010.10.002

Searle, I. R., Men, A. E., Laniya, T. S., Buzas, D. M., Iturbe-Ormaetxe, I., Carroll, B. J., et al. (2003). Long-distance signaling in nodulation directed by a CLAVATA1-Like receptor kinase. *Science* 299, 109–112. doi: 10.1126/science.1077937

Seo, M., Kim, H., and Lee, J. Y. (2020). Information on the move: vascular tissue development in space and time during postembryonic root growth. *Curr. Opin. Plant Biol.* 57, 110–117. doi: 10.1016/j.pbi.2020.08.002

Shimamura, M. (2016). Marchantia polymorpha: taxonomy, phylogeny and morphology of a model system. *Plant Cell Physiol.* 57, 230–256. doi: 10.1093/pcp/pcv192

Shinohara, H., and Matsubayashi, Y. (2015). Reevaluation of the CLV3-receptor interaction in the shoot apical meristem: dissection of the CLV3 signaling pathway from a direct ligand-binding point of view. *Plant J.* 82, 328–336. doi: 10.1111/tpj.12817

Shinohara, H., Moriyama, Y., Ohyama, K., and Matsubayashi, Y. (2012). Biochemical mapping of a ligand-binding domain within Arabidopsis BAM1 reveals diversified ligand recognition mechanisms of plant LRR-RKs. *Plant J.* 70, 845–854. doi: 10.1111/j.1365-313X.2012.04934.x

Somssich, M., Ma, Q., Weidtkamp-Peters, S., Stahl, Y., Felekyan, S., Bleckmann, A., et al. (2015). Real-time dynamics of peptide ligand-dependent receptor complex formation in planta. *Sci. Signal.* 8:ra76. doi: 10.1126/scisignal.aab0598

Stahl, Y., Wink, R. H., Ingram, G. C., and Simon, R. (2009). A signaling module controlling the stem cell niche in Arabidopsis root meristems. *Curr. Biol.* 19, 909–914. doi: 10.1016/j.cub.2009.03.060

Stührwohldt, N., Scholl, S., Lang, L., Katzenberger, J., Schumacher, K., and Schaller, A. (2020). The biogenesis of CLEL peptides involves several processing events in consecutive compartments of the secretory pathway. *Elife* 9:e55580. doi: 10.7554/eLife.55580

Su, C. J., Murugan, A., Linton, J. M., Yeluri, A., Bois, J., Klumpe, H., et al. (2022). Ligand-receptor promiscuity enables cellular addressing. *Cell Syst.* 13, 408.e12–425.e12. doi: 10.1016/j.cels.2022.03.001

Suzaki, T., Yano, K., Ito, M., Umehara, Y., Suganuma, N., and Kawaguchi, M. (2012). Positive and negative regulation of cortical cell division during root nodule development in Lotus japonicus is accompanied by auxin response. *Development* 139, 3997–4006. doi: 10.1242/dev.084079

Takahara, M., Magori, S., Soyano, T., Okamoto, S., Yoshida, C., Yano, K., et al. (2013). Too much love, a novel Kelch repeat-containing F-box protein, functions in the long-distance regulation of the legume-rhizobium symbiosis. *Plant Cell Physiol.* 54, 433–447. doi: 10.1093/pcp/pct022

Takahashi, F., Suzuki, T., Osakabe, Y., Betsuyaku, S., Kondo, Y., Dohmae, N., et al. (2018). A small peptide modulates stomatal control via abscisic acid in long-distance signalling. *Nature* 556, 235–238. doi: 10.1038/s41586-018-0009-2

Torres-Martínez, H. H., Rodríguez-Alonso, G., Shishkova, S., and Dubrovsky, J. G. (2019). Lateral root primordium morphogenesis in angiosperms. *Front. Plant Sci.* 10:206. doi: 10.3389/fpls.2019.00206

Tsai, C. J., Ma, B., and Nussinov, R. (2009). Protein-protein interaction networks: how can a hub protein bind so many different partners? *Trends Biochem. Sci.* 34, 594–600. doi: 10.1016/j.tibs.2009.07.007

Tsikou, D., Yan, Z., Holt, D. B., Abel, N. B., Reid, D. E., Madsen, L. H., et al. (2018). Systemic control of legume susceptibility to rhizobial infection by a mobile microRNA. *Science* 362, 233–236. doi: 10.1126/science.aat6907

Van Norman, J. M., Breakfield, N. W., and Benfey, P. N. (2011). Intercellular communication during plant development. *Plant Cell* 23, 855–864. doi: 10.1105/tpc.111.082982

Wang, X., Mitchum, M. G., Gao, B., Li, C., Diab, H., Baum, T. J., et al. (2005). A parasitism gene from a plant-parasitic nematode with function similar to CLAVATA3/ESR (CLE) of *Arabidopsis thaliana*. *Mol. Plant Pathol.* 6, 187–191. doi: 10.1111/j.1364-3703.2005.00270.x

Whitewoods, C. D. (2021). Evolution of CLE peptide signalling. *Semin. Cell Dev. Biol.* 109, 12–19. doi: 10.1016/j.semcdb.2020.04.022

Whitewoods, C. D., Cammarata, J., Nemec Venza, Z., Sang, S., Crook, A. D., Aoyama, T., et al. (2018). CLAVATA was a genetic novelty for the morphological innovation of 3D growth in land plants. *Curr. Biol.* 28, 2365.e5–2376.e5. doi: 10.1016/j.cub.2018.05.068

Whitford, R., Fernandez, A., De Groodt, R., Ortega, E., and Hilson, P. (2008). Plant CLE peptides from two distinct functional classes synergistically induce division of vascular cells. *Proc. Natl. Acad. Sci. U. S. A.* 105, 18625–18630. doi: 10.1073/pnas.0809395105

Willoughby, A. C., and Nimchuk, Z. L. (2021). WOX going on: CLE peptides in plant development. *Curr. Opin. Plant Biol.* 63:102056. doi: 10.1016/j.pbi.2021.102056

Xu, X., Smaczniak, C., Muino, J. M., and Kaufmann, K. (2021). Cell identity specification in plants: lessons from flower development. *J. Exp. Bot.* 72, 4202–4217. doi: 10.1093/jxb/erab110

Yadav, R. K., Perales, M., Gruel, J., Girke, T., Jönsson, H., and Reddy, G. V. (2011). WUSCHEL protein movement mediates stem cell homeostasis in the Arabidopsis shoot apex. *Genes Dev.* 25, 2025–2030. doi: 10.1101/gad.17258511

Yamaguchi, Y. L., Suzuki, R., Cabrera, J., Nakagami, S., Sagara, T., Ejima, C., et al. (2017). Root-knot and cyst nematodes activate Procambium-associated genes in Arabidopsis roots. *Front. Plant Sci.* 8:1195. doi: 10.3389/fpls.2017.01195

Yang, S., Bai, J., and Wang, J. (2020). TDIF peptides regulate root growth by affecting auxin homeostasis and PINs expression in *Arabidopsis thaliana*. *Planta* 251:109. doi: 10.1007/s00425-020-03406-1

Yosef, E., Politi, R., Choi, M. H., and Shifman, J. M. (2009). Computational design of calmodulin mutants with up to 900-fold increase in binding specificity. *J. Mol. Biol.* 385, 1470–1480. doi: 10.1016/j.jmb.2008.09.053

Zhang, L., Shi, X., Zhang, Y., Wang, J., Yang, J., Ishida, T., et al. (2019). CLE9 peptide-induced stomatal closure is mediated by abscisic acid, hydrogen peroxide, and nitric oxide in *Arabidopsis thaliana*. *Plant Cell Environ.* 42, 1033–1044. doi: 10.1111/pce.13475

Zhu, Y., Song, D., Zhang, R., Luo, L., Cao, S., Huang, C., et al. (2020). A xylem-produced peptide PtrCLE20 inhibits vascular cambium activity in Populus. *Plant Biotechnol. J.* 18, 195–206. doi: 10.1111/pbi.13187

frontiers | Frontiers in Plant Science

TYPE Original Research
PUBLISHED 02 September 2022
DOI 10.3389/fpls.2022.980138

OPEN ACCESS

EDITED BY
Neusa Steiner,
Federal University of Santa Catarina, Brazil

REVIEWED BY
Karl H. Hasenstein,
University of Louisiana at Lafayette, United States
Nhut Tan Duong,
Vietnam Academy of Science and Technology, Vietnam

*CORRESPONDENCE
Hirokazu Tsukaya
tsukaya@bs.s.u-tokyo.ac.jp

SPECIALTY SECTION
This article was submitted to Plant Development and EvoDevo, a section of the journal Frontiers in Plant Science

RECEIVED 28 June 2022
ACCEPTED 17 August 2022
PUBLISHED 02 September 2022

CITATION
Kinoshita A and Tsukaya H (2022) Auxin and cytokinin control fate determination of cotyledons in the one-leaf plant *Monophyllaea glabra*.
Front. Plant Sci. 13:980138.
doi: 10.3389/fpls.2022.980138

Auxin and cytokinin control fate determination of cotyledons in the one-leaf plant *Monophyllaea glabra*

Ayaka Kinoshita and Hirokazu Tsukaya*

Graduate School of Science, The University of Tokyo, Tokyo, Japan

One-leaf plants in the Gesneriaceae family initially have two cotyledons of identical size; one cotyledon stops growing shortly after germination, whereas the other continues indeterminate growth. Factors involved in the unequal growth have been investigated, and a competitive relationship between the two cotyledons was previously proposed. However, questions regarding the fate determination of the two cotyledons remain: Why does only one cotyledon grow indeterminately while the other stops; is the fate of the cotyledons reversible; and what role does light quality play in the fate determination of the cotyledons? In this study, physiological experiments using the one-leaf plant species *Monophyllaea glabra* suggest that a biased auxin concentration between the two cotyledons and subsequent cytokinin levels may determine the fate of the cotyledons. In addition, observation of relatively mature individuals without hormone treatment and younger individuals with cytokinin treatment under laboratory growth conditions revealed that the fate determination of the microcotyledon is reversible. Although light quality has been suggested to be important for the determination of cotyledon fate in *Streptocarpus rexii*, an anisocotylous species, we conclude that light quality is not important in *M. glabra*.

KEYWORDS

auxin, cytokinin, fate determination, indeterminate growth, one-leaf plant, *Monophyllaea glabra*

Introduction

Typical seed plants produce a shoot (composed of stems, leaves, and axial buds) with indeterminate growth from the shoot apical meristem (SAM). However, lateral organs, such as leaves, show determinate development. One-leaf plants in Gesneriaceae, which include all members of the genus *Monophyllaea* and some members of the genus *Streptocarpus*, have contrasting development compared to typical plants: One-leaf plants do not produce new leaves or stems after germination; instead, one of the cotyledons grows indeterminately.

Notably, one-leaf plants have two cotyledons of identical size just after germination as typical eudicots do, called the isocotylous stage. However, after initial development, one of the cotyledons (the microcotyledon) stops growing, whereas the other cotyledon (the macrocotyledon) continues to grow; this is called the anisocotylous stage. Although such indeterminate growth of the cotyledon is an extreme case represented by one-leaf plants, unequal growth of the two cotyledons is observed among plants in the Didymocarpoideae in Gesneriaceae, to which both the known one-leaf plants genera belong. The other subfamilies in Gesneriaceae do not show the unequal growth between two cotyledons. The unequal growth of two cotyledons, called anisocotyly (Fritsch, 1904), in one-leaf plants has attracted scientific interest for more than 100 years (Crocker, 1860; Chifflot, 1909).

To interpret the unique development of plants in the Gesneriaceae, including one-leaf plants, a concept called the phyllomorph, which is thought to correspond to the shoot (Kinoshita and Tsukaya, 2018), was introduced (Jong, 1970; Jong and Burtt, 1975). A phyllomorph is composed of an indeterminately growing leaf and a petiole-like structure. Basically, a one-leaf plant is composed of only one phyllomorph derived from a macrocotyledon, a cotyledonary phyllomorph. In *Streptocarpus*, there is a rosulate species, *S. rexii*, composed of multiple phyllomorphs including a macrocotyledon, arranged in an irregular rosette. Although this species is not a one-leaf plant, the growth of the macrocotyledon and newly produced leaves of phyllomorphs persist for long time.

There are three kinds of unique meristems in the basal part of the macrocotyledon, the groove meristem (GM), the basal meristem (BM), and the petiolode meristem, which are thought to contribute to the development of the inflorescence, lamina expansion, and elongation of the petiole-like stalk (petiolode), respectively (Jong, 1970; Jong and Burtt, 1975). The GM and the BM are thought to correspond to the SAM and leaf meristem of typical seed plants, respectively, based on studies of histological characters and gene expression (Jong and Burtt, 1975; Imaichi et al., 2000, 2001; Ayano et al., 2005; Ishikawa et al., 2017; Kinoshita et al., 2020). However, the GM is different from the SAM in that it does not produce new organs in the vegetative phase; the BM is different from the leaf meristem in that the cell proliferative activity is indeterminate.

Regarding the timing of the cotyledon fate determination, Oehlkers (1923) suggested that the two cotyledons have the same physiological features just after germination. This hypothesis was supported by Tsukaya (1997), who removed the cotyledons of *Monophyllaea horsfieldii* just after germination and observed that the remaining cotyledon differentiated into the macrocotyledon. From this result, Tsukaya (1997) proposed that the two cotyledons compete with each other, similar to apical dominance in which removal of the apical shoot induces the growth of lateral shoots. It has also been reported that some one-leaf plants in the genus *Streptocarpus* and *Monophyllaea*, both cotyledons occasionally grow continuously (Burtt, 1978; Tsukaya, 1997), again suggesting that the cotyledons have the same potential, at least just after germination.

Tsukaya (1997) also revealed that the likelihood of growth of the remaining cotyledon after the other is removed decreases as the timing of the removal is delayed, suggesting that the fate of the cotyledons becomes gradually irreversible as development progresses. However, substantial growth of the microcotyledons under greenhouse conditions has also been reported (Chifflot, 1909), although they remain smaller than macrocotyledons, suggesting a possibility that microcotyledons can retain a macrocotyledon-like nature.

Some phytohormones induce curious effects in the cotyledon growth of anisocotylous plants. For example, in species in *Monophyllaea* and *Streptocarpus*, the application of exogenous cytokinin to culture medium or soil can cause both cotyledons to grow (Rosenblum and Basile, 1984; Nishii et al., 2004, 2012b; Mantegazza et al., 2007, 2009). Light quality is also known to affect the determination of the cotyledon fate in *S. rexii*, as typical anisocotyly was observed under blue light, whereas the two cotyledons remained small under red light (Saueregger and Weber, 2003; Nishii et al., 2012a). By contrast, red light enhanced anisocotyly of *Microchirita lavandulacea*, an anisocotylous species in Didymocarpoideae (Saueregger and Weber, 2003).

Despite the experiments and observation performed to this time to reveal the nature of anisocotyly, the underlying molecular mechanisms controlling cotyledon fate are still unclear. Furthermore, whether fate determination is reversible or not is controversial. Moreover, whether environmental factors known to affect anisocotyly in some taxa also affect anisocotyly in *Monophyllaea* has not been investigated. In addition it is noteworthy that molecular systems behind the BM activity may differ between the two one-leaf plant genera, because expression pattern of Class I KNOX gene, a key factor for formation and maintenance of SAM, differs between them (Kinoshita et al., 2020).

In this study, to investigate the role of phytohormones in each cotyledon, we used lanolin paste to apply phytohormones to the cotyledons of *M. glabra*, which has been well established as a model one-leaf plant species (Ishikawa et al., 2017; Kinoshita and Tsukaya, 2018; Kinoshita et al., 2020). Our results suggest that the cotyledon with a higher auxin concentration becomes the microcotyledon, whereas a certain cytokinin concentration induces growth of the macrocotyledon. In addition, observation of relatively mature individuals without phytohormone treatment and younger individuals with cytokinin treatment in the anisocotylous stage, both under our laboratory conditions, showed that the fate determination of the microcotyledon is reversible. Moreover, both red and blue light could induce anisocotyly in *M. glabra* as they did in *Microchirita lavandulacea*, an anisocotylous Gesneriaceae species, although previous research showed that anisocotyly was suppressed under

red light in *S. rexii*, suggesting that the quality of light might not be a critical factor in fate determination of anisocotylous species in Gesneriaceae in general.

Results

Both cotyledons have the same potential to become macrocotyledons just after germination in *Monophyllaea glabra*

In *M. horsfieldii*, when one of the cotyledons was removed in the early isocotylous stage, the other cotyledon survived and became the macrocotyledon (Tsukaya, 1997), suggesting that both cotyledons of *M. horsfieldii* initially have the potential to grow indeterminately. We conducted a similar experiment using *M. glabra* to test whether this nature was conserved among species in the genus *Monophyllaea*. We removed one of the cotyledons just after (within 24 h) unfolding of cotyledons (**Figures 1A,C**). Intact individuals were also prepared as controls (**Figure 1E**). Ten days after cutting, the remaining cotyledon grew as a macrocotyledon in 18 out of 20 samples (**Figure 1B**), suggesting that both cotyledons initially had the same potential to become macrocotyledons, consistent with the result of Tsukaya (1997). The remaining cotyledon did not grow in the other two samples (**Figure 1D**). In all the control individuals, one of the cotyledons grew larger than the other and became the macrocotyledon (**Figure 1F**). These results strongly suggest that the fate of the two cotyledons is variable just after germination in *M. glabra*; a similar result was obtained in *M. horsfieldii* (Tsukaya, 1997); therefore, it is likely that this plastic character of the cotyledons in the isocotylous stage just after germination is conserved at least in the genus *Monophyllaea*.

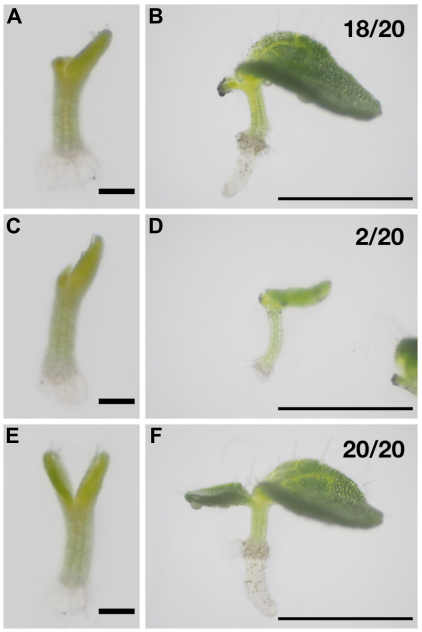

FIGURE 1
Both of the cotyledons have the same potential to become a macrocotyledon at the early isocotylous stage in *M. glabra*. **(A, B)** One of the cotyledons was removed at 6 DAS **(A)**, and the remaining cotyledon became the macrocotyledon by 10 days after cutting (DAC) **(B)**. **(C,D)** One of the cotyledons was removed at 6 DAS **(C)**, and the remaining cotyledon became the microcotyledon by 10 DAC **(D)**. **(E,F)** A control sample. 6 DAS **(E)** and 16 DAS **(F)**. Bar = 1 mm in **(A,C,E)** and 1 cm in **(B,D,F)**.

Auxin suppresses—and cytokinin promotes—the growth of cotyledons when applied to cotyledons in the isocotylous stage

To test whether the bias of the concentration of phytohormones between the two cotyledons affects their fate, we used lanolin, an oil from wool, to apply phytohormones to a single cotyledon; this method of exogenous phytohormone application is widely used in plant research (e.g., Watahiki and Yamamoto, 1997; Reinhardt et al., 2000; Scarpella et al., 2006). In a previous study, the authors applied phytohormones to each cotyledon on a species of *Streptocarpus* using aquaphore, whose main component is also oil. However, the application of aquaphore to both cotyledons inhibited the growth of both cotyledons (Rosenblum and Basile, 1984). Therefore, it was necessary to improve the experimental system. To prevent harmful effects as much as possible from both physical and physiological aspects, the lanolin paste treatments were applied to the edge of the cotyledon but not on the top surface of the cotyledon (**Figure 2D**). When the lanolin, containing ethanol (EtOH), used in the cytokinin experiments as a solvent and here as a control, was applied to only one cotyledon, it seemed to have no effect on its fate, as statistically significant difference was not detected in the number between micro- and macrocotyledons were formed from the treated cotyledons (**Figures 2A–C**; EtOH). Furthermore, when lanolin was applied to both cotyledons, one of the cotyledons became larger than the other cotyledon in all the individuals, similar to the non-treated plants (**Figure 2A**; EtOH both). These results suggest that the fate determination of the cotyledons was not affected by lanolin application in the experimental system. Here, we judged the differentiation of macro- and microcotyledons not only by the size of the leaf lamina but also by the presence of a petiole-like narrow part at the proximal end, which is made by elongation of differentiate cells and the absence of further cell proliferation (**Figures 2E,F**).

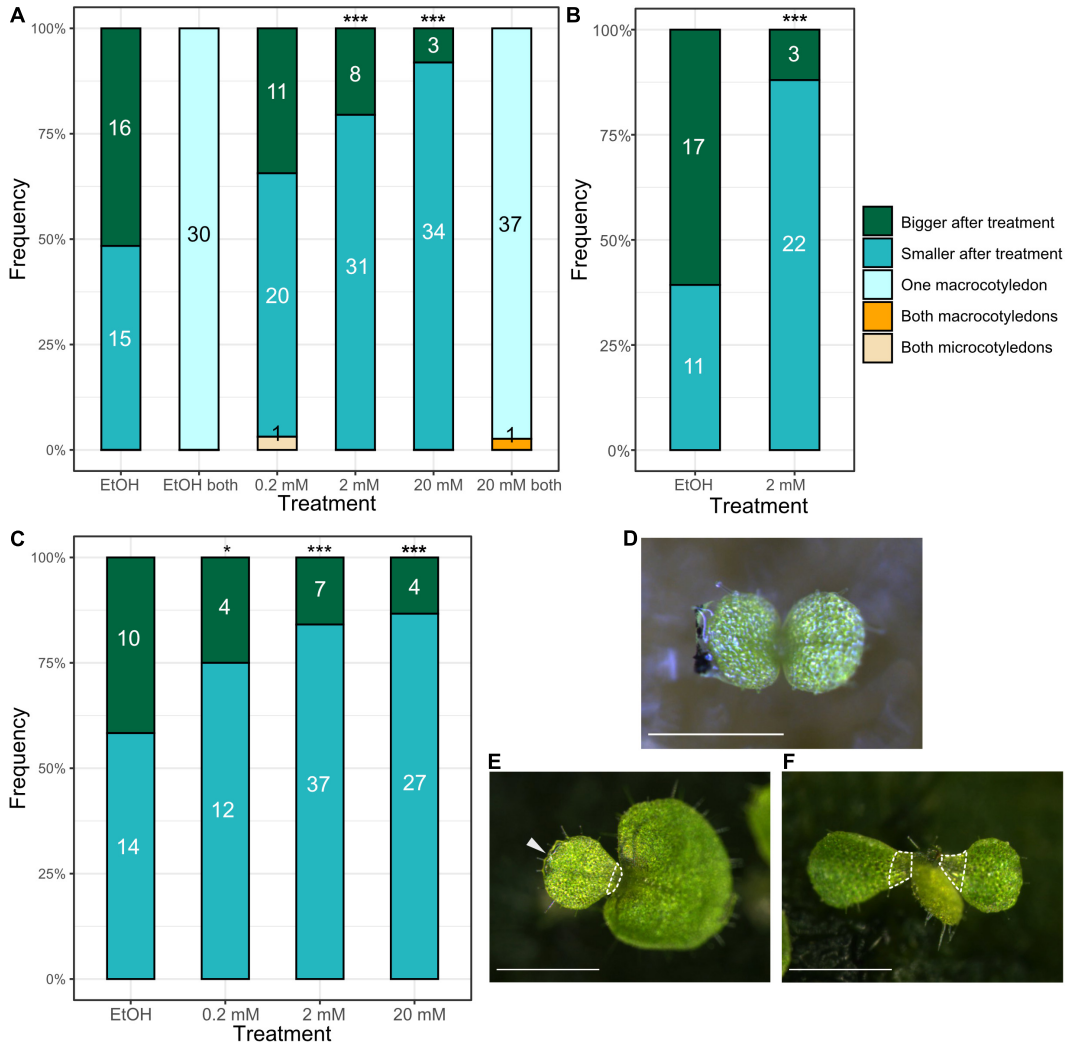

FIGURE 2
Auxin treatment of cotyledons in the isocotylous stage reveals that a higher concentration in one of the cotyledons induces the microcotyledon fate. **(A–C)** The results of three independent auxin application experiments. "Bigger after treatment" and "Smaller after treatment" indicate individuals in which the cotyledon treated with the lanolin paste grew larger (macrocotyledon) and those that stopped growth (microcotyledon) after treatment, respectively. "One macrocotyledon" indicates that one of the cotyledons differentiated into a macrocotyledon and the other differentiated into a microcotyledon. "Both macrocotyledons" and "Both microcotyledons" indicate individuals that harbored two macrocotyledons and two microcotyledons, respectively. The numbers in the bars indicate the absolute number of individuals in each category. The x-axis shows the types of treatment: "EtOH" indicates the treatment with lanolin only containing ethanol, used to dilute IAAK. "0.2 mM," "2 mM," and "20 mM" indicate the concentration of auxin dissolved in the lanolin in the treatment. On the x axis, "both" indicates that the lanolin was applied to both of the cotyledons. **(D)** The stage at which the lanolin treatment was conducted. Lanolin was applied to the edge of the individual cotyledon, and black carbon particles were stuck on the lanolin to make it easier to show the position of the lanolin. **(E)** One of the individuals treated with 20 mM IAAK, observed in experiment **(A)**. The arrow indicates the lanolin, which can be seen on the cotyledon on the left (microcotyledon). The hatched white line shows narrower part in the microcotyledon lamina. **(F)** The individual harboring both microcotyledons in experiment **(A)**. A new organ was produced between the two cotyledons. The hatched white line shows narrower part in the microcotyledon lamina. *$p < 0.05$, ***$p < 0.001$ in a binomial test of "Bigger after treatment" and "Smaller after treatment" (The number of occurrences of "Both macrocotyledons" and "Both microcotyledons" is not included because they are very rare). Bar = 0.5 mm in **(D)** and 1 mm in **(E,F)**.

The effect of auxin on the fate determination of the cotyledons was investigated using this lanolin paste experimental system. Lanolin paste containing different concentrations of auxin [indole-3-acetic acid potassium salt (IAAK); 0.2, 2, and 20 mM] was applied to one of the cotyledons. The auxin-treated cotyledons differentiated into microcotyledons more frequently than into macrocotyledons, and this tendency was more obvious when the auxin concentration was higher (Figures 2A–C). Strikingly, when 2 and 20 mM IAAK was used, 31 out of 39 (79%) and 34 out of 37 individuals (92%) with the auxin-treated cotyledons, respectively, differentiated into microcotyledons (Figure 2A);

a binomial test indicated that the percentage of the number of cotyledons differentiating into the microcotyledons was significantly higher than at random. We conducted two more independent experiments, and all the experiments showed the same tendency: In a second experiment, 22 out of 25 individuals with the auxin-treated cotyledons differentiated into microcotyledons when 2 mM IAAK was applied (**Figure 2B**); in the third experiment, 37 out of 44 and 27 out of 31 individuals with the auxin-treated cotyledons differentiated into microcotyledons when they were treated with 2 and 20 mM IAAK, respectively (**Figure 2C**). Furthermore, when 20 mM IAAK was applied to both cotyledons, one grew as a macrocotyledon and the other grew as a microcotyledon in most of the individuals (37 out of 38 individuals), similar to the non-treated plants (**Figure 2A**; 20 mM both). Notably, when both cotyledons were treated with 0.2 mM IAAK, we observed an individual in which both cotyledons differentiated into microcotyledons and a phyllomorph-like structure was produced between the two cotyledons (**Figure 2F**).

The effect of cytokinin was also examined in the same manner. We applied 6-benzylaminopurine (BAP), a synthetic cytokinin, at a concentration of 5 mM in lanolin to one of the cotyledons. This resulted in the similar growth of both cotyledons in all individuals (**Figures 3A,C**). Both cotyledons had lateral veins and a wide leaf lamina in the basal part, which are characteristic of macrocotyledons. By contrast, when lanolin containing only dimethyl sulfoxide (DMSO), a solvent for BAP, was applied, one of the cotyledons remained small and the leaf lamina of the cotyledon became narrower in the basal part due to cell elongation without further cell proliferation, similar to in the non-treated plants (**Figure 3B**).

These results suggest that a higher concentration of auxin in one cotyledon than the other suppresses the fate of the macrocotyledon and that cytokinin above a threshold level promotes the fate of the macrocotyledon.

Microcotyledons resume growth without hormone treatment under laboratory conditions

Although *Monophyllaea* species are called one-leaf plants, under certain cultivation conditions, the microcotyledon, which remains small or withers away in wild habitats, grows to some extent (Chifflot, 1909; Oehlkers, 1923). However, it is not known whether the microcotyledon growth continues throughout the life of the plant or if it pauses for a time and then restarts.

We noticed growth of the microcotyledon in *M. glabra* in our laboratory conditions where we grow *M. glabra* for collecting seeds or other research purposes (continuous light, 22–23°C) (Kinoshita and Tsukaya, 2018; Kinoshita et al., 2020), so we decided to observe the process of the growth carefully. We observed five individuals of *M. glabra* from 82 to 201 days after sowing (DAS) and determined that all the microcotyledons grew to some extent during this time (**Figures 4A–E** and **Table 1**). Especially for four individuals at 201 DAS the length of the microcotyledon was more than 50 times longer than the length at 82 DAS (**Figure 4A1, A6, A7** and **Table 1**).

Also, at 101 DAS, the length of the microcotyledons was slightly longer than that at 82 DAS (**Figures 4A–E** and **Table 1**). The elongation occurred in the petiole-like part of the microcotyledons where the color was whiter (more colorless) than that of the leaf lamina. At 115 DAS, drastic changes in the microcotyledons started to appear in three individuals, ("A", "B", and "D" in **Figure 4A4, B4, D4**). Greener tissues and wider lamina with longer trichomes than the petiole-like part were produced in the basal part of the microcotyledon, leaving the initial microcotyledon lamina in the distal part. This phenomenon also became evident in another individual by 125 DAS ("E" in **Figure 4E5**). After these drastic changes at 125 DAS, the growth rate increased considerably (**Figure 4F**).

The drastic changes of microcotyledon growth in the four individuals suggested that this was due to resumed growth after a pause rather than a continuation of growth. To test whether the growth of the microcotyledon stops in earlier stages, we observed 10 other individuals grown under the same conditions and measured the length of the microcotyledons. The length reached a plateau around 40 DAS (**Figure 4G**) in all individuals. The microcotyledon length was around 0.8 to 1.5 mm, which was almost the same as in the other five individuals at 82 DAS (**Table 1**), suggesting that growth of microcotyledons almost stopped around 40–80 DAS when grown under the laboratory conditions. In summary, in our laboratory conditions, the microcotyledon of *M. glabra* stops growing for a while, but resumes growth just as macrocotyledons without plant hormone treatment.

Cytokinin induces the resumption of the microcotyledon growth even when it is applied to microcotyledons in the anisocotylous stage

As mentioned above, we observed a pause in growth followed by resumed growth of microcotyledons in our laboratory conditions. However, the factors that control this restart of growth have yet to be revealed. Since cytokinin can induce both cotyledons to become macrocotyledons when applied in the isocotylous stage, we suspected that exogeneous cytokinin can make fate-determined microcotyledons grow as macrocotyledons.

To investigate this, lanolin containing cytokinin (BAP) or DMSO as a control was applied to the microcotyledon of individual plants in the anisocotylous stage (25 DAS, **Figures 5A,E**). In this stage, the shape of the microcotyledon was petiole-like in the basal part, whereas the basal part of

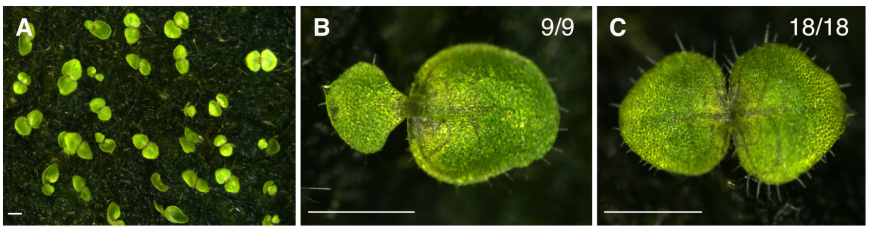

FIGURE 3
Application of cytokinin to one of the cotyledons in the isocotylous stage induces both cotyledons to grow as macrocotyledons. **(A,C)** Individuals treated with lanolin containing cytokinin. All the individuals (18 out of 18) treated with cytokinin had two cotyledons with lateral veins and a wide leaf lamina in the basal part. **(B)** All the individuals (9 out of 9) treated with lanolin containing DMSO showed clear anisocotyly. Bar = 1 mm.

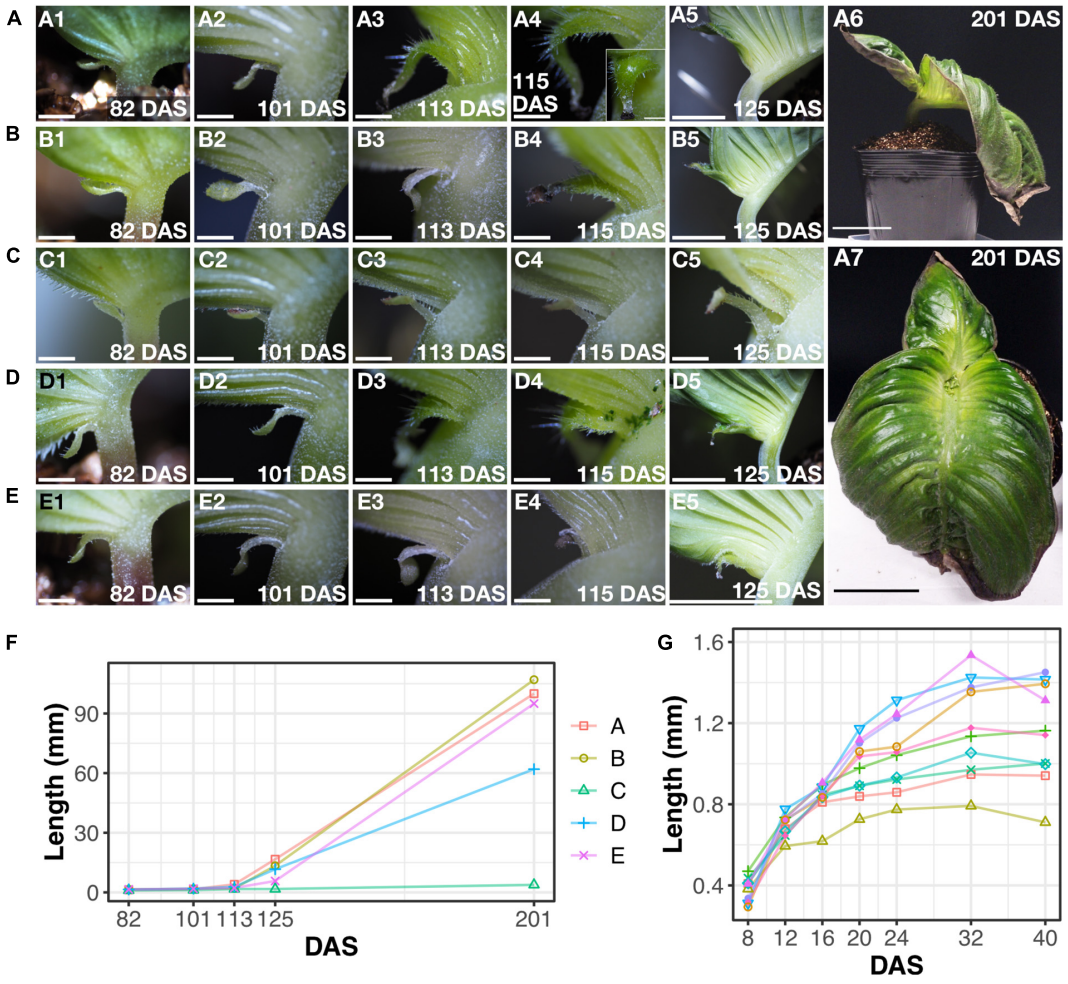

FIGURE 4
Microcotyledons resume growth under laboratory conditions. **(A–E)** Five individuals, **(A–E)** at 82, 101, 113, 115, 125, and 201 [only for **(A)**] DAS (1–6). The inset in (A4) is a view from the adaxial side of the microcotyledon. (A7) is the frontal view of the individual in (A6). **(F)** The length of the microcotyledons of each individual, **(A–E)**. **(G)** The length of microcotyledons in 10 additional individuals at 8–40 DAS. Bar = 1 mm in (1–4) in **(A–E)** and (C5), 1 cm in (5) in **(A,B,D,E)**, and 5 cm in (A6, A7).

the macrocotyledon was rounded. Ten days after treatment (DAT), at 35 DAS, the basal part of the microcotyledon seemed slightly wider in cytokinin treated individuals than the control, but the difference was not clear (Figures 5B,F). At 17 DAT, obvious microcotyledon growth, which was marked by new lateral veins (clearly observed in 16 out of 18 individuals)

TABLE 1 Length of the microcotyledon.

Individual	DAS				
	82	101	113	125	201
A	1.26	1.57	4.03	16.7	100
B	1.50	1.80	1.99	13.4	107
C	1.02	1.18	1.70	1.70	3.79
D	1.47	1.90	2.79	11.7	62.0
E	1.47	1.82	2.24	5.72	95.0

Each individual (A–E) corresponds to the individuals A–E in Figure 4. Length of unit: mm.

and/or longer trichomes were observed in the cytokinin-treated individuals, whereas no such phenotype was observed among all 16 individuals in the control condition (**Figures 5C,D,G,H**). In a cytokinin-treated sample at 17 DAT, the GM-like and the BM-like tissues, which are composed of small cells, which positioned in the same way as the GM and the BM in macrocotyledon (Imaichi et al., 2001; Ayano et al., 2005) were observed in the basal part of the microcotyledon (**Figures 5I,J**). Before the resumption of the growth of the microcotyledon, it has been observed in *M. glabra* that cells in the basal part of the microcotyledons are expanded, suggesting they are differentiated (Ayano et al., 2005; Kinoshita et al., 2020). At 62 DAT, in some individuals, microcotyledons grew to the extent that they were difficult to distinguish from macrocotyledons (**Figures 5K–N**). Therefore, cotyledons seem to retain the potential to grow like a macrocotyledon even after fate-determination as a microcotyledon.

Anisocotyly can be induced under both red and blue light

The effect of light quality on anisocotyly has been investigated in several Gesneriaceae species. Although all of them belong to the subfamily Didymoracpoideae, their reaction to red or blue light seems to differ among species. In *S. rexii*, typical anisocotyly was induced under blue light, whereas an isocotylous phenotype was observed under red light (Saueregger and Weber, 2003; Nishii et al., 2012a). Contrarily, the anisocotylous phenotype was enhanced in *M. lavandulacea* (Saueregger and Weber, 2003) under red light. Therefore, there is a possibility that the external factors that induce anisocotyly may differ among anisocotylous species. Therefore, we examined the reaction of *M. glabra* to different qualities of light.

Red-light, blue-light, white-light, and dark conditions (see Materials and methods) were examined. For the red- and blue-light treatments, we compared two conditions: Seeds were irradiated with red or blue light just after sowing, or seeds irradiated with white light for 7 days were transferred to red or blue light.

We observed that anisocotyly was induced among almost all the individuals under all the tested conditions (**Figures 6A–E**),

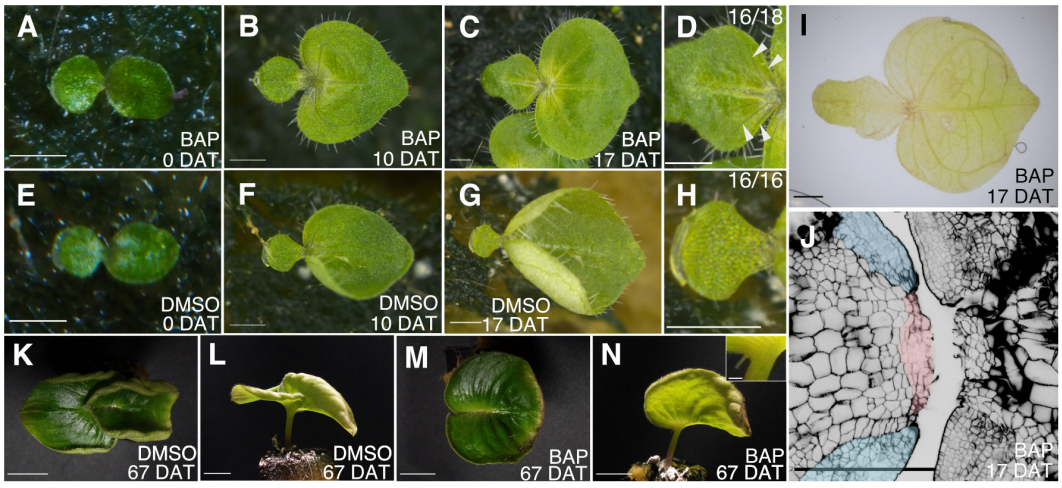

FIGURE 5
Application of cytokinin to microcotyledons in the anisocotylous stage induces resumption of the growth of microcotyledons. An individual plant treated with lanolin containing cytokinin **(A–D)**; an individual plant treated with lanolin containing DMSO **(E–H)**. 0 days after treatment (DAT) **(A,E)**, 10 DAT **(B,F)**, and 17 DAT **(C,D,G,H)**. The microcotyledons in **(C)** and **(G)** are magnified in **(D)** and **(H)**, respectively. The arrowheads in **(D)** point to lateral veins. **(I)** An individual treated with lanolin containing cytokinin fixed at 17 DAT. **(J)** The outline of epidermal and subepidermal cells in the basal part of macro- and microcotyledons in the same individual as **(I)**. The pink and blue shaded areas are the putative GM and BM, respectively, in the microcotyledon resuming growth. **(K–N)** Individuals treated with cytokinin **(K,L)** or DMSO **(M,N)** at 67 DAT. Top views **(K,M)** and side views **(L,N)**. The inset in **(N)** is the magnified view of the microcotyledon of the individual in **(N)**. Bar = 1 mm in **(A–J)**, 1 cm in **(K–N)**, and 100 μm in the inset of **(N)**.

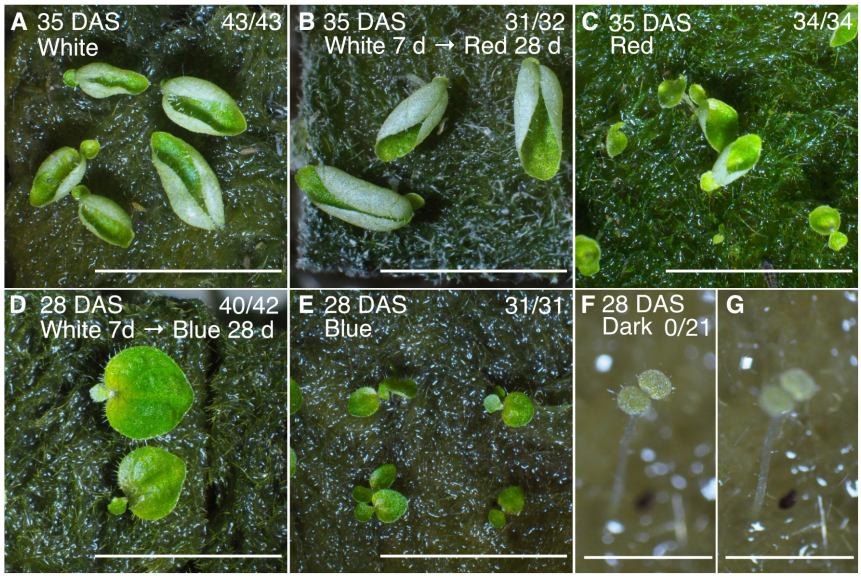

FIGURE 6
Anisocotylous growth of *M. glabra* is observed both under red and blue light conditions. **(A)** Individuals at 35 DAS grown under white fluorescent light. **(B)** Individuals at 35 DAS grown under white fluorescent light for the first 7 days and red light for the subsequent 28 days. **(C)** Individuals at 28 DAS grown under red light. **(D)** Individuals at 35 DAS grown under white fluorescent light for the first 7 days and blue light for the subsequent 28 days. **(E)** Individuals at 28 DAS grown under blue light. **(F,G)** An individual at 28 DAS grown under dark conditions. The focus is on the cotyledons in **(F)** and on the petiolode in **(G)**. The denominator and numerator at the top right in each figure indicate the number of individuals germinated and the number of anisocotyl individuals, respectively. Bar = 1 cm in **(A–E)** and 1 mm in **(F,G)**.

except for the dark condition (Figure 6F). The individuals grown under red light had macrocotyledons that curled up to the adaxial side (Figure 6C), whereas when grown under blue light, the macrocotyledons grew flat (Figures 6D,E). All individuals germinated under the dark condition showed an isocotylous phenotype with an elongated petiolode (Figures 6F,G). In summary, both red and blue light can induce the anisocotyly in *M. glabra*.

Discussion

Cotyledon growth is suppressed by auxin and promoted by cytokinin

In this study, we examined the effects of phytohormones on the fate determination of cotyledons in *M. glabra.* Auxin treatment of one cotyledon resulted in a greater propensity for that cotyledon to differentiate into a microcotyledon, and this tendency increased as the concentration of auxin increased. These results suggest that auxin may have a suppressive role in the growth of the cotyledons in *M. glabra*. Auxin appears to be working in a relative manner between the two cotyledons, rather than in an absolute dose-dependent manner, because application of a high concentration auxin to both did not affect the fate determination (Figure 2A). The difference in the concentration of auxin between two cotyledons might be a molecular background of the proposed "competition" (Tsukaya, 1997).

There were, however, some exceptions. In all three independent experiments, the auxin-treated cotyledon became the macrocotyledon in a few individuals even when the concentration of auxin was considerably high (20 mM). This might be because the fate of these cotyledons in these individuals had already been determined before the treatment; thus, they were not affected by exogenous auxin. Similarly, when one of the cotyledons was removed, even within 24 h after the unfolding of the two cotyledons, the remaining cotyledon in 2 out of 20 individuals did not grow as the macrocotyledon. Therefore, cotyledon fate may be determined at a very early stage; alternatively, these plants may have germinated slightly earlier than the other individuals, and thus they were at a slightly more advanced developmental stage at the time of the auxin treatment.

Although auxin suppressed cotyledon growth when it was applied to only one cotyledon, when both cotyledons were treated it did not cause both cotyledons to become microcotyledons. This suggests that the microcotyledon fate is induced when auxin concentration in the cotyledon is higher than the other cotyledon but not when absolute auxin concentration exceed a certain threshold.

Cytokinin treatment to only one of the cotyledons resulted in the growth of both cotyledons. This may suggest that the growth of a cotyledon occurs when cytokinin

levels exceed a certain threshold, and the difference in the concentration between two cotyledons is not important for the fate determination.

Apical dominance is achieved by the suppression of cytokinin synthesis by auxin (Tanaka et al., 2006). If the endogenous auxin and cytokinin work in the same way as the exogenous auxin applications in *Monophyllaea*, it is possible that a similar mechanism as that in apical dominance underlies the competitive phenotype of the cotyledons in the following steps: (1) A stochastic difference in the auxin level between two cotyledons is somehow amplified; (2) cytokinin synthesis is then initiated in the cotyledon with a lower auxin level, whereas its production is suppressed in the cotyledon with higher auxin; and 3) cell division in the proximal part is induced in the cotyledon with a higher cytokinin level due to promotion of the expression of cyclin genes by cytokinin signaling (Riou-Khamlichi et al., 1999) (**Figure 7**). In step 1, auxin transport to the cells with higher auxin levels from the adjacent cells with lower auxin, as explained in the up-the-gradient model (Smith et al., 2006; reviewed in van Berkel et al., 2013), is a possible underlying molecular mechanism for the growth of the macrocotyledon.

Ability of the microcotyledon to restart growth

Substantial growth of the microcotyledon has been observed in some cultivation conditions in previous studies but has not been observed in wild habitats. In this study, we also observed enhanced growth of the microcotyledons in relatively older individuals under our laboratory growth conditions, and the resumption of growth was induced at a much earlier stage by applying cytokinin to already fate-determined microcotyledons under the same environment.

In our growth conditions, the observation of microcotyledon growth without exogenous application of phytohormones suggested that the growth of the microcotyledon pauses briefly after initial development, but active growth resumes in a later stage. Moreover, we observed the growth of the lamina in the basal part of the microcotyledon. This suggests that cells in the basal part of the microcotyledon retain the potential to become an active leaf meristem or new meristematic cells are provided to the basal part. The substantial growth of microcotyledons has been observed in our laboratory cultivation conditions or in a greenhouse in the previous study (Chifflot, 1909), but not in the wild habitat, so some environmental factors likely affect whether the microcotyledons restart growth. The wild habitat of *Monophyllaea* is often in limestone caves (Burtt, 1978; Kinoshita and Tsukaya, 2018), so it is possible that nutrition and light are more plentiful in the laboratory conditions or in the green house than in the wild habitat, which may promote the unusual development of the microcotyledon.

In the artificially induced growth of the microcotyledon by application of cytokinin, microcotyledons started to produce lamina with long trichomes and lateral veins. Nishii et al. (2004) reported that also in *M. glabra*, the enlarging macrocotyledon in the anisocotylous stage has traits not observed in the isocotylous stage: long trichomes and lateral veins. Therefore, our observations suggest that the growing microcotyledon gained the same identity as the enlarging macrocotyledons. Moreover, the GM- and the BM-like tissues, which comprised small cells, were observed in the basal part of the microcotyledon after the cytokinin treatment, again suggesting that the microcotyledons gained the same identity as the macrocotyledons. Indeed, at 67 DAT, both cotyledons were almost indistinguishable in some individuals. Although Tsukaya (1997) proposed that the fate determination is irreversible by showing that excision of the macrocotyledon did not induce microcotyledon growth, our report of the growth of the microcotyledons suggests that microcotyledons retain the potential for indeterminate growth even after fate determination.

The observation of microcotyledon growth with and without exogenous cytokinin suggests that the restart of the growth of the microcotyledon is related to cytokinin signaling. When microcotyledons resumed growth without exogeneous cytokinin, endogenous cytokinin may be overproduced.

It has been reported that cytokinin promotes cell division in the cotyledons in *Arabidopsis thaliana* (Stoynova-Bakalova et al., 2004), but the role of cytokinin in the establishment of meristematic tissues or indeterminate growth in cotyledons has not been reported. Therefore, the indeterminate growth of the microcotyledon induced by cytokinin is likely to be unique for species in *Monophyllaea* or other species with indeterminately growing leaves. As cytokinin signaling positively regulates class I KNOTTED LIKE HOMEOBOX (KNOX I) gene expression (Rupp et al., 1999; Hamant et al., 2002; Tsuda et al., 2011) and KNOX I promotes cytokinin biosynthesis (Jasinski et al., 2005; Yanai et al., 2005; Sakamoto et al., 2006) resulting in positive feedback, a higher concentration of cytokinin might induce the expression of *SHOOT MERISTEMLESS (STM)*, one of the KNOX I genes, in the basal part of the microcotyledon. If this is true, as *STM* is essential for the formation and maintenance of the SAM (Barton and Poethig, 1993; Endrizzi et al., 1996; Long et al., 1996; Long and Barton, 1998), the corresponding tissue of the SAM in *Monophyllaea*, the GM, may be formed in the microcotyledon in response to cytokinin, leading to the indeterminate growth. Indeed, it has been confirmed that an *STM* ortholog is expressed in the GM of macrocotyledons of *MN. Glabra* (Ishikawa et al., 2017; Kinoshita et al., 2020). The BM may be produced from the GM (Ishikawa et al., 2017), as the leaf meristem is produced from the SAM in typical plants. Therefore, the establishment of the GM may be enough to explain the resumption of indeterminate growth of the microcotyledon.

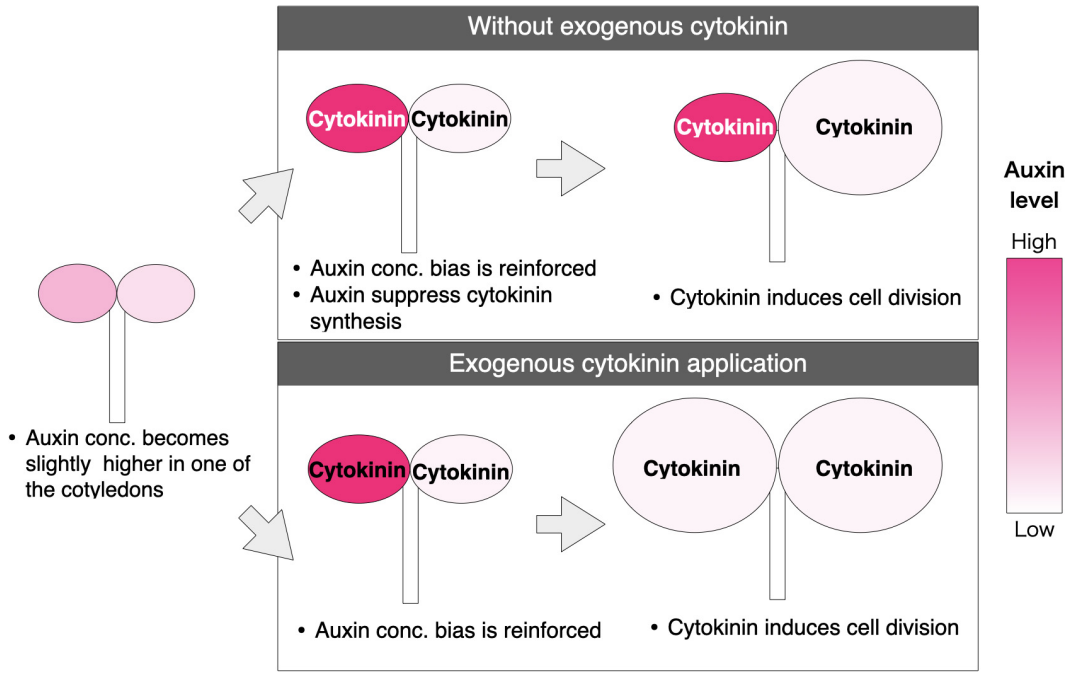

FIGURE 7
Proposed model for fate determination of the two cotyledons in *M. glabra*. The red color indicates the concentration of auxin. The darker color indicates higher concentration. The black and white color of the letters, "Cytokinin" indicates the high and low concentration of cytokinin in the cotyledons, respectively. The developmental process indicated in the upper part is under a non-treated condition; auxin concentration is slightly different between the two cotyledons in the isocotylous stage. After some time, the difference of the auxin level is enforced due to "up-the-gradient" mechanisms supported by auxin polar transport. Then, cytokinin is produced less in the cotyledon where the auxin level is higher due to the inhibition of cytokinin synthesis by auxin signaling. This results in only one of the cotyledons with a higher cytokinin level becoming a macrocotyledon. The diagram on the bottom shows a developmental process where cytokinin is applied exogenously; when the cytokinin level exceeds a certain threshold in both cotyledons, regardless of the auxin level, both cotyledons can become macrocotyledons.

Growth of the cotyledon and organ formation

In one-leaf *Streptocarpus* species, it has been observed that new organs are produced between two cotyledons when the growth of both cotyledons is suppressed, such as by application of gibberellic acid, whereas no new organ is produced during the vegetative phase without such a treatment (Nishii et al., 2012b). This phenomenon has been interpreted as a release from apical suppression of the basal meristem (Nishii et al., 2012b).

Although this phenotype has not been induced by gibberellic acid in *Monophyllaea* (Imaichi, 2001), a similar phenomenon was observed in this study when both of the cotyledons were treated with auxin: When the growth of the both cotyledons was suppressed, a new phyllomorph was formed between the two cotyledons. This suggests that, at least in the vegetative phase, the BM also has a suppressive role on the GM in *Monophyllaea* in terms of the formation of new organs. This may also explain the formation of new phyllomorphs after removing the macrocotyledon, although this observation is rare (Tsukaya, 1997).

Effect of red and blue light on the growth of the cotyledons

We observed that anisocotyly of *M. glabra* was induced under both red- and blue-light conditions, whereas an isocotylous phenotype was observed when grown under dark conditions. Therefore, light is necessary for the anisocotylous development of *M. glabra*. Notably, the reaction to red light differs among species: In *S. rexii*, red light did not induce anisocotyly (Saueregger and Weber, 2003; Nishii et al., 2012a), whereas red light enhanced anisocotyly in *Microchirita lavandulacea* (Saueregger and Weber, 2003). Phylogenetically, *Streptocarpus* and *Microchirita* are more closely related, belonging to the same tribe, Trichosporeae, whereas *Monophyllaea* is relatively distantly related to these genera, belonging to another tribe, Trichosporeae. Therefore, in general, the quality of light might not be important for anisocotyly, but light itself is important. For example, both red and blue light are used for photosynthesis; thus, photosynthetic products, such as sucrose, might be important for anisocotyl growth. Since the intensity and wavelength of the light or whether light receptors are saturated affect the

downstream, knocking-out the light-receptors-related genes would be necessary in the future to get solid conclusion on whether light receptors are involved in the determination of the cotyledons.

We also observed that the macrocotyledons curled upward when grown under red light, whereas they grew flat under the blue-light condition. This is consistent with the previous research showing that signaling from the phytochrome, which perceives red light, promotes curling (Kozuka et al., 2013), while the signal from phototropin, which perceives blue light, suppresses curling (Sakamoto and Briggs, 2002; de Carbonnel et al., 2010). However, the direction of curling is opposite in *M. glabra* when compared to *A. thaliana*. It has been suggested in *A. thaliana* that the curling is caused by a lack of cell expansion in the abaxial side (Kozuka et al., 2013). Therefore, *M. glabra* may differ from *A. thaliana* in terms of which side of the epidermal cells reacts to the light.

In conclusion, we have revealed that auxin and cytokinin control the fate determination of cotyledons of the one-leaf plant *Monophyllaea glabra*. In particular, we proposed a new hypothesis that the difference of auxin concentration and subsequent cytokinin concentration between the two cotyledons is important for the competition-like growth of the two cotyledons. Moreover, we demonstrated the ability of the microcotyledon to restart growth as a macrocotyledon. Finally, we revealed that both blue and red light can induce anisocotyly of *M. glabra*. These findings contribute to our understanding of the development of one-leaf plants; furthermore, as one-leaf plants can be regarded as mutants of typical plants with shoots, the elucidation of one-leaf plant development provides general insight into the developmental of typical seed plants.

Materials and methods

Plant materials and growth conditions

Seeds of *Monophyllaea glabra* were originally collected at Srakaew Cave, Thailand and have succeeded generation by generation in the laboratory and maintained the strain by collecting seeds in growth chambers (Ishikawa et al., 2017). Seeds were sown on either a block of rockwool or 1/3 MS0 medium adjusted to pH 7.0 by potassium hydroxide with 0.8% (w/v) agar (Wako, Osaka, Japan) depending on experiments. When plants were grown on rockwool for more than 2 months, they were replanted into pots with vermiculite. Plants grown on rockwool or vermiculite were provided with 0.5% (w/w) fine powder hyponex (Hyponex, Osaka, Japan) in tap water. Those plants were grown at 22–23°C under white light provided by fluorescent lamps under continuous-light conditions (Kinoshita and Tsukaya, 2018). The light intensity was ∼45 μmol m^{-2} s^{-1}.

Preparation and application of lanolin paste

Indole acetic acid potassium salt (IAAK; Nacalai Tesque, Kyoto, Japan) was dissolved in Milli-Q water to prepare a 2 M IAAK stock solution. To prepare the lanolin paste containing the final concentrations of 0.2, 2, and 20 mM IAAK, IAAK solutions diluted with 99.5% ethanol were added to lanolin (Wako, Osaka, Japan), heated to 50°C, and vigorously mixed. 6-Benzylaminopurine (BAP; Wako, Osaka, Japan) was dissolved in dimethyl sulfoxide (DMSO; Nacalai Tesque, Kyoto, Japan) to prepare a 500 mM stock solution. Then, 5 mM BAP lanolin paste was prepared by dissolving the stock solution in lanolin. As the controls, we prepared lanolin pastes with only ethanol or DMSO of the same concentration to the corresponding hormone treatments. The lanolin was cooled down to room temperature and picked with an injection needle. A small amount of the lanolin was put on the edge of cotyledons under a dissecting microscope.

Cultivation under different qualities of light

To test whether the quality of light affects anisocotyly of *M. glabra*, individuals were grown under blue monochromatic light-emitting diode (LED) lights (470 nm) (15–30 μmol s^{-2}), red monochromatic LED lights (660 nm) (15–30 μmol s^{-2}), white fluorescent lights (15–30 μmol s^{-2}), or in darkness. The temperature was kept at 22–23°C. For blue and red light, two conditions were compared: Seeds were kept under the white light condition from just after sowing to 7 DAS and subsequently placed under the blue- or red-light condition; also, seeds were placed under the red- or blue-light condition just after sowing (within 3 h).

Microscopy

Most of the individuals were observed under a SZ61 dissecting microscope (Olympus, Tokyo, Japan), and the images were taken by an OM-D E-M10 digital camera (Olympus, Tokyo, Japan). For smaller samples, a MZ16 stereomicroscope (Leica Microsystems GmbH, Wetzlar, Germany) was also used. For samples large enough for observation with the naked eye, pictures were taken by a Ricoh WG-4 camera (Ricoh, Tokyo, Japan). To image the basal part of the cells in the microcotyledons in the individuals treated with cytokinin in the anisocotylous stage, the individuals were fixed with 4% PFA with 15% DMSO and 0.1% Tween-20 at 18 days after treatment (DAT). After more than 1 day of the fixation, the sample was immersed in 1% (v/v) calcofluor white stain (Sigma-Aldrich, St. Louis, MO, United States) in ClearSee solution

(Kurihara et al., 2015) for more than overnight and observed with a Fluoview FV10i confocal microscope (Olympus, Tokyo, Japan).

Data availability statement

The original contributions presented in this study are included in the article. Further inquiries can be directed to the corresponding author.

Author contributions

AK designed the study and performed the experiments. AK and HT directed the study and wrote the manuscript. Both authors contributed to the article and approved the submitted version.

Funding

This research was supported by a Grant-in-Aid for JSPS Fellows (AK, JP19J14140) and a Grant-in-Aid for Scientific Research on Innovation Areas (HT, JP25113002 and JP19H05672) from MEXT and GPLLI/WINGS-LST of the University of Tokyo (AK).

Acknowledgments

We thank Yuta Otsuka from the University of Tokyo for helping us conduct experiments using lanolin.

Conflict of interest

The authors declare that the research was conducted in the absence of any commercial or financial relationships that could be construed as a potential conflict of interest.

Publisher's note

References

Ayano, M., Imaichi, R., and Kato, M. (2005). Developmental morphology of the Asian one-leaf plant, *Monophyllaea glabra* (Gesneriaceae) with emphasis on inflorescence morphology. *J. Plant Res.* 118, 99–109. doi: 10.1007/s10265-005-0195-5

Barton, M. K., and Poethig, R. S. (1993). Formation of the shoot apical meristem in *Arabidopsis thaliana*: An analysis of development in the wild type and in the shoot meristemless mutant. *Development* 119, 823–831. doi: 10.1242/dev.119.3.823

Burtt, B. L. (1978). Studies in the Gesneriaceae of the Old World. XLV. A preliminary revision of *Monophyllaea*. *R. Bot. Gard. Edinburgh* 37, 1–59.

Chifflot, M. (1909). Sur quelques variations du *Monophyllaea horsfieldii*. *R. Br. Comptes Rendus l'Académie Des Sci.* 148, 939–941.

Crocker, C. W. (1860). Notes on the Germination of certain species of Cyrtandreae. *J. Proc. Linn. Soc. London Bot.* 5, 65–67. doi: 10.1111/j.1095-8312.1860.tb01039.x

de Carbonnel, M., Davis, P., Roelfsema, M. R. G., Inoue, S., Schepens, I., Lariguet, P., et al. (2010). The *Arabidopsis* PHYTOCHROME KINASE SUBSTRATE2 protein is a phototropin signaling element that regulates leaf flattening and leaf positioning. *Plant Physiol.* 152, 1391–1405. doi: 10.1104/pp.109.150441

Endrizzi, K., Moussian, B., Haecker, A., Levin, J. Z., and Laux, T. (1996). The SHOOT MERISTEMLESS gene is required for maintenance of undifferentiated cells in *Arabidopsis* shoot and floral meristems and acts at a different regulatory level than the meristem genes WUSCHEL and ZWILLE. *Plant J.* 10, 967–979. doi: 10.1046/j.1365-313X.1996.10060967.x

Fritsch, K. (1904). *Die Keimpflanzen der Gesneriaceae mit besonderer Berücksichtigung von Streptocarpus, nebst vergleichenden Studien über die Morphologie dieser Familie*. Jena: Fisher.

Hamant, O., Nogué, F., Belles-Boix, E., Jublot, D., Grandjean, O., Traas, J., et al. (2002). The KNAT2 homeodomain protein interacts with ethylene and cytokinin signaling. *Plant Physiol.* 130, 657–665. doi: 10.1104/pp.004564

Imaichi, R. (2001). Evolutionary morphology of one-leaf plants (Gesneriaceae). *Plant Morphol.* 13, 45–50. doi: 10.5685/plmorphol.13.41

Imaichi, R., Inokuchi, S., and Kato, M. (2001). Developmental morphology of one-leaf plant *Monophyllaea singularis* (Gesneriaceae). *Plant Syst. Evol.* 229, 171–185. doi: 10.1007/s006060170010

Imaichi, R., Nagumo, S., and Kato, M. (2000). Ontogenetic anatomy of *Streptocarpus grandis* (Gesneriaceae) with implications for evolution of monophylly. *Ann. Bot.* 86, 37–46. doi: 10.1006/anbo.2000.1155

Ishikawa, N., Takahashi, H., Nakazono, M., and Tsukaya, H. (2017). Molecular bases for phyllomorph development in a one-leaf plant, *Monophyllaea glabra*. *Am. J. Bot.* 104, 233–240. doi: 10.3732/ajb.1600303

Jasinski, S., Piazza, P., Craft, J., Hay, A., Woolley, L., Rieu, I., et al. (2005). KNOX action in *Arabidopsis* is mediated by coordinate regulation of cytokinin and gibberellin activities. *Curr. Biol.* 15, 1560–1565. doi: 10.1016/j.cub.2005.07.023

Jong, K. (1970). *Developmental Aspects of Vegetative Morphology in Streptocarpus*. Edinburgh: The University of Edinburgh.

Jong, K., and Burtt, B. L. (1975). The evolution of morphological novelty exemplified in the growth patterns of some Gesneriaceae. *New Phytol.* 75, 297–311. doi: 10.1111/j.1469-8137.1975.tb01400.x

Kinoshita, A., Koga, H., and Tsukaya, H. (2020). Expression profiles of ANGUSTIFOLIA3 and SHOOT MERISTEMLESS, key genes for meristematic activity in a one-leaf plant *Monophyllaea glabra*, revealed by whole-mount in situ hybridization. *Front. Plant Sci.* 11:1160. doi: 10.3389/fpls.2020.01160

Kinoshita, A., and Tsukaya, H. (2018). One-leaf plants in the Gesneriaceae: Natural mutants of the typical shoot system. *Dev. Growth Differ.* 61, 25–33. doi: 10.1111/dgd.12582

Kozuka, T., Suetsugu, N., Wada, M., and Nagatani, A. (2013). Antagonistic regulation of leaf flattening by phytochrome B and phototropin in *Arabidopsis thaliana*. *Plant Cell Physiol.* 54, 69–79. doi: 10.1093/pcp/pcs134

Kurihara, D., Mizuta, Y., Sato, Y., and Higashiyama, T. (2015). ClearSee: A rapid optical clearing reagent for whole-plant fluorescence imaging. *Development* 142, 4168–4179. doi: 10.1242/dev.127613

Long, J. A., and Barton, M. K. (1998). The development of apical embryonic pattern in *Arabidopsis*. *Development* 125, 3027–3035. doi: 10.1242/dev.125.16.3027

Long, J. A., Moan, E. I., Medford, J. I., and Barton, M. K. (1996). A member of the KNOTTED class of homeodomain proteins encoded by the STM gene of *Arabidopsis*. *Nature* 379, 66–69. doi: 10.1038/379066a0

Mantegazza, R., Möller, M., Jill Harrison, C., Fior, S., De Luca, C., and Spada, A. (2007). Anisocotyly and meristem initiation in an unorthodox plant, *Streptocarpus rexii* (Gesneriaceae). *Planta* 225, 653–663. doi: 10.1007/s00425-006-0389-7

Mantegazza, R., Tononi, P., Möller, M., and Spada, A. (2009). WUS and STM homologs are linked to the expression of lateral dominance in the acaulescent *Streptocarpus rexii* (Gesneriaceae). *Planta* 230, 529–542. doi: 10.1007/s00425-009-0965-8

Nishii, K., Kuwabara, A., and Nagata, T. (2004). Characterization of anisocotylous leaf formation in *Streptocarpus wendlandii* (Gesneriaceae): Significance of plant growth regulators. *Ann. Bot.* 94, 457–467. doi: 10.1093/aob/mch160

Nishii, K., Nagata, T., Wang, C. N., and Möller, M. (2012a). Light as environmental regulator for germination and macrocotyledon development in *Streptocarpus rexii* (Gesneriaceae). *S. Afr. J. Bot.* 81, 50–60. doi: 10.1016/j.sajb.2012.05.003

Nishii, K., Wang, C. N., Spada, A., Nagata, T., and Möller, M. (2012b). Gibberellin as a suppressor of lateral dominance and inducer of apical growth in the unifoliate *Streptocarpus wendlandii* (Gesneriaceae). *New Zeal J Bot* 50, 267–287. doi: 10.1080/0028825X.2012.671775

Oehlkers, F. (1923). Entwicklungsgeschichte von *Monophyllaea horsfieldii*. *Beihefte Zum Bot. Cent. Orig. Arb.* 39, 128–151.

Reinhardt, D., Mandel, T., and Kuhlemeier, C. (2000). Auxin regulates the initiation and radial position of plant lateral organs. *Plant Cell* 12, 507–518. doi: 10.1105/tpc.12.4.507

Riou-Khamlichi, C., Huntley, R., Jacqmard, A., and Murray, J. A. H. (1999). Cytokinin activation of *Arabidopsis* cell division through a D-type cyclin. *Science* 283, 1541–1544. doi: 10.1126/science.283.5407.1541

Rosenblum, I. M., and Basile, D. V. (1984). Hormonal regulation of morphogenesis in *Streptocarpus* and its relevance to evolutionary history of the Gesneriaceae. *Am. J Bot.* 71, 52–64. doi: 10.1002/j.1537-2197.1984.tb12484.x

Rupp, H. M., Frank, M., Werner, T., Strnad, M., and Schmülling, T. (1999). Increased steady state mRNA levels of the STM and KNAT1 homeobox genes in cytokinin overproducing *Arabidopsis thaliana* indicate a role for cytokinins in the shoot apical meristem. *Plant J.* 18, 557–563. doi: 10.1046/j.1365-313X.1999.00472.x

Sakamoto, K., and Briggs, W. R. (2002). Cellular and subcellular localization of Phototropin 1. *Plant Cell* 14, 1723–1735. doi: 10.1105/tpc.003293

Sakamoto, T., Sakakibara, H., Kojima, M., Yamamoto, Y., Nagasaki, H., Inukai, Y., et al. (2006). Ectopic expression of KNOTTED1-like homeobox protein induces expression of cytokinin biosynthesis genes in rice. *Plant Physiol.* 142, 54–62. doi: 10.1104/pp.106.085811

Saueregger, J., and Weber, A. (2003). Factors controlling initiation and orientation of the macrocotyledon in anisocotylous Gesneriaceae. *Edinburgh J. Bot.* 60, 467–482. doi: 10.1017/S0960428603000350

Scarpella, E., Marcos, D., Friml, J., and Berleth, T. (2006). Control of leaf vascular patterning by polar auxin transport. *Genes Dev.* 20, 1015–1027. doi: 10.1101/gad.1402406

Smith, R. S., Guyomarc'h, S., Mandel, T., Reinhardt, D., Kuhlemeier, C., and Prusinkiewicz, P. (2006). A plausible model of phyllotaxis. *Proc. Natl. Acad. Sci. U.S.A.* 103, 1301–1306. doi: 10.1073/pnas.0510457103

Stoynova-Bakalova, E., Karanov, E., Petrov, P., and Hall, M. A. (2004). Cell division and cell expansion in cotyledons of *Arabidopsis* seedlings. *New Phytol.* 162, 471–479. doi: 10.1111/j.1469-8137.2004.01031.x

Tanaka, M., Takei, K., Kojima, M., Sakakibara, H., and Mori, H. (2006). Auxin controls local cytokinin biosynthesis in the nodal stem in apical dominance. *Plant J.* 45, 1028–1036. doi: 10.1111/j.1365-313X.2006.02656.x

Tsuda, K., Ito, Y., Sato, Y., and Kurata, N. (2011). Positive autoregulation of a KNOX gene is essential for shoot apical meristem maintenance in rice. *Plant Cell* 23, 4368–4381. doi: 10.1105/tpc.111.090050

Tsukaya, H. (1997). Determination of the unequal fate of cotyledons of a one-leaf plant, *Monophyllaea*. *Development* 124, 1275–1280. doi: 10.1242/dev.124.7.1275

van Berkel, K., de Boer, R. J., Scheres, B., and ten Tusscher, K. (2013). Polar auxin transport: models and mechanisms. *Development* 140, 2253–2268. doi: 10.1242/dev.079111

Watahiki, M. K., and Yamamoto, K. T. (1997). The massugu1 mutation of *Arabidopsis* identified with failure of auxin-induced growth curvature of hypocotyl confers auxin insensitivity to hypocotyl and leaf. *Plant Physiol.* 115, 419–426. doi: 10.1104/pp.115.2.419

Yanai, O., Shani, E., Dolezal, K., Tarkowski, P., Sablowski, R., Sandberg, G., et al. (2005). *Arabidopsis* KNOXI proteins activate cytokinin biosynthesis. *Curr. Biol.* 15, 1566–1571. doi: 10.1016/j.cub.2005.07.060

frontiers | Frontiers in Plant Science

TYPE Original Research
PUBLISHED 03 October 2022
DOI 10.3389/fpls.2022.971235

OPEN ACCESS

EDITED BY
Jana Krajnakova,
New Zealand Forest Research Institute Limited (Scion), New Zealand

REVIEWED BY
Lloyd Alister Donaldson,
New Zealand Forest Research Institute Limited (Scion), New Zealand
Simone Pádua Teixeira,
University of São Paulo, Brazil

*CORRESPONDENCE
Maria Camila Medina
camiliny@usp.br
Diego Demarco
diegodemarco@usp.br

SPECIALTY SECTION
This article was submitted to Plant Development and EvoDevo, a section of the journal Frontiers in Plant Science

RECEIVED 16 June 2022
ACCEPTED 25 August 2022
PUBLISHED 03 October 2022

CITATION
Medina MC, Sousa-Baena MS, Van Sluys M-A and Demarco D (2022) Laticifer growth pattern is guided by cytoskeleton organization.
Front. Plant Sci. 13:971235.
doi: 10.3389/fpls.2022.971235

Laticifer growth pattern is guided by cytoskeleton organization

Maria Camila Medina*, Mariane S. Sousa-Baena, Marie-Anne Van Sluys and Diego Demarco*

Departamento de Botânica, Instituto de Biociências, Universidade de São Paulo, São Paulo, SP, Brazil

Laticifers are secretory structures that produce latex, forming a specialized defense system against herbivory. Studies using anatomical approaches to investigate laticifer growth patterns have described their origin; however, their mode of growth, i.e., whether growth is intrusive or diffuse, remains unclear. Studies investigating how cytoskeleton filaments may influence laticifer shape establishment and growth patterns are lacking. In this study, we combined microtubule immunostaining and developmental anatomy to investigate the growth patterns in different types of laticifers. Standard anatomical methods were used to study laticifer development. Microtubules were labelled through immunolocalization of α-tubulin in three types of laticifers from three different plant species: nonanastomosing (*Urvillea ulmacea*), anastomosing unbranched with partial degradation of terminal cell walls (*Ipomoea nil*), and anastomosing branched laticifers with early and complete degradation of terminal cell walls (*Asclepias curassavica*). In both nonanastomosing and anastomosing laticifers, as well as in differentiating meristematic cells, parenchyma cells and idioblasts, microtubules were perpendicularly aligned to the cell growth axis. The analyses of laticifer microtubule orientation revealed an arrangement that corresponds to those cells that grow diffusely within the plant body. Nonanastomosing and anastomosing laticifers, branched or not, have a pattern which indicates diffuse growth. This innovative study on secretory structures represents a major advance in the knowledge of laticifers and their growth mode.

KEYWORDS

laticifers, cytoskeleton, microtubules, development, apical growth

Introduction

Laticifers are formed by specialized cells which contain latex and form a defense system, sealing wounds, blocking microorganisms, and avoiding herbivory (Fahn, 1988; Agrawal and Fishbein, 2006; Demarco et al., 2013; Ramos et al., 2019, 2020). Laticifers can be a single cell (nonarticulated) or a row of cells (articulated). In the latter, the terminal walls of each cell in the row may remain intact (nonanastomosing) or can be partially or completely (anastomosing) dissolved (Fahn, 1979). In some cases, anastomosing laticifers can also branch through lateral anastomosis between two laticifer rows, forming an interconnected system of tubes throughout the entire plant (Demarco et al., 2006; Ramos et al., 2019; Johnson et al., 2021). Although these general aspects of laticifer development

are well-known, how the laticifers grow is a question that is still postulated (Gama et al., 2017; Johnson et al., 2021).

Two concurrent hypotheses based on observations from anatomical and developmental studies have been debated to explain their mode of growth in the plant body: (1) Laticifers grow through apical intrusive growth in meristematic regions, dissolving the middle lamella through enzymatic activity and growing intrusively between cells (Mahlberg, 1993; Canaveze and Machado, 2016; Castelblanque et al., 2016; Canaveze et al., 2019). In this case laticifers might combine two types of cell expansion, diffuse growth followed by polarized growth, as described for some fibers (Snegireva et al., 2010; Gorshkova et al., 2012; Majda et al., 2021); (2) Laticifers may grow through the addition of new cells in the laticifer system followed by cell expansion, thus not through apical growth. Evidence supporting this view is the fact that laticifer apices (the region of the laticifer system where new cells that have just differentiated are added to the system) are found close to the shoot apical meristem but never penetrate this tissue (Milanez, 1960, 1977, 1978; Demarco and Castro, 2008; Demarco et al., 2013; Gama et al., 2017; Ramos et al., 2019; Naidoo et al., 2020).

Plant cells can grow diffusely or apically. The first process is typically anisotropic and occurs in almost all cells (Hamada, 2014). The second one is considered an extreme form of cell growth that is concentrated at the apex of the cell, which gives it the ability to grow extensively in a polarized way (Anderhag et al., 2000; Wasteneys and Galway, 2003). Apical growth has been associated with the search for nutrients, as observed in root hairs (Hepler et al., 2001; Sieberer et al., 2005) and also in pollen tubes searching for the ovule (Cai et al., 2017). Both root hairs and pollen tubes are models of apical growth for which important processes involving the cytoskeleton are well-characterized (Gu and Nielsen, 2013). Additionally, some plant cells display an apical intrusive growth where the plant cell grows differentially at its tip. Intrusive growth implies that a part of the cell maintains cell-to-cell contact with their neighboring cells, and another part of the cell (the tip) invades new locations (Lev-Yadun, 2001), provoking changes not only in cytoskeleton patterns but also in the middle lamella of the surrounding cells, as well as disrupting their plasmodesmata connections (Lev-Yadun, 2001; Majda et al., 2021; Box 1). The apical intrusive growth has also been used to explain the way laticifers might grow within the plant, i.e., combining an initial phase of diffuse growth and then a phase of apical growth during their development, as is observed in vascular fibers (Ageeva et al., 2005; Snegireva et al., 2010; Gorshkova et al., 2018; Gorshkov et al., 2019; Majda et al., 2021; Sousa-Baena and Onyenedum, 2022).

The main characteristic of apical growth is the expansion of a single region of the wall independently of the rest of cell. This extremely polarized type of growth is mediated and directed by the cytoskeleton (Wasteneys and Galway, 2003; Smith and Oppenheimer, 2005; Li et al., 2017). Cells with apical growth usually have microtubules in longitudinal or slightly helical organization in the cortical and endoplasmic cell regions. Apparently, this organization facilitates the transport of secretory vesicles containing mainly pectin, which is deposited in the apical cell wall region (Anderhag et al., 2000). This local increment of wall constituents enlarges the cell, which maintains its cylindrical shape (Hepler et al., 2001), an essential feature for the preservation of apical growth both in roots and in pollen tubes (Gu and Nielsen, 2013).

BOX 1. Defining terms of plant cell growth modes.

Polarized growth: It is a mode of growth in which cells expand in a unidirectional way due to an asymmetrical distribution of molecules and structures at the subcellular level. Different types and levels of polarity exist even in the same plant cell. Polarized growth occurs in plant cells with diffuse growth (anisotropic) and with tip growth.

Diffuse growth: This is the most common mode of growth in plant cells in which wall extension and incorporation of new wall material occurs uniformly across the cell surface. It can be isotropic (considered transitory in plant cell growth) or anisotropic.

Apical or tip growth: This is an extremely polarized mode of cell growth where wall synthesis occurs at a single site on the cell surface (e.g., pollen tubes or root hairs).

Intrusive growth: The plant cell has an apical growth that can be unidirectional or bidirectional, and the region that is differentially growing loses the cell-to-cell contact and invades intercellular spaces, damaging the middle lamella (e.g., some xylem fibers, phloem fibers, and gelatinous fibers).

Laticifer development has been widely studied using anatomical approaches. However, laticifers may grow in a diverse mode, with ramifications and turns inside the plant body, which is difficult to follow and interpret using exclusively structural ontogenetic methodologies. The observation of an acute apex in some laticifers has frequently been interpreted as evidence that they have apical growth; however, the acute shape of the cell tip in the apical region of the laticifer may, in fact, be the result of an oblique section of the sinuous apical portion of the laticifers (Gama et al., 2017). Therefore, new approaches are required to assess this question.

It is well known that cytoskeleton plays a crucial role in plant cell developmental processes and in the establishment of polarized growth (Kost et al., 1999), but no cytoskeleton analyses have been made in laticifers so far. Thus, we performed a comparative study of the role of microtubules in the growth mode of different types of laticifers in three species: (1) *Asclepias curassavica* L. (Apocynaceae), whose laticifers are anastomosing branched with early and complete degradation of terminal walls (Demarco and Castro, 2008), (2) *Ipomoea nil* (L.) Roth (Convolvulaceae), which has anastomosing unbranched laticifers with a partial degradation of terminal walls (pers. obs.) and (3) *Urvillea ulmacea* Kunth (Sapindaceae) with nonanastomosing laticifers (Medina et al., 2021).

Materials and methods

Sampling and cultivation

Shoots of *Asclepias curassavica* L. (Apocynaceae) and *Urvillea ulmacea* Kunth (Sapindaceae) were collected on the campus of the Universidade de São Paulo (USP) in São Paulo/SP (Brazil); vouchers for these specimens were deposited in the Herbarium SPF (SPF 150070 and SPF 227683, respectively). Shoots from *Ipomoea nil* (L.) Roth (Convolvulaceae) were collected from plants cultivated in the greenhouse from seeds acquired from Cosmos Agrícola Produção e Serviços Rurais Ltda. (Engenheiro Coelho/SP, Brazil).

Developmental analysis

Shoot apices of *Asclepias*, *Ipomoea* and *Urvillea* were isolated and fixed in formalin-acetic acid-50% alcohol (FAA) for 24 h (Johansen, 1940) and stored in 70% ethanol. Then, the material was dehydrated in an ascending butyl series (Johansen, 1940) and embedded in Paraplast (Leica Microsystems, Heidelberg, Germany). All samples were longitudinally sectioned using a Microm HM340E rotary microtome (Microm, Walldorf, Germany) and then stained with 1% astra blue and 1% safranin (Gerlach, 1984). Slides were mounted in Permount resin (Fisher Scientific, Pittsburgh, PA, United States) and photographed using a Leica DMLB light microscope.

Microtubules immunolocalization

A modified protocol based on Wasteneys et al. (1997) and Celler et al. (2016) was used for microtubule labelling. Peelings of the shoot apices of the three species, containing epidermis plus some stem cortical layers, were gently collected with forceps and then fixed in PMET buffer (100 mM PIPES, 5 mM EGTA, 1 mM magnesium sulfate, pH 6.9) containing 0.5% glutaraldehyde, 1.5% formaldehyde fixative solution for 40 min. Then, the peels were washed in PMET buffer (100 mM PIPES, 5 mM EGTA, 1 mM magnesium sulfate, 0.05% triton X-100, pH 6.9). A freeze-shattering procedure was performed following Wasteneys et al. (1997). An enzymatic cell wall digestion step was subsequently done using a 0.1% pectinase solution (0.1% pectinase from *Aspergillus aculeatus* Sigma-Aldrich, 0.4 M mannitol, 1% BSA and 1xPBS) for 20 min at room temperature. After rinsing off the pectinase solution with PMET buffer, samples were incubated for 3 h in the permeabilization buffer (PBS, 1% Triton X-100 in 1x PBS, pH 7.5) at room temperature. After washing in PBS, samples were incubated in a sodium borohydride solution (1 mg/mL sodium borohydride in 1x PBS) and then transferred to blocking buffer (1% BSA, 50 mM glycine in 1 x PBS).

All samples were incubated in a 1.5 mL Eppendorf tube with a solution 1:1000 of the monoclonal mouse anti-α-tubulin antibody, clone B 512 (Sigma-Aldrich catalogue number T6199) in blocking buffer at 4°C overnight. Five washes of 10 min each in the incubation buffer (50 mM glycine in 1x PBS) were carried out, and then the samples were transferred to the blocking buffer for 30 min. After that, the samples were incubated in a 1.5 mL Eppendorf tube with the secondary antibody in a 1:100 solution of Alexa 488-conjugated goat anti-mouse IgG antibody (Invitrogen catalogue number A28175) in blocking buffer for 3 h at 37°C. Samples were washed in PBS and mounted in antifade mounting medium (glycerin in PBS). The slides were analyzed using a Zeiss LSM880 confocal laser microscope at 488 nm wavelength. To observe the organization of microtubules in meristematic regions during development, z-stack images were created.

Results

Laticifer characterization and development

Branched laticifers

In the shoot system of *Asclepias curassavica*, whose laticifers are anastomosing branched with early and complete degradation of terminal walls, laticifers are found in the stem cortex, vascular system and pith and in the mesophyll and vascular system of leaves (Figure 1A). They are originated from the ground meristem and procambium, and their apices are located near the shoot apical meristem (SAM) and within leaf primordia (Figures 1B,C). Each laticifer is formed by a row of cells and develop in meristematic regions, where intercellular spaces are absent. The apical cells of the laticifer differentiate rapidly, and their walls are thicker than the adjacent cells (Figures 1D,E). The dissolution of the terminal walls (transverse walls located between two laticifer cells) within the laticifer occurs early in development, and only a few cells with entire terminal walls are observed in apical portions of the shoot. Even in portions very close to the SAM, the terminal walls of some laticifers were already dissolved, with the laticifer forming a continuous tube-like structure (Figures 1B–E). In the same way, the production of latex, as well as laticifer branching, begins early, still in the meristematic region of the stem (Figure 1E).

Unbranched laticifers

Similar to laticifers of *Asclepias*, laticifers of *Ipomoea*, which are anastomosing unbranched with a partial degradation of terminal walls, and *Urvillea*, which are nonanastomosing, are formed and grow in the shoot apices, but in such species, they are originated only from the ground meristem in the cortex and pith (Figures 1F,G). They are formed by a row of cells, more or less straight, and can be distinguished from neighboring cells by latex content which is precociously produced (Figure 1H). Laticifers of *Ipomoea* are anastomosed with partial, late disintegration of the terminal walls, whose debris can be observed in mature portions of the laticifer (Figure 1I). Conversely, laticifers of *Urvillea* are

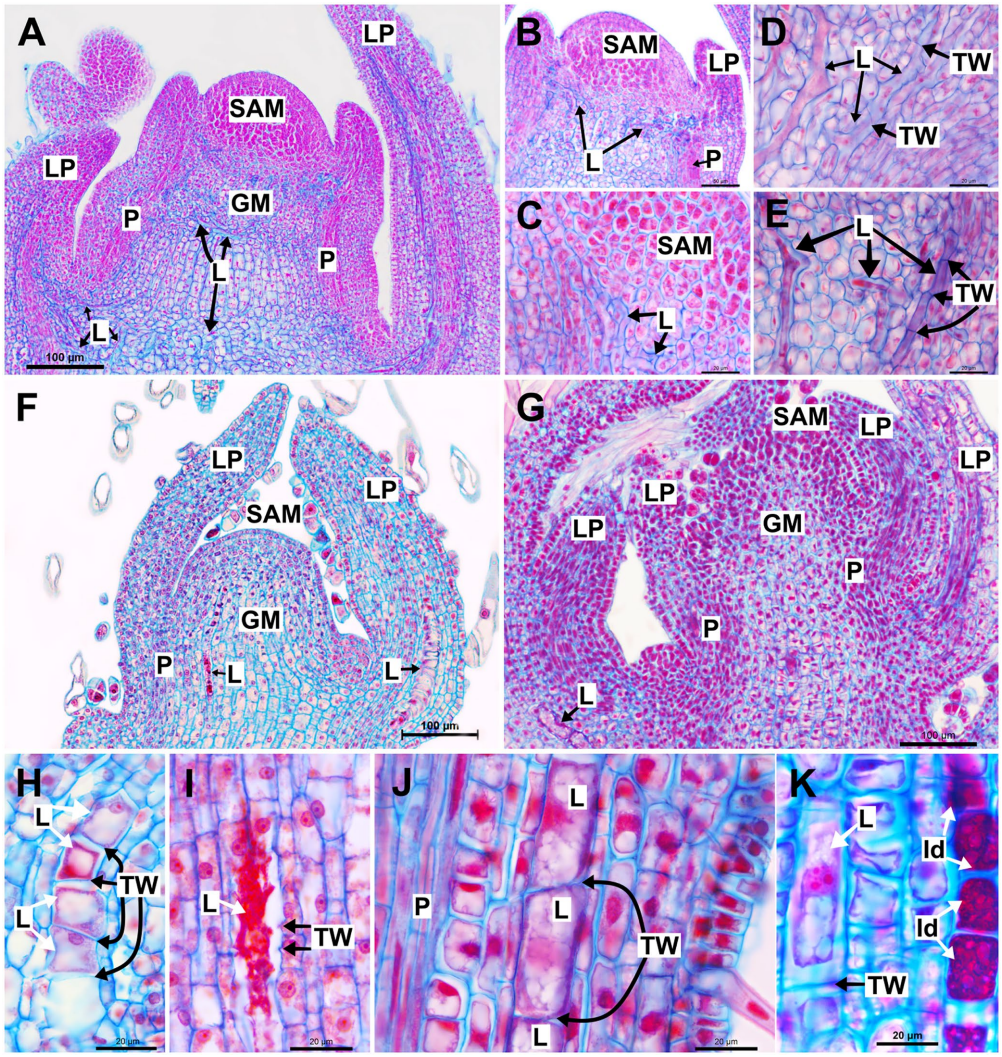

FIGURE 1
Structure and development of laticifers in *Asclepias curassavica*, *Ipomoea nil* and *Urvillea ulmacea*. **(A–E)** Anastomosing branched laticifers of *A. curassavica*. **(F,H,I)** Anastomosing unbranched laticifers of *I. nil*. **(G,J,K)** Nonanastomosing unbranched laticifers of *U. ulmacea*. (GM, ground meristem; Id: idioblast; L, laticifer; LP, leaf primordia; N, nucleus; P, procambium; SAM, shoot apical meristem; TW, terminal wall).

nonanastomosing, maintaining the terminal walls intact throughout development (Figure 1J). It is noteworthy that the laticifers of Ipomoea and *Urvillea* are much larger in expanding leaf primordia when compared to those of *Asclepias* (Figures 1F,G). Unlike *Asclepias* and *Ipomoea*, *Urvillea* also have idioblasts in the shoot system, a secretory structure constituted by a single cell that produces mainly phenolic compounds (Figure 1K).

Laticifer microtubules organization

In all species, developing and mature laticifers have cortical microtubules arranged perpendicular to the cell growth axis (Figures 2–5). A dense network of endoplasmic microtubules was also observed in developing laticifers of *Asclepias* (Figures 2A,C) idioblasts of *Urvillea* (Figures 3D,E) and meristematic cells (Figure 4F). Perpendicularly-oriented cortical microtubules were also observed in idioblasts cells (Figure 3D), parenchyma (Figures 4A–C) and ground meristem (Figures 4D,F).

Nuclei were evident in developing laticifers of all species (Figures 2G, 3A,B,D). Nuclei are parietally located due to the displacement caused by the expanding vacuole as observed in laticifers of *Ipomoea* (Figure 3A) and centrally located as in laticifers and idioblasts in *U. ulmacea* and parenchyma (Figures 3D,E). In laticifers, the displacement of nuclei to a parietal position is due to the production and accumulation of latex constituents within the vacuole, which compresses the nucleus against the wall. Microtubules were also observed as mitotic spindles and phragmoplasts in many meristematic cells in all species (Figures 4D–F).

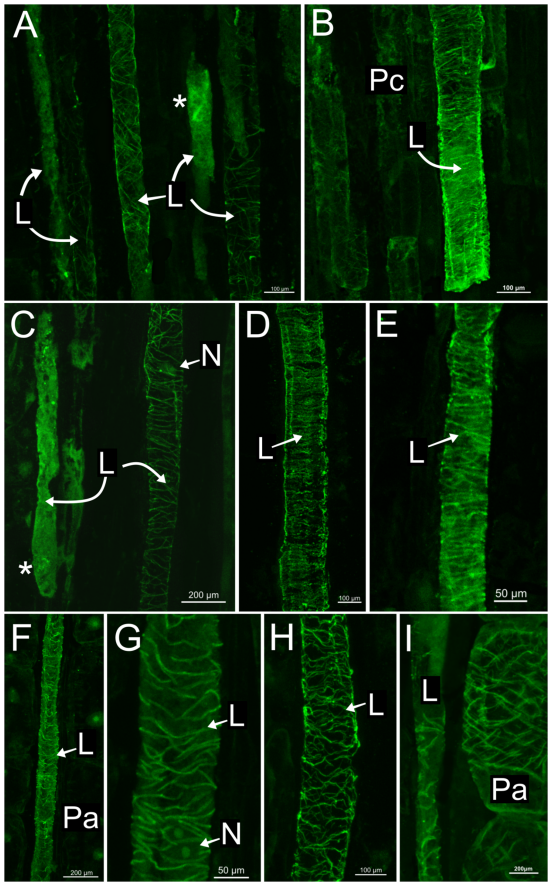

FIGURE 2
Immunolocalization of microtubules in articulated anastomosing laticifers of the shoot apex of *Asclepias* curassavica. **(A)** Procambial laticifers with cortical microtubules in transversal orientation to the cell axis. **(B,C,H,I)** Procambial laticifers showing a well-preserved transverse cortical microtubule orientation. Note the nucleus and a laticifer full of latex without microtubule detection in C. **(D,E)** Laticifers in the pith of stem exhibiting similar transverse microtubule arrangement. **(F,G)** Laticifer in cortex region of stem with some cortical microtubules. Note the nucleus in G. **(I)** Parenchyma cell with a transverse microtubule arrangement similar to the adjacent laticifer (asterisk, endoplasmic microtubules; L, laticifer; N, nucleus; Pa, parenchyma cell; Pc, procambium).

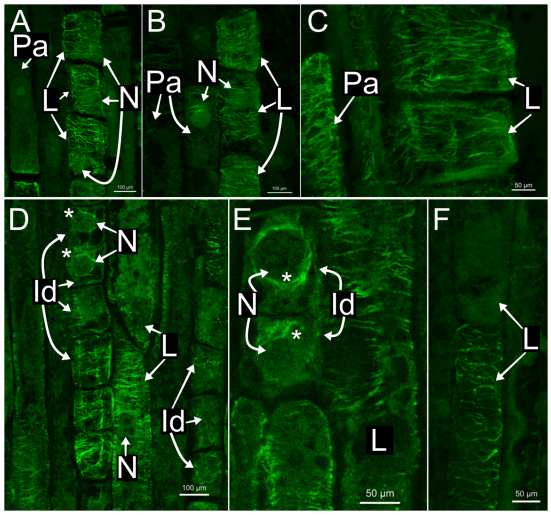

FIGURE 3
Immunolocalization of microtubules in articulated anastomosing laticifers of the shoot apices of *Ipomoea nil* **(A–C)** and *Urvillea ulmacea* **(D–F)**. Laticifers with transverse microtubule orientation in both species. **(A,B)** Laticifer nuclei are displaced to a parietal position due to the enlargement of the vacuole. **(C–E)** Both parenchyma cells and idioblasts with transverse microtubule arrangement similar to the adjacent laticifers. **(D,E)** Endoplasmic microtubules (asterisk) surrounding the nuclei of idioblasts (Id, idioblast; L, laticifer; N, nucleus; Pa, parenchyma cell).

See Figure 5 for a summary of the type of development of unbranched and branched laticifers and their pattern of microtubule arrangement.

Discussion

In this study we show that cortical microtubules have the same arrangement, i.e., being organized perpendicular to the cell growth axis, in the three types of laticifers present in the different species analyzed in this study, as well as in the meristematic cells of ground meristem, in subepidermal parenchyma cells and phenolic idioblasts. Although both diffuse and polarized growth have been associated with laticifers, we found that cortical microtubules in nonanastomosing and anastomosing laticifers exhibited a transverse arrangement, commonly associated with diffuse growth, as opposed to a longitudinal organization, historically associated with apical and intrusive growth in other cell types, which strongly suggest that laticifers grow mainly through diffuse growth.

Laticifers maintain adhesion to neighboring cell walls throughout development

Our analyses show that laticifers grow synchronously with other meristematic cells in the meristematic regions, as the middle lamella keeps the cells united across the whole process. Hence, the surface contact area increases at a similar rate, even when some cells assume different positions and shapes. This type of growth was described as symplastic growth by Fahn (1990). In particular, we observed that nonanastomosing laticifers can be longer and wider than the neighboring cells, which is probably related with differences in turgor pressure in the laticifer cells, which have a unique and distinct metabolism, and with their cell wall composition, as laticifer walls can be more acidic and thicker than neighboring cells in meristematic regions and also exhibit singular mechanical properties (Demarco et al., 2006; Palin and Geitmann, 2012; Demarco, 2015; Medina et al., 2021).

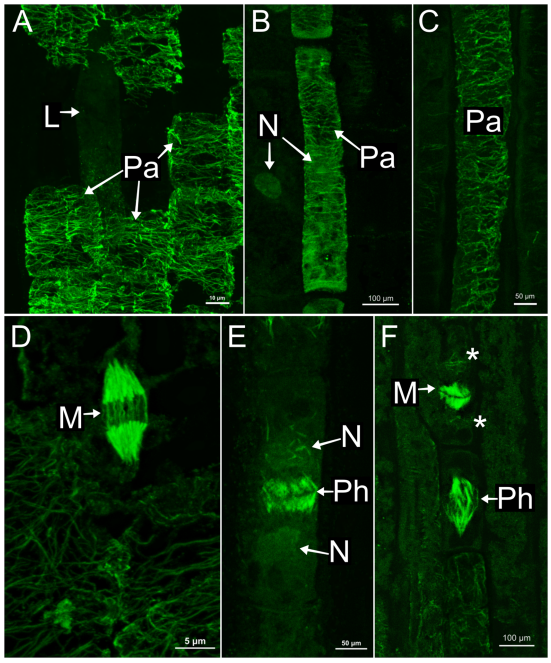

FIGURE 4
Immunolocalization of microtubules in parenchyma cells of the shoot apices. **(A,D)** *Asclepias* curassavica. **(B,E)** *Ipomoea nil*. **(C,F)** *Urvillea ulmacea*. **(A–C)** Cortical microtubules arranged perpendicularly to the cell axis. **(D–F)** Mitotic activity in meristematic regions. **(D,F)** Microtubules of the mitotic spindles. **(E)** Microtubules of the phragmoplast. (L, laticifer; M, mitosis; N, nucleus; Pa, parenchyma cell; Ph, phragmoplast).

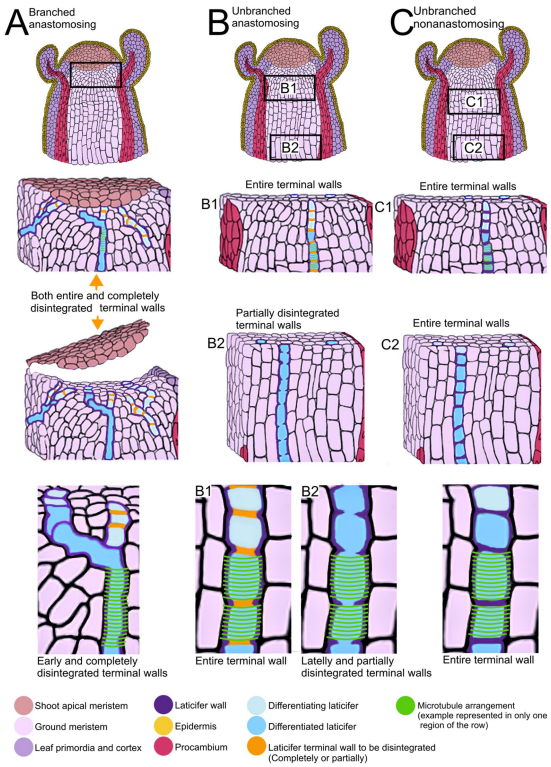

FIGURE 5
Summary of developmental processes of articulated laticifers and their microtubule patterns. **(A)** Articulated anastomosing branched laticifers. These laticifers differentiate early in development, branching and dissolving their terminal walls near the shoot apical meristem. **(B)** Articulated anastomosing unbranched laticifers. This type of laticifer forms more or less straight rows of cells, whose terminal walls may remain entire in meristematic regions (B1) but partially disintegrate lately, forming a continuous tube (B2). **(C)** Articulated nonanastomosing unbranched laticifers. This type of laticifer is differentiated in regions a little further from the shoot apical meristem (C1) and forms more or less straight rows of cells, whose terminal walls remain entire (C2).

The apical intrusive growth of internal cells might require neighboring cells forming intercellular spaces by detachment of middle lamella in order to intrusively grow between the spaces formed. In that case, the region of the cell which is intrusively growing detaches from the neighboring walls. That process was observed, for instance, during xylary fiber tip growth (Majda et al., 2021). In phloem bast fibers, a higher rate of elongation in comparison with the neighboring cells has been also observed. In early stages of development, bast fibers have a symplastic growth from the region right below the SAM to a portion of the stem called "snap point" in flax (also observed in hemp and ramie; Sousa-Baena and Onyenedum, 2022); they start to grow in a polarized manner, displaying an intrusive growth with synchronous nuclear divisions. In addition, the transcriptome profile of isolated phloem bast fibers during their intrusive stage corroborate their intrusive nature as many genes, transcripts and miRNAs linked to cell wall modification are differentially expressed (Gorshkova et al., 2018; Gorshkov et al., 2019). Modification of walls to form intercellular spaces is also observed in the development of leaf mesophyll cells that present a multipolar type of growth (Panteris and Galatis, 2005). These cells present a variety of shapes during their development, which is driven by microtubules and actin filaments. They go from being densely packed polyhedral cells without intercellular spaces, to large, branched and separated from each other by intercellular spaces with indentations and lobed regions (Panteris et al., 1993). The lobes are the regions with tip growth where microtubules are organized perpendicularly to the cell axis in the base of the lobes but are absent in the tip where additional actin filaments are abundant, similar to pollen tubes (Zhang et al., 2021).

In laticifer development, cell division in ground meristem originates a daughter cell through the formation of the cell plate and not by nuclear divisions. Then, the daughter cell differentiates into a laticiferous cell whose terminal walls may be observed in the laticifer apex (Milanez, 1960, 1977; Gama et al., 2017). We observed that in the apical region, intercellular spaces are absent between laticifer and neighboring cells, corroborating observations from other studies (Milanez, 1959; Demarco et al., 2006; Demarco and Castro, 2008; Medina et al., 2021). In particular, in the case of branched laticifers of *Asclepias*, where the laticifer cells can be a sinuous cylinder, they maintain the

cell-to-cell wall adhesion with neighboring cells, contrary to the pattern observed in mesophyll cells, and the transverse arrangement of microtubules is uniform throughout the entire row of cells, not displaying differential growth or any different patterns that could promote polarized growth, as observed in unbranched laticifers. Sousa-Baena et al. (2021) observed cortical microtubules transversally arranged in hypocotyl epidermal cells in *Ipomoea nil*, a very similar pattern observed in cortical microtubules of both branched and unbranched laticifers in this study.

Laticifers grow diffusely and display transversally oriented microtubules

Although laticifers are not essential for basic plant development (Castelblanque et al., 2016; Benninghaus et al., 2020), they are important in providing defense through the production of latex, which is, in fact, energetically expensive to produce in both primary and secondary metabolism (Agrawal and Konno, 2009). It is important to consider that during laticifer development and elongation, the latex production occurs simultaneously. Depending on the species, terminal walls are also being dissolved at the same time. It can represent a very high cost to the plant if, at the same time, modifications to the organization of cortical microtubules are required for polarized growth, as occur in pollen tubes. Li et al. (2017) describe this as an extreme polarized mode of plant cell growth that requires a high activity in the tip to penetrate the style and reach the ovule through intrusive growth. In pollen tubes, microtubules are organized in longitudinal bundles along the tube elongation axis and are absent in its apical and subapical regions (Cai et al., 2017). Conversely, we show that the cortical microtubules of laticifers are transversally arranged, following a pattern that is considered the default organization which allows the cell to organize the cytoskeleton during organ elongation (Wasteneys, 2004).

Laticifer terminal wall degradation and the branching could also be mediated by microtubules. In pit formation on vessel elements of *Aesculus hippocastanum*, cortical microtubules form rings around the perforation but not in the pit; instead, they are randomly arranged between the adjacent pits (Chaffey et al., 1997). A similar process was observed in pit formations of fibers in the hybrid *Populus tremula*×*P. tremuloides* (Chaffey et al., 2002). In protoxylem (Schneider et al., 2021) and metaxylem (Schneider et al., 2017) formation in *Arabidopsis*, microtubules form the template for cell wall deposition, and in areas where the cortical microtubules density is reduced, the cell wall is thinner. Canaveze et al. (2019) observed that meristematic cells in contact with laticifers, which subsequently may be incorporated into the laticifer system, presented microtubules perpendicularly oriented with respect to axis growth. However, more studies are necessary to better understand the role of microtubules in branched laticifers.

Our study showed that laticifers have a coordinated growth with the neighboring cells, in which the cortical microtubules are arranged in a perpendicular orientation to the cell axis. The same microtubule arrangement was observed in ground meristem, parenchyma and secretory idioblasts, indicating that all these cells have diffuse growth. No sign of polarized growth was observed in laticifers. This is the first study of microtubules in laticifers and living image technologies; transcriptomic studies of laticifers could be also a good strategy to investigate the developmental process and mode of growth of these complex secretory cells.

Data availability statement

The original contributions presented in the study are included in the article/supplementary material, further inquiries can be directed to the corresponding authors.

Author contributions

MM: conceptualization, data curation, formal analysis, investigation, methodology, and writing—original draft, and writing—review and editing. MS-B: data curation, formal analysis, methodology, and writing—review and editing. M-AS: data curation and writing—review and editing. DD: conceptualization, data curation, formal analysis, methodology, funding acquisition, project administration, supervision, writing—original draft, and writing—review and editing. All authors contributed to the article and approved the submitted version.

Funding

This work was funded by CAPES—Coordenação de Aperfeiçoamento de Pessoal de Nível Superior (Grant number 001), Conselho Nacional de Desenvolvimento Científico e Tecnológico (CNPq proc. #304297/2021–6), and FAPESP—Fundação de Amparo à Pesquisa do Estado de São Paulo (proc. #2017/23882–0 and #2022/11286-1).

Acknowledgments

The authors thank CAPES, CNPq and FAPESP for financial support and Centro de Aquisição de Imagens e Microscopia do Instituto de Biociências—CAIMi/IB for their assistance with confocal microscopy.

Conflict of interest

The authors declare that the research was conducted in the absence of any commercial or financial relationships that could be construed as a potential conflict of interest.

The reviewer ST declared a shared affiliation with the authors to the handling editor at the time of review.

Publisher's note

References

Ageeva, M. V., Petrovská, B., Kieft, H., Sal'nikov, V. V., Snegireva, A. V., van Dam, J. E. G. G., et al. (2005). Intrusive growth of flax phloem fibers is of intercalary type. *Planta* 222, 565–574. doi: 10.1007/s00425-005-1536-2

Agrawal, A. A., and Fishbein, M. (2006). Plant defense syndromes. *Ecology* 87, S132–S149. doi: 10.1890/0012-9658(2006)87[132:PDS]2.0.CO;2

Agrawal, A. A., and Konno, K. (2009). Latex: a model for understanding mechanisms, ecology, and evolution of plant defense against herbivory. *Annu. Rev. Ecol. Evol. Syst.* 40, 311–331. doi: 10.1146/annurev.ecolsys.110308.120307

Anderhag, P., Hepler, P. K., and Lazzaro, M. D. (2000). Microtubules and microfilaments are both responsible for pollen tube elongation in the conifer Picea abies (Norway spruce). *Protoplasma* 214, 141–157. doi: 10.1007/BF01279059

Benninghaus, V. A., Van Deenen, N., Müller, B., Roelfs, K. U., Lassowskat, I., Finkemeier, I., et al. (2020). Comparative proteome and metabolome analyses of latex-exuding and non-exuding *Taraxacum koksaghyz* roots provide insights into laticifer biology. *J. Exp. Bot.* 71, 1278–1293. doi: 10.1093/jxb/erz512

Cai, G., Parrotta, L., Cresti, M., Parrota, L., Cresti, M., Parrotta, L., et al. (2017). "The cytoskeleton of pollen tubes and how it determines the physico-mechanical properties of cell wall," in *Pollen Tip Growth: From Biophysical Aspects to Systems Biology*. eds. G. Obermeyer and J. Feijó (Cham: Springer International Publishing), 1–424.

Canaveze, Y., and Machado, S. R. (2016). The occurrence of intrusive growth associated with articulated laticifers in *Tabernaemontana catharinensis* A.DC., a new record for Apocynaceae. *Int. J. Plant Sci.* 177, 458–467. doi: 10.1086/685446

Canaveze, Y., Mastroberti, A. A., de Araujo Mariath, J. E., and Machado, S. R. (2019). Cytological differentiation and cell wall involvement in the growth mechanisms of articulated laticifers in *Tabernaemontana catharinensis* A.DC. (Apocynaceae). *Protoplasma* 256, 131–146. doi: 10.1007/s00709-018-1284-3

Castelblanque, L., Balaguer, B., Martí, C., Rodríguez, J. J., Orozco, M., and Vera, P. (2016). Novel insights into the organization of laticifer cells: a cell comprising a unified whole system. *Plant Physiol.* 172, 1032–1044. doi: 10.1104/pp.16.00954

Celler, K., Fujita, M., Kawamura, E., Ambrose, C., Herburger, K., Holzinger, A., et al. (2016). "Microtubules in plant cells: strategies and methods for immunofluorescence, transmission electron microscopy, and live cell imaging", in *Cytoskeleton Methods and Protocols. Methods in Molecular Biology*. ed. R. Gavin (New York: Humana Press). 155–184.

Chaffey, N., Barlow, P., and Sundberg, B. (2002). Understanding the role of the cytoskeleton in wood formation in angiosperm trees: hybrid aspen (*Populus tremula* × *P. tremuloides*) as the model species. *Tree Physiol.* 22, 239–249. doi: 10.1093/treephys/22.4.239

Chaffey, N. J., Barnett, J. R., and Barlow, P. W. (1997). Cortical microtubule involvement in bordered pit formation in secondary xylem vessel elements of *Aesculus hippocastanum* L. (Hippocastanaceae): a correlative study using electron microscopy and indirect immunofluorescence microscopy. *Protoplasma* 197, 64–75. doi: 10.1007/BF01279885

Demarco, D. (2015). Micromorphology and histochemistry of the laticifers from vegetative organs of Asclepiadoideae species (Apocynaceae). *Acta biol. Colomb.* 20, 57–65. doi: 10.15446/abc.v20n1.42375

Demarco, D., and Castro, M. D. M. (2008). Laticíferos articulados anastomosados em espécies de Asclepiadeae (Asclepiadoideae, Apocynaceae) e suas implicações ecológicas. *Rev. Bras. Botânica* 31, 701–713. doi: 10.1590/S0100-84042008000400015

Demarco, D., Castro, M. D. M., and Ascensao, L. (2013). *Two laticifer systems in Sapium haematospermum*—new records for Euphorbiaceae. *Botany* 91, 545–554. doi: 10.1139/cjb-2012-0277

Demarco, D., Kinoshita, L. S., and Castro, M. D. M. (2006). Laticíferos articulados anastomosados: novos registros para Apocynaceae. *Rev. Bras. Botânica* 29, 133–144. doi: 10.1590/S0100-84042006000100012

Fahn, A. (1979). *Secretory Tissues in Plants*. London, New York, NY, San Francisco, CA: Academic Press INC.

Fahn, A. (1988). Secretory tissues in vascular plants. *New Phytol.* 108, 229–257. doi: 10.1111/j.1469-8137.1988.tb04159.x

Fahn, A. (1990). *Plant Anatomy. 4th Edn.* Oxford: Pergamon Press.

Gama, T. d. S. S., Rubiano, V. S., and Demarco, D. (2017). Laticifer development and its growth mode in *Allamanda blanchetii* A. DC. (Apocynaceae). *J. Torrey Bot. Soc.* 144, 303–312. doi: 10.3159/TORREY-D-16-00050

Gerlach, D. (1984). *Botanische Mikrotechnik: Eine Einführung. 3rd Edn.* Stuttgart: Georg Thieme.

Gorshkov, O., Chernova, T., Mokshina, N., Gogoleva, N., Suslov, D., Tkachenko, A., et al. (2019). Intrusive growth of phloem fibers in flax stem: integrated analysis of miRNA and mRNA expression profiles. *Plan. Theory* 8, 1–23. doi: 10.3390/plants8020047

Gorshkova, T., Brutch, N., Chabbert, B., Deyholos, M., Hayashi, T., Lev-Yadun, S., et al. (2012). Plant fiber formation: state of the art, recent and expected progress, and open questions. *CRC. Crit. Rev. Plant Sci.* 31, 201–228. doi: 10.1080/07352689.2011.616096

Gorshkova, T., Chernova, T., Mokshina, N., Gorshkov, V., Kozlova, L., and Gorshkov, O. (2018). Transcriptome analysis of intrusively growing flax fibers isolated by laser microdissection. *Sci. Rep.* 8, 1–17. doi: 10.1038/s41598-018-32869-2

Gu, F., and Nielsen, E. (2013). Targeting and regulation of cell wall synthesis during tip growth in plants. *J. Integr. Plant Biol.* 55, 835–846. doi: 10.1111/jipb.12077

Hamada, T. (2014). "Microtubule organization and microtubule-associated proteins in plant cells," in *International Review of Cell and Molecular Biology*. ed. W. J. Kwang (San Diego, CA: Elsevier Inc.), 1–52.

Hepler, P. K., Vidali, L., and Cheung, A. Y. (2001). Polarized cell growth in higher plants. *Annu. Rev. Cell Dev. Biol.* 17, 159–187. doi: 10.1146/annurev.cellbio.17.1.159

Johansen, D. A. (1940). *Plant Microtechnique*. New York: McGraw-Hill.

Johnson, A. R., Moghe, G. D., and Frank, M. H. (2021). Growing a glue factory: open questions in laticifer development. *Curr. Opin. Plant Biol.* 64:102096. doi: 10.1016/j.pbi.2021.102096

Kost, B., Mathur, J., and Chua, N. H. (1999). Cytoskeleton in plant development. *Curr. Opin. Plant Biol.* 2, 462–470. doi: 10.1016/S1369-5266(99)00024-2

Lev-Yadun, S. (2001). Intrusive growth - the plant analog of dendrite and axon growth in animals. *New Phytol.* 150, 508–512. doi: 10.1046/j.1469-8137.2001.00143.x

Li, S., Dong, H., Pei, W., Liu, C., Zhang, S., Sun, T., et al. (2017). LlFH1-mediated interaction between actin fringe and exocytic vesicles is involved in pollen tube tip growth. *New Phytol.* 214, 745–761. doi: 10.1111/nph.14395

Mahlberg, P. G. (1993). Laticifers: an historical perspective. *Bot. Rev.* 59, 1–23. doi: 10.1007/BF02856611

Majda, M., Kozlova, L., Banasiak, A., Derba-Maceluch, M., Iashchishyn, I. A., Morozova-Roche, L. A., et al. (2021). Elongation of wood fibers combines features of diffuse and tip growth. *New Phytol.* 232, 673–691. doi: 10.1111/nph.17468

Medina, M. C., Sousa-Baena, M. S., Prado, E., Acevedo-Rodríguez, P., Dias, P., and Demarco, D. (2021). Laticifers in Sapindaceae: structure, evolution and phylogenetic importance. *Front. Plant Sci.* 11:612985 doi: 10.3389/fpls.2020.612985

Milanez, F. R. (1959). Contribuição ao conhecimento anatômico de *Cryptostegia grandiflora* III: nota sobre a estrutura secundária. *Rodriguésia* 25, 335–349.

Milanez, F. R. (1960). Contribuição ao conhecimento anatômico de *Cryptostegia grandiflora* II: sôbre os laticíferos da estrutura primária (Asclepiadaceae). *Rodriguésia* 35, 99–128.

Milanez, F. R. (1977). "Ontogênese dos laticíferos contínuos de *Nerium oleander* L." in *Trabalhos do XXVI Congresso Nacional de Botânica*, Rio de Janeiro, 343–379.

Milanez, F. R. (1978). Ontogênese dos laticíferos contínuos. *Arq. do Jard. Botânico do Rio Janeiro* 23, 47–114.

Naidoo, C., Naidoo, Y., and Dewir, Y. H. (2020). The secretory apparatus of *Tabernaemontana ventricosa* Hochst. ex A.DC. (Apocynaceae): laticifer identification, characterization and distribution. *Plants* 9:686. doi: 10.3390/plants9060686

Palin, R., and Geitmann, A. (2012). The role of pectin in plant morphogenesis. *Biosystems* 109, 397–402. doi: 10.1016/j.biosystems.2012.04.006

Panteris, E., Apostolakos, P., and Galatis, B. (1993). Microtubule organization, mesophyll cell morphogenesis, and intercellular space formation in *Adiantum capillus* veneris leaflets. *Protoplasma* 172, 97–110. doi: 10.1007/BF01379367

Panteris, E., and Galatis, B. (2005). The morphogenesis of lobed plant cells in the mesopyll and epidermis: organization and distinct roles of cortical microtubules and actin filaments. *New Phytol.* 167, 721–732. doi: 10.1111/j.1469-8137.2005.01464.x

Ramos, M. V., Demarco, D., da Costa Souza, I. C., and de Freitas, C. D. T. (2019). Laticifers, latex, and their role in plant defense. *Trends Plant Sci.* 24, 553–567. doi: 10.1016/j.tplants.2019.03.006

Ramos, M. V., Freitas, C. D. T., Morais, F. S., Prado, E., Medina, M. C., and Demarco, D. (2020). "Plant latex and latex-borne defense," in *Advances in Botanical Research*. ed. R. Nawrot (Amsterdan: Elsevier Ltd), 1–25.

Schneider, R., Klooster, K., Picard Van't, K. L., van der Gucht, J., Demura, T., Janson, M., et al. (2021). Long-term single-cell imaging and simulations of microtubules reveal principles behind wall patterning during proto-xylem development. *Nat. Commun.* 12, 669–612. doi: 10.1038/s41467-021-20894-1

Schneider, R., Tang, L., Lampugnani, E. R., Barkwill, S., Lathe, R., Zhang, Y., et al. (2017). Two complementary mechanisms underpin cell wall patterning during xylem vessel development. *Plant Cell* 29, 2433–2449. doi: 10.1105/tpc.17.00309

Sieberer, B. J., Ketelaar, T., Esseling, J. J., and Emons, A. M. C. (2005). Microtubules guide root hair tip growth. *New Phytol.* 167, 711–719. doi: 10.1111/j.1469-8137.2005.01506.x

Smith, L. G., and Oppenheimer, D. G. (2005). Spatial control of cell expansion by the plant cytoskeleton. *Annu. Rev. Cell Dev. Biol.* 21, 271–295. doi: 10.1146/annurev.cellbio.21.122303.114901

Snegireva, A. V., Ageeva, M. V., Amenitskii, S. I., Chernova, T. E., Ebskamp, M., and Gorshkova, T. A. (2010). Intrusive growth of sclerenchyma fibers. *Russ. J. Plant Physiol.* 57, 342–355. doi: 10.1134/S1021443710030052

Sousa-Baena, M. S., Hernandes-Lopes, J., and Van Sluys, M. A. (2021). Reaching the top through a tortuous path: helical growth in climbing plants. *Curr. Opin. Plant Biol.* 59, 101982–101988. doi: 10.1016/j.pbi.2020.101982

Sousa-Baena, M. S., and Onyenedum, J. G. (2022). Bouncing back stronger: diversity, structure, and molecular regulation of gelatinous fiber development. *Curr. Opin. Plant Biol.* 67:102198. doi: 10.1016/j.pbi.2022.102198

Wasteneys, G. O. (2004). Progress in understanding the role of microtubules in plant cells. *Curr. Opin. Plant Biol.* 7, 651–660. doi: 10.1016/j.pbi.2004.09.008

Wasteneys, G. O., and Galway, M. E. (2003). Remodeling the cytoskeleton for growth and form: an overview with some new views. *Annu. Rev. Plant Biol.* 54, 691–722. doi: 10.1146/annurev.arplant.54.031902.134818

Wasteneys, G. O., Theune-Willingale, , and Menzel, D. (1997). Freeze shattering: a simple and effective method for permeabilizing higher plant cell walls. *J. Microsc.* 188, 51–61. doi: 10.1046/j.1365-2818.1977.2390796.x

Zhang, L., McEvoy, D., Le, Y., and Ambrose, C. (2021). Live imaging of microtubule organization, cell expansion, and intercellular space formation in *Arabidopsis* leaf spongy mesophyll cells. *Plant Cell* 33, 623–641. doi: 10.1093/plcell/koaa036

frontiers | Frontiers in Plant Science

TYPE Original Research
PUBLISHED 13 October 2022
DOI 10.3389/fpls.2022.950936

OPEN ACCESS

EDITED BY
Jiangqi Wen,
Oklahoma State University,
United States

REVIEWED BY
Juhua Liu,
Chinese Academy of Tropical Agricultural Sciences, China
Qiaoli Xie,
Chongqing University, China

*CORRESPONDENCE
Er-pei Lin
zjulep@hotmail.com
Huahong Huang
huanghh@zafu.edu.cn

SPECIALTY SECTION
This article was submitted to Plant Development and EvoDevo, a section of the journal Frontiers in Plant Science

RECEIVED 23 May 2022
ACCEPTED 22 September 2022
PUBLISHED 13 October 2022

CITATION
Borah P, Ni F, Ying W, Zhuang H, Chong S-L, Hu X-G, Yang J, Lin E-p and Huang H (2022) Genome-wide identification and characterization of OVATE family proteins in *Betula luminifera* reveals involvement of *BlOFP3* and *BlOFP5* genes in leaf development. *Front. Plant Sci.* 13:950936. doi: 10.3389/fpls.2022.950936

Genome-wide identification and characterization of OVATE family proteins in *Betula luminifera* reveals involvement of *BlOFP3* and *BlOFP5* genes in leaf development

Priyanka Borah[1], Fei Ni[1], Weiyang Ying[1], Hebi Zhuang[1], Sun-Li Chong[1], Xian-Ge Hu[1], Jun Yang[2], Er-pei Lin[1]* and Huahong Huang[1]*

[1]State Key Laboratory of Subtropical Silviculture, Zhejiang A&F University, Hangzhou, China, [2]Shanghai Key Laboratory of Plant Functional Genomics and Resources, Shanghai Chenshan Plant Science Research Center, Chinese Academy of Sciences, Shanghai, China

Ovate family proteins (OFP) are plant-specific transcription factors involved in regulating morphologies of the lateral organs, plant growth and development. However, the functional roles of *OFP* genes in *Betula luminifera*, an important timber tree species, are not well studied. In this study, we identified 20 *BlOFP* genes and analyzed their phylogenetic relationship, gene structure, conserved motifs, and *cis*-elements. Further, expression analysis indicates that *BlOFP* genes were up-regulated in leaves on the one-year-old branch compared to leaves on the current-year branch and bract, except *BlOFP7*, *BlOFP11*, *BlOFP14* and *BlOFP12*. The overexpression of *BlOFP3* and *BlOFP5* in *Arabidopsis thaliana* not only resulted in a slower growth rate but also produced sawtooth shape, flatter and darker green rosette leaves. Further investigation showed that the leaf thickness of the transgenic plants was more than double that of the wild type, which was caused by the increasement in the number and size of palisade tissue cells. Furthermore, the expression analysis also indicated that the expressions of several genes related to leaf development were significantly changed in the transgene plants. These results suggested the significant roles of *BlOFP3* and *BlOFP5* in leaf development. Moreover, protein-protein interaction studies showed that BlOFP3 interacts with BlKNAT5, and BlOFP5 interacts with BlKNAT5, BlBLH6 and BlBLH7. In conclusion, our study demonstrates that BlOFP3 and BlOFP5 were involved in leaf shape and thickness regulation by forming a complex with BlKNAT5, BlBLH6 and BlBLH7. In addition, our study serves as a guide for future functional genomic studies of *OFP* genes of the *B. luminifera*.

KEYWORDS

***Betula luminifera*, ovate family protein, expression analysis, protein-protein interaction, transmission electron microscopy**

Introduction

The OVATE Family Proteins (OFP) are unique plant-specific transcription factors containing a ~70 amino acids long conserved C-terminal OVATE domain (DUF623) (Schmitz et al., 2015). Based on the similarity of the OVATE domain, OFPs were identified in monocots, dicots, bryophytes and lycophytes (Liu et al., 2014). The first *OFP* gene was cloned by Liu et al. (2002) from tomatoes, and they reported that a point mutation in the *OFP* gene resulted in pear-shaped tomatoes, and overexpression causes abnormal phenotypes like slower plant growth, exserted stigmas, and altered floral and vegetative architecture. Later, the function of *OFP* genes was studied in many plant species and identified that *OFP* genes exhibit various roles in the different stages of a plant's growth and development. For example, in *Arabidopsis thaliana*, an overexpression study of *AtOFP1* exhibits round and curly leaves and kidney-shaped cotyledons. Moreover, the expression of *AtOFP1* also inhibits the expression of *AtGA20ox1*, an essential gene for gibberellin biosynthesis, and prevents cell elongation (Wang et al., 2007). Besides, Wang et al. (2011) reported that in *A. thaliana*, *AtOFPs* act as transcriptional repressors regulating the morphology of cotyledons and true leaves, flower formation, and seed development. Further, overexpression of *OsOFP2* in rice leads to a decrease in plant height and changes in leaf morphology and seed shape (Schmitz et al., 2015). Likewise, genetic transformation experiments revealed that rice *OsOFP19* could affect architecture and seed shape by regulating the BR signalling pathway (Yang et al., 2018).

OFP proteins form complexes with other proteins and directly or indirectly affect the transcription of target genes to regulate plant growth and development. For example, *A. thaliana* OFPs can interact with TALE (three-amino-acid-loop-extension) superfamily members to form a complex and play an essential regulatory role in growth and development (Hackbusch et al., 2005). Further, AtOFP1 and AtBLH3 form a protein complex that regulates the transition time from vegetative growth to reproductive development of *A. thaliana* (Zhang et al., 2016). Moreover, AtOFP4 interacts with AtKNAT7 protein and acts as a transcriptional inhibitor to regulate the formation of the secondary cell wall of the inflorescence stem in *A. thaliana* (Li et al., 2011; Li et al., 2012). In addition, AtOFP5 interacts with AtBLH1 and AtKNAT3 and coordinately regulates embryo sac development (Pagnussat et al., 2007). Besides this, AtOFP1 also interacts with DNA double-strand break repair-related protein AtKu and jointly regulates the DNA double-strand break repair process (Wang et al., 2010). Further, rice OsOFP8 phosphorylates OsGSK2 protein and plays a role in growth and development by participating in the BR signalling pathway (Yang et al., 2016). Likewise, OsOFP19 forms a complex with OSH1 (a member of the KNOX subfamily protein) and DLT (DWARF AND LOW-TILLERING) protein. The complex of these three proteins plays a vital role in regulating BR signalling and determining cell division patterns (Yang et al., 2018).

Betula luminifera H. Winkler is a deciduous tree of the Betulaceae family, distributed in 14 provinces of southern China (Li et al., 2018). It grows fast and has strong adaptability with a high yield rate (Li et al., 2018). In addition to these traits, it has a short juvenile period. The one-and-a-half-year-old young plants can bloom under natural conditions, making the corresponding breeding and research cycle faster than other tree species (Li et al., 2018). Further, the complete genome sequence of the same genus, *Betula pendula* has been published (Salojarvi et al., 2017). These special characteristics make *B. luminifera* an ideal plant species for forest genetic and molecular biology studies. In recent years, bioinformatics and molecular biology studies of *B. luminifera* have also been conducted, such as RNA-seq analysis and gene family studies (Cai et al., 2018; Li et al., 2018). However, so far, there are no research findings involving the OFP transcription factor of *B. luminifera*. Therefore, in this study, we identified the *OFP* gene family in *B. luminifera* and analyzed their gene structure, conserved domains, evolutionary relationships, and expression patterns in different developmental stages of leaves. Moreover, functional studies for *BlOFP3* and *BlOFP5* were performed through ectopic expression in *A. thaliana* and protein-protein interactions. The present results provide a basis for functional studies of *OFP* genes in *B. luminifera*.

Materials and methods

Plant materials

The material used in this study is *B. luminifera* 1-V-25-2 clone, planted in the Pingshan nursery of Zhejiang A & F University. The leaves of three different developmental stages were collected from a healthy plant and named Brt (bracts), YL1 (young leaf from the current-year branch), and YL2 (young leaf from the one-year-old branch). The sample was collected in April 2021. The *A. thaliana* Columbia-0 (Col-0) was used for gene transformation. Seeds of Col-0 were sterilized twice with 75% alcohol and grown on ½ MS media until leaves reached the four-leaf stage in an artificial incubator (at 25°C, light for 16 h, dark for 8 h, with an average light intensity of 12,000 lx). Then the seedlings were transplanted to the peat moss (peat soil: vermiculite: perlite is 3:1:1) and grew at 22°C under photoperiod (16h light/8h dark) in a growth chamber.

Identification of *OFP* genes

The Hidden Markov Model (HMM) profile of the OVATE domain (PF04844) was obtained from the Pfam database (Mistry et al., 2021). Putative OFP protein sequences were identified by

HMMER search against the *B. luminifera* genome and the publicly available *B. pendula* genome (Salojarvi et al., 2017). In cases of multiple putative proteins from the same gene locus, the most extended variant was kept for further analysis. Editseq module in the DNAStar package was used to predict the amino acid sequence, molecular weight, and isoelectric point of the deduced protein. The identified gene sequences are provided in Supplementary Table 1.

Gene structure, genome location and *cis*-elements analysis of *BlOFPs*

The gene structure and genomic location of *BlOFPs* were searched in the genomic database, and the localization of the *BlOFP* genes on the chromosomes was generated using TBtools (Chen et al., 2020). The PlantCARE webtool (http://bioinformatics.psb.ugent.be/webtools/plantcare/html/) was used to analyze the *cis*-acting elements in the promoter sequence.

Phylogenetic analysis and conserved motif analysis of BlOFP proteins

The phylogenetic tree was constructed using MEGA-X using the Maximum likelihood method (Kumar et al., 2018). The aligned peptide sequences of OVATE domains from *B. luminifera*, *B. pendula*, *A. thaliana*, *Oryza sativa* and *P. trichocarpa* OFP proteins were used to generate phylogenetic analysis. The bootstrap value of 1000 replicates was used to evaluate the statistical significance. The conserved motifs were identified by the online program MEME (http://meme-suite.org/tools/meme) and visualized using the TBtools (Chen et al., 2020).

RNA isolation

According to the manufacturer's instructions, the total RNA was extracted from tissues using PureLinkTM Plant RNA Reagent (Invitrogen, Carlsbad, CA, USA). The concentration of RNA samples was analyzed by spectrophotometer (Nanodrop ND-2000), and purity and integrity were analyzed by agarose gel electrophoresis. Promega's RQ1 RNase-Free DNase was used to remove the DNA contamination following the manufacturer's instructions.

Real-time qRT-PCR

The cDNA was synthesized using Takara's PrimeScript™ RT reagent Kit (Perfect Real Time) as per the manufacturer's instructions. Oligo7.0 software was used to design fluorescent quantitative PCR primers (Supplementary Table 2). The TB green premix ex Taq II (Tli RNase H Plus) (Takara) was used for qRT-PCR amplification in the CFX96™ Real-Time PCR detection system (Bio-Rad, USA). All PCR reactions were performed in triplicate. The *BlEF1a* gene was used as an internal reference for *B. luminifera* samples, and the *Actin* gene was used as an internal reference in qRT-PCR for *Arabidopsis* samples. All the primers used in qRT-PCR were listed in Supplementary Table 2. The relative expression levels were determined with CFX96 Manager™ software (version 1.6; Bio-Rad, USA) using the delta-delta Ct method (Livak and Schmittgen, 2001). GraphPad Prism (Version 5.01) was used to draw the graphs of the quantitative results.

Production of transgenic *A. thaliana* plants

For the construction of the overexpression vector, the open reading frame (ORF) of *BlOFP3* and *BlOFP5* genes were inserted into the pCAMBIA13011 vector, respectively. The generated vectors *pCAMBIA13011-BlOFP3* and *pCAMBIA13011-BlOFP5* were transferred to *Agrobacterium tumefaciens* (GV3101). Transformation of transgenic *A. thaliana* plants was performed using the floral dip method (Clough and Bent, 1998), and transgenic plant selection was performed on MS agar medium supplemented with hygromycin. The transgenic plants were transplanted to peat moss and grown as mentioned above for wild-type (WT) plants. The transgenic *A. thaliana* plants were also verified by PCR and qRT-PCR, and homozygous T3 generation plants were used for further analysis.

Phenotyping of transgenic plants

To observe the growth and leaf development of transgenic plants, the young (21-day-old) and mature (42-day-old) transgenic plants were photographed and compared with WT. The relative chlorophyll content of leaves was measured using a SPAD (soil plant analysis development) meter. To measure the leaf thickness and cell number, the cross-section of about 8 µm thick from rosette leaves of 42-day-old plants was obtained by microtome (Leica). The sections were stained with 0.02% toluidine blue for 5 minutes and rinsed with distilled water until the wash solution was clear. Finally, the sections were observed under a light microscope (Zeiss). At least 8 sections (8 replicates) of each sample were used to determine the leaf thickness and cell number.

Transmission electron microscopy

To measure cell size, the rosette leaves of a 42-day-old plant were fixed in 0.1 M phosphate buffer (pH 7.2) with 2.5%

glutaraldehyde at 4°C overnight. Then, the samples were washed with 0.1 M phosphate buffer and treated with 1.0% osmium tetroxide for 1h. After that, the samples were rinsed twice in deionized water and dehydrated in a graded ethanol series. After dehydration, the samples were infiltrated and embedded in epon-araldite. Ultra-thin sections (70 nm) were sliced with a diamond knife (Reichert-Jung, Germany), stained with uranyl acetate and lead citrate, and mounted on nickel grids for examination in the transmission electron microscope (FEI Titan G2 80-200 ChemiSTEM, USA). At least 10 photos for each sample were analyzed.

Yeast two-hybrid assay

Y2H experiment was performed according to the manufacturer's instructions of Matchmaker™ gold yeast two-hybrid system (Clontech). Briefly, the ORFs of *BlOFPs* were cloned into bait vector pGBKT7, respectively. The ORFs of *BlKNOXs* and *BlBLHs* genes were constructed into prey vector pGADT7, respectively. The recombinant bait and prey vectors were transformed into the Y2H gold strain and Y187 strain, and the protein interaction was tested through yeast mating according to the manufacturer's instructions. The pGADT7-T+pGBKT7-Lam and pGADT7-T+pGBKT7-53 were used as negative and positive controls, respectively. The gene sequences used in Y2H were provided in Supplementary Table 1, and the primers used in Y2H were also listed in Supplementary Table 2.

Bimolecular fluorescence complementation assay

The ORF of BlOFP3, BlOFP5, BlKNOX5, BlKNOX9, BlBLH6, BlKNOX5, BlKNOX9 and BlBLH7 were cloned into the pSAT1- nEYFP-C1 and pSAT4-cEYFP-C1-B vectors using ClonExpress® II One Step Cloning Kit (Vazyme). The recombinant vectors transiently co-expressed in *Arabidopsis* protoplast cells through PEG-mediated transformation (Yoo et al., 2007). The images of transformed protoplast cells were captured on a Laser confocal microscope (Carl Zeiss LSM880) to observe and detect protein interaction signals. The primers used in BiFC were listed in Supplementary Table 2.

Statistical analysis

The significant differences in experimental data were compared by the Duncan algorithm. All calculations are based on Data Processing System Software (V15.10), and differences were considered significant at a p-value ≤ 0.05 level.

Results

Identification of *OFP* genes in *B. luminifera* and *B. pendula*

Our lab has developed *B. luminifera* genome reads using PacBio's RS II platform, and the assembled genome contained 9,332 contigs with an N50 of 247 kb (unpublished data). Using this contigs information, we have identified a total of 20 *B. luminifera BlOFPs* (*BlOFP1-B1OFP20*) genes using the HMM model. Further, we also identified the 20 *BpOFPs* of silver birch (*B. pendula*) using the published genome (Salojarvi et al., 2017). The 20 B1OFP proteins consist of 106-422 amino acid residues, with a molecular weight of 12.08-48.21 kDa and an isoelectric point of 4.38-9.79 (Table 1). Further, multiple sequence alignment indicated that all the 20 BlOFP proteins contain an OVATE domain, which was not highly conserved among these proteins (Supplementary Figure 1). The gene structure of *BlOFP* genes is also analyzed and identified that the ORF size in the genomic DNA ranged from 321 - 1269 bp. Out of 20 *BlOFP* genes, 18 *BlOFPs* genes are intron-free. While *BlOFP19* and *BlOFP20* have an intron of 2506 bp and 110 bp in length, respectively (Figure 1). Based on the published genome database of *B. pendula* (Salojarvi et al., 2017), we analyzed the distribution of *BpOFPs* genes on the chromosomes (Figure 2). The 16 *BpOFPs* genes are mapped to 9 chromosomes of *B. pendula*, of which chromosomes 6 and 8 have the highest number of genes, i.e. three *OFPs*. In addition, *BpOFP5*, *BpOFP11*, *BpOFP15*, and *BpOFP17* were found to be located on unanchored contig796, contig419 and contig230 (Figure 2).

Phylogenetic analysis of birch OFP proteins

In order to analyze the phylogenetic relationship of OFP proteins, a phylogenetic tree containing 102 OFP proteins (BlOFPs, BpOFPs, AtOFPs, OsOFPs and PtOFPs) is constructed. All OFP proteins can be divided into eight sub-groups from the topological structure: Subgroup I, Subgroup II, Subgroup III, Subgroup IV, Subgroup V, Subgroup VI, Subgroup VII and Subgroup VIII (Figure 3). Except for BlOFP18 and BpOFP18, other BlOFP and BpOFP proteins are placed next to each other in all clades, indicating that these OFP proteins have a certain degree of differentiation during evolution. The two concerned BlOFPs of the present study, i.e., BlOFP3 and BlOFP5, were placed in the same subgroup, Subgroup-I. Along with BlOFP3 and BlOFP5, AtOFP6 and AtOFP19 from *A. thaliana* and OsOFP8 and OsOFP20 from *O. sativa* are grouped in the same subgroup, indicating their close homologous relationships (Liu et al., 2014). Further, most monocot OFP proteins (OsOFPs) are divided into six subgroups, except Subgroup II and VIII.

TABLE 1 Physical and chemical properties of *BlOFP* genes in *B.luminifera*.

S. No	cDNA	ORF size (bp)	Predicted protein length/ m.w.(kDa)	Isoelectric point	S. No	cDNA	ORF size (bp)	Predicted protein Length/m.w.(kDa)	Isoelectric point
1	BlOFP1	981	326/36.60	9.79	1	BpOFP1	981	326/36.59	9.94
2	BlOFP2	345	114/12.92	4.53	2	BpOFP2	345	114/12.92	4.53
3	BlOFP3	543	180/20.67	8.7	3	BpOFP3	543	180/20.70	8.7
4	BlOFP4	720	239/26.47	4.38	4	BpOFP4	720	239/26.58	4.29
5	BlOFP5	543	180/20.24	5.11	5	BpOFP5	543	180/20.14	4.87
6	BlOFP6	804	267/29.53	4.5	6	BpOFP6	729	242/26.70	4.3
7	BlOFP7	1062	353/39.98	9.6	7	BpOFP7	1062	353/40.10	9.54
8	BlOFP8	1023	340/38.03	9.38	8	BpOFP8	1020	339/38.00	9.33
9	BlOFP9	987	328/38.21	9.71	9	BpOFP9	894	297/34.64	9.64
10	BlOFP10	486	161/18.68	7.9	10	BpOFP10	474	157/18.21	8.74
11	BlOFP11	720	239/26.42	5.63	11	BpOFP11	720	239/26.46	5.96
12	BlOFP12	711	236/26.69	6.97	12	BpOFP12	711	236/26.67	6.59
13	BlOFP13	846	281/31.58	6.12	13	BpOFP13	846	281/31.69	6.62
14	BlOFP14	855	284/32.78	8.15	14	BpOFP14	777	258/29.74	9.35
15	BlOFP15	636	211/24.15	8.86	15	BpOFP15	642	213/24.21	8.9
16	BlOFP16	321	106/12.08	4.54	16	BpOFP16	324	107/12.26	4.54
17	BlOFP17	1269	422/48.21	9.21	17	BpOFP17	1197	398/45.57	9.4
18	BlOFP18	645	214/24.35	6.07	18	BpOFP18	645	214/24.16	5.23
19	BlOFP19	585	194/23.02	8.54	19	BpOFP19	561	186/21.64	7.69
20	BlOFP20	1143	381/43.12	9.36	20	BpOFP20	330	110/12.82	10.29

Prediction of conserved motifs in birch OFP proteins

Studying the conserved motifs can reveal the functional diversity of OFP proteins. Through conserved motif analysis, fifteen conserved motifs of BlOFPs were identified. Among these motifs, OVATE domains are present in the C-terminal of OFP proteins, while other motifs are upstream of the OVATE domain (Figure 3). Interestingly, the OsOFP23 in Subgroup III, OsOFP11 in Subgroup VI and BlOFP2, BpOFP2, PtOFP28,

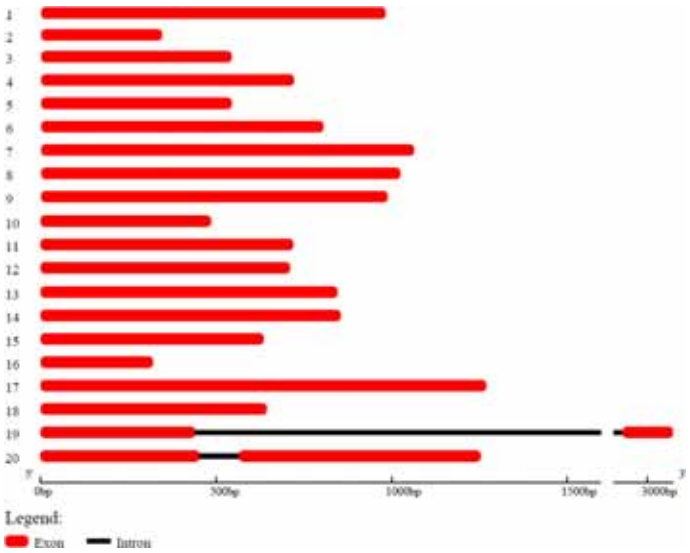

FIGURE 1
Gene structure analysis of *BlOFP* genes. The scale bar is shown at the bottom.

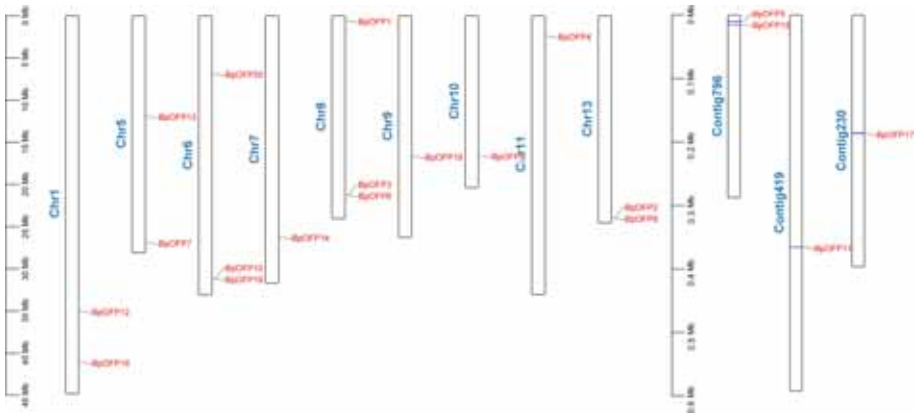

FIGURE 2
Physical location of *BpOFP* genes on the Chromosomes and scaffolds of *B. pendula*.

AtOFP17 and AtOFP20 in the Subgroup VIII don't contain the complete OVATE domain (Figure 3). These results suggest that the OVATE domain is not that conserved during evolution. Further, most OFP proteins in the same subgroup have similar motif distributions (Figure 3). These results show that the motifs of members within the same subgroup are conserved, which implies they may perform similar functions.

Analysis of *cis*-acting elements in the promoter region of *BlOFP* genes

The *cis*-acting elements play a vital role in regulating gene transcription during plant growth, development, and stress. Therefore, studying the *cis*-elements in *BlOFP* genes will help understand their role in plant growth and development. Hence, we analyzed the 1500 bp upstream region of the 20 *BlOFPs* genes. We classified the *cis*-acting elements into eight types based on the functions of *cis*-elements: light-responsive elements, induction-specific elements, plant tissue-specific elements, binding site-specific elements, transcription-related elements, process-specific elements, regulatory-specific elements, and environment-specific elements (Figure 4A). The promoter regions of *BlOFPs* genes contain at least six different types of *cis*-acting elements. Although the regulatory-specific *cis*-elements are the most abundant among the different *cis*-elements analyzed, the process-specific elements (plant hormone-related *cis*-acting elements) seem to be essential. Further, ABRE, ERE, GARE motif, TCA-element, TC-rich repeats, and TGA elements were found in abundance compared to other process-specific elements (Figure 4B).

Expression of *BlOFP* genes during leaf development in *B. luminifera*

The *OFP* genes are reported to be involved in the regulation of leaf development (Yang et al., 2016; Sun et al., 2020). So to identify the expression pattern of *BlOFP* genes in leaf development, we performed qRT-PCR in *B. luminifera* leaves with three developmental stages: Brt, YL1, and YL2. Most *BlOFP* genes have increased expression in YL2 except *BlOFP7*, *BlOFP11*, *BlOFP14*, and *BlOFP12* (Figure 5). The *BlOFP7* and *BlOFP12* showed their highest relative expressions in Brt, and the *BlOFP11* and *BlOFP14* showed their highest expressions in YL1 (Figure 5). Interestingly, our qRT-PCR analysis showed that the *BlOFP9* and *BlOFP20* gene expression in YL2 was 228 and 184 times to the Brt, and 63 and 162 times to YL1, respectively. Further, *BlOFP3* and *BlOFP5* in YL2 were 6.9 and 4.4 times to the Brt and 9.6 and 6.2 times to the YL1, respectively (Figure 5).

Phenotype and anatomic analysis of *Arabidopsis* overexpressing *BlOFP3* and *BlOFP5*

In our study, through phylogenetic and motif analysis, we identified that *AtOFP6* and *OsOFP8* are closely related to *BlOFP3* and *BlOFP5*. Furthermore, sequence alignment of AtOFP6, BlOFP3 and BlOFP5 showed that conserved OVATE domain among these sequences (Supplementary Figure 2). Considering the function of *AtOFP6* in leaf development (Wang et al., 2011), the role of *BlOFP3* and *BlOFP5* genes was first investigated through ectopic expression in *A. thaliana* plants. The transgenic plants were screened out and confirmed

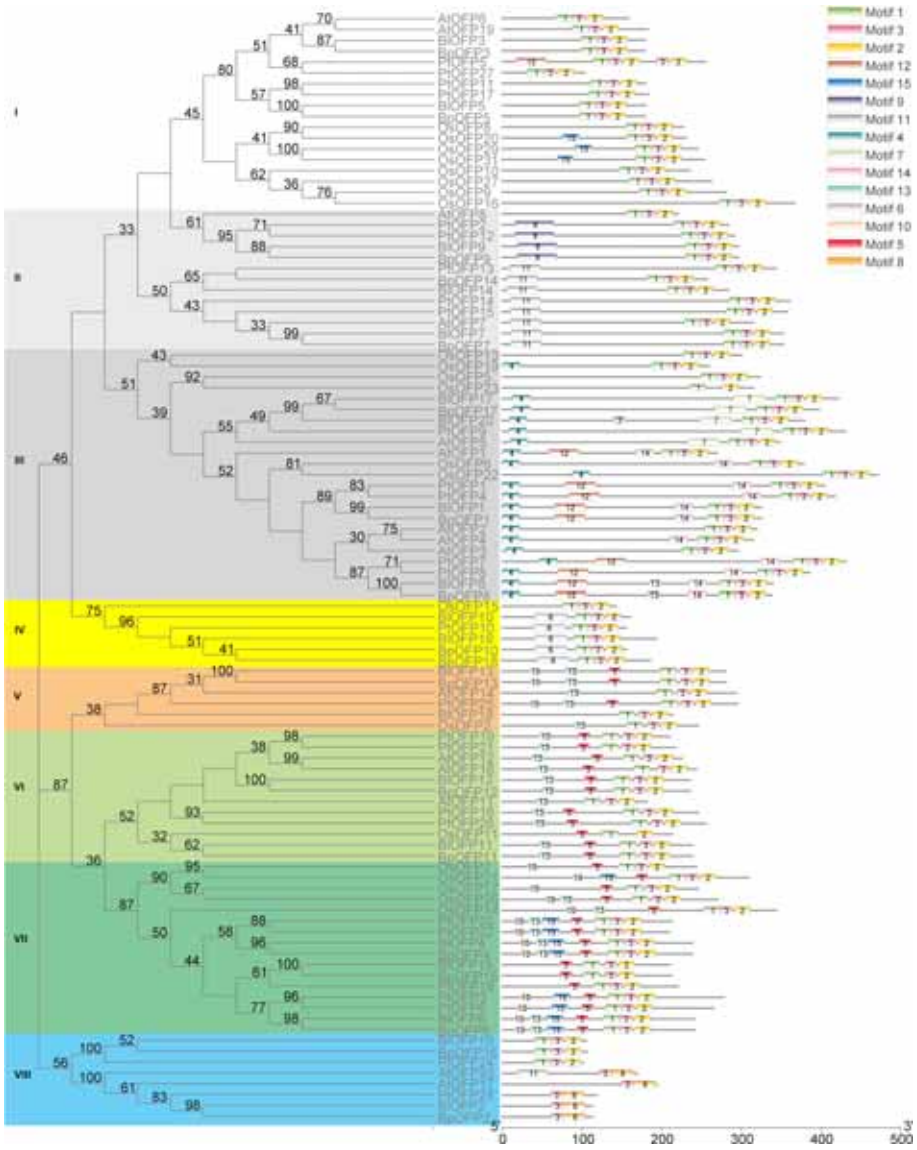

FIGURE 3
Phylogenetic relationship and conserved motif analysis of BlOFPs from *B. luminifera*. The phylogenetic tree was constructed using aligned OVATE domains sequences of *B. luminifera* (Bl), *B. pendula* (Bp), *A. thaliana* (At), *Oryza sativa* (Os) and *P. trichocarpa* (Pt). All the eight subgroups are indicated in different colours. The conserved motifs (1-15) are indicated in 15 different colour boxes.

using PCR detection on two reporter genes and BlOFP3/5 (Supplementary Figure 3), and then homologous T3 generations were used for phenotypic observation and anatomical analysis. The expression of *BlOFP3* and *BlOFP5* genes are also investigated by qRT-PCR in T3 generation transgenic plants. The results showed that *BlOFP3* and *BlOFP5* were strongly expressed in the transgenic plants (Supplementary Figure 3). Phenotype observation showed that overexpressing of *BlOFP3* and *BlOFP5* caused apparent differences in growth rate and leaf shape (Figure 6). The plant height of 42-day-old transgenic plants was 13.04 cm (35S::*BlOFP3*) and 13.08 cm (35S::*BlOFP5*), respectively, while the plant height of WT was 15.60 cm, which indicated that the growth of transgenic plants was slower (Figure 6E). Moreover, the rosette leaves of the two transgenic lines were flatter, darker green in colour, and a more obvious sawtooth appeared near the leaf stalk (Figures 6A, B). Measurement of the leaf area of 21-day-old and 42-day-old plants showed that the plants overexpressing *BlOFP3* and *BlOFP5* have considerably less leaf area (Figure 6C).

Furthermore, the SPAD values indicated that the relative chlorophyll content of leaves in transgenic plants is significantly higher than that in WT (Figure 6D). And the anatomic analysis

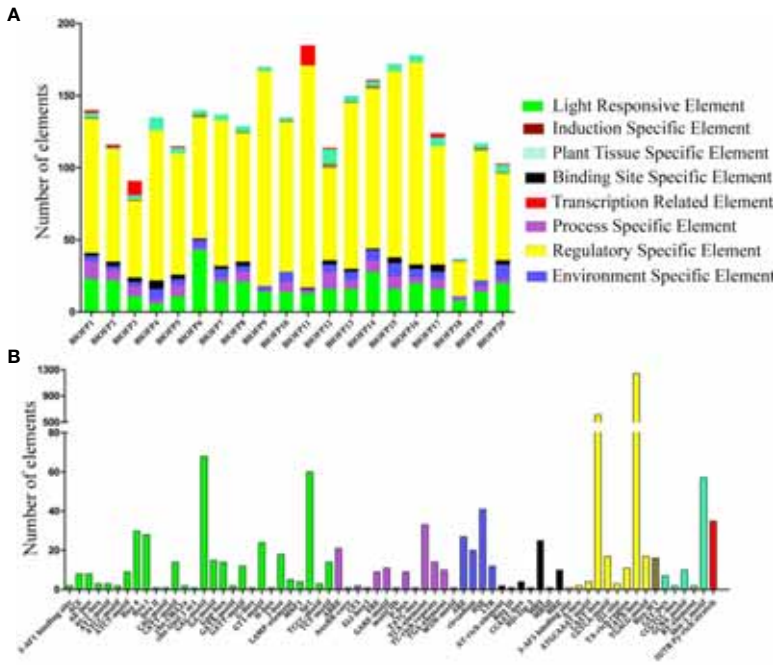

FIGURE 4
Analysis of conserved *cis*-acting elements in the promoter region of BlOFPs. Elements were identified in the 1500 bp sequences upstream of the start codon of *BlOFP* genes. **(A)** The elements involved in specific functions are indicated by different colours for each gene. **(B)** Number of different conserved elements.

revealed that the leaf thickness of plants overexpressing *BlOFP3* and *BlOFP5* is more than two times of the WT (Figures 7A, C). Meanwhile, an obvious increase in the number and size of palisade tissue cells is also observed in transgenic plants (Figures 7A, D, E). The increase in the size of palisade tissue cells was confirmed using transmission electron microscopy (TEM) (Figure 7B). Besides, the expression of *AtOFP6*, the endogenous homolog for *BlOFP3* and *BlOFP5*, was not altered in the plants overexpressing *BlOFP3* and *BlOFP5* (Supplementary Figure 4). These results suggest that *BlOFP3* and *BlOFP5* may play essential roles in leaf development by regulating the cell's number and size in palisade tissue.

Expression analysis of genes associated with leaf development in transgenic *Arabidopsis*

To explore the molecular mechanism of *BlOFP3* and *BlOFP5* in leaf development, six genes, including *KNAT2*, *KNAT6*, *AS1*, *CLV1*, *GA20ox1*, *PIN1* and *CUC2* genes, have been proved as crucial genes in leaf development (Long et al., 1996; Belles-Boix et al., 2006; Wang et al., 2021; Zhou et al., 2022), were chosen for expression analysis in the transgenic *A. thaliana* plants. As shown in figure 8, the expressions of *KNAT2* and *KNAT6* were both drastically inhibited in plants overexpressing *BlOFP3* and *BlOFP5* (Figure 8). At the same time, the expression of *CLV1*, *GA20ox1*, *PIN1* and *CUC2* genes up-regulated in the transgenic plants (Figure 8). These results further support the essential roles of *BlOFP3* and *BlOFP5* in leaf development. It also implies that these two genes may perform redundant functions through similar pathways in the leaf development of *B.luminifera*.

Interaction analysis of BlOFP3 and BlOFP5 with TALE homeodomain protein

In previous studies, OFP proteins have been shown to interact with various TALE (KNOX and BLH) proteins, forming a TALE-OFP protein complex to regulate different biological processes (Hackbusch et al., 2005; Li et al., 2011; Liu and Douglas, 2015). In this study, the interactions between these two BlOFP proteins (BlOFP3 and BlOFP5), eight BlKNOX proteins and nine BlBLH proteins were first analyzed using the Y2H method, respectively. As shown in figure 9, strong interactions between BlOFP3 and BlKNOX5, BlOFP3 and BlBLH6, BlOFP5 and BlKNOX5 as well as BlOFP5 and BlBLH6 were detected, and weak interactions between BlOFP3 and BlKNOX9, and BlOFP5 and BlBLH7 were also identified. However, in the present experiment, all other members of TALE

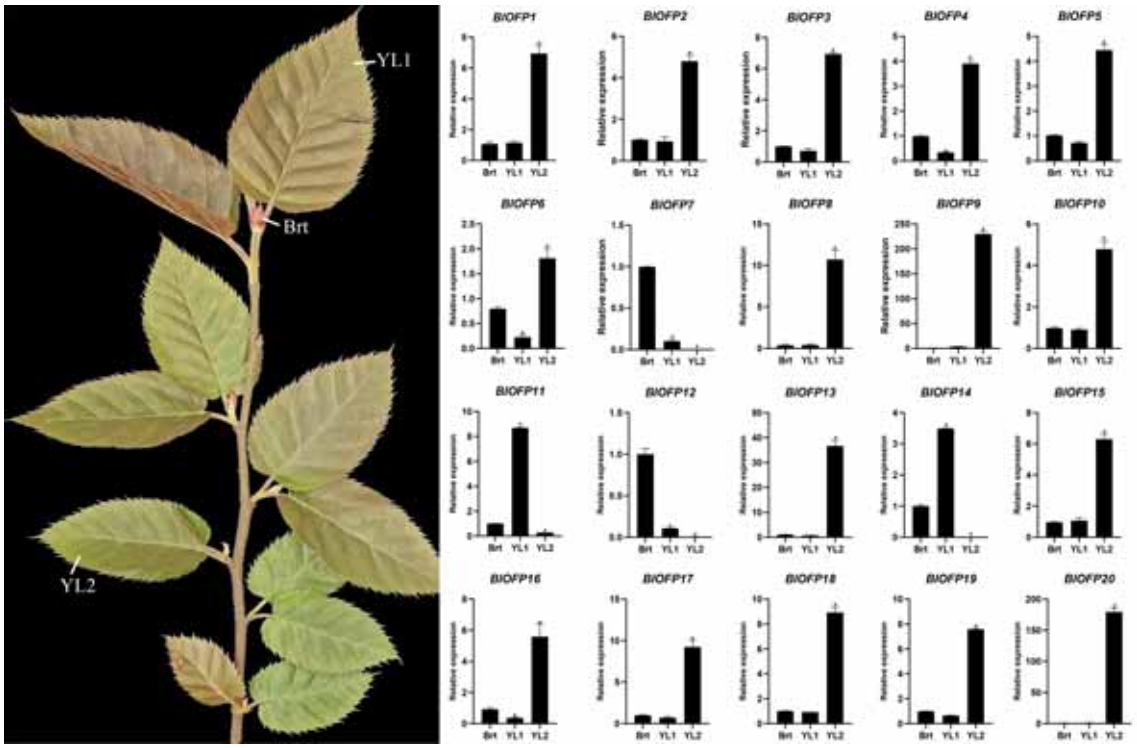

FIGURE 5
Expression analysis of *BlOFP* genes for leaf development. qRT-PCR analysis of 20 *BlOFP* genes in three developmental stages of *B. luminifera* leaves. The error bar represents the standard deviation from three biological replicates. The asterisk indicates significant difference compared to Brt at $p<0.05$ level.

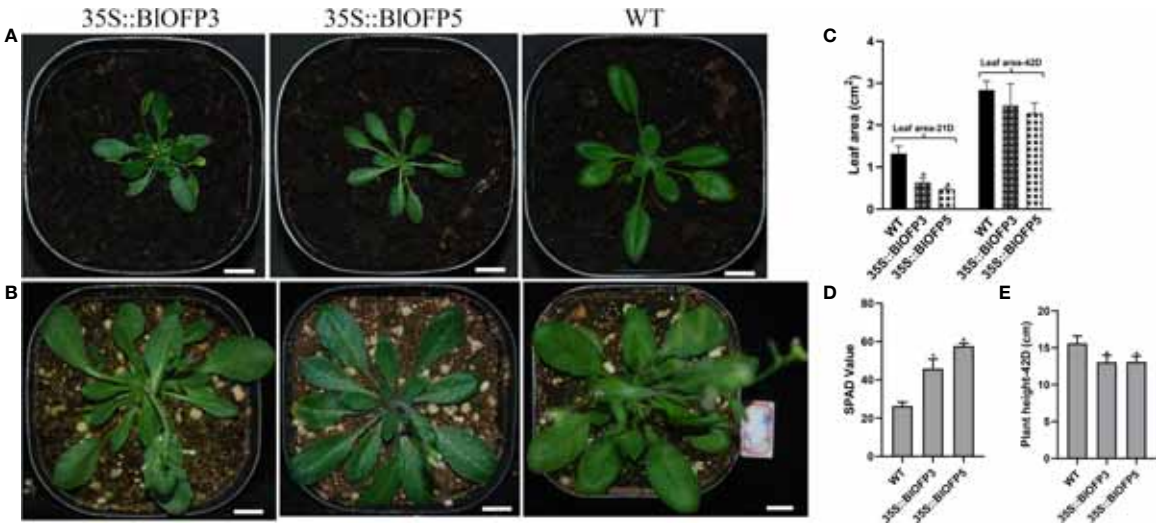

FIGURE 6
Phenotype observation on transgenic plants overexpressing *BlOFP3* and *BlOFP5* in *A. thaliana*. **(A)** 21-day-old transgenic plants transformed with 35S::BlOFP3 (left), 35S::BlOFP5 (middle), and WT plants (right). **(B)** 42-day-old transgenic plants transformed with 35S::BlOFP3 (left), 35S::BlOFP5 (middle), and WT plants (right). **(C)** Leaf area of 21-day and 42-day-old plants. **(D)** SPAD values of plants. **(E)** Plant height of 42-day-old plants. Bar = 1cm. The asterisk indicates significant difference compared to WT at $p<0.05$ level.

10.3389/fpls.2022.950936

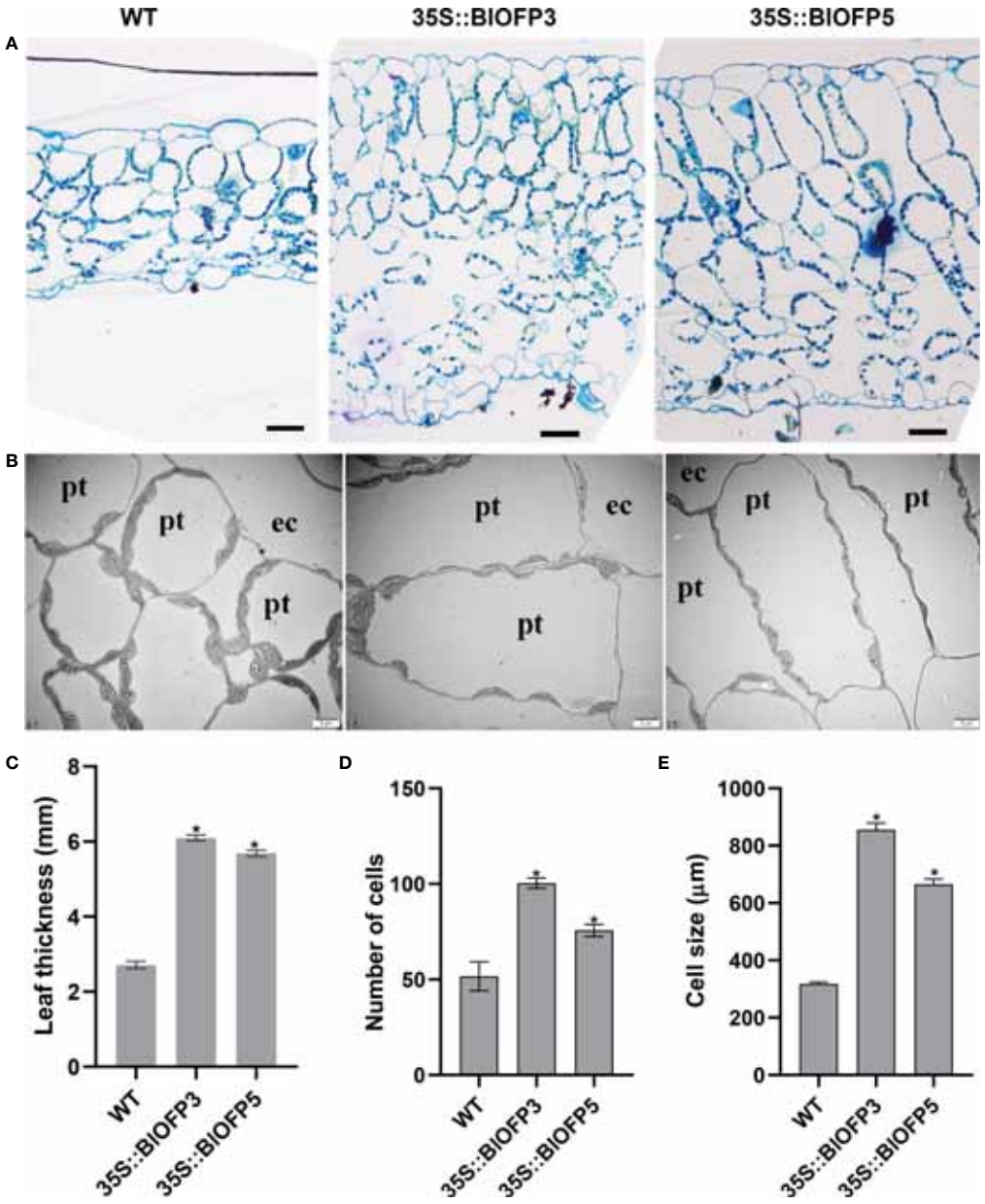

FIGURE 7
Anatomical characterization of transgenic Arabidopsis leaves. **(A)** Transverse sections of leaves from WT and transgenic *A. thaliana* plants stained with toluidine blue. Bar = 50 µm. **(B)** The TEM analysis of transgenic *A. thaliana* leaves. Bar = 5 µm. **(C)** Leaf thickness of WT and transgenic plants. **(D)** Number of palisade tissue cells. **(E)** Size of palisade tissue cells The asterisk indicates significant difference compared to WT at $p<0.05$ level.

homeodomain proteins did not show any interactions with BlOFP3 and BlOFP5 (Figure 9). This means there is interaction specificity exists between OFP and TALE homeodomain proteins.

Furthermore, the interactions obtained from Y2H were then verified by the BiFC assay in mesophyll protoplast cells of *A. thaliana*. Similar to the Y2H assay, the protoplast cells co-expressing BlOFP3-cEYFP with BlKNOX5-nEYFP, BlOFP5-cEYFP with BlKNOX5-nEYFP, as well as BlOFP5-cEYFP with BlBLH6-nEYFP exhibited intense fluorescence signals (Figure 10). In addition, a weak fluorescence signal was detected in the protoplast cells co-expressing BlOFP5-cEYFP with BlBLH7-nEYFP (Figure 10). These results were consistent with the Y2H interactions. However, in contrast to Y2H results, the fluorescence signal was absent in protoplast cells co-expressing BlOFP3-cEYFP with BlKNOX9-nEYFP and

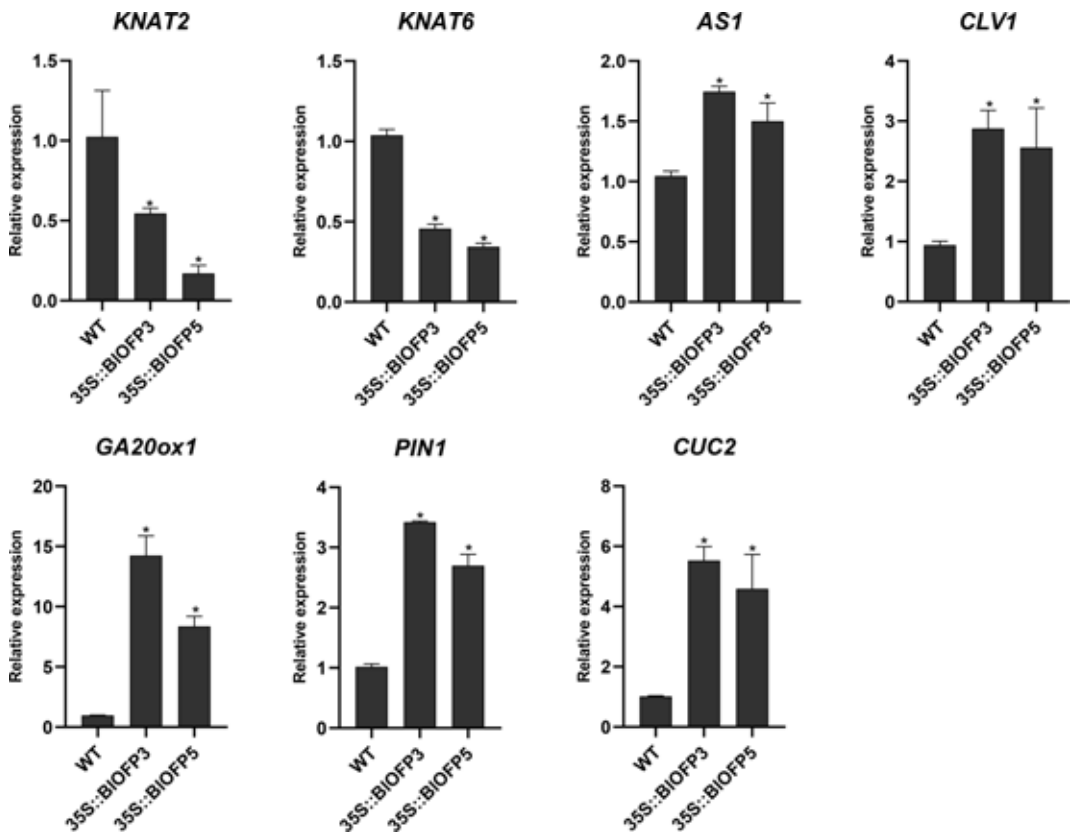

FIGURE 8
Expression analysis of genes involved in leaf development. qRT-PCR analysis of *KNAT2*, *KNAT6*, *AS1*, *CLV1*, *GA20ox1*, *PIN1* and *CUC2* genes normalized with *Actin*. The error bar indicates the standard deviation from three biological replicates. The asterisk indicates significant difference compared to WT at $p<0.05$ level.

BlOFP3-cEYFP with BlBLH6-nEYFP (Figure 10). Based on the above results, we hypothesized that at least BlKNOX5 is a common partner for BlOFP3 and BlOFP5, forming a functional complex to regulate leaf development in *B.luminifera*.

Discussion

OFPs, encoding a class of plant-specific transcription regulators, have been identified in many plants (Wang et al., 2010; Rodríguez et al., 2011; Tsaballa et al., 2011; Wang et al., 2011; Wang et al., 2016; Yang et al., 2016; Yang et al., 2018). This study identified and characterized 20 genes encoding OFP proteins in *B. luminifera*. As indicated by phylogenetic analysis, 20 OFP proteins in *B. luminifera* are distributed into eight subgroups based on their sequence similarity (Figure 3). The two studied BlOFPs of the present study, i.e., BlOFP3 and BlOFP5, showed close homologous relationships with AtOFP6 and AtOFP19 from *A. thaliana*. Domains and motifs are the key elements for the structure and functions of a protein or protein family (Moore et al., 2008; Forslund and Sonnhammer, 2012). In this study, 15 conserved motifs were identified, and most of these motifs showed similar distribution patterns to their homologs within the same subgroup (Figure 3). Moreover, the OVATE domain was also identified to be present at the end of 20 BlOFPs (Figure 3), which is consistent with the previous studies (Liu et al., 2014; Li et al., 2019). Since BlOFPs and BpOFPs share almost identical OVATE domain sequences, all BlOFPs and BpOFPs are positioned next to each other except BlOFP18 and BpOFP18. Divergent expansion might be considered the reason behind the presence of BlOFP18 and BpOFP18 in different subgroups (Liu et al., 2014). In the current study, hormone-specific *cis*-acting elements, including ABRE, TCA-element, TC-rich repeats, and TGA elements, which are associated with abscisic acid (ABA), salicylic acid (SA), gibberellin (GA) and auxin (IAA) responses, respectively, were found to be distributed in the promoter region of the *BlOFPs* genes (Figure 4). These hormone-responsive regulatory elements in the promoter regions suggest that *BlOFP* genes might be involved in response to various plant hormones and developmental processes (Liu and Douglas, 2015; Tang et al., 2018; Wu et al., 2018).

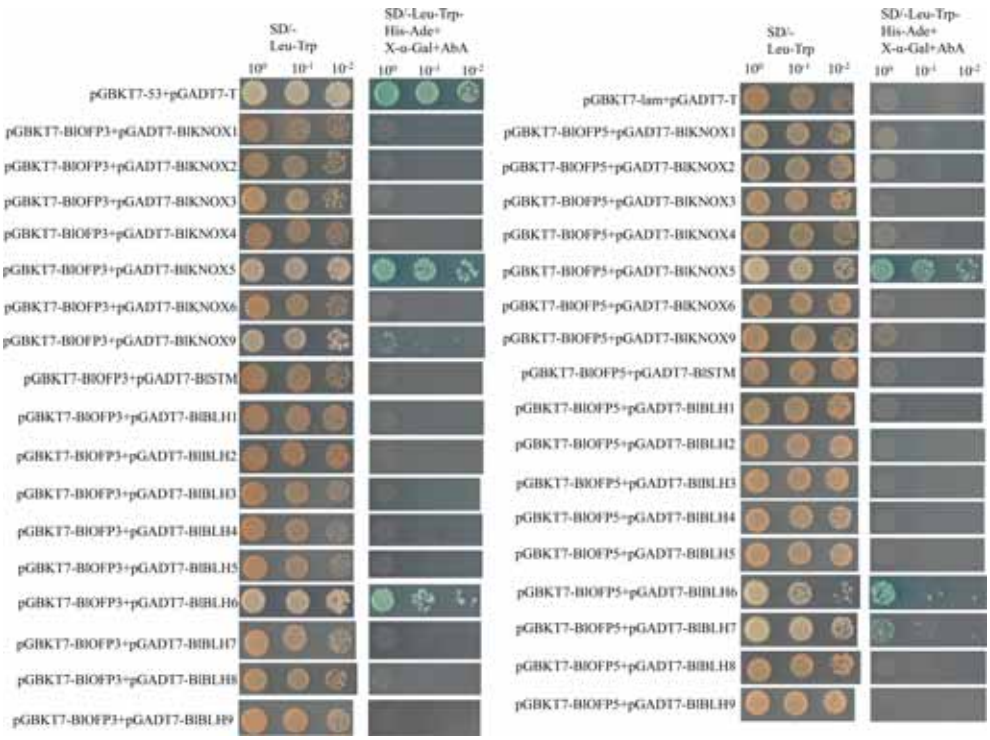

FIGURE 9
Protein-protein interactions of BlOFP3 and BlOFP5 with eight BlKNOX proteins and nine BlBLH proteins tested by Y2H. Yeast cells co-transformed with pGBKT7-53 and pGADT7-T were used as the positive control, and pGBKT7-lam and pGADT7-T were used as a negative control. Positive interactions were specified by the ability of cells to grow on SD-Leu-Trp-His-Ade plates supplemented with 40 μg/ml X-α-Gal and 125 ng/ml Aureobasidin A. Images were taken after 5 days of incubation at 30°C.

OFPs play diverse roles at different stages of plant growth and development (Wang et al., 2016; Knaap and Ostergaard, 2018). Regulation of leaf development is one of those important functions for plant *OFP* genes. For example, Wang et al. (2011) reported that overexpression of the *AtOFP6* gene resulted in flat, thick and cyan rosette leaves in *A. thaliana*. In the current study, transgenic *A. thaliana* overexpressing *BlOFP3* and *BlOFP5* genes showed flat, thicker leaves with higher relative chlorophyll content (Figure 6). Likewise, Zhou et al. (2019) found that tomato plants overexpressing *SlOFP20* genes showed shorter compound leaves and contained more chlorophyll than wild plants. These observations indicate that these *OFP* genes, including *BlOFP3* and *BlOFP5*, are essential regulators for leaf development. Moreover, in transgenic *Arabidopsis* plants overexpressing *BlOFP3* and *BlOFP5*, the expressions of several essential leaf development genes (*KNAT2*, *KNAT6*, *AS1*, *CLV1*, *GA20ox1*, *PIN1*, and *CUC2*) were considerably changed (Figure 8). As a critical TF in plant growth and development, the class I *KNOX* genes (*KNAT2*, *KNAT6*) maintain the function of shoot apical meristem (SAM) by regulating other key genes involved in leaf development. Prior studies have reported that AS1 and AS2 form a protein complex that inhibits the expression of *KNAT2*, resulting in regular leaf morphology (Li et al., 2016; Li et al., 2017). In the current study, the expression analysis of *KNAT2* and *KNAT6* in transgenic plants has shown an antagonistic relationship with *AS1* expression (Figure 8). There is an antagonism that exists between auxin and KNOX too. At the same time, auxins are transported by *PIN1*. The interaction among AS1, auxin and KNOX1 may directly affect the process of leaf initiation as well as leaf morphology (Hay et al., 2006). Likewise, the *GA20ox1* is involved in forming the boundary between SAM and the primary leaf primordia, which results from inhibition of the synthesis of GA by KNOX (Rosin et al., 2003; Hay and Tsiantis, 2009; Nakayama et al., 2014). Our study identified that the *GA20ox1* expression is also significantly changed in transgenic lines. At the same time, *CLV1* promotes stem cell activity in the SAM. Similarly, *CUC2* genes are also involved in leaf primordia initiation and affect the leaves' morphology (Hasson et al., 2011). In the current study, *CUC2* expression is also found to be up-regulated in the transgenic lines (Figure 8). These results further demonstrated that *BlOFP3* and *BlOFP5* probably regulate leaf development through various molecular pathways.

The TALE homeodomain proteins are fundamental regulators of plant leaf development and meristem function (Blanco et al., 2009). These homeodomain TFs is conserved in animals, plants, and fungi. In plants, TALE proteins are comprised of two classes, KNOTTED1-LIKE homeobox (KNOX) and BEL1-

like homeobox (BELL), which are involved in the determination and morphological development of leaves, stems, and inflorescences (Kumar et al., 2007; Hamant and Pautot, 2010; Hay and Tsiantis, 2010). The KNOX/BELL homo- and heterodimerization play an essential role in general TALE protein function (Hackbusch et al., 2005). Further, Hackbusch et al. (2005) also demonstrated that KNOX and BELL proteins interact with nine AtOFP proteins, regulating plant meristem and leaf development. Many other studies also showed that OFP proteins could interact with KNOX and BLH to regulate plant growth and development (Pagnussat et al., 2007; Li et al., 2011). Therefore, it is well-established that OFPs could act as the central point to interact with multiple proteins to form different regulatory complex to accurately and efficiently regulate plant growth and development. In our study, the physical interaction between BlOFP3 and BlKNOX5 as well as BlOFP5 and BlKNOX5 was detected by Y2H and BiFC experiments (Figures 9, 10). This implies that BlKNOX5 should be a significant component for the complex formed by BlOFP3 or BlOFP5. Besides, several other TALE proteins, including BlKNOX5, BlKNOX9, BlBLH6 and BlBLH7 proteins, were identified to interact with BlOFP3 or BlOFP5 by either Y2H or BiFC (Figures 9, 10). Although no consistent results were obtained from Y2H and BiFC, it is possible that BlOFP3 or BlOFP5 could interact with these TALE proteins to form various complexes, which may be associated with different biological processes in *B. luminifera*, but further experiments are needed to analyze the underlying molecular mechanism.

Conclusion

In the current study, we identified 20 *BlOFP* genes and analyzed the phylogenetic analysis, conserved motifs and *cis*-elements. The qRT-PCR analysis reveals that most *BlOFP* genes were up-regulated in YL2 compared to YL1 and bract. The overexpression of *BlOFP3* and *BlOFP5* genes in *A. thaliana* produces sawtooth shape, flatter, darker green rosette leaves, indicating their involvement in leaf development. Moreover, TEM results showing a significant increase in the number and size of palisade tissue cells in transgenic plants, which resulted in an increasement in leaf thickness. Besides, expression analysis also indicated that the expressions of several genes related to leaf development were considerably changed in transgenic plants. Furthermore, physical interactions between BlOFP3, BlOFP5 and several TALE proteins were also identified. On the basis of the interaction assay, we hypothesized that at least BlKNOX5 is a

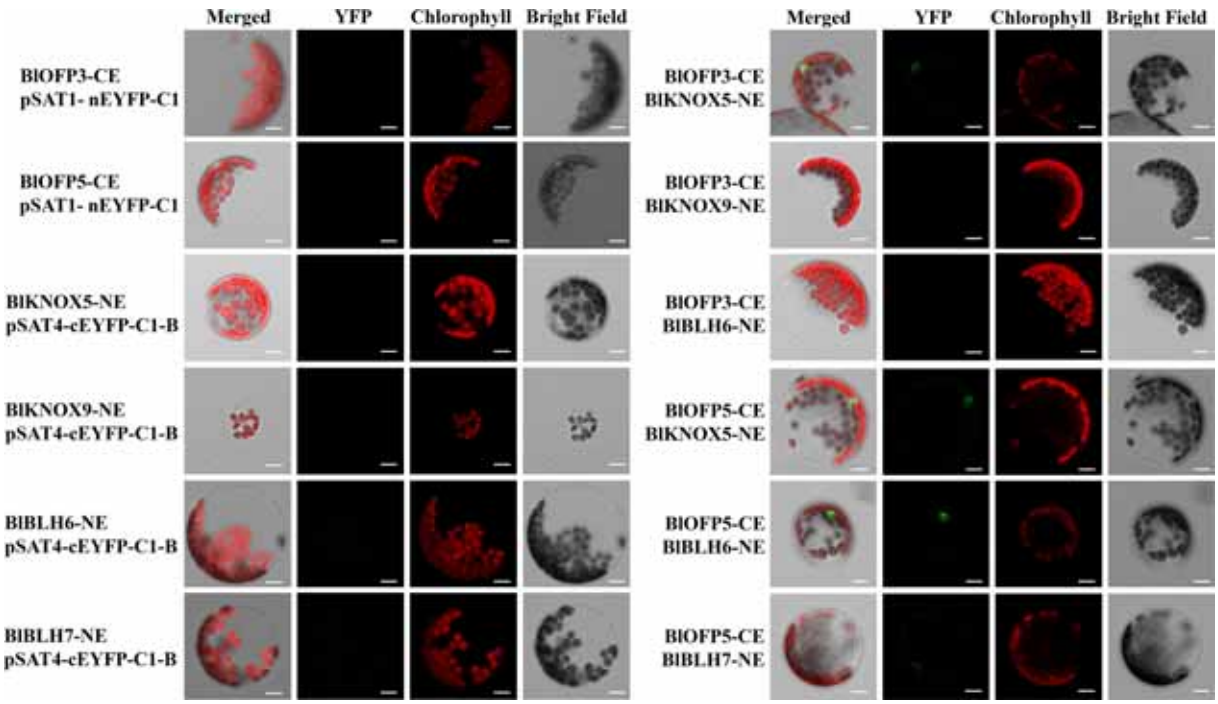

FIGURE 10
Verification of positive interactions of BlOFP3 and BlOFP5 with TALE proteins by BiFC assay in protoplast cells of *A. thaliana*. Proteins fused to the N- or C-terminal fragments of EYFP (NE or CE, respectively) were co-expressed transiently in protoplasts. Fluorescence signal indicating reconstitution of YFP was analyzed by confocal laser scanning microscopy. Empty vectors and corresponding recombinant vectors were co-expressed as negative control. Bar = 10 μm.

common interacting protein for BlOFP3 and BlOFP5, forming a functional complex to regulate leaf development in *B. luminifera*.

Data availability statement

The datasets presented in this study can be found in online repositories. The names of the repository/repositories and accession number(s) can be found in the article/Supplementary Material.

Author contributions

EL and HH designed the research. PB, FN, WY and HZ performed the experiments. JY performed the BiFC assay and revised the manuscript. PB, FN, WY, HZ, SC and XH analyzed the data. PB, EL and HH wrote the manuscript with comments from all authors. All authors contributed to the article and approved the submitted version.

Funding

This work was supported in part by the National Key Research and Development Program of China (No. 2021YFD2200304-2), the National Natural Science Foundation of China (No. 31470674) and the State Key Laboratory of Subtropical Silviculture (No. KF201902).

Acknowledgments

We thank Dr. Naresh Vasupalli, State Key Laboratory of Subtropical Silviculture, Zhejiang A & F University, for helping to revise the manuscript.

Conflict of interest

The authors declare that the research was conducted in the absence of any commercial or financial relationships that could be construed as a potential conflict of interest.

Publisher's note

Supplementary material

The Supplementary Material for this article can be found online at: https://www.frontiersin.org/articles/10.3389/fpls.2022.950936/full#supplementary-material

SUPPLEMENTARY FIGURE 1
OVATE domain alignment of BlOFP proteins.

SUPPLEMENTARY FIGURE 2
Sequence alignment of AtOFP6, BlOFP3 and BlOFP6.

SUPPLEMENTARY FIGURE 3
Transgenic *Arabidopsis* plants confirmation with PCR and qRT-PCR. **(A)** PCR amplification of *BlOFP3* and *BlOFP5* genes in transgenic lines and WT. **(B)** PCR amplification of hygromycin and GUS in WT and 35S::BlOFP3 transgenic lines. **(C)** PCR amplification of hygromycin and GUS in WT and 35S::BlOFP5 transgenic lines. **(D)** Expression analysis of *BlOFP3* in 35S::BlOFP3 transgenic lines by qRT-PCR. **(E)** Expression analysis of *BlOFP5* in 35S::BlOFP5 transgenic lines by qRT-PCR. The size of the PCR products indicated in Kb. The asterisk indicates significant difference compared to WT at $p<0.05$ level.

SUPPLEMENTARY FIGURE 4
Expression analysis of *AtOFP6* in transgenic plants.

References

Belles-Boix, E., Hamant, O., Witiak, S. M., Morin, H., Traas, J., and Pautot, V. (2006). KNAT6: An arabidopsis homeobox gene involved in meristem activity and organ separation. *Plant Cell* 18 (8), 1900–1907. doi: 10.1105/tpc.106.041988

Blanco, F., Salinas, P., Cecchini, N. M., Jordana, X., Van Hummelen, P., Alvarez, M. E., et al. (2009). Early genomic responses to salicylic acid in arabidopsis. *Plant Mol. Biol.* 70, 79–102. doi: 10.1007/s11103-009-9458-1

Cai, M., Huang, H., Ni, F., Tong, Z., Lin, E., and Zhu, M. (2018). RNA-Seq analysis of differential gene expression in betula luminifera xylem during the early stages of tension wood formation. *PeerJ* 6, e5427. doi: 10.7717/peerj.5427

Chen, C., Chen, H., Zhang, Y., Thomas, H. R., Frank, M. H., He, Y., et al. (2020). TBtools: An integrative toolkit developed for interactive analyses of big biological data. *Mol. Plant* 13, 1194–1202. doi: 10.1016/j.molp.2020.06.009

Clough, S. J., and Bent, A. F. (1998). Floral dip: A simplified method for agrobacterium-mediated transformation of arabidopsis thaliana. *Plant J.* 16, 735–743. doi: 10.1046/j.1365-313x.1998.00343.x

Forslund, K., and Sonnhammer, E.L.J.E.G. (2012). "Evolution of protein domain architectures," in *Evolutionary genomics. methods in molecular biology*, vol. 856. Ed. M. Anisimova (Totowa, New Jersey, USA: Humana Press), 187–216.

Hackbusch, J., Richter, K., Müller, J., Salamini, F., and Uhrig, J. F. (2005). A central role of arabidopsis thaliana ovate family proteins in networking and subcellular localization of 3-aa loop extension homeodomain proteins. *PNAS* 102, 4908–4912. doi: 10.1073/pnas.0501181102

Hamant, O., and Pautot, V. (2010). Plant development: A TALE story. *C. R. Biol.* 333 (4), 371–381. doi: 10.1016/j.crvi.2010.01.015

Hasson, A., Plessis, A., Blein, T., Adroher, B., Grigg, S., Tsiantis, M., et al. (2011). Evolution and diverse roles of the CUP-SHAPED COTYLEDON genes in arabidopsis leaf development. *Plant Cell* 23 (1), 54–68. doi: 10.1105/tpc.110.081448

Hay, A., Barkoulas, M., and Tsiantis, M. (2006). ASYMMETRIC LEAVES1 and auxin activities converge to repress *BREVIPEDICELLUS* expression and promote leaf development in *Arabidopsis*. 133, 20, 3955–3961. doi: 10.1242/dev.02545

Hay, A., and Tsiantis, M. (2009). A KNOX family tale. *Curr. Opin. Plant Biol.* 12 (5), 593–598. doi: 10.1016/j.pbi.2009.06.006

Hay, A., and Tsiantis, M. (2010). KNOX genes: Versatile regulators of plant development and diversity. *Development* 137 (19), 3153–3165. doi: 10.1242/dev.030049

Knaap, E. V. D., and Ostergaard, L. (2018). Shaping a fruit: Developmental pathways that impact growth patterns. *Semin. Cell Dev. Biol.* 79, 27–36. doi: 10.1016/j.semcdb.2017.10.028

Kumar, R., Kushalappa, K., Godt, D., Pidkowich, M. S., Pastorelli, S., Hepworth, S. R., et al. (2007). The arabidopsis BEL1-LIKE HOMEODOMAIN proteins SAW1 and SAW2 act redundantly to regulate KNOX expression spatially in leaf margins. *Plant Cell* 19 (9), 2719–2735. doi: 10.1105/tpc.106.048769

Kumar, S., Stecher, G., Li, M., Knyaz, C., and Tamura, K. (2018). MEGA X: Molecular evolutionary genetics analysis across computing platforms. *Mol. Biol. Evol.* 35, 1547–1549. doi: 10.1093/molbev/msy096

Li, E., Bhargava, A., Qiang, W., Friedmann, M. C., Forneris, N., Savidge, R. A., et al. (2012). The class II KNOX gene KNAT7 negatively regulates secondary wall formation in arabidopsis and is functionally conserved in populus. *New Phytol.* 194, 102–115. doi: 10.1111/j.1469-8137.2011.04016.x

Li, H., Dong, Q., Zhu, X., Zhao, Q., and Ran, K. (2019). Genome-wide identification, expression, and interaction analysis for ovate family proteins in peach. *Mol. Biol. Rep.* 46 (4), 3755–3764. doi: 10.1007/s11033-019-04817-4

Li, Z., Li, B., Liu, J., Guo, Z., Liu, Y., Li, Y., et al. (2016). Transcription factors AS1 and AS2 interact with LHP1 to repress KNOX genes in arabidopsis. *J. Integr. Plant Biol.* 58 (12), 959–970. doi: 10.1111/jipb.12485

Li, X. Y., Lin, E. P., Huang, H. H., Niu, M. Y., Tong, Z. K., and Zhang, J. H. (2018). Molecular characterization of SQUAMOSA PROMOTER BINDING PROTEIN-LIKE (SPL) gene family in betula luminifera. *Front. Plant Sci.* 9, 608. doi: 10.3389/fpls.2018.00608

Li, Z., Li, B., Shen, W. H., Huang, H., and Dong, A. (2017). TCP Transcription factors interact with AS2 in the repression of class-I KNOX genes in arabidopsis thaliana. *Plant J.* 71 (1), 99–107. doi: 10.1111/j.1365-313X.2012.04973.x

Liu, Y., and Douglas, C. J. (2015). A role for OVATE FAMILY PROTEIN1 (OFP1) and OFP4 in a BLH6-KNAT7 multi-protein complex regulating secondary cell wall formation in arabidopsis thaliana. *Plant Signal Behav.* 10, e1033126. doi: 10.1080/15592324.2015.1033126

Liu, D., Sun, W., Yuan, Y., Zhang, N., Hayward, A., Liu, Y., et al. (2014). Phylogenetic analyses provide the first insights into the evolution of OVATE family proteins in land plants. *Ann. Bot.* 113, 1219–1233. doi: 10.1093/aob/mcu061

Liu, J., Van Eck, J., Cong, B., and Tanksley, S. D. (2002). A new class of regulatory genes underlying the cause of pear-shaped tomato fruit. *PNAS* 99, 13302–13306. doi: 10.1073/pnas.162485999

Livak, K. J., and Schmittgen, T. D. (2001). Analysis of relative gene expression data using real-time quantitative PCR and the 2– ΔΔCT method. *Methods* 25, 402–408. doi: 10.1006/meth.2001.1262

Li, E., Wang, S., Liu, Y., Chen, J. G., and Douglas, C. J. (2011). OVATE FAMILY PROTEIN4 (OFP4) interaction with KNAT7 regulates secondary cell wall formation in arabidopsis thaliana. *Plant J.* 67(2), 328–341. doi: 10.1111/j.1365-313X.2011.04595.x

Long, J. A., Moan, E. I., Medford, J. I., and Barton, M. K. (1996). A member of the KNOTTED class of homeodomain proteins encoded by the STM gene of arabidopsis. *Nature* 379 (6560), 66–69. doi: 10.1038/379066a0

Mistry, J., Chuguransky, S., Williams, L., Qureshi, M., Salazar, G. A., Sonnhammer, E. L., et al. (2021). Pfam: The protein families database in 2021. *Nucleic Acids Res.* 49 (D1), D412–D419. doi: 10.1093/nar/gkaa913

Moore, A. D., Björklund, Å.K., Ekman, D., Bornberg-Bauer, E., and Elofsson, A. (2008). Arrangements in the modular evolution of proteins. *Trends Biochem. Sci.* 33, 444–451. doi: 10.1016/j.tibs.2008.05.008

Nakayama, H., Nakayama, N., Seiki, S., Kojima, M., Sakakibara, H., Sinha, N., et al. (2014). Regulation of the KNOX-GA gene module induces heterophyllic alteration in north American lake cress. *Plant Cell* 26 (12), 4733–4748. doi: 10.1105/tpc.114.130229

Pagnussat, G. C., Yu, H. J., and Sundaresan, V. (2007). Cell-fate switch of synergid to egg cell in arabidopsis eostre mutant embryo sacs arises from misexpression of the BEL1-like homeodomain gene BLH1. *Plant Cell* 19, 3578–3592. doi: 10.1105/tpc.107.054890

Rodríguez, G. R., Muños, S., Anderson, C., Sim, S. C., Michel, A., Causse, M., et al. (2011). Distribution of SUN, OVATE, LC, and FAS in the tomato germplasm and the relationship to fruit shape diversity. *Plant Physiol.* 156 (1), 275–285. doi: 10.1104/pp.110.167577

Rosin, F. M., Hart, J. K., Horner, H. T., Davies, P. J., and Hannapel, D. J. (2003). Overexpression of a knotted-like homeobox gene of potato alters vegetative development by decreasing gibberellin accumulation. *Plant Physiol.* 132 (1), 106–117. doi: 10.1104/pp.102.015560

Salojarvi, J., Smolander, O. P., Nieminen, K., Rajaraman, S., Safronov, O., Safdari, P., et al. (2017). Genome sequencing and population genomic analyses provide insights into the adaptive landscape of silver birch. *Nat. Genet.* 49, 904–912. doi: 10.1038/ng.3862

Schmitz, A. J., Begcy, K., Sarath, G., and Walia, H. (2015). Rice ovate family protein 2 (OFP2) alters hormonal homeostasis and vasculature development. *Plant Sci.* 241, 177–188. doi: 10.1016/j.plantsci.2015.10.011

Sun, X., Ma, Y., Yang, C., and Li, J. (2020). Rice OVATE family protein 6 regulates leaf angle by modulating secondary cell wall biosynthesis. *Plant Mol. Biol.* 104, 249–261. doi: 10.1007/s11103-020-01039-2

Tang, Y., Zhang, W., Yin, Y. L., Feng, P., Li, H. L., and Chang, Y. (2018). Expression of ovate family protein 8 affects epicuticular waxes accumulation in arabidopsis thaliana. *Bot. Stud.* 59, 12. doi: 10.1186/s40529-018-0228-8

Tsaballa, A., Pasentsis, K., Darzentas, N., and Tsaftaris, A. S. (2011). Multiple evidence for the role of an ovate-like gene in determining fruit shape in pepper. *BMC Plant Biol.* 11 (1), 1–16. doi: 10.1186/1471-2229-11-46

Wang, S., Chang, Y., and Ellis, B. (2016). Overview of OVATE FAMILY PROTEINS, a novel class of plant-specific growth regulators. *Front. Plant Sci.* 7, 417. doi: 10.3389/fpls.2016.00417

Wang, S., Chang, Y., Guo, J., and Chen, J. G. (2007). Arabidopsis ovate family protein 1 is a transcriptional repressor that suppresses cell elongation. *Plant J.* 50, 858–872. doi: 10.1111/j.1365-313X.2007.03096.x

Wang, S., Chang, Y., Guo, J., Zeng, Q., Ellis, B. E., and Chen, J. G. (2011). Arabidopsis ovate family proteins, a novel transcriptional repressor family, control multiple aspects of plant growth and development. *PloS One* 6, e23896. doi: 10.1371/journal.pone.0023896

Wang, Y. K., Chang, W. C., Liu, P. F., Hsiao, M. K., Lin, C. T., Lin, S. M., et al. (2010). Ovate family protein 1 as a plant Ku70 interacting protein involving in DNA double-strand break repair. *Plant Mol. Biol.* 74, 453–466. doi: 10.1007/s11103-010-9685-5

Wang, H., Kong, F., and Zhou, C. (2021). From genes to networks: The genetic control of leaf development. *J. Integr. Plant Bio.* 63 (7), 1181–1196. doi: 10.1111/jipb.13084

Wu, S., Zhang, B., Keyhaninejad, N., Rodriguez, G. R., Kim, H. J., Chakrabarti, M., et al. (2018). A common genetic mechanism underlies morphological diversity in fruits and other plant organs. *Nat. Commun.* 9, 4734. doi: 10.1038/s41467-018-07216-8

Yang, C., Ma, Y., He, Y., Tian, Z., and Li, J. (2018). OsOFP19 modulates plant architecture by integrating the cell division pattern and brassinosteroid signaling. *Plant J.* 93, 489–501. doi: 10.1111/tpj.13793

Yang, C., Shen, W., He, Y., Tian, Z., and Li, J. (2016). OVATE family protein 8 positively mediates brassinosteroid signaling through interacting with the GSK3-like kinase in rice. *PloS Genet.* 12, e1006118. doi: 10.1371/journal.pgen.1006118

Yoo, S. D., Cho, Y. H., and Sheen, J. (2007). Arabidopsis mesophyll protoplasts: A versatile cell system for transient gene expression analysis. *Nat. Protoc.* 2, 1565–1572. doi: 10.1038/nprot.2007.199

Zhang, L., Zhang, X., Ju, H., Chen, J., Wang, S., Wang, H., et al. (2016). Ovate family protein1 interaction with BLH3 regulates transition timing from vegetative to reproductive phase in arabidopsis. *Biochem. Biophys. Res. Commun.* 470, 492–497. doi: 10.1016/j.bbrc.2016.01.135

Zhou, S., Cheng, X., Li, F., Feng, P., Hu, G., Chen, G., et al. (2019). Overexpression of SlOFP20 in tomato affects plant growth, chlorophyll accumulation, and leaf senescence. *Front. Plant Sci.* 10, 510. doi: 10.3389/fpls.2019.01510

Zhou, R., Fan, M., Zhao, M., Jiang, X., and Liu, Q. (2022). Overexpression of *LtKNOX1* from *Lilium tsingtauense* in *Nicotiana benthamiana* affects the development of leaf morphology. *Plant Signal Behav.* 17, 1. doi: 10.1080/15592324.2022.2031783

frontiers | Frontiers in Plant Science

TYPE Original Research
PUBLISHED 04 January 2023
DOI 10.3389/fpls.2022.1058522

OPEN ACCESS

EDITED BY
Jana Krajnakova,
New Zealand Forest Research Institute Limited (Scion), New Zealand

REVIEWED BY
Maria Pilar Valles,
Aula Dei Experimental Station (CSIC), Spain
Polina Yu. Novikova,
Max Planck Institute for Plant Breeding Research, Germany

*CORRESPONDENCE
Rie Shimizu-Inatsugi
rie.inatsugi@ieu.uzh.ch

SPECIALTY SECTION
This article was submitted to Plant Development and EvoDevo, a section of the journal Frontiers in Plant Science

RECEIVED 30 September 2022
ACCEPTED 30 November 2022
PUBLISHED 04 January 2023

CITATION
Shimizu-Inatsugi R, Morishima A, Mourato B, Shimizu KK and Sato Y (2023) Phenotypic variation of a new synthetic allotetraploid *Arabidopsis kamchatica* enhanced in natural environment. *Front. Plant Sci.* 13:1058522. doi: 10.3389/fpls.2022.1058522

Phenotypic variation of a new synthetic allotetraploid *Arabidopsis kamchatica* enhanced in natural environment

Rie Shimizu-Inatsugi[1]*, Aki Morishima[1], Beatriz Mourato[1], Kentaro K. Shimizu[1,2] and Yasuhiro Sato[1]

[1]Department of Evolutionary Biology and Environmental Studies, University of Zurich, Zurich, Switzerland, [2]Kihara Institute for Biological Research, Yokohama City University, Yokohama, Japan

The phenotypic variation of vegetative organs and reproductive organs of newly synthesized and natural *Arabidopsis kamchatica* genotypes was investigated in both a controlled environment and a natural environment in an experimental garden. When we compared the variation of their leaf shape as a vegetative organ, the synthetic *A. kamchatica* individuals grown in the garden showed larger variation compared with the individuals incubated in a growth chamber, suggesting enhanced phenotypic variation in a natural fluctuating environment. In contrast, the natural *A. kamchatica* genotypes did not show significant change in variation by growth condition. The phenotypic variation of floral organs by growth condition was much smaller in both synthetic and natural *A. kamchatica* genotypes, and the difference in variation width between the growth chamber and the garden was not significant in each genotype as well as among genotypes. The higher phenotypic variation in synthetic leaf may imply flexible transcriptomic regulation of a newly synthesized polyploid compared with a natural polyploid.

KEYWORDS

polyploid, neopolyploid, phenotypic variation, vegetative organ, *in natura*, *Arabidopsis*

Introduction

Allopolyploid species have been considered to possess higher intraspecific phenotypic diversity, as a nature of its merged genomes from two closely relative but distinct species (Paterson, 2005; Van de Peer et al., 2017). The allopolyploid genome can be considered as a permanent heterozygote in this sense. In fact, many agriculturally or ecologically important polyploid plants are reported to have transgressive, intermediate,

or wider phenotypes beyond progenitors (Comai, 2005; Gallego-Tévar et al., 2018; Shimizu, 2022). For this reason, polyploidization has been considered as one of the most important motive forces for evolution by expanding phenotypic diversity. However, polyploidization accompanies a genetic bottleneck due to the limited number of progenitors involved in the establishment of a polyploid population. Thus, the genetic variation could have only limited contribution to the phenotypic diversity of a newly synthesized polyploid group. Even if the genetic diversity will be restored by introgression, multiple origins, and new mutations gradually (Shimizu-Inatsugi et al., 2009; Novikova et al., 2017; Paape et al., 2018), the newly synthesized polyploid should cope with the reduced genetic diversity for speciation. Thus, in addition to genetic diversity, phenotypic variation within the same genotype would be more important at the beginning of a new polyploid group. The intraspecific phenotypic diversity might also contribute to widen the habitat range of a species (Westerband et al., 2021), most probably by higher adaptive ability for dispersal. In fact, some invasive species have been found to have higher phenotypic diversity than natives (Funk, 2008; Hiatt and Flory, 2020). It is also consistent with the theoretically expected wider distribution of polyploid species or the distribution at extreme environments (Rice et al., 2019), assuming that polyploid had higher phenotypic diversity.

Several factors can cause phenotypic diversity within the same genotype. Developmental noise in ontogeny would be an important factor to realize the phenotypic diversity within the same genotype, which could also be stimulated by environmental factors (Westerband et al., 2021). In addition, epigenetic diversity may be another important factor for phenotypic diversity, which is also supported by a previous study showing phenotypic disturbance in the mutant line lacking DNA methylase (Kakutani et al., 1996) as well as by famous examples of phenotypic variation caused by single epialleles in floral symmetry of antirrhinum (Cubas et al., 1999) or fruit ripening (Manning et al., 2006). At the early stage of polyploid species with reduced genetic diversity, epigenetic diversity produced by the genome merge would play a crucial role to generate high phenotypic diversity as reviewed by Shimizu (2022).

In this study, we quantitatively investigated the difference in phenotypic variation between new and established polyploids and statistically evaluated how the environment can influence their variation. We regenerated a new allotetraploid by crossing *A. halleri* subsp. *gemmifera* and *A. lyrata* subsp. *petraea* mimicking the natural allotetraploid species *A. kamchatica*. By using selfing lines, we can focus on phenotypic variation within the same genotype. The natural and synthetic *A. kamchatica* were incubated in continuous and stable conditions in a growth chamber and in a fluctuating natural environment in an experimental garden. The range of phenotypic diversity between synthetic and established lines as well as the change of that range according to environments are compared by examining two hypotheses: 1) Does the range of phenotypic variation differ between new and established polyploids? 2) Is the phenotypic variation higher in naturally fluctuating environments than in regulated chambers? At last, we will discuss the evolutionary significance of polyploid phenotypic variation.

Materials and methods

Plant incubation

We incubated two natural *A. kamchatica* lines, from Alaska, US (ALK, GPS coordinates: 63.42, 145.84) and Murodo, Japan (MRD, GPS coordinates: 36.58, 137.60), and two synthetic *A. kamchatica* lines (RS2 and RS7). The natural lines were self-fertilized for at least twice in the laboratory after the collection from natural populations. Considering that they are selfing species, additional selfings in the lab should have made them highly homogeneous. The synthetic lines are produced by crossing *A. halleri* subsp. *gemmifera* (Japan) (maternal, GPS coordinates: 35.10, 134.92) and *A. lyrata* subsp. *petraea* (Russia, GPS coordinates: 68.8, 160.3) (paternal). Both of the diploid lines are also nearly homogenous because the former was repeatedly self-fertilized by bud pollination and the latter is originally self-compatible and self-fertilized twice in the laboratory (Briskine et al., 2017; Paape et al., 2018). The F1 hybrid diploid individuals were polyploidized by colchicine treatment on seedling (RS2) or autonomously without colchicine treatment (RS7), and the second generation of a selfed tetraploid offspring was used for this experiment, which also made these lines highly homogeneous. They were incubated either in a growth chamber (22˚C / 20˚C, 16 h light/8 h dark, 60% relative humidity) or in the experimental garden located at the Irchel campus of University of Zurich (Zurich, Switzerland) in 2015 and 2016, independently. For the garden experiment, the plants were first incubated in the chamber for 2–3 weeks and then transplanted to the garden plot in November to be incubated there until July the next year.

Leaf and flower collection and measurement

The leaf samples (except for ALK in 2015 in the garden) and flower samples (except for 2015 in the garden) were collected soon after they started flowering. It was about 4 months after the germination (including 6 weeks of vernalization at 4˚C as seedlings) for the chamber individuals and from February to June for the garden individuals. We selected mature leaves and fully and newly open flowers for sampling. The sample sizes (summarized in Supplementary Table S1) were unbalanced among lines (5 to 104 in leaf and 7 to 79 in flower) due to the high variation of growth speed as

well as flowering period among lines. Leaves were pressed and fixed on a paper by transparent sticky tape immediately after the collection (as seen in Figure 1A). Flowers were immediately dissected into each organ, and all parts were pressed and fixed on a paper by transparent sticky tape (as seen in Figure 1B). Each trait was measured on the specimen using a digital caliper. The detailed position of each trait is shown in Figures 1B, C (flower) and Figure 1D (leaf). We counted the number of each organ in one flower. For petals and sepals, we measured the length and width and measured the length of stamens and pistils. Blade length represents the distance from the tip of the blade to the bottom of the last lobe. Top represents the distance from the tip of the blade to the widest point of the blade. These traits as well as blade width were independently measured on the right and left sides, and thus two values of R (right) and L (left) are available.

To calculate the ratio of the two factors, we first calculated the ratio of each leaf/side to take the average of all replicates. To calculate the leaf shape uniformity on R and L, we first took the difference between the two values (R and L) to calculate the difference from their mid-value in percent figures and then took the average among replicates.

All the visualization and statistical analyses were performed using R version 4.0.3 (R Core Team, 2020). The coefficient of variation (i.e., CV = standard deviation/average) was first calculated as an index of phenotypic variation. To statistically test whether the phenotypic variation in each trait was significantly different among the genotypes (comparing four genotypes in the same growth condition) or among the growth conditions (comparing the same genotype between two or among three growth conditions), we then used the Levene test to compare variance among the groups. The null hypothesis of

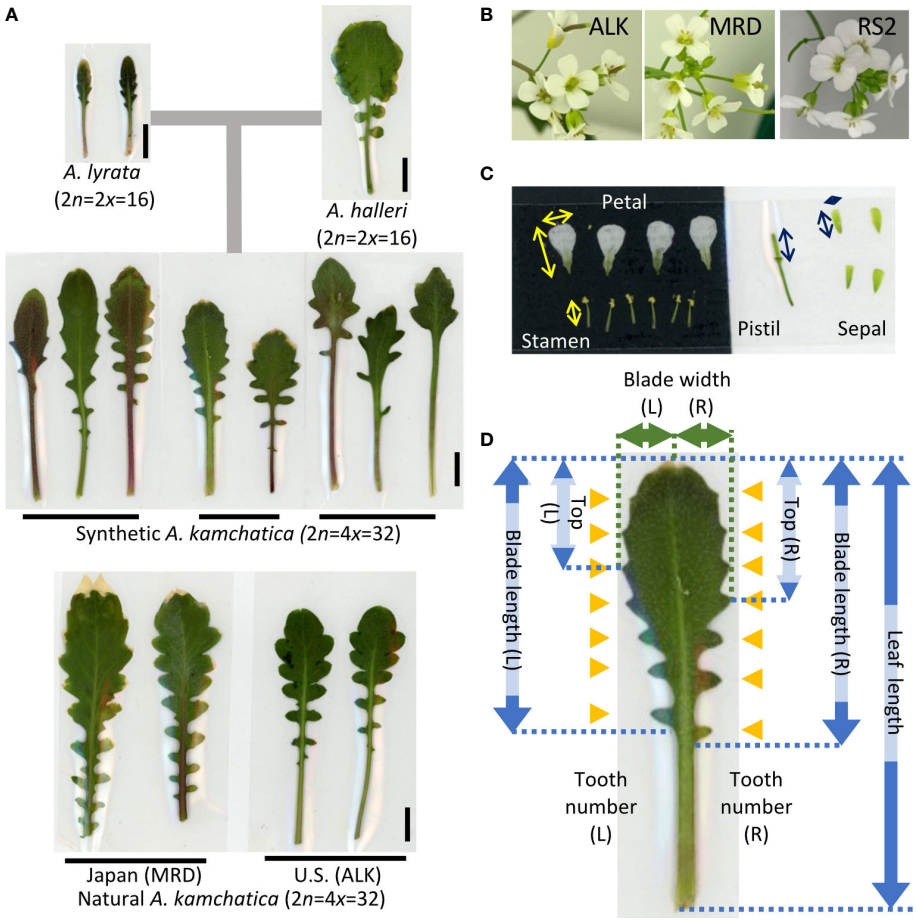

FIGURE 1
Representative leaf and flower shape of *A. kamchatica* and the traits used for the analysis. **(A)** Representative leaves of diploid progenitors, and synthetic and natural *A. kamchatica* genotypes grown in the chamber. The horizontal lines suggest the leaves collected from the same individual. The vertical lines indicate 1 cm. **(B)** Representative flowers of *A. kamchatica*, ALK, MRD and RS2. **(C)** An example of pressed floral organs. The arrows indicate the measured positions of each organ, vertical (length) and horizontal (width). **(D)** The positions of measured traits on leaf morphology. The arrows indicate the length or width of each trait, and the orange triangles indicate the position of leaf tooth on R (right) and L (left) sides, respectively.

the Levene test was equal phenotypic variation among the groups. The alternative hypothesis indicated statistically significant differences of phenotypic variation among the groups. To make the Levene test robust against the distribution of each phenotype, we combined Brown–Forsythe tests for the group median (Brown and Forsythe, 1974) with zero correction (Noguchi and Gel, 2010). *P*-values were determined by 1,000-times bootstraps to deal with the unbalanced sample size. To perform this robust-type Levene test, we used the levene.test function of the lawtest package (Gastwirth et al., 2020) implemented in R. The result of the Levene test is summarized in Supplementary Tables S2, S3 as the category of *P*-values ($P < 0.05$, $P < 0.01$, $P < 0.001$), and the result among genotypes is referred in text as needed.

Results

Leaf morphology

We first compared the traits that were directly measured, i.e., leaf size and shape, of each genotype in different growth conditions, i.e., in a growth chamber and in an experimental garden, for two seasons of 2015 and 2016. As many of the leaves were not perfectly symmetrical, we measured some traits independently on both the right side (R) and left side (L). Generally, the leaf lengths of all genotypes of synthetic and natural lines are longer in the chamber compared with those in the garden (Figure 2A). A similar trend was observed in the blade length and blade width except for ALK (Figures 2B, C),

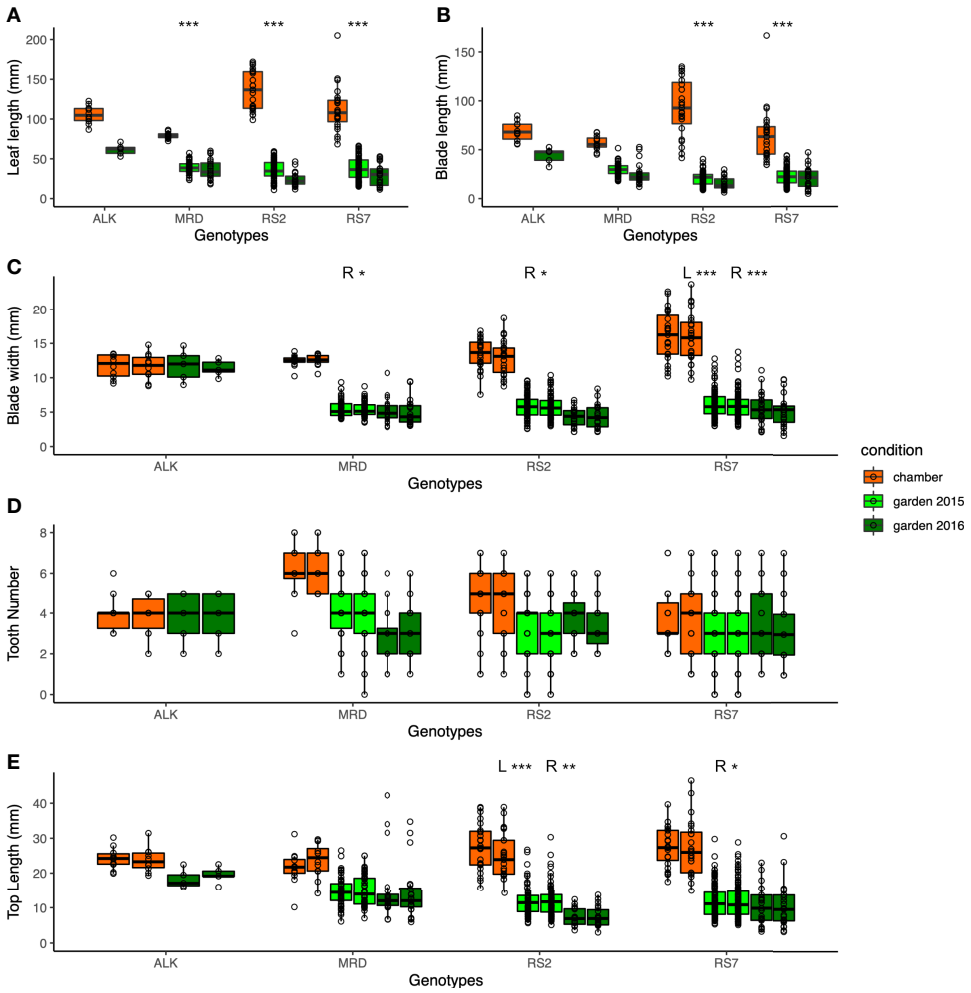

FIGURE 2
The traits representing the size and the shape of leaves. **(A)** Leaf length (mm). **(B)** Blade length (mm). **(C)** Blade width (mm). **(D)** Tooth number. **(E)** Top length (mm). Two neighboring columns in the same color in **(C–E)** represent the values of the left side (left) and right side (right) of leaves. The number of asterisks above the columns represents the category of *P* values (*$P < 0.05$; **$P < 0.01$; ***$P < 0.001$) by Levene test to examine the statistical significance of variation in each trait among growth conditions. When the test is conducted independently on the left and right sides, the result is shown as L and R.

suggesting the harsher condition of the garden generally making the leaf size smaller. We also evaluated the statistical significance of the width of variation by Levene test whether each genotype shows different phenotypic variation between the growth conditions, except for ALK due to its small sample size as well as lack of incubation in the garden in 2015. The other three genotypes showed high significance in leaf length, and two synthetic lines but not MRD showed significant difference between the growth conditions when the blade length and blade width on one or both sides were analyzed (Table S2).

As a proxy of the complexity of the pinnately lobed leaf, we counted the number of tooth points on R and L of the leaf blade, representing the lobe number. Compared with the blade size change, the tooth number on each blade showed smaller change except for a few lines. In the chamber, the tooth number was generally similar between R and L in natural lines but the synthetic lines had a slightly wider variation (Figure 2D). The variation became slightly greater in natural lines in the garden in 2015 and 2016, but no statistical significance was detected by Levene test (Table S2). Another trait representing the leaf complexity, the length from the tip to the widest point of each blade (top length), showed a large decrease in the garden than in the chamber in synthetic lines, but not in ALK and MRD (Figure 2E).

In all leaf morphology traits, the synthetic lines generally showed a larger decrease in the garden compared with the chamber. In addition, the range of each trait as calculated by CV value was larger in the garden than in the chamber (Table 1) in most traits and genotypes, suggesting the larger variation of phenotype. Levene test also supported these differences in phenotypic variation between the growth conditions for many of the traits (Table S2). In summary, among the four genotypes, two synthetic lines showed larger changes and variations against growth conditions.

Leaf shape balance on right and left sides

As the measured values of leaf length and width turned out to be vulnerable to the environment, we investigated the aspect ratio and right-and-left balance of the blade as proxies of leaf shape variation. We calculated the aspect ratio of the blade (blade length/sum of right and left width) (Figure 3A) as well as the top and blade length ratio for each right and left sides (Figure 3B). While ALK and RS2 showed a decrease in blade aspect ratio in the garden, MRD and RS7 did not show a big change in the value. The top and blade length ratio changed drastically only in RS2 but not in the other three genotypes. In the sense of phenotypic variation between the growth conditions, Levene test detected a significant difference in variation for the blade aspect ratio only in RS2 and for the top and blade length ratio in both RS2 and RS7. These results suggest the wider phenotypic variation of leaf morphology in synthetic lines in the garden than in the chamber, whereas that of natural lines was similar between garden and chamber. On the other hand, the variation among the genotypes showed a significant difference in chamber and garden 2015 conditions in many traits (Table S2), supporting the difference among the genotypes.

We also investigated the leaf shape unevenness on the right side and left side by calculating the difference (%) of R and L of each factor in each leaf (Table 2), in which the larger number suggests the larger imbalance between the right and left sides. The unevenness in blade width, tooth number, top length, and blade W/L ratio was higher in synthetic lines than in natural ones in the chamber. The unevenness was slightly enhanced in natural lines, but not in the synthetic lines in the garden. This result suggests that the leaf shape unevenness of right and left sides in synthetic lines is high regardless of environment and that of natural lines is low in stable conditions but can be enhanced by fluctuating conditions.

TABLE 1 CV values of each leaf trait.

Genotype	Incubation	Leaf length	Blade length	Blade width		Tooth number		Top length	
				Left	Right	Left	Right	Left	Right
ALK	Chamber	0.11	0.15	0.15	0.17	0.24	0.25	0.13	0.15
ALK	2016 garden	0.11	0.19	0.20	0.10	0.34	0.34	0.15	0.12
MRD	Chamber	0.05	0.13	0.07	0.07	0.23	0.18	0.23	0.21
MRD	2015 garden	0.19	0.22	0.23	0.21	0.31	0.38	0.29	0.30
MRD	2016 garden	0.35	0.45	0.35	0.38	0.46	0.42	0.62	0.56
RS2	Chamber	0.18	0.31	0.17	0.20	0.37	0.37	0.25	0.27
RS2	2015 garden	0.35	0.33	0.28	0.28	0.39	0.43	0.36	0.37
RS2	2016 garden	0.38	0.43	0.32	0.40	0.34	0.38	0.35	0.40
RS7	Chamber	0.26	0.44	0.23	0.23	0.39	0.48	0.21	0.30
RS7	2015 garden	0.36	0.36	0.32	0.33	0.48	0.46	0.39	0.42
RS7	2016 garden	0.45	0.54	0.42	0.44	0.49	0.52	0.53	0.62

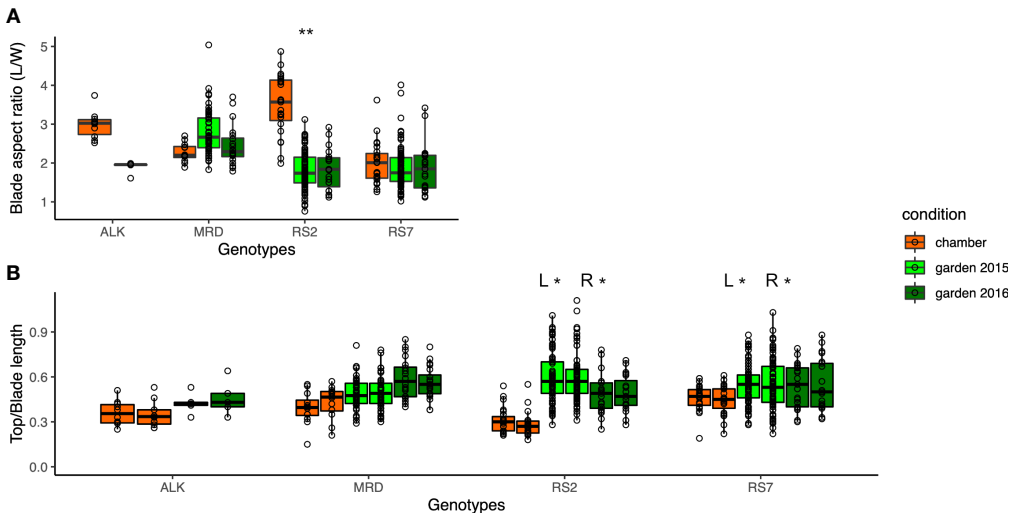

FIGURE 3
The traits representing the balance of the blade shape. **(A)** Blade aspect ratio is calculated by dividing the blade length by the sum of the left- and right-blade width. **(B)** Ratio of top length is calculated by dividing the top length by the blade length, representing the relative size of the upper round part of the leaf. The asterisk represents the P-value by Levene test (*: P<0.05; **: P<0.01; ***: P<0.001).

Flower morphology

In comparison with the shape of leaf as a vegetative organ, we also analyzed the phenotypic variation of flower as a reproductive organ. The number and size of four floral organs (sepal, petal, stamen, and pistil) were measured after dissection. The number of each organ was largely stable in both chamber and garden except for few flowers (Table 3). The variation was found only in the sepal and petal numbers of synthetic lines in chamber, and the stamen number was the most variable found in all genotypes in either or both chamber and garden. We did not find any variation of pistil number in any lines and conditions. Overall, the variation in floral organ number was very limited, suggesting the robustness in flower whorl development against external stimuli. The variations of floral organ numbers were not significant among the four genotypes grown in the same condition (chamber or garden) (Levene test, $p > 0.05$), except for the stamen number among four genotypes in chamber ($p < 0.001$).

The size of each organ tends to be smaller in the garden than in the chamber. Compared with leaf size, which could be less than half in the garden than in the chamber, the decrease in floral organ size was smaller. The petal length and width, which might reflect the flower size the best, decreased most drastically in RS7 but less in RS2 and natural lines (Figures 4A–D). A similar level of decrease was found in stamen and pistil sizes (Figures 4E, F). The decrease in their size was slightly smaller in

TABLE 2 The unevenness of the right side and left side of a leaf.

		Blade width			Tooth number			Top			Blade length/width		
Genotype	Incubation	Average (%)		SD	Average (%)		SD	Average (%)		SD	Average (%)		SD
ALK	Chamber	1.33	±	0.89	2.01	±	3.51	2.32	±	1.23	1.33	±	0.89
ALK	2016 garden	3.41	±	2.12	4.00	±	5.48	1.79	±	2.24	3.41	±	2.12
MRD	Chamber	0.86	±	0.70	1.98	±	3.72	4.22	±	3.74	0.86	±	0.70
MRD	2015 garden	2.43	±	1.87	5.10	±	9.05	3.77	±	3.00	2.43	±	1.87
MRD	2016 garden	4.97	±	4.47	7.24	±	9.63	4.31	±	4.38	4.97	±	4.47
RS2	Chamber	3.36	±	3.62	3.96	±	5.41	4.52	±	4.09	3.36	±	3.62
RS2	2015 garden	2.87	±	2.39	5.97	±	10.27	4.28	±	3.85	2.87	±	2.39
RS2	2016 garden	3.94	±	3.50	3.58	±	4.09	2.24	±	1.99	3.94	±	3.50
RS7	Chamber	2.21	±	1.77	6.75	±	6.40	4.40	±	2.95	2.21	±	1.77
RS7	2015 garden	2.34	±	2.00	5.40	±	10.53	4.48	±	3.82	2.34	±	2.00
RS7	2016 garden	2.82	±	2.09	5.08	±	6.54	2.91	±	2.78	2.82	±	2.09

TABLE 3 The number of floral organs.

		Sepal			Petal			Stamen		
Genotype	Incubation	Average (%)		SD	Average (%)		SD	Average (%)		SD
ALK	Chamber	4.00	±	0.00	4.00	±	0.00	5.98	±	0.16
ALK	2016 garden	4.00	±	0.00	4.00	±	0.00	6.00	±	0.00
MRD	Chamber	4.00	±	0.00	4.00	±	0.00	6.00	±	0.00
MRD	2016 garden	4.00	±	0.00	4.00	±	0.00	5.88	±	0.35
RS2	Chamber	3.97	±	0.16	3.96	±	0.19	5.73	±	0.55
RS2	2016 garden	4.00	±	0.00	4.00	±	0.00	6.00	±	0.00
RS7	Chamber	4.05	±	0.28	4.04	±	0.41	6.01	±	0.38
RS7	2016 garden	4.00	±	0.00	4.00	±	0.00	5.89	±	0.33

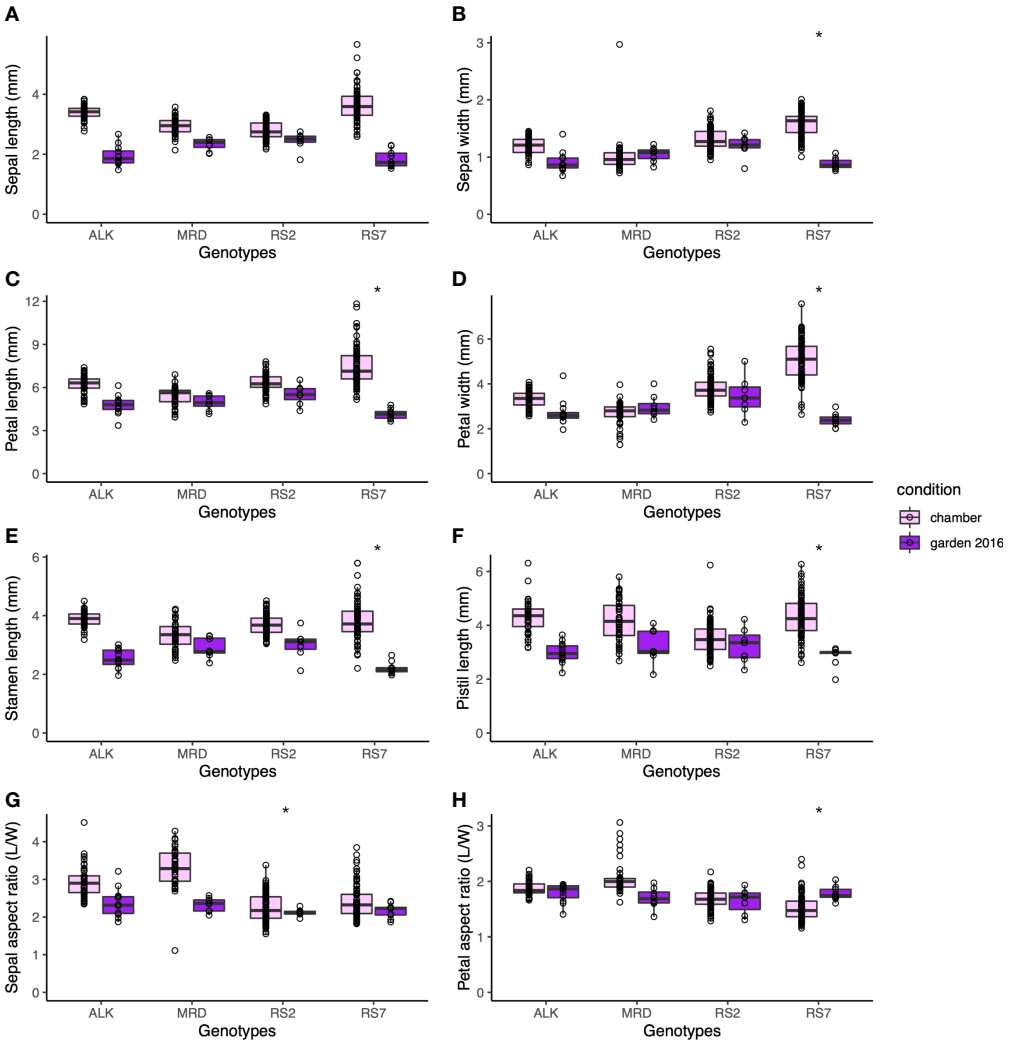

FIGURE 4
The traits representing the size and shape of floral organs. Sepal length **(A)** and width **(B)**. Petal length **(C)** and width **(D)**. **(E)** Stamen length. **(F)** Pistil length. **(G)** Sepal aspect ratio, length divided by width. **(H)** Petal aspect ratio, length divided by width. The asterisk represents the P-value by Levene test (*: P<0.05; **: P<0.01; ***: P<0.001).

MRD and RS2 than in ALK and RS7, but statistical significance was only detected in most organs in RS7. These results suggest that the effect of the environment on floral organ shape in each genotype was smaller than that on leaf shape. In other words, floral organ shape had higher stability against external stimuli, and a small variation in phenotypic plasticity among conditions was found only in RS7 (Table S3, $p < 0.05$).

Consistent with the robustness of length of each factor, the aspect ratios of sepal and petal were also stable among genotypes and conditions (Figures 4G, H). Compared with the sepal aspect ratio for which natural lines showed a slight change in the two conditions, the petal aspect ratio was very similar to each other in all genotypes and conditions. Levene test detected the significant difference in variation between conditions only in the sepal aspect ratio of RS2 (Table S3, $p < 0.05$). This result means that even if the ultimate size of the floral organs changes according to conditions, their shape hardly changes.

Size balance between reproductive organs

We next focused on the relative size between floral organs, as it may affect the auto-pollination of *A. kamchatica* as a selfing species. We calculated three indices of the relative length, stamen/petal, pistil/petal, and stamen/pistil, depending on their lengths. All indices did not show a significant difference among genotypes and between conditions (Figure 5). It suggests that the relative positions of these organs were maintained in spite of the size variation of these organs. In addition, the variations of each index did not have a significant difference in variation between conditions except for the stamen/pistil of MRD ($p < 0.001$), in which the variation was bigger in the garden. Nevertheless, the morphology of floral organs was much less variable among genotypes and between conditions compared with the leaf shape (Figure 3), and most of all, the phenotypic variation in the same genotype was not affected by growth condition. This result implies the developmental robustness of the morphology of floral organs by strict genetic control behind.

Discussion

Phenotypic variation of vegetative organs larger in a natural environment than in a chamber

In this study, we investigated the width of phenotypic variation of both leaves and flowers, using two natural and two synthetic genotypes of allotetraploid species *A. kamchatica*. We examined the difference of phenotypic variation in constant growth conditions in a chamber and in naturally fluctuating conditions in an experimental garden. Floral organs showed similar sizes and shapes between conditions as well as among genotypes (Figure 4). In addition, the width of phenotypic variation between two conditions was not significantly different in most traits in both natural and synthetic lines (Table S2). In contrast, a wider range of organ size as well as organ shape was found in leaves among genotypes and conditions, which we could detect as larger values of CV in leaf (Table 1) than those in flower (Table 4). Especially, the

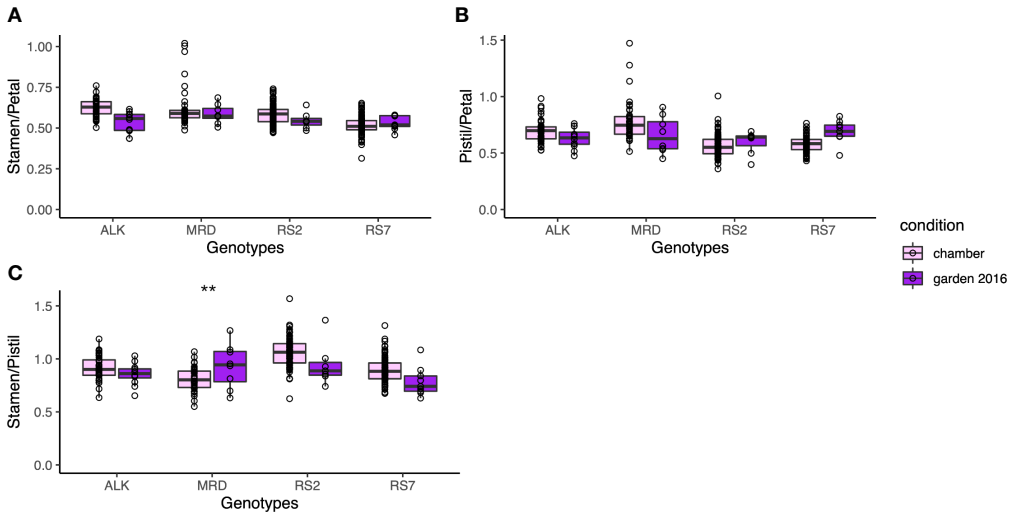

FIGURE 5
The traits representing the relative position of each organ. **(A)** Ratio of stamen length and petal length. **(B)** Ratio of pistil length and petal length. **(C)** Ratio of stamen length and pistil length. The asterisk represents the P-value by Levene test (*: P<0.05; **: P<0.01; ***: P<0.001).

phenotypic variation of many leaf shape traits was amplified by a natural condition, detected as much lower *p*-values by Levene test among growth conditions in synthetic genotypes than natural genotypes (Figure 2 and Table S2).

Furthermore, even when significant variation was found in the actual size of floral organ among genotypes or conditions, the traits representing the relative length between organs or the shape of each organ showed more uniform values among genotypes. The relative length of stamens and a pistil was stable around 1.0 without significant difference among genotypes and conditions (Figure 5), suggesting the importance of keeping their ratio close for successful self-pollination. On the other hand, the petal aspect ratio was also one of the least variable traits among genotypes. The fact that the flower sizes of natural allotetraploid with old origin of approximately 0.1 M years old (Tsuchimatsu et al., 2012; Paape et al., 2018) and synthetic tetraploid with new origin are very similar may also support the importance of outcrossing, instead of flower downsizing by selfing syndrome. Assuming that the flower shape is most largely influenced by petal size and shape, this may imply the significance of outcrossing even in this self-compatible species.

In previous studies, large intraspecific phenotypic variation of flower tended to attract more interest of studies and thus many reports about outstanding phenotypic variations, e.g., dimorphism (Potente et al., 2022), color shift (Gómez et al., 2020), and impact of environment on phenotype (March-Salas et al., 2021), have been published. In contrast, reports dealing with the lack of phenotypic variation can be barely found. Yet, in some species, lack of phenotypic variation in reproductive organs might also represent an important significance in evolution, reflecting some selective pressure.

While leaf morphology showed generally larger variations in size and shape than floral organs among genotypes as well as conditions, the synthetic lines tend to have larger variations in most traits. Most importantly, the range of phenotypic variation of synthetic lines but not natural lines was amplified by fluctuating conditions in the garden, in spite of the lack of genetic variation among individuals. In the previous study evaluating phenotypic plasticity of worldwide genotype collection of allopolyploid and diploid wild strawberry, no difference in plasticity was found between ploidy levels (Wei et al., 2019). These results may suggest that established polyploid species reduce their plasticity at the early step of "diploidization of polyploid" or adaptation. Our study further adds an insight about the difference between established and new polyploids, showing higher phenotypic variation of new polyploids than established polyploids. When we compared the balance of size between right and left sides of a leaf, the unevenness of synthetic lines was only slightly larger than that of the natural lines (Table 2), suggesting that the symmetrical development is still under some regulation if not perfect. This suggests that these variations in synthetic *A. kamchatica* did not occur stochastically as evoked by the idea of "genome shock" by polyploidization (Bird et al., 2018).

How does new polyploid show larger phenotypic variation, and can it be advantageous?

Although generally large phenotypic variation or instability of newly synthesized polyploid has been recognized and reported so far (Madlung et al., 2002; Chen, 2007), this is the first study to compare the effect of the environment to examine the magnifying effect of the fluctuating environment on the width of variation. Although some previous papers report large polyploid variation in controlled conditions, the variation might have been even larger if they had been conducted in the wild environment.

The genetic variation in natural lines should be low due to multiple times self-fertilization in the lab, and that of synthetic lines should be even lower, theoretically null, due to their diploid hybrid origins before polyploidization. In spite of lower genetic variation, both of the two synthetic lines showed significantly larger variation in most leaf phenotypic traits than natural lines. These high phenotypic variations may be attributed to the variation of the epigenetic status (Chen, 2007; Schmid et al., 2018). Allopolyploidization is known to change the progenitors' patterns of DNA methylation, generating a new pattern in early

TABLE 4 CV values of each flower trait.

Genotype	Incubation	Sepal length	Sepal width	Petal length	Petal width	Stamen length	Pistil length
ALK	Chamber	0.07	0.12	0.10	0.11	0.07	0.14
ALK	2016 garden	0.17	0.20	0.14	0.22	0.13	0.13
MRD	Chamber	0.10	0.34	0.13	0.19	0.14	0.19
MRD	2016 garden	0.09	0.12	0.10	0.17	0.12	0.19
RS2	Chamber	0.10	0.14	0.10	0.16	0.09	0.17
RS2	2016 garden	0.12	0.17	0.13	0.25	0.17	0.20
RS7	Chamber	0.15	0.14	0.18	0.18	0.17	0.17
RS7	2016 garden	0.16	0.11	0.09	0.13	0.10	0.13

generations of allopolyploids (Yuan et al., 2020; Jiang et al., 2021). Even though the direct effect of DNA methylome variation on phenotype (Seymour and Becker, 2017) as well as the effect of a fluctuating environment on DNA methylation is not clear yet, our results imply that a fluctuating environment may stimulate the width of epigenetic status.

Considering the fact that a polyploidization event changes the epigenetic patterns of progenitors genomes in the new polyploid genome, this enhancement of variation should be derived from the wider transcriptomic pattern of neopolyploids in natural condition. This phenotypic enhancement could contribute to the adaptation of neopolyploids. Indeed, in our preliminary analysis of transcriptomic patterns of new synthetic polyploids of *A. kamchatica*, a larger variation among biological triplicates compared with natural polyploids has been observed (unpublished data), which is consistent with this idea. Polyploidization usually works as a genetic bottleneck in evolution, as only a limited number and genotype of progenitors contribute to the establishment of a new polyploid species (Shimizu-Inatsugi et al., 2009; Novikova et al., 2017). Nevertheless, polyploidization was considered as a motive force in evolution. A higher phenotypic variation of a new polyploid might contribute to solve this contradiction.

After polyploidization, offspring of early generations may undergo adaptation to new habitats. As a consequence, the epigenetic status should be stabilized according to time. This might be the reason we detected less phenotypic variation among conditions in established natural genotypes in this study or in a previous report (Wei et al., 2019). In addition, the difference in the reaction norm of our two natural populations could be attributed to their distinct adaptation measures to distinct habitats, ALK from a high-latitude population in Alaska and MRD from a low-latitude but high-altitude population in Japan.

In conclusion, we propose the positive effect of a fluctuating environment on the wider possibility of phenotypic diversification in polyploid species. The higher phenotypic variation of the polyploid in nature at the early stage of speciation may provide higher chances of adaptation to a wider habitat, assuming that epigenetic variation can be inherited. They will undergo natural selection in each habitat, and their epigenetic status will get stabilized again in the course of time, expanding the habitat to a wider (Akiyama et al., 2021) or even harsher environment (Rice et al., 2019) than progenitors. They will also obtain their own genetic variation advantageous in each habitat, but the speed of genetic evolution is much slower than that of epigenetic evolution, and thus epigenetic variation may be a major contributing factor at the early stage of speciation. The epigenetic variation among isogenic individuals right after polyploidization as well as its significance on phenotypes should be addressed in future studies. In addition, the investigation of not only morphological but also physiological variation would be needed to further understand the significance of polyploidy in evolution.

Data availability statement

The original contributions presented in the study are included in the article/Supplementary Material. Further inquiries can be directed to the corresponding author.

Author contributions

RS-I planned the experiment. AM and BM acquired the phenotypic data. RS-I and YS analyzed the data. KS, YS, and RS-I wrote the manuscript. All authors contributed to the article and approved the submitted version.

Funding

This study was supported by the Swiss National Science Foundation (31003A_182318, 31003A_159767), JST CREST (PMJCR16O3), JSPS Kakenhi 22H05179, URPP Evolution in Action, and URPP Global Change and Biodiversity of the University of Zurich.

Acknowledgments

We thank Dr. Reiko Akiyama and Dr. Lucas Mohn for their kind support for the plant incubation at the experimental garden.

Conflict of interest

The authors declare that the research was conducted in the absence of any commercial or financial relationships that could be construed as a potential conflict of interest.

Publisher's note

Supplementary material

The Supplementary Material for this article can be found online at: https://www.frontiersin.org/articles/10.3389/fpls.2022.1058522/full#supplementary-material

References

Akiyama, R., Sun, J., Hatakeyama, M., Lischer, H. E.L., Briskine, R. V., Hay, A., et al. (2021). Fine-scale empirical data on niche divergence and homeolog expression patterns in an allopolyploid and its diploid progenitor species. *New Phytol.* 229 (6), 3587–3601. doi: 10.1111/nph.17101

Bird, K. A., VanBuren, R., Puzey, J. R., and Edger, P. P. (2018). The causes and consequences of subgenome dominance in hybrids and recent polyploids. *New Phytologist.* 220 (1), 87–93. doi: 10.1111/nph.15256

Briskine, R. V., Paape, T., Shimizu-Inatsugi, R., Nishiyama, T., Akama, S., Sese, J., et al. (2017). Genome assembly and annotation of arabidopsis halleri, a model for heavy metal hyperaccumulation and evolutionary ecology. *Mol. Ecol. Resour.* 17 (5), 1025–1036. doi: 10.1111/1755-0998.12604

Brown, M. B., and Forsythe, A. B. (1974). Robust tests for the equality of variances. *J. Am. Stat. Assoc.* 69 (346), 364–367. doi: 10.1080/01621459.1974.10482955

Chen, Z. J. (2007). Genetic and epigenetic mechanisms for gene expression and phenotypic variation in plant polyploids. *Annu. Rev. Plant Biol* 58, 377–406. doi: 10.1146/annurev.arplant.58.032806.103835

Comai, L. (2005). The advantages and disadvantages of being polyploid. *Nat. Rev. Genet* 6, 836–846. doi: 10.1038/nrg1711

Cubas, P., Vincent, C., and Coen, E. (1999). An epigenetic mutation responsible for natural variation in floral symmetry. *Nature.* 401 (6749), 157–161. doi: 10.1038/43657

Funk, J. L. (2008). Differences in plasticity between invasive and native plants from a low resource environment. *J. Ecol.* 96, 1162–1173. doi: 10.1111/j.1365-2745.2008.01435.x

Gallego-Tévar, B., Rubio-Casal, A. E., de Cires, A., Figueroa, E., Grewell, B. J., Castillo, J. M., et al. (2018). Phenotypic plasticity of polyploid plant species promotes transgressive behaviour in their hybrids. *AoB Plants.* 10 (5). doi: 10.1093/aobpla/ply055

Gastwirth, J. L., Gel, Y. R., Hui, W. L. W., Lyubchich, V., Miao, W., Noguchi, K., et al. (2020). 'lawstat: Tools for biostatistics, public policy, and law," in *R package version 3.4.*

Gómez, J. M., Perfectti, F., Armas, C., Narbona, E., González-Megías, A., Navarro, L., et al. (2020). Within-individual phenotypic plasticity in flowers fosters pollination niche shift. *Nat. Commun.* 11 (1). doi: 10.1038/s41467-020-17875-1

Hiatt, D., and Flory, S. L. (2020). Populations of a widespread invader and co-occurring native species vary in phenotypic plasticity1. *New Phytol.* 225, 584–594. doi: 10.1111/nph.16225

Jiang, X., Song, Q., Ye, W., and Chen, Z. J. (2021). Concerted genomic and epigenomic changes accompany stabilization of arabidopsis allopolyploids. *Nat. Ecol. Evol.* 5, 1382–1393. doi: 10.1038/s41559-021-01523-y

Kakutani, T., Jeddeloh, J. A., Flowers, S. K., Munakata, K., and Richards, E. J. (1996). Developmental abnormalities and epimutations associated with DNA hypomethylation mutations. *Proc. Natl. Acad. Sci. United States America.* 93 (22), 12406–12411. doi: 10.1073/pnas.93.22.12406

Madlung, A., Masuelli, R. W., Watson, B., Reynolds, S. H., Davison, J., Comai, L., et al. (2002). Remodeling of DNA methylation and phenotypic and transcriptional changes in synthetic arabidopsis allotetraploids. *Plant Physiol.* 129 (2), 733–746. doi: 10.1104/pp.003095

Manning, K., Tör, M., Poole, M., Hong, Y., Thompson, A. J., King, G. J., et al. (2006). A naturally occurring epigenetic mutation in a gene encoding an SBP-box transcription factor inhibits tomato fruit ripening. *Nat. Genet.* 38 (8), 948–952. doi: 10.1038/ng1841

March-Salas, M., Fandos, G., and Fitze, P. S. (2021). Effects of intrinsic environmental predictability on intra-individual and intra-population variability of plant reproductive traits and eco-evolutionary consequences. *Ann. Bot.* 127 (4), 413–423. doi: 10.1093/aob/mcaa096

Noguchi, K., and Gel, Y. R. (2010). Combination of levene-type tests and a finite-intersection method for testing equality of variances against ordered alternatives. *J. Nonparametr. Stat.* 22 (7), 897–913. doi: 10.1080/10485251003698505

Novikova, P. Y., Tsuchimatsu, T., Simon, S., Nizhynska, V., Voronin, V., Burns, R., et al. (2017a). Genome sequencing reveals the origin of the allotetraploid arabidopsis suecica. *Mol. Biol. Evol.* 34 (4), 957–968. doi: 10.1093/molbev/msw299

Novikova, P. Y., Tsuchimatsu, T., Simon, S., Nizhynska, V., Voronin, V., Burns, R., et al. (2017b). Genome sequencing reveals the origin of the allotetraploid Arabidopsis suecica. *Mol. Biol. Evol.* 34, msw299. doi: 10.1093/molbev/msw299

Paape, T., Briskine, R. V., Halstead-Nussloch, G., Lischer, H. E.L., Shimizu-Inatsugi, R., Hatakeyama, M., et al. (2018). Patterns of polymorphism and selection in the subgenomes of the allopolyploid Arabidopsis kamchatica. *Nat. Commun.* 9 (1), 3909. doi: 10.1038/s41467-018-06108-1

Paterson, A. H. (2005). Polyploidy, evolutionary opportunity, and crop adaptation. *Genetica (Springer)* 123, 191–196. doi: 10.1007/s10709-003-2742-0

Potente, G., Léveillé-Bourret, É., Yousefi, N., Choudhury, R. R., Keller, B., Diop, S. I., et al. (2022). Comparative genomics elucidates the origin of a supergene controlling floral heteromorphism. *Mol. Biol. Evol.* 39 (2). doi: 10.1093/molbev/msac035

R Core Team (2020). *R: A language and environment for statistical computing* (Vienna, Austria: R Foundation for Statistical Computing). Available at: https://www.r-project.org/.

Rice, A., Šmarda, P., Novosolov, M., Drori, M., Glick, L., Sabath, N., et al. (2019). The global biogeography of polyploid plants. *Nat. Ecol. Evol.* 3 (2), 265–273. doi: 10.1038/s41559-018-0787-9

Schmid, M. W., Heichinger, C., Coman Schmid, D., Guthörl, D., Gagliardini, V., Bruggmann, R., et al. (2018). Contribution of epigenetic variation to adaptation in arabidopsis. *Nat. Commun.* 9 (1), 1–12. doi: 10.1038/s41467-018-06932-5

Seymour, D. K., and Becker, C. (2017). The causes and consequences of DNA methylome variation in plants. *Curr. Opin. Plant Biol.* 36, 56–63. doi: 10.1016/j.pbi.2017.01.005

Shimizu-Inatsugi, K. K. (2022). Robustness and the generalist niche of polyploid species: Genome shock or gradual evolution? *Curr. Opin. Plant Biol.* 69, 102292. doi: 10.1016/j.pbi.2022.102292

Shimizu-Inatsugi, R., LihovÁ, J., Iwanaga, H., Kudoh, H., Marhold, K., Savolainen, O., et al. (2009). The allopolyploid arabidopsis kamchatica originated from multiple individuals of Arabidopsis lyrata and Arabidopsis halleri. *Mol. Ecol.* 18 (19), 4024–4048. doi: 10.1111/j.1365-294X.2009.04329.x

Tsuchimatsu, T., Kaiser, P., Yew, C.-L., Bachelier, J. B., Shimizu, K. K., et al. (2012). Recent loss of self-incompatibility by degradation of the Male component in allotetraploid arabidopsis kamchatica. *PloS Genet.* 8 (7), e1002838. doi: 10.1371/journal.pgen.1002838

Van de Peer, Y., Mizrachi, E., and Marchal, K. (2017). The evolutionary significance of polyploidy. *Nat. Rev. Genet.* 18 (7), 411–424. doi: 10.1038/nrg.2017.26

Wei, N., Cronn, R., Liston, A., and and Ashman, T. L. (2019). Functional trait divergence and trait plasticity confer polyploid advantage in heterogeneous environments. *New Phytologist.* 221 (4), 2286–2297. doi: 10.1111/nph.15508

Westerband, A. C., Funk, J. L., and Barton, K. E. (2021). Intraspecific trait variation in plants: A renewed focus on its role in ecological processes. *Ann. Bot.* 127, 397–410. doi: 10.1093/aob/mcab011

Yuan, J., Jiao, W., Liu, Y., Ye, W., Wang, X., Liu, B., et al. (2020). Dynamic and reversible DNA methylation changes induced by genome separation and merger of polyploid wheat. *BMC Biol.* 18 (1), 171. doi: 10.1186/s12915-020-00909-x

frontiers | Frontiers in Plant Science

TYPE Original Research
PUBLISHED 09 January 2023
DOI 10.3389/fpls.2022.1058421

OPEN ACCESS

EDITED BY
Jana Krajnakova,
New Zealand Forest Research Institute Limited (Scion), New Zealand

REVIEWED BY
Giorgio Perrella,
University of Milan, Italy
Reeta Bhatia,
Indian Agricultural Statistics Research Institute (ICAR), India
Barbara Wójcikowska,
University of Silesia, Poland

*CORRESPONDENCE
Maria Pilar Vallés
valles@eead.csic.es

SPECIALTY SECTION
This article was submitted to Plant Development and EvoDevo, a section of the journal Frontiers in Plant Science

RECEIVED 30 September 2022
ACCEPTED 07 December 2022
PUBLISHED 09 January 2023

CITATION
Valero-Rubira I, Castillo AM, Burrell MA and Vallés MP (2023) Microspore embryogenesis induction by mannitol and TSA results in a complex regulation of epigenetic dynamics and gene expression in bread wheat. *Front. Plant Sci.* 13:1058421. doi: 10.3389/fpls.2022.1058421

Microspore embryogenesis induction by mannitol and TSA results in a complex regulation of epigenetic dynamics and gene expression in bread wheat

Isabel Valero-Rubira[1], Ana María Castillo[1], María Ángela Burrell[2] and Maria Pilar Vallés[1]*

[1]Departamento de Genética y Producción Vegetal, Estación Experimental de Aula Dei, Consejo Superior de Investigaciones Científicas (EEAD-CSIC), Zaragoza, Spain, [2]Departamento de Patología, Anatomía y Fisiología, Facultad de Ciencias, Universidad de Navarra, Pamplona, Spain

Reprogramming of microspores development towards embryogenesis mediated by stress treatment constitutes the basis of doubled haploid production. Recently, compounds that alter histone post-translational modifications (PTMs) have been reported to enhance microspore embryogenesis (ME), by altering histones acetylation or methylation. However, epigenetic mechanisms underlying ME induction efficiency are poorly understood. In this study, the epigenetic dynamics and the expression of genes associated with histone PTMs and ME induction were studied in two bread wheat cultivars with different ME response. Microspores isolated at 0, 3 and 5 days, treated with 0.7M mannitol (MAN) and 0.7M mannitol plus 0.4μM trichostatin A (TSA), which induced ME more efficiently, were analyzed. An additional control of gametophytic development was included. Microspores epigenetic state at the onset of ME induction was distinctive between cultivars by the ratio of H3 variants and their acetylated forms, the localization and percentage of labeled microspores with H3K9ac, H4K5ac, H4K16ac, H3K9me2 and H3K27me3, and the expression of genes related to pollen development. These results indicated that microspores of the high responding cultivar could be at a less advanced stage in pollen development. MAN and TSA resulted in a hyperacetylation of H3.2, with a greater effect of TSA. Histone PTMs were differentially affected by both treatments, with acetylation being most concerned. The effect of TSA was observed in the H4K5ac localization pattern at 3dT in the mid-low responding cultivar. Three gene networks linked to ME response were identified. *TaHDT1, TaHAG2, TaYAO*, *TaNFD6-A*, *TabZIPF1* and *TaAGO802-B*, associated with pollen development, were down-regulated. *TaHDA15*, *TaHAG3*, *TaHAM, TaYUC11D*, *Ta-2B-LBD16 TaMS1* and *TaDRM3* constituted a network implicated in morphological changes by auxin signaling and cell wall modification up-regulated at 3dT. The last network included *TaHDA18, TaHAC1, TaHAC4, TaABI5*, *TaATG18fD, TaSDG1a-7A* and

was related to ABA and ethylene hormone signaling pathways, DNA methylation and autophagy processes, reaching the highest expression at 5dT. The results indicated that TSA mainly modified the regulation of genes related to pollen and auxin signaling. This study represents a breakthrough in identifying the epigenetic dynamics and the molecular mechanisms governing ME induction efficiency, with relevance to recalcitrant wheat genotypes and other crops.

KEYWORDS

bread wheat, microspore embryogenesis, mannitol, trichostatin A, histones, epigenetics, gene expression

Introduction

Microspore embryogenesis (ME) constitutes a process in which the microspore changes its developmental pathway from a gametophytic towards a sporophytic. This change is triggered by a stress treatment, followed by an *in vitro* culture phase in which embryos and haploid plants are finally formed (Soriano et al., 2013). Doubled haploid (DH) plants can be obtained spontaneously by nuclear fusion or endoreduplication, during the first microspore divisions, or can be induced by the action of chromosome doubling agents (González-Melendi et al., 2005; Griggs and Zheng, 2016). DH plants have a great value to produce new varieties or inbred lines because complete homozygosis is achieved in one generation.

In recent years, increasing evidence has been accumulated on how the dynamics of epigenetic processes regulates gene expression and establishes genomic elements in adaptive responses to developmental transitions. Epigenetic modifications have been reported to play an important role in reproductive development, abiotic stress response and plant regeneration, processes which are involved in ME (Begcy and Dresselhaus, 2018; Lee and Seo, 2018; Mozgova et al., 2019; Ono and Kinoshita, 2021).

Changes in histone post-translational modifications (PTMs), DNA methylation as well as regulation of small RNA and long noncoding RNA pathways have been described as the major epigenetic mechanisms in plants (Pikaard and Scheid, 2014). PTMs of histone-tails can alter the interaction between histones and DNA directly or by recruiting specific effectors such as transcriptional regulators or chromatin remodelers (for review see Tessarz and Kouzarides, 2014). Acetylation and methylation are the two most common histone PTMs involved in activation and repression of transcription, respectively. Histone deacetylases (HDAC) and acetyltransferases (HAT) regulate the balance of histone acetylation by modifying lysine residues, leading to a chromatin compaction/decompaction that facilitates the repression/activation of gene transcription (for review see Bannister and Kouzarides, 2011). Histone lysine residues can be mono-, di- or tri-methylated in a dynamic way by the action of histone lysine methyltransferases (HKMT) and histone demethylases (for review see Bannister and Kouzarides, 2011).

Histone hyperacetylation and DNA hypomethylation have been directly associated to ME induction by the application of a heat stress treatment in the model species *Brassica napus* (Solis et al., 2012; Li et al., 2014a). Furthermore, the application of inhibitors of enzymes involved in the modification of epigenetic marks has been shown to be a successful strategy to increase the efficiency of ME (for review see Testillano, 2019). Thus, trichostatin A (TSA), a HDAC inhibitor acting over acetylation of histones and other proteins related to cytoskeleton, increased the efficiency of microspore reprogramming in *Brassica* (Li et al., 2014a; Zhang et al., 2016) and barley (Pandey et al., 2017). Studies performed in barley indicated that there was a very intricate interaction between the histone acetylation and methylation after TSA application (Pandey et al., 2017). Other histone deacetylases inhibitors such as suberoylanilide hydroxamic acid (SAHA) and sodium butyrate have also been used to enhance ME in *Brassica* (Zhang et al., 2016). Also, the application of 5-azacytidine, which causes a global DNA demethylation, or BIX, a histone lysine methyltransferase inhibitor, promotes ME in *Brassica*, barley and triticale (Solis et al., 2015; Berenguer et al., 2017; Nowicka et al., 2019).

Different approaches have been described for the application of TSA to increase ME efficiency in wheat. Thus, green plant regeneration was enhanced in different cultivars applying TSA in the microspore isolation procedure or in the culture medium, after a cold stress treatment (Jiang et al., 2017; Wang et al., 2019). However, a comparison of different strategies showed that the application of 0.4 μM TSA simultaneously with 0.7 M mannitol for 5 days was the most efficient for DH production, increasing twice and four times the number of green plants compared to mannitol in a high and a mid-low responding bread wheat cultivars, respectively (Castillo et al., 2020).

Although different protocols are available for ME in wheat (Castillo et al., 2021; Jensen et al., 2022), their efficiency depends largely on the genotype (Lantos et al., 2013; Weigt et al., 2019; Castillo et al., 2019). The genetic control of ME is quite complex (Muñoz-Amatriaín et al., 2008; Nielsen et al., 2015; Abd ElFath et al., 2020). Besides the genetic control, the epigenetic state of the microspores before ME induction could also play and important role. Thus, microspores from a high ME responding line of triticale had a higher level of DNA methylation than a low responding one (Nowicka et al., 2019). Different levels of endogenous ABA as well as gene transcripts related to ME have been also described in genotypes with different ME response in *Brassica*, wheat and triticale (Dubas et al., 2013; Sánchez-Díaz et al., 2013; Nowicka et al., 2019).

Little is known about the dynamics of histone PTMs and their impact on transcriptional regulation of wheat ME. A recent study applying TSA after a cold treatment shows that TSA up-regulates genes involved in cell division, DNA organization, signaling cascades, hormone mediated signaling, and cell wall and cytoskeleton modifications (Jensen, 2021). To provide new insights into wheat ME induction mechanisms, the dynamics of acetylation and methylation histone PTMs was analyzed with a mannitol and a mannitol plus TSA treatment, which induced ME more efficiently, in two bread wheat cultivars with different ME response. The expression of genes involved in PTMs and key genes for ME and their correlations were also studied. For the first time, the epigenetic dynamics and gene regulation are discussed in wheat ME induction depending on cultivars and treatments.

Material and methods

Material, growing conditions of the donor plants and harvest of the spikes

The spring cultivars (cvs) of bread wheat Pavon and Caramba, which have a high and a mid-low ME response, respectively, were used in this study. Growth conditions of the mother plants and harvest and sterilization of spikes were performed as described by Castillo et al. (2021). Anthers containing most microspores at the mid to late uninucleated stage, determined by DAPI (4′, 6-Diamidine-2'-phenylindole dihydrochloride) staining were excised and brought under stress treatments. For selection of the spikes at this stage of development, tillers with 3-5 cm length from the distal part of the spike to the basal part of the flag leaf were harvested. Some spikes were harvested two days later to allow microspores to progress into gametophytic development (GD).

Application of TSA in combination with a mannitol stress treatment

Comparison of different TSA application strategies showed that the incorporation of TSA in a mannitol treatment was the best to enhance wheat ME (Castillo et al., 2020). Therefore, the effect of 0.4 μM TSA (Sigma T8852) in combination with 0.7 M mannitol stress treatment was assayed. TSA was dissolved in 1% DMSO (final concentration in the medium). Freshly excised anthers were randomly distributed in 6 cm Ø Petri dishes containing solidified 0.7 M mannitol stress medium (SM medium, Castillo et al., 2021) (MAN) or in mannitol plus 0.4 μM TSA (TSA) (Castillo et al., 2020) and placed in the dark at 25°C. Microspores from anthers after 3 and 5 days of MAN (3dT-MAN, 5dT-MAN) and TSA (3dT-TSA, 5dT-TSA) treatments from Pavon and Caramba were isolated following the protocol described by Castillo et al. (2000). Isolated microspores from freshly harvested anthers (0dT) were used as control. In addition, isolated microspores at GD were used as a second control to discriminate the gametophytic and the sporophytic pathways.

Protein Analysis by Western blot

Isolated microspores of Pavon and Caramba from 0dT, GD, 3dT-MAN, 5dT-MAN, 3dT-TSA, and 5dT-TSA were used. Leaves from 30 day-old plants, young embryos (14 days after pollination) and pollen grains were also included in this analysis. Proteins were extracted using the buffer containing 150 mM NaCl, 2 mM EDTA and 50 mM NaH_2PO_4, 2% SDS, pH 6. After homogenization, samples were boiled (95°C 10 min) and centrifuged twice at 15000 g, 10 min at 4°C. Protein extracts were quantified using Qubit Protein BR Assay kit following manufacturer's instructions in fluorimeter Qubit4. Ten μg of total proteins from all samples, except from embryos (5 μg), were electrophoresed on a Mini-PROTEAN TGX 12% SDS-PAGE gel under reducing conditions. Proteins were transferred to a polyvinylidene difluoride membrane and blocked with 5% BSA in TBS-T (20 mM Tris, 150 mM NaCl, pH 7.5, and 0.1% Tween 20). The blots were incubated for 2 h with anti-histone H3 (clone A3S, Millipore), anti-histone H4 (clone 62-141-13, Millipore), anti-pan-acetyl-histone H3 (K9, K14, K18, K23, K27) (ab47915, Abcam) or anti-pan-acetyl-histone H4 (K5, K8, K12, K16) (PA1-84526 Invitrogen), all of them at 1:1000 dilution. Secondary goat anti-rabbit IgG peroxidase conjugated antibody (AP132P, Millipore) was used at a 1:1000 dilution and signals were detected using enhanced chemiluminescence (Clarity Western ECL substrate, BIORAD). Western blot was performed in two independent biological replicates.

Immunofluorescence analysis

Isolated microspores of both cultivars from 0dT, GD, 3dT-MAN, 5dT-MAN, 3dT-TSA, and 5dT-TSA were fixed in 4% paraformaldehyde and 2% sucrose in PBS, pH 7.3, overnight at 4°C. After three washes in PBS for 10 min, microspores were pre-embedded in 2% agarose and post-fixed in the same fixative solution during 2 h at 4°C. The samples were washed twice in PBS before being dehydrated in an ethanol series (30, 50 and 70%) at 4°C, processed in an automatic Vacuum Infiltration Processor (Sakura 4893-Floor E150, BAYER, Barcelona, Spain), and embedded in paraffin blocks. Four µm-thick sections were cut using a rotary microtome (Microm HM 340E, Bio Optica, Milan, Italy) with steel blades, and were collected on special slides (Menzel-Glaser, J1800AMNN, Braunschweig, Germany) to facilitate their adherence and avoid their loss during the performance of the immunohistochemical techniques.

The sections were deparaffinized with xylene and rehydrated with graded ethanol to water. Before the incubation with the primary antibodies, samples were treated with 0.05 M NH_4Cl and 0.05 M $NaBH_4$ in TBS (0.05 M TRIS, 0.5 M NaCl, pH 7.36) to partially reduce the autofluorescence of aldehydes (highly abundant in the exine of microspores) and were blocked with a 2% BSA solution at RT. The following primary antibodies, raised in rabbit, were used: anti-histone H3K9ac (EMD Millipore, Cat. No. 06-942; dilution 1:100), anti-histone H4K5ac (EMD Millipore, Cat. No. 07-327; dilution 1:100), anti-histone H4K16ac (EMD Millipore, Cat. No. 07-329; dilution 1:100), anti-histone H3K9me2 (EMD Millipore, Cat. No. 07-441; dilution 1:100) and anti-histone H3K27me3 (EMD Millipore, Cat. No. 07-449; dilution 1:50). The samples were incubated with primary antibodies overnight at 4°C. Goat anti-rabbit Alexa Fluor 488 (Sigma, Cat. No. SAB4600044; dilution 1:100) was applied as secondary antibody during 30 min at RT. Fluoromount G with DAPI (Invitrogen, Cat. No. 00-4959-52) was used as an aqueous mounting medium.

To study the localization pattern of epigenetic marks and to quantify the number of labeled microspores and nuclei, an inverted microscope Nikon Eclipse-T300 was used and fluorochrome Alexa Fluor 488 was excited at 460 nm, and emission was detected with a 505-520 nm long-pass filter. Microspores nuclei were counterstained with DAPI, excited at 350 nm in combination with a 400-420 nm long-pass filter. Images were recorded by the Digital sight DS-5MC camera with NIS-D software. Immunohistochemical analysis was performed in two independent biological replicates, containing an average of five technical replicates for each mark (H3K9ac, H4K5ac, H4K16ac, H3K9me2 and H3K27me3). An average of 1500 and 1000 microspores and 400 and 250 nuclei from Pavon and Caramba were analyzed, respectively.

Identification of selected genes in the wheat genome

Genes associated with ME induction response were selected based on a previous study performed in barley (Sánchez-Díaz, 2014). In this study, an Affymetrix Barley1 GeneChip microarray analysis was carried out on anthers before stress treatment, after 4 days of 0.7 M mannitol treatment, and after 4 and 8 days of culture, following the procedures described in Muñoz-Amatriaín et al. (2006). Identification and clustering of the differentially expressed genes allowed the selection of candidate genes that characterized barley ME induction. Among them, 20 barley probe set related to HDACs, HATs, and major processes involved in ME induction were selected (Supplementary Table 1).

Wheat genes with homology to barley probe set were identified based on sequence homology by BLASTN of barley sequences exported from HarvEST : Barley version 2.26 (http://www.harvest.ucr.edu), against *Triticum aestivum* IWGSC (Genomic sequence) on Ensembl Plants, which hosts the RefSeq v1.0 assembly from the IWGSC (http://plants.ensembl.org/Triticum_aestivum/Tools/Blast) or against WheatExp: An Expression Database for Polyploid Wheat (https://wheat.pw.usda.gov/WheatExp/). Overlapping genes with higher scores were selected, and homologues genes in bread wheat and orthologues in *Arabidopsis thaliana* and *Oryza sativa* Japonica Group were identified on Ensembl Plants. Only *TaMS1* gene was directly selected from literature (Supplementary Table 1).

If primers were not available in the literature, the cDNA sequence of genes based on Ensembl Plants/*Triticum_aestivum* was used for designing specific primer pairs by Primer-BLAST (NCBI), which uses Primer3 (Ye et al., 2012) (Supplementary Table 2).

Selected genes ontology analyses were performed based on RefSeq v1.0 assembly by AgriGO v2.0, a database (Tian et al., 2017) (Supplementary Table 3).

Transcript level analysis by quantitative RT-PCR

Total RNA of three independent biological replicates from 0dT, GD, 3dT-MAN, 5dT-MAN, 3dT-TSA, and 5dT-TSA from Pavon and Caramba was isolated using TRIzol Reagent (Ambion, Life technologies) and passed through RNeasy columns (Qiagen) for further clean up. Double-stranded cDNA was synthesized using the M-MLV Reverse Transcriptase kit from Promega. qRT-PCR reactions were performed with PowerUp SYBR Green Master Mix (Applied Biosystems) and ROX (ROX Reference Dye, Invitrogen). The reaction conditions were optimized at: 95°C for 10 min, followed by 40 cycles of 95°C for 15 s and 60°C for 1 min, in the QuantStudio3 System (Applied Biosystems), using the *Ta.27771* and *Ta.2291* as reference genes (Paolacci et al., 2009). Two technical replicates were performed for each biological replicate in each gene.

Gene expression pattern in different stresses and tissues in a wheat *in silico* analysis

The expVIP Wheat Expression Browser (http://www.wheat-expression.com) was used to study the expression of selected genes in different studies (Ramírez-González et al., 2018). The relative transcript abundance (per 10 million reads) from each gene obtained from the databases was presented as a heat map (Graphad Prism 7).

Statistical analysis

A densitometry analysis was performed on images of western blotting membranes, obtained in the ChemiDoc Imaging System (BIO-RAD), using the gel analyzer tool from Image-J software. Densitometry data allowed the estimation of the H3.1/H3.2, H3.1ac/H3.1, H3.2ac/H3.2 and H4ac/H4 ratios. In the immunofluorescence analysis, the following variables were calculated: the percentage of labeled microspores, that is, the number of microspores with each epigenetic marks over the total number of microspores, and the percentage of labeled nuclei, that is, the number of microspores with each epigenetic marks in the nuclei over the total number of microspores stained with DAPI. Normality and homogeneity of variance were tested using the Shapiro-Wilk and Levene´s tests, respectively. Data from the qRT-PCR reactions were analyzed using the Livak (2-ΔΔCT) calculation method (Livak and Schmittgen, 2001). For the calculation of the standard errors, the values of the relative expression level (2-ΔΔCT) were used. For statistical analysis, the values of fold change (2 -ΔΔCT) were transformed with log2 to correct the heterogeneity of variance. A one-way analysis of variance (ANOVA) was used, and significant differences among treatments were determined by the Duncan test ($p \leq 0.05$). Statistical analysis of these variables was performed using IBM SPSS statistics version 27.0.1. (IBM Corp, 2020).

All possible pairwise correlations of the expression of the studied genes over samples were calculated using Pearson´s coefficient. A principal component analysis (PCA) was performed to analyze the association between relative gene expression and the course of ME inducing treatments, using the program R 4.1.3 (R Core Team, 2021).

Results

Histone H3 and H4 acetylation dynamics in microspore embryogenesis induction

To determine if MAN and TSA treatments modified microspores global histone acetylation, a western blot assay was performed using a pan-acetylated Lys antibody for histones H3 and H4 (Figures 1A, B). Antibodies against unmodified histone H3 and H4 were used as controls. In the text, only statistically significant differences were described. However, in some cases a tendency to statistical significance has been described as slight.

Two histone H3 variants with different molecular weight (17 KDa and 14 KDa, approximately) were detected in both cultivars (Figure 1A). These proteins corresponded to the major H3.1 variant and the minor H3.2 variant (H3.3-type, Waterborg, 1991). Quantitative analysis of the H3.1/H3.2 ratio showed a low value at 0dT, which increased greatly with MAN and TSA treatments, reaching the highest value at 5dT (Figure 1C). This ratio was higher with TSA than with MAN in both cultivars at 3dT. Given the change in the H3.1/H3.2 ratio during ME induction, the study was extended to young zygotic embryos, leaves, and GD, including mature pollen grains (Supplementary Figure 1A). The two variants were observed in all samples, although there were differences between cultivars, particularly in leaves (Supplementary Figures 1A, B). It was noteworthy the increase of H3.1/H3.2 in mature pollen (P) in both cultivars (Supplementary Figure 1B). Embryos showed the highest and the lowest amount of H3.1 and H3.2 variants, respectively, but quantification of H3.1/H3.2 was not possible.

Acetylation of both H3.1 and H3.2 variants was observed in all microspore samples (Figure 1A). The highest H3.1ac/H3.2ac ratio was showed at 0dT, and treatments reduced this ratio in both cultivars, especially at 3dT (Figure 1D). However, it increased greatly at 5dT-MAN in Pavon. Acetylation ratio of each variant was also studied (Figures 1E, F). At 0dT, H3.1ac/H3.1 was twice higher in Caramba than in Pavon. MAN and TSA treatments increased this ratio in Pavon but decreased it in Caramba (Figure 1E). H3.2ac/H3.2 had low and similar values at 0dT, but MAN and TSA induced H3.2 acetylation in both cultivars (Figure 1F). However, TSA enhanced acetylation up to approximately 4-fold over MAN at 3dT and 5dT in Pavon, but 1.5-fold only at 3dT in Caramba.

Analysis with H4 antibody showed that it was acetylated in all samples at a similar ratio to those of H3.1 variant (Figures 1B, E, G). It should be noted that MAN caused a slight decrease in H4 acetylation at 3dT in both cultivars, followed by an increase at 5dT in Caramba, reaching similar values in both cultivars (Figure 1G). The acetylation ratio at 3dT-TSA was slightly higher than at 3dT-MAN, but similar values were observed at 5dT.

Immunolocalization and dynamics of epigenetic marks in wheat microspores

Epigenetic dynamics were characterized by the pattern of intracellular localization and the percentage of labeled

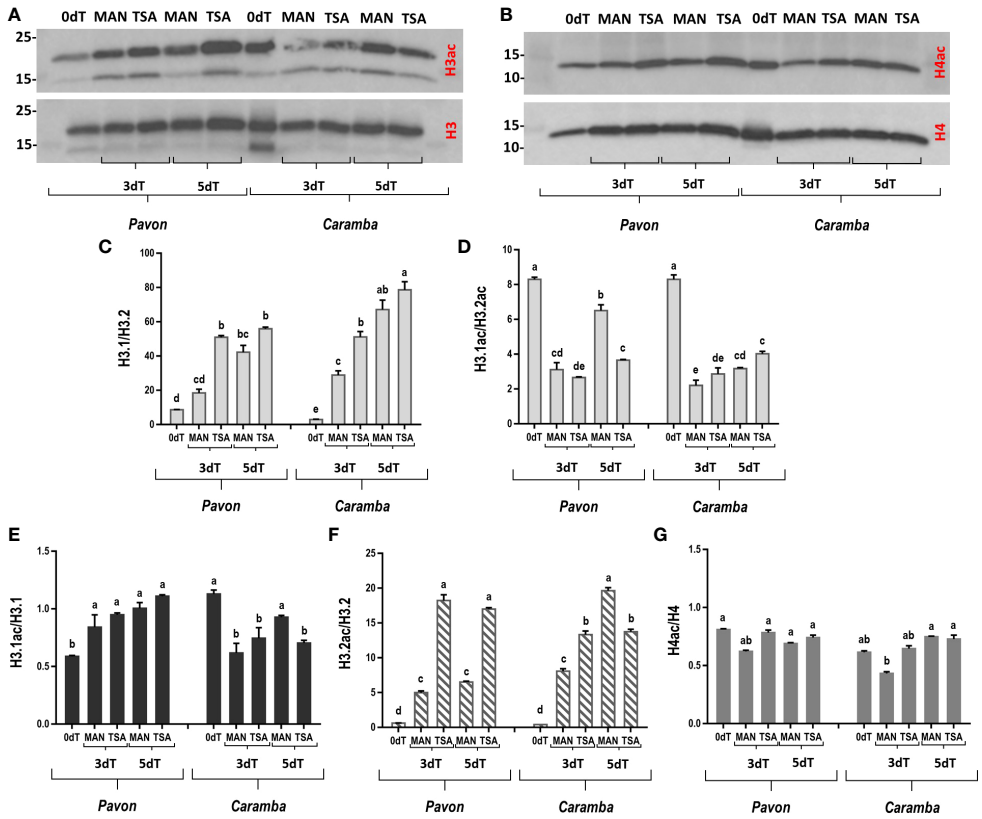

FIGURE 1
Effect of MAN and TSA treatments on histones H3 and H4 acetylation. **(A, B)** Immunoblot of histones H3 and H4 and pan-acetylated H3 and H4 (H3ac and H4ac, respectively). **(C, D)** Quantitative analysis of the H3.1/H3.2 and H3.1ac/H3.2ac ratios, respectively. **(E, F)** Quantitative analysis of the H3.1 and H3.2 acetylation ratio **(G)** Quantitative analysis of the H4 acetylation ratio. Microspores before stress treatment (0dT), after 3 and 5 days with mannitol treatment (3dT-MAN, 5dT-MAN), and after 3 and 5 days with mannitol plus TSA treatment (3dT-TSA, 5dT-TSA) from Pavon (on the left) and Caramba (on the right). Bars represent the standard errors of the means. Histone H3.1/H3.2, H3.1ac/H3.2ac, H3.1ac/H3.1, H3.2ac/H3.2 and H4ac/H4 ratios with the same letter within each ratio are not significantly different (P<0.05) according to the Duncan test.

microspores or nuclei with specific antibodies for histone acetylation (H3K9ac, H4K5ac, H4K16ac) and methylation (H3K9me2 and H3K27me3). The percentage of labeled nuclei was only noted if it was different from that of the labeled microspores.

Uninucleate microspores from the two cultivars at 0dT showed large differences in epigenetic state, although they were at a similar morphological stage of development according to microscopic visualization. The sum of the percentages of microspores with acetylation marks was 35.85% in Pavon but only 9.29% in Caramba, with the values for each mark being lower in Caramba (Figure 2A). In contrast to acetylation, the sum of the percentages of microspores with methylation marks was lower in Pavon (12.89%) than in Caramba (33.14%) (Figure 2C). It should be noted the low number of microspores with H3K27me3 and the absence of H3K9me2 mark in Pavon. Furthermore, all acetylation marks were exclusively located in the nucleus in both cultivars (Figures 3A, B). H3K27me3 was observed in the cytoplasm (including the vacuole) in both cultivars and only in the nucleus in Pavon (Figures 3A, B).

Differences in the dynamics of PTMs at GD were also observed between cultivars. The sum of percentages of acetylation decreased in Pavon as compared with 0dT (28.39% vs 35.85%), mainly due to the lower value of H3K9ac (6.03% vs 11.40%) (Figure 2A). There was a global increase of acetylation in Caramba (14.01%) due to H4K5ac (12.07%), which reached similar percentages to Pavon (13.25%). H4K5ac mark was observed in the nucleus and the cytoplasm (including the vacuole) in both cultivars and H3K9ac was absent in Caramba (Figures 3A, B). Concerning methylation, H3K9me2 was detected in a low percentage of nuclei (7.31%) in Pavon and was absent in Caramba (Figure 2D), and H3K27me3 was localized in the cytoplasm (including the vacuole) in both cultivars (Figure 3B).

Induction treatment with MAN modified the epigenetic state of microspores compared to 0dT and GD, and determined differences between cultivars. In Pavon, the sum of the

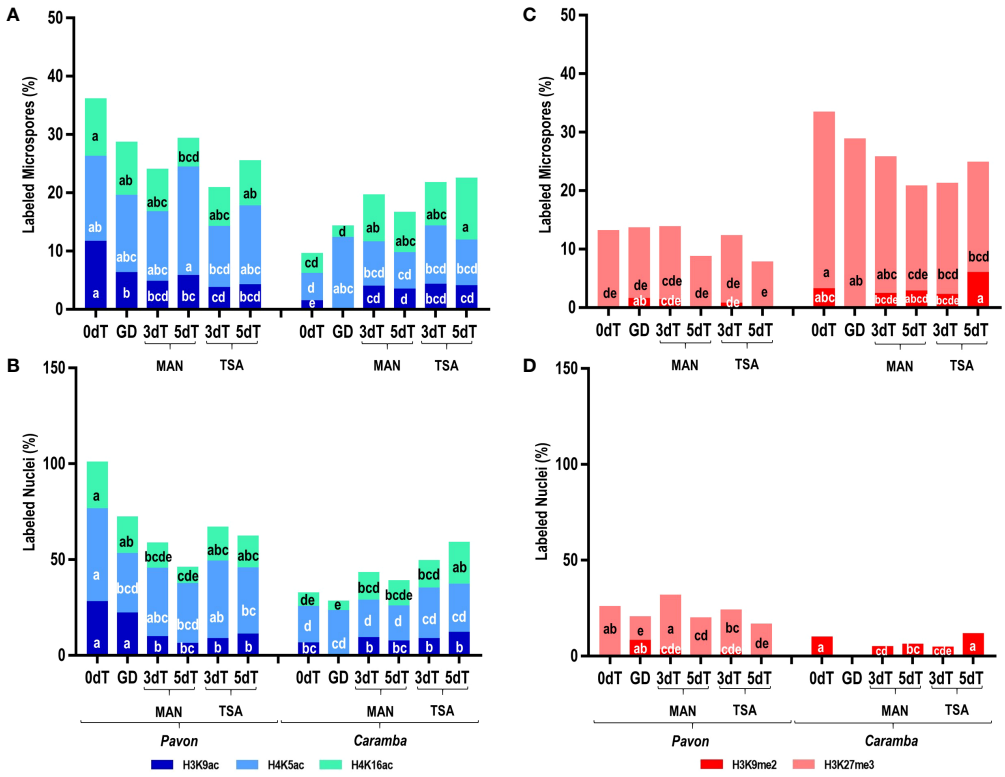

FIGURE 2
Effect of MAN and TSA on histone PTMs. **(A, B)** Percentage of labeled microspores and nuclei, respectively, with the acetylation marks H3K9ac (dark blue), H4K5ac (light blue), H4K16ac (green). **(C, D)** Percentage of labeled microspores and nuclei, respectively, with the methylation marks H3K9me2 (red), H3K27me3 (pink). Microspores before stress treatment (0dT), microspores under gametophyte development (GD), microspores after 3 and 5 days with mannitol treatment (3dT-MAN, 5dT-MAN) and after 3 and 5 days with mannitol plus TSA treatment (3dT-TSA, 5dT-TSA) from Pavon (on the left) and Caramba (on the right). Percentages of labeled microspore and nuclei with the same letter within each epigenetic mark are not significantly different (P<0.05) according to the Duncan test.

percentages of acetylated microspores at 3dT (23.76%) decreased as compared to 0dT (35.85%) or GD (28.39%), mainly due to lower value of H3K9ac (4.51% vs 11.40%) (Figure 2A). A decrease was also observed in the percentage of labeled nuclei with H4K16ac (Figure 2B). However, the percentage of acetylated microspores rose at 5dT-MAN (29.07%), mainly due to the H4K5ac mark, although this percentage decreased in the nuclei (Figure 2B). In Caramba, the dynamics of epigenetic marks was different from that of Pavon. An increase in the percentage of acetylated microspores was observed at 3dT with respect to 0dT (19.36% vs 9.29%), being significant for H3K9ac (3.67% vs 1.19%) and H4K16ac (8.06% vs 3.42%) (Figure 2A). Nevertheless, the differences were not significant in the nuclei (Figure 2B). A slight decrease in all acetylation marks was noticed at 5dT (Figure 2A).

Regarding methylation, the percentage of labeled microspores with H3K9me2 was very low at 3dT-MAN (1.08%), and it was absent at 5dT-MAN in Pavon (Figure 2C). In Caramba, this percentage was not modified with MAN, but the percentage of labeled nuclei decreased (Figure 2D). Furthermore, the percentage of microspores with H3K27me3 decreased at 5dT (17.98%) compared to 0dT (30.18%).

The localization of H4K5ac and H3K27me3 with MAN also revealed differences between the two cultivars. H4K5ac was detected in the nucleus and cytoplasm at both 3dT and 5dT in Pavon (Figure 3A). In Caramba, it was only observed in the nucleus at 3dT, but also in the cytoplasm at 5dT (Figure 3B). H3K27me3 was present in the nucleus and cytoplasm in Pavon (Figure 3A), but only in the cytoplasm in Caramba (Figure 3B).

TSA treatment produced modifications in the epigenetic state of the microspores compared to MAN. TSA decreased the percentages of microspores with acetylation marks in Pavon (20.61% at 3dT-TSA and 25.25% at 5dT-TSA vs 23.76% at 3dT-MAN and 29.07% at 5dT-MAN) (Figure 2A). However, the sum of the percentages of labeled nuclei was higher at 5dT-TSA than at 5dT-MAN, mainly due to the H4K16ac mark (Figure 2B). In Caramba, higher percentages of acetylated microspores were observed with TSA than with MAN, especially at 5dT (22.24% vs 16.37%), highlighting the increase of the H4K16ac mark. The most remarkable change produced by TSA was the localization

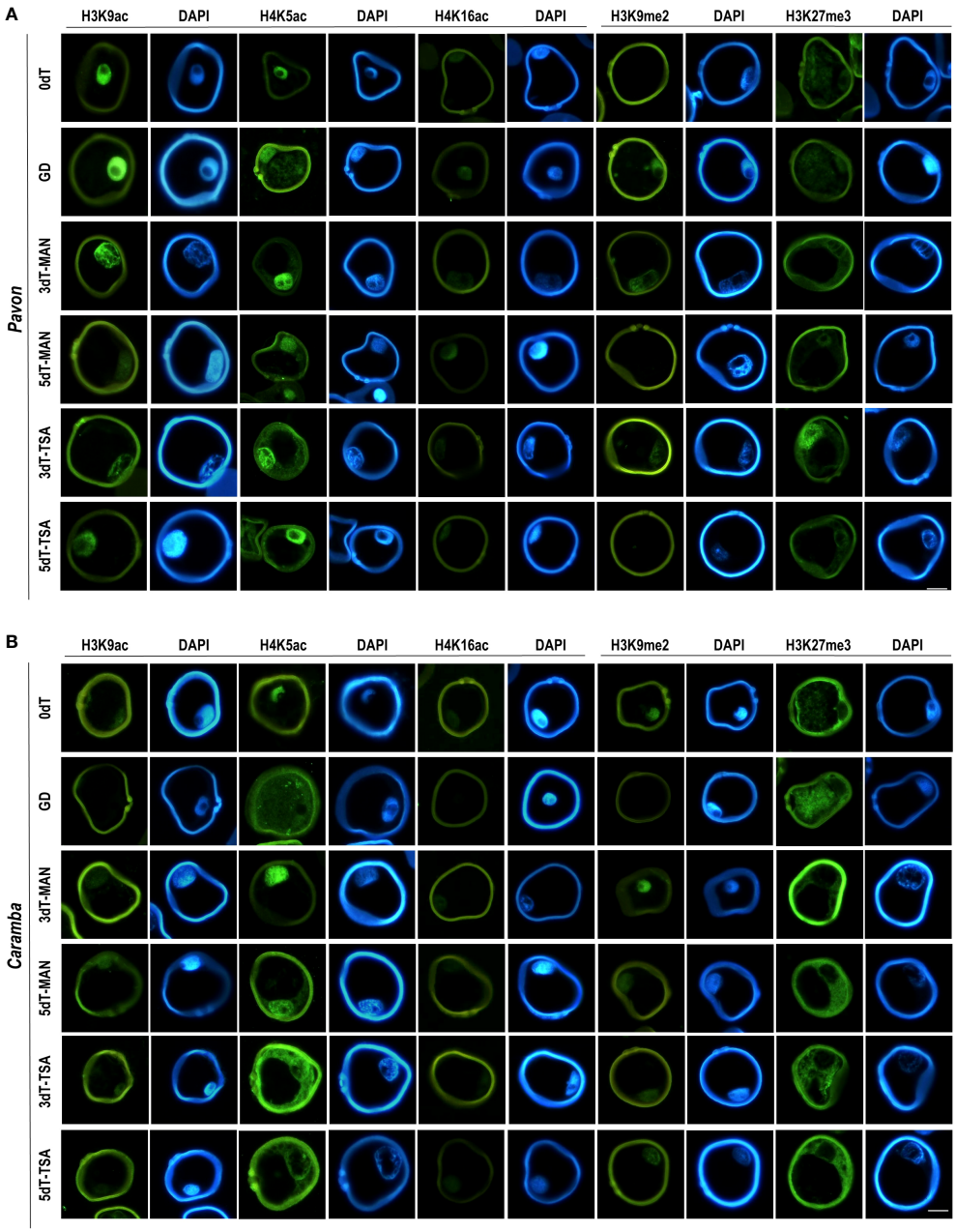

FIGURE 3
Immunolocalization of histone PTMs in microspores before stress treatment (0dT), microspores under gametophytic development (GD), microspores after 3 and 5 days with mannitol treatment (3dT-MAN, 5dT-MAN) and after 3 and 5 days with mannitol plus TSA treatment (3dT-TSA, 5dT-TSA) from Pavon **(A)** and Caramba **(B)**. H3K9ac, H4K5ac, H4K16ac, H3K9me2 and H3K27me3 antibodies labeling in green, DAPI in blue. Scale bar = 20 μm.

of H4K5ac in both the nucleus and cytoplasm at 3dT-TSA in Caramba (Figure 3B). Finally, TSA resulted in an increase in the percentage of labeled nuclei with H3K9me2 at 5dT-TSA compared to 5dT-MAN in Caramba, and a decrease in the percentage of nuclei with H3K27me3 at 3dT-TSA in Pavon (Figure 2D).

Transcriptional changes associated to microspore embryogenesis induction by MAN and TSA treatments

The immunohistochemical analysis revealed that MAN and TSA modified the epigenetic state of microspores. Therefore, the

dynamics of transcriptional changes in genes controlling histone acetylation state and genes involved in key processes of ME induction produced by treatments was studied. The candidate genes were selected based on a previous study on barley ME induction (Sánchez-Díaz, 2014). Genes were associated with GO terms as a source of information about gene functions (Supplementary Table 3).

Expression of histone deacetylases and acetyltransferases genes

Histone acetylation depends on the balance between HDAC and HAT. In this study, six wheat HDAC genes (*TaHDA8*, *TaHDA15*, *TaHDA18*, *TaHDT1*, *TaHDT2* and *TaTAF14*) and five HAT genes (*TaHAG2*, *TaHAG3*, *TaHAM*, *TaHAC1* and *TaHAC4*) were studied. Three HDAC genes were not considered for further analysis as *TaHDA8* was not amplified, and *TaHDT2* and *TaTAF14* showed no differences between the samples.

In microspores at 0dT, only two HATs genes (*TaHAC4* and *TaHAG2*) showed differential expression between the two cultivars. Both genes were expressed at a lower level in Pavon, although the differences were only significant in *TaHAC4* (Figure 4). Also noteworthy was the high expression level of *TaHDT1* in both cultivars. In microspores at GD, *TaHDT1* was down-regulated in both cultivars, *TaHAG2* in Caramba, and *TaHAC4* was up-regulated in Pavon (Figure 4).

MAN treatment modified the expression of most HDAC and HAT genes (Figure 4). The decrease in *TaHDT1*, compared to 0dT, was even higher than at GD, reaching the lowest values at 5dT in both cultivars. A similar decrease in *TaHAG2* throughout MAN treatment was observed in Caramba, whereas this gene was only slightly down-regulated at 3dT in Pavon. The *TaHDA18* and four HAT genes (*TaHAG3*, *TaHAM*, *TaHAC1* and *TaHAC4)* were up-regulated at 3dT in both cultivars. The expression at 3dT and 5dT in most of the above mentioned

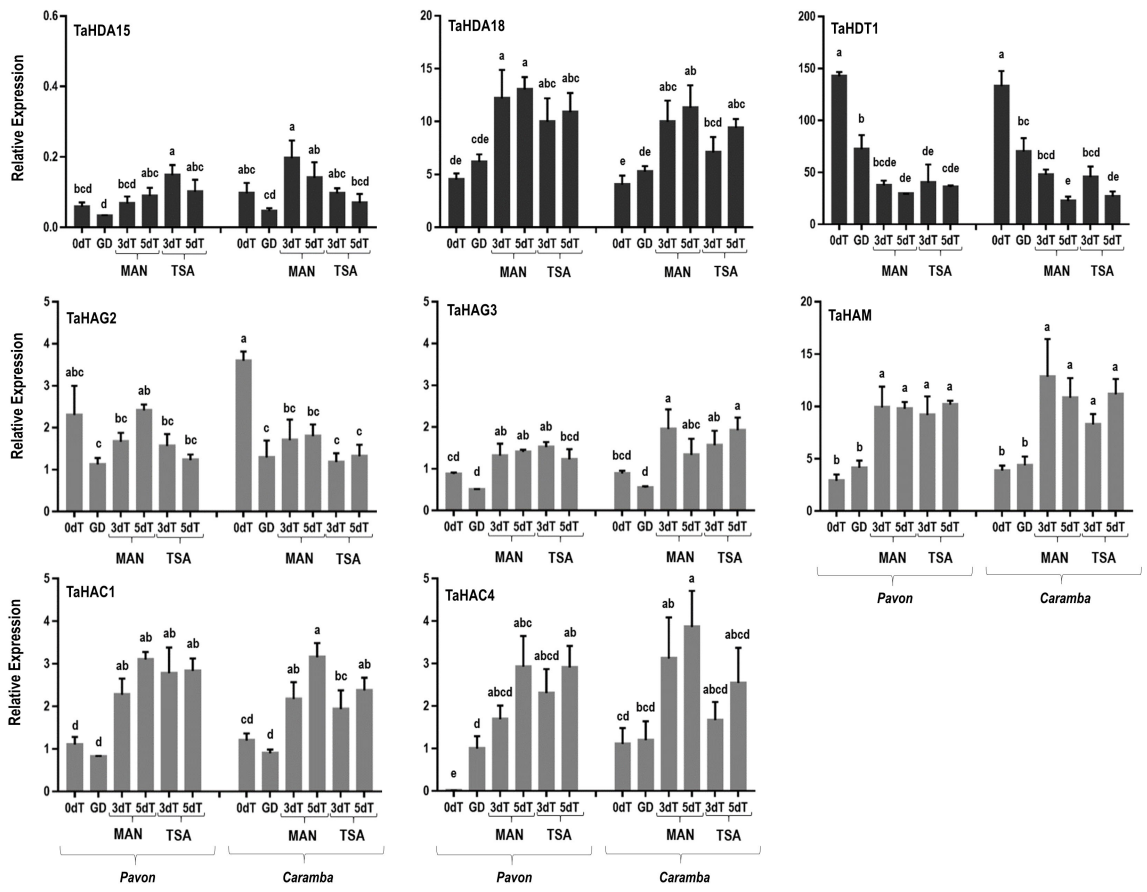

FIGURE 4
qRT-PCR analysis of histone deacetylases genes (*TaHDA15*, *TaHDA18*, *TaHDT1*, *TaHDT2*, *TaTAF14*) and histone acetyltransferases genes (*TaHAG2*, *TaHAG3*, *TaHAM*, *TaHAC1*, *TaHAC4*) in microspore before stress treatment (0dT), microspores under gametophytic development (GD), microspores after 3 and 5 days with mannitol treatment (3dT-MAN, 5dT-MAN) and after 3 and 5 days with mannitol plus TSA treatment (3dT-TSA, 5dT-TSA) from Pavon (on the left) and Caramba (on the right). Data were normalized using *Ta.27771* and *Ta.2291* as endogenous control genes. Bars represent the standard errors of the means. Relative expression values with the same letter are not significantly different (P<0.05) according to the Duncan test.

genes were similar in both cultivars. *TaHDA15* was not induced in any cultivar, but Pavon showed a lower expression level than Caramba at 3dT (Figure 4).

TSA showed a tendency to up-regulate most genes in Pavon and to down-regulate them in Caramba, compared to MAN (Figure 4). Notably, TSA treatment caused an increase in *TaHDA15* expression at 3dT in Pavon. In addition, Pavon showed a lower *TaHAG3* expression than Caramba at 5dT-TSA.

The transcriptome and RNA-Seq data set available on the expVIP Wheat Expression Browser was used to analyze the expression of the selected genes under different stresses and in different wheat tissues (Supplementary Figure 2). *TaHDA15* and *TaHAG2* were specifically expressed in the spike, whereas a low expression of *TaHAC1* and *TaHAC4* was observed in all tissues. In the RNA-Seq data of bread wheat cv Svilena microspores induced to ME by cold, only *TaHAG3* and *TaHAM* were up-regulated after stress (Supplementary Figure 3).

Expression of candidate genes involved in microspore embryogenesis induction

Candidate genes involved in key processes associated with ME induction, such as histone methylation, DNA silencing, nuclear fusion, pollen wall development, autophagy, ABA signaling, auxin synthesis, and stress tolerance were also examined.

In microspores at 0dT, four genes showed differential expression between cultivars: *TaDRM3* (*DOMAINS REARRANGED METHYLTRANSFERASE 3*), encoding a DNA methyltransferase; *TaMS1* (*MALE STERILITY 1*), that encodes a protein required for exine development; *TaATG18fD* (*AUTOPHAGY-ASSOCIATED 18fD*); and *Ta-2B-LBD16* (*LATERAL ORGAN BOUNDARIES DOMAIN 16*), encoding a plant-specific transcription factor (Figure 5). Pavon showed higher expression of *TaMS1* and *Ta-2B-LBD16* and lower expression of *TaDRM3* and *TaATG18fD* than Caramba (Figure 5). Two genes *TaABI5* (*ABCISIC ACID-INSENSITIVE 5*) and *TaYUC11D* (*INDOLE-3-PYRUVATE MONOOXYGENASE YUCCA 11D*), that encode a basic leucine zipper transcription factor and an auxin synthesis limiting enzyme, respectively, were also differentially expressed between cultivars at a very low level. *TaNFD6-A* (*NUCLEAR FUSION DEFECTIVE 6-A*), encoding a mitochondrial ribosomal protein involved in nuclear membrane fusion, showed a slightly down-regulation in Pavon.

Changes in the expression of several genes were observed when comparing GD with 0dT (Figure 5). A reduction in *TaMS1* expression was shown in Pavon. *TaYAO* (*YAOZHE*), that encodes a protein involved in rRNA processing, and *Ta-2B*-LBD16 were down-regulated in both cultivars. In contrast, up-regulation of *TaMPK3* (*MITOGEN-ACTIVATED PROTEIN KINASE 3*) in Pavon and *TaATG18fD* in both cultivars was observed. Genes *TaDRM3*, *TaYAO*, *TaNFD6-A*, *TaATG18fD* and *TaYUC11D* were differentially expressed between cultivars, with Pavon showing a lower level.

MAN treatment at 3dT increased the expression of most genes (*TaMS1*, *TaATG18fD, TaMPK3, TaABI5, TaYUC11D,* and *Ta-2B-LBD16*) compared to 0dT in both cultivars (Figure 5). Interestingly, *TaSDG1a-7A* (*SET DOMAIN GENE 1a-7A*), encoding a histone methyltransferase, was up-regulated only in Caramba and *TaYAO* was the only gene down-regulated in Pavon. Differences between cultivars were also observed in *TaAGO802-B, TaDRM3, TaYAO,* and *TaYUC11D*, being *TaYUC11D* the only one with a higher expression in Pavon. When MAN treatment was extended from 3 to 5 days, some genes changed their expression. *TaSDG1a-7A* increased in Pavon, and *TaATG18fD* in Caramba. Also, *TaYAO*, *TabZIPF1* (*BASIC LEUCINE ZIPPER F1*), described as an *E2F-RELATED* (*E2F*) transcription factor, and *Ta-2B-LBD16* were down-regulated in Caramba. Differences between cultivars were also noticed at 5dT-MAN, with *Ta-2B*-LBD16 showing higher expression, and *TaNFD6-A* and *TaATG18fD* lower in Pavon.

TSA only resulted in small changes at 3dT compared to MAN in Caramba. A higher expression of *TaYUC11D* was accompanied by a slightly lower expression of *TaAGO802-B*. Furthermore, *TabZIPF1* in Pavon and *TaYAO* and *Ta-2B-LBD16* in Caramba were up-regulated at 5dT-TSA (Figure 5).

The analysis of the transcriptome and RNA-Seq data set available showed that all genes had a low expression level, except *TaAGO802-B*, *TabZIPF1*, *TaMPK3* and *Ta-2B-LBD16* (Supplementary Figure 2). Some of these genes were associated with stress response, such as *TaMPK3* and *Ta-2B-LBD16*, while *TaABI5* and *TaNFD6*-A were specifically expressed in grains and roots, respectively, and *TaAGO802-B* and *TaMS1* in spikes. Differences in the expression between homologues of *TaMS1*, *TabZIPF1* and *TaMPK3* were also detected. In the RNA-Seq data of ME induction, few of the studied genes were expressed. *TaAGO802-B* was shown as a constitutive gene, whereas *TaYAO* was mainly expressed in embryogenic microspores, *TaATG18fD* in cold treated and embryogenic microspores, and *TabZIPF1* in fresh and cold treated microspores (Supplementary Figure 3).

Gene expression correlations and their association with ME induction

Pearson correlation coefficients were calculated to examine the association between the relative expression of genes determining histone acetylation status and genes involved in processes related to ME induction. The data from all samples (0dT, GD, 3dT-MAN, 5dT-MAN, 3dT-TSA, and 5dT-TSA) in the two cultivars were used.

Two groups could be clearly distinguished in the correlation matrix (Figure 6A). The first revealed a strong positive correlation between the histone deacetylase *TaHDT1* gene and the set of genes *TaYAO*, *TaNFD6-A* and *TabZIPF1*, and a negative correlation with most of the other genes. *TaHAG2* acetyltransferase was positively correlated with *TaHDT1* and *TaYAO* but was independent of *TaDRM3*, *TaNFD6-A* and *TabZIPF1*. The majority of HDACs

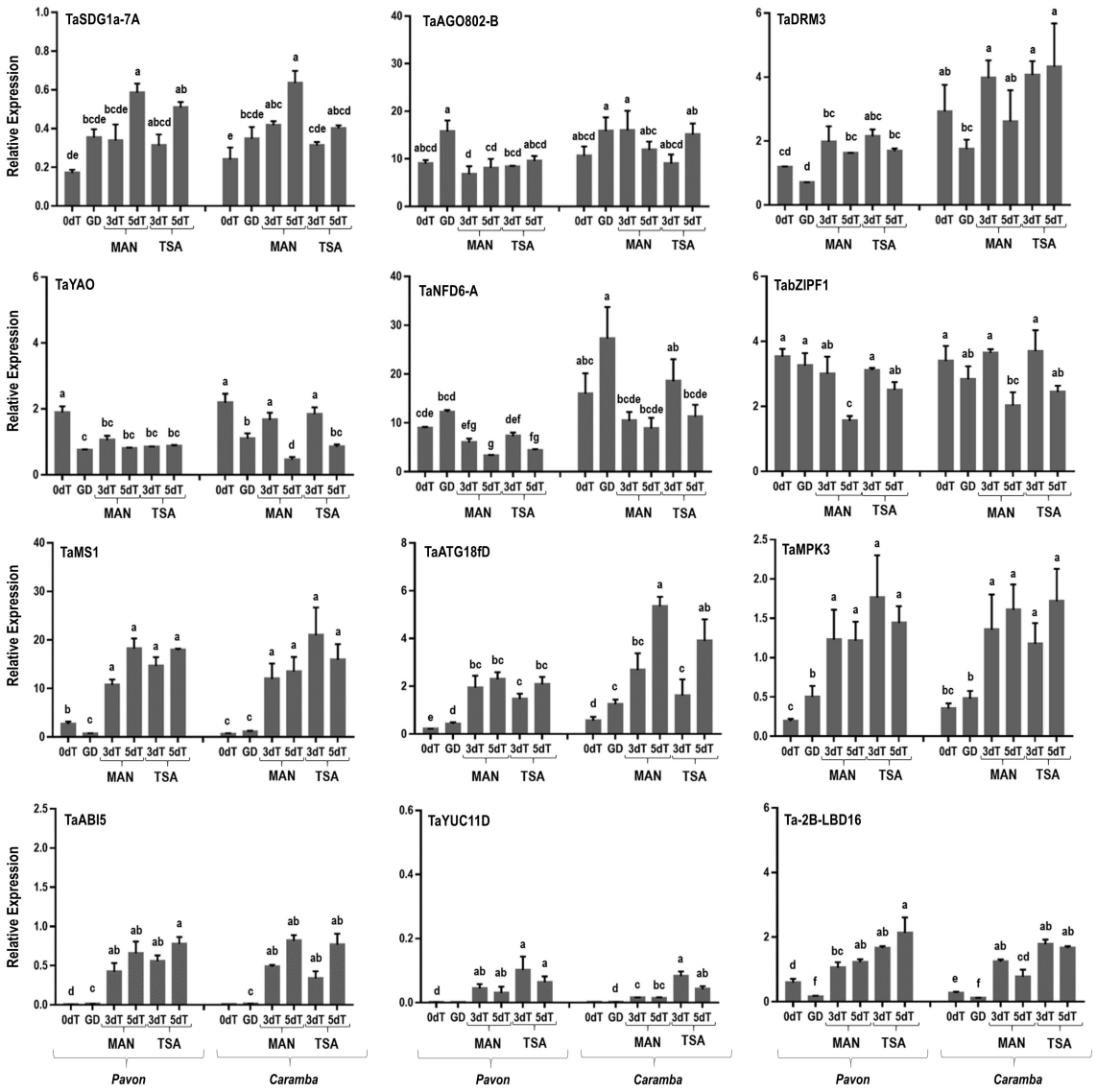

FIGURE 5
qRT-PCR analysis of key genes involved in microspore embryogenesis induction. Microspores before stress treatment (0dT), microspores under gametophytic development (GD), microspores after 3 and 5 days with mannitol treatment (3dT-MAN, 5dT-MAN) and after 3 and 5 days with mannitol plus TSA treatment (3dT-TSA, 5dT-TSA) from Pavon (on the left) and Caramba (on the right). Data were normalized using *Ta.27771* and *Ta.2291* as endogenous genes control. Bars represent the standard errors of the means. Relative expression values with the same letter are not significantly different (P<0.05) according to the Duncan test.

and HATs (*TaHDA15* and *TaHDA18*, *TaHAG3*, *TaHAM*, *TaHAC1* and *TaHAC4)* were in the second group that was positively associated with *TaSDG1a-7A*, *TaMS1*, *TaATG18fD*, *TaMPK3*, *TaABI5*, *TaYUC11D* and *Ta-2B-LBD16* (Figure 6A).

Principal component analysis (PCA) was performed to identify the genes associated with wheat ME induction. The data set included the relative expression of the genes in all samples from Pavon and Caramba (Figure 6B). The two components analysis accounted for 70.4% of the total variance, 55.9% explained by PC1 and 14.5% by PC2. PC1 was mainly determined by *TaHDA18*, *TaHDT1*, *TaHAM*, *TaHAC1*, *TaHAC4*, *TaMS1*, *TaMPK3* and *TaABI5* genes, and PC2 by TaHDA15, *TaHAG3*, *TaSDG1a-7A*, *TaDRM3*, *TaYAO*, *TabZIPF1*, *TaYUC11D* and *Ta-2B-LBD16* genes.

PC1 differentiated untreated (0dT) and GD from MAN and TSA microspores of both cultivars, on the right and left respectively (Figure 6B). PC1 showed that *TaHDT1* was strongly associated with microspores at 0dT and GD.

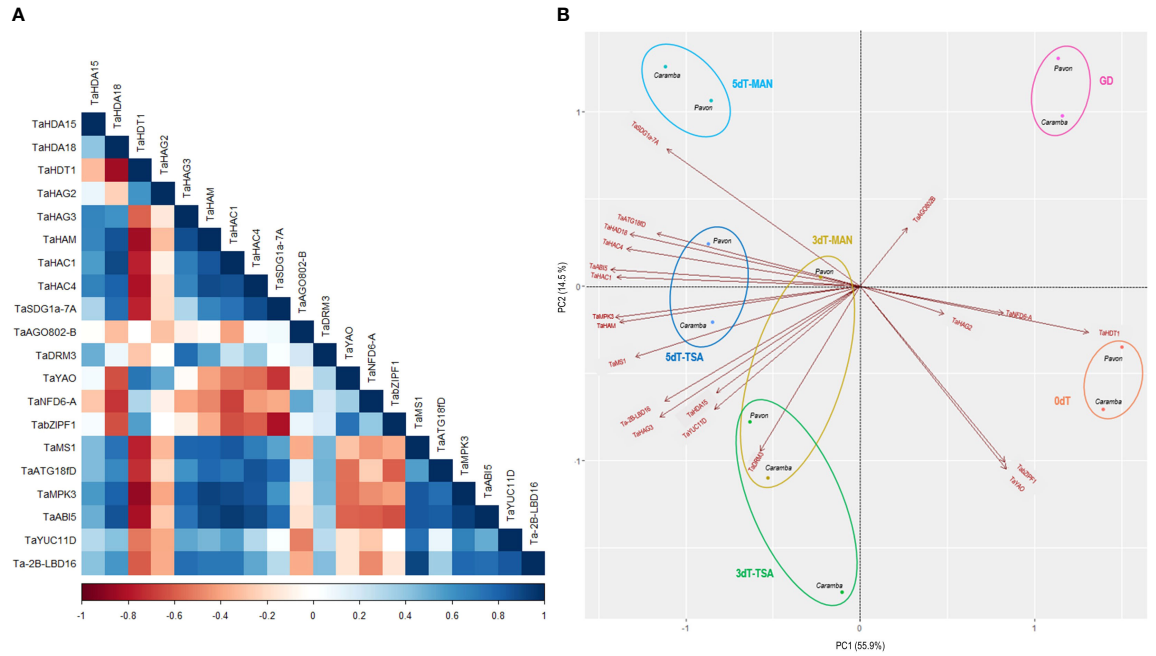

FIGURE 6
(A) Pearson correlation coefficients of histone deacetylases, histone acetyltransferases and key genes involved in ME induction, considering all samples of the two cultivars. **(B)** Principal component analysis (PCA) plot of the 20 genes in Pavon and Caramba. Microspores before stress treatment (0dT), microspores under gametophytic development (GD), microspores after3 and 5 days with mannitol treatment (3dT-MAN, 5dT-MAN) and after 3 and 5 days with mannitol plus TSA treatment (3dT-TSA, 5dT-TSA).

TaYAO and *TabZIPF1* contributed to the differentiation between 0dT and GD microspores. On the opposite position in PC1, *TaHDA18*, *TaHAM*, *TaHAC1*, and *TaHAC4* were positively associated with stress treated microspores, accompanied by *TaMS1*, *TaMPK3*, *TaABI5*. The differences between 3dT and 5dT were determined by a strong contribution of *TaSDG1a-7A*, *TaHDA15*, *TaHAG3*, *TaDRM3*, *TaYUC11D and Ta-2B-LBD16*.

Discussion

Increasing evidence indicates that epigenetic changes are involved in the regulation of biological processes including stress response and developmental reprogramming, both implicated in ME induction (for review see Lloyd and Lister, 2022). Histone PTMs, mainly acetylation and methylation, and DNA methylation have been directly associated with ME induction. Our previous report showed that the simultaneous application of mannitol and TSA increased ME efficiency compared to mannitol in two bread wheat cultivars with different ME response (Castillo et al., 2020). However, it remains a challenge to ascertain the mechanisms by which chromatin organization responds to transcriptional requirements and how TSA modifies them during ME induction.

Microspores from cultivars with different ME response have a distinctive epigenetic state before induction

Pollen development is characterized by specific chromatin changes, including the dynamics of H3 variants, the progressive loss of active histone marks and the accumulation of repressive marks (Borg and Berger, 2015). Furthermore, transcriptome complexity is significantly reduced after pollen mitosis I (PMI) (Liu et al., 2018a). However, uninucleate microspores (0dT) become transcriptionally active just before PMI, initiating the transition from sporophyte to gametophyte (Nelms and Walbot, 2022).

Histone variants contribute to define different chromatin states (for a review see Probst et al., 2020). The replicative histone H3.1 variant is associated with gene silencing in heterochromatin and the replacement H3.3 variant with active transcription and euchromatin regions (for a review see Probst et al., 2020). The H3.2 identified in wheat belongs to the histone H3.3 class (Waterborg, 1991). According to Otero et al. (2016), the ratio between H3.1 and H3.3 could be related to a proliferative state of the cell in *Arabidopsis*. Interestingly, the H3.1/H3.2 ratio was higher in Pavon than in Caramba at 0dT, that could indicate an elevated cell division potential of Pavon (Otero et al., 2016). Differences in H3.1 acetylation have been

associated with diverse heterochromatin domains and compaction levels (Jasencakova et al., 2001). The lower H3.1 acetylation suggests a higher heterochromatin compaction in Pavon (Figure 1).

One of the major epigenetic differences between cultivars at 0dT was the higher percentages of acetylated microspores in Pavon, highlighting the percentage of H3K9ac (Figure 3A). At GD, the percentage of labeled microspores with H3K9ac decreased in Pavon whereas this mark was absent in Caramba (Figure 3A). It is known that H3K9ac mark is present in microspores but is removed during pollen development (Pandey et al., 2013; Liu et al., 2018a). In accordance, Pavon microspores could be at a less advanced stage in pollen development. Curiously, H4K5ac was localized in the cytoplasm, including the vacuole, in both cultivars at GD (Figure 2), the increase of labeled microspores with this mark in Caramba being noteworthy (Figure 3A). The presence of H4K5ac in the cytoplasm has been previously described in barley and *Brachypodium* (Braszewska-Zalewska et al., 2013; Wolny et al., 2014). These authors propose that newly synthetized acetylated H4, prior to DNA replication, is present in the cytoplasm while the recycling of acetylated H4 takes place in the vacuole. Differences in H4K5ac dynamics suggests that Pavon is less primed to enter in DNA replication. Histone acetylation depends on the balance between HDAC and HAT. No major differences in *HDAC* or *HAT* expression were observed between cultivars at 0dT, except for *TaHAC4* that showed a lower level in Pavon (Figure 4). *TaHAC4* has been associated with the enrichment of H3K9ac in *Arabidopsis* (Li et al., 2022). In contrast, the expression level of this gene was negatively correlated with the percentage of microspores with H3K9ac in both cultivars.

In *Arabidopsis*, the diploid to haploid transition is governed by the loss of H3K9me2 mark, and the transition back to diploid by the loss of H3K27me3 (Borg et al., 2021). However, H3K9me2 mark persisted throughout pollen development in rye and barley (Houben et al., 2011; Pandey et al., 2013). In this study, H3K9me2 was absent in Pavon and present in Caramba at 0dT, and the opposite was observed at GD (Figure 2). This could be associated with small adjustments to control transposon reactivation in the two cultivars during pollen development (Pecinka et al., 2010). Interestingly, in Caramba, H3K27me3 was exclusively in the cytoplasm that could also be related to an accumulation of histones prior to DNA replication as indicated in barley (Pandey et al., 2017). However, the progressive decrease of the percentage of labeled nuclei and the enrichment of H3K27me3 in the cytoplasm reinforce the less advanced stage in pollen development of Pavon microspores.

Differences in the epigenetic state of the cultivars at 0dT were barely reflected at the transcriptional level of the genes involved in ME induction, with the exception of *TaDRM3* and *TaNFD6-A*. *DRM3* participates in *de novo* DNA methylation *via* RNA (RdDM) and is crucial to maintain CHH methylation, although the levels in microspores are low (Henderson et al., 2010; Gehring, 2019). *TaNFD6-A* encodes a protein related to nuclear membrane fusion, playing an important role in female and male gametogenesis (Portereiko et al., 2006). At 0dT, Caramba microspores had a higher expression of both genes, but *TaDRM3* decreased and *TaNFD6-A* increased in both cultivars at GD. Other genes related to pollen development, as *TaMS1* and *Ta-2B-LBD16* (Li et al., 2021; Xu et al., 2021), had a higher expression at 0dT in Pavon and were down-regulated at GD in both cultivars. The expression pattern of these genes confirmed that Pavon microspores were more delayed in pollen development.

MAN and TSA treatments modified the epigenetic state of microspores initiating a new cell fate

The relationship between epigenetic modifications, transcriptional changes and ME induction is largely unknown. The analysis of epigenetic dynamics in coordination with gene regulation offers new opportunities to study the mechanisms underlying microspore reprogramming towards embryogenesis.

MAN and TSA treatments modified the H3 variants ratio and H3 and H4 acetylation

H3 variants are involved in transcriptional regulation in response to stress (Yung et al., 2021). However, no previous information about the role of histone variants in ME induction is available. In this study, MAN and TSA raised the H3.1/H3.2 ratio in both cultivars, highlighting the TSA effect at 3dT (Figure 1). These results agreed with a high cell division potential (Otero et al., 2016), and with the higher number of pro-embryos produced by TSA (Castillo et al., 2020). Histone hyperacetylation processes were observed in MAN and TSA (Figure 1), accordingly with previous results reported in *Brassica* ME induction by heat and TSA (Li et al., 2014a). The results obtained in this study confirm the higher hyperacetylation capacity of the H3.2 variant described by Waterborg (1991). The effect of TSA on H3.2 hyperacetylation enhancement at 3dT (Figure 1) could be an important factor for ME induction in both cultivars. MAN and TSA caused only minor H4 deacetylation/acetylation processes, although H4 acetylation was slightly higher with TSA in both cultivars at 3dT.

The dynamics of PTMs in response to MAN and TSA changed microspore epigenetic state

Long-duration and medium-intensity stress treatments have epigenetic characteristics that allow for a greater adaptation and survival (Pecinka et al., 2010). Thus, acetylation is positively associated with the activation of stress response genes in plants

(Kong et al, 2020), but deacetylation is also essential to cause growth responses to warm temperature (Tasset et al., 2018).

In this study, the effect of the MAN and TSA on histone acetylation depended on the epigenetic state of the microspores at 0dT. A strong decrease in the percentage of microspores with H3K9ac in Pavon and a large increase in H3K9ac and H4K16ac in Caramba were observed at 3dT (Figure 3A). Interestingly, both PTMs were detected in the nuclei after treatments in this study, whereas H3K9ac was mainly located in the cytoplasm in barley (Pandey et al., 2017). The cytoplasmic H4K5ac did prove to be distinctive between treatments in Caramba, emerging at 3dT with TSA but at 5dT with MAN (Figure 2B). As mentioned above, the presence of H4K5ac in the cytoplasm could point out to a nascent acetylated H4 for DNA synthesis. Therefore, TSA could accelerate the replication processes in the mid-low responding cultivar. Curiously, one effect of TSA in maize seedlings is the hyperacetylation of H4K5, which is associated with cell cycle arrest in prophase (Wang et al., 2016). Furthermore, DNA replication arrested in G1 is related to the accumulation of the cytoplasmic H4K5ac signals in dry seeds of *Brachypodium* (Wolny et al., 2014).

The percentages of labeled microspores with H3K9me2 and H3K27me3 silencing marks during treatments seemed to be determined by the cultivar and the epigenetic state of the microspore at 0dT, similarly to histone acetylation. In MAN and TSA, H3K9me2 emerged at 3dT in Pavon but it was present in Caramba at 0dT and throughout treatments. A striking increase in the percentage of labeled microspores at 5dT-TSA was observed in Caramba (Figure 3B). However, the presence of H3K9me2 was noticed during ME induction in a high responding barley cultivar (Pandey et al., 2017). The loss of H3K27me3 accompanies callus induction and plant regeneration in *Arabidopsis* (He et al., 2012; Yan et al., 2020). In this study, the presence of this mark in Pavon nuclei could indicate some level of silencing, which is not contradictory to an active response to ME induction. In Caramba, H3K27me3 is restrictive to the cytoplasm as in a barley high responding cultivar to ME (Pandey et al., 2017). Even if there were differences between cultivars, it was not possible to establish a direct correlation between methylation marks and ME induced by MAN and TSA.

MAN and TSA caused transcriptional changes for the elimination of gametophytic pathway and the initiation of a new developmental program

The gene networks regulated by histone PTMs are still poorly characterized (Kumar et al., 2021). In addition, few reports are focused on transcriptional changes accompanying wheat ME induction (Seifert et al., 2016; Jensen, 2021), and the direct impact of PTMs dynamics on key genes related to ME is unknown.

After 3 days of MAN or TSA treatments, most genes studied were up-regulated compared to 0dT and GD. Only a few genes associated with 0dT or GD in PCA analysis, *TaHDT1, TaHAG2, TaYAO*, *TaNFD6-A*, *TabZIPF1* and *TaAGO802-B* were down-regulated (Figures 4, 5, 6). *TaYAO*, *TaNFD6-A*, *TabZIPF1* and *TaAGO802* were directly related to different pollen development processes as 18S pre-rRNA processing, zinc homeostasis, DNA silencing, or other unknown functions (Portereiko et al., 2006; Li et al., 2010; Evens et al., 2017; Akond et al., 2020). Disruption of the gametophytic developmental pathway has been reported as a key process in barley ME induction with mannitol (Muñoz-Amatriaín et al., 2006; Muñoz-Amatriaín et al., 2009). In this study, a progressive down-regulation of most genes associated with the disruption of the gametophytic development was observed, with a tendency to be faster in Pavon. Surprisingly, TSA caused a slower down-regulation of *TaYAO* and *TaNFD6-A* in Caramba, and *TabZIPF1* in Pavon. *TaAGO802-B* deserves an especial mention, since it exhibited a remarkable difference between MAN and TSA, with opposite expression in Caramba at 3dT (Figure 5).

The epigenetic control of the transcriptional regulation of these genes could be associated with *TaHDT1* and *TaHAG2*. *TaHDT1* sharply decreased at 3dT in both treatments and cultivars as compared to 0dT. This gene is a negative regulator of biotic defense response in wheat (Zhi et al., 2020). Accordingly, the activation of pathogen defense genes has been previously described in barley and wheat ME induction (Muñoz-Amatriaín et al., 2006; Soriano, 2008). Moreover, *HDT1* binds to the *YAO* promoter during rRNA processing (Luo et al., 2022). Therefore, the down-regulation of *TaHDT1* could lead to a reduction on rRNA processing, allowing the elimination of gametophytic development by prioritizing the synthesis of stress-response RNAs. *TaHAG2* is activated in response to drought and medium temperature stresses (Gao et al., 2021; Li et al., 2022). In this study, *TaHAG2* was down-regulated with the stress, showing only slight differences between treatments.

TaHDA15, *TaHAG3*, *TaHAM, TaYUC11D*, *Ta-2B-LBD16, TaMS1* and *TaDRM3* constitute a network according to a PCA analysis (Figure 6), characterized by activation a 3dT and few expression changes at 5dT (Figures 4, 5). *TaYUC11D* is a limiting enzyme in auxin synthesis (Yang et al., 2021). In ME, auxin accumulation is localized in uninucleate microspores after induction in *Brassica* (Dubas et al., 2014; Soriano et al., 2014). *De novo* auxin biosynthesis is noticed at early multicellular embryo in barley and *Brassica* ME, increasing during embryo development. (Rodríguez-Sanz et al., 2014; Pérez-Pérez et al., 2019). In addition, it has been suggested that *YUC11* is responsible of auxin biosynthesis require for zygotic embryo polarization in *Arabidopsis* (Larsson et al., 2017). Furthermore, *YUCCA* genes also play a crucial role in morphology changes associated with survival in a medium-long temperature stress (Casal and Balasubramanian, 2019). Interestingly, TSA increased the expression of *TaYUC11D*, particularly in the mid-low responding cultivar Caramba (Figure 5). These results agree with the up-regulation of auxin-related genes produced by

TSA in *Brassica* ME (Li et al., 2014a). Moreover, TSA also caused an up-regulation of the auxin related gene *Ta-2B-LBD16*, in Caramba at 5dT. *Ta-2B-LBD16* is an orthologist of *AtLBD40* that promotes auxin signaling-dependent lateral organ development (Zentella et al., 2007; Okushima et al., 2007). TSA has also been associated with an up-regulation of genes encoding cell wall mobilization enzymes in *Brassica* ME (Li et al., 2014a). In this study, *TaMS1*, which is required for pollen exine development (Liu et al., 2018b), was up-regulated not only by TSA but also by MAN. A special mention of *TaDRM3*, a DNA silencing component, should also be made since it was up-regulated by treatments, maintaining the differences between cultivars previously observed at 0dT.

Diverse histone acetylation regulatory genes are included in this network, but only *TaHAG3* and *TaHAM* showed slight differences between treatments in Caramba, highlighting *HAG3* expression at 5dT-TSA (Figure 4). Interestingly, orthologists of *TaHDA15*, *TaHAG3* and *TaHAM* have been described to promote hypocotyl elongation by up-regulation of auxin response and cell wall modifications genes in darkness in *Arabidopsis* (Tang et al., 2017; Woloszynska et al., 2018; Peng et al., 2018). Therefore, histone acetylation could be directly involved in the up-regulation of auxin related genes in this network.

The last network was characterized by the highest expression levels at 5dT, including *TaABI5*, *TaATG18fD, TaSDG1a-7A*, *TaHDA18, TaHAC1* and *TaHAC4* (Figure 6). The role of ABA in ME induction is unclear (for review see Żur et al., 2015). It has been proposed that each genotype requires a basal level of ABA to initiate a signaling cascade for ME (Żur et al., 2012). However, *TaABI5* was expressed at low levels at 0dT, and slightly increased throughout the treatments at a similar rate in the two cultivars. This could be in line with the requirement of the novo ABA synthesis to induce barley ME reported by Hoekstra et al. (1996). The up-regulation of *BnATG8*, accompanied by an accumulation of autophagosomes, has been previously described in *Brassica* ME (Berenguer et al., 2020). In this study, the mid-low responding cultivar had a higher expression of *TaATG18fD*, suggesting a greater cellular component recycling in stress response. Finally, the gene *TaSDG1a-7A*, an orthologist of AtCLF (*CURLY LEAF*) (Strejčková et al., 2020) that is a PRC2 component (polycomb repressive complex 2), was up-regulated particularly at 5dT-MAN. The CLF/H3K27me3 complex could play a role in controlling the transcription of developmental genes in stress-response (Avramova, 2015). The up-regulation of *CLF* has been previously associated with ME induction by mannitol in barley (Muñoz-Amatriaín et al., 2009), and by cold in perennial ryegrass (Begheyn et al., 2018).

The *TaHDA18, TaHAC1* and *TaHAC4* genes could be implicated in the epigenetic control of the network. It has been reported that they are related to the regulation of developmental processes mediated by hormone signaling, including ABA, ethylene or auxins (Xu et al., 2005; Li et al., 2014b; Li et al., 2022). These genes showed a slightly higher expression with MAN than TSA, especially in Caramba.

In this report, for the first time, a comprehensive analysis of the epigenetic dynamics involved in ME induction has been performed applying two treatments of different efficiency, in two bread wheat cultivars with different response. The epigenetic state of the microspores before induction was distinctive between cultivars. Evidences obtained in this study allow us to conclude that microspores of the high responding cultivar at the onset of ME induction were at a less advanced stage in pollen development and had a higher cell division potential. The initial differences determined the dynamics of histone PTMs to MAN and TSA. A response pattern could be established for the percentages of acetylation but not for methylation, during treatments. MAN and TSA increased the H3.1/H3.2 ratio and the hyperacetylation of H3. Moreover, there was a down-regulation of pollen developmental genes and an up-regulation of genes related to stress and hormonal response and morphological changes. The effect of TSA pointed out the most significant processes for wheat ME induction. In the mid-low responding cultivar, TSA enhanced histone hyperacetylation and cell division potential, and promoted an early initiation of DNA replication mechanisms. In addition, the down-regulation of pollen development genes was slowed down whereas the expression of genes associated with morphological changes, mainly mediated by auxin signaling, was increased. This study answers key questions about the role of epigenetic modifications and their relationship with transcriptional requirements in wheat ME induction, and it is a starting point for new studies and approaches to improve ME efficiency in a wide range of wheat genotypes and other crops.

Data availability statement

The original contributions presented in the study are included in the article/Supplementary Materials. Further inquiries can be directed to the corresponding author.

Author contributions

Conceptualization AMC and MPV; methodology IV-R, AMC, MAB, and MPV; microspore and RNA sampling IV-R, AMC, and MPV; immunofluorescence analysis IV-R, AMC, and MAB; gene expression analysis IV-R and MPV; writing-original draft

preparation IV-R, AMC, and MPV; writing-review and editing IV-R, AMC, MAB, and MPV; supervisor, project administration and funding acquisition AMC and MPV. All authors contributed to the article and approved the submitted version.

Funding

This research was supported by Project AGL2016-77211-R and PID2020-119540RB-100 from State R&D Program Oriented to the Challenges of the Spanish Society and funds for Reference Research Groups recognized by Diputación General de Aragón, Spain (Group A08-20R). IV-R was funded by the Spanish Ministry of Science and Innovation grant no. BES-2017-080970 (linked to the project AGL2016-77211-R).

Acknowledgments

The authors would like to thank Asunción Costar for her assistance growing the plant material and Begoña Echávarri and Patricia Fustero for their assistance collecting microspores samples.

Conflict of interest

The authors declare that the research was conducted in the absence of any commercial or financial relationships that could be construed as a potential conflict of interest.

Publisher's note

Supplementary material

The Supplementary Material for this article can be found online at: https://www.frontiersin.org/articles/10.3389/fpls.2022.1058421/full#supplementary-material

References

Abd ElFatah, B. E. S., Sayed, M. A., and ElSanusy, S. A. (2020). Genetic analysis of anther culture response and identification of QTLs associated with response traits in wheat (*Triticum aestivum l.*). *Mol. Biol. Rep.* 47, 9289–9300. doi: 10.1007/s11033-020-06007-z

Akond, Z., Rahman, H., Ahsan, M. A., Mosharaf, M. P., Alam, M., and Mollah, M. N. H. (2020). Bioinformatic analysis based genome-wide identification, characterization, diversification and regulatory transcription components of RNA silencing machinery genes in wheat (*Triticum aestivum l.*). *bioRxiv*. doi: 10.1101/2020.05.21.108100

Avramova, Z. (2015). Transcriptional 'memory' of a stress: transient chromatin and memory (epigenetic) marks at stress-response genes. *Plant J.* 83, 149–159. doi: 10.1111/tpj.12832

Bannister, A., and Kouzarides, T. (2011). Regulation of chromatin by histone modifications. *Cell Res.* 21, 381–395. doi: 10.1038/cr.2011.22

Batra, R., Gautam, T., Pal, S., Chaturvedi, D., Jan, I., Balyan, H. S., et al. (2020). Identification and characterization of SET domain family genes in bread wheat (*Triticum aestivum l.*). *Sci. Rep.* 10, 1–14. doi: 10.1038/s41598-020-71526-5

Begcy, K., and Dresselhaus, T. (2018). Epigenetic responses to abiotic stresses during reproductive development in cereals. *Plant Reprod.* 31, 343–355. doi: 10.1007/s00497-018-0343-4

Begheyn, R. F., Yates, S. A., Sykes, T., and Studer, B. (2018). Genetic loci governing androgenic capacity in perennial ryegrass (*Lolium perenne l.*). *G3: Genes Genomes Genet.* 8, 1897–1908. doi: 10.1534/g3.117.300550

Berenguer, E., Bárány, I., Solís, M. T., Pérez-Pérez, Y., Risueño, M. C., and Testillano, P. S. (2017). Inhibition of histone H3K9 methylation by BIX-01294 promotes stress-induced microspore totipotency and enhances embryogenesis initiation. *Front. Plant Sci.* 8, 1161. doi: 10.3389/fpls.2017.01161

Berenguer, E., Minina, E. A., Carneros, E., Bárány, I., Bozhkov, P. V., and Testillano, P. S. (2020). Suppression of metacaspase-and autophagy-dependent cell death improves stress-induced microspore embryogenesis in *Brassica napus*. *Plant Cell Physiol.* 61, 2097–2110. doi: 10.1093/pcp/pcaa128

Borg, M., and Berger, F. (2015). Chromatin remodelling during male gametophyte development. *Plant J.* 83, 177–188. doi: 10.1111/tpj.12856

Borg, M., Jiang, D., and Berger, F. (2021). Histone variants take center stage in shaping the epigenome. *Curr. Opin. Plant Biol.* 61, 101991. doi: 10.1016/j.pbi.2020.101991

Braszewska-Zalewska, A. J., Wolny, E. A., Smialek, L., and Hasterok, R. (2013). Tissue-specific epigenetic modifications in root apical meristem cells of hordeum vulgare. *PloS One* 8, e69204. doi: 10.1371/journal.pone.0069204

Casal, J. J., and Balasubramanian, S. (2019). Thermomorphogenesis. *Annu. Rev. Plant Biol.* 70, 321–346. doi: 10.1146/annurev-arplant-050718-095919

Castillo, A. M., Allué, S., Costar, A., Álvaro, F., and Vallés, M. P. (2019). Doubled haploid production from Spanish and central European spelt by anther culture. *J. Agric. Sci. Technol.* 21, 1313–1324.

Castillo, A. M., Valero-Rubira, I., Allué, S., Costar, A., and Vallés, M. P. (2021). "Bread wheat doubled haploid production by anther culture". *Doubled haploid Technology: Methods Protocols* ed J. M. Seguí-Simarro (Humana New York NY) 227–244.

Castillo, A. M., Valero-Rubira, I., Burrell, M. A., Allué, S., Costar, A., and Vallés, M. P. (2020). Trichostatin a affects developmental reprogrammning of bread wheat microspores towarsd an embryogenic route. *Plants* 9, 1442.

Castillo, A. M., Valles, M. P., and Cistué, L. (2000). Comparison of anther and isolated microspore cultures in barley. effects of culture density and regeneration medium. *Euphytica* 113, 1–8. doi: 10.1023/A:1003937530907

Dubas, E., Janowiak, F., Krzewska, M., Hura, T., and Żur, I. (2013). Endogenous ABA concentration and cytoplasmic membrane fluidity in microspores of oilseed rape (*Brassica napus l.*) genotypes differing in responsiveness to androgenesis induction. *Plant Cell Rep.* 32, 1465–1475. doi: 10.1007/s00299-013-1458-6

Dubas, E., Moravčíková, J., Libantová, J., Matušíková, I., and Benková, E. (2014). Żur, IThe influence of heat stress on auxin distribution in transgenic *B. napus* microspores and microspore-derived embryos. *alProtoplasma* 251, 1077–1087. doi: 10.1007/s00709-014-0616-1

Evens, N. P., Buchner, P., Williams, L. E., and Hawkesford, M. J. (2017). The role of ZIP transporters and group f bZIP transcription factors in the zn-deficiency response of wheat (*Triticum aestivum*). *Plant J.* 92, 291–304. doi: 10.1111/tpj.13655

Gao, S., Li, L., Han, X., Liu, T., Jin, P., Cai, L., et al. (2021). Genome-wide identification of the histone acetyltransferase gene family in *Triticum aestivum*. *BMC Genomics* 22, 1–17. doi: 10.1186/s12864-020-07348-6

Gehring, M. (2019). Epigenetic dynamics during flowering plant reproduction: evidence for reprogramming? *New Phytol.* 224, 91–96. doi: 10.1111/nph.15856

González-Melendi, P., Ramirez, C., Testillano, P. S., Kumlehn, J., and Risueño, M. C. (2005). Three dimensional confocal and electron microscopy imaging define the

dynamics and mechanisms of diploidisation at early stages of barley microspore-derived embryogenesis. *Planta* 222, 47–57. doi: 10.1007/s00425-005-1515-7

Griggs, R., and Zheng, M. Y. (2016). Nuclear fusion during early stage of microspore embryogenesis indicates chromosome doubling in wheat (*Triticum aestivum*). *Am. J. Plant Sci.* 7, 489–499. doi: 10.4236/ajps.2016.73043

He, C., Chen, X., Huang, H., and Xu, L. (2012). Reprogramming of H3K27me3 is critical for acquisition of pluripotency from cultured arabidopsis tissues. *PloS Genet.* 8, e1002911. doi: 10.1371/journal.pgen.1002911

Henderson, I. R., Deleris, A., Wong, W., Zhong, X., Chin, H. G., Horwitz, G. A., et al. (2010). The *de novo* cytosine methyltransferase DRM2 requires intact UBA domains and a catalytically mutated paralog DRM3 during RNA–directed DNA methylation in arabidopsis thaliana. *PloS Genet.* 6, e1001182. doi: 10.1371/journal.pgen.1001182

Hoekstra, S., Hoekstra, I. R., Hoekstra, R. A., and Hoekstra, E. (1996). The interaction of 2, 4-d application and mannitol pretreatment in anther and microspore culture *of hordeum vulgareL.* cv. igri. *J. Plant Physiol.* 148, 696–700. doi: 10.1016/S0176-1617(96)80370-1

Houben, A., Kumke, K., Nagaki, K., and Hause, G. (2011). CENH3 distribution and differential chromatin modifications during pollen development in rye (Secale cereale l.). *Chromosome Res.* 19, 471–480. doi: 10.1007/s10577-011-9207-6

IBM Corp (2020). *IBM SPSS Statistics for windows* (Armonk, NY: IBM Corp).

Jasencakova, Z., Meister, A., and Schubert, I. (2001). Chromatin organization and its relation to replication and histone acetylation during the cell cycle in barley. *Chromosoma* 110, 83–92. doi: 10.1007/s004120100132

Jensen, T. (2021). The impact of cold and trichostatin a treatment on the transcriptome of wheat microspores. university of lethbridge (Canada). *ProQuest Dissertations Theses* 137.

Jensen, T., Bodell, K., Jiang, F., and Laurie, J. D. (2022). "Doubled haploid production through microspore culture," in *Accelerated breeding of cereal crops*. Eds. A. Bilichak and J. D. Laurie(Humana, New York, NY), 151–166.

Jiang, F., Ryabova, D., Diedhiou, J., Hucl, P., Randhawa, H., Marillia, E. F., et al. (2017). Trichostatin a increases embryo and green plant regeneration in wheat. *Plant Cell Rep.* 36, 1701–1706. doi: 10.1007/s00299-017-2183-3

Jin, P., Gao, S., He, L., Xu, M., Zhang, T., Zhang, F., et al. (2020). Genome-wide identification and expression analysis of the histone deacetylase gene family in wheat (*Triticum aestivum l.*). *Plants* 10, 19. doi: 10.3390/plants10010019

Kong, L., Liu, Y., Wang, X., and Chang, C. (2020). Insight into the role of epigenetic processes in abiotic and biotic stress response in wheat and barley. *Int. J. Mol. Sci.* 21, 1480. doi: 10.3390/ijms21041480

Kumar, V., Thakur, J. K., and Prasad, M. (2021). Histone acetylation dynamics regulating plant development and stress responses. *Cell. Mol. Life Sci.* 78, 4467–4486. doi: 10.1007/s00018-021-03794-x

Lantos, C., Weyen, J., Orsini, J. M., Gnad, H., Schlieter, B., Lein, V., et al. (2013). Efficient application of *in vitro* anther culture for different European winter wheat (*Triticum aestivum l.*) breeding programmes. *Plant Breed.* 132, 149–154. doi: 10.1111/pbr.12032

Larsson, E., Vivian-Smith, A., Offringa, R., and Sundberg, E. (2017). Auxin homeostasis in arabidopsis ovules is anther-dependent at maturation and changes dynamically upon fertilization. *Front. Plant Sci.* 8, 1735. doi: 10.3389/fpls.2017.01735

Lee, K., and Seo, P. J. (2018). Dynamic epigenetic changes during plant regeneration. *Trends Plant Sci.* 23, 235–247. doi: 10.1016/j.tplants.2017.11.009

Li, H., Liu, H., Pei, X., Chen, H., Li, X., Wang, J., et al. (2022). Comparative genome-wide analysis and expression profiling of histone acetyltransferases and histone deacetylases involved in the response to drought in wheat. *J. Plant Growth Regul.* 41, 1065–1078. doi: 10.1007/s00344-021-10364-9

Li, H. J., Liu, N. Y., Shi, D. Q., Liu, J., and Yang, W. C. (2010). YAO is a nucleolar WD40-repeat protein critical for embryogenesis and gametogenesis in arabidopsis. *BMC Plant Biol.* 10, 1–12. doi: 10.1186/1471-2229-10-169

Li, H., Soriano, M., Cordewener, J., Muiño, J. M., Riksen, T., Fukuoka, H., et al. (2014a). The histone deacetylase inhibitor trichostatin a promotes totipotency in the Male gametophyte. *Plant Cell* 26, 195–209. doi: 10.1105/tpc.113.116491

Liu, L., Lu, Y., Wei, L., Yu, H., Cao, Y., Li, Y., et al. (2018a). Transcriptomics analyses reveal the molecular roadmap and long non-coding RNA landscape of sperm cell lineage development. *Plant J.* 96, 421–437. doi: 10.1111/tpj.14041

Liu, H., Wang, J., Li, C., Qiao, L., Wang, X., Li, J., et al. (2018b). Phenotype characterisation and analysis of expression patterns of genes related mainly to carbohydrate metabolism and sporopollenin in male-sterile anthers induced by high temperature in wheat (*Triticum aestivum*). *Crop Pasture Sci.* 69, 469–478. doi: 10.1071/CP18034

Livak, K. J., and Schmittgen, T. D. (2001). Analysis of relative gene expression data using real-time quantitative PCR and the 2– ΔΔCT method. *Methods* 25, 402–408. doi: 10.1006/meth.2001.1262

Li, J., Wang, Z., Chang, Z., He, H., Tang, X., Ma, L., et al. (2021). A functional characterization of TaMs1 orthologs in poaceae plants. *Crop J.* 9, 1291–1300. doi: 10.1016/j.cj.2020.12.002

Li, C., Xu, J., Li, J., Li, Q., and Yang, H. (2014b). Involvement of arabidopsis HAC family genes in pleiotropic developmental processes. *Plant Signaling Behav.* 9, 426–435. doi: 10.1093/pcp/pct180

Lloyd, J. P., and Lister, R. (2022). Epigenome plasticity in plants. *Nat. Rev. Genet.* 23, 55–68. doi: 10.1038/s41576-021-00407-y

Luo, Y., Shi, D. Q., Jia, P. F., Bao, Y., Li, H. J., and Yang, W. C. (2022). Nucleolar histone deacetylases HDT1, HDT2, and HDT3 regulate plant reproductive development. *J. Genet. Genomics* 49, 30–39. doi: 10.1016/j.jgg.2021.10.002

Mozgova, I., Mikulski, P., Pecinka, A., and Farrona, S. (2019). Epigenetic mechanisms of abiotic stress response and memory in plants. *Epigenet. Plants Agronomic Importance: Fundamentals Appl.* Eds. R. Alvarez-Venegas, C. De-la-Peña and J. Casas-Mollano (Springer, Cham), 1–64. doi: 10.1007/978-3-030-14760-0_1

Muñoz-Amatriaín, M., Castillo, A. M., Cistué, L., and Vallés, M. P. (2008). Identification and validation of QTLs for green plant percentage in barley (*Hordeum vulgare l.*) anther culture. *Mol. Breed.* 22, 119–129. doi: 10.1007/s11032-008-9161-y

Muñoz-Amatriaín, M., Svensson, J. T., Castillo, A. M., Cistué, L., Close, T. J., and Vallés, M. P. (2006). Transcriptome analysis of barley anthers: effect of mannitol treatment on microspore embryogenesis. *Physiologia Plantarum* 127, 551–560. doi: 10.1111/j.1399-3054.2006.00729.x

Muñoz-Amatriaín, M., Svesson, J. T., Castillo, A. M., Cistué, L., Close, T. J., and Vallés, M. P. (2009). "Expression profiles in barley microspore embryogenesis," in *Advanced in haploid production in higher plants*. Eds. A. Touraev, B. P. Forster and S. M. Jain (Dordrecht: Springer), 127–134.

Nelms, B., and Walbot, V. (2022). Gametophyte genome activation occurs at pollen mitosis I in maize. *Science* 375, 424–429. doi: 10.1126/science.abl7392

Nielsen, N. H., Andersen, S. U., Stougaard, J., Jensen, A., Backes, G., and Jahoor, A. (2015). Chromosomal regions associated with the *in vitro* culture response of wheat *(Triticum aestivum l.*) microspores. *Plant Breed.* 134, 255–263. doi: 10.1111/pbr.12257

Nowicka, A., Juzoń, K., Krzewska, M., Dziurka, M., Dubas, E., Kopeć, P., et al. (2019). Chemically-induced DNA de-methylation alters the effectiveness of microspore embryogenesis in triticale. *Plant Sci.* 287, 110189. doi: 10.1016/j.plantsci.2019.110189

Okushima, Y., Fukaki, H., Onoda, M., Theologis, A., and Tasaka, M. (2007). ARF7 and ARF19 regulate lateral root formation *via* direct activation of LBD/ASL genes in arabidopsis. *Plant Cell* 19, 118–130. doi: 10.1105/tpc.106.047761

Ono, A., and Kinoshita, T. (2021). Epigenetics and plant reproduction: Multiple steps for responsibly handling succession. *Curr. Opin. Plant Biol.* 61, 102032. doi: 10.1016/j.pbi.2021.102032

Otero, S., Desvoyes, B., Peiró, R., and Gutierrez, C. (2016). Histone H3 dynamics reveal domains with distinct proliferation potential in the arabidopsis root. *Plant Cell* 28, 1361–1371. doi: 10.1105/tpc.15.01003

Pandey, P., Daghma, D. S., Houben, A., Kumlehn, J., Melzer, M., and Rutten, T. (2017). Dynamics of post-translationally modified histones during barley pollen embryogenesis in the presence or absence of the epi-drug trichostatin a. *Plant Reprod.* 30, 95–105. doi: 10.1007/s00497-017-0302-5

Pandey, P., Houben, A., Kumlehn, J., Melzer, M., and Rutten, T. (2013). Chromatin alterations during pollen development in hordeum vulgare. *Cytogenetic Genome Res.* 141, 50–57. doi: 10.1159/000351211

Paolacci, A. R., Tanzarella, O. A., Porceddu, E., and Ciaffi, M. (2009). Identification and validation of reference genes for quantitative RT-PCR normalization in wheat. *BMC Mol. Biol.* 10, 1–27. doi: 10.1186/1471-2199-10-11

Pecinka, A., Dinh, H. Q., Baubec, T., Rosa, M., Lettner, N., and Scheid, O. M. (2010). Epigenetic regulation of repetitive elements is attenuated by prolonged heat stress in arabidopsis. *Plant Cell* 22, 3118–3129. doi: 10.1105/tpc.110.078493

Peng, M., Li, Z., Zhou, N., Ma, M., Jiang, Y., Dong, A., et al. (2018). Linking PHYTOCHROME-INTERACTING FACTOR to histone modification in plant shade avoidance. *Plant Physiol.* 176, 1341–1351. doi: 10.1104/pp.17.01189

Pérez-Pérez, Y., El-Tantawy, A. A., Solís, M. T., Risueño, M. C., and Testillano, P. S. (20191200). Stress-induced microspore embryogenesis requires endogenous auxin synthesis and polar transport in barley. *Front. Plant Sci.* 10.

Pikaard, C. S., and Scheid, O. M. (2014). Epigenetic regulation in plants. *Cold Spring Harbor Perspect. Biol.* 6, a019315. doi: 10.1101/cshperspect.a019315

Placido, D. F., Campbell, M. T., Folsom, J. J., Cui, X., Kruger, G. R., Baenziger, P. S., et al. (2013). Introgression of novel traits from a wild wheat relative improves drought adaptation in wheat. *Plant Physiol.* 161, 1806–1819. doi: 10.1104/pp.113.214262

Portereiko, M. F., Sandaklie-Nikolova, L., Lloyd, A., Dever, C. A., Otsuga, D., and Drews, G. N. (2006). NUCLEAR FUSION DEFECTIVE1 encodes the arabidopsis RPL21M protein and is required for karyogamy during female

gametophyte development and fertilization. *Plant Physiol.* 141, 957–965. doi: 10.1104/pp.106.079319

Probst, A. V., Desvoyes, B., and Gutierrez, C. (2020). Similar yet critically different: the distribution, dynamics and function of histone variants. *J. Exp. Bot.* 71, 5191–5204. doi: 10.1093/jxb/eraa230

Ramírez-González, R. H., Borrill, P., Lang, D., Harrington, S. A., Brinton, J., Venturini, L., et al. (2018). The transcriptional landscape of polyploid wheat. *Science* 361, eaar6089.

R Core Team (2021). *R: A language and environment for statistical computing* (Vienna, Austria: R Foundation for Statistical Computing). Available at: https://www.R-project.org/.

Rodríguez-Sanz, H., Solís, M. T., López, M. F., Gómez-Cadenas, A., Risueño, M. C., and Testillano, P. S. (2014). Auxin biosynthesis, accumulation, action and transport are involved in stress-induced microspore embryogenesis initiation and progression in *Brassica napus*. *Plant Cell Physiol.* 56, 1401–1417. doi: 10.1093/pcp/pcv058

Sánchez-Díaz, R. A. (2014). *Estudio de los mecanismos moleculares implicados en la embriogénesis de la microspora en cebad y trigo* (University of Zaragoza – Estación Experimental Aula Dei (Spain). http://hdl.handle.net/10261/94534

Sánchez-Díaz, R. A., Castillo, A. M., and Vallés, M. P. (2013). Microspore embryogenesis in wheat: New marker genes for early, middle and late stages of embryo development. *Plant Reprod.* 26, 287–296. doi: 10.1007/s00497-013-0225-8

Seifert, F., Bössow, S., Kumlehn, J., Gnad, H., and Scholten, S. (2016). Analysis of wheat microspore embryogenesis induction by transcriptome and small RNA sequencing using the highly responsive cultivar "Svilena. *BMC Plant Biol.* 16, 1–16. doi: 10.1186/s12870-016-0782-8

Singh, M., Singh, S., Randhawa, H., and Singh, J. (2013). Polymorphic homoeolog of key gene of RdDM pathway, ARGONAUTE4_9 class is associated with pre-harvest sprouting in wheat (*Triticum aestivum l.*). *PloS One* 8, e77009. doi: 10.1371/journal.pone.0077009

Solís, M. T., El-Tantawy, A. A., Cano, V., Risueño, M. C., and Testillano, P. S. (2015). 5-azacytidine promotes microspore embryogenesis initiation by decreasing global DNA methylation, but prevents subsequent embryo development in rapeseed and barley. *Front. Plant Sci.* 6, 472. doi: 10.3389/fpls.2015.00472

Solís, M. T., Rodríguez-Serrano, M., Meijón, M., Cañal, M. J., Cifuentes, A., Risueño, M. C., et al. (2012). DNA Methylation dynamics and MET1a-like gene expression changes during stress-induced pollen reprogramming to embryogenesis. *J. Exp. Bot.* 63, 6431–6444. doi: 10.1093/jxb/ers298

Soriano, M. (2008). *Embriogénesis de la microspora en trigo panadero: optimización de la producción de plantas doblehaploides y estudio de genes de estrés durante el pretratamiento* (University of Zaragoza – Estación Experimental Aula Dei (Spain).

Soriano, M., Li, H., and Boutilier, K. (2013). Microspore embryogenesis: Establishment of embryo identity and pattern in culture. *Plant Reprod.* 26, 181–196. doi: 10.1007/s00497-013-0226-7

Soriano, M., Li, H., Jacquard, C., Angenent, G. C., Krochko, J., Offringa, R., et al. (2014). Plasticity in cell division patterns and auxin transport dependency during *in vitro* embryogenesis in brassica napus. *Plant Cell* 26 (6), 2568–2581. doi: 10.1105/tpc.114.126300

Strejčková, B., Čegan, R., Pecinka, A., Milec, Z., and Šafář, J. (2020). Identification of polycomb repressive complex 1 and 2 core components in hexaploid bread wheat. *BMC Plant Biol.* 20, 1–13.

Tang, Y., Liu, X., Liu, X., Li, Y., Wu, K., and Hou, X. (2017). Arabidopsis NF-YCs mediate the light-controlled hypocotyl elongation *via* modulating histone acetylation. *Mol. Plant* 10, 260–273. doi: 10.1016/j.molp.2016.11.007

Tasset, C., Singh Yadav, A., Sureshkumar, S., Singh, R., van der Woude, L., Nekrasov, M., et al. (2018). POWERDRESS-mediated histone deacetylation is essential for thermomorphogenesis in arabidopsis thaliana. *PloS Genet.* 14, e1007280. doi: 10.1371/journal.pgen.1007280

Tessarz, P., and Kouzarides, T. (2014). Histone core modifications regulating nucleosome structure and dynamics. *Nat. Rev. Mol. Cell Biol.* 15, 703–708. doi: 10.1038/nrm3890

Testillano, P. S. (2019). Microspore embryogenesis: targeting the determinant factors of stress-induced cell reprogramming for crop improvement. *J. Exp. Bot.* 70, 2965–2978. doi: 10.1093/jxb/ery464

Tian, T., Liu, Y., Yan, H., You, Q., Yi, X., Du, Z., et al. (2017). agriGO v2.0: a GO analysis toolkit for the agricultural community. *Nucleic Acids Res.* 45, 122–129. doi: 10.1093/nar/gkx382

Wang, H. M., Enns, J. L., Nelson, K. L., Brost, J. M., Orr, T. D., and Ferrie, A. M. R. (2019). Improving the efficiency of wheat microspore culture methodology: Evaluation of pretreatments, gradients, and epigenetic chemicals. *Plant Cell Tissue Organ Culture* 139, 589–599. doi: 10.1007/s11240-019-01704-5

Wang, Z., Li, J., Chen, S., Heng, Y., Chen, Z., Yang, J., et al. (2017). Poaceae-specific MS1 encodes a phospholipid-binding protein for male fertility in bread wheat. *Proc. Natl. Acad. Sci.* 114, 12614–12619. doi: 10.1073/pnas.1715570114

Wang, Z., Zhang, R., Cheng, Y., Lei, P., Song, W., Zheng, W., et al. (2021). Genome-wide identification, evolution, and expression analysis of LBD transcription factor family in bread wheat (*Triticum aestivum l.*). *Front. Plant Sci.* 12, 1870. doi: 10.3389/fpls.2021.721253

Wang, P., Zhang, H., Hou, H., Wang, Q., Li, Y., Huang, Y., et al. (2016). Cell cycle arrest induced by inhibitors of epigenetic modifications in maize (Zea mays) seedling leaves: characterization of the process and possible mechanisms involved. *New Phytol.* 211, 646–657. doi: 10.1111/nph.13942

Waterborg, J. H. (1991). Multiplicity of histone h3 variants in wheat, barley, rice, and maize. *Plant Physiol.* 96, 453–458. doi: 10.1104/pp.96.2.453

Weigt, D., Kiel, A., Siatkowski, I., Zyprych-Walczak, J., Tomkowiak, A., and Kwiatek, M. (2019). Comparison of the androgenic response of spring and winter wheat (*Triticum aestivum l.*). *Plants* 9, 49. doi: 10.3390/plants9010049

Wolny, E., Braszewska-Zalewska, A., and Hasterok, R. (2014). Spatial distribution of epigenetic modifications in brachypodium distachyon embryos during seed maturation and germination. *PloS One* 9, e101246. doi: 10.1371/journal.pone.0101246

Woloszynska, M., Gagliardi, O., Vandenbussche, F., De Groeve, S., Alonso Baez, L., Neyt, P., et al. (2018). The elongator complex regulates hypocotyl growth in darkness and during photomorphogenesis. *J. Cell Sci.* 131, jcs203927.

Xu, J., Hu, P., Tao, Y., Song, P., Gao, H., and Guan, Y. (2021). Genome-wide identification and characterization of the lateral organ boundaries domain (LBD) gene family in polyploid wheat and related species. *Peer J.* 9, e11811. doi: 10.7717/peerj.11811

Xu, C. R., Liu, C., Wang, Y. L., Li, L. C., Chen, W. Q., Xu, Z. H., et al. (2005). Histone acetylation affects expression of cellular patterning genes in the arabidopsis root epidermis. *Proc. Natl. Acad. Sci.* 102, 14469–14474. doi: 10.1073/pnas.0503143102

Yan, A., Borg, M., Berger, F., and Chen, Z. (2020). The atypical histone variant H3. 15 promotes callus formation in arabidopsis thaliana. *Development* 147, dev184895.

Yang, Y., Xu, T., Wang, H., and Feng, D. (2021). Genome-wide identification and expression analysis of the TaYUCCA gene family in wheat. *Mol. Biol. Rep.* 48, 1269–1279. doi: 10.1007/s11033-021-06197-0

Yan, J., Su, P., Wei, Z., Nevo, E., and Kong, L. (2017). Genome-wide identification, classification, evolutionary analysis and gene expression patterns of the protein kinase gene family in wheat and *Aegilops tauschii*. *Plant Mol. Biol.* 95, 227–242. doi: 10.1007/s11103-017-0637-1

Ye, J., Coulouris, G., Zaretskaya, I., Cutcutache, I., Rozen, S., and Madden, T. L. (2012). Primer-BLAST: a tool to design target-specific primers for polymerase chain reaction. *BMC Bioinf.* 13, 1–11. doi: 10.1186/1471-2105-13-S6-S1

Yung, W. S., Li, M. W., Sze, C. C., Wang, Q., and Lam, H. M. (2021). Histone modifications and chromatin remodelling in plants in response to salt stress. *Physiologia Plantarum* 173, 1495–1513. doi: 10.1111/ppl.13467

Zentella, R., Zhang, Z. L., Park, M., Thomas, S. G., Endo, A., Murase, K., et al. (2007). Global analysis of DELLA direct targets in early gibberellin signaling in arabidopsis. *Plant Cell* 19, 3037–3057. doi: 10.1105/tpc.107.054999

Zhang, T., Liu, P., Zhong, K., Zhang, F., and Xu, M. He, l.et al). wheat yellow mosaic virus NIb interacting with host light induced protein (LIP) facilitates its infection through perturbing the abscisic acid pathway in wheat. *Biology* 8, 80. doi: 10.3390/biology8040080

Zhang, L., Zhang, Y., Gao, Y., Jiang, X., Zhang, M., Wu, H., et al. (2016). Effects of histone deacetylase inhibitors on microspore embryogenesis and plant regeneration in pakchoi (Brassica rapa ssp. *chinensis L.) Sci. Hortic.* 209, 61–66. doi: 10.1016/j.scienta.2016.05.001

Zhi, P., Kong, L., Liu, J., Zhang, X., Wang, X., Li, H., et al. (2020). Histone deacetylase TaHDT701 functions in TaHDA6-TaHOS15 complex to regulate wheat defense responses to *Blumeria graminis* f. *sp tritici Int. J. Mol. Sci.* 21, 2640. doi: 10.3390/ijms21072640

Zur, I., Dubas, E., Krzewska, M., and Janowiak, F. (2015). Current insights into hormonal regulation of microspore embryogenesis. *Front. Plant Sci.* 6, 424.

Zur, I., Krzewska, M., Dubas, E., Janowiak, F., Golemiec, E., and Golebiowska-Pikania, G. (2012). The possible role of ABA in androgenesis induction in triticale (x Triticosecale Wittm.). *Acta biologica cracoviensia. Ser. Botanica Supplement* 54, 91.

Frontiers in Plant Science

Cultivates the science of plant biology and its applications

The most cited plant science journal, which advances our understanding of plant biology for sustainable food security, functional ecosystems and human health.

Discover the latest Research Topics

See more →

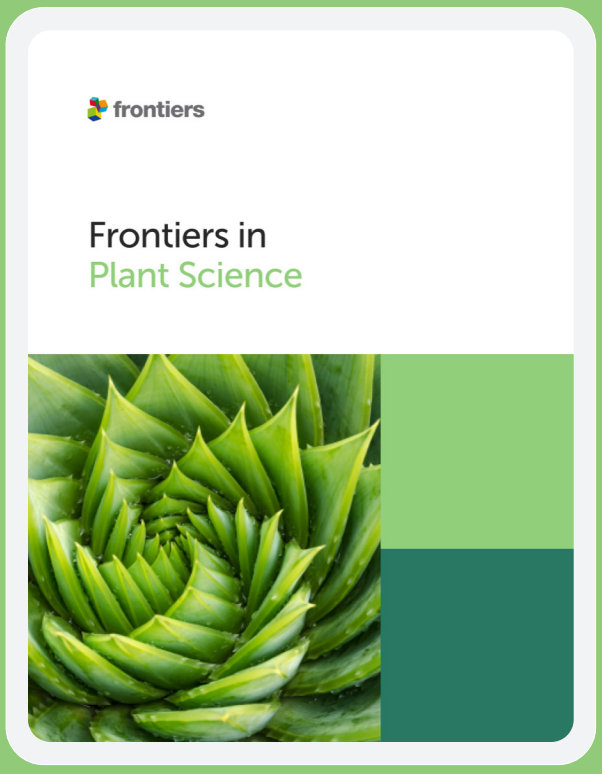

Frontiers

Avenue du Tribunal-Fédéral 34
1005 Lausanne, Switzerland
frontiersin.org

Contact us

+41 (0)21 510 17 00
frontiersin.org/about/contact